Measurement of chaperone-mediated effects on polyglutamine protein aggregation by the filter trap assay

van Waarde-Verhagen, Maria A.W.H.; Kampinga, Harm H.

Published in:
Methods in Molecular Biology

DOI:
10.1007/978-1-4939-7477-1_5

Publication date:
2018

Methods in Molecular Biology 1709

Springer Protocols

Stuart K. Calderwood
Thomas L. Prince
Editors

Chaperones

Methods and Protocols

Humana Press

METHODS IN MOLECULAR BIOLOGY

Series Editor
John M. Walker
School of Life and Medical Sciences
University of Hertfordshire
Hatfield, Hertfordshire, AL10 9AB, UK

For further volumes:
http://www.springer.com/series/7651

Chaperones

Methods and Protocols

Edited by

Stuart K. Calderwood

Department of Radiation Oncology, Beth Israel Deaconess Medical Center Harvard Medical School Boston, MA, USA

Thomas L. Prince

Department of Urology Weis Center for Research Geisinger Clinic Danville, PA, USA

Humana Press

Editors
Stuart K. Calderwood
Department of Radiation
Oncology, Beth Israel Deaconess
Medical Center
Harvard Medical School
Boston, MA, USA

Thomas L. Prince
Department of Urology
Weis Center for Research
Geisinger Clinic
Danville, PA, USA

ISSN 1064-3745 ISSN 1940-6029 (electronic)
Methods in Molecular Biology
ISBN 978-1-4939-7476-4 ISBN 978-1-4939-7477-1 (eBook)
https://doi.org/10.1007/978-1-4939-7477-1

Library of Congress Control Number: 2017958738

Printed on acid-free paper

This Humana Press imprint is published by Springer Nature
The registered company is Springer Science+Business Media, LLC
The registered company address is: 233 Spring Street, New York, NY 10013, U.S.A.

Dedication

I (T.L.P.) would like to dedicate this book to my lovely wife Bourdana, our son Jessup, and the memory of my mother Suzanne Irene Prince.

The book is also dedicated to my family (S.K.C.), including my wife Laura, daughter Roxanne, and son Alexander, in recognition of their patience during the long hours I had to spend away from them while in the laboratory or traveling.

Preface

Life is a complex and dynamic interplay of energy and mass within space and time. Biological life depends on proteins to carry out the reactions and processes that allow communities of cells to cooperate and compete to propagate their genetic information. Proteins are complex linear polymers that fold into specific structures that give them function. Molecular chaperones are a family of proteins that help fold and maintain the 3-dimensional structure of a significant portion of proteins in the proteome. The cellular stress response is the mechanism for acutely initiating the expression of molecular chaperones, often referred to as Heat Shock Proteins (HSPs), to refold and process aggregated proteins when proteostasis is perturbed. Molecular chaperones and the cellular stress response affect all aspects of our lives. Increased chaperone capacity and a hijacked stress response enable cancer to grow more malignant and strike down our youth, family providers, and thoughtful leaders. In contrast, reduced chaperone activity allows for the formation of protein aggregates that result in the neurodegeneration of our aged citizens and sometimes the politically powerful. How an organism or population responds to stress determines its evolution. The state of knowledge concerning molecular chaperones reflects our actual knowledge of biology, health, and disease.

This volume of methods and topics is a compilation of laboratory protocols and methodology required for the study of molecular chaperones and the cellular stress response. Our authors devoted their expertise, time, and energy into each chapter. Some chapters are extensive; some chapters are succinct; all address an important area of molecular chaperone research. We greatly appreciate each author's contribution and hope that this volume aids in the education of the next generation of scientists studying molecular chaperones and the cellular stress response.

We begin this volume with the study of the cellular stress response and its initiation by heat shock transcription factors (HSFs) that bind to the promoters in HSP genes and induce expression. In Chapter 1, Mivechi and colleagues describe the generation of key resources for studying the stress response in Hsf1, Hsf2, and Hsf4 knockout mice. We next provide an overview of techniques that have laid the foundation for the study of HSF function and activity in Chapter 2. In Chapter 3, we describe a method for real-time monitoring of the degree and duration of the transcribed heat shock response and its alteration by drugs.

The next two chapters describe powerful methods for mapping HSP interaction networks and testing chaperone function. In Chapter 4, Mikko Taipale explains the use of the luminescence-based mammalian interactome (LUMIER) assay to define the interactome of the molecular chaperone, Hsp90, providing insight into the role of Hsp90 as a network hub in diseases such as cancer. In Chapter 5, Kampinga and van Waarde-Verhagen describe the application of a filter trap assay for studying the ability of HSPs to prevent poly-Q protein aggregations that occur in neurodegenerative diseases.

Methods for screening small molecule libraries for modulators of chaperone function are also addressed. The importance of this area of research has grown with our understanding of the role of molecular chaperones in health and disease. In Chapter 6, Timothy

Haystead reviews Hsp70 biology and explains the use of the fluorescence-linked enzyme chemoproteomic strategy (FLECS) for identifying new Hsp70 inhibitors. In Chapter 7, Bob Matts and colleagues describe a cell-free, high-throughput, luciferase assay that exploits the protein folding activity of Hsp90.

The next section follows the course of using cell culture models to test the cytotoxicity of HSP inhibitors as described by Lee et al. in Chapter 8 and Kabakov and Gabai in Chapter 9. HSP inhibitors may also be combined with other targeted therapies, such as kinase inhibitors, to achieve synergistic tumor toxicity as explained by Gibbs and Sourbier in Chapter 10. These inhibitor treatments can then be profiled at the level of the proteome to ultimately determine their mechanisms of action as detailed by Hartson and colleagues in Chapter 11.

The following chapters describe methods for the biochemical characterization of HSPs. In Chapter 12, Patrick Arrigo describes the analysis of the oligomerization and phosphorylation state of the small HSP, HspB1. Mayer and Rampelt explain the chaperone binding cycle of Hsp70 and the study of nucleotide exchange factors (NEFs) in Chapter 13. In Chapter 14, Michael Reidy describes how glucocorticoid receptor activity in yeast can be used to assess chaperone function. The Wickner lab explains the use of bacterial Hsp90 ATPase assays in Chapter 15. Finally, Mollapour and coworkers in Chapter 16 write about the detection of Hsp90 post-translational modifications by Western blot analysis.

The use of next-generation sequencing techniques is showcased in the following chapters. Yoveva and Sawarkar expand on the role of the Hsp90 machine in the nucleus with ChIP-Seq analysis in Chapter 17. In Chapter 18, Lang and Holton detail the use of RNA-Seq to study the effects of altered chaperone activity.

Computational analysis of chaperone interactions at the biophysical level and interactome are described in Chapters 19 and 20. Gennady Verkhivker reviews and explains computational approaches for modeling allosteric Hsp90 interactions with individual cochaperones, client proteins, and small molecule inhibitors. Kumar and Rizzolo provide protocols for finding chaperone interacting proteins and building comprehensive interaction networks that may be explored to identify biologically significant protein complexes.

In Chapters 21–23, methods for the detection and localization of HSPs are described. Macario and colleagues explain the role of the mitochondrial chaperonin, Hsp60, in autoimmune disorders and cancer along with Hsp60 detection by immunohistochemistry in clinical samples. Stangl et al. profile the stress-inducible form of Hsp70 in cancer and explain its cytosolic detection in formalin-fixed paraffin-embedded sections and detection of plasma membrane-associated Hsp70 by multiparametric flow cytometry. And Bourboulia and coworkers summarize the study of extracellular Hsp90 and its detection by immunoprecipitation-Western blot analysis.

Methods surrounding the role of HSPs in immunity and vaccine development are outlined in Chapters 24–26. Murshid and colleagues describe the investigation of receptors that bind extracellular HSPs that influence adaptive immunity. A method for creating cancer vaccines using large HSPs to prime professional antigen presenting cells by Guo et al. is presented in Chapter 25. Then Weng et al. describe how to prepare Hsp70-based vaccines derived from dendritic-tumor fusion cells.

The last section comprising Chapters 27–29 extensively reviews the biologies of Hsp70 and Hsp90 along with the targeting of their function in the clinic. Boudesco et al. write about the oncogenesis enabling properties of Hsp70 as both an extra- and intracellular agent along with strategies for inhibiting its activity. Next Johnson and Cox elucidate the Hsp90 chaperone machine and its network of cochaperones that regulate and direct its function. Finally, Trepel and colleagues provide an overview of the use of Hsp90 inhibitors in the cancer clinic and the use of pharmacodynamics assays to track efficacy.

Boston, MA, USA — *Stuart K. Calderwood*
Danville, PA, USA — *Thomas L. Prince*

Contents

Preface ..... *vii*
Contributors ..... *xv*

1 Targeted Deletion of Hsf1, 2, and 4 Genes in Mice 1
Xiongjie Jin, Binnur Eroglu, Demetrius Moskophidis, and Nahid F. Mivechi

2 Role of Heat Shock Factors in Stress-Induced Transcription 23
Ayesha Murshid, Thomas L. Prince, Ben Lang, and Stuart K. Calderwood

3 Monitoring of the Heat Shock Response with a Real-Time Luciferase Reporter 35
Toshiki Kijima, Takanori Eguchi, Len Neckers, and Thomas L. Prince

4 Quantitative Profiling of Chaperone/Client Interactions with LUMIER Assay 47
Mikko Taipale

5 Measurement of Chaperone-Mediated Effects on Polyglutamine Protein Aggregation by the Filter Trap Assay 59
Maria A.W.H. van Waarde-Verhagen and Harm H. Kampinga

6 Fluorescent-Linked Enzyme Chemoproteomic Strategy (FLECS) for Identifying HSP70 Inhibitors 75
T.A. J. Haystead

7 A High-Throughput Screen for Inhibitors of the Hsp90-Chaperone Machine 87
Jason Davenport, Lakshmi Galam, and Robert L. Matts

8 Primary Colorectal Cells Culture as a Translational Research Model 97
Sheah Lin Lee, Nina Claire Dempsey-Hibbert, Dale Vimalachandran, Terence David Wardle, Paul A. Sutton, and John H.H. Williams

9 Cell Death and Survival Assays 107
Alexander E. Kabakov and Vladimir L. Gabai

10 Detecting the Potential Pharmacological Synergy of Drug Combination by Viability Assays In Vitro 129
Benjamin K. Gibbs and Carole Sourbier

11 Proteomic Profiling of Hsp90 Inhibitors 139
Sudhakar Voruganti, Jake T. Kline, Maurie J. Balch, Janet Rogers, Robert L. Matts, and Steven D. Hartson

12 Analysis of HspB1 (Hsp27) Oligomerization and Phosphorylation Patterns and Its Interaction with Specific Client Polypeptides 163
André-Patrick Arrigo

13 Nucleotide Exchange Factors for Hsp70 Chaperones 179
Heike Rampelt, Matthias P. Mayer, and Bernd Bukau

14 Determination of Hsp90 Activity Through Activation of Glucocorticoid Receptors in Yeast 189
Michael Reidy

15 Bacterial Hsp90 ATPase Assays 199
Joel R. Hoskins, Sue Wickner, and Shannon M. Doyle

16 Detecting Posttranslational Modifications of Hsp90. 209
Rebecca A. Sager, Mark R. Woodford, Len Neckers, and Mehdi Mollapour

17 Chromatin Immunoprecipitation (ChIP) of Heat Shock Protein 90 (Hsp90) 221
Aneliya Yoveva and Ritwick Sawarkar

18 A Workflow Guide to RNA-seq Analysis of Chaperone Function and Beyond 233
Benjamin J. Lang, Kristina M. Holton, Jianlin Gong, and Stuart K. Calderwood

19 Computational Modeling of the Hsp90 Interactions with Cochaperones and Small-Molecule Inhibitors. 253
Gennady M. Verkhivker

20 Computational Analysis of the Chaperone Interaction Networks. 275
Ashwani Kumar, Kamran Rizzolo, Sandra Zilles, Mohan Babu, and Walid A. Houry

21 Immunohistochemistry of Human Hsp60 in Health and Disease: From Autoimmunity to Cancer 293
Francesco Cappello, Everly Conway de Macario, Francesca Rappa, Giovanni Zummo, and Alberto J.L. Macario

22 Immunohistochemical and Flow Cytometric Analysis of Intracellular and Membrane-Bound Hsp70, as a Putative Biomarker of Glioblastoma Multiforme, Using the cmHsp70.1 Monoclonal Antibody 307
Stefan Stangl, Gemma A. Foulds, Helena Fellinger, Geoffrey J. Pilkington, A. Graham Pockley, and Gabriele Multhoff

23 Detection and Analysis of Extracellular Hsp90 (eHsp90) 321
Stephanie Cortes, Alexander J. Baker-Williams, Mehdi Mollapour, and Dimitra Bourboulia

24 Molecular Chaperone Receptors 331
Ayesha Murshid, Jimmy Theriault, Jianlin Gong, and Stuart K. Calderwood

25 Creation of Recombinant Chaperone Vaccine Using Large Heat Shock Protein for Antigen-Targeted Cancer Immunotherapy. 345
Chunqing Guo, John R. Subjeck, and Xiang-Yang Wang

26 A Novel Heat Shock Protein 70-based Vaccine Prepared from DC-Tumor Fusion Cells 359
Desheng Weng, Stuart K. Calderwood, and Jianlin Gong

27 Hsp70: A Cancer Target Inside and Outside the Cell. 371
Christophe Boudesco, Sebastien Cause, Gaëtan Jego, and Carmen Garrido

28 Evidence for Hsp90 Co-chaperones in Regulating Hsp90 Function and Promoting Client Protein Folding 397
Marc B. Cox and Jill L. Johnson

29 Clinical Evaluation and Biomarker Profiling of Hsp90 Inhibitors 423
Akira Yuno, Min-Jung Lee, Sunmin Lee, Yusuke Tomita, David Rekhtman, Brittni Moore, and Jane B. Trepel

Index *443*

Contributors

André-Patrick Arrigo • *Cancer and Development Laboratory, Lyon Cancer Research Center, Centre Léon Bérard, UMR INSERM 1052-CNRS 5286, Claude Bernard University, Lyon, France*

Mohan Babu • *Department of Biochemistry, Research and Innovation Centre, University of Regina, Regina, SK, Canada*

Alexander J. Baker-Williams • *Department of Urology, SUNY Upstate Medical University, Syracuse, NY, USA; Department of Biochemistry and Molecular Biology, SUNY Upstate Medical University, Syracuse, NY, USA*

Maurie J. Balch • *Department of Biochemistry and Molecular Biology, Oklahoma State University, Stillwater, OK, USA*

Christophe Boudesco • *Univ. Bourgogne Franche-Comté, LNC UMR1231, Dijon, France; INSERM, LNC UMR1231, Dijon, France; Equipe Labellisée par la Ligue Nationale Contre le Cancer, INSERM, LNC UMR1231, Dijon, France; LipSTIC LabEx, Fondation de Coopération Scientifique Bourgogne Franche-Comté, Dijon, France*

Dimitra Bourboulia • *Department of Urology, SUNY Upstate Medical University, Syracuse, NY, USA; Department of Biochemistry and Molecular Biology, SUNY Upstate Medical University, Syracuse, NY, USA; Cancer Research Institute, SUNY Upstate Medical University, Syracuse, NY, USA*

Bernd Bukau • *Center for Molecular Biology of Heidelberg University (ZMBH), DKFZ-ZMBH Alliance, Heidelberg, Germany*

Stuart K. Calderwood • *Department of Radiation Oncology, Beth Israel Deaconess Medical Center, Harvard Medical School, Boston, MA, USA*

Francesco Cappello • *Human Anatomy Section, Department of Experimental Biomedicine and Clinical Neurosciences, University of Palermo, Palermo, Italy; Euro-Mediterranean Institute of Science and Technology (IEMEST), Palermo, Italy*

Sebastien Cause • *Univ. Bourgogne Franche-Comté, LNC UMR1231, Dijon, France; INSERM, LNC UMR1231, Dijon, France; Equipe Labellisée par la Ligue Nationale Contre le Cancer, INSERM, LNC UMR1231, Dijon, France; LipSTIC LabEx, Fondation de Coopération Scientifique Bourgogne Franche-Comté, Dijon, France*

Everly Conway de Macario • *Euro-Mediterranean Institute of Science and Technology (IEMEST), Palermo, Italy; Department of Microbiology and Immunology, School of Medicine, University of Maryland at Baltimore, and IMET, Columbus Center, Baltimore, MD, USA*

Stephanie Cortes • *Department of Urology, SUNY Upstate Medical University, Syracuse, NY, USA; College of Medicine, SUNY Upstate Medical University, Syracuse, NY, USA*

Marc B. Cox • *Department of Biological Sciences, University of Texas at El Paso and the Border Biomedical Research Center, El Paso, TX, USA*

Jason Davenport • *Department of Biochemistry and Molecular Biology, Oklahoma State University, Stillwater, OK, USA; SensiQ Technologies, Inc., Oklahoma City, OK, USA*

Nina Claire Dempsey-Hibbert • *Chester Centre for Stress Research, Institute of Medicine, University of Chester, Chester, UK; Centre for Biomedicine Research, Manchester Metropolitan University, Manchester, UK*

Shannon M. Doyle • *Laboratory of Molecular Biology, National Cancer Institute, National Institutes of Health, Bethesda, MD, USA*
Takanori Eguchi • *Department of Dental Pharmacology, Graduate School of Medicine, Dentistry and Pharmaceutical Sciences, Okayama University, Okayama, Japan*
Binnur Eroglu • *Molecular Chaperone Biology, Medical College of Georgia, Augusta University, Georgia Cancer Center, Augusta, GA, USA*
Helena Fellinger • *Department of Radiation Oncology, Klinikum Rechts der Isar, Technische Universität München, Munich, Germany*
Gemma A. Foulds • *John van Geest Cancer Research Centre, School of Science and Technology, Nottingham Trent University, Nottingham, UK*
Vladimir L. Gabai • *Department of Biochemistry, Boston University Medical School, Boston, MA, USA*
Lakshmi Galam • *Department of Biochemistry and Molecular Biology, Oklahoma State University, Stillwater, OK, USA; University of South Florida School of Medicine, Tampa, FL, USA*
Carmen Garrido • *Univ. Bourgogne Franche-Comté, LNC UMR1231, Dijon, France; INSERM, LNC UMR1231, Dijon, France; Equipe Labellisée par la Ligue Nationale Contre le Cancer, INSERM, LNC UMR1231, Dijon, France; LipSTIC LabEx, Fondation de Coopération Scientifique Bourgogne Franche-Comté, Dijon, France*
Benjamin K. Gibbs • *Urologic Oncology Branch, Center for Cancer Research, National Cancer Institute, Bethesda, MD, USA*
Jianlin Gong • *Department of Medicine, Boston University School of Medicine, Boston, MA, USA*
Chunqing Guo • *Department of Human Molecular Genetics, Virginia Commonwealth University, Richmond, VA, USA; Massey Cancer Center, Virginia Commonwealth University, Richmond, VA, USA; Institute of Molecular Medicine, Virginia Commonwealth University, Richmond, VA, USA*
Steven D. Hartson • *Department of Biochemistry and Molecular Biology, Oklahoma State University, Stillwater, OK, USA*
T.A.J. Haystead • *Department of Pharmacology and Cancer Biology, Duke University, Durham, NC, USA*
Kristina M. Holton • *Research Computing, Harvard Medical School, Boston, MA, USA*
Joel R. Hoskins • *Laboratory of Molecular Biology, National Cancer Institute, National Institutes of Health, Bethesda, MD, USA*
Walid A. Houry • *Department of Biochemistry, University of Toronto, Toronto, ON, Canada; Department of Chemistry, University of Toronto, Toronto, ON, Canada; Department of Biochemistry, Faculty of Medicine, University of Toronto, Toronto, ON, Canada*
Gaëtan Jego • *Univ. Bourgogne Franche-Comté, LNC UMR1231, Dijon, France; INSERM, LNC UMR1231, Dijon, France; Equipe Labellisée par la Ligue Nationale Contre le Cancer, INSERM, LNC UMR1231, Dijon, France; LipSTIC LabEx, Fondation de Coopération Scientifique Bourgogne Franche-Comté, Dijon, France*
Xiongjie Jin • *Molecular Chaperone Biology, Medical College of Georgia, Augusta University, Georgia Cancer Center, Augusta, GA, USA*
Jill L. Johnson • *Department of Biological Sciences and the Center for Reproductive Biology, University of Idaho, Moscow, ID, USA*
Alexander E. Kabakov • *Department of Radiation Biochemistry, A. Tsyb Medical Radiology Research Center, Obninsk, Russia*

Harm H. Kampinga • *University Medical Center Groningen, University of Groningen, Department of Cell Biology, Groningen, The Netherlands*
Toshiki Kijima • *Department of Urology, Tokyo Medical and Dental University Graduate School, Tokyo, Japan*
Jake T. Kline • *Department of Biochemistry and Molecular Biology, Oklahoma State University, Stillwater, OK, USA*
Ashwani Kumar • *Department of Computer Science, University of Regina, Regina, SK, Canada*
Ben Lang • *Molecular and Cellular Radiation Oncology, Beth Israel Deaconess Medical Center, Harvard Medical School, Boston, MA, USA*
Benjamin J. Lang • *Department of Radiation Oncology, Beth Israel Deaconess Medical Center, Harvard Medical School, Boston, MA, USA*
Min-Jung Lee • *Developmental Therapeutics Branch, Center for Cancer Research, NCI, NIH, Bethesda, MD, USA*
Sheah Lin Lee • *Chester Centre for Stress Research, Institute of Medicine, University of Chester, Chester, UK; University Hospital Southampton, Southampton, UK*
Sunmin Lee • *Developmental Therapeutics Branch, Center for Cancer Research, NCI, NIH, Bethesda, MD, USA*
Alberto J.L. Macario • *Euro-Mediterranean Institute of Science and Technology (IEMEST), Palermo, Italy; Department of Microbiology and Immunology, School of Medicine, University of Maryland at Baltimore, and IMET, Columbus Center, Baltimore, MD, USA*
Robert L. Matts • *Department of Biochemistry and Molecular Biology, Oklahoma State University, Stillwater, OK, USA*
Matthias P. Mayer • *Center for Molecular Biology of Heidelberg University (ZMBH), DKFZ-ZMBH Alliance, Heidelberg, Germany*
Nahid F. Mivechi • *Molecular Chaperone Biology, Medical College of Georgia, Augusta University, Georgia Cancer Center, Augusta, GA, USA*
Mehdi Mollapour • *Department of Urology, SUNY Upstate Medical University, Syracuse, NY, USA; Upstate Cancer Center, SUNY Upstate Medical University, Syracuse, NY, USA; Department of Biochemistry and Molecular Biology, SUNY Upstate Medical University, Syracuse, NY, USA*
Brittni Moore • *Developmental Therapeutics Branch, Center for Cancer Research, NCI, NIH, Bethesda, MD, USA*
Demetrius Moskophidis • *Molecular Chaperone Biology, Medical College of Georgia, Augusta University, Georgia Cancer Center, Augusta, GA, USA*
Gabriele Multhoff • *Department of Radiation Oncology, Klinikum Rechts der Isar, Technische Universität München, Munich, Germany; CCG-Innate Immunity in Tumor Biology, Helmholtz Zentrum München, Neuherberg, Germany*
Ayesha Murshid • *Molecular and Cellular Radiation Oncology, Beth Israel Deaconess Medical Center, Harvard Medical School, Boston, MA, USA*
Len Neckers • *Urologic Oncology Branch, Center for Cancer Research, National Cancer Institute, National Institutes of Health, Bethesda, MD, USA*
Geoffrey J. Pilkington • *Brain Tumour Research Centre, Institute of Biomedical and Biomolecular Sciences, School of Pharmacy and Biomedical Sciences, University of Portsmouth, Portsmouth, UK*

A. Graham Pockley • *Department of Radiation Oncology, Klinikum Rechts der Isar, Technische Universität München, Munich, Germany; John van Geest Cancer Research Centre, School of Science and Technology, Nottingham Trent University, Nottingham, UK*
Thomas L. Prince • *Department of Urology, Weis Center for Research, Geisinger Clinic, Danville, PA, USA*
Heike Rampelt • *Center for Molecular Biology of Heidelberg University (ZMBH), DKFZ-ZMBH Alliance, Heidelberg, Germany; Faculty of Medicine, Institute of Biochemistry and Molecular Biology, ZMBZ, Freiburg, Germany*
Francesca Rappa • *Human Anatomy Section, Department of Experimental Biomedicine and Clinical Neurosciences, University of Palermo, Palermo, Italy; Euro-Mediterranean Institute of Science and Technology (IEMEST), Palermo, Italy*
Michael Reidy • *Laboratory of Biochemistry and Genetics, National Institute of Diabetes, Digestive and Kidney Diseases, National Institutes of Health, Bethesda, MD, USA*
David Rekhtman • *Developmental Therapeutics Branch, Center for Cancer Research, NCI, NIH, Bethesda, MD, USA*
Kamran Rizzolo • *Department of Biochemistry, University of Toronto, Toronto, ON, Canada*
Janet Rogers • *Department of Biochemistry and Molecular Biology, Oklahoma State University, Stillwater, OK, USA*
Rebecca A. Sager • *Department of Urology, SUNY Upstate Medical University, Syracuse, NY, USA; Upstate Cancer Center, SUNY Upstate Medical University, Syracuse, NY, USA; Department of Biochemistry and Molecular Biology, SUNY Upstate Medical University, Syracuse, NY, USA*
Ritwick Sawarkar • *Max Planck Institute of Immunobiology and Epigenetics, Freiburg, Germany*
Carole Sourbier • *Urologic Oncology Branch, Center for Cancer Research, National Cancer Institute, Bethesda, MD, USA*
Stefan Stangl • *Department of Radiation Oncology, Klinikum Rechts der Isar, Technische Universität München, Munich, Germany*
John R. Subjeck • *Department of Cellular Stress Biology, Roswell Park Cancer Institute, Buffalo, NY, USA*
Paul A. Sutton • *Countess of Chester Hospital, Chester, UK*
Mikko Taipale • *Donnelly Centre for Cellular and Biomolecular Research, University of Toronto, Toronto, ON, Canada*
Jimmy Theriault • *Molecular and Cellular Radiation Oncology, Beth Israel Deaconess Medical Center, Harvard Medical School, Boston, MA, USA*
Yusuke Tomita • *Developmental Therapeutics Branch, Center for Cancer Research, NCI, NIH, Bethesda, MD, USA*
Jane B. Trepel • *Developmental Therapeutics Branch, CCR, NCI, NIH, Bethesda, MD, USA*
Gennady M. Verkhivker • *Schmid College of Science and Technology, Chapman University, Orange, CA, USA; Chapman University School of Pharmacy, Irvine, CA, USA*
Dale Vimalachandran • *Countess of Chester Hospital, Chester, UK*
Sudhakar Voruganti • *Department of Biochemistry and Molecular Biology, Oklahoma State University, Stillwater, OK, USA; Bristol-Myers Squibb, Pennington, NJ, USA*
Maria A.W.H. van Waarde-Verhagen • *University Medical Center Groningen, University of Groningen, Department of Cell Biology, Groningen, The Netherlands*

Xiang-Yang Wang • *Department of Human Molecular Genetics, Virginia Commonwealth University, Richmond, VA, USA; Massey Cancer Center, Virginia Commonwealth University, Richmond, VA, USA; Institute of Molecular Medicine, Virginia Commonwealth University, Richmond, VA, USA*
Terence David Wardle • *Countess of Chester Hospital, Chester, UK*
Desheng Weng • *Department of Medicine, Boston University School of Medicine, Boston, MA, USA*
Sue Wickner • *Laboratory of Molecular Biology, National Cancer Institute, National Institutes of Health, Bethesda, MD, USA*
John H.H. Williams • *Chester Centre for Stress Research, Institute of Medicine, University of Chester, Chester, UK*
Mark R. Woodford • *Department of Urology, SUNY Upstate Medical University, Syracuse, NY, USA; Upstate Cancer Center, SUNY Upstate Medical University, Syracuse, NY, USA*
Aneliya Yoveva • *Max Planck Institute of Immunobiology and Epigenetics, Freiburg, Germany*
Akira Yuno • *Developmental Therapeutics Branch, Center for Cancer Research, NCI, NIH, Bethesda, MD, USA*
Sandra Zilles • *Department of Computer Science, University of Regina, Regina, SK, Canada*
Giovanni Zummo • *Human Anatomy Section, Department of Experimental Biomedicine and Clinical Neurosciences, University of Palermo, Palermo, Italy*

Chapter 1

Targeted Deletion of Hsf1, 2, and 4 Genes in Mice

Xiongjie Jin, Binnur Eroglu, Demetrius Moskophidis, and Nahid F. Mivechi

Abstract

Heat shock transcription factors (Hsfs) regulate transcription of heat shock proteins as well as other genes whose promoters contain heat shock elements (HSEs). There are at least five Hsfs in mammalian cells, Hsf1, Hsf2, Hsf3, Hsf4, and Hsfy (Wu, Annu Rev Cell Dev Biol 11:441–469, 1995; Morimoto, Genes Dev 12:3788–3796, 1998; Tessari et al., Mol Hum Repord 4:253–258, 2004; Fujimoto et al., Mol Biol Cell 21:106–116, 2010; Nakai et al., Mol Cell Biol 17:469–481, 1997; Sarge et al., Genes Dev 5:1902–1911, 1991). To understand the physiological roles of Hsf1, Hsf2, and Hsf4 in vivo, we generated knockout mouse lines for these factors (Zhang et al., J Cell Biochem 86:376–393, 2002; Wang et al., Genesis 36:48–61, 2003; Min et al., Genesis 40:205–217, 2004). Numbers of other laboratories have also generated Hsf1 (Xiao et al., EMBO J 18:5943–5952, 1999; Sugahara et al., Hear Res 182:88–96, 2003), Hsf2 (McMillan et al., Mol Cell Biol 22:8005–8014, 2002; Kallio et al., EMBO J 21:2591–2601, 2002), and Hsf4 (Fujimoto et al., EMBO J 23:4297–4306, 2004) knockout mouse models. In this chapter, we describe the design of the targeting vectors, the plasmids used, and the successful generation of mice lacking the individual genes. We also briefly describe what we have learned about the physiological functions of these genes in vivo.

Key words Hsf1, Hsf2, Hsf4, Knockout mice, Targeting vector, Hsf4-EGFP

1 Introduction

Transcription of the genome is controlled by a class of proteins known as transcription factors. Transcription factors bind to specific DNA sequences and enhance (or repress) expression of specific genes. These factors usually share a high level of overlap in their DNA recognition sequence. The Hsf family members (Hsf-1, -2, and -4) bind to HSEs (5′-nGAAn-3′ units) and regulate transcription of Hsps and other molecular chaperones [1–3]. Comparisons between Hsf protein sequences between different organisms indicate the presence of a conserved DNA binding domain and three hydrophobic heptad repeats known as the trimerization domain. These domains are located within the amino-terminal portion of the protein. The transcriptional activation domain is located toward

Stuart K. Calderwood and Thomas L. Prince (eds.), *Chaperones: Methods and Protocols*, Methods in Molecular Biology, vol. 1709, https://doi.org/10.1007/978-1-4939-7477-1_1,

the carboxyl-terminus end of the molecule. The intra-molecular interactions between the amino- and carboxyl-terminal domains keep Hsf1 in an inactive state under non-stress conditions [1]. The expression of Hsf2 and Hsf4 in the cell correlates with their increased DNA binding activity [2, 4, 5]. Number of studies has provided evidence for the role of Hsf1 in tumorigenesis and metabolism. Hsf1-deficient mice are significantly resistant to Ha-Ras and mutant p53-induced tumorigenesis [6], p53-loss-induced lymphomas [7], and carcinogen-induced liver cancer [8]. Hsf1-deficient mice are also resistant to ErbB2-induced mammary tumorigenesis [9, 10]. Contribution of other Hsfs to tumorigenesis remains less explored. We have shown that deletion of Hsf4-deficient mice is resistant to p53-loss-induced lymphomas [11]. Hsf2 expression has been shown to be reduced in number tumor types and knockdown of Hsf2 increases the invasion ability of prostate cancer cell line [12].

Gene targeting in mice by homologous recombination in embryonic stem (ES) cells has become a routine procedure [13–16]. Gene targeting alters the mouse genome at specific selective locus. A targeting vector that carries a specific portion of the gene to be targeted is normally flanked by a neomycin gene, most often containing its own promoter sequence. Other strategies where neomycin expression is under the control of an endogenous gene have also been used. The neomycin gene is used as a positive selectable marker for the isolation of embryonic stem cells that carry the targeted allele. Neomycin gene may be flanked by loxP sites so that it can be deleted following the generation of the knockout mouse line [15, 16]. The targeting vector may also contain one or two thymidine kinase (TK) genes that can be used as a negative selectable marker. Following electroporation of the targeting vector into the ES cells, if the targeting vector is randomly inserted into the genome by nonhomologous recombination, the TK genes will also be inserted and the gene is expressed. Treatment of the ES cells with ganciclovir ensures the removal of the cells containing the random integration of the targeting constructs. In contrast, if the targeting vector is inserted into the genome by homologous recombination, the TK genes will not be inserted into the genome and the ES clones will survive the treatment with ganciclovir. The strategy we used was to generate mutant *hsf1*, *hsf2*, and *hsf4* targeting vectors containing a neomycin gene flanked by two loxP sites and two TK genes.

In this chapter, we describe the targeting vectors and generation of *hsf1*, *hsf2*, and *hsf4*-deficient mouse lines. We will also briefly describe the phenotype of the *hsf* knockout mice generated in our laboratory.

2 Materials

2.1 Genomic DNA Identification, Isolation, and Analyses

At the time when we began constructing targeting vectors for the *hsf* genes, the mouse genome had not been entirely sequenced. Therefore, we cloned these genes as described in the following sections. However, currently, a BAC clone has been identified that encodes the murine *hsf* genes. To identify the BAC clone number that contains specific gene, one can go to the NCBI Web site "Clone Registry" and search for the gene of interest. After clicking the BAC clone number, the Web sites for the *hsf1*, *2*, and *4* clones are indicated.

1. The BAC clone containing the *hsf1* gene can be found at: https://www.ncbi.nlm.nih.gov/clone/684469/.
2. The BAC clone containing the *hsf2* gene can be found at: https://www.ncbi.nlm.nih.gov/clone/666759/.
3. The BAC clone containing the *hsf4* gene can be found at: https://www.ncbi.nlm.nih.gov/clone/599701/.
4. Clones can be obtained from http://bacpac.chori.org.

One method of using a BAC clone to construct the targeting vector is from the available sequencing information, first design the targeting vector, and then fragments that are needed can be amplified by PCR. Any fragment that is amplified via PCR must be sequenced entirely to detect the presence of any errors. For PCR of genomic DNA, use of a high-fidelity TAQ polymerase is highly recommended. For the conventional knockout strategy, presence of more than one or two base pairs differences per kb pairs of DNA may reduce homologous recombination. For the conditional cre-loxP techniques, even one change in the DNA bases may be detrimental in proper expression of the gene under study and should be avoided.

2.2 Plasmids and Phages

Conventional plasmids can be used for the manipulation of the DNA fragments. For the final targeting vector we used Lamda DASH II-254-2TK Phage (Stratagene, and a modified version was provided by Drs. NR Manley, Department of Genetics, University of Georgia, Athens, GA 30602, USA). A map of Lamda DASH II-254-2TK has been provided in Fig. 1. It contains Stuffer sequences that can be removed by restriction enzyme (XhoI) digestion, and the gene fragments (in two or three pieces) of interest can then be inserted. If three fragments are inserted into the final phage, it is advisable to use different restriction enzymes for each fragment to avoid excessive self ligation.

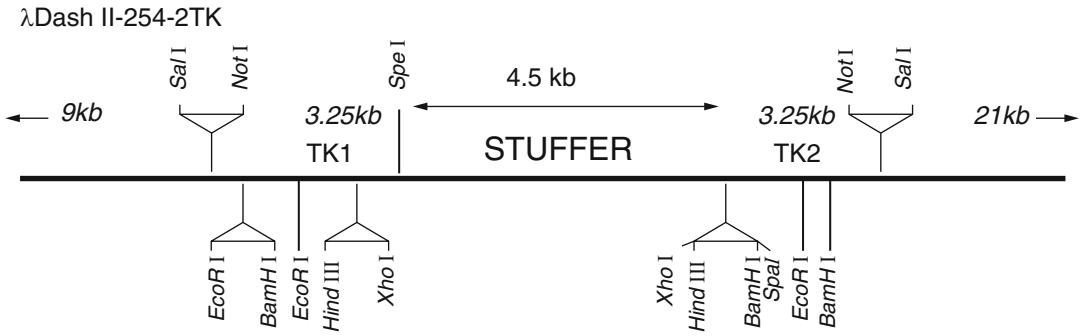

Fig. 1 Schematic presentation of Lambda Dash II-254-2TK Vector. The portion of the map of lambda-Dash II-254-2TK is presented. The stuffer sequence can be removed and the targeting vector can be ligated into the phage DNA in two or three fragments

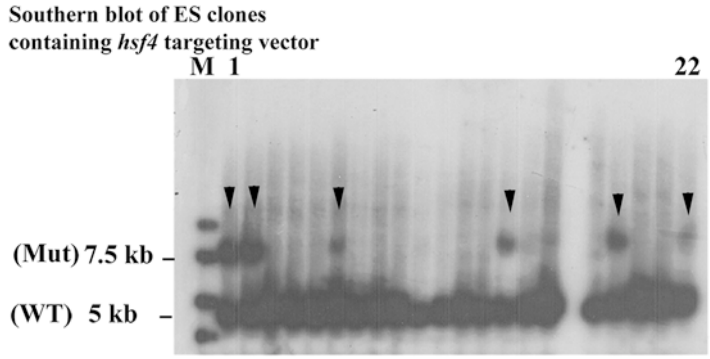

Fig. 2 Southern blot analyses of ES cells electroporated with *hsf4* targeting vector. From 22 clones presented, six clones carried the correct targeting for the *hsf4* mutant (*arrow heads*). WT is wild-type band (5 kb) and Mut is the *hsf4* mutant band at 7.5 kb

2.3 ES Electroporation, Southern Blotting of ES Clones, and Identification of Positively Targeted ES Clones

For the identification of ES clones with correct targeting, Southern blotting from a small amount of DNA (may be as low as 2 μg) is essential. For Southern blotting, we follow the procedure in the Molecular Cloning, Laboratory Manual [17]. Figure 2 represents Southern blotting of 22 clones of ES cells obtained for targeting of the *hsf4* gene. As the data indicate from 22 clones, six clones were found to be positive. Other methods of this section have been briefly described for each knockout mouse line; however, the methodology can be found in detail in the following references 13–16, 18.

2.4 ES Cell Microinjection into Blastocysts, Generation of Chimeras, and Germline Transmission

This section has been briefly described for each knockout mouse line; however, the methodology can be found in more detail in the following references [13–16, 18] (*see* **Notes 1–8**).

3 Methods

3.1 Knockout of hsf1 Gene

Hsf1 gene structure: The mouse Hsf1 gene (*hsf1*) is located on chromosome 15 and encodes a Hsf1 protein that contains 503 amino acids [19, 20]. The mouse *hsf1* gene has 12 exons. Exon 1 contains 274 base pairs (bp), and the start codon (ATG) is located at 158 bp, i.e., exon 1 encodes 39 amino acids. The distance between exon 1 and exon 2 (intron 1) is 18 kb (18, 254 bp). The remaining exons (exon 2 through exon 12) are located compactly in a 4.6 kb region. The entire *hsf1* gene is 23.5 kb.

1. *Design of the targeting vector to delete hsf1*: To target the *hsf1* gene, the cloned fragment containing *hsf1* was sequenced and analyzed for the presence of unique restriction enzyme sites. In our targeting strategy, we selected to delete a portion of the exon 2 of the *hsf1* gene for the reasons provided below: (1) In the *hsf1* gene, exon 1 is located 18 kb apart from other exons. (2) Intron 1 encodes the promoter of another gene (known as Bop1), as we have previously reported [20]. Disruption of exon 1 (plus insertion of neomycin gene in this exon) could potentially disrupt the expression of the Bop1 gene. (3) Since the distance between exon 1 and exon 2 is 18 kb, deletion of both exons would have been impossible. (4) If only exon 1 was deleted, there would be a possibility that a truncated Hsf1 mRNA and protein encoded by other exons (from exon 2 to exon 12) would be generated. This truncated Hsf1 would potentially contain amino acid residues 40–503 due to the presence of an ATG at amino acid 40. (5) For the *hsf1* targeting construct, we planned that a LacZ gene could be inserted under control of the *hsf1* promoter. The best strategy would have been to insert the LacZ gene at the first ATG. However, for the reasons noted above, we inserted the LacZ gene into the *hsf1* exon 2.

   The amino acid sequence encoded by exon 2 is critical for the DNA binding domain of Hsf1 protein. If exon 2 was deleted, the Hsf1 DNA binding domain would be disrupted and Hsf1 could not bind to the DNA. Furthermore, if exon 2 was deleted, the *hsf1* open reading frame (i.e., a cDNA

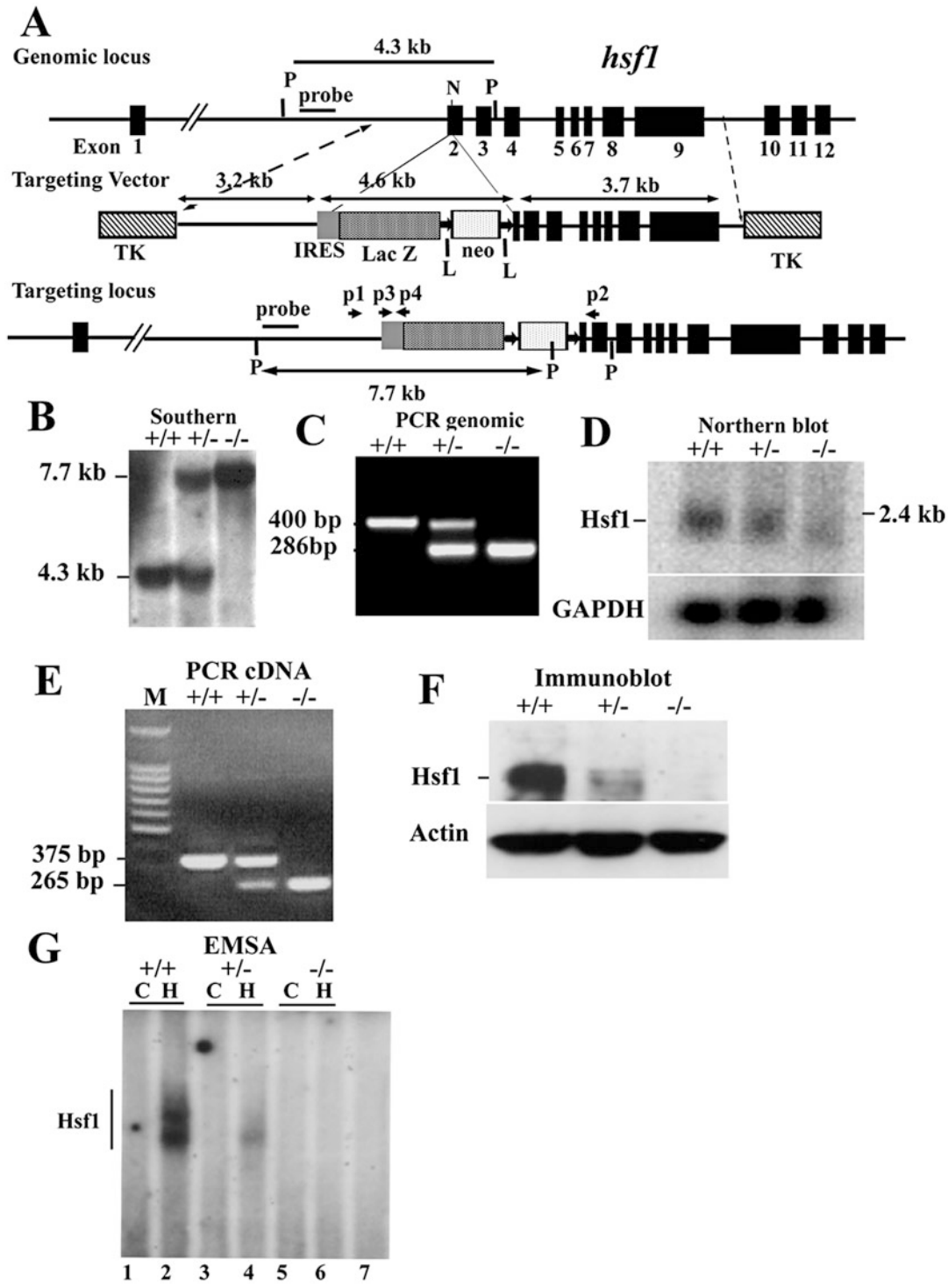

Fig. 3 Targeted disruption of *hsf1* by homologous recombination. (**a**) Schematic of segment of the *hsf1* locus, targeting construct, and targeted locus. Coding exons are indicated as *black boxes*, beginning with exon 2 [20]. Targeting construct replaces the coding region for 55 bp of exon 2. *LoxP* flanked, PKG-neomycin

encoding exon 1 and exons 3–12) will shift and a stop codon will appear immediately at amino acid residue 49 in exon 2. Three more stop codons are also present within the next 100 bps. Therefore, the deletion of exon 2 will completely disrupt the Hsf1 protein structure and function. According to these criteria, we designed an *hsf1* targeting vector with the deletion of 55 bp of exon 2. The final targeting vector contains a 3.2 kb proximal fragment with homology to *hsf1*, a 3.2 kb IRES-LacZ-neomycin fragment, and a 3.7 kb distal fragment with homology to *hsf1* (Fig. 3) [19].

2. *Targeting vector*: Cloning of the *hsf1* gene: An 18 kb clone containing a portion of the *hsf1* gene fragment (exon 2–exon 12) was isolated following screening a 129/SvJ mouse genomic library in Lambda Fix II vector (Stratagene) using Hsf1 cDNA as a probe [20]. This 18 kb DNA fragment was used as a template for constructing the *hsf1* targeting vector.

   External probe for the detection of correct targeting: To identify homologous recombination, an external probe was designed to screen the *hsf1* mutant ES clones and eventually the *hsf1*-deficient mice. The external probe should hybridize to the DNA region that is close to, but not included in the targeting vector. According to our targeting strategy, we designed a 1 kb probe that hybridized to the 5′ region of the targeting vector as presented in Fig. 3a. The probe was tested on genomic DNA prepared from wild-type mouse tail that was digested by the restriction enzyme PstI. PstI was selected

Fig. 3 (continued) cassette with upstream *IRES-LacZ* is indicated. Two TK genes were used for negative selection. "Outside probe or external probe" was used for screening ES cell clones to distinguish between endogenous and targeted alleles. The 3.2 and 3.7 kb fragments are the proximal and distal *hsf1* homologous segments in the targeting vector [19]. The final insert between the two TK genes is 13 kb. N and P represent NheI and PstI sites, respectively. Primers p2, p2, p3, and p4 are used for genotyping. (**b**) Southern blot analysis of genomic DNA prepared from tails of wild-type (+) and targeted mutant mice (−). The 7.7 and 4.3 kb bands are PstI digested fragments corresponding to the targeted (−) and wild-type (+) alleles, respectively. (**c**) PCR analysis of tail DNA derived from wild-type (+) and targeted mutant mice (−) showing 420 and 890 bp fragments derived from wild-type and targeted alleles, respectively. (**d**) Northern blot analysis of total RNA derived from mouse embryo fibroblasts (MEFs) of wild-type (+) or mutant (−) mice. Full-length murine *hsf1* cDNA was used as a probe. Hsf1 generates an approximately 2.4 kb fragment. GAPDH is shown for equal loading. (**e**) cDNA from wild-type (+) and *hsf1* mutant (−) mice were amplified using forward primer located in exon 1 and reverse primers located in exon 3. Sequencing the 375 bp (+) and 265 bp (−) fragment indicated normal splicing of exons 1, 2, and, 3 and splicing of exon 1 to exon 3, respectively. (**f**) Immunoblot analysis of extracts of MEFs derived from wild-type (+) or mutant (−) *hsf1* analyzed by SDS-PAGE using antibody to Hsf1. Actin is presented as an indicator of loading. (**g**) Electrophoretic mobility shift assays (EMSA) [19]. Nuclear extracts of wild-type (+) or *hsf1* mutant (−) MEFs were prepared from untreated control (C) or heated (43 °C for 20 min plus 30 min recovery at 37 °C to ensure Hsf1 activation). *Lanes 1* and *2*, *3* and *4*, *5* and *6* represent untreated control (C) and heated (H) samples, respectively. *Lane 7* is the same extract as in *lane 2* but with 200× excess cold HSE to show specificity

because of its suitability of detecting the correct targeting of ES cell clones.

Vector construct: A 3.2 kb proximal fragment with homology to *hsf1* was amplified by PCR using the isolated 18 kb *hsf1* clone as a template using forward primer: 5′-CTG CAG AAC CAA TGC ATT GGC GGC CGC TCG AGA ACA CAG CAT TC TTG AAA GAA A-3′ that included BstXI, NotI, EagI, and XhoI restriction enzyme sites, and a reverse primer: 5′-GAA TCG GCC GTG GTC AAA CAC GTG GAA GCT GTT-3′ that included an EagI restriction enzyme site. The PCR product was sequenced to confirm DNA sequence fidelity. The PCR product was digested by EagI for subcloning.

A plasmid containing an IRES-lacZ-neomycin cassette was used to insert an IRES-lacZ-neomycin fragment in the targeting vector (Fig. 3a) [19]. The neomycin gene (used as a positive selectable marker) was driven by the phosphoglycerate kinase (PKG) promoter and contained an SV40 poly-(A) signal and a stop codon. The neomycin gene was flanked by Cre recombinase recognition sequences (loxP) to allow the removal of the neomycin gene in the mutant mice. The lacZ gene contained sequences of the picornaviral Internal Ribosomal Entry Site (IRES) at its 5′-end and a poly-(A) signal and a stop codon at its 3′-end (clones encoding sequences for lacZ and IRES were the gift of Dr. A. Smith (Univ. of Edinburgh, Scotland)). Since the decision was made to insert the lacZ gene (containing its own ATG) into exon 2, it was possible that Hsf1 transcripts that start from exon 1 would interfere with the lacZ expression. Therefore, an IRES was inserted before the lacZ gene to direct translation of the reporter gene. However, as we have noted in our previous publication [19], in *hsf1*-deficient mice, the lacZ gene (plus the entire exon 2) is spliced out, fusing exon 1 directly to exon 3 and making a shorter transcript that excluded exon 2. Since we had predicted this may occur in vivo, we still went with such a design since fusion of exon 1–exon 3 would generate an Hsf1 transcript that would be out-of-frame and no protein could be generated from this transcript (as noted above). As such, cells deficient in the *hsf1* gene do not express the lacZ gene [19].

The proximal 3.2 kb fragment was subcloned into the IRES-lacZ-neomycin plasmid. The resulting plasmid was then digested with XhoI/NruI to release the 7.8 kb proximal fragment. For the distal 3.7-kb fragment with homology to *hsf1*, the 18-kb genomic clone was digested with NheI to release a 7.5-kb fragment, which was subcloned into plasmid pBlue-Script at an EcoRV site. This plasmid was then digested with HindIII to remove a 3.8-kb fragment. The remaining 3.7 kb fragment (portion of exons 2–9) was subsequently released by SmaI/XhoI digestion.

The proximal fragment containing the IRES-lacZ-neomycin cassette and the 3.7 kb distal fragment were then ligated into the phage DNA vector λDASHII-254-2TK at XhoI site [19]. The targeting construct is flanked by 2TK genes, which are used as a negative selectable marker. The vector was packaged into phage and the positive phage clones were selected by PCR and restriction enzyme digestion. Several positive phage DNA clones were digested by NotI (*see* Fig. 1) to release the final vector that contained the targeting vector and the 2TK genes. This final vector can be recircularized into a plasmid that could be amplified in bacteria. After amplification, the final vector was linearized with NotI digestion for ES cell transfection.

3. *ES cell electroporation*: ES (D3; Incyte Genomics, St. Louis, MO) cells were cultured as described previously [18, 19]. The ES cells were electroporated (BioRad Gene Plus, 250 V, 950 μF) with the linearized targeting vector and cultured in the presence of neomycin (200 μg/ml) and ganciclovir (2 μM) for 10 days. The ES cell clones were isolated and expanded. Following Southern blotting using the external probe, two doubly resistant ES cell clones (Fig. 3b) (from 167 clones tested) were selected and expanded.
4. *Generation of hsf1 mutant mice*: The two ES clones that were found to be positive by Southern blotting were microinjected into C57BL/6 blastocysts, and germline-transmitting chimeric mice were obtained. The chimeric mice were then crossed with C57BL/6 mice to obtain *hsf1*$^{+/-}$ mice that were interbred to generate *hsf1*$^{-/-}$ mice.
5. *Genotyping of mutant mice*: Southern blotting: ES clones, germline-transmitting chimeric mice, and the first several litters of mice were genotyped by Southern blotting. Mouse genomic DNA was isolated and digested with the restriction enzyme PstI. Southern blotting was performed using an external probe (indicated in Fig. 3b) [19]. This generates a 7.7 kb fragment for the targeted locus and a 4.3 kb fragment for the wild-type locus.

   PCR: When the *hsf1* mutant mouse line was established after screening by Southern blotting (Fig. 3b), mice were subsequently routinely genotyped by PCR (Fig. 3c). Genomic DNA isolated from mouse tail was used as a template. Two sets of primers were used to identify wild-type and mutant alleles: for wild type, forward primer (P1): 5′-GAG ATG ACC AGA ATG CTG TGG GTG-3′ and reverse primer (P2): 5′-GCA AGC ATA GCA TCC TGA AAG AG-3′; for mutant alleles (the primers to amplify IRES region): forward primer (P3): 5′-ACT GGC CGA AGC CGC TTG GAA TAA-3′ and reverse primer (P4): 5′-ATA CAC GTG GCT TTT GGC CGC

AGA-3′. These PCR reactions generated a 400 bp fragment for wild type and a 285 bp fragment for mutants (Fig. 3) [19].

Figure 3d–g show analyses of *hsf1*$^{-/-}$ tissues confirming no Hsf1 protein was produced.

3.2 Knockout of hsf2 Gene

Hsf2 gene structure: The mouse *hsf2* gene (*mhsf2*) is located on chromosome 10 and encodes Hsf2 protein that contains 517 amino acids. The mouse *hsf2* gene contains 12 exons. Exon 1 contains 117 base pairs (bp) and the start codon (ATG) begins at 25 bp. Exon1 and exon 2 are separated by a 9.4 kb intron [21].

1. *Design of the targeting vector to delete hsf2*: To disrupt the mouse *hsf2* gene, we designed a targeting vector in which 67 bp from the start codon were deleted. An EGFP reporter gene with a start and stop codons was inserted into this region of the *hsf2* gene. The removal of the first 67 bp from exon I of the *hsf2* gene results in an out-of-frame shift in the cDNA. Since EGFP inserted in exon 1 of the *hsf2* gene contained a stop codon, it is therefore unlikely that the truncated Hsf2 cDNA could be translated. Therefore, the deletion of 67 bp from exon I of the *hsf2* gene will completely disrupt the *hsf2* gene. The final targeting vector contained a 2.8 kb proximal fragment with homology to the *hsf2* gene, a 2.2 kb EGFP-neomycin fragment, and a 6.1 kb distal fragment with homology to *hsf2* (Fig. 4) [21].
2. *Targeting vector*: Isolation of the *hsf2* gene: A 22 kb DNA fragment containing 3.8 kb of the promoter region and the first 6 of the 12 exons of the murine *hsf2* gene was isolated from a 129/SvJ mouse genomic library in Lambda FixII vector (Stratagene, La Jolla, CA) by hybridization with a mouse *hsf2* exon 1 cDNA as a probe. This genomic clone was used to construct a targeting vector [21].

   External probe for the detection of correct targeting: To identify the homologous recombination, a 500 bp external probe was generated by PCR using primers: 5′-GTT TCT GCA CTG AGC CCT TG-3′ and 5′-CAA GGA TTC AAT AAT CGT GAC AC-3′. This probe hybridizes to a fragment of the *hsf2* gene that is located in the 5′ region of the targeting vector (Fig. 4a). The probe was tested on wild-type genomic DNA digested with PvuII restriction enzyme.

   A 2.8 kb proximal fragment including part of the *hsf2* promoter and the *hsf2* start codon was amplified by PCR using the following primers: 5-AGT CCG CTC GAG GAG AGG TGG TAT ACA TAA ACA AGG (included a *Xho*I site, underlined) and 5-GAA CTC GGA TCC ATT GTT AGC CCG GTG CAG GGA TTC CAA ATT CTA CTA CCG AAC GCG GAG GTC GCA GCG GCG GCG G (included a BamHI

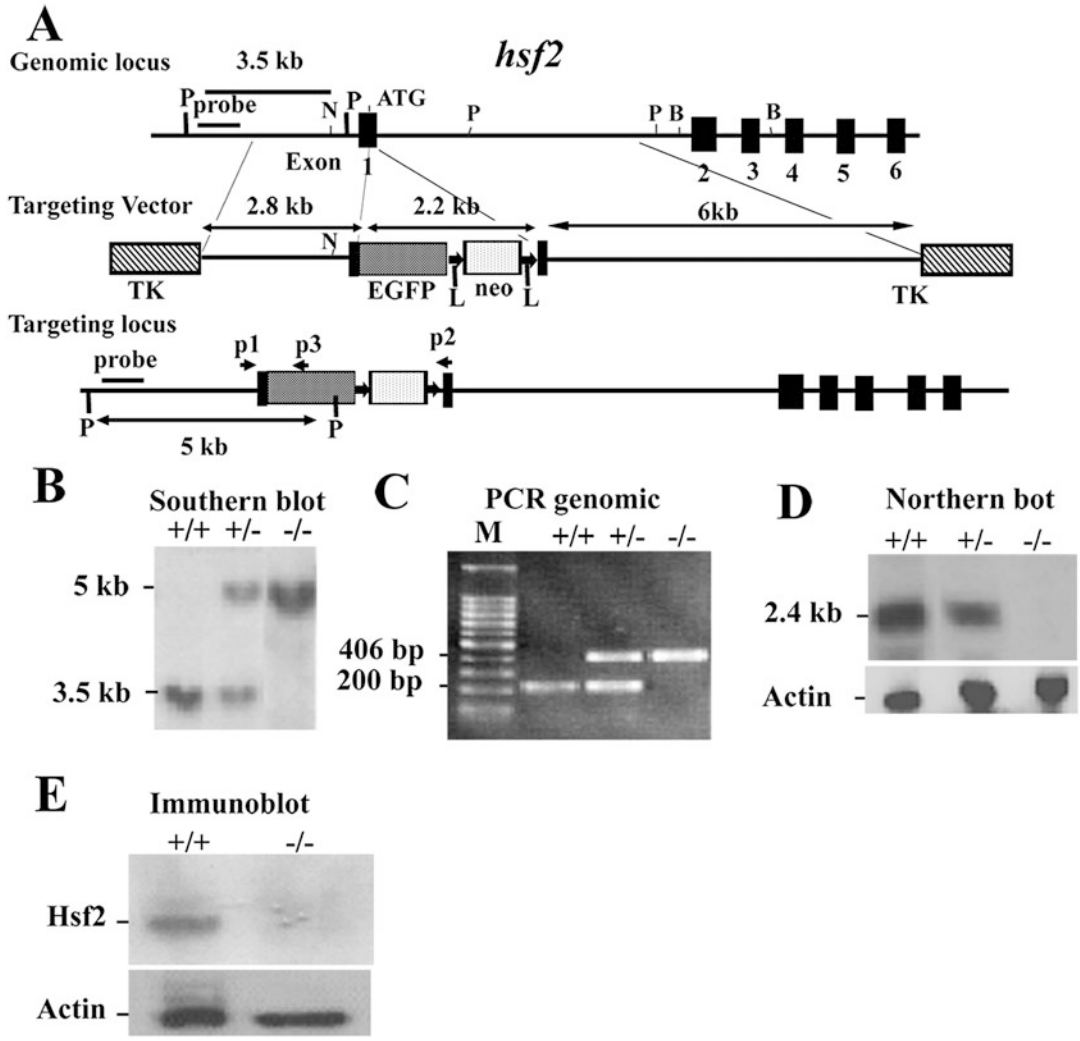

Fig. 4 Targeting strategy for the *hsf2* genomic locus and generation of *hsf2*-deficient mice. (**a**) Restriction map of the *hsf2* gene, showing the wild-type allele (*top*), targeting vector (*middle*), and the predicted targeted allele following homologous recombination (*bottom*). The ATG indicates the start codon (*top*). The position of the *EGFP-neo* and TK cassettes, probes for Southern blotting, and PCR primers P1, P2, and P3 are indicated. The vectors were designed so that the promoter of *hsf2* gene drives *EGFP* expression. Note that the Pvu II restriction enzyme site located upstream of exon 1 was destroyed in the targeting vector. The restriction enzymes are designated: P, PvuII; N, NheI; B, BamHI [21]. (**b**) Southern blotting analysis of tail DNA derived from wild-type (+/+), heterozygous (+/−), or homozygous (−/−) *hsf2* mice. PvuII-digested genomic DNA was hybridized with an external probe to yield bands of 3.5 and 5 kb for the *hsf2* wild type and targeted loci, respectively. (**c**) PCR-based genotyping assay amplifies wild-type and targeted *hsf2* locus fragments of 200 and 406 bp, respectively. (**d**) Northern blotting analysis. Total RNA extracted from the livers of 8-weeks-old mice of wild-type (+/+), heterozygous (+/−), or homozygous (−/−) for the targeted *hsf2* allele adult mice was hybridized with a full-length murine *hsf2* cDNA probe. The expected 2.4 kb *hsf2* transcript was present in the wild-type and heterozygous mice but absent in mice homozygous for the targeted *hsf2* allele. The level of actin mRNA is shown to indicate equal loading of RNA. (**e**) Western blot analysis. Equal amount of protein from cell extracts from the liver extracts of 8-weeks-old mice of wild-type (+/+) or homozygous (−/−) for the targeted *hsf2* allele adult mice was analyzed using SDS-PAGE followed by immunoblotting using antibody to Hsf2. The level of actin is shown to indicate equal loading of protein

site, underlined). This fragment lacks an unwanted PvuII site present 99 bp upstream of the start codon. This PCR fragment was digested by XhoI and BamHI and cloned into pBluescript II KS plasmid for amplification, and was sequenced to confirm the DNA sequence fidelity. The 2.8 kb proximal fragment was released by XhoI and BamHI digestion for subcloning into the final targeting vector.

A plasmid containing the 2.2 kb EGFP-neo cassette was digested with BamHI and ClaI to release the EGFP-neo fragment. The *EGFP* gene with the poly(A) signal was driven by the *hsf2* promoter (EGFP was from Clontech; Neomycin was modified by the addition of two loxP sites by Dr. M. Capecchi's laboratory) [22, 23]. Neomycin gene was driven by the TK promoter with a simian virus 40 poly(A) signal.

A 6 kb distal fragment including the C-terminal 26 bp of exon 1 extending into the first intron was PCR-amplified using the following primers: 5′-CCA TCG ATC CAA CGA GTT CAT CAC CTG GAG TC (included a ClaI site) and 5′-CTC ATA CTC GAG TTA ACT AAA CCA ATG CAT TCA ACTG-3′ (include XhoI site).

The 2.8 kb proximal fragment, 2.2 kb EGFP-neo fragment, and 6 kb distal fragment were ligated to phage DNA vector λDASHII-254-2TK at XhoI site flanked by 2TK genes (Fig. 1). The vector was then packaged into phage and the positive phage clones were selected by PCR and restriction enzyme digestion. The positive phage DNA was digested by NotI to release the final targeting vector containing 2TK genes. This final vector could be recircularized into a plasmid and could be amplified in bacteria. After amplification, the final vector was linearized with NotI and was purified for the transfection into the ES cells.

3. *ES cell electroporation*: ES (D3; Incyte Genomics, St. Louis, MO) cells were cultured as described previously. The ES cells that were electroporated (BioRad Gene Plus, 250 V, 950 μF) with the linearized targeting vector were double selected by G418 (200 μg/ml) and ganciclovir (2 μM) [18, 21]. Double-resistant ES cell clones were selected and expanded. Genomic DNA was isolated as described in Molecular Cloning [17].
4. *Generation of mutant mice*: Positive ES clones were selected by Southern blotting (Fig. 4b). The positive clones were microinjected into C57BL/6 blastocysts and germline-transmitting chimeric mice were obtained. The chimeric mice were then crossed with the wild-type mice to obtain *hsf2*$^{+/-}$ mice, which were intercrossed to generate *hsf2*$^{-/-}$ mice [21].
5. *Genotyping of mutant mice*: Southern blotting: ES clones, germline-transmitting chimeric mice, and first several litters of mice were genotyped by Southern blotting. Mouse genomic

DNA was isolated [17] and was digested with PvuII. Southern blotting was performed using an external probe (Fig. 4b) [21]. This generates a 5 kb fragment for the targeted locus and a 3.5 kb fragment for the wild-type locus. PCR: When the *hsf2* mutant mouse line was established after Southern blotting, mice were genotyped routinely by PCR (4C). Genomic DNA isolated from mouse tail was used as a template. PCR was performed using one common (i.e., recognized by both wild type and mutant) primer (P1; 5′-GTGGTGTGCGTT CCCCGGAG-3′), a primer located in the wild-type locus (P2; 5′-TGACTCCAGGTGATGAACTC-3′) to identify the untargeted allele, and a primer (P3; 5′-CTTCGGGCAT GGCGGACTTG-3′) located in the EGFP to identify the mutant gene. The locations of the primers P1, P2, and P3 are indicated by the arrows in Fig. 4a. The expected PCR products for wild-type and targeted *hsf2* loci are fragments of 200 bp, and 406 bp, respectively (Fig. 4c).

Figure 4d and e show cells deficient in Hsf2 do not express Hsf2 mRNA or protein.

3.3 Knockout of hsf4 Gene

Hsf4 gene structure: The mouse *hsf4* gene (*mhsf4*) is located on chromosome 8 and contains 13 exons (Fig. 5a) [24].

1. *Design of the targeting vector to delete hsf4*: To disrupt the *hsf4* gene, we designed a targeting vector by inserting the *EGFP-neo* cassette after the start codon. Ligation of the EGFP-neo fragment with the proximal fragment of the *hsf4* gene would result in an out-of-frame cDNA product for the *hsf4* gene by the disruption of the gene at the ATG. The final targeting vector contains a 2.8 kb proximal fragment with homology to *hsf4*, a 2.2 kb *EGFP-neo* cassette [22, 23], and a 5.5 kb distal fragment with homology to *hsf4* [24].
2. *Targeting vector*: To generate the *hsf4* targeting vector, a 129/SvJ mouse genomic DNA phage library (Lambda FixII vector, Stratagene, La Jolla, CA) was used to identify clones containing the *hsf4* gene using a mouse *hsf4* cDNA probe. The isolated *hsf4* gene contained 13 exons within a 5.9 kb fragment, as well as several kb flanking sequences at both the 5′ and 3′ regions.

   The proximal 3.2 kb region was amplified by PCR using the following primers:

   5′-TTCCCACGCGTCGACCCCTCCAGTCCCATTCTTTT GTTG-3′ and 5′-GAAGATCTGCCATGGCGCAGTCT CGGCCGGCCGG-3′ (included BglII site, underlined). Because of the existence of a Sal I site within the amplified product, digestion with Sal I and Bgl II gives the final 2.8 kb proximal gene product.

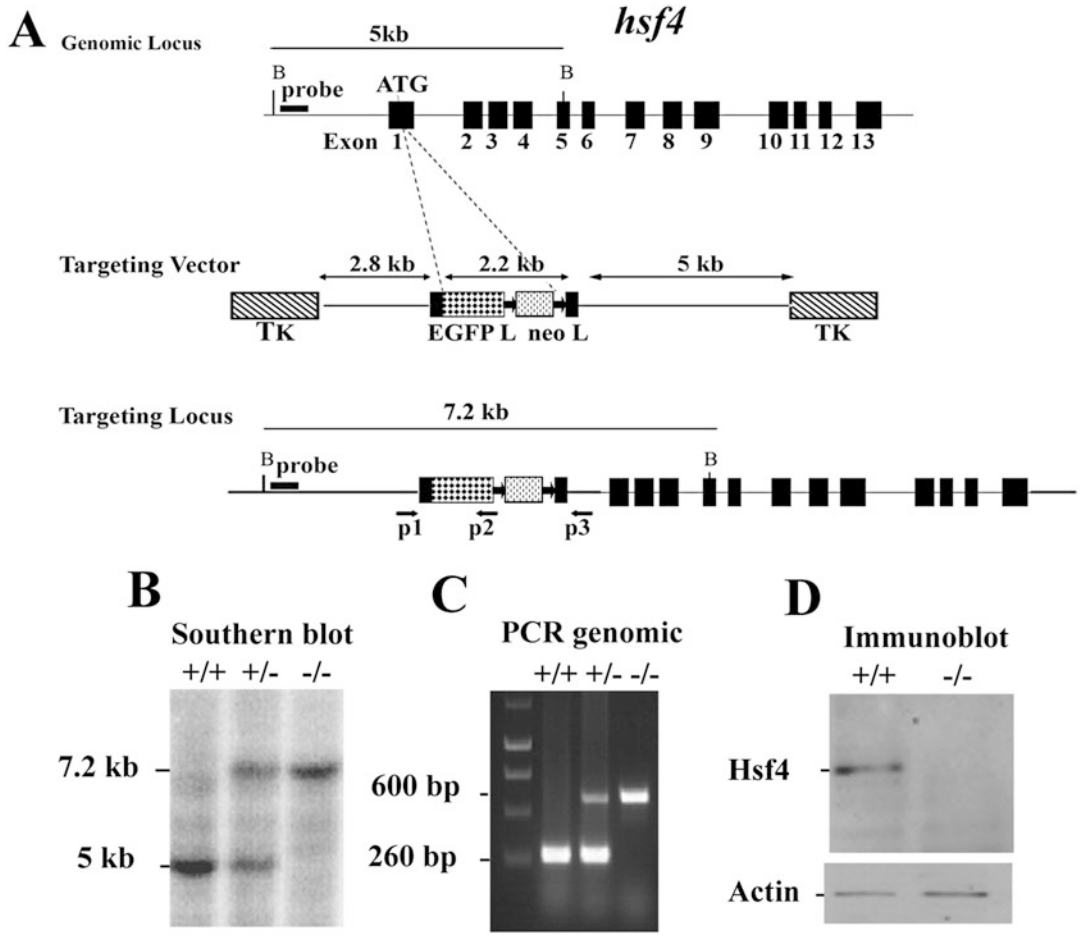

Fig. 5 Targeted disruption of the *hsf4* gene. (**a**) Wild-type *hsf4* locus, targeting vector, and the predicted targeted allele following homologous recombination are shown. Exons are presented by *black boxes*. The probe used for Southern blotting and PCR primers P1, P2, and P3 are indicated by *arrows* below the targeted allele [24]. (**b**) Bgl II-digested tail DNA (10 μg) from wild-type (+/+), or *hsf4*$^{+/-}$ (+/−) or *hsf4*$^{-/-}$ (−/−) mice was hybridized with an external probe to yield bands of 5 and 7.2 kb for the wild-type and targeted *hsf4* loci, accordingly. (**c**) PCR-based genotyping assay amplifies fragments of 260- and 600-bp for wild-type and targeted *hsf4* allele, respectively. (**d**) 50 μg protein from lens extracts of wild-type (+/+) or *hsf4*$^{-/-}$ (−/−) mice at P28 was analyzed by Western blotting using antibody specific to Hsf4b. As a control for equal protein loading, the blot was probed for β-actin

A plasmid containing a 2.2 kb *EGFP-neo* cassette was digested with BamHI and ClaI to release the *EGFP-neo* fragment. The *EGFP* gene with the poly(A) signal was driven by the *hsf4* promoter, followed by the neomycin resistance gene, which was flanked by two loxP sites to allow its removal by cre recombinase, and was driven by the TK promoter, with a Simian virus 40 poly(A) signal.

The distal 5.5 kb was PCR amplified by using the following primers:

5′-CCATCGATGGCAGGAAGCGCCAGCTGCGCTGCC-3′ (included ClaI site, underlined), and 5′-CCGCTCGAG CGGGGCAGGGTCTTGTTGCATAGCCT-3′ (included Xho I site, underlined).

The 2.8 kb proximal fragment, 2.2 kb EGFP-neo fragment, and the 5.5 kb distal fragment were subcloned into phage DNA vector (λDASHII-254-2TK) at the XhoI sites to flank the targeting construct with 2TK genes. The vector was then packaged into phage, and the positive phage clones were selected by PCR digested using restriction enzyme. The positive phage DNA was digested by NotI to release the final targeting vector that contained the 2TK genes. This vector could be circularized into a plasmid and amplified in bacteria. After amplification, the final vector was linearized by NotI digestion and used for electroporation of 129/SvJ ES cells [24].

3. *ES cell electroporation*: ES cells (D3; Incyte Genomics, St. Louis, MO) were electroporated with the linearized targeting vector. The ES cells were then selected by G418 (200 μg/ml) and ganciclovir. The double-resistant ES cell clones were selected and expanded for screening by Southern blotting [17].
4. *Genotyping of mutant mice*: Southern Blotting: Mouse genomic DNA from the ES cells was isolated and digested with BglII. Restriction enzyme-digested genomic DNA was then hybridized with an external probe located upstream of the targeting vector, yielding 5 kb and 7.2 kb fragments for wild-type and *hsf4*-targeted alleles, respectively. From the 141 isolated ES clones that were analyzed by Southern blotting, 33 clones contained the correctly targeted allele (Fig. 2) [24]. Two positive ES clones were injected into C57BL/6J blastocysts, and the resulting chimeric male mice were crossed with C57BL/6J females to generate germ-line transmission. Homozygous mice were obtained by interbreeding of F1 heterozygous mice (Fig. 5b).

   Primers used for genotyping: For routine genotyping of mice, DNA extracted from tail was used for PCR analysis to verify a 260 bp wild-type and a 600 bp targeted *hsf4* fragments using the following primers: P1: 5′-GCAAACGCAG CACTTTCGCG-3′; P2: 5′-CGGATCTTGAAGT TCACCTTGAT-3′; P3: 5′-TGGACAGGGGTGTTCACG ACA-3′ (Fig. 5c).

   Immunoblotting of lens extracts of *hsf4*-deficient mice showed no Hsf4 expression (Fig. 5d).

3.4 Physiological Function of Mice with a Targeted Disruption of the hsf1, hsf2, or hsf4 Gene

In this section, we will briefly describe the major phenotypes of the *hsf1*-, *hsf2*- and *hsf4*-deficient mice generated in our laboratory. Additionally, since some of our *hsf*-deficient mouse lines encode a reporter gene and we have also generated *hsp25*$^{-/-}$-lacZ and *hsp70.3*$^{-/-}$-lacZ [25, 26] knock-in reporter genes, we will briefly describe the beneficial uses of knockout mice containing reporter genes in investigating the effects of hsf deletions on the expression of their downstream target gene in vivo.

In addition to the *hsf* knockout mice that we have generated [19, 21, 24], there are two other *hsf1* [27, 28], two other *hsf2* [29, 30], and one other *hsf4* [31] mutant mouse lines that have been generated in other laboratories. The phenotypes of all the mouse lines are almost comparable with each other. *Hsf1*-deficient mice generated in our laboratory exhibit complete female infertility (unpublished data). This phenotype was reported by Christians, et al. [32], and the cause appears to be the inability of the *hsf1*$^{-/-}$ zygote to undergo zygotic gene activation following fertilization [32]. Another major phenotype of *hsf1*$^{-/-}$ mice is their inability to mount a heat-shock response in every tissue that has been tested using immunoblotting or following crossing of *hsf1*$^{-/-}$ mice with *hsp70.3*$^{-/-}$-lacZ reporter mice [19]. *Hsf1*$^{-/-}$ mice exhibit an age-dependent demyelinating disease [33], and cells deficient in *hsf1* exhibit accumulation of ubiquitinated proteins, including wild-type and mutant p53 proteins [33, 34]. In addition to supporting stress response, Hsf1 in cooperation with mTORC1 regulates sizes of the cell, organ, and body [35]. *Hsf1*$^{-/-}$ mice in p53-deficient background (*hsf1*$^{-/-}$*p53*$^{-/-}$) exhibit a delay in the development of lymphomas compared to *p53*$^{-/-}$ mice. There is a change in tumor spectrum that is observed in *hsf1*$^{-/-}$*p53*$^{-/-}$ mice compared to *p53*$^{-/-}$ mice, and double-knockout mice exhibit reduced lymphomas (7.9% in *hsf1*$^{-/-}$*p53*$^{-/-}$ mice versus 72.2% in *p53*$^{-/-}$ mice) [7]. As noted above, Hsf1-deficient mice are also resistant to ErbB2-induced breast cancer [9, 10] and carcinogen-induced liver cancer and exhibit altered glucose and lipid metabolism [8]. *Hsf2*$^{-/-}$ mice exhibit defects in spermatogenesis, and males exhibit reduced fertility a few months after birth and in the background of *hsf1* deficiency, all males are infertile due to complete disruption in spermatogenesis [36]. Hsf2 also expresses at high levels in the brain, and *hsf2*$^{-/-}$ mice exhibit developmental defects in the central nervous system (CNS) [21]. Further studies on these mice are needed to reveal additional functions of Hsf2 in mammalian organisms. Before we generated *hsf4*$^{-/-}$ mice, there was no information on how Hsf4 becomes transcriptionally activated or in which tissues or cells it expresses. Previous reports indicated that the *hsf4* gene was mutated in humans, and humans who carry the mutation exhibit lamellar and marner cataracts [37]. Interestingly, *hsf4*$^{-/-}$ mice exhibit developmental defects in fiber cell

differentiation in the lens, which leads to blindness in 100% of the progeny [24]. Hsf4 activity was, for the first time, detected in the lens epithelial cells at 3 days postnatally [24]. The activation of Hsf4 leads to the expression of Hsp25, which was 1000-fold lower in *hsf4*$^{-/-}$ lens [24].

1. *Hsf4-EGFP is expressed in many tissues.* Addition of a reporter gene (EGFP) under control of the *hsf2* and *hsf4* promoters has been a powerful means of revealing in which cell types these transcription factors express in vivo. As we already have reported, Hsf2-EGFP expression can be detected in the testis during spermatogenesis using flow cytometry [21]. Flow cytometry and immunoblotting experiments also show that *hsf4-EGFP* (knockout/knock-in mice) is expressed in a number of adult tissues (Fig. 6). The expression of *hsf4-EGFP* was analyzed in spleen and found to be expressed in mature CD4+, CD8+, and CD3+ (T cell receptor) thymocytes, GR-1-positive granulocytes (not presented), neutrophils/macrophages (CD11b+), and dendritic cells (CD11c+) (Fig. 6). Interestingly, Hsf4 does not express in B cells or immature $CD4^{-}CD8^{-}$ or $CD4^{+}CD8^{+}$ T cells (Fig. 6, thymus), but it is expressed in spleen and peripheral lymph nodes (Fig. 6a and b). Interestingly, Hsf4-EGFP expression can only be detected once T cells leave the thymus and enter the periphery.
2. *Hsf4 regulation of Hsp25 expression in vivo*: Another unique use of analyzing knockout mice expressing a reporter gene is the use of intercrossing Hsfs with their downstream target genes that express LacZ (or EGFP when possible) under their endogenous promoters to determine the extent that they regulate each downstream target gene in vivo. In one study, we crossed *hsf4*-deficient mice with *hsp25*$^{-/-}$-lacZ reporter mice [26]. We found that *hsp25-lacZ* is a downstream target of the *hsf4* gene in the lens. As we described earlier, Hsf4 DNA binding and transcriptional activity was demonstrated in developing lens epithelial cells [24]. Using gel mobility shift assays, Hsf4 DNA binding activity could be detected between postnatal days P1-P5 lens extracts (data not presented, please *see* [24]). Using *hsp25*$^{+/-}$*-LacZ* knockin mice, we were able to demonstrate that Hsp25-lacZ expression coincides with the onset of Hsf4 activity in the lens epithelium and fiber cells (Fig. 7, upper panel, X-gal staining). Crossing *hsf4*$^{-/-}$ mice with *hsp25*$^{-/-}$ mice we were able to completely eliminate the Hsp25 promoter-driven β-galactosidase (β-gal) expression, suggesting that Hsp25 is a downstream target of the *hsf4* gene during lens epithelial cell differentiation.

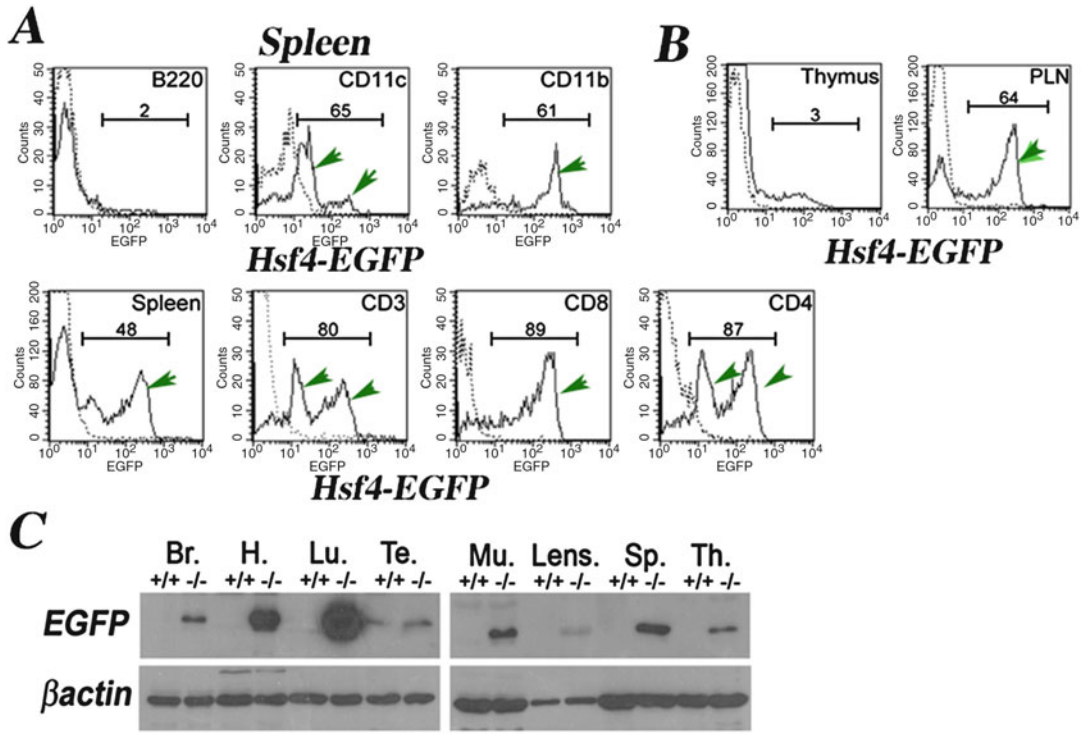

Fig. 6 Hsf4-EGFP is expressed in adult normal tissues. (**a**) Cells from *hsf4*$^{-/-}$ spleen were immunostained to detect a specific cell population expressing Hsf4-EGFP as indicated. B220 detects B cell population; CD11c detects dendritic cells; CD11b detects neutrophils/ macrophages; CD3+, CD4+, or CD8+ are T cell-specific markers. *Dotted lines* are immunostained +/+ cells (no EGFP). (**b**) Cells from *hsf4*$^{-/-}$ thymus or peripheral lymph nodes (PLNs) were analyzed by flow cytometry for expression of EGFP. In panels (**a**) and (**b**), the numbers represent percentages of cells expressing EGFP, and these populations are indicated by *green arrows*. (**C**) 30 μg of indicated adult tissue extracts from wild-type or *hsf4*$^{-/-}$ mice were used in immunoblotting experiments using antibody to EGFP. Hsf4-EGFP expression can be detected in the brain (Br), heart (H), lung (Lu), testis (Te), muscle (Mu), lens, spleen (Sp), and thymus (Th). Wild type (+/+), *hsf4*$^{-/-}$(−/−). Note that EGFP expression is an indication of Hsf4-driven transcription

4 Notes

General considerations to knockout hsf1, hsf2, or hsf4 genes

The following points are important considerations for successful gene targeting.

1. The genomic DNA source must be the same as the ES cells to be used. This will facilitate homologous recombination.
2. Purchase a BAC clone containing the gene of interest (http://bacpac.chori.org).
3. For designing the targeting vector, the lengths of the 5′ and 3′ fragments are important in facilitating homologous recombination. Sizes between 0.8 and 5 kb have been successfully used.

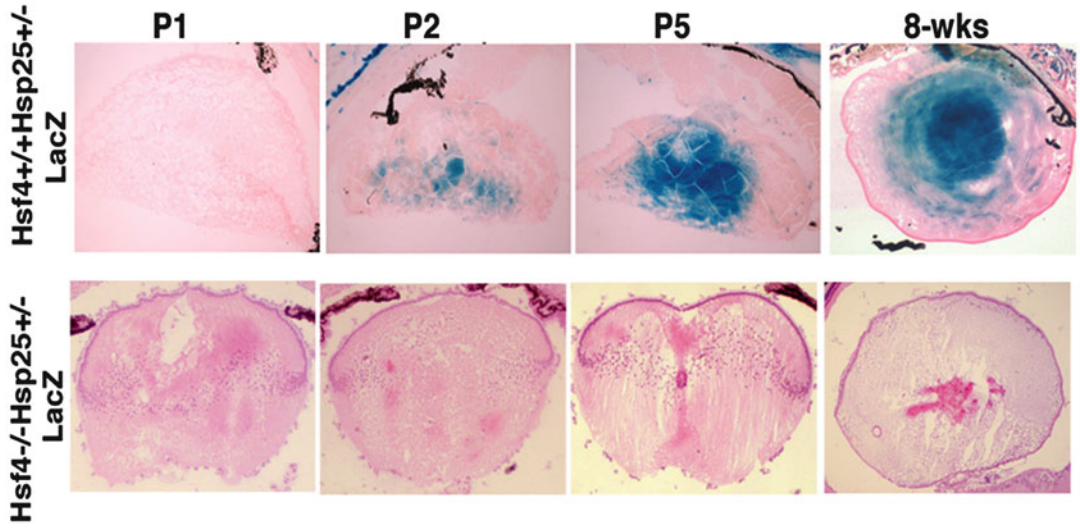

Fig. 7 Hsf4 controls the expression of Hsp25 in the lens during development. Histological analyses of *hsf4*$^{+/+}$*hsp25*$^{+/-}$*-LacZ* lens at P1 to 8-weeks old mice to show the expression of β-gal in developing and mature lens. Note the positive X-gal staining in *hsf4*$^{+/+}$*hsp25*$^{+/-}$*-lacZ* P2 stage, while no X-gal staining can be detected in lenses of *hsf4*$^{-/-}$*hsp25*$^{+/-}$*-lacZ*

The total size of the fragment that can be inserted into the final vector needs to be considered before constructing the vector. The λDash II-254-2TK phage used by our laboratory can accommodate approximately 14 kb. Therefore, the sizes of the 5′ and 3′ fragments plus the neomycin gene that is required for positive selection of ES cells and a reporter gene (such as green fluorescent protein (EGFP) or β-galactosidase) should not exceed more than 14 kilobase pairs. Before attempting to construct the targeting vector, it is best to schematically draw the entire plan for the construct to be made. This should include all the restriction enzymes to be used.

4. It is best to insert the EGFP or LacZ genes at the ATG of the gene that is targeted. This design will ensure that expression of EGFP or LacZ is under the direct control of the promoter of the gene to be targeted.
5. Although the insertion of the EGFP or LacZ gene at the ATG interrupts the gene of interest, the design of the targeting construct could be such that a portion of the gene to be targeted is also deleted to ensure complete disruption of the gene.
6. Two probes need to be designed for the detection of ES cell clones following electroporation of the targeting vector into the ES cells. The external probe is located outside of the 5′ and 3′ fragments. A restriction enzyme must be selected so that the external probe can detect correct targeting into the intended

locus. Sometimes, creating a unique restriction enzyme before the EGFP (or LacZ genes) or between the EGFP and neomycin genes (or after neomycin) is an option. Another consideration is that the fragment size created following restriction enzyme digest will not be larger than 12–15 kb since large fragments will be more difficult to detect by Southern blotting. Once the outside probe (best size is 500 bp to 1 kb) is selected, it is best to perform Southern blotting using the genomic DNA following digestion with one or two restriction enzymes to ensure the probe generates a predicted band for the wild-type locus.

7. It is best that the neomycin gene is flanked by two loxP sites so that it can be removed following the generation of the knockout mouse by crossing with transgenic female mouse expressing Cre recombinase (Splicer mice [38], Jackson laboratory).
8. The identity of all the fragments that have been amplified by PCR needs to be verified by DNA sequencing. The ligation sites of the final targeting vector also need to be confirmed by sequencing since deletions may occur during the ligation.

Acknowledgements

This work was supported by VA Award 1I01BX000161 and NIH grants CA062130 and CA132640 (N.F.M.) and CA121951 and CA121951-07S2 (D.M.). For generation of hsf knockout mice, the microinjection of ES cells and generation of chimeras were conducted in the Medical College of Georgia (Augusta University) Embryonic Stem Cell and Transgenic Core Facility.

References

1. Wu C (1995) Heat shock transcription factors: structure and regulation. Annu Rev Cell Dev Biol 11:441–469
2. Morimoto RI (1998) Regulation of the heat shock transcriptional response: cross talk between a family of heat shock factors, molecular chaperones, and negative regulators. Genes Dev 12:3788–3796
3. Anckar J, Sistonen L (2011) Regulation of HSF1 function in the heat stress response: implications in aging and disease. Annu Rev Biochem 80:1089–1115
4. Nakai A, Tanabe M, Kawazoe Y, Inazawa J, Morimoto RI, Nagata K (1997) HSF-4, a new member of the human heat shock factor family which lacks properties of a transcriptional activator. Mol Cell Biol 17:469–481
5. Hu Y, Mivechi NF (2006) Association and regulation of heat shock transcription factor 4b with both extracellular signal-regulated kinase mitogen-activated protein kinase and dual-specificity tyrosine phosphatase DUSP26. Mol Cell Biol 8:3282–3294
6. Dai C, Whitesell L, Rogers AB, Lindquist S (2007) Heat shock factor 1 is a powerful multifaceted modifier of carcinogenesis. Cell 130:1005–1018
7. Min J-N, Huang L, Zimonjic D, Moskophidis D, Mivechi NF (2007) Selective suppression of lymphomas by functional loss of hsf1 in a p53-deficient mouse model of spontaneous tumors. Oncogene 26(35):5086–5097
8. Jin X, Moskophidis D, Mivechi NF (2011) Heat shock transcription factor 1 is a key

determinant of HCC development by regulating hepatic steatosis and metabolic syndrome. Cell Metab 14:91–103

9. Xi C, Hu Y, Buckhaults P, Moskophidis D, Mivechi NF (2012) Heat shock factor Hsf1 cooperates with ErbB2 (Her2/Neu) protein to promote mammary tumorigenesis and metastasis. J Biol Chem 287:35646–35657
10. Gabai VL et al (2012) Heat shock transcription factor Hsf1 is involved in tumor progression via regulation of hypoxia-inducible factor 1 and RNA-binding protein HuR. Mol Cell Biol 32:929–940
11. Jin X et al (2012) Inactivation of heat shock factor Hsf4 induces cellular senescence and suppresses tumorigenesis in vivo. Mol Cancer Res 10:523–534
12. Bjork JK et al (2016) Heat-shock factor 2 is a suppressor of prostate cancer invasion. Oncogene 35:1770–1784
13. Muller U (1999) Ten years of gene targeting: targeted mouse mutants, from vector design to phenootype analysis. Mech Dev 82:3–21
14. Van Der Weyden L, Adams DJ, Bradley A (2002) Tools for targeted manipulation of the mouse genome. Physiol Genomics 11:133–164
15. Bockamp E, Sprengel R, Eshkind L, Lehmann T, Braun JM, Emmrich F, Hengstler JG (2008) Conditional transgenic mouse models: from the basics to genome-wide sets of knockouts and current studies of tissue regeneration. Regen Med 3:217–235
16. Bockamp E, Maringer M, Spangenberg C, Fees S, Fraser S, Eshkind L, Oesch F, Zabel B (2002) Of mice and models: improved animal models for biomedical research. Physiol Genomics 11:115–132
17. Sambrook J, Fritsch EF, Maniatis T (1989) Molecular cloning: a laboratroy manual, 2nd edn. Cold Spring Harbor Laboratory Press, Cold Spring Harbor, NY
18. Limaye A, Hall B, Kulkarni AB (2009) Manipulation of mouse embryonic stem cells for knockout mouse production. Curr Protoc Cell Biol; Chapter 19:Unit 19.13 19.13.1–24
19. Zhang Y, Huang L, Zhang J, Moskophidis D, Mivechi NF (2002) Targeted disruption of hsf1 leads to lack of thermotolerance and defines tissue-specific regulation for stress-inducible Hsp molecular chaperones. J Cell Biochem 86:376–393
20. Zhang Y, Koushik S, Dai R, Mivechi NF (1998) Structural organization and promoter analysis of murine heat shock transcription factor-1 gene. J Biol Chem 273:32514–32521
21. Wang G, Zhang J, Moskophidis D, Mivechi NF (2003) Targeted disruption of the heat shock transcription factor (hsf)-2 gene results in increased embryonic lethality, neuronal defects, and reduced spermatogenesis. Genesis 36:48–61
22. Thomas KR, Capecchi MR (1987) Site-directed mutagenesis by gene targeting in mouse embryo-derived stem cells. Cell 51:503–512
23. Godwin AR, Stadler HS, Nakamura K, Capecchi MR (1998) Detection of targeted GFP-Hox gene fusions during mouse embryogenesis. Proc Natl Acad Sci U S A 95:13042–13047
24. Min J, Zhang Y, Moskophidis D, Mivechi NF (2004) Unique contribution of heat shock transcription factor 4 in ocular lens development and fiber cell differentiation. Genesis 40:205–217
25. Huang L, Mivechi NF, Moskophidis D (2001) Insights into regulation and function of the major stress-induced hsp70 molecular chaperone in vivo: analysis of mice with targeted gene disruption of the hsp70.1 or hsp70.3 genes. Mol Cell Biol 21:8575–8591
26. Huang L, Min J, Maters S, Mivechi NF, Moskophidis DI (2007) Insights into the function and regulation and of small hsp25 (HSPB1) in mouse model with targeted gene disruption. Genesis 45:487–501
27. Xiao X, Zuo X, Davis AA, McMillan DR, Curry BB, Richardson JA, Benjamin IJ (1999) HSF1 is required for extra-embryonic development, postnatal growth and protection during inflammatory responses in mice. EMBO J 18:5943–5952
28. Sugahara K, Inouye S, Izu H, Katoh Y, Katsuki K, Takemoto T, Shimogori H, Yamashita H, Nakai A (2003) Heat shock transcription factor HSF1 is required for survival of sensory hair cells against acoustic overexposure. Hear Res 182:88–96
29. McMillan DR, Christians E, Forster M, Xiao X, Connell P, Plumier JC, Zuo X, Richardson J, Morgan S, Benjamin IJ (2002) Heat shock transcription factor 2 is not essential for embryonic development, fertility, or adult cognitive and psychomotor function in mice. Mol Cell Biol 22:8005–8014
30. Kallio M, Chang Y, Manuel M, Alastalo TP, Rallu M, Gitton Y, Pirkkala L, Loones MT, Paslaru L, Larney S, Hiard S, Morange M, Sistonen L, Mezger V (2002) Brain abnormalities, defective meiotic chromosome synapsis and female subfertility in HSF2 null mice. EMBO J 21:2591–2601

31. Kurokawa H et al (2000) Inhibition of HER2/neu (erbB-2) and mitogen-activated protein kinases enhances tamoxifen action against HER2-overexpressing, tamoxifen-resistant breast cancer cells. Cancer Res 60:5887–5894
32. Christians E, Davis AA, Thomas SD, Benjamin IJ (2000) Maternal effect of Hsf1 on reproductive success. Nature 407:693–694
33. Homma S et al (2007) Demyelination, astrogliosis, and accumulation of ubiquitinated proteins, hallmarks of CNS disease in hsf1-deficient mice. J Neurosci 27:7974–7986
34. Jin X, Moskophidis D, Hu Y, Phillips A, Mivechi NF (2009) Heat shock factor 1 deficiency via its downstream target gene alphaB-crystallin (Hspb5) impairs p53 degradation. J Cell Biochem 107:504–515
35. Su KH et al (2016) HSF1 critically attunes proteotoxic stress sensing by mTORC1 to combat stress and promote growth. Nat Cell Biol 18:527–539
36. Wang G, Ying Z, Jin X, Tu N, Zhang Y, Phillips M, Moskophidis D, Mivechi NF (2004) Essentail requirement for both *hsf1* and *hsf2* transcriptional activity activity in spermatogenesis and male fertility. Genesis 38:66–80
37. Bu L et al (2002) Mutant DNA-binding domain of HSF4 is associated with autosomal dominant lamellar and Marner cataract. Nat Genet 31:276–278
38. Koni PA, Joshi SK, Temann UA, Olson D, Burkly L, Flavell RA (2001) Conditional vascular cell adhesion molecule 1 deletion in mice: impaired lymphocyte migration to bone marrow. J Exp Med 193:741–754
39. Tessari A, Salata E, Ferlin E, Bartoloni L, Slongo ML, Foresta C (2004) Characterization of HSFY, a novel AZFb gene on the Y chromosome with a possible role in human spermatogenesis. Mol Hum Repord 4:253–258
40. Fujimoto M, Hayashida N, Katoh T, Oshima K, Shinkawa T, Prakasam R, Tan K, Inouye S, Takii R, Nakai A (2010) A novel mouse HSF3 has the potential to activate non-classical heat shock genes during heat shock. Mol Biol Cell 21(1):106–116
41. Sarge KD, Zimarino V, Holm K, Wu C, Morimoto RI (1991) Cloning and characterization of two mouse heat shock factors with distinct inducible and constitutive DNA-binding ability. Genes Dev 5:1902–1911
42. Fujimoto M, Izu H, Seki K, Fukuda K, Nishida T, Yamada S, Kato K, Yonemura S, Inouye S, Nakai A (2004) HSF4 is required for normal cell growth and differentiation during mouse lens development. EMBO J 23 (21):4297–4306

Chapter 2

Role of Heat Shock Factors in Stress-Induced Transcription

Ayesha Murshid, Thomas L. Prince, Ben Lang, and Stuart K. Calderwood

Abstract

Heat shock proteins (HSP) are rapidly induced after stresses such as heat shock and accumulate at high concentrations in cells. HSP induction involves primarily a family of heat shock transcription factors (HSF) that bind the heat shock elements of the *HSP* genes and mediate transcription *in trans*. We discuss methods for the study of HSP binding to *HSP* promoters and the consequent increases in HSP gene expression in vitro and in vivo.

Key words Heat shock factor, Binding, Purification, Transcription, Heat shock protein, Nuclear run on, Chromatin immunoprecipitation

1 Introduction

Heat shock factor (HSF) was first discovered in yeast as a sequence-specific transcription factor that binds to the promoters of heat shock protein (HSP) genes [1]. HSF was shown to bind as a trimer to three inverted repeats of the sequence nGAAn at high affinity, an activity that was later shown in *Drosophila* HSF and human HSF1 [2–5]. In more complex organisms, there are at least four members of the family in avian and mammalian species and multiple members in higher plants [6–11]. The current consensus in mammalian cells is that HSF1 is the most potent regulator of the heat shock response with the remaining factors playing supplementary roles in stress and perhaps more significant roles in development [6, 12, 13]. The mechanisms by which HSF1 is triggered by stress are not entirely clear. HSF1 is thought to be constitutively repressed by the products of its transcriptional activity—HSPs through a feedback inhibition mechanism [14, 15]. Activation is thus envisaged as a reversal of such inhibi-

Ayesha Murshid, Thomas L. Prince, Ben Lang and Stuart K. Calderwood contributed equally to this work.

Stuart K. Calderwood and Thomas L. Prince (eds.), *Chaperones: Methods and Protocols*, Methods in Molecular Biology, vol. 1709, https://doi.org/10.1007/978-1-4939-7477-1_2,

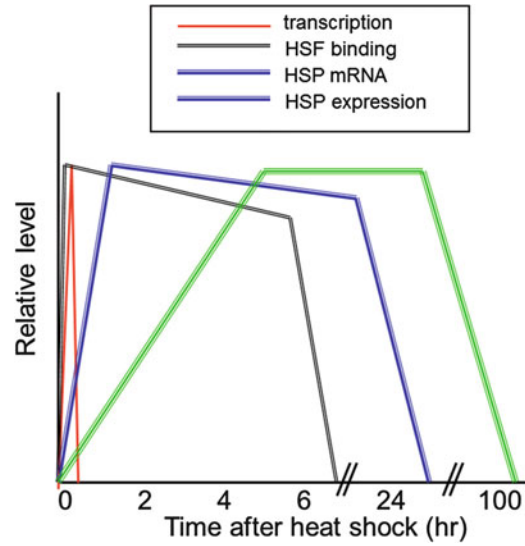

Fig. 1 Relative kinetics of *hsp* gene transcription, HSF binding, HSP mRNA expression, and heat shock protein expression after heat shock

tion as denatured proteins sequester HSPs during heat shock and HSF1 becomes liberated to bind to HSE elements in *HSP* genes. However, alternative/overlapping hypotheses have been proposed involving stress-mediated HSF1 phosphorylation, binding to large noncoding RNA, and regulation at the level of posttranscriptional pausing [16–19]. HSF1 and HSF2 are predicted to encode at least two splicing variants, with HSF2A and HSF2b showing differential expression during erythroid differentiation [6]. HSF2A appears to be active in transcriptional regulation while HSF2B appears to be inactive [6].

Heat shock causes a rapid increase in HSF1 binding to *HSP* gene promoters and an acute elevation in the transcription of *HSP* genes (relative rates are indicated in Fig. 1) [16]. Transcription decays rapidly after initiation, while HSF continues to bind to HSE for several hours [20, 21]. HSP mRNAs are then observed within 1 h of activation and are maintained at these high levels for up to 24 h due to enhanced stabilization after stress [22]. After acute stress, HSP protein expression in mammalian cells is delayed due to initial translational inhibition, then Hsp70, Hsp90, and Hsp110 are observed by 2–6 h after a 43 °C heat shock and can persist in most cells for up to 100 h [23] (Fig. 1). In this report, we are concerned with the early phase of HSP gene expression, involving HSF1 binding to *HSP* genes and activation of transcription.

2 Materials

2.1 Purification of HSF2 and Electrophoretic Mobility Shift Assay (EMSA)

2.1.1 Primers

For human HSF2:

Forward primer was 5′–3′ GC[GAATCC]ATGAAGCAGAG TTCGA.

Reverse primer 5′–3′ AAA[GTCGAC]TTCCTGGGGATTT AGCTA.

For murine HSF2:

Forward primer 5′–3′ GG[GAATCC]ATGAAGCAGAGTT CGAACG.

Reverse primer 5′–3′ AGT[GTCGAC]TTGGGAGTTTAA CTATCT.

EMSA oligonucleotides:

Hsp70 HSE top strand: 5′-CACCTCGGCTGGAATATTCCCGA CCTGGCAGCCGA-3′.

2.2 Mutant Oligonucleotides

5′-CACCTCGGCTG**C**A**A**TAA**T**CCCGACCTGGCAGCCGA-3′.

Cells: BL21 (DE3) *E. coli, Human HeLa*.

Columns and filters.

20 ml glutathione-sepharose (Pierce Chemicals).

Mono-Q HR 5/5 (Pharmacia).

Centricon 10 ultrafilter.

2.3 Buffers

E. coli Lysis buffer: 7 M guanidine-HCl in 0.1 M potassium phosphate buffer pH 7.4 containing 50 mM DTT and 0.05% NP-40.

Dialysis buffer: 50 mM potassium phosphate buffer containing 0.1 M KCl and 2 mM DTT.

BSA Solution: 0.1 mg/ml bovine serum albumin.

EMSA lysis buffer: 10 mM (HEPES), 10 mM NaCl, 0.1 mM EDTA, 1.0 mM dithiothreitol (DTT), 1.0 mM phenylmethylsulfonyl fluoride (PMSF), 2.0 mg/ml aprotinin, leupeptin, 20 mM NaF and 2.0 mM Na_3VO_4 (pH 7.9).

HSF extraction buffer: aprotinin, leupeptin, 20 mM NaF and 2.0 mM Na_3VO_4 (pH 7.9) on ice. Cells are then lysed by the addition of Nonidet P-40 to 0.6% and lysates clarified by spinning at 12,000 × g. Nuclear pellets.

EMSA incubation buffer: (12 μl) contained 2.0 μl nuclear extract or recombinant protein, 2.0 mg/ml bovine serum albumin, 2.0 mg/ml poly dI-dC, 0.5–1.0 ng ^{32}-P-labeled, double-stranded oligonucleotide probe, 12 mM Hepes, 12% glycerol, 0.12 mM EDTA, 0.9 mM $MgCl_2$, 0.6 mM DTT, 0.6 mM PMSF and 2.0 mg/ml aprotinin and leupeptin (pH 7.9).

2.4 ChIP Assay

ChIP Dilution Buffer (1.1% Triton X-100, 1.2 mM EDTA, 16.7 mM Tris–HCl, pH 8.0, and 167 mM NaCl).

Protein A Agarose Slurry (Sigma Chemicals, St Louis, MO).

ChIP Washing buffers:

Washing buffer 1 (20 mM Tris–HCl, pH 8.0, 150 mM NaCl, 1% Triton X-100, 2 mM EDTA, and 0.1% SDS).

Washing buffer 2 (20 mM Tris–HCl, pH 8.0, 500 mM NaCl, 1% Triton X-100, 2 mM EDTA, and 0.1% SDS).

Washing buffer 3 (10 mM Tris–HCl, pH 8.0, 250 mM LiCl, 1% NP-40, 1% sodium deoxycholate, and 1 mM EDTA), TE (10 mM Tris–HCl, pH 7.5, 1 mM EDTA).

ChIP elution buffer (1% SDS, 0.1 M $NaHCO_3$).

5 M NaCl.

ChIP Uncrosslinking Buffer: 0.5 M EDTA, 10 μl of 1 M Tris–HCl, pH 6.5, and 2 μl Proteinase K.

ChIP hsp70.1 primers: exon region forward primers: {*hsp70.1* exn Forward: 5′ ggacatcagccagaacaagc 3′ *hsp70.1* exn Reverse: 5′ aagtcgatgccctca aac ag 3′.

hsp70.1 HSE Reverse:5′ cggcttttataagtcgtcgt 3′ *hsp70.1* HSE Forward: 5′ aggcgaaacccctggaata 3′}.

2.5 Run-on Transcription

Run-on Lysis Buffer: 10 mM Tris–HCl (pH 7.4), 10 mM NaCl, 3 mM $MgCl_2$ and 0.5% nonidet-P40.

Run-On Storage Buffer: 50 mM Tris (pH 8.30), 40% glycerol, 5 mM $MgCl_2$ and 40 units of RNAsin (Roche Molecular Biochemicals).

Run-on Reaction Buffer: 10 mM Tris–HCl (pH 8.0), 5 mM $MgCl_2$, 0.3 M KCl, 5 mM DTT, 1 mM ATP, 1 mM CTP, 1 mM GTP, and 50 uCi [α-^{32}P] UTP (3000 Ci/mmol).

Hybridization Solution: UltraHyb solution (*Ambion*).

Hybridization Washing Buffers: (1) 2× SSC, 0.1% SDS, (2) high stringency solution (1× SSC, 0.1% SDS), (3) 2× SSC, 0.1% SDS with 10 μg RNase A.

3 Purification of Heat Shock Factors and In Vitro EMSA

In order to study the properties of HSF family members in vitro we have prepared purified, recombinant HSF1 and HSF2.

3.1 Complementary DNA Cloning of Human and Mouse HSF2A and HSF2B

RNA was isolated from NIH-3 T3 (mouse) or HeLa (human cells) and messenger RNA prepared by poly-T affinity chromatography (PolyAtract system, Promega, Madison, WI). cDNA was then prepared from the mRNA using the AMV reverse transcriptase system (Promega) and HSF2 cDNAs amplified using Taq polymerase and the polymerase chain reaction using the following primer sets mentioned above [6]:

Forward primers contain Eco-R1 restriction site consensus sequences [marked in boxes] and the reverse primers contain Sal-1 sequences for subsequent cloning of amplified DNAs into the PGEX5 prokaryotic expression vector (Pharmacia). After transformation and growth of competent bacteria, colonies are screened for either total HSF2 using oligonucleotides (1764–1785; CAGGAGCAAGTTCACATAAATA and 1786–1807; GGCATATCACTATCCAGAGGTG) predicted to detect all forms of HSF2 or for the larger form (HSF2A) using oligonucleotides predicted to hybridize specifically with this species (1420–1440; TTGTATTATTGATGTAATCT and (1392–1412; CATCTGCACAGAACTAG TGA). Oligonucleotides are then end-labeled with ^{32}-P ATP and T4 polynucleotide kinase. Plasmids detected using these probes are isolated, screened for the presence of inserts and for the production of HSF2-glutathione transferase fusion proteins from representative cDNAs in bacteria exposed to the inducing agent IPTG (Pharmacia). After induction, bacterial lysates are prepared and screened by immunoblot with anti-GST antibodies (St Cruz Antibodies) and anti-HSF2 antibody Ab-3158 prepared in the Calderwood lab. Representative clones from human HSF2A and HSF2B and murine HSF2A and HSF2B are then further analyzed by dideoxynucleotide sequencing.

3.2 Purification of HSF2 Proteins

HSF2 variants are cloned into the pGEX-5 expression vector, between the Eco RI and Sal I sites and the resulting plasmids are used to transform BL21 (DE3) *E. coli* bacteria. HSF2 was thus expressed as a fusion protein with glutathione-S transferase. All the purification steps are carried out at 4 °C. Briefly, IPTG-induced bacteria are pelleted and dissolved in *E. coli* Lysis Buffer and dialyzed against *E. coli* Lysis Buffer. The samples are centrifuged at 2500 × *g* for 5 min and the supernatant loaded on a 20 ml volume glutathione-Sepharose column at a flow rate of 0.5 ml/min, washed extensively with Dialysis Buffer, and eluted with this buffer A containing 10 mM reduced glutathione. The eluate was loaded onto a Mono-Q HR 5/5 ion-exchange chromatography column at a flow rate of 0.8 ml/min and eluted with a 24 ml linear gradient from 0.1 to 1.0 M KCl final concentration of KCl in buffer A. Absorbance was monitored at 280 nm and the fractions corresponding to HSF2 assayed for binding to HSE, pooled and concentrated with a Centricon 10 ultrafilter in the presence of 0.1 mg/ml bovine serum albumin. Relative concentrations of active HSF2 are estimated by quantitative EMSA (Fig. 1).

GST-HSF1 is purified using a similar protocol [24]. Alternatively, we have described a detailed method for purifying recombinant HSF1 after expression in *E. coli* from the pET7.1 vector [25]. Recombinant HSF1 without a GST tag is prepared by ammonium sulfate precipitation, heparin-agarose affinity, and ion

exchange chromatography in a pure form as assessed by SDS-PAGE and reverse-phase HPLC [25].

Activity of purified GST-HSF2A, GST-HSF2B, or GST-HSF1 is estimated by EMSA. Proteins are incubated with ^{32}P-labeled HSE at a range of dilutions and then subjected to EMSA analysis as described below. GST-HSF2A and GST-HSF2B are serially diluted 1/2200, 1/660, 1/220, 1/66, 1/22, and 3/22 prior to EMSA.

4 Nuclear Extraction from Tissue Culture Cells and EMSA

EMSA is carried out using purified recombinant HSF or after the extraction of intracellular HSF complexes from either whole cell or nuclear extracts from heat shocked cells and incubation of complexes with double-stranded oligonucleotides encoding heat shock elements in HSP genes (HSE) (*see* **Note 1**). To prepare HSF from cells growing in vitro, nuclear extracts are prepared according to Schreiber [26]. In our standard assay, the cells are incubated for 15 min in 200–800 μl of EMSA Lysis Buffer on ice. The cells are then lysed by the addition of Nonidet P-40 to 0.6% and lysates clarified by spinning at 12,000 × *g*. The nuclear pellets are then resuspended in 25 μl ice-cold EMSA extraction buffer. Extracts containing HSF are then aliquoted and stored at −80 °C.

For incubation with oligonucleotide probe, each binding mixture (12 μl) contained 2.0 μl nuclear extract or recombinant protein, 2.0 mg/ml bovine serum albumin in EMSA Incubation Buffer. Samples are incubated at room temperature for 15 min, and then fractionated by electrophoresis on 4.0% polyacrylamide, 1× TBE gels. Oligonucleotide hHSE was synthesized, annealed, and labeled by end filling with ^{32}P-dCTP at 6000 Ci/mmol (DuPont, NEN) to an activity of 100, 000 cpm/ng. hHSE contains the heat shock element (HSE) from the top strand of the human *HSP70.1* promoter [27]. (We have found that double-stranded oligonucleotide end filling with Klenow fragment or end labeling of single-stranded oligonucleotides with T4 kinase to be equally effective.) The oligonucleotide shown in Subheading 2 (575 ng) and the complementary oligonucleotide (2300 ng) (resulting in 1150 ng double stranded oligo) are made up to 25 ng/μl in 46 μl of TE buffer, annealed by incubation at 100 °C for 5 min, and cooled overnight. As a control, we carried out the EMSA procedure with a similar oligonucleotide containing mutations in the HSE elements, indicated in bold in the sequence shown in Subheading 2. For experiments on cell extracts, a number of controls are used standardly. To determine specific binding of HSF1 to labeled HSE, we examine the ability to inhibit HSE-HSF association with a tenfold excess of unlabeled wild-type oligonucleotide included in the incubation. In addition, specific binding is further indicated by failure of

a tenfold excess of the mutant HSE shown above to inhibit binding. The protein (HSF) in the HSF-HSE complex can be identified by the addition of specific anti-HSF1 or anti-HSF2 antibodies to the reaction mix. We used a 1:100 dilution of anti-HSF1 antibody 68-3 prepared in our laboratory to positively identify HSF1 in the complexes [28, 29]. As a control, we use pre-immune antiserum obtained from the same rabbit. For commercially obtained antibodies, a serial dilution approach was used to determine optimal antibody concentrations.

HSF1 from heat shocked cells is contained in large complexes of at least 600 kDa and is fractionated on 4% tris-borate non-denaturing gels [30, 31]. For most purposes, we found that the mini-gel (Bio-Rad, CA) format was quite adequate for separation, although for supershift assay and higher resolution a larger format was used [32].

5 Measuring HSF1 Binding to HSP Promoters In Vivo by the Chromatin Immunoprecipitation (ChIP) Assay

ChIP (Chromatin Immunoprecipitation) offers an attractive solution to transcription analysis by combining the specificity of immunoprecipitation and the sensitivity of PCR [19] (*see* **Note 2**).

The method allows monitoring of the interactions between DNA and transcription factors and/or components of chromatin remodeling complexes, but it is technically challenging due to the low abundance and/or only temporary interactions of these proteins [33].

Our ChIP assays were performed as described in previous publication Run-on transcription with some modifications [34, 35]. For each ChIP assay, heat shocked or control 10^6 Hela cells were formaldehyde (1% final) fixed for 10 min. (Note that the optimal cross-linking concentration and duration need to be determined empirically with different tissues or cell types, state, and even intensity. Other protocols could rely either on other chemical reagents or UV-mediated physical cross-linking to preserve native nuclear structures for subsequent biochemical and molecular analysis.) After neutralization with 0.125 M glycine, the cell pellets were lyzed in 200 µl *ChIP Lysis Buffer* with protease inhibitors. Samples were sonicated and then diluted into1800 µl ChIP Dilution Buffer. ChIP was carried out with precipitating antibodies either anti-HSF1, or anti-IgG as control from Stressgen (Vancouver, CA, USA) added to precleared chromatin with protein A agarose slurry at 4C overnight. (Note that the optimal concentration of the primary antibody for ChIP must be determined empirically even with different lot of "same name antibody".) Then four sequential washings were performed by adding the washing buffer

1, washing buffer 2, and washing buffer finally elution in 500 μl elution buffer (1% SDS, 0.1 M $NaHCO_3$). To reverse the cross-linking fixation, 20 μl of 5 M NaCl were added and the mixture incubated at 65 °C for 4 h. Afterward, we added 10 μl of Uncross-linking Buffer and incubated at 45 °C for 1 h, and then purified the DNAs. The immunoprecipitated DNA is now analyzed by PCR amplification using appropriate primer pairs for the HSE consensus region and the control region in the hsp70.1 exon. A total of 27–30 cycles of PCR were carried out with 2 μl of eluted DNA and primers to amplify the exon region (from +752 to +878) and the HSE containing region from −334 to −233. The amplified PCR products were analyzed by agarose gel/ethidium bromide. The input was used as positive control and anti-IgG mock ChIP as negative control. Alternatively, the PCR products were quantified by using ABI 7300 real-time PCR system and $2^{-\Delta\Delta Ct}$ method for the fold increase in the ChIP PCR products compared with the control (anti-IgG) was plotted for the respective region of hsp70.1. (Note for some transcription factors, if a specific antibody is unavailable, a tagged construct could be made and transfect the cells and obtain its overexpression in cells.) Then the ChIP assay could be performed by using commercially available antibody, which is against such a tag.

6 Measuring the Contribution of HSF1-HSE Binding to Transcription

6.1 Luciferase Reporter Assays for HSF Activity

To construct an intracellular reporter of HSF activity (pGL.hsp70B), we used 1.44 kB of the human *HSP70B* gene inserted into the pGL.Basic plasmid (*Promega*) (*see* **Note 3**). The *HSP70B* gene is almost entirely silent at physiological temperatures but powerfully activated by heat shock [36]. pGL.hsp70B was constructed by digestion with Bgl*II* and Hind*III* and cloning into pGL.Basic. We have also used the human Hsp27 gene by a similar process, inserting the 730 kB Bgl*II* and Hind*III* digest of a HSP27 promoter fragment into pGL.Basic. For overexpression of HSF1, human HSF1 cDNA [37] is inserted into the pcDNA3.1 (−) expression vector (*Invitrogen*) at the *Xho*I and *Eco*RI sites [38]. Human HSF2A was inserted into the pcDNA3.1(+) vector at the *Xho*I and *Eco*RI sites to produce pHSF2A [39].

To assay HSF1 transcriptional activity in HeLa cells, the cells are maintained in HAM's F-12 (Mediatech) with 10% heat inactivated fetal bovine serum (FBS). HeLa cells (2.5×10^5 cells/well) in 6-well plates are transfected with the pGL.hsp70B or pGL.hsp27 plasmids [40]. pCMV-β-*lacZ* plasmid is co-transfected as an internal control for transfection efficiency. The pHM6 empty vector is used as a blank plasmid to balance the amount of DNA transfected in transient transfection. Luciferase and β-galactosidase activity assays are performed after 24 h of transfection according to the

Promega protocol. Luciferase activity is normalized to β-galactosidase activity. Results are expressed as relative luciferase (relative light units) activity of the appropriate control.

6.2 Nuclear Run on Assay of Rate of Hsp70 Gene Transcription

To determine the HSP70 gene transcriptional rate, the cells are treated according to the experiment and then quenched in ice-cold phosphate-buffered saline, pH 7.4 (PBS) on ice (*see* **Note 4**). Cells are next washed in PBS and lysed in Run-On Lysis Buffer Nuclei that are collected by centrifuge (500 × *g*, 5 min) at 4 °C and resuspended in storage buffer.

To assay rate of transcription, 100 μl of nuclei and 100 μl of Run-on Reaction Buffer are added and the samples incubated for 30 min at 30 °C with shaking. RNA is then extracted from the reaction mix using Trizol (*invitrogen*) according to the manufacturer's protocol.

The hsp70 DNA containing cDNA probe [41] or control β-actin probe are linearized and purified by phenol/chloroform extraction and ethanol precipitation. Probes are then denatured and slot-blotted onto Hybond N+ membrane. (Membranes are first pre-hybridized with UltraHyb solution (*Ambion*) for 2 h at 42 °C, before equivalent counts of newly transcribed RNA (10^6 cpm) are added to the solution). Hybridization is then carried out for 24 h at 42 °C. Membranes are then washed twice for 20 min at 42 °C in a low stringency solution (2× SSC, 0.1% SDS), twice for 20 min in a high stringency solution (1× SSC, 0.1% SDS), and once for 30 min at 37 °C in a low stringency solution containing 10 μg RNase A. Membranes are then rinsed in a low stringency solution and analyzed by incubation with X-ray film. We have successfully used this protocol for the assay of transcription of the mouse *hsp70.1*, c-*fms*, IL-1β, and TNF-α genes [42].

7 Notes

1. *The EMSA technique* has the advantages that it is rapid, sensitive, and straightforward to carry out. For assessing the significance of the transcription factor-response element interaction, it is however lacking in that response elements in chromatin are wound along nucleosomes and may not be available for binding. The EMSA reaction is carried out using naked DNA. In addition, as ChIP on CHIP and ChIP-seq studies begin to accumulate it is evident that response elements for particular factors are more flexible than suspected from early studies [21].
2. Some of these problems can be avoided using the *ChIP assay* that measures HSF binding to chromosomal DNA in vivo. This technique is highly dependent on availability of high affinity and specific antibodies for transcription factors. This can be

overcome by the overexpression of the factor with a seuqence tag and carrying out ChIP with anti-TAG antibody. However, this can introduce potential artifacts involved with protein overexpression [16].

3. To assess the results of HSF-DNA binding we have used two approaches. We have used transfection of *reporter constructs* containing either HSP promoters or HSE coupled to reporter genes CAT or luciferase. The assays have the advantages of being rapid and permitting accumulation of plentiful data. The promoter portion of the construct can be tailored to assess the activity of a single transcription factor such as HSF1. The assay is however indirect and does not measure the transcription of the native, chromosomally embedded gene. There are other potential complications, as reporters require to be translated and yield enzymatically active proteins [22].
4. Transcriptional rate of HSP genes can be assessed directly by run-on assay. This assay indicates joint activities of all the response elements in the *HSP* gene promoters. Although genes such as *HSP70B* respond only to HSF1 or heat shock, others such as *HSP70A* have more complex promoters [42].

Acknowledgments

This work was supported by NIH research grants RO-1CA047407, R01CA119045 and RO-1CA094397.

References

1. Sorger PK, Pelham HRB (1987) Purification and characterization of a heat-shock element binding protein from yeast. EMBO J 6:3035–3041
2. Sorger PK, Nelson HCM (1989) Trimerization of a yeast transcriptional activator via a coiled-coil motif. Cell 59:807–813
3. Sorger PK, Pelham HRB (1988) Yeast heat shock factor is an essential DNA-binding protein that exhibits temperature-dependent phosphorylation. Cell 54:855–864
4. Rabindran SK et al (1993) Regulation of heat shock factor trimer formation: role of a conserved leucine zipper. Science 259:230–234
5. Wu C (1995) Heat shock transcription factors: structure and regulation. Annu Rev Cell Dev Biol 11:441–469
6. He H et al (2003) Elevated expression of heat shock factor (HSF) 2A stimulates HSF1-induced transcription during stress. J Biol Chem 278(37):35465–35475
7. Fujimoto M et al (2009) A novel mouse HSF3 has the potential to activate non-classical heat shock genes during heat shock. Mol Biol Cell 21(1):106–116
8. Tanabe M et al (1998) Disruption of the HSF3 gene results in the severe reduction of heat shock gene expression and loss of thermotolerance. EMBO J 17(6):1750–1758
9. Tanabe M et al (1999) The mammalian HSF4 gene generates both an activator and a repressor of heat shock genes by alternative splicing. J Biol Chem 274(39):27845–27856
10. Kumar M et al (2009) Heat shock factors HsfB1 and HsfB2b are involved in the regulation of Pdf1.2 expression and pathogen resistance in Arabidopsis. Mol Plant 2(1):152–165
11. Scharf KD et al (1990) Three tomato genes code for heat stress transcription factors with a region of remarkable homology to the DNA-binding domain of the yeast HSF. EMBO J 9(13):4495–4501

12. McMillan DR et al (1998) Targeted disruption of heat shock transcription factor 1 abolishes thermotolerance and protection against heat-inducible apoptosis. J Biol Chem 273:7523–7528
13. Morange M (2006) HSFs in development. Handb Exp Pharmacol 172:153–169
14. Abravaya K et al (1992) The human heat shock protein hsp70 interacts with HSF, the transcription factor that regulates heat shock protein expression. Genes Dev 6:1153–1164
15. Zou J et al (1998) Repression of heat shock transcription factor HSF1 activation by HSP90 (HSP90 complex) that forms a stress-sensitive complex with HSF1. Cell 94(4):471–480
16. Bunch H et al (2014) TRIM28 regulates RNA polymerase II promoter-proximal pausing and pause release. Nat Struct Mol Biol 21 (10):876–883
17. Guettouche T et al (2005) Analysis of phosphorylation of human heat shock factor 1 in cells experiencing a stress. BMC Biochem 6 (1):4
18. Shamovsky I et al (2006) RNA-mediated response to heat shock in mammalian cells. Nature 440(7083):556–560
19. Bunch H et al (2015) Transcriptional elongation requires DNA break-induced signalling. Nat Commun 6:10191
20. Mosser DD et al (1997) Role of the human heat shock protein hsp70 in protection against stress-induced apoptosis. Mol Cell Biol 17 (9):5317–5327
21. Price BD, Calderwood SK (1992) Heat-induced transcription from RNA polymerases II and III and HSF binding are co-ordinately regulated by the products of the heat shock genes. J Cell Physiol 153:392–401
22. Zhao M et al (2002) Double-stranded RNA--dependent protein kinase (pkr) is essential for thermotolerance, accumulation of HSP70, and stabilization of ARE-containing HSP70 mRNA during stress. J Biol Chem 277 (46):44539–44547
23. Subjeck JR, Sciandra JJ, Johnson RJ (1982) Heat shock proteins and thermotolerance; a comparison of induction kinetics. Br J Radiol 55(656):579–584
24. Wang X et al (2006) Phosphorylation of HSF1 by MAPK-activated protein kinase 2 on serine 121, inhibits transcriptional activity and promotes HSP90 binding. J Biol Chem 281 (2):782–791
25. Soncin F, Prevelige R, Calderwood SK (1997) Expression and purification of human heat-shock transcription factor 1. Protein Expr Purif 9(1):27–32
26. Schreiber E et al (1989) Rapid detection of octamer binding proteins with "mini-extracts" prepared from a small number of cells. Nucleic Acids Res 17:6419
27. Wu B, Hunt C, Morimoto RI (1985) Structure and expression of the human gene encoding the major heat shock protein HSP70. Mol Cell Biol 5:330–341
28. Bruce JL et al (1999) Activation of heat shock transcription factor 1 to a DNA binding form during the G(1)phase of the cell cycle. Cell Stress Chaperones 4(1):36–45
29. Cahill CM et al (1996) Transcriptional repression of the prointerleukin 1beta gene by heat shock factor 1. J Biol Chem 271 (40):24874–24879
30. Nunes SL, Calderwood SK (1995) Heat shock factor-1 and the heat shock cognate 70 protein associate in high molecular weight complexes in the cytoplasm of NIH-3T3 cells. Biochem Biophys Res Commun 213(1):1–6
31. Westwood T, Wu C (1993) Activation of drosophila heat shock factor: conformational changes associated with monomer-to-trimer transition. Mol Cell Biol 13:3481–3486
32. Xie Y et al (2003) Heat shock factor 1 contains two functional domains that mediate transcriptional repression of the c-fos and c-fms genes. J Biol Chem 278(7):4687–4698
33. Solomon MJ, Varshavsky A (1985) Formaldehyde-mediated DNA-protein cross-linking: a probe for in vivo chromatin structures. Proc Natl Acad Sci U S A 82 (19):6470–6474
34. Takacs-Vellai K et al (2007) Transcriptional control of Notch signaling by a HOX and a PBX/EXD protein during vulval development in C. elegans. Dev Biol 302(2):661–669
35. Khaleque MA et al (2008) Heat shock factor 1 represses estrogen-dependent transcription through association with MTA1. Oncogene 27(13):1886–1893
36. Tang D et al (2005) Expression of heat shock proteins and heat shock protein messenger ribonucleic acid in human prostate carcinoma in vitro and in tumors in vivo. Cell Stress Chaperones 10(1):46–58
37. Rabindran SK et al (1991) Molecular cloning and expression of a human heat shock factor, HSF1. Proc Natl Acad Sci U S A 88:6906–6910
38. Oesterreich S et al (1996) Basal regulatory promoter elements in the hsp27 gene in

human breast carcinoma cells. Biochem Biophys Res Commun 222:155–163

39. Chen C et al (1997) Heat shock factor 1 represses Ras-induced transcriptional activation of the c-fos gene. J Biol Chem 272 (43):26803–26806
40. Wang XZ, Asea A, Xie Y, Kabingu E, Stevenson MA, Calderwood SK (2000) RSK2 represses HSF1 activation during heat shock. Cell Stress Chaperones 5:432–437
41. Hunt C, Calderwood SK (1990) Characterization and sequence of a mouse HSP70 gene and its expression in mouse cell lines. Gene 87:199–204
42. Xie Y et al (2002) Heat shock factor 1 represses transcription of the IL-1beta gene through physical interaction with the nuclear factor of interleukin 6. J Biol Chem 277 (14):11802–11810

Chapter 3

Monitoring of the Heat Shock Response with a Real-Time Luciferase Reporter

Toshiki Kijima, Takanori Eguchi, Len Neckers, and Thomas L. Prince

Abstract

The heat shock response (HSR) is a cellular mechanism for counteracting acute proteotoxic stress. In eukaryotes, transcriptional activation of the HSR is regulated by heat shock factor 1 (HSF1). Activation of HSF1 induces the expression of heat shock proteins (HSPs) that function as molecular chaperones to fold and maintain the three-dimensional structure of misfolded proteins. The regulation of the degree and duration of the HSR is controlled by multiple biochemical mechanisms that include posttranslational modification of HSF1 and numerous protein-protein interactions. In this chapter, we describe a method to evaluate the activation and deactivation of the HSR at the transcriptional level using a short half-life luciferase reporter assay. This assay can be used to further characterize the HSR or as a screen for small-molecule inducers, amplifiers, or repressors.

Key words Heat shock response, Heat shock factor 1 (HSF1), Heat shock protein 90 (HSP90), Luciferase assay, Real-time, Drug screen

1 Introduction

The heat shock response (HSR) is an evolutionarily conserved cytoprotective mechanism for maintaining proteostasis. Heat shock factor 1 (HSF1) is the master transcription factor responsible for initiating the HSR and inducing the expression of a variety of genes, most notably heat shock proteins (HSPs) [1, 2]. Through a mechanism not completely understood, proteotoxic stress activates HSF1 to homotrimerize, translocate from the cytosol into the nucleus, and bind heat shock elements (HSE) within the promoters of its target genes. This induces paused RNA polymerase II to resume transcription elongation resulting in the rapid production of HSP mRNA transcripts [3, 4]. Once the stress has abated and proteostasis restored, HSF1 is dissembled and translocated back into the cytosol. Throughout this process, HSF1 is heavily post-translationally modified and interacts with numerous cellular components, such as newly expressed HSPs [5–7]. These modifications

Stuart K. Calderwood and Thomas L. Prince (eds.), *Chaperones: Methods and Protocols*, Methods in Molecular Biology, vol. 1709, https://doi.org/10.1007/978-1-4939-7477-1_3,

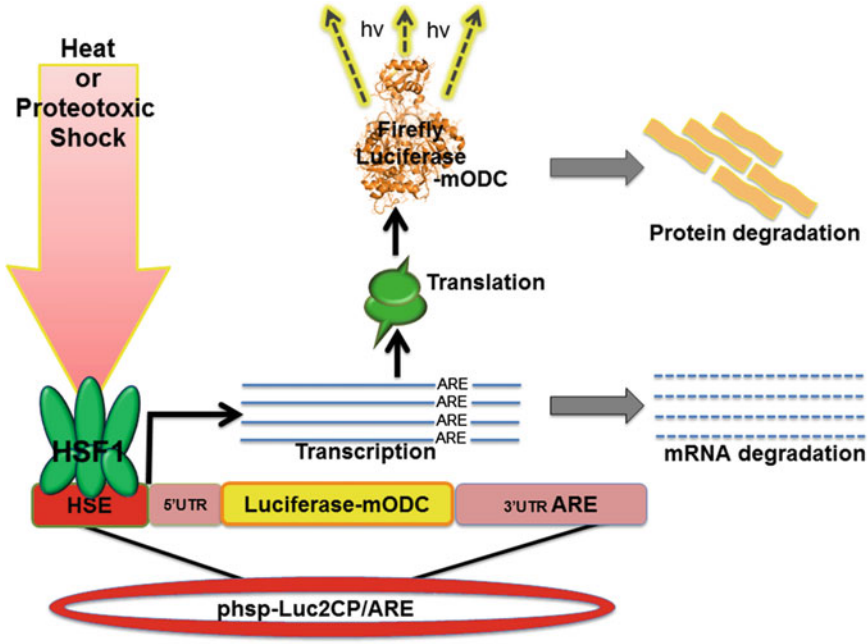

Fig. 1 Cartoon of real-time detection of induction of the HSR using destabilized luciferase reporter

and interactions affect the degree and duration of the HSR that is often amplified in cancer and reduced in neurodegenerative diseases [8, 9]. Understanding how to effectively modulate the HSR through small-molecule therapies and lifestyle has the potential to positively influence disease outcomes and improve overall health.

Being able to monitor real-time expression of *HSP* gene products is essential for determining the degree and duration of the HSR. Previous versions of luciferase reporter assays are useful for measuring the induction and degree of the HSR but not effective at determining the attenuation of transcription and the actual duration of the response. Here, we describe the use of a destabilized luciferase reporter assay driven by the heat inducible *HSP70B* gene promoter for real-time monitoring of the HSR in mammalian cell culture (Fig. 1). The *HSP70B* gene (*HSPA7* locus) is one of the most strongly expressed human transcripts induced by proteotoxic stress, despite not encoding a functional protein product [10]. The reporter assay is based on a plasmid encoding an *HSP70B* promoter-driven firefly luciferase transcript linked to an RNA decay element and a protein-destabilizing domain. An AU-rich element (ARE) in the 3′ untranslated region (UTR) induces rapid decay of the mRNA transcript, while a mouse ornithine decarboxylase (mODC) PEST domain linked to the C-terminus of the luciferase peptide results in prompt ubiquitination and degradation (Fig. 1). These features promote rapid turnover of the luciferase within the cell and thereby provide a real-time readout of HSR

transcription. With this assay, screens for the effects of small-molecule drugs or transiently expressed HSPs and HSF1 mutants on the HSR can readily be developed. The method described here is modified from the assay developed by Younnis et al. [11].

Our method essentially involves the transfection of plasmids into cells, treating with drugs (optional), heat shock and then allowing the cells to recover for specific periods of time before harvesting and assaying for luciferase activity. Differences in luciferase activity at each time point will reflect the intensity and stage of the HSR. In Human embryonic kidney (HEK) 293 cells transcription of the *HSP70B* promoter typically attenuates after 2 h when heat shocked for 30 min at 42 °C, however, in other cell lines these times may vary. Treating the cells with drugs before, during, or after the heat shock may alter the HSR by shortening, extending, and/or amplifying it. Some drugs such as proteasome inhibitors may also induce the HSR [12]. Furthermore, transiently overexpressing other protein components such as HSF1 mutants or HSPs can alter the HSR and provide a mechanism for evaluating the effects of genetic alterations or posttranslational modifications.

2 Materials

All the solutions should be prepared with double-deionized water. Chemicals should be molecular biology grade or above. Follow your institutions' waste disposal guidelines when discarding used reagents.

2.1 Cell Culture and Transfection

1. HEK293 cells.
2. Dulbecco's modified Eagle medium (DMEM), serum free for transfecting and supplemented with 10% fetal calf serum (FCS), and 100 U/mL penicillin-streptomycin (optional) for growing cells.
3. X-tremeGENE 9 DNA Transfection Reagent (Roche).

2.2 Plastic Ware

1. 96-Well clear cell culture plates.
2. 96-Well white assay plates.
3. Parafilm.

2.3 Plasmids

1. Standard positive control luciferase, pGL3-CMV-Luc (Promega).
2. Transfection normalization β-Galactosidase control, pGL3-CMV-βGal (Promega).
3. *HSP70B*-promoter luciferase reporter plasmid, pHsp70b-Luc, was made for an earlier project [13].

4. Short half-life luciferase expression plasmid, pCMV-Luc2CP/ARE, with two protein-destabilizing sequences (2CP) at the C-terminus of a luciferase protein along with a 3′UTR AU-rich element (ARE) for rapid mRNA turnover was made and deposited into Addgene (#62857) by Dr. Gideon Dreyfuss [11].
5. The heat shock inducible reporter plasmid, pHsp70b-Luc2CP/ARE, was constructed by substituting the CMV promoter sequence in pCMV-Luc2CP/ARE with the *HSP70B* gene promoter sequence by Gibson assembly [14].

2.4 Buffers and Reagents

1. Reporter lysis buffer (RLB): 25 mM Bicine (pH 7.6), 0.05% Tween20, 0.05% Tween80. Store at 4 °C.
2. Luciferase assay reagent (LAR): 25 mM Glycine, 15 mM KPO_4, 15 mM $MgSO_4$, 4 mM EGTA, 2 mM ATP, 1 mM DTT, 1.7 mM K-Luciferin. Aliquot and store at −20 °C.
3. β-Galactosidase assay reagent (BAR): 200 mM $NaPO_4$ (pH 7.3), 2 mM $MgCl_2$, 100 mM β-mercaptoethanol, 1.33 mg/mL o-nitrophenyl-β-D-galactopyranoside (ONPG). Aliquot and store at −20 °C.
4. β-Galactosidase stop (BGS): 1 M Na_2CO_3. Store at 4 °C.
5. 17-AAG: 1 mM stock dissolved in DMSO. Aliquot and store at −20 °C.

2.5 Equipment

1. Set of single and multichannel pipettes.
2. Cell culture incubator (37 °C, 5% CO_2).
3. Laboratory water bath (42 °C).
4. 96-Well plate reader with luminometer and UV-Vis absorbance.
5. −20 °C and/or −80 °C freezers.

3 Methods

Care should be taken when working with any biological material. The plasmids and cell lines used in this method are not known to be infectious; however, proper personal protection equipment should be worn. All cell lysate, media, and chemicals should be treated and disposed of per the institution guidelines. Prepare all the reagents in a sterile environment such as a cell culture hood.

3.1 Cell Plating

A separate 96-well plate is needed for each time point in the experiment. For studying the HSR with this assay, five time points suffices: Control No HS, 1 h post HS, 2 h post HS, 4 h post HS, 6 h post HS. This allows the experiment to be done in a single workday; however for most experiments more time points are better.

The density at which the cells are plated may influence transfection levels and overall HSR reporter signal. Moreover, each cell line divides at a different rate. Varying the cell plating density to optimize the HSR signal may be a worthwhile preliminary experiment. As a general rule, plating HEK293 cells at 30–40% confluency the night before transfecting works well.

1. Aliquot 12,000 cells in 100 μL of supplemented DMEM per well into each 96-well plate.
2. Incubated overnight this gives a confluency of 50–80% the next day at the time of transfection (*see* **Note 1**).

3.2 Transfection

Transfect the cells with a mixture of the following: 0.05 μg of DNA + 0.15 μL of X-tremeGENE + 20 μL of serum-free DMEM for each well (*see* **Note 2**). The 0.05 μg of DNA includes all the plasmids to be transfected. Adjusting all the plasmids to the same concentration is rather helpful. The ratio of each plasmid can be varied to optimize the assay. Typically, less pCMV-βGal is required compared to other plasmids in the experiment. The ratio of phsp70b-Luc2CP/ARE and effector HSF1 or HSP plasmid can be varied to test for mutation or regulatory effects. It is advised to repeat each condition as many times as possible but avoid the perimeter (*see* **Note 3**). Setting up a spreadsheet to calculate plasmid and reagent amounts is advised (Fig. 2a). Plasmids to be used: pCMV-βGal (transfection normalization control), pCMV-LUC (positive luciferase control), phsp70B-Luc (stable HSR control), phsp70b-Luc2CP/ARE (experimental, real-time reporter), and optional pcDNA3-HSF1 or -HSP (effector constructs).

1. Aliquot and mix X-tremeGENE, serum-free DMEM, and plasmids in a separate sterile 96-well plate with each well corresponding to a different sample condition.
2. Using a multichannel pipette distribute the ~20 μL of transfection mix into each well on the 96-well plates containing the cultured cells.
3. Incubate the cells and transfection mix for 16–24 h.

3.3 Drug Treatment (Optional)

To test the effects of drugs on the HSR, the transfected cells can be treated with small-molecule inhibitors for 1 h before heat shocking. Treatment time can be varied but at least 45 min is needed to allow the drugs to accumulate in the cells. The number of plates and wells per plate to be treated will determine the amount of drugs to be pre-diluted in DMEM and aliquoted. Here, we use the HSP90 N-terminal inhibitor 17-AAG as an example.

1. For 17-AAG at a final concentration of ~1 μM in 16 wells (two columns of eight) across five plates, a total of 12 μL of 1 mM

A

Experiment:	Effect of HSP90 Inhibitors on the HSR							Date:	TODAY	
Cell line:	HEK293									
Conditions:	12									
Time points	5									
Repeats:	8									
Wells/condition:	40			Condition	Plasmid 1	Plasmid 2	1 (uL)	2 (uL)	Drug	[Final]
Plasmids:	2			1	CMV-βGal	CMV-Luc	3.73	7.47	DMSO	na
[DNA] µg/µL:	0.25			2	CMV-βGal	hsp70b-Luc	3.73	7.47	DMSO	na
				3	CMV-βGal	hsp70b-Luc2CP/ARE	3.73	7.47	DMSO	na
	/well	/sample	Total	4	CMV-βGal	hsp70b-Luc2CP/ARE	3.73	7.47	17-AAG	1 µM
DNA (µg):	0.07	2.8		5	CMV-βGal	hsp70b-Luc2CP/ARE	3.73	7.47	STA-9090	1 µM
X-tremeGene (µL):	0.21	9.24	111	6	CMV-βGal	hsp70b-Luc2CP/ARE	3.73	7.47	KU32	10 µM
media (µL):	20	880	10560	7	CMV-βGal	hsp70b-Luc2CP/ARE	3.73	7.47	SNX2112	1 µM
				8	CMV-βGal	hsp70b-Luc2CP/ARE	3.73	7.47	DMSO	na
Total DNA (µL):	11.2			9	CMV-βGal	hsp70b-Luc2CP/ARE	3.73	7.47	17-AAG	1 µM
Plasmid 1 (µL):	3.73	1/3		10	CMV-βGal	hsp70b-Luc	3.73	7.47	17-AAG	1 µM
Plasmid 2 (µL):	7.47	2/3		11	CMV-βGal	CMV-Luc	3.73	7.47	DMSO	1 µM
				12	CMV-βGal	CMV-Luc	3.73	7.47	DMSO	na
							44.8			

B

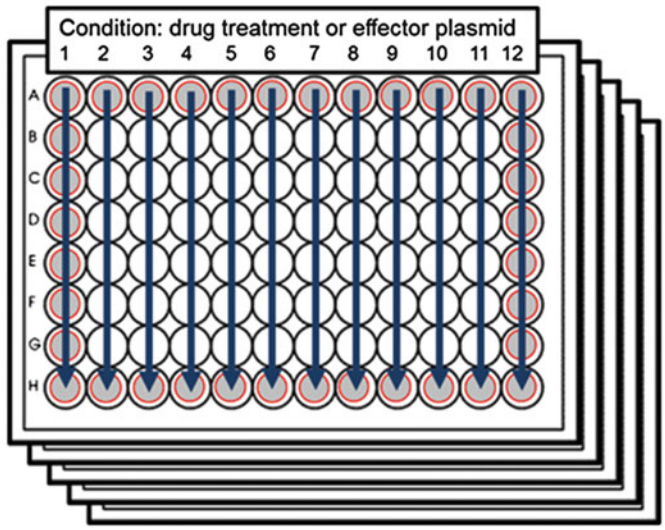

Fig. 2 Preparation of 96-well plates for transfection and drug treatment. (**a**) Sample spreadsheet for aliquoting reagents and arranging conditions. (**b**) Schematic for 12 drug treatment conditions across five time points. *Gray circles* indicate perimeter wells that should not typically be used for experimental testing

stock 17-AAG dissolved in DMSO should be added to 1700 µL of DMEM.

2. Once mixed, 20 µL of pre-diluted 17-AAG is added to each well.
3. DMSO is used as the vehicle control (Fig. 2a and b).

3.4 Heat Shock

There are few different ways to heat shock cells depending on available equipment (*see* **Note 4**):

1. Wrap each plate tightly with Parafilm.
2. Float each plate in a water bath heated to 42 °C for 30 min.

3. If using a common lab water bath, before unwrapping and placing back into the 37 °C incubator, each plate must be thoroughly sprayed and wiped with a 70% Ethanol and then dried to prevent contaminating cell culture incubator.

Or

1. Preheat a separate incubator to 43 °C.
2. Place the plates in the incubator for 45–60 min to induce a robust heat shock.
3. Place the cells back into the 37 °C incubator to recover.

3.5 Cell Lysis and Sample Storage

To harvest the cells at each time point:

1. Remove the plate from the incubator and aspirate off all media but be careful not to dislodge the cells from the plate.
2. Add 110 μL of RLB to each well and place in a freezer for at least 45 min. Samples can also be stored until the time course is complete. For longer term storage samples should be placed in an −80 °C freezer.
3. A single freeze-thaw cycle should efficiently lyse the cells.

3.6 Luciferase Assay

To determine the level of induced gene expression:

1. Allow all the plates to completely thaw on ice.
2. Once thawed, the plates can be spun down on a large bench top centrifuge at 4 °C to aggregate cell debris and ensure uniform lysis (optional).
3. Thaw both LAR and BAR making sure both the reagents are warm and completely dissolved.
4. Turn on the plate reader luminometer and load proper program for analysis.
5. When ready use a multichannel pipette to transfer 50 μL of lysate from each well to the corresponding well in a clean white 96-well plate.
6. Add 50 μL of LAR to each well. Let the plate set for 10 min at room temperature.
7. Read the plate on the luminometer and record the results.
8. Repeat the process of aliquoting the lysate, adding the LAR, allowing to set for 10 min, and reading the luciferase activity for each plate in the time course.
9. Due to changes in luciferase activity overtime, make sure the timing between adding the LAR and reading luciferase activity is consistent for each plate. This will ensure consistent and accurate readings of HSR induction at each time point (*see* **Note 5**).

3.7 β-Galactosidase Assay

To determine the transfection efficiency for each well:

1. For each plate pipette 50 μL of lysate from each well into a corresponding well in a clear 96-well plate. Do this for all the plates in the time course.
2. Add 35 μL of BAR to each well and incubate all the plates at 37 °C for 20 min or until the lysate mix turns yellow.
3. Add 50 μL of BGS to all the wells to terminate the enzyme reaction. This will ensure that the β-galactosidase reaction time is the same across all the plates.
4. Read each plate for absorbance at 420 nM and record the results (*see* **Note 6**).

3.8 Normalization and Statistics

To determine the luciferase activity relative to the amount of plasmid transfected into the cells:

1. Divide the luciferase readout value by the β-galactosidase value using a spreadsheet program.
2. Identify the baseline reporter signal, in this case, the Control No HS plate and no drugs sample set and then calculate the average.
3. Divide all the other wells in all other plates by this control value. This makes all reporter readout signals relative to the average of the baseline signal.
4. For each sample condition set of repeats determine the average and standard deviation.
5. Sample values can finally be graphed +/− standard deviation at each time point and *p*-values calculated using Student's *t*-tests between each time point and/or condition (Fig. 3).
6. If utilizing the assay as a high-throughput screen a *Z*-factor score can be calculated for a specific time point where a value greater than 0.5 indicates significance [15].

3.9 Results

Differences in HSR transcription rates were observed between DMSO and 17-AAG pretreatments in HEK293 cells. For DMSO control cells the HSR increased over time with a maximum at 120 min and then decreased to baseline at 360 min. For 17-AAG pretreated cells the HSR increased over time with a maximum around 240 min and remained above baseline at 360 min indicating that HSP90 N-terminal inhibition increased the degree and duration of the HSR. At 240 min the difference between DMSO and 17-AAG-treated cells gave a *Z*-factor of 0.65, suggesting that 17-AAG warrants further attention as an amplifier of the HSR. Results for only DMSO and 17-AAG treatment are shown (Fig. 3). Despite the reliance of firefly luciferase on HSP90 chaperone function as described by Dr. Robert Matts and colleagues

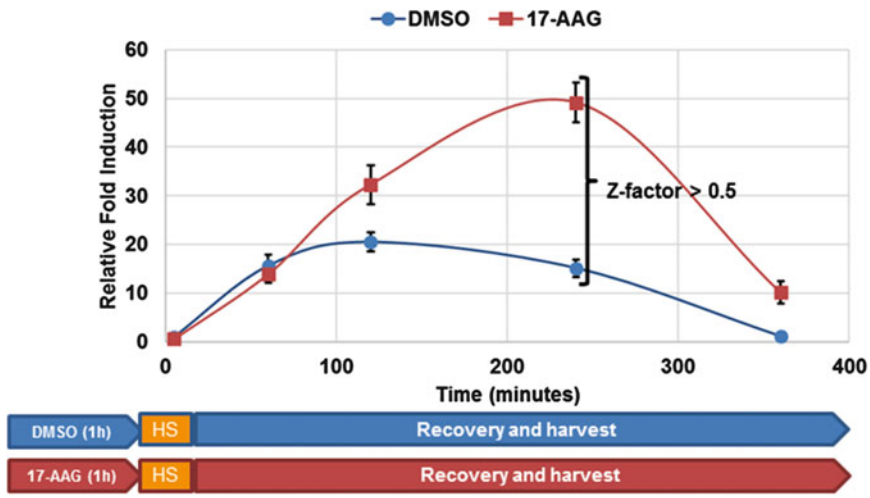

Fig. 3 Effect of 17-AAG pretreatment on HSR degree and duration. Cells were incubated with DMSO or 1 μM 17-AAG for 1 h and then heat shocked for 30 min at 42 °C, allowed to recover and then harvested at designated time points

(Chapter 7, [16]), the newly synthesized luciferase enzymes within whole cells were still able to produce a strong signal as compared to denatured luciferase in cell-free rabbit reticulocyte lysate (*see* **Note 7**).

4 Notes

1. Transfection and Luciferase/β-galactosidase assays work well in 96-well plate with HEK293 cells. For cell lines with low transfection efficiency scale up to 12- or 24-well plates to increase cell numbers.
2. We have used X-tremeGENE 9 and Lipofectamine 3000 as transfection reagents with equal success.
3. Due to exposure and evaporation issues, use the wells on the perimeter of the plate as control repeats and not for experimental testing.
4. Each cell line is different in regards to inducing the HSR, some cell lines may require higher temperatures for longer periods of time. Preliminary testing may be required using the 2-h post-HS time point.
5. It is essential that all the plates are assayed and read in the same manner and timing after the addition of LAR. This is to ensure that the substrate concentration and luciferase activity are the same for each time point. The pre-read incubation time can be adjusted to 5 min and staggered depending on setup.

6. In HEK293 cells, 10–20 min incubation is long enough for the β-Galactosidase assay before adding BGS. Do not incubate the plates too long at 37 °C as the reaction can be saturated. For a time-course assay with multiple plates, it is extremely important to measure β-galactosidase activity of each plate with the same incubation time.
7. Since firefly luciferase depends on HSP90 for folding, inhibitors such as 17-AAG may be predicted to reduce the luciferase activity in our real-time cell reporter assay. However, in whole cell models the drug concentration throughout cells will vary due to efflux pumps transporting 17-AAG out of the cells. The induction of the HSR also increases the number of HSP90 peptides available to chaperone newly synthesizing luciferase. Moreover, only a fraction of the population of HSP90 within the cell may bind 17-AAG possibly due to alterations in the posttranslational modification state of HSP90 [17]. This contrasts with the robust assay developed by Dr. Robert Matts where the drug concentration and perhaps HSP90 population is uniform throughout the rabbit reticulocyte cell lysate and the denatured luciferase must be refolded as a complete peptide.

Acknowledgments

This work was supported by the Mowad Endowment for New Discoveries at Geisinger Health Systems, the JSPS Research Fellowship for Japanese Biomedical and Behavioral Research at NIH, and the Intramural Research Program at the National Cancer Institute.

References

1. Vihervaara A, Sistonen L (2014) HSF1 at a glance. J Cell Sci 127(Pt 2):261–266
2. Dayalan Naidu S, Dinkova-Kostova AT (2017) Regulation of the mammalian heat shock factor 1. FEBS J 284(11):1606–1627
3. Brown SA, Kingston RE (1997) Disruption of downstream chromatin directed by a transcriptional activator. Genes Dev 11(23):3116–3121
4. Bunch H et al (2014) TRIM28 regulates RNA polymerase II promoter-proximal pausing and pause release. Nat Struct Mol Biol 21 (10):876–883
5. Zou J, Guo Y, Guettouche T, Smith DF, Voellmy R (1998) Repression of heat shock transcription factor HSF1 activation by HSP90 (HSP90 complex) that forms a stress-sensitive complex with HSF1. Cell 94 (4):471–480
6. Guettouche T, Boellmann F, Lane WS, Voellmy R (2005) Analysis of phosphorylation of human heat shock factor 1 in cells experiencing a stress. BMC Biochem 6:4
7. Xu YM, Huang DY, Chiu JF, Lau AT (2012) Post-translational modification of human heat shock factors and their functions: a recent update by proteomic approach. J Proteome Res 11(5):2625–2634
8. Mendillo ML et al (2012) HSF1 drives a transcriptional program distinct from heat shock to support highly malignant human cancers. Cell 150(3):549–562
9. Calderwood SK, Murshid A, Prince T (2009) The shock of aging: molecular chaperones and the heat shock response in longevity and aging—a mini-review. Gerontology 55 (5):550–558

10. Parsian AJ et al (2000) The human Hsp70B gene at the HSPA7 locus of chromosome 1 is transcribed but non-functional. Biochim Biophys Acta 1494(1–2):201–205
11. Younis I et al (2010) Rapid-response splicing reporter screens identify differential regulators of constitutive and alternative splicing. Mol Cell Biol 30(7):1718–1728
12. Kim D, Kim SH, Li GC (1999) Proteasome inhibitors MG132 and lactacystin hyperphosphorylate HSF1 and induce hsp70 and hsp27 expression. Biochem Biophys Res Commun 254(1):264–268
13. Murshid A et al (2010) Protein kinase A binds and activates heat shock factor 1. PLoS One 5 (11):e13830
14. Gibson DG et al (2009) Enzymatic assembly of DNA molecules up to several hundred kilobases. Nat Methods 6(5):343–345
15. Zhang JH, Chung TD, Oldenburg KR (1999) A simple statistical parameter for use in evaluation and validation of high throughput screening assays. J Biomol Screen 4(2):67–73
16. Galam L et al (2007) High-throughput assay for the identification of Hsp90 inhibitors based on Hsp90-dependent refolding of firefly luciferase. Bioorg Med Chem 15(5):1939–1946
17. Beebe K et al (2013) Posttranslational modification and conformational state of heat shock protein 90 differentially affect binding of chemically diverse small molecule inhibitors. Oncotarget 4(7):1065–1074

Chapter 4

Quantitative Profiling of Chaperone/Client Interactions with LUMIER Assay

Mikko Taipale

Abstract

Chaperones associate with hundreds or thousands of diverse client proteins and regulate their function. Chaperone/client interactions are generally very transient and involve a highly orchestrated assembly and disassembly of regulatory co-factors. This poses specific challenges for identifying and characterizing these interactions in a scalable and sensitive manner. LUMIER assay, which takes advantage of the high sensitivity and linear range of luminescence-based detection, has proven to be an ideal assay to quantitatively profile chaperone/client interactions in a high-throughput manner. This article provides step-by-step instructions for quantitatively profiling these interactions with LUMIER.

Key words Protein/protein interactions, Proteomics, LUMIER, Chaperone/client interactions, Chaperones, Protein homeostasis

1 Introduction

Anyone interested in finding novel interaction partners to their favorite protein can today look into the ever-expanding toolbox of protein/protein interaction (PPI) assays and pick the right tool for the job [1]. However, while appreciating the diversity of the options, it is important to keep in mind that every assay has its own quirks. Selecting the right assay is particularly important for some types of proteins and interactions. For example, transient interactions are difficult to capture with many methods, as are those between membrane proteins or within large multiprotein complexes. Hsp90/client protein interactions—and chaperone/client interactions more generally—are among such tricky interactions. First, Hsp90/client interactions are typically very transient and not well captured by, e.g., yeast two-hybrid assays. Second, most client proteins are unstable and their chaperone interactions require the presence of a large but often poorly defined cohort of

Stuart K. Calderwood and Thomas L. Prince (eds.), *Chaperones: Methods and Protocols*, Methods in Molecular Biology, vol. 1709, https://doi.org/10.1007/978-1-4939-7477-1_4,

co-chaperones, making, e.g., in vitro binding assays challenging. Third, at any given moment the cellular Hsp90 pool is engaged in hundreds of different interactions, and thus detecting a single, low-abundance client protein among these by, e.g., Hsp90 affinity purification and mass spectrometry is difficult due to low signal-to-noise ratio.

To address these challenges, we have used LUMIER assays to quantitatively characterize interactions between Hsp90 and its co-chaperones and clients. Originally developed by the Wrana lab [2], LUMIER takes advantage of the exceptional sensitivity and linear range of luciferases. In the assay, the bait protein is tagged with an epitope tag like FLAG and the prey protein is fused to *Renilla reniformis* luciferase. After co-expression of both bait and prey proteins, the bait protein is immunoprecipitated with an antibody against the bait protein (e.g., anti-FLAG). If the two proteins interact, it can be detected as luminescence. Although the amount of luminescence does not directly reflect fundamental biophysical parameters of the interaction, it does give an idea about the strength or robustness of the interaction and allows investigators to survey PPIs in a more quantitative manner compared to, e.g., yeast two-hybrid assays.

The original LUMIER assay is based on co-transfection of bait and prey protein constructs followed by immunoprecipitation with anti-FLAG-coated beads. While this approach is relatively straightforward and certainly sufficient to detect interactions for most purposes (*see* **Note 1**), we introduced several modifications to the original LUMIER assay to make it more quantitative and increase its throughput [3–5]. Most notably, LUMIER with BACON (bait control) uses stable cell lines expressing the luciferase-fused prey protein and adds an additional step to measure the amount of the FLAG tagged bait protein with ELISA (Fig. 1). Using a stable cell line expressing the prey protein significantly reduces well-to-well variation arising from variable co-transfection efficiency, while accounting for bait protein abundance can provide a more quantitative readout for the strength or the robustness of the interaction. There are also other variants of the original LUMIER assay, such as DLR-PD [6] and DULIP [7]. In these variants, prey and bait proteins are fused to different luciferases (Renilla or Firefly luciferase), facilitating the quantitation of both proteins with a dual luciferase assay. Although these variants have not been tested with chaperone/client interactions, it is likely that they also work well.

Finally, it is important to bear in mind that there is no such thing as the best PPI assay, as each assay has its characteristic advantages and disadvantages that need to be carefully considered [8]. Thus, it is always recommended to validate interactions identified with one method with an orthogonal approach.

The advantages and disadvantages of the LUMIER assay include the following:

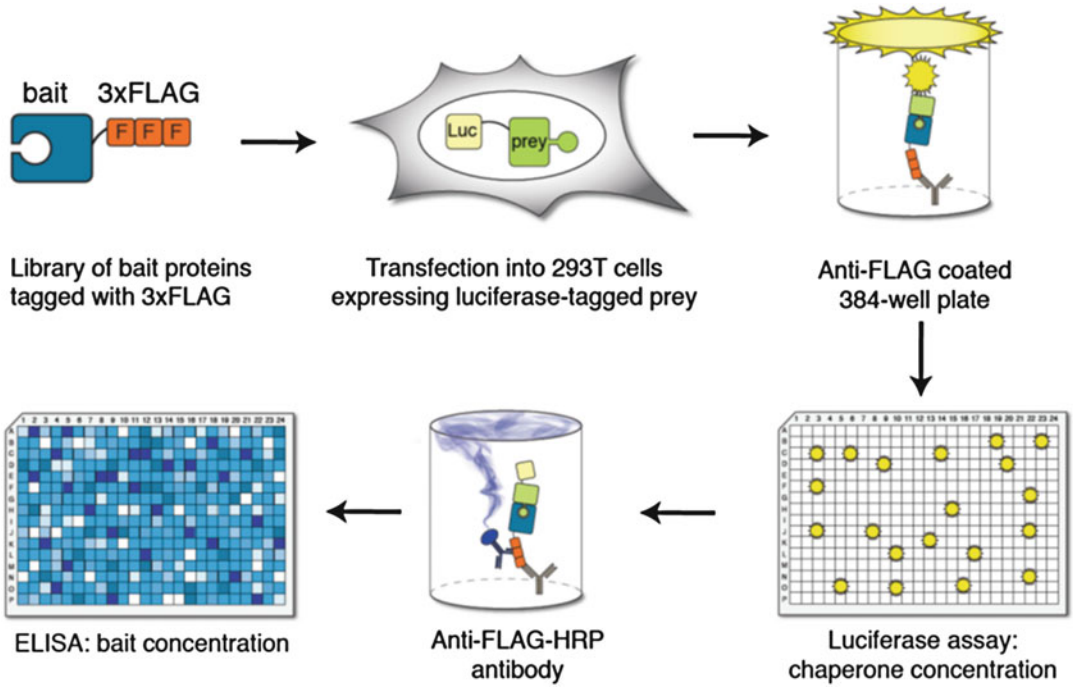

Fig. 1 Principle of the LUMIER assay. 3xFLAG tagged bait proteins are transfected in 96-well format into 293T cells expressing the prey (chaperone) protein fused to Renilla luciferase. Two days after transfection, lysates are incubated on 384- or 96-well plates coated with anti-FLAG antibody, which captures the bait protein. The interaction of the bait protein with the prey can be detected as luminescence. In the second step, ELISA with anti-FLAG antibody conjugated to horseradish peroxidase is used to measure the amount of bait protein in the well

1.1 Advantages

Proteins are expressed in their native physiological context.

Quantitative readout facilitates robust comparison of interaction profiles.

Quantitative readout for every tested protein pair enables adjustment of cutoff values, depending on, e.g., tolerance for false positives.

High throughput: laboratory automation enables assaying thousands of pairwise interactions/day.

The assay is compatible with drug treatments, growth factor treatments, etc.

The assay can be used to measure EC50 values of compounds, growth factors, etc. on protein/protein interactions.

1.2 Disadvantages

Overexpression of proteins can lead to artificial interactions due to mass action.

It requires cell lysis with detergents, which can lead to loss of weak interactions and membrane protein interactions.

Introducing epitope tags or folded domains to proteins can disrupt their function or native interactions.

It is not possible to distinguish between direct and indirect interactions.

Laboratory automation may not be available in many laboratories.

2 Materials

1. Expression plasmids for bait (client) proteins tagged with 3xFLAG (backbone vectors available from Addgene) (*see* **Note 2**).
2. Lentiviral plasmid expressing prey protein (chaperone) fused to Renilla luciferase or another luciferase (backbone vectors available from Addgene) (*see* **Note 3**).
3. Second generation lentiviral packaging plasmid psPAX2 (Addgene #12260).
4. Viral envelope plasmid pCMV-VSV-G (Addgene #8454).
5. HEK293T cells.
6. Polyethylenimine "MAX" (Polysciences) (*see* **Note 4**).
7. Polybrene (hexadimethrine bromide).
8. 3 ml syringes.
9. 0.45 μm syringe filters.
10. Lumitrac 600 white high-binding 384-well microplates *or* Lumitrac 600 white high-binding 96-well microplates (Greiner Bio-One).
11. 96-Well flat-bottom tissue culture plates (e.g., Corning).
12. Saerstedt 96-well V-bottom plates (Saerstedt).
13. Coelenterazine-h (Goldbio) (*see* **Note 5**).
14. Mouse anti-FLAG M2 antibody (Sigma).
15. Mouse anti-FLAG M2 antibody, HRP conjugate (Sigma).
16. SuperSignal ELISA Pico Chemiluminescent Substrate, 250 ml (Thermo Fisher).
17. Goat serum (Thermo Fisher).
18. OptiMEM serum reduced media (Invitrogen).
19. Polybrene stock solution: Dissolve 100 mg polybrene into 10 ml sterile water and filter sterilize. Store in 1 ml aliquots at −20 °C.
20. Polyethylenimine transfection reagent: 1 mg/ml polyethylenimine. Dissolve 100 mg polyethylenimine "MAX" into 100 ml water. Filter sterilize. The stock solution can be stored at 4 °C for months and at −20 °C for years (*see* **Note 6**).

21. HENG buffer for cell lysis and washes: 20 mM Hepes-KOH pH 7.9, 150 mM NaCl, 2 mM EDTA pH 8.0, 20 mM sodium molybdate, 0.5% Triton X-100, 5% glycerol. Add protease inhibitors aprotinin, leupeptin, pepstatin (1 μg/ml each), and 0.2 mM PMSF to cell lysis buffer before use (*see* **Note 7**). Protease inhibitors are not required at subsequent wash steps.
22. Blocking buffer: 1xPBS, 1% BSA, 5% sucrose, 0.5% Tween 20.
23. ELISA wash buffer (PBST): 1xPBS, 0.01% Tween 20.
24. Coelenterazine stock solution: 1 mM coelenterazine-h in acidified methanol (200 μl 3 N HCl in 10 ml methanol). Stock solution should be stored at −80 °C, preferably under nitrogen.
25. Luciferase assay buffer: 20 mM Tris–HCl pH 7.5, 1 mM EDTA, 150 mM KCl, 0.5% Tergitol NP9. Dilute coelenterazine stock solution 1:200 (final coelenterazine-h concentration 5 μM) into assay buffer 10 min before use.
26. ELISA buffer: 1xPBS, 1% Tween 20, 1% goat serum.
27. Plate washer.
28. Plate reader.
29. Liquid handling robot with a 96-well arm.
30. Reagent dispenser.

3 Methods

Here, a polyclonal stable cell line is generated by viral transduction. Please check with your local biosafety office for the requirements for working with lentiviral constructs, as they often require higher biosafety levels such as BL2+/CL2+.

3.1 Viral Packaging

1. Seed fresh 293T cells to 12-well plates so that they are ~90% confluent on the day of transfection (this corresponds to ~300,000 cells/well the day before transfection).
2. Mix 500 ng lentiviral prey protein/Renilla luciferase fusion construct, 375 ng psPAX2, and 125 ng pVSV-G in a sterile Eppendorf tube and add 50 μl Opti-MEM. Mix well.
3. Mix 3 μl polyethylenimine (PEI) solution with 50 μl Opti-MEM in another Eppendorf tube.
4. Incubate both tubes for 5 min at room temperature.
5. Add the PEI/Opti-MEM mix to DNA/Opti-MEM, mix well, and incubate for 20 min at room temperature.
6. Add the transfection mix to 293T cells.

7. After overnight incubation, replace the medium with 1 ml fresh cell culture medium.
8. Two days after transfection, collect the supernatant with a 3 ml syringe and filter it through a 0.45 μm filter. This is the filtered viral supernatant that can be used immediately or frozen at −80°C.

3.2 Establishing Stable Cell Lines

1. Seed fresh 293T cells on a 6-well plate so that they are ~30–50% confluent on the day of infection (this corresponds to ~300,000 cells/well the day before infection).
2. Before infection, replace the medium with 2 ml fresh medium containing 8 μg/ml polybrene.
3. Add 2, 20, and 200 μl filtered virus into separate wells of the 6-well plate (*see* **Note 8**). Leave at least one well uninfected as a control.
4. One day after transfection, trypsinize infected cells on 6-well plates and transfer everything onto a 100 mm cell culture dish. Transfer also one noninfected well as a control.
5. Two days after transfection, add selection antibiotic to each plate (1.5 μg/ml puromycin or 6 μg/ml blasticidin). Control cells should die in 2–3 days (puromycin) or 3–5 days (blasticidin) (*see* **Note 9**).
6. When all control cells are dead, replace the medium with a fresh medium without selection antibotic. Of three dilutions, select the one that resulted in <20% infection efficiency, ensuring single viral integration in most cells.
7. Freeze down several aliquots of cells (*see* **Note 10**).
8. Validate the expression level of the tagged protein with luciferase assay and with western blotting.

3.3 Transfection

1. Seed stable cells expressing the prey protein into 96-well plates so that they are ~80% confluent on the day of transfection (for 293T cells, this corresponds to ~30,000 cells/well 1 day before transfection, or ~15,000 cells/well 2 days before transfection).
2. Array 150 ng of 3xFLAG-tagged bait protein expression plasmids into each well of a V-bottom 96-well plate with a liquid handler or a multichannel. Include multiple, preferably at least 8, negative control plasmids without FLAG tag (e.g., empty vector).
3. Prepare PEI/OptiMEM mix: add 60 μl PEI into 6 ml OptiMEM in a sterile 15 ml conical tube and incubate for 5 min at room temperature (*see* **Note 4**).
4. Using a reagent dispenser or a trough and a multichannel pipette, add 50 μl of PEI/OptiMEM to each well with DNA and mix well.

5. Incubate the DNA/PEI/OptiMEM mix for 20 min (incubation can be extended to up to 2 h).
6. Transfer 45 µl of the mix to each well of the 96-well cell culture plate with a liquid handler or a multichannel pipette.
7. Remember to coat the LUMIER assay plate with anti-FLAG antibody (Subheading 3.4)!
8. Two days after transfection, proceed to LUMIER assay.

3.4 Coating and Blocking Assay Plates

1. On the day of transfection, prepare an antibody coating solution. For each 384-well plate, prepare 9 ml 10 µg/ml anti-FLAG M2 in 1xPBS. For each 96-well plate, prepare 7 ml 4 µg/ml anti-FLAG M2 in 1xPBS (*see* **Note 11**).
2. Add 20 µl/well antibody solution to a 384-well plate or 60 µl/well to a 96-well plate with a reagent dispenser or a multichannel pipette.
3. Cover the plate tightly with parafilm and incubate overnight on a shaking platform.
4. Aspirate all buffer and flick off any remaining liquid.
5. Add 80 µl blocking buffer to a 384-well plate or 250 µl to a 96-well plate with a reagent dispenser or a multichannel pipette.
6. Incubate the plate for 1 h at room temperature on a plate shaker. Plates do not need to be covered at this point.
7. Aspirate all blocking buffer and flick off any remaining liquid.
8. Cover the plate tightly with a sealing tape or parafilm and store at 4 °C until needed. Plates can be stored for at least 2 months at 4 °C.

3.5 LUMIER Assay

1. If required, treat the cells with inhibitors, growth factors, or other compounds prior to lysis.
2. Prepare lysis buffer by adding protease inhibitors to ice-cold HENG buffer.
3. Wash the cells three times with 100 µl cold 1xPBS with a plate washer or with a multichannel pipette.
4. Add 80 µl HENG buffer to the plate with a reagent dispenser or a multichannel pipette and incubate for 5 min on ice to lyse cells.
5. Transfer 60 µl lysate to an anti-FLAG-coated 384-well plate or a 96-well plate with a liquid handler or a multichannel pipette.
6. Incubate 384-well or 96-well plates for 3 h at 4 °C on a plate shaker.
7. Wash the plate seven times with 80 µl (384-well plate) or 250 µl (96-well plate) ice-cold HENG buffer using a plate washer. No

protease inhibitors are needed at this point. If using a multichannel pipette, wash the 96-well plates four times with 250 µl HENG buffer, incubating the wash buffer for 5 min each time. After the last wash, flick off any remaining liquid.

8. Add coelenterazine-h to luciferase assay buffer and wait 10 min to let autoluminescence decrease.
9. Add 20 µl (384-well plate) or 60 µl (96-well plate) luciferase assay buffer to each well with a reagent dispenser or quickly with a multichannel (*see* **Note 12**).
10. Wait 2 min before measuring luminescence with a plate reader (100 ms read time per well; *see* **Note 7**).
11. After reading luminescence, flick off the luciferase reagent.
12. Dilute anti-FLAG M2 HRP antibody 1:10,000 into ELISA buffer and add 20 µl (384-well plate) or 60 µl (96-well plate) to each well with a reagent dispenser or a multichannel pipette.
13. Incubate the plate for 90 min at room temperature on a plate shaker.
14. Wash the plate seven times with 80 µl (384-well plate) or 250 µl (96-well plate) PBST. After the last wash, flick off any remaining liquid. If using a multichannel, wash the 96-well plates four times with 250 µl PBST, incubating the wash buffer for 5 min each time. After the last wash, flick off any remaining liquid.
15. Dilute ELISA Pico stable peroxidase and luminol reagent each 1:10 in water (e.g., 1 ml peroxidase, 1 ml luminol, 8 ml water) and add 20 µl (384-well plate) or 60 µl (96-well plate) to each well with a reagent dispenser or a multichannel pipette.
16. Read luminescence with a plate reader (100 ms read time per well).

3.6 Data Analysis

There are multiple different ways to calculate interaction scores. In our first study, we calculated the luciferase/ELISA signal ratio for each interaction [4]. However, such ratios are challenging in cases where ELISA signal is very low, leading to high interaction scores even if luciferase signal is barely above cutoff. Therefore, we prefer using the ELISA signal to filter out baits that were not expressed (i.e., potential false negatives) and use *Z*-score or control normalized luminescence as the interaction metric (Fig. 2).

3.7 Z Score

Z score is the most robust metric if a large number of baits (several hundred) are assayed and most of them are not expected to interact with the prey (*see* Fig. 2 and **Note 13**).

1. Transform all luminescence values to base-2 logarithm. (Background luminescence follows log-normal distribution.) If multiple plates are analyzed, normalize each plate separately to control for plate effects.

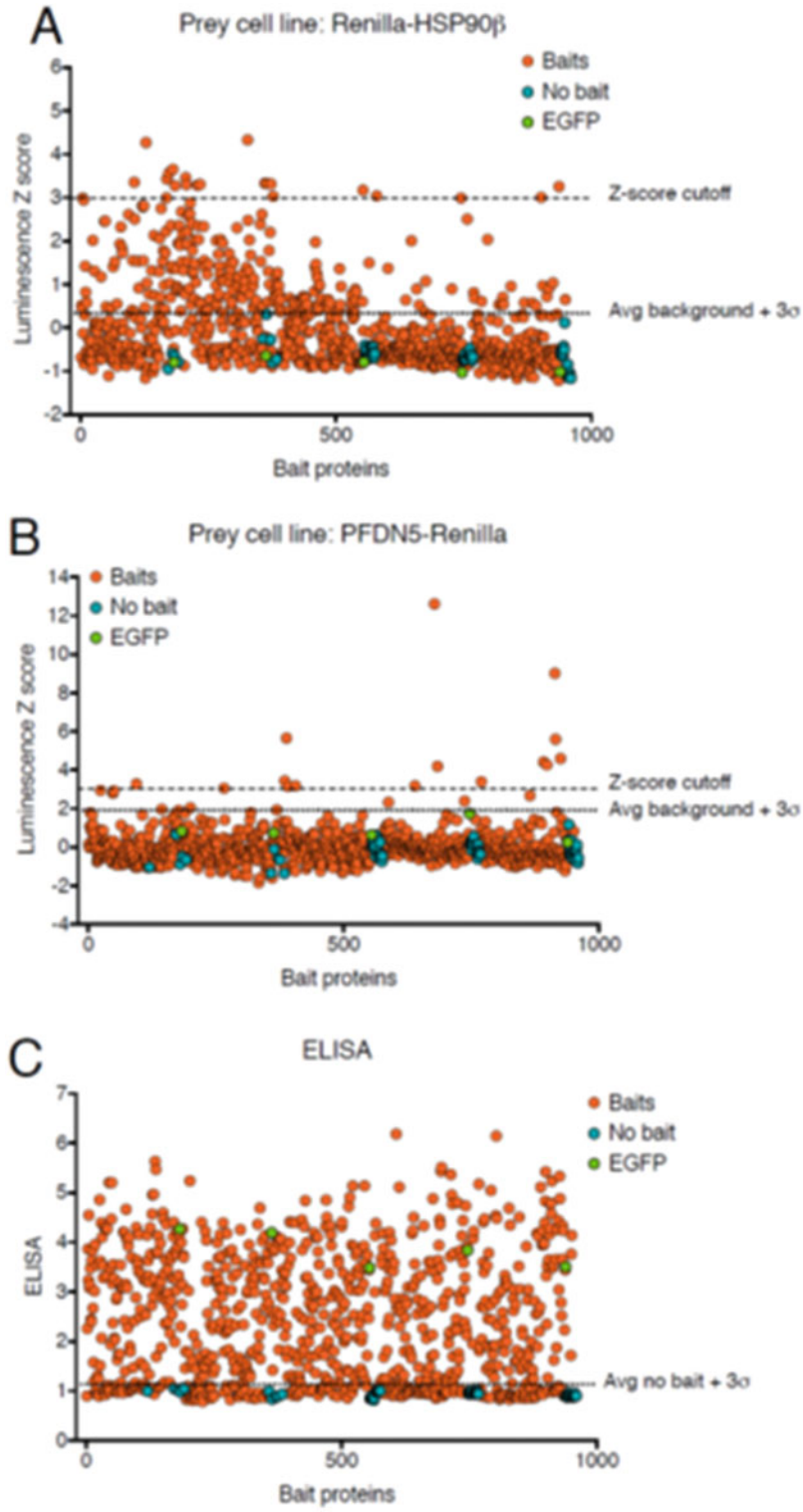

Fig. 2 Example of LUMIER data and analysis methods. 960 bait proteins were assayed for interaction with Hsp90 (**a**) or the prefoldin subunit PFDN5 (**b**). Luminescence was converted to *Z* scores. Dashed line indicates cutoff based on *Z*-score > 3. *Dotted line* indicates cutoff based on average control background $+3$ standard

2. Calculate average luminescence and standard deviation of all wells.
3. Subtract average luminescence from each luminescence value and divide this value by standard deviation. Z score > 3 generally corresponds to a robust interaction (*see* Fig. 2 and **Note 13**).
4. Calculate average ELISA signal and standard deviation of negative controls.
5. Filter out all the samples with ELISA signal below background +3SD (or another suitable cutoff). These are non-expressed baits (potential false negatives).

3.8 Normalization with Negative Controls

If there are fewer samples (tens to a few hundred), specific negative controls can be used to normalize the luminescence values. Confidence cutoffs can also be calculated, provided that enough negative controls are tested.

1. Transform all luminescence values to base-2 logarithm. (Background luminescence follows log-normal distribution.) If multiple plates are analyzed, normalize each plate separately to control for plate effects.
2. Calculate average luminescence and standard deviation of all control wells.
3. Subtract average control luminescence from each luminescence value. Normalized luminescence values over 2–3 × SD generally correspond to a robust interaction.
4. Calculate average ELISA signal and standard deviation of negative controls.
5. Filter out all the samples with ELISA signal below background +3SD (or another suitable cutoff). These are non-expressed baits (potential false negatives).

4 Notes

1. Should I generate stable cell lines for LUMIER assays? In general, stable cell lines are recommended for large-scale experiments where many (>200 up to thousands)

Fig. 2 (continued) deviations. Average was calculated from all no bait (empty) wells and EGFP negative control. Because Hsp90 interacts with a large fraction of the bait proteins, *Z*-score is likely too conservative a metric for distinguishing true positives from false positives. Therefore, cutoff based on average control background is more appropriate in this case. In contrast, PFDN5 interacts with only few bait proteins, and consequently, cutoffs based on different metrics are much more similar. ELISA values for the same bait proteins (**c**) show the distribution of bait protein expression. Cutoff based on average empty well ELISA luminescence +3 standard deviations separates nonexpressed baits from expressed baits relatively well

bait proteins are tested against a few (5–20) prey proteins. However, for many-vs-many interaction matrices (e.g., 96 baits against 96 preys on a single 96-well plate), co-transfection is likely a more cost-effective method. This protocol assumes that stable cell lines are used. However, the protocol can be used for co-transfection as well. In that case, bait and prey proteins are transfected in a 1:1 ratio (that is, 75 ng bait +75 ng prey for one well of a 96-well plate). It is important to include multiple "prey only" controls to account for the nonspecific binding of the prey protein to the plate. *See*, e.g., [8] for details on calculating interaction scores from co-transfection experiments.

2. Due to stoichiometric imbalance, it is better to fuse the chaperone to luciferase and capture the potential client protein with anti-FLAG. Because only a fraction of the cellular chaperone pool is engaged in interaction with the potential bait protein, the signal-to-noise ratio is significantly higher in this way than when the chaperone is captured with anti-FLAG.
3. This protocol and most LUMIER variants use *Renilla* luciferase, but other luciferases can also be used. For Nanoluc luciferase [9], the protocol is identical except for the luciferase substrate, which is furimazine (Promega) instead of coelenterazine-h. Similarly, for *Gaussia princeps* luciferase [10], replace coelenterazine-h with native coelenterazine.
4. This protocol uses affordable alternatives to commercial reagents, including polyethylenimine (PEI) instead of commercial transfection reagents. However, PEI can be replaced by any commercial reagent such as Lipofectamine 3000 (Thermo Fisher) or Effectene (Qiagen).
5. This protocol uses an affordable alternative to commercial luciferase assays. However, commercial luciferase assays such as Renilla-Glo Luciferase Assay System (Promega) or BioLux Gaussia Luciferase Assay Kit (New England Biolabs; also compatible with Renilla luciferase) work at least equally well. However, e.g., the Promega assay buffer contains reducing agents that will strip the anti-FLAG antibody off the plate, leading to loss of ELISA signal in the second part of the LUMIER with BACON assay.
6. The optimal concentration of each batch of PEI stock solution should be experimentally tested by transfecting a reporter protein such as GFP and the protocol modified accordingly.
7. Separate protease inhibitors can be replaced with commercial reagents such as cOmplete Protease Inhibitor Cocktail (Sigma-Aldrich).
8. Here, the cells are transduced with several dilutions of the virus to ensure that at least one results in 10–20% transduction

efficiency. Lentiviruses can also be titrated more accurately but for purposes of generating stable cell lines, this is generally not required.

9. If the cells get confluent before selection, antibiotics do not work efficiently. In that case, trypsinize the cells and passage them 1:5 into another cell culture dish. Continue selection 1 day after passaging (adding the antibiotic immediately after trypsinization can be toxic to the cells).
10. If the expression level of the prey protein needs to be titrated, polyclonal cell lines can be single-cell sorted by flow cytometry to derive clonal lineages.
11. All the pipetting steps on 96-well plates can be done with an 8-well or 12-well multichannel pipette. However, for laboratory automation (in particular an automated plate washer) will dramatically increase the throughput and decrease well-to-well variation. For 384-well plates, automation is essentially required.
12. Because luminescence signal decays relatively rapidly (half-life $T_{1/2} \sim 15$ min in the assay buffer), it is important that add the reagent as quickly as possible to the samples and also read the plate with short integration time per well (e.g., 100 ms).
13. *Z*-score calculations assume that most tested bait proteins do not interact with the prey, so that average luminescence is very close to negative control luminescence. If this is not the case, median luminescence can be calculated solely from negative controls and subtracted from all luminescence values.

References

1. Snider J, Kotlyar M, Saraon P et al (2015) Fundamentals of protein interaction network mapping. Mol Syst Biol 11:848–848
2. Barrios-Rodiles M, Brown KR, Ozdamar B et al (2005) High-throughput mapping of a dynamic signaling network in mammalian cells. Science (New York, NY) 307:1621–1625
3. Taipale M, Tucker G, Peng J et al (2014) A quantitative chaperone interaction network reveals the architecture of cellular protein homeostasis pathways. Cell 158:434–448
4. Taipale M, Krykbaeva I, Koeva M et al (2012) Quantitative analysis of hsp90-client interactions reveals principles of substrate recognition. Cell 150:987–1001
5. Taipale M, Krykbaeva I, Whitesell L et al (2013) Chaperones as thermodynamic sensors of drug-target interactions reveal kinase inhibitor specificities in living cells. Nat Biotechnol 31:630–637
6. Jia S, Peng J, Gao B et al (2011) Relative quantification of protein-protein interactions using a dual luciferase reporter pull-down assay system. PLoS One 6:e26414
7. Trepte P, Buntru A, Klockmeier K et al (2015) DULIP: a dual luminescence-based co-immunoprecipitation assay for interactome mapping in mammalian cells. J Mol Biol 427:3375–3388
8. Braun P, Tasan M, Dreze M et al (2009) An experimentally derived confidence score for binary protein-protein interactions. Nat Methods 6:91–97
9. Hall MP, Unch J, Binkowski BF et al (2012) Engineered luciferase reporter from a deep sea shrimp utilizing a novel imidazopyrazinone substrate. ACS Chem Biol 7:1848–1857
10. Tannous BA, Kim D-E, Fernandez JL et al (2005) Codon-optimized Gaussia luciferase cDNA for mammalian gene expression in culture and in vivo. Mol Ther 11:435–443

Chapter 5

Measurement of Chaperone-Mediated Effects on Polyglutamine Protein Aggregation by the Filter Trap Assay

Maria A.W.H. van Waarde-Verhagen and Harm H. Kampinga

Abstract

The formation of aggregates by polyglutamine-containing (polyQ) proteins in neurons is a key to the pathogenesis of several progressive neurodegenerative diseases such as Huntington's disease (HD) spinocerebellar ataxias (SCAs), and spinal and bulbar muscular atrophy (SBMA). In order to study whether the members of the heat shock protein (HSP) families, by virtue of their molecular chaperone activity, can inhibit the formation of polyQ aggregates, we developed a cell culture model expressing the GFP tagged fragment of exon1 of the huntingtin gene with an expanded polyQ chain and tetracycline inducible chaperones. Expression of mutated Huntington's protein leads to the formation of 2% SDS insoluble high molecular weight polyQ aggregates that are retarded on a cellulose acetate membrane in the so-called filter trap assay (FTA). This chapter explains in detail the protocols of the FTA and how it can be a useful tool to study the effect of HSPs or their functional mutants on aggregation of polyglutamine proteins. Moreover, the assay is useful to investigate how externally added polyQ peptides can act as nucleation seeds for internally expressed polyQ proteins.

Key words Protein aggregation, Huntington's disease, Polyglutamine diseases, Filter retardation assay, polyQ peptides, Prion-like seeding

1 Introduction

In trinucleotide (CAG) repeat expansion disorders, which include Huntington's disease (HD), spinocerebellar ataxias (SCAs), and spinal and bulbar muscular atrophy (SBMA), proteins containing polyglutamine (polyQ) stretches aggregate and form pathological structures such as amyloid fibrils and their precursors [1, 2]. For this paper, we will focus on Huntington's disease (HD), but the principles related to what we describe apply to all CAG repeat diseases. HD results from a CAG repeat expansion (>36) in exon 1 of the huntingtin (htt) gene. In brain tissues of affected patients, protein aggregates accumulate in the cytoplasm and nucleus of neurons. The principal component of these aggregates is an N-terminal fragment of htt that contains the polyglutamine tract

Stuart K. Calderwood and Thomas L. Prince (eds.), *Chaperones: Methods and Protocols*, Methods in Molecular Biology, vol. 1709, https://doi.org/10.1007/978-1-4939-7477-1_5,

[3]. In the polyQ diseases, the length of the polyQ expansion is strongly linked with aggregation propensity and is also inversely correlated with the age at the onset of the disease [4] and it is clear that aggregates drive the pathogenesis of the disease as various modulations of aggregation delay disease progression in model systems [5–8]. Thus, accurate quantitative measurements of aggregation are important tools to study these diseases.

Heat shock proteins, by virtue of their chaperone function whereby they support protein folding and timely protein degradation, form the first line of defense against protein aggregation [7]. Therefore, in several studies, the potential of HSPs to inhibit the formation of polyQ aggregates has been investigated [7, 9, 10]. In this paper, we will use a chaperone of the DNAJ (hsp40) family, DNAJB6, as an example of a very potent inhibitor of polyQ aggregation [11, 12] to illustrate the usefulness of the FTA for investigating the contribution of chaperones.

One of the characteristics of the disease-related polyglutamine (polyQ) aggregates in Huntington's disease is that the aggregates are insoluble in SDS, even in high concentrations SDS up to 2% [13–15]. The filter trap assay (FTA) or filter retardation assay as described in this chapter is an adaptation of a procedure developed in the laboratory of Dr. Erich Wanker to detect and quantify aggregates of the mutant huntingtin protein [13, 16], but also can be used for detection of aggregates generated by other polyQ containing proteins. Detection of the 2% SDS insoluble aggregated expanded polyQ proteins is based on its retardation on a cellulose acetate membrane with 0.22 μm pores. Comparable to slot-blotting where all proteins from a cell lysate are trapped on a nitrocellulose membrane, the FTA uses the same equipment with the exception of the type of membrane. Note that not all aggregation-related proteins causing neurodegenerative diseases can be detected by this assay. E.g., aggregates caused by mutations in superoxide dismutase-1 (SOD-1) that cause amyotrophic lateral sclerosis (SOD-1) are not detected by the protocol as we described here (data not shown) as these types of aggregates are SDS-soluble.

To study the effect of chaperones on the formation of aggregates, a toolbox of expression constructs of tagged exon1-mutant Huntington client proteins and chaperones was constructed [17]. Chaperones (or their mutants) were cloned in a pcDNA5/FRT/TO vector and, after transfection in a Flp-In T-Rex HEK-293 cell line, the expression can be regulated by tetracycline to directly compare the effect of the chaperone with the control situation [12]. The tagging of the HSPs allows for direct intercomparison of their effectiveness at equal (over)expression levels. Of course, the presence or type of the tag linked to the HSPs has to be checked for potential negative effects by confirmation of data using untagged versions. For the N-terminally tagged DNAJs used in our studies,

we so far did not find (major) influences on their anti-aggregation activity [12, 17].

The rate of aggregation of the exon1-mutant Huntingtin (and all polyQ proteins) depends on the length of the polyQ-stretch. After transfection with a plasmid encoding for a Q-length of 119 glutamines (pHttQ119-eYFP), microscopically visible aggregation is already seen within 1 day whereas detectable aggregation of HttQ74 takes 2 days [11, 16, 18]. This feature makes it possible to distinguish different chaperone potencies: strong "anti-polyQ aggregation chaperones" will be able to prevent aggregation of exon1-HttQ119, while inhibitory effects (of e.g. HSPB1) could be minor, yet not negligible and should be studied with, e.g., the exon1-HttQ74 or exon1-HttQ43 fragments [11, 12]. As a control, we always include a non-pathological exon1-HttQ23 fragment that does not form aggregates and should not be retained on the membranes in the FTA.

After expression of polyQ and HSPs (usually 1 day after transfection for HttQ119 and 2–3 days for HttQ74 or HttQ43), the cells are lysed in a 2% SDS buffer and the lysates are applied on a cellulose-acetate membrane (0.22 μm pores). We generally use three serial dilutions (1×, 5×, 25×) to allow (semi-quantitative) quantification. Only the aggregates are trapped and after some wash steps, to remove soluble (polyQ) proteins, the detection takes place [13, 14]. After blocking for a-specific binding, the bands can be detected immunologically as in westerns, followed by densitometric quantification using standard imaging programs (we typically use free software like image-J).

Besides its use in studying aggregation inhibition by chaperones on endogenously expressed proteins, the FTA can also be used to study the putative suppressive effect of chaperones on the seeding effect of externally added polyglutamine peptides. It has been suggested for many aggregation-prone proteins, including polyQ containing proteins, that they can be released from (dying) cells and be taken up by neighboring cells in a prion-like manner [19]. To study this, polyQ peptides are added to the culture medium. These have been shown to be internalized in cells and to be capable of seeding intracellular expressed polyQ containing proteins resulting in the formation of homotypic fibrillar polyglutamine aggregates [20]. In fact, such external peptides can even induce FTA-detectable aggregation of Huntington fragments with non-pathological polyQ stretches (e.g., HttQ23) that normally do not form aggregates [20, 21].

The FTA described here is robust and in several research projects in our lab, we have shown that the level of aggregation as detected in the filter trap assay correlates very well with microscopic quantification of intracellular inclusions and even generally correlates well with high molecular weight (HMW) material that remains in the stacking gel of western blots where the SDS insoluble

aggregates are detectable [12, 18]. Even more so, chaperone effects detected with this assay (especially of those having effects on the larger Q119 fragments) translate to disease-delaying effects in model organisms such as Xenopus [12], Drosophila [5, 22, 23], and even mouse [21]. The advantages over microscopy are that the FTA is more objective and easier to quantify. Its quantification is also more accurate and better reproducible than the analysis of HMW aggregates in stacking gels of westerns or of cell fractionation experiments [24]. Moreover, the method is not very labor intensive, not very time consuming nor does require specialized laboratory skills or expensive equipment. One limitation is that its capacity is relatively low—on one membrane 16 samples (as triplicates in serial dilution) can be quantified—which makes the method less suitable for high-throughput (compound) screens.

2 Materials

Prepare all the solutions using demineralized water and analytical grade reagents. Store all the reagents at room temperature unless indicated otherwise. Accurately follow all the waste disposal rules when disposing waste materials.

2.1 Cell Culture and Transfection

1. Cell Culture Plates, 6-wells.
2. 0.001% Poly-L-lysine: dilute a stock 0.1% poly-L-lysine (Sigma) 1:100 in sterile water. Store at 4 °C for maximal 3 months.
3. Flp-In T-REx HEK-293 cell line, Invitrogen.
4. Dulbecco's modified Eagle's medium (DMEM), supplemented with 10% fetal calf serum (FCS). Store at 4 °C.
5. Plasmids: cmv-(GFP)tagged-exon1-Huntingtin-polyglutamine with different Q-lengths and pcDNA5/FRT/TO-(V5) tagged chaperones [12, 17]. Store at −20 °C.
6. Lipofectamine, Invitrogen. Store at 4 °C.

2.2 Cell Lysis and Sample Preparation

1. Phosphate-Buffered Saline (PBS) pH 7.4: 137 mM NaCl, 2.7 mM KCl, 10 mM Na_2HPO_4 and 1.8 mM KH_2PO_4. Store at 4 °C.
2. Filter Trap Assay buffer (FTA buffer) pH 8.0: 10 mM Tris–Cl and 150 mM NaCl.
3. Stock solution of 20% sodium-dodecyl sulfate (SDS): dilute to appropriate working solutions.
4. Lysis buffer: FTA buffer + 2% SDS. Dilute SDS 20% stock 1:10 in FTA buffer.
5. Dithiothreitol (DTT) 1 M stock in Lysis buffer. Prepare fresh.

6. Lysis buffer + 50 mM DTT: dilute DTT 1 M stock 1:20 in Lysis buffer. Prepare fresh.
7. Disposable cell scrapers (Corning).
8. Micro-tip Sonifier (B-12, Branson Sonic Power Company).
9. DC Protein Assay, protein concentration assay (Bio-Rad).
10. Urea 8 M: dissolve 4.8 g Urea (Sigma) in 100 ml demineralized water. Prepare fresh.

2.3 Filter Trap

1. Wash buffer: FTA buffer + 0.1% SDS. Dilute SDS 20% stock 1:200 in FTA buffer.
2. Bio-Dot SF microfiltration apparatus (Bio-Rad Laboratories, Inc.).
3. Vacuum pomp (MEDAP P7050).
4. Bio-Dot thick filter paper, 11.3 × 7.7 cm (Bio-Rad).
5. Cellulose Acetate membrane, pore size 0.22 μm (Maine manufacturing).
6. Multichannel pipette (Costar).

2.4 Immunodetection and Quantification

1. PBS containing 0.1% Tween-20 (PBST). Dilute Tween-20 stock 1:1000 in PBS. Store at 4 °C.
2. Blocking buffer: 5% nonfat dry milk powder in PBST. Store at 4 °C for maximal 2 days.
3. Mouse anti-GFP (JL-8, Clontech) 1:5000 in PBST supplemented with 3% Bovine Serum Albumin (BSA). When stored at −20 °C the diluted antibody can be used several times.
4. Second antibody: Anti-mouse IgG HRP-conjugated 1:5000 in blocking buffer. Prepare fresh.
5. Enhanced Chemiluminescence (ECL) substrate (Pierce). Store at 4 °C.
6. ChemiDoc Touch Imaging system (Bio-Rad).
7. Quantification software Image Lab 5.2.1.

2.5 Testing the Seeding Effect of Externally Added Peptides

1. PolyQ-peptides (K2Q45K2) were kindly provided by Prof. Dr. R. Melki, Gif-sur-Yvette, France and were generated as described in [20]. Stock 100 μM solutions in PBS are stored at −80 °C.

3 Methods

Safety precautions: Safety rules have to be followed since, like other disease-associated, aggregation-prone proteins, polyQ proteins and polyQ peptides are suggested to be capable of acting as prion-like

proteins capable of infiltrating cells [25, 26], although an "infectious" property of polyQ proteins has not been demonstrated yet. Precautions include wearing protective gloves and facemasks. Carry out all handling of samples, especially cell lysis and sonication, in a safety cabinet. 8 M Urea or 1% SDS [26] is used to clean the working area and to inactivate liquid waste. All waste generated during work with aggregation-prone proteins should be autoclaved for 30 min at 121 °C.

3.1 Cell Culture and Transfection

One day before transfection the cells are seeded in (precoated) multi-well dishes. The protocol described here uses the tetracycline regulated expression system of Flp-In T-Rex HEK-293 cells with tagged pcDNA5/FRT/TO chaperones [12]. In the experimental setup (Fig. 1a) it is shown how the effects on polyglutamine-aggregation without and with chaperones can be directly compared. Figure 1b shows the setup of a seeding experiment where aggregation is induced by the addition of external peptides (for details about the protocol for a seeding experiment, *see* Subheading 3.5).

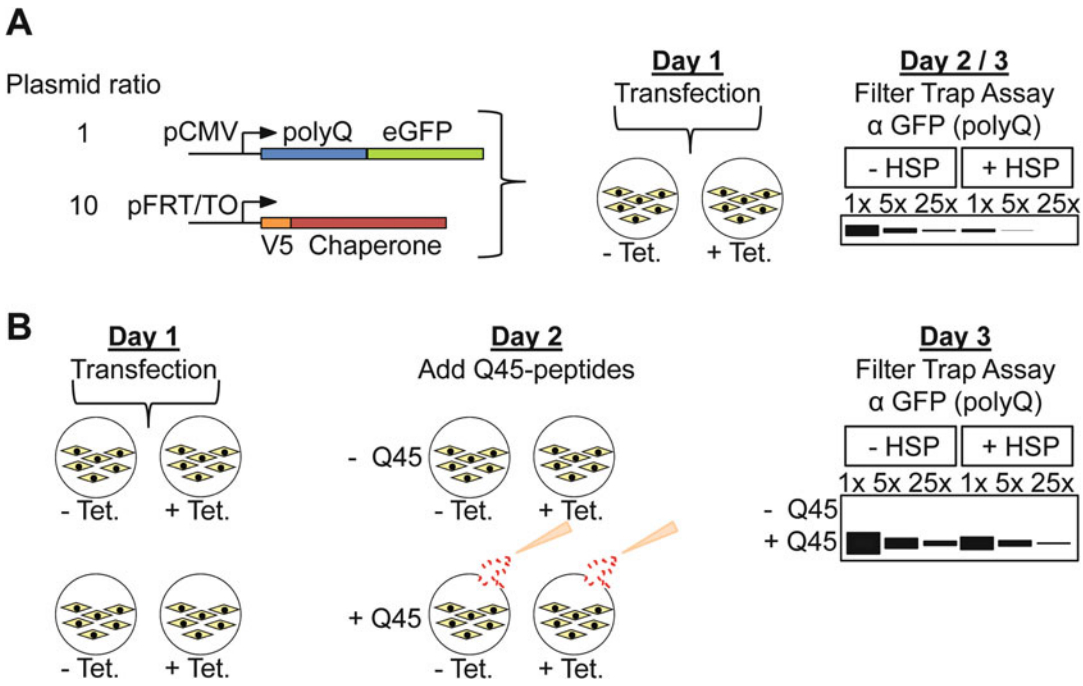

Fig. 1 Experimental setup for the Filter Trap Assay (FTA). (**a**) Schematic representation of the plasmids used. One day after seeding, the HEK293 cells are co-transfected with constructs encoding HttQ119-eYFP or eGFP-HttQ74 and a tetracycline inducible chaperone. After 24 or 48 h, this allows for direct comparison of the extent of aggregation without and with chaperone in the FTA. (**b**) In a seeding experiment, external peptides are added 1 day after transfection of the cells with constructs encoding HttQ23-eGFP alone or with a chaperone. 3–24 h after peptide addition, the filter trap assay allows for the detection of the extent of aggregation without and with extracellularly added Q-peptides. Note that intracellular expression of HttQ23 without extracellular Q-peptides does not lead to aggregate formation

Depending on the Q-length of the expanded exon1-Huntingtin fragment the cells are incubated for 1 or 2 days after transfection. Standard procedures for mammalian cell culture and transfection are followed.

1. Before seeding cells coat 6-well plates (or 3.5 cm culture dishes) with 1 ml 0.001% poly-L-lysine. Remove after 10 min the poly-L-lysine and wash the wells 3× with sterile water (*see* **Note 1**).
2. Seed 3×10^5 HEK293 cells/well in 2 ml culture medium (*see* **Note 2**).
3. On the day after seeding, transfect the cells by a method of choice, according to the manufacturer's instructions, with plasmids encoding for exon1-mutated Huntingtin protein and (tetracycline inducible) chaperones. Commonly a plasmid ratio of 1:10 is used. Replace the transfection-medium after 3–4 h by culture-medium and add tetracycline to a final concentration of 1 μg/ml in the wells which require chaperone expression (*see* **Note 3**).
4. Harvest the cells 24–48 h after transfection depending on the expected rate and extent of aggregation as described in Subheading 3.2.

3.2 Cell Lysis and Sample Preparation

The cells are harvested when microscopically visible aggregates are detected; commonly this is 1 or 2 days after transfection with pHttQ119-eYFP or peGFP-HttQ74 respectively. Since the polyQ fragments are tagged with a fluorescent tag, aggregation can be checked regularly using a standard fluorescence microscope without the need of harvesting and fixing the cells. Protein extracts are prepared by scraping the cells in a lysis buffer containing 2% SDS at room temperature in a safety cabinet. Samples can be stored at −20 °C at any moment after each of the **steps 4–8** below. Take care that after thawing the samples are mixed very well by vortexing, to solidify the SDS (*see* **Note 4**).

1. Remove the culture medium from the multi-well plate by aspiration. Never allow the monolayer to dry but immediately add 1 ml PBS.
2. Wash the cell layer twice with 1 ml PBS.
3. Add 200 μl lysis buffer to each well (*see* **Note 5**).
4. Scrape the surface of the well with a cell scraper and transfer the entire cell lysate to an Eppendorf vial (*see* **Note 6**).
5. Sonicate each lysate 5 s at 50 W with a microtip sonifier in a safety cabinet. Attention: ear protection is required.

6. At this point measure the protein concentrations in the solubilized samples with a commercially available protein assay (*see* **Note 7**).
7. Bring the samples to equal protein level of 40 μg/100 μl with lysis buffer; dilute the samples to obtain a total volume of 400 μl. These are the stock samples (1× sample) for preparing the serial dilution (*see* **Note 8**).
8. Add 1 M DTT to a final concentration of 50 mM (dilution 1:20) to the stock samples. Heat the samples in a boiling water bath or heating block for 5 min (*see* **Note 9**).
9. Make serial dilutions (typically 1:5 and 1:25) from the boiled stock samples with lysis buffer + DTT 50 mM; dilute the samples to obtain a final volume of 400 μl (*see* **Note 10**).

3.3 Filter Trap

When the serial dilutions are ready, the samples can be applied on the filter trap apparatus (*see* **Note 11**). After the samples are aspirated, the slots have to be washed thoroughly in order to remove soluble proteins which can disturb the results. The setup of the Bio-Dot SF apparatus is illustrated in Fig. 2. For more detailed guidelines we refer to the manufacturer's Instruction Manual.

1. Prepare the bottom part of the apparatus by inserting the gasket support plate into the vacuum manifold and place the sealing gasket. Presoak 2 Trans-Blot filter papers in wash buffer and place them onto the top of the bottom part. Then place a

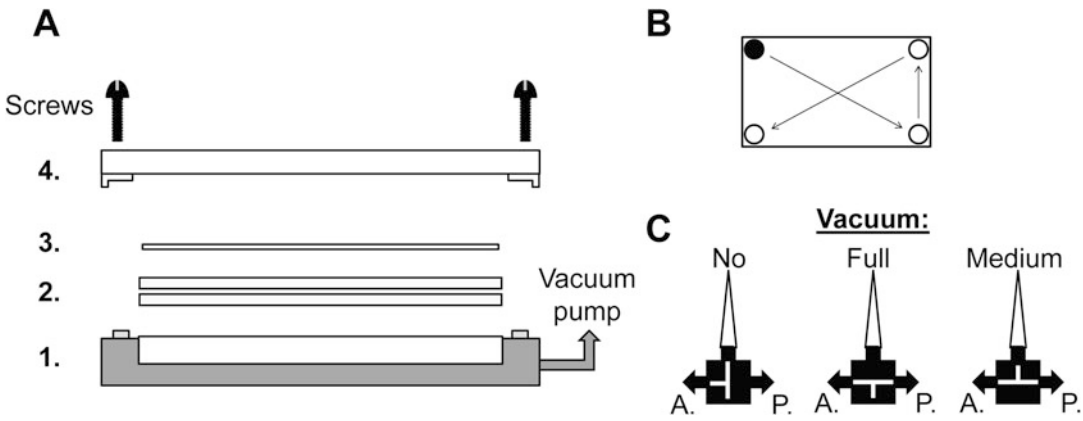

Fig. 2 Setup of the Filter Trap Apparatus. (**a**) Schematic representation of the Cellulose-acetate membrane assembly in the Filter Trap Apparatus. A presoaked cellulose acetate membrane (*3*) is put on top of two thick filter papers (*2*) and clamped between the bottom-part (*1*) and the slotted lid (*4*). (**b**) After clamping the membrane, the screws on the top of the lid are tightened diagonally to establish equal pressure. (**c**) Between the vacuum pump (P) and the apparatus (A), the vacuum can be regulated by a valve. During the application of the samples or wash buffer, the vacuum pump should be off. Full vacuum is only used for tightening the screws. Medium vacuum is required to aspirate the samples and the wash buffer

presoaked 0.22 μm Cellulose Acetate membrane on the top of the filter papers (Fig. 2a) (*see* **Note 12**).

2. Use a glass rod to remove air bubbles.
3. Put the slotted lid onto the top of the membrane and tighten the screws diagonally (Fig. 2b) to provide equal force.
4. Apply vacuum, and tighten the screws further under full vacuum (Fig. 2c).
5. Fill all the slots with 100 μl wash buffer with a multi-channel pipette and apply mild vacuum (Fig. 2c) to pre-equilibrate the membrane.
6. Vortex the samples before loading. Turn the vacuum off (Fig. 2c) and carefully load 100 μl sample with the pipet tip touching the side of the slot to prevent the formation of air bubbles. Apply mild vacuum till the samples are completely aspirated (*see* **Note 13**).
7. Wash the slots three times with 100 μl wash buffer, followed each time by mild vacuum (*see* **Note 14**).
8. Disassemble the blotting apparatus, remove the membrane, and wash it shortly in PBST before starting immunodetection (*see* **Note 15**).

3.4 Immunodetection and Quantification

After the membrane is removed from the Bio-Dot apparatus, it can either be dried between filter papers or used immediately for immunodetection. From this point on, a standard immunodetection protocol as used for western blotting can be used. Below, a brief description is provided for the antibody incubation followed by ECL detection on a ChemiDoc Touch Imaging System (Bio-Rad). For densitometric quantification, we routinely use the program Image Lab 5.2, but other freeware should serve the same purpose.

1. Block the membrane with 5% skimmed milk powder in PBST 0.1% by shaking for 45 min at room temperature.
2. Wash the membrane for three times (5 min each) with PBST 0.1%.
3. Incubate with mouse GFP primary antibody (dilution 1:5000, *see* Subheading 2.4, **item 3**) in a cold room with shaking overnight.
4. Wash the membrane for three times (10 min each) with PBST 0.1%.
5. Incubate with secondary antibody, anti-mouse IgG HRP-conjugated (dilution 1:5000, *see* Subheading 2.4, **item 4**) for 1 h on a shaker at room temperature.
6. Wash the membrane for three times (10 min each) with PBST 0.1%.

7. Apply ECL substrate and detect chemiluminescence on the ChemiDoc Touch according to the manufacturer's instructions. By making images at different time points, the best exposure can be selected later.
8. Accurate quantification of the bands is accomplished by software program Image Lab 5.2.1. Ignore overexposed bands (as highlighted in red in the program). Correct for background staining, according to the User's Manual. Check linearity of the signal using the serial dilutions.

3.5 Testing the Seeding Effect of Externally Added Peptides

The experimental setup for a seeding experiment with externally added peptides (Fig. 1b) does not differ very much from a regular experiment. Below we describe the differences in the protocol in more detail. For all other steps the protocols as described in Subheading 3.1 till 3.4 can be followed.

1. For testing the seeding effect of Q-peptides, transfect the cells with plasmids encoding for chaperones and peGFP-HttQ23 according to the schedule in Fig. 1b. Replace the transfection medium after 3–4 h by the culture medium. For chaperone expression, add tetracycline to a final concentration of 1 μg/ml (*see* **Note 16**).
2. One day after transfection add extracellular peptides to the culture medium in the appropriate wells (Fig. 1b) to a typical final concentration of 1 μM. Add the same volume of solvent (PBS) to the control wells. *Attention*: Prior to the addition of the peptides to the culture medium, the peptide-stock solution should be homogenized thoroughly by vortexing and repeated pipetting.
3. Since seeding-induced aggregation is rapid, the cells can be harvested between 3 and 24 h after peptide addition. Prepare the cell lysates in the same way as described in Subheading 3.2. Care should be taken to wash away the culture medium (*see* Subheading 3.2, **step 2**) thoroughly by two wash steps with 2 ml PBS each, since the remaining peptides could associate with endogenous polyglutamine proteins after lysis and increase aggregation (*see* **Note 17**).
4. After this point, there are no differences in the protocols for working with cell lysates obtained after the addition of external Q-peptides compared to regular samples.

3.6 Illustrations of Typical Results

To illustrate our findings, some typical results obtained with the above-mentioned protocols are presented in Figs. 3–5.

Figure 3a demonstrates that aggregation kinetics occur in a polyQ length-dependent manner: 48 h of transient expression of non-pathogenic HttQ23 leads to no detectable aggregates. HttQ74 shows some detectable aggregation whereas HttQ119

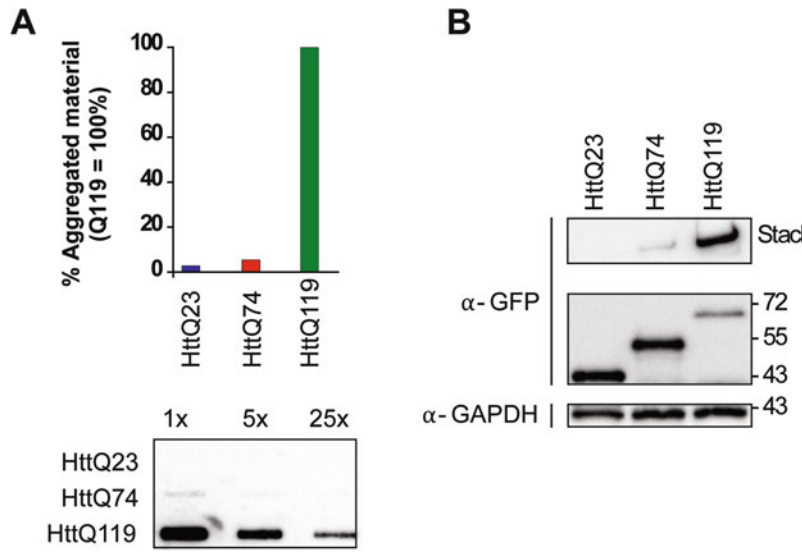

Fig. 3 Aggregation is dependent on the polyQ-length. (**a**) Filter trap assay of HEK293 cell extracts expressing GFP tagged Htt-exon1 with different polyQ lengths. Cells were lysed 48 h after transfection. Serial five-fold dilutions of cell lysate were loaded on cellulose-acetate membranes and probed with anti-GFP. Quantification was done using the aggregation of HttQ119 as a reference (=100%). (**b**) Cell lysates were also loaded onto 12.5% SDS-PAA gels and processed for immunoblotting with anti-GFP for analysis of Htt-exon1 expression and aggregation (high molecular weight material in the stacking gel). GAPDH is used as a loading control

shows massive aggregation. Figure 3b shows the expression levels of the various Htt constructs and also shows that for HttQ74 some and for Htt119 a lot of the protein remains as aggregates in the stacking gel.

The effect of chaperones is illustrated in Fig. 4. Here tetracycline inducible DNAJB1 or DNAJB6 constructs were co-transfected with exon1-HttQ119eYFP. Increasing the concentration of tetracycline induces increasing expression of DNAJB1 or DNAJB6 (Fig. 4b), which is accompanied by a parallel concentration-dependent reduction in the level of aggregation of HttQ119 (Fig. 4a). The data also show that DNAJB6 is more potent than DNAJB1 in reducing HttQ119 aggregation, as found before [12].

In Fig. 5, the effect of addition of extracellular Q45-peptides on the aggregation of endogenously expressed Htt-PolyQ is shown. The Q45-peptides were added immediately after transfection (*see* Subheading 3.5, **step 1**). The Q45-peptides form extracellular fibrils [21] that can enter the cells and act as seeds that dramatically enhance the aggregation of intracellularly expressed Htt. In fact, they even lead to the aggregation of a non-pathogenic HttQ23. Post lysis control experiments (Fig. 5c) have to be done to exclude potential artifacts (*see* **Note 17**).

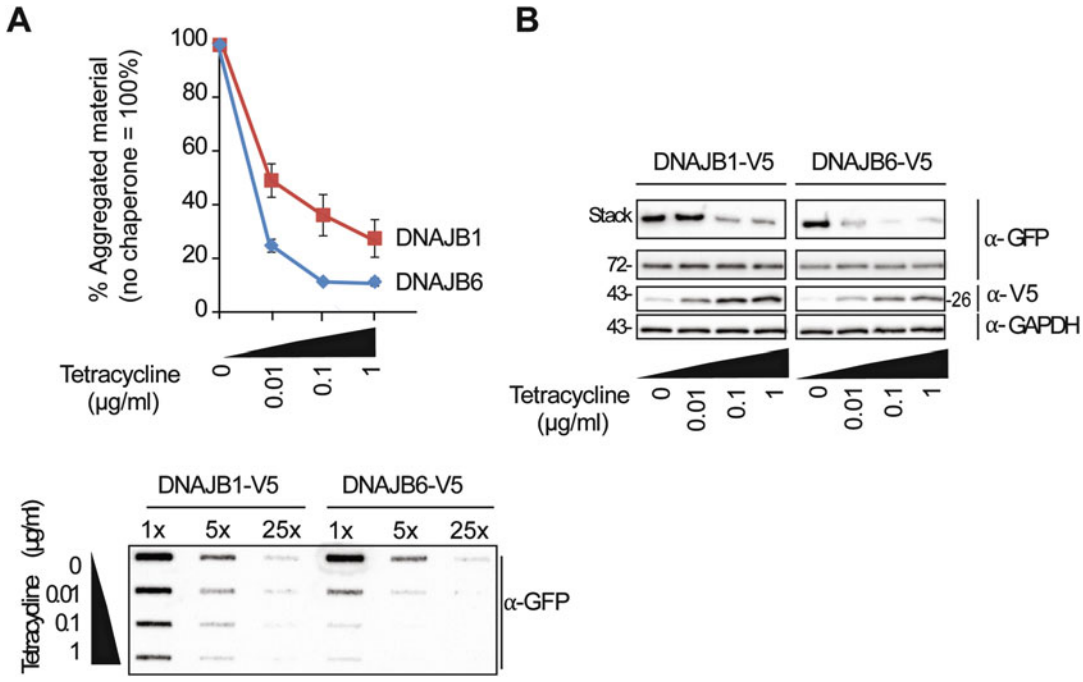

Fig. 4 Anti-aggregation effect of tetracycline regulated DNAJB1 and DNAJB6. (**a**) Filter trap assay of HEK293 cell extracts co-expressing HttQ119-eYFP and DNAJB1 or DNAJB6. Cells were lysed 48 h after transfection. The level of expression of the chaperones was regulated by the concentration of tetracycline. Serial fivefold dilutions of cell lysates were loaded on cellulose-acetate membranes and probed with anti-GFP. Quantification was done using the aggregation of HttQ119 without chaperones (no tetracycline) as a reference (=100%). (**b**) Cell lysates were also loaded onto 12.5% SDS-PAA gels and processed for immunoblotting with GFP antibodies for analysis of Htt-exon1 expression and aggregation (high molecular weight material in the stacking gel) and with V5 antibodies for the detection of V5-tagged chaperones. GAPDH is used as a loading control

4 Notes

1. To improve cell adhesion and transfection efficiency, the wells are first coated with 1 ml 0.001% poly-L-lysine for 10 min at room temperature. Since poly-L-lysine is very toxic to the cells, after coating the wells should be washed thoroughly by three wash steps with 2 ml/well sterile water.
2. The number of cells used for seeding is dependent on the density needed for the transfection method on the next day and the required duration of culture time after transfection. In a typical experiment when the HEK293 cells are transfected with pHttQ119-eYFP and harvested after 1 day, we seed 3.5×10^5 cells/well; for a transfection with pEGFP-HttQ74 and harvesting after 2 days, we seed 2.8×10^5 cells/well.

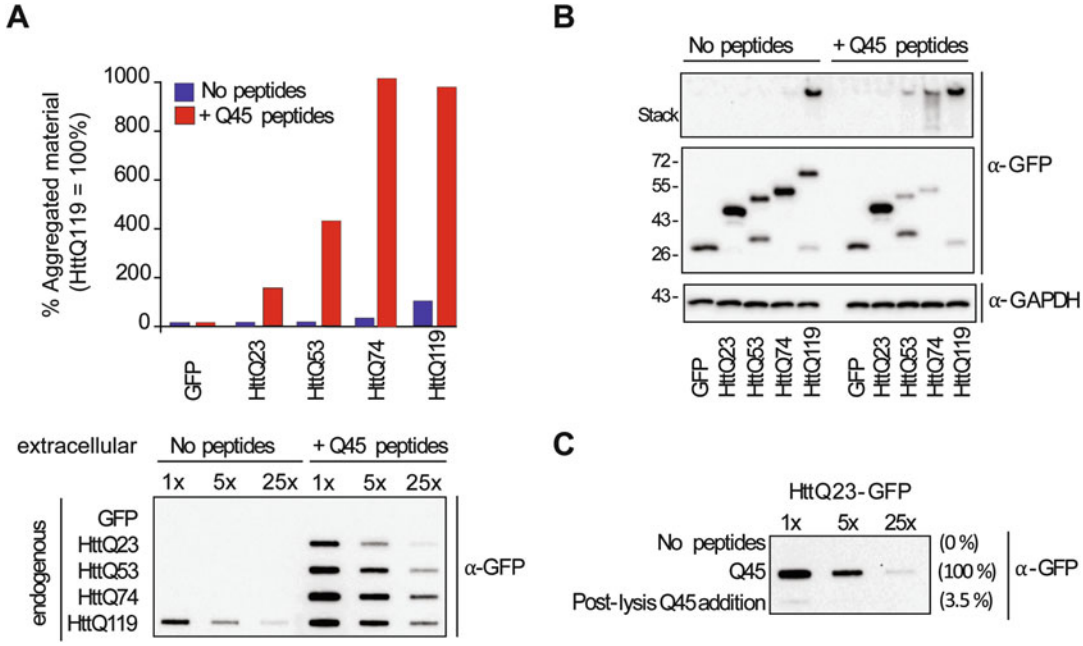

Fig. 5 Extracellular Q-peptides "seed" aggregation of cytoplasmic Htt-polyQ proteins. (**a**) Filter trap assay of HEK293 cells expressing Htt-exon1 with different polyQ lengths. Q-peptides (1 μM) were added immediately after transfection. After 24 h serial fivefold dilutions of cell lysates were loaded on cellulose-acetate membranes and probed with anti-GFP. Quantification was done using the aggregation of HttQ119 without added Q-peptides as a reference (=100%). (**b**) Cell lysates were also loaded onto 12.5% SDS-PAA gels and processed for immunoblotting with GFP antibodies for the analysis of Htt-exon1 expression and aggregation (high molecular weight material in the stacking gel). GAPDH is used as a loading control. (**c**) Filter trap assay of HEK293 cell extracts expressing eGFP-HttQ23. A post lysis control was made by adding Q45 peptides after the cell lysis (*see* **Note 17**). This should not and did not lead to detectable aggregation of eGFP-HttQ23. As a reference, cell lysates of eGFP-HttQ23 expressing cells without or with incubation with Q45 peptides for 24 h during culture are shown

3. The use of 1 μg/ml tetracycline in the culture medium to induce chaperone expression is sufficient to reach maximal expression. When milder expression is aimed for this can be regulated by reducing the concentration of tetracycline.
4. All the sample preparation steps are carried out at room temperature because SDS crystallizes at low temperature. Since the concentration of SDS is rather high and no lengthy extraction procedure is necessary, the addition of protease inhibitors to inhibit protein and protein aggregate breakdown is not essential.
5. The 200 μl lysis buffer is a convenient volume for solubilizing HEK293, U2Os, and Hela cells, grown to an approximate density of 0.5–1.5 $\times$ 10^6 cells/well. Since the proteins are not diluted to such an extent that the volume is too large, it

increases flexibility to make concentrated samples to apply on the filter trap assay.

6. In order to transfer the entire volume of the viscous lysate aspirate slowly, using a blue tip of a 1 ml pipette. Make sure to avoid air-bubbles.
7. Measuring the protein concentration in the lysates can be done using a commercially available Tris/SDS-compatible protein assay such as the DC Protein Assay (BioRad).
8. The concentration of protein in the cell lysate of 40 μg/100 μl is used to detect aggregation of polyQ with a length of 119 Q's after 1 day. Depending on the level of aggregation microscopically observed, the protein concentration can be varied between 10 and 100 μg/100 μl [16]. A cell lysate with a final volume of 400 μl is sufficient to repeat the FTA with the same samples at least twice for intra-experimental duplicates.
9. Boiling of the cell lysates for 5 min at 100 °C is very important for optimal detection. In case a boiling water bath is not available, a heat block heated to 100 °C can be used.
10. Once the stock 1×–sample has been boiled, there is no need to boil the diluted samples again. The fivefold serial dilution (1:5 and 1:25) was shown to give the best information in a wide range of aggregation levels. Dependent on the application one can decide to lower or increase the dilution level, e.g., to a twofold or a tenfold serial dilution.
11. The method described here uses the slot format (SF) of the Bio-Dot microfiltration apparatus (Bio-Rad). The Bio-Dot SF apparatus focuses the sample on a thin line instead of a circle (in the 96-well dot format), making quantification by densitometry more reproducible. The Bio-Dot SF has 48 slots and a capacity of 50–500 μl sample volume per slot.
12. Depending on the goal of the experiment, different membranes can be used. For the detection of polyQ aggregates, a Cellulose Acetate membrane is used with pore holes of 0.2 μM [13, 14].
13. It is recommended to fill the wells that are not used for cell lysates with identical volume of wash buffer before applying vacuum to deliver steady pressure on each well. From here on, only apply mild vacuum (Fig. 2c) till the samples or wash buffer are completely aspirated. Do not aspirate longer than necessary.
14. After the lysates have been applied on the cellulose acetate membrane, it is very important to thoroughly wash at least three times to ensure removal of soluble (polyQ) proteins. To check for possible clogging of the cellulose acetate membrane pores by the aggregated proteins, cell lysates with aggregated

polyQ (e.g., HA-tagged HttQ74) can be loaded on the filter, followed by loading a cell lysate of cells expressing a soluble protein with another tag (e.g., GFP) in the same slot. When, after three washes, no GFP is detected, clogging can be excluded. The same protocol can be used to check if enhanced aggregation caused by extracellular polyQ peptides would block the passage of soluble intracellular (polyQ) proteins.

15. After usage, it is very important to intensively clean the Bio-Dot apparatus with water and a mild soap and to rinse with distilled water. Prevent scratching with sharp tools to avoid damage to the surface.
16. To examine the seeding effect of Q-peptides, transfection with plasmids encoding for short endogenous polyQ-lengths can be used; even non-self-aggregating polyQ stretches with 23 glutamines (eGFP-HttQ23) will be induced to aggregate and thus an accurate information on seeding-induced aggregation can be obtained. Note that it is important that the chaperone is already expressed at the time when extracellular peptides are added.
17. After incubating the cells with external Q-peptides, the culture medium has to be washed away carefully to prevent a possible co-aggregation of remaining peptides from the culture medium with endogenous polyglutamine proteins during cells lysis. Hereto post-lysis controls can be included by adding Q-peptides (final concentration of 0.2 μM) to a lysate of cells expressing eGFP-HttQ23. As shown in Fig. 5c only minor post lysis aggregation is usually found, indicating that the observed increase in aggregation of the endogenous HttQ23 is not an artifact of sample preparation.

Acknowledgments

This work was supported by a grant from Senter Novem (IOP-IGE07004) and a Stimulation Grant from the Nederlandse Hersenstichting (project 15F07(2)-58) awarded to H.H.K. The authors wish to thank Dr. M.A. Rujano and Dr. J. Hageman for their contribution to the introduction of the Filter Trap Assay in our lab. The corrections and suggestions after careful reading of the manuscript by E. Preusser de Mattos are very much appreciated.

References

1. Chiti F, Dobson CM (2006) Protein misfolding, functional amyloid, and human disease. Annu Rev Biochem 75:333–366
2. Zoghbi HY, Orr HT (2000) Glutamine repeats and neurodegeneration. Annu Rev Neurosci 23:217–247
3. Schilling G, Klevytska A, Tebbenkamp ATN et al (2007) Characterization of huntingtin pathologic fragments in human Huntington disease, transgenic mice, and cell models. J Neuropathol Exp Neurol 66:313–320

4. Gusella JF, MacDonald ME (2000) Molecular genetics: unmasking polyglutamine triggers in neurodegenerative disease. Nat Rev Neurosci 1:109–115
5. Neef DW, Turski ML, Thiele DJ (2010) Modulation of heat shock transcription factor 1 as a therapeutic target for small molecule intervention in neurodegenerative disease. PLoS Biol 8: e1000291
6. Warrick JM, Chan HY, Gray-Board GL et al (1999) Suppression of polyglutamine-mediated neurodegeneration in Drosophila by the molecular chaperone HSP70. Nat Genet 23:425–428
7. Kampinga HH, Bergink S (2016) Heat shock proteins as potential targets for protective strategies in neurodegeneration. Lancet Neurol 15:748–759
8. Labbadia J, Morimoto RI (2013) Huntington's disease: underlying molecular mechanisms and emerging concepts. Trends Biochem Sci 38:378–385
9. Kakkar V, Meister-Broekema M, Minoia M et al (2014) Barcoding heat shock proteins to human diseases: looking beyond the heat shock response. Dis Model Mech 7:421–434
10. Kakkar V, Prins L, Kampinga H (2012) DNAJ proteins and protein aggregation diseases. Curr Top Med Chem 12:1873–4294. Review
11. Vos MJ, Zijlstra MP, Kanon B et al (2010) HSPB7 is the most potent polyQ aggregation suppressor within the HSPB family of molecular chaperones. Hum Mol Genet 19:4677–4693
12. Hageman J, Rujano MA, van Waarde MAWH et al (2010) A DNAJB chaperone subfamily with HDAC-dependent activities suppresses toxic protein aggregation. Mol Cell 37:355–369
13. Scherzinger E, Lurz R, Turmaine M et al (1997) Huntingtin encoded polyglutamine expansions form amyloid-like protein aggregates *in vitro* and *in vivo*. Cell 90:549–558
14. Bailey CK, Andriola IFM, Kampinga HH et al (2002) Molecular chaperones enhance the degradation of expanded polyglutamine repeat androgen receptor in a cellular model of spinal and bulbar muscular atrophy. Hum Mol Genet 11:515–523
15. Carra S, Sivilotti M, Zobel ATC et al (2005) HspB8, a small heat shock protein mutated in human neuromuscular disorders, has in vivo chaperone activity in cultured cells. Hum Mol Genet 14:1659–1669
16. Scherzinger E, Sittler A, Schweiger K et al (1999) Self-assembly of polyglutamine-containing huntingtin fragments into amyloid-like fibrils: implications for Huntington's disease pathology. Proc Natl Acad Sci U S A 96:4604–4609
17. Hageman J, Kampinga HH (2009) Computational analysis of the human HSPH/HSPA/DNAJ family and cloning of a human HSPH/HSPA/DNAJ expression library. Cell Stress Chaperones 14:1–21
18. Rujano MA, Kampinga HH, Salomons FA (2007) Modulation of polyglutamine inclusion formation by the Hsp70 chaperone machine. Exp Cell Res 313:3568–3578
19. Brundin P, Melki R, Kopito R (2010) Prion-like transmission of protein aggregates in neurodegenerative diseases. Nat Rev Mol Cell Biol 11:301–307
20. Ren P-H, Lauckner JE, Kachirskaia I et al (2009) Cytoplasmic penetration and persistent infection of mammalian cells by polyglutamine aggregates. Nat Cell Biol 11:219–225
21. Kakkar V, Månsson C, de Mattos EP et al (2016) The S/T-rich motif in the DNAJB6 chaperone delays polyglutamine aggregation and the onset of disease in a mouse model. Mol Cell 62:272–283
22. Fujikake N, Nagai Y, Popiel HA et al (2008) Heat shock transcription factor 1-activating compounds suppress polyglutamine-induced neurodegeneration through induction of multiple molecular chaperones. J Biol Chem 283:26188–26197
23. Vos MJ, Carra S, Kanon B et al (2016) Specific protein homeostatic functions of small heat-shock proteins increase lifespan. Aging Cell 15:217–226
24. Tebbenkamp ATN, Borchelt DR (2009) Neuroproteomics. Protein Aggregate Characterization in Models of Neurodegenerative Disease 566:85–91
25. Peelaerts W, Bousset L, Van der Perren A et al (2015) α-Synuclein strains cause distinct synucleinopathies after local and systemic administration. Nature 522:340–344
26. Bousset L, Brundin P, Böckmann A et al (2016) An efficient procedure for removal and inactivation of alpha-synuclein assemblies from laboratory materials. J Parkinsons Dis 6:143–151

Chapter 6

Fluorescent-Linked Enzyme Chemoproteomic Strategy (FLECS) for Identifying HSP70 Inhibitors

T.A.J. Haystead

Abstract

Activation of the heat shock response, and in particular upregulation of stress-inducible Hsp70, herein referred to as Hsp70i, in newly transformed cells, appears to protect against protein damaging stimuli, induction of premature oncogene-induced terminal senescence (OIS), and apoptosis, thereby enabling tumor initiation and progression to an aggressive phenotype. Expressed at very low or undetectable levels in normal tissue, the cytoprotective effects of Hsp70i appear to be mediated through its activity as a molecular chaperone allowing proper folding of mutated proteins, and by blocking cell signaling pathways that regulate OIS and apoptosis. Identification of small-molecule inhibitors selective for Hsp70i could provide new therapeutic tools for cancer treatment. However, identification of selective inhibitors of Hsp70i has proven challenging largely because of the affinity of the protein for ATP. Additionally, its chaperone functions do not lend the protein amenable to traditional enzymatic high-throughput screens. Here, we describe the use of fluorescence-linked enzyme chemoproteomic strategy (FLECS) to identify Hsp70i inhibitors. The FLECS assay is a simple binding assay that enables proteins tagged with fluorophors to be rapidly and quantitative screened against small-molecule libraries. We show several case history examples of the methodology that led to the discovery of the Fatty acid synthase inhibitor, FASNALL, the DAPK3 inhibitor HS38, and HS72, an allosteric inhibitor selective for Hsp70i.

Key words Heat shock protein 70, Fluorescence linked enzyme chemoproteomic strategy

1 Introduction

The Heat shock protein 70 (Hsp70) family have broad chaperone functions in cells that include folding of nascent proteins, refolding of misfolded proteins, protein transport, regulation of breakdown of unstable proteins, removal of protein complexes, and control of regulatory proteins [1, 2]. These functions are driven by ATP hydrolysis in the N-terminal nucleotide-binding domain (NBD) of Hsp70. The Hsp70s are evolutionary conserved across species and there are eight mammalian Hsp70 family members [3]. The inducible form of Hsp70 (Hsp70i, also called Hsp72, Hsp70-1, HspA1A/HspA1B) is present in low or undetectable levels in most unstressed normal cells and tissues; however, expression levels

Stuart K. Calderwood and Thomas L. Prince (eds.), *Chaperones: Methods and Protocols*, Methods in Molecular Biology, vol. 1709, https://doi.org/10.1007/978-1-4939-7477-1_6,

rapidly increase in response to cellular stresses such as heat shock or transformation. Deletion of its immediate paralog, constitutively active heat shock protein cognate 70 (Hsc70), is developmentally lethal, whereas deletion of Hsp70i results in sterility of male mice, but no other overt phenotype in unstressed mice [4, 5]. Hsp70i and Hsc70 are highly related, sharing 90% over all sequence identity; however, most of the sequence variability is confined to the NBD (<80% identity). The close sequence similarity between Hsp70i and Hsc70 has certainly contributed to past difficulties in distinguishing the biological functions of the two proteins using both pharmacologic and RNA interference approaches. The broad structural organization of the Hsp70's is similar; consisting of three functional domains, the NBD in the N-terminal region, a substrate-binding domain (SBD) in the C-terminal region, and a linker in the middle [6]. The chaperone activity of Hsp70i is a function of the C-terminus in cooperation with other co-chaperones such as Hsp40, Hip, Hop, CHIP, and Bag1 [6]. Crystallographic and NMR studies have shown that Hsp70i has distinct open and closed conformational states that change based on the presence of nucleotides and some of its co-chaperones [2, 7, 8]. When complexed with ADP and substrate, there is little interaction between the NBD, SBD, and linker region. Upon substrate and ADP release and rebinding of ATP, the linker region and SBD make contact with the NBD [9]. There is also allosteric regulation of ATP hydrolysis between the domains [10].

1.1 Hsp70 Inhibitor Prior Art

The involvement of Hsp70i in maintaining tumor stability and its potential to synergize with Hsp90 to selectively kill tumors have been driving factors to develop inhibitors specifically targeting the protein in vivo [9, 11]. Confounding factors in the discovery of Hsp70i inhibitors include its affinity for ATP/ADP and their conformational influences, the close sequence similarity within the NBD with Hsc70. Indeed, conventional approaches have failed to consider off target binding to Hsc70, which could account for the poor performance in vivo of current Hsp70 inhibitors. Current inhibitors identified to target mammalian Hsp70 include NSC 630668-R/1, VER-155008, MAL3-101, MKT-077, Pifithrin, and Apoptozole (Fig. 1). There is considerable structural diversity among the prior inhibitors, reflecting the various methodologies that were employed to define them, as well as whether they target the NBD or SBD on Hsp70 (30-33). The NDB domain is most favored for inhibitor development, albeit challenging. Inhibitors targeting the NBD to date have either employed rationale design approaches based on partial crystallographic structures with bound nucleotide or have relied on coupled enzymatic assays measuring ATP depletion. The polar interactions present in the NBD and its low μM affinity for ADP have certainly contributed to difficulties in selective inhibitor discovery [12]. The crystal structure of the active

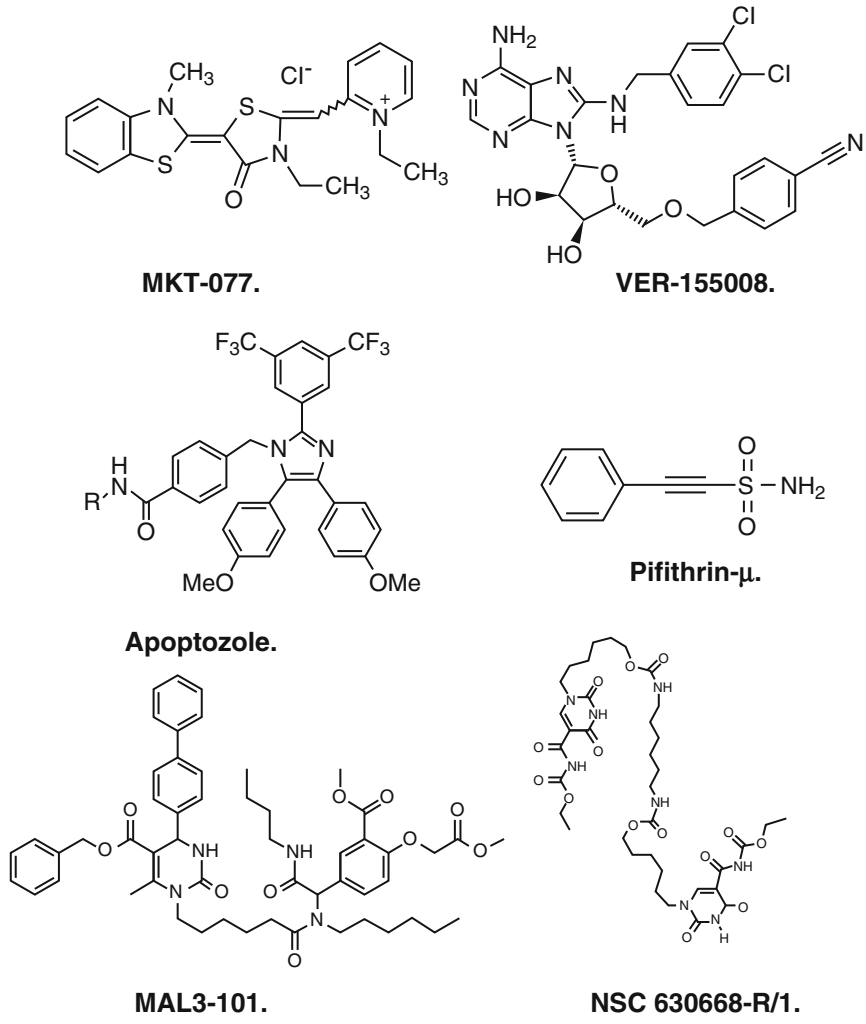

Fig. 1 Prior art inhibitors reported to target heat shock protein 70

form of Hsp70i shows the NBD to be completely enclosed around the nucleotide with almost no solvent accessibility to the surface [13]. Aside from the nuances associated with targeting the NBD, none of the approaches adopted thus far by other groups have been able to separate Hsp70 family members, especially Hsp70i from Hsc70. NSC 630668-R/1 inhibits ATPase activity but does not discriminate Hsp70i from Hsc70 [14]. VER-155008 shows broad specificity with other Hsp family members, largely because it is a nucleotide derivative. It also contains two potentially labile (perhaps by design) benzyl groups [12]. MAL3-101 has been shown to stimulate Hsp70 ATPase function, suggesting it is an allosteric regulator, although the exact binding site of this molecule remains unknown [15]. Like NSC 630668-R/1, MAL3-101 is quite large and has a number of labile ester groups. MKT-077 targets the NBD

and inhibits proliferation in tumor cell lines; however, severe renal dysfunction in patients was observed in phase I clinical trials [16, 17]. Pifithrin, binds to the SBD of both Hsc70 and Hsp70i disrupting client protein interaction in vitro. In tumor cells the molecule promotes caspase-dependent cell death in tumor cells only suggesting it has some specificity to Hsp70i in vivo, although p53 binding has also been shown, which could explain its antitumor actions [18]. MKT-O77 and Pifithrin have potential reactive groups that render them covalent modifiers, which may contribute to side effects in vivo. More promising inhibitors of the Hsp70 class are second and third generation MKT-077 analogs JG18 and JG40. Their mechanism of action and specificity lies in interaction with Hsp70 co-chaperones such as NEF [19].

1.2 Discovery of HS-72 by FLECS

In Howe et al. [20] we reported the results of screening Hsp70i by fluorescent-linked enzyme chemoproteomic strategy (FLECS) and identified several novel inhibitors that appeared to act by allosterically affecting the Hsp70i's affinity for ATP. The most promising of these was HS-72 a ((S)-N-(1-propyl-1H-benzo[*d*]imidazol-2-yl)-1-(pyrazin-2-yl)piperidine-3-carboxamide (Fig. 2). The FLECS screen is a variation of proteome mining technology utilized in the discovery of the Hsp90 inhibitor SNX5422 [21]. Proteome mining was designed to screen all purine binding proteins (the purinome) expressed in cells/tissues *en masse* against large directed chemical libraries, matching early chemical starting points with targets [22, 23]. The power of this approach enabled not only hundreds of diverse enzymes to be screened at a single step but also enabled the selectivity of a particular hit molecule to be determined simultaneously. The same assay could also then be used in subsequent iterative campaigns to monitor or improve selectivity as one strived to improve the molecules potency and bioavailability. The hypothesis is that this would avoid later stage failures due to unpredicted toxicity during in vivo studies in animals. This approach was put into practice in the discovery and development of SNX5422, and orally bioavailable inhibitor for Hsp90 that is currently advancing in clinical trials [21]. A cell/tissue extract is

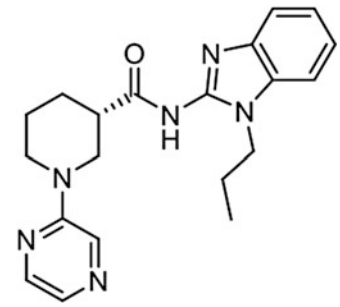

Fig. 2 Structure of HS-72

applied to an ATP affinity resin in which the nucleotide is immobilized through its gamma-phosphate [21–23]. This orientation favors reversible binding of proteins that bind purines through multiple contacts with the adenosine ribose moiety with the gamma phosphate showing solvent accessibility at the surface (the kinase orientation). This orientation of the purine is highly conserved across multiple gene families including protein kinases, non-protein kinases, dehydrogenases, hydrolyases formylases, most metabolic enzymes, helicases, DNA and RNA binding proteins, transcription factors, and chaperones such as Hsp90. Over the years, by MS analysis we have documented several hundreds proteins that reversibly bind to ATP when tethered by its gamma phosphate from human, mammalian, and pathogen sources. Typically, we estimate that up to 10% of the expressed genome of most species express protein that bind the purine in the "kinase orientation." In human tissues this represents up to 2000 distinct proteins. Importantly, the majority of the enzymes captured on this media are considered intractable to conventional methods of high-throughput (HT) screening. They often require radioisotopes to follow activity or have functions that do not lend themselves readily amenable HT screening, e.g., protein folding. The method is a simple universal binding assay that enables ATP competitive inhibitors to be identified directly.

The FLECS assay is a variation on the proteome mining approach and is more targeted from the outset, yet still retains the selectivity profiling capabilities of proteome mining [20, 24, 25]. Moreover, FLECS is more suited to academic-based drug discovery than the original proteome mining approach which was really designed to identify chemical starting points that would likely derive novel composition of matter claims. For a FLECS screen one expresses the targeted purine binding protein of choice as a recombinant GFP-fusion protein (one could use YFP or RFP) either in a bacterial, yeast, or mammalian cell line. The expressing cells are then lysed, homogenized, clarified and the entire extract applied to gamma phosphate ATP resin without further purification. The bound proteins are washed with high salt to remove any nonspecifically associated proteins. To verify that the GFP-fusion protein has a functional ATP binding site the GFP-fusion protein charged resin is serially eluted with increasing concentrations of ATP [1–100 mM]. The resin flow though is collected and aliquots measured for fluorescence in a plate reader. This method can also be used to determine the dissociation constant (K_d) of the bound fluorescent protein for ATP as described [25]. Once competitive binding is established one is ready to screen the fusion protein against large libraries of small molecules. Figure 3 illustrates the diversity of proteins we have screened using the FLECS assay. In some instances native proteins can also be screened after labeling them with reactive fluorophors directly while bound to the ATP

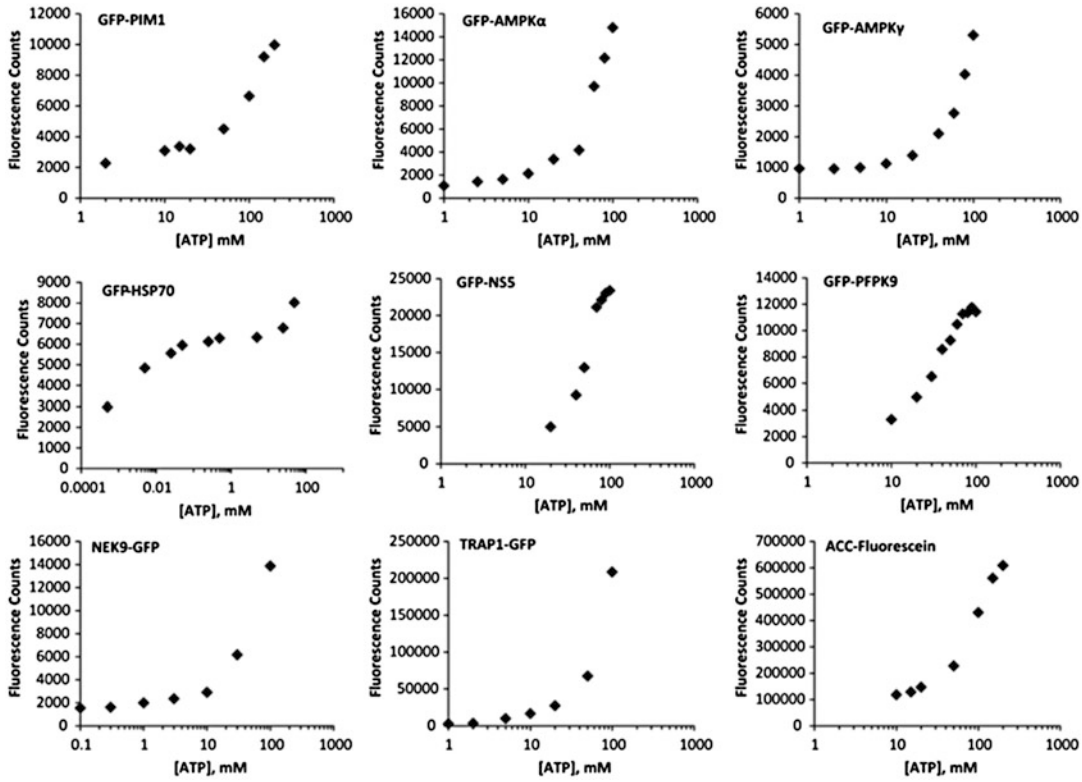

Fig. 3 FLECS is a Universal assay that enables purine utilizing proteins of diverse function to be screened against small molecule libraries. The indicated GFP-fusion proteins were expressed in various cell lines and captured from homogenates on ATP media. The proteins were then tested for their ability to be competitively released from the media with increasing concentrations of free ATP. GFP proteins tested—*PIMK* Pim kinase 1, *AMPKα* α subunit AMP activated protein kinase, *AMPKγ* γ regulatory subunit AMPK, *GFP-Hsp70* inducible form of heat shock protein 70, *NS5* non-structural protein 5 of Dengue virus, *PfPK9 Plasmodium falciparum* Protein kinase 9, *NEK9* NEK9 protein kinase, *TRAP1* TNF Receptor Associated Protein 1, *ACC* Acetyl CoA Carboxylase. Figure previously reported in Carlson et al. ACS Chem Biol 8, 2715–2723

resin. This approach was used to identify fatty acid synthase (FASN) inhibitor Fasnall [24]. Briefly, lactating pig mammary gland extract was applied to the ATP resin and the bound proteins labeled with cysteine reactive fluor probe [24]. The reader should note that FASN is highly induced in the lactating mammary gland and constitutes ~25% of the soluble cellular protein fraction.

1.3 Hsp70 and ATP Binding

The Hsp70 family have a very low affinity for ATP (<10 μM) compared with most ATP binding proteins we have examined and its ATPase activity turns over rapidly. Interestingly, based on the crystal structure of Hsc70 with bound nucleotide one would predict that the protein is sterically hindered from binding ATP tethered through its gamma phosphate. This is because the protein normally binds the nucleotide in the opposite direction to the majority of purine utilizing enzymes such as protein kinases or

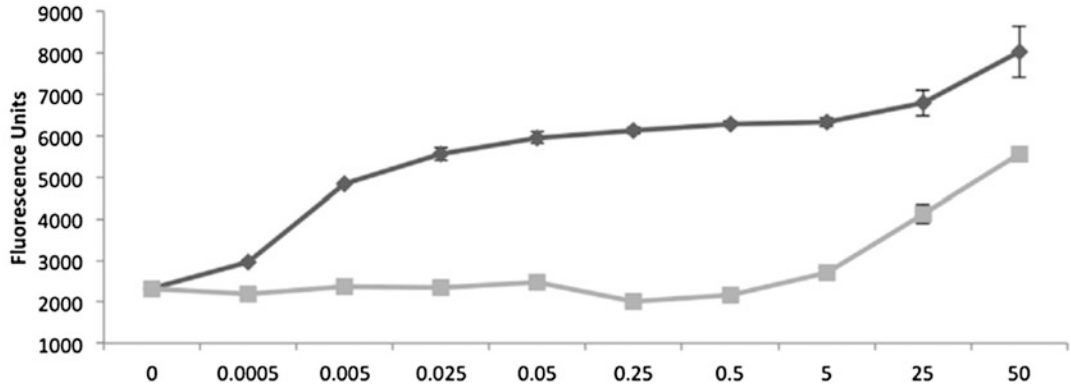

Fig. 4 Nucleotide binding of the inducible form of Hsp70 is allosterically regulated. GFP-Hsp 70 bound to γ-phosphate linked ATP is selectively released with low [μM] ATP compared with high mM [ADP], suggesting that the protein is allosterically regulated by ATP. Figure was previously reported in Howe et al. Chem Biol. 2014 Dec 18; 21 (12):1648–59

Hsp90. However, when one mixes cellular extract with gamma-phosphate linked ATP resin one can efficiently bind native forms of Hsp70. Interestingly however if one performs a titration experiment against ATP and ADP from μM to high [mM], one observes a strikingly different pattern of elution compared with the majority of proteins bound to gamma phosphate-linked ATP resin (Fig. 4). Figure 4 shows that very low [μM] of ATP are required to elute GFP-Hsp70i from gamma phosphate-linked ATP compared to very high [mM] of ADP. This contrast with proteins like Hsp90 which generally requires [mM] ATP to be released from the same resin. The underlying mechanisms for these different elution patterns are related to distinct mechanism of binding and release from the media. In the case of Hsp90 binding is due to first order binding to the immobilized ATP and the amount of free ATP required to release is therefore a function of the ligand density (10 μmol/mL) and the proteins affinity for ATP (<10 μM). In the case of Hsp70, the nucleotide is bound in the opposite orientation. Therefore, in order for Hsp70 to bind ATP tethered through its gamma phosphate the protein would have to first be in its "apo" open conformation state. Once bound the protein cannot be released by simple nucleotide competition as shown by the high [ADP] required to liberate the protein. However, as shown in Fig. 5, when exposed to even low [μM] ATP the protein turns over and is released. Since it is unlikely that the low ATP (<10 μM) is able to compete with high ligand density, the only possible mode of release is through an allosteric effect, i.e., the protein is regulated allosterically via a nucleotide-binding site distinct from its active site. For these reasons, when screening for inhibitors of Hsp70 using the FLECS assay one is unlikely to identify inhibitors that directly compete at its active site.

2 Materials

1. *γ-Linked ATP Sepharose Media (see* ***Note 1****)*: Dry CNBr-Activated Sepharose 4B media (28.6 g, GE Healthcare) was equilibrated in HCl (1 mM, 333 mL) for 5–15 min, washed with HCl (1 mM, 600 mL) followed by deionized water (333 mL). The media was added to mixture A ($NaHCO_3$, 0.97 g; NaCl, 3.4 g; H_2O, 115 mL; 1,4-dioxane, 29 mL; 1,10-diaminodecane, 3.6 g; ethanolamine, 3.6 mL) and shaken for 2 h. Meanwhile, reaction mixture B (H_2O, 143 mL; ATP, disodium salt, 7 g; 1-methylimidazole, 5.2 mL; EDC, 12 g) was stirred for 1 h. Mixture A was removed and the media was washed with HCl (1 mM, 600 mL) and then deionized water (333 mL). Mixture B and the media were combined and rotated for 24 h. The resulting ATP Sepharose media was filtered and washed with HCl (1 mM, 600 mL), then deionized water (333 mL) and stored at 4 °C in phosphate buffer (0.1 M, pH 7.4) containing NaN_3 (3 mM).
2. *Cell Lysis Buffer*: 150 mM NaCl, 50 mM Tris pH 7.5, 1% Triton X-100, 1 mM EDTA, 1 mM dithiothreitol (DTT]).
3. *Low Salt Buffer*: 150 mM NaCl, 25 mM Tris pH 7.5, and 60 mM $MgCl_2$.
4. *High-Stringency Wash Buffer*: 1 M NaCl, 25 mM Tris pH 7.5, 60 mM $MgCl_2$, and 1 mM DTT.
5. *Low-Stringency Wash Buffer*: 150 mM NaCl, 25 mM Tris pH 7.5, 60 mM MgCl2, and 1 mM DTT.

3 Methods

Screening compounds by FLECS. Figure 5 illustrates the steps and equipment required to complete the FLECS assay. ATP media (25 mL) is charged with clarified cellular extract expressing an N terminal GFP fused to Hsp70i. Typically for screening 1000 compounds we recommend charging the media with 1×10^7 cells/mL of ATP media. The media is washed with high and low ionic strength buffers to remove nonspecifically bound proteins. Next, one determines the signal-to-noise ratio for the assay by parsing out the charged resin *without further purification* into a 96-well filter plate (0.2 μm cutoff) and eluting the bound proteins with increasing [ATP, 0–100 mM] (*see* **Note 2**). As shown in Fig. 5, following addition of ATP (or drug) solution (50 μL), the elution plate containing the resin is placed over a catch plate and centrifuged ($3000 \times g$) for 5 min. The eluted proteins are measured in a fluorescent plate reader. Signal-to-noise ratio is determined from the maximal signal one obtains with ATP and should be 10- to

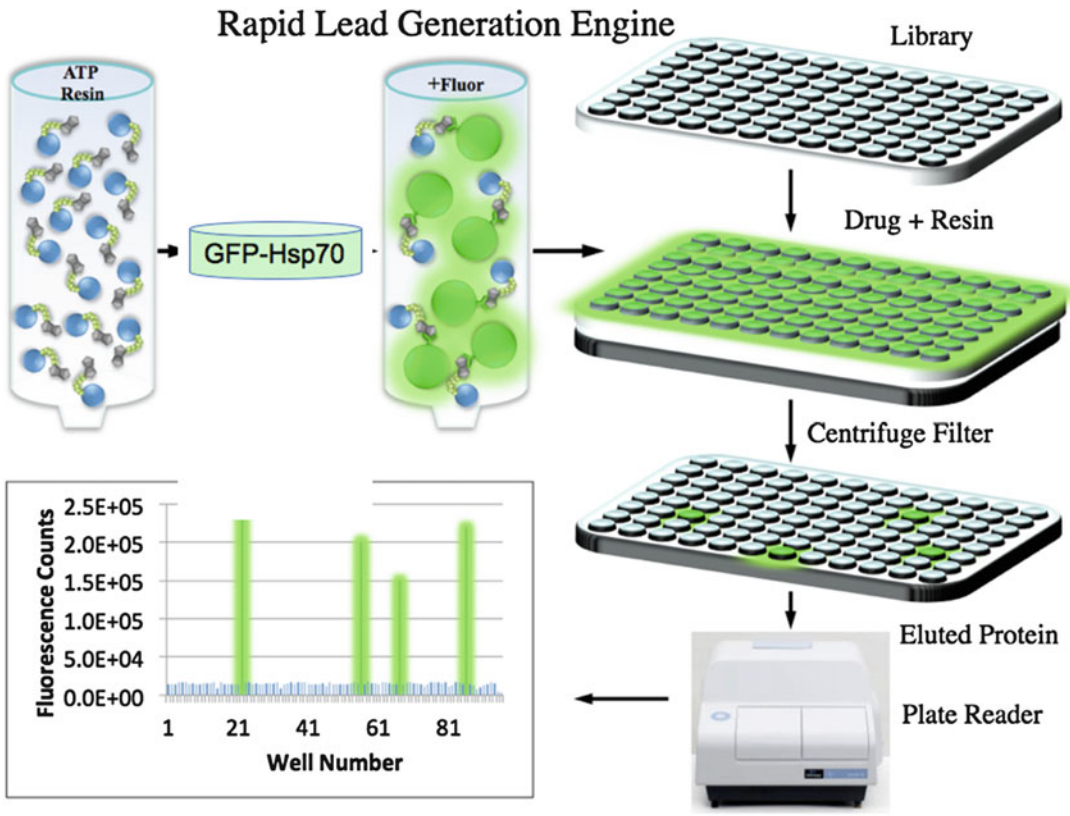

Fig. 5 Steps involved in screening for inhibitors of Hsp70 by FLECS. Extracts are prepared from cells expressing GFP-Hsp70 and mixed with a column of ATP resin. Following washing, the resin with bound protein is parsed into a 96 well filter plate and each well eluted by centrifugation with a drug like molecule. The eluted proteins are captured in a 96 well titer plate and measured for fluorescence in a standard fluorescence plate reader

15-fold above background. Once one has established that the assay is working one is ready to screen small-molecule libraries for compounds that will affect Hsp70i affinity for ATP. In the discovery of HS-72, we screened a ~4000 member library of purine-like analogs against GFP-Hsp70i *en masse*. Following parsing of the charged resin into filter plates, 50 μL of 350 μM solution (in 10% DMSO) of each compound from the library was added to each well. The plate was placed over the catch plate and centrifuged resulting in 96 compounds screened simultaneously for potential Hsp70i inhibitors. This operation can be carried out either manually or using a standard liquid-handling robot. All the compounds yielding significant fluorescence should be verified by repeating the assay preferably in titration experiments. In our HS-72 study the primary screen identified 197 hits from the library, which were first sorted by their specificity toward GFP-Hsp70i over other purinome members that had also been screened against the same chemical library by FLECS.

The compounds that were active in multiple assays were removed from consideration since these were considered non-selective. Next, the presence of GFP-Hsp70i in the eluates from the 197 primary hits was determined by Western blot. This reduced the collection to 60 compounds and also eliminated autofluorescent false-positive molecules. Then, we tested the ability of the 60 compounds for the elution of native Hsp70 from the ATP resin using pig bladder extracts, a rich source of native Hsp70i, reducing the final collection to 22 diverse structures (0.65% of the library). This collection contained several diverse chemical structures which were further prioritized in a series of cell-based assays of Hsp70i function that defined HS-72 as the most promising molecule.

3.1 FLECS Screen

A pEGFP-tagged Hsp70i was (plasmid 15215; Addgene) used in the FLECS assay and was originally cloned by Evan Eisenburg [26]. ATP 200 mM stock was prepared with low salt buffer. FuGENE 6 transfection reagent (Roche) was used for transfection of GFP-Hsp70i into HEK293T cells, following the manufacturer's protocol. The transfection ensued for 48 h, upon which time the cells were harvested and lysed in cell lysis buffer and one tablet Complete Mini protease inhibitor [Roche]). Cell lysates were stored at −80 °C until further use. After binding, the resin lysates were washed three times with high-stringency wash buffer and three times with low-stringency wash buffer. Next, the resin with bound proteins (50 μL) was transferred to 0.2 μm polyvinylidene fluoride filter 96-well plate (Corning) sitting on the top of a black flat-bottomed 96-well catch plate (Corning). Inhibitors or ATP were added to each well (50 μL) and the plates were centrifuged using an Eppendorf Centrifuge5810 at 1000 × *g* for 2 min.

4 Notes

1. As with any synthesis batches of gamma-phosphate-linked ATP resin can vary considerably if protocols are not followed rigorously. The methods outlined give a specific density of ATP/mL of resin, typically 10 μmol/mL. If the density is increased by twofold this increases the avidity of the media considerably reducing the sensitivity of the assay. This also leads to size exclusion due to ligand crowding, i.e., high molecular proteins >50 kDa start to be occluded. If one reduces the ligand density to 1 μmol/mL, the resin begins to lose capacity. A lower density media can however be used with more purified proteins. We prefer the 10 μmol/mL for three reasons; (1) this mimics intracellular ATP concentration (~10 mM most cells); (2) this reduces the sensitivity of the assay to only define more potent inhibitors; (3) this enables both the GFP-fusion protein to be recovered as well as the entire cellular purinome. Later

one can evaluate the intrinsic selectivity of a hit as well as its potency.

2. The major issue with the FLECs assay is the quality of the recombinant GFP-protein and ensuring adequate expression to complete the screen. One typically wants to achieve a signal-to-noise ratio of 10:1 over base line. This is determined by expressing the protein of interest, making a cell extract and applying the clarified mixture directly to the ATP resin. The resin is washed and the bound protein eluted with high Mg/ATP (60 mM/100 mM). The eluate is collected and amount of liberated GFP-fusion protein determined by fluorescence over low-stringency buffer elution. Although it is possible to carry out the assay at lower ratios, we would not recommend it. Once one has established an effective level of expression one should calculate how much expressed GFP fusion protein one requires to complete the entire screen, i.e., how much extract needs to be applied to routinely give a signal-to-noise ratio of 10:1 or > for every compound in the library. One should then scale up expression to enable complete screening of the library in a single batch.

Acknowledgements

This work was supported by NIH grants R01-AI089526-04 to T.A.J.H. and a Department of Defense Transformative Vision Award to T.A.J.H.

References

1. Daugaard M, Rohde M, Jaattela M (2007) The heat shock protein 70 family: highly homologous proteins with overlapping and distinct functions. FEBS Lett 581:3702–3710
2. Evans CG, Chang L, Gestwicki JE (2010) Heat shock protein 70 (hsp70) as an emerging drug target. J Med Chem 53:4585–4602
3. Hunt C, Morimoto RI (1985) Conserved features of eukaryotic hsp70 genes revealed by comparison with the nucleotide sequence of human hsp70. Proc Natl Acad Sci U S A 82:6455–6459
4. Dix DJ, Allen JW, Collins BW et al (1996) Targeted gene disruption of Hsp70-2 results in failed meiosis, germ cell apoptosis, and male infertility. Proc Natl Acad Sci U S A 93:3264–3268
5. Wacker JL, Huang SY, Steele AD et al (2009) Loss of Hsp70 exacerbates pathogenesis but not levels of fibrillar aggregates in a mouse model of Huntington's disease. J Neurosci 29:9104–9114
6. Tavaria M, Gabriele T, Kola I, Anderson RL (1996) A hitchhiker's guide to the human Hsp70 family. Cell Stress Chaperones 1:23–28
7. Ramos C (2011) Molecular chaperones and protein quality control. Protein Pept Lett 18:100
8. Mayer MP, Bukau B (2005) Hsp70 chaperones: cellular functions and molecular mechanism. Cell Mol Life Sci 62:670–684
9. Powers MV, Jones K, Barillari C, Westwood I, van Montfort RL, Workman P (2010) Targeting HSP70: the second potentially druggable

heat shock protein and molecular chaperone? Cell Cycle 9:1542–1550

10. Swain JF, Dinler G, Sivendran R, Montgomery DL, Stotz M, Gierasch LM (2007) Hsp70 chaperone ligands control domain association via an allosteric mechanism mediated by the interdomain linker. Mol Cell 26:27–39
11. Powers MV, Clarke PA, Workman P (2009) Death by chaperone: HSP90, HSP70 or both? Cell Cycle 8:518–526
12. Massey AJ (2010) ATPases as drug targets: insights from heat shock proteins 70 and 90. J Med Chem 53:7280–7286
13. Qi R, Sarbeng EB, Liu Q et al (2013) Allosteric opening of the polypeptide-binding site when an Hsp70 binds ATP. Nat Struct Mol Biol 20 (7):900
14. Fewell SW, Day BW, Brodsky JL (2001) Identification of an inhibitor of hsc70-mediated protein translocation and ATP hydrolysis. J Biol Chem 276:910–914
15. Braunstein MJ, Scott SS, Scott CM et al (2011) Antimyeloma effects of the heat shock protein 70 molecular chaperone inhibitor MAL3-101. J Oncol 2011:232037
16. Propper DJ, Braybrooke JP, Taylor DJ et al (1999) Phase I trial of the selective mitochondrial toxin MKT077 in chemo-resistant solid tumours. Ann Oncol 10:923–927
17. Britten CD, Rowinsky EK, Baker SD et al (2000) A phase I and pharmacokinetic study of the mitochondrial-specific rhodacyanine dye analog MKT 077. Clin Cancer Res 6:42–49
18. Leu JI, Pimkina J, Frank A, Murphy ME, George DL (2009) A small molecule inhibitor of inducible heat shock protein 70. Mol Cell 36:15–27
19. Taguwa S, Frydman J (2015) The significance of Hsp70 subnetwork for Dengue virus life-cycle. Uirusu 65:179–186
20. Howe MK, Bodoor K, Carlson DA et al (2014) Identification of an allosteric small-molecule inhibitor selective for the inducible form of heat shock protein 70. Chem Biol 21:1648–1659
21. Fadden P, Huang KH, Veal JM et al (2010) Application of chemoproteomics to drug discovery: identification of a clinical candidate targeting hsp90. Chem Biol 17:686–694
22. Haystead TA (2006) The purinome, a complex mix of drug and toxicity targets. Curr Top Med Chem 6:1117–1127
23. Graves PR, Kwiek JJ, Fadden P et al (2002) Discovery of novel targets of quinoline drugs in the human purine binding proteome. Mol Pharmacol 62:1364–1372
24. Alwarawrah Y, Hughes P, Loiselle D et al (2016) Fasnall, a selective FASN inhibitor, shows potent anti-tumor activity in the MMTV-Neu model of HER2(+) breast cancer. Cell Chem Biol 23:678–688
25. Carlson DA, Franke AS, Weitzel DH et al (2013) Fluorescence linked enzyme chemoproteomic strategy for discovery of a potent and selective DAPK1 and ZIPK inhibitor. ACS Chem Biol 8:2715–2723
26. Zeng XC, Bhasin S, Wu X, Lee JG, Maffi S, Nichols CJ, Lee KJ, Taylor JP, Greene LE, Eisenberg E (2004) Hsp70 dynamics in vivo: effect of heat shock and protein aggregation. J Cell Sci 117:4991–5000

Chapter 7

A High-Throughput Screen for Inhibitors of the Hsp90-Chaperone Machine

Jason Davenport, Lakshmi Galam, and Robert L. Matts

Abstract

Hsp90 has emerged as a key chemotherapeutic target for the development of drugs for the treatment of cancer and neurodegenerative diseases. The shortcomings of many of the Hsp90 inhibitors that have made it to clinical trials have bolstered the need to identify new lead compounds with superior properties. Here, we describe a high-throughput screen for the identification of Hsp90 inhibitors based on the refolding of thermally denatured firefly luciferase.

Key words Hsp90, Co-chaperones, High-throughput screen, Firefly luciferase, Protein refolding

1 Introduction

In 1994, Whitesell and coworkers reported that the putative tyrosine kinase inhibitor geldanamycin did not directly inhibit v-src, but rather bound Hsp90 and inhibited its interaction with v-src: an interaction that is required for v-src to acquire its active conformation [1]. With this tool in hand, it rapidly became apparent that the numerous proteins involved in tumorigenesis required the action of Hsp90 to attain their functional conformation. Indeed, it was soon evident that there were Hsp90-dependent proteins that are represented in all six [2] [now eight [3]] hallmarks of cancer [4, 5]. Thus, Hsp90 became an exciting new druggable target for the treatment of cancer, as an Hsp90 inhibitor has that ability to incapacitate multiple oncogenic pathways simultaneously.

The binding and hydrolysis of ATP was demonstrated to be required for Hsp90 to facilitate the folding of Hsp90-dependent proteins, and geldanamycin and radicicol were demonstrated to bind to the ATP-binding site that was present in the N-terminal domain of Hsp90 and inhibits its function [6]. With the publication of the co-crystal structures of geldanamycin and radicicol bound to Hsp90's N-terminal domain [7], the pathway to rational drug

Stuart K. Calderwood and Thomas L. Prince (eds.), *Chaperones: Methods and Protocols*, Methods in Molecular Biology, vol. 1709, https://doi.org/10.1007/978-1-4939-7477-1_7,

design was opened, and numerous Hsp90 inhibitors were synthesized, based on the gelanamycin, radicicol, and purine scaffolds, among others. Several Hsp90 inhibitors have moved into more than 20 clinical trials, and while some limited efficacy has been observed in several trials [8], reports of ocular, hepato- and cardio-toxicity, and peripheral neuropathy have dampened the enthusiasm for Hsp90 as a drug target.

Thus, the search for less toxic and more efficacious Hsp90 inhibitors continues. Here, we describe an Hsp90-inhibitor screen that can be carried out in any laboratory with access to multichannel pipettors, and a luminescent plate reader using 96-well plates, which we have used to screen natural product libraries [9]. It can also be scaled to 384-well plates to screen large chemical libraries with the special equipment available at High Throughput Screening Core Facilities [10]. The advantage of this assay over assays that are based on inhibition of Hsp90's ATPase activity or displacement of fluorescent ligands from Hsp90's ATP binding pocket is that it can detect inhibitors that do not bind to Hsp90's ATP binding site, such as inhibitors that bind to the C-terminal domain of Hsp90 [10, 11], or inhibitors that target other components of the Hsp90 super-chaperone machine, such as Hsc70 or DNAJA1 [12–14].

2 Materials

2.1 Reagents

1. Rabbit reticulocyte 1:2, one volume of packed cell lysed in two volumes sterile deionized water (*see* **Note 1**) prepared as previously described [15–19].
2. D-Luciferin sodium salt and dithiothreitol (DTT) (*see* **Note 1**).
3. Recombinant firefly (*Photinus pyralis*) luciferase (*see* **Note 1**).
4. Molecular biology grade acetylated bovine serum albumin (BSA), Tricine, Triton X-100, ATP, coenzyme A trilithium salt, creatine phosphate, creatine kinase (Type I from rabbit muscle).
5. DMSO (sterile cell culture grade).

2.2 Stock Solutions

2.2.1 Stock Solutions for Preparing Native and Denatured Luciferase, Refolding Buffer and the Assay Buffer (AB) Are Made with Nano-Pure Deionized Water

1. Tricine–HCl (1 M, pH 7.8): sterile filtered and stored at 4 °C or −20 °C for short-term or long-term storage, respectively.
2. $MgSO_4$ (1 M): sterile filtered and stored at 4 °C.
3. Sodium EDTA (0.5 M, pH 8.0): sterile filtered and stored at 4 °C.
4. DTT (0.2 M): prepared fresh with deionized water the day of use.
5. ATP (0.1 M): prepared in deionized water and stored in 2.0 mL aliquots at −80 °C.

6. Coenzyme A, trilithium salt (40 mg/mL; 50 mM): prepared in deionized water and stored in 3 mL aliquots at −80 °C.
7. D-Luciferin, sodium salt (6.5 mg/mL; 20 mM): prepared in deionized water, snap frozen in liquid nitrogen, and stored in 3.5 mL aliquots at −80 °C.
8. Triton X-100 (10%): prepared in deionized water and stored at 4 °C.
9. Acetylated BSA (50 mg/mL): prepared in sterile deionized water and stored in 2 mL aliquots at −20 °C (*see* **Note 2**).
10. Tris–HCl (1 M, pH 7.8): prepared in deionized water, sterile filtered and stored at 4 °C.
11. $Mg(OAc)_2$ (1 M): prepared in deionized water, sterile filtered and stored at 4 °C.
12. KCl (1 M): prepared in deionized water, sterile filtered and stored at 4 °C.
13. Creatine Phosphate (0.1 M): prepared in sterile deionized water and stored in 5 mL aliquots at −20 °C
14. Creatine kinase (10 mg/mL): prepared in 50% glycerol and stored at −20 °C.

2.3 Compounds/ Drugs for Screening

Compounds purchased in 96-well plates at constant μg quantities were reconstituted to 1 mg/mL in sterile DMSO. Compounds purchased in 96-well plates at constant μmol quantities were reconstituted to 4 mM in sterile DMSO.

2.4 Rabbit Reticulocyte (RRL) Reagent

RRL dilution buffer: 25 mM Tris–HCl, pH 7.8 with 75 mM KCl. Prepare by diluting 2 mL of 1 M Tris–HCl (pH 7.8) and 7.5 mL of 1 M KCl into 100 mL in deionized water. RRL is rapidly thawed and three volumes of RRL is diluted with one volume of RRL dilution buffer (*see* **Note 3**), which is flash frozen and stored in liquid nitrogen.

2.5 Luciferase Reagent for the Preparation of Denatured Luciferase

Combine 0.25 mL 1 M Tricine–HCl pH 7.8, 80 μL 1 M $MgSO_4$, 2 mL 50 mg/mL acetylated BSA, 2 μL 0.5 M NaEDTA, and 5 mL deionized water. Add 5 mg luciferase to the mixture, and after the luciferase is dissolved add 1 mL 10% Triton X-100 and 2 mL of 50% glycerol and bring the final volume to 10 mL (*see* **Note 4**). The final concentrations of the components are: 25 mM Tricine–HCl (pH 7.8), 8 mM MgSO4, 0.1 mM NaEDTA, 10% glycerol, 1% Triton X-100, and 10 mg/mL acetylated BSA (referred to a stability buffer) and 0.5 mg/mL luciferase.

2.6 Refolding Assay Reagent

Combine 0.8 mL 1 M Tricine–HCl pH 7.8, 0.08 mL 1 M $MgSO_4$, 3 mL 1 M KCl, 1.2 mL 0.1 M ATP, 2 mL 0.1 M creatine phosphate, and 0.8 mL 10 mg/mL creatine kinase, and dilute to 10 mL

with deionized water. The final concentrations of the components are: 80 mM Tris–HCl, pH 7.7, 8 mM $Mg(OAc)_2$, 300 mM KCl, 12 mM ATP, and 20 mM creatine phosphate, and 0.8 mg/mL creatine phosphokinase. The denatured luciferase reagent for the refolding assay is prepared by adding 18.75 µL of the 0.5 mg/mL denatured luciferase solution (prepared as described in Subheading 3.1) to 1.5 mL of the refolding assay reagent (*see* **Note 5**).

2.7 Assay Buffer

Combine 7.5 mL 1 M Tricine–HCl, 2.4 mL 1 M $MgSO_4$, 60 µL 0.5 M NaEDTA, 1 mL 0.2 M DTT, 1.565 mL 20 mM D-luciferin, 1.28 mL 50 mM Coenzyme A, 0.66 mL 1 M ATP, 15 mL 1 M KCl, 10 mL Triton X-100, 20 mL Glycerol, and 3.5 mL DMSO and dilute to 100 mL with deionized water (*see* **Note 6**). The final concentrations of the components are: 75 mM Tricine–HCl, pH 7.8, 24 mM $MgSO_4$, 300 µM EDTA, 2 mM DTT, 313 µM D-luciferin, 640 µM coenzyme A, 660 µM ATP, 150 mM KCl, 10% (*v*/*v*) Triton X-100, 20% (*v*/*v*) glycerol, and 3.5% DMSO.

Assay buffer for native luciferase additionally contains 4 mg/L acetylated BSA.

2.8 Native Luciferase Reagent

Combine 0.25 mL 1 M Tricine–HCl pH 7.8, 80 µL 1 M $MgSO_4$, 2 mL 50 mg/mL acetylated BSA, 2 µL 0.5 M NaEDTA, 3 mL 10% Triton X-100, and 3 mL of glycerol and bring the final volume to 10 mL, then add 1 µL of non-denatured luciferase reagent prepared as described in 2.5 (*see* **Note 7**). The final concentrations of the components are: 25 mM Tricine–HCl, pH 7.8, 8 mM $MgSO_4$, 0.1 mM NaEDTA, 30% glycerol, 3% Triton X-100, 10 mg/mL BSA, and 50 ng/mL of native luciferase.

2.9 Negative Control Reagent

Combine 0.1 g Hemoglobin, 0.4 g BSA, 0.2 mL 1 M Tris–HCl pH 7.8, 1.5 mL 1 M KCl and dilute to 10 mL with deionized water. The final concentrations of the components are 1% (w/v) hemoglobin, 4% (w/v) BSA in 20 mM Tris–HCl pH 7.8, and 150 mM KCl (*see* **Note 8**).

2.10 Equipment

1. Water bath.
2. Lumac 3 M bioluminometer.
3. Lumacuvets from Celsis (Monmouth Junction, NJ).
4. Biohit multi-channel pipettors: 0.2–10 µL, and 5–100 µL.
5. Variable volume pipettors: 0.1–10 µL, 2–20 µL, 20–200 µL.
6. $LMax^{384}$ luminescence plate reader, Molecular Devices.

3 Methods

3.1 Preparation of Denatured Luciferase

1. Luciferase prepared as described in 2.5 is heated at 41 °C in a water bath with inversion of the tube several times a minute for the first 3 min to insure homogeneous heating.
2. Luciferase activity is measured before the 41 °C incubation, and at 1 min intervals by adding 0.1 μL of the luciferase mix to 50 mL of assay buffer in a lumacuvet, followed by a brief vortexing, and reading of light units for an integration time of 10 s in the Lumac 3M bioluminometer.
3. Once the luciferase activity reaches >1% of its original activity the mixture is placed on ice (*see* **Note 9**).

3.2 Preparation of Screening Plates

1. Thirty microliters of nano-pure deionized water are added to the wells of white 96-well plates using a multi-channel pipettor.
2. A 0.75 μL aliquot of DMSO is added to the first column (#1) of the plate, while the other 11 columns of the plate receive 0.75 μL of the drugs to be screen (either the 4 mM or 1 mg/mL concentrations) to give a concentration of the drugs of 100 μM or 25 μg/mL. The plates are mixed on a rotary shaker of 5 min.
3. Four wells (A–D) of the first column of each plate receive 15 μL of the hemoglobin/BSA negative control reagent and the second 4 wells (E–H) of column #1 receive 15 μL of RRL reagent (positive control) (*see* **Note 10**), while the other 11 columns of the plate receive 15 μL of RRL reagent using a multichannel pipettor. The plate is then mixed on a rotary shaker for 5 min.

3.3 Screening of the Drug Plates

1. While the plate is shaking, 1.5 μL of the refolding assay reagent is unthawed and 18.75 μL of thawed denatured luciferase reagent is added (*see* **Note 11**).
2. Fifteen microliters of the reagent is added to each well of the 96-well plate, and the plate is mixed on a rotary shaker for 5 min, and incubated at room temperature for 3 h. The final concentrations of the drugs are 12.5 μg/mL or 50 μM.
3. After the incubation, 60 μL of assay buffer is added to each well with a multichannel pipettor, the plate is placed in the LMax^{384} plate reader and agitated for mixing, followed by immediate reading of the plate reader with an integration time of 10 s (*see* **Note 12**).
4. Drug-induced inhibition of luciferase refolding is measured as % of the positive control.

3.4 Counter Screen for Direct Luciferase Inhibitors and Approximate IC_{50} for Drug-Induced Inhibition of Luciferase Refolding

1. Setup of the screening plates: For preparing serial dilutions of the drugs, 40 μL of deionized water is added to the first and seventh columns of a 96 well of the screening plate while the remaining ten rows received 30 μL. One microliter of the 16 drug stocks that were found to inhibit luciferase refolding by 66% or greater are pipetted into the first and seventh columns of the plate with each row (A–H) receiving a different drug (*see* **Note 13**). The wells were mixed by repeated drawing of the stock into and out of a multi-channel pipette, and then 10 μL were removed and pipetted into the adjacent columns wells (e.g., columns 2 and 8). This process was repeated until the first and last five adjacent columns have 1:3 serial dilutions of the drugs. Ten milliliters were removed from the sixth and 12th columns to give a final volume of 30 μL.
2. Screen for direct luciferase inhibitors: The effect of each compound on the activity of native luciferase is determined by the addition of 10 μL of native luciferase mix, followed by 5 min of mixing on a rotary shaker. Assay buffer that has been supplemented with 4 mg/mL BSA as described in 2.7 is then added, followed by immediately placing the plate in the LMax384 plate reader. The plate is agitated in the plate reader for mixing followed by an immediate read of the plate with a 10 s integration time.
3. Screening for the concentration of compound that inhibits luciferase refolding by 50% (IC_{50}): The concentration-dependent inhibition of luciferase refolding is carried out as described in Subheading 3.3. RRL reagent (15 μL) is dispensed into each well of the plate, the plate is shaken, followed by the addition of 15 μL of the denatured luciferase (refolding reagent) into each well. The plates are shaken, and then after a 3 h incubation 60 μL of assay buffer is added to each well and the plates are agitated in the plate reader and then read with an integration time of 10 s.

   A third plate is prepared by the addition of 30 μL of 2.5% DMSO in deionized water into the first three columns of the plate. Fifteen microliters of the hemoglobin/BSA negative control reagent is added to the wells of the first column, and 15 μL of the RRL reagent (positive control) is added to the wells of the second column. The denature luciferase refolding reagent (15 μL) is then added to each well of the first two columns and the plate is incubated at room temperature for 3 h. After 3 h, 10 μL of the native luciferase reagent is added to each well of the third column, followed by the addition of 60 μL of assay buffer to each well of the first two columns and 30 μL of assay buffer supplemented with 4 mg/mL BSA to each well of the third column. The plate is then placed in the plate reader, agitated and read immediately with a 10 s

integration time. The first column indicates the light unit produces upon 100% inhibition of luciferase refolding. The second column is used to calculate % inhibition of refolding, and the third column is used to calculate % inhibition of native luciferase: to detect drugs that directly inhibit luciferase (*see* **Note 14**). The data is graphed out in Graph Pad which calculates the estimated IC_{50} for each drug.

3.5 Secondary Screens

The results from the luciferase refolding screen only indicate that a compound has the potential to inhibit the Hsp90 chaperone machine. Secondary screens are required to demonstrate that the compound is an inhibitor of the Hsp90 chaperone machine. We have reviewed these criteria in a previous review article [20]. These criteria include but are not limited to the compounds: effects on cell proliferation/cytotoxicity; ability to deplete cells of Hsp90-dependent proteins; capacity to inhibit Hsp90-dependent activation of a client's biological activity; ability to alter Hsp90's conformation as measured by protease nicking; effects on the stability of client binding and interactions with co-chaperones; and ability to inhibit Hsp90's ATPase activity or to binding known inhibitors.

4 Notes

1. Green Hectares, GoldBio, and Promega have the most economical prices for the purchase of RRL, D-luciferin, and firefly luciferase.
2. Luciferase refolding rates vary with the grade of BSA used to make the reagent. Luciferase also aggregates in the presence of certain lots of BSA. We find the best results are obtained using molecular biology grade acetylated BSA.
3. RRL is rapidly thawed in a 30 °C water bath with continual mixing until only a small amount of frozen material is visible, to ensure that the RRL is never heated above 4 °C. Twelve milliliters of RRL diluted with 4 mL 25 mM Tris–HCl, pH 7.8 with 75 mM KCl will yield enough reagent to screen ten plates with reagent to spare. For one 96-well plate 1.5 mL is sufficient with 60 μL to spare. We flash freeze the RRL reagent in liquid nitrogen in 1.5 mL aliquots, or multiples thereof, depending on the size of the library we are planning to screen.
4. To completely solubilize luciferase, it is added to the buffer prior to the addition of the Triton X-100 and glygerol. The reagent can be stored in 0.125 mL aliquots that are flash frozen in liquid nitrogen and stored at −80 °C.
5. For one 96-well plate 1.5 mL of the refolding reagent is sufficient with 60 μL to spare. We flash freeze the reagent in liquid

nitrogen in 1.5 mL aliquots or multiple thereof, depending on the size of the library we are planning to screen, and store at −80 °C. Denatured luciferase is added to the reagent prior to the assay.

6. Six milliliters of the assay buffer is sufficient to assay 1 96-well plate. We flash freeze the reagent in liquid nitrogen in 6 mL aliquots or multiple thereof, depending on the size of the library we are planning to screen and store at −80 °C in light tight boxes. Luciferin is light sensitive, so tubes are covered with foil when removed for use to protect them from light.
7. Depending on the specific activity of the lot of native luciferase and the sensitivity of the plate reader used, the volume of native luciferase added to the 10 mL of reagent may need to be adjusted up or down. For one 96-well plate 1.5 mL of the native luciferase reagent is sufficient with 60 μL to spare. We flash freeze the reagent in liquid nitrogen in 1.5 mL aliquots or multiple thereof, and store at −80 °C.
8. We snap freeze the hemoglobin/ BSA negative control reagent in 0.15 mL aliquots, and store at −80 °C.
9. The time of incubation for the preparation of denatured luciferase is usually 10 min. However, the actual temperature and time used is very important. We have found that laboratory thermometers can vary by up to 1 °C, thus affecting the rate and degree of denaturation. Overly denatured luciferase will not refold, "under"-denatured luciferase will refold through an Hsp90-independent, Hsc70-dependent pathway. Therefore, we monitor the degree of denaturation to prevent having to discard an expensive reagent. The reagent is stored 0.1 mL aliquots, which are flash frozen in liquid nitrogen and stored at −80 °C.
10. The first column (#1) of the plates contains the negative control (no Hsp90-dependent refolding, A–D) and the positive control (no inhibition of Hsp90 refolding, E–H) that are used to calculate the Z value for the assay. RRL reagent is rapidly thawed in a 30 °C water bath with continual mixing until only a small amount of frozen material is visible, to ensure that the reagent never is heated above 4 °C. The reagent is then centrifuged at 25,000 × g for 20 min to remove any particulates. Dispensing of the RRL reagent generally takes less than 15 s. V-shaped trough containers the width of the multi-channel pipettors are used to contain the reagents for dispensing into the plates.
11. This volume of the denatured luciferase reagent is sufficient to screen one 96-well plate, and is scaled up if more plates are to be screened. Dispensing of the denatured luciferase reagent generally takes less than 15 s.

12. We predetermine in pilot assays that the rate of luciferase renaturation is linear over a 3 h time point, and that the glow phase of the luciferase reaction decays by less than 2% over the time required to read the 96-well plate [10]. Dispensing of the assay reagent generally takes less than 15 s. If multiple plates are being assayed, assay buffer is not added to the next plate until the reading of the first plate is complete.
13. A value of 66% inhibition is arbitrary, and the cutoff can be raised or lowered. We have used a cutoff of 60% [9] and 70% [10], previously.
14. Duplicate plates are made for the serial dilutions of the drugs, so that both the assays can be carried out in parallel. The plates for determining the ability of the drugs to directly inhibit luciferase activity are assayed, while the plates used to calculate the IC_{50} for each drug are incubating for the 3 h.

References

1. Whitesell L, Mimnaugh EG, De Costa B, Myers CE, Neckers LM (1994) Inhibition of heat shock protein HSP90-pp60v-src heteroprotein complex formation by benzoquinone ansamycins: essential role for stress proteins in oncogenic transformation. Proc Natl Acad Sci U S A 91:8324–8328
2. Hanahan D, Weinberg RA (2000) The hallmarks of cancer. Cell 100:57–70
3. Hanahan D, Weinberg RA (2011) Hallmarks of cancer: the next generation. Cell 144:646–674
4. Bishop SC, Burlison JA, Blagg BS (2007) Hsp90: a novel target for the disruption of multiple signaling cascades. Curr Cancer Drug Targets 7:369–388
5. Koga F, Kihara K, Neckers L (2009) Inhibition of cancer invasion and metastasis by targeting the molecular chaperone heat-shock protein 90. Anticancer Res 29:797–807
6. Grenert JP, Johnson BD, Toft DO (1999) The importance of ATP binding and hydrolysis by hsp90 in formation and function of protein heterocomplexes. J Biol Chem 274:17525–17533
7. Roe SM, Prodromou C, O'Brien R, Ladbury JE, Piper PW, Pearl LH (1999) Structural basis for inhibition of the Hsp90 molecular chaperone by the antitumor antibiotics radicicol and geldanamycin. J Med Chem 42:260–266
8. Neckers L, Workman P (2012) Hsp90 molecular chaperone inhibitors: are we there yet? Clin Cancer Res 18:64–76
9. Davenport J, Balch M, Galam L, Girgis A, Hall J, Blagg BS, Matts RL (2014) High-throughput screen of natural product libraries for hsp90 inhibitors. Biology (Basel) 3:101–138
10. Galam L, Hadden MK, Ma Z, Ye QZ, Yun BG, Blagg BS, Matts RL (2007) High-throughput assay for the identification of Hsp90 inhibitors based on Hsp90-dependent refolding of firefly luciferase. Bioorg Med Chem 15:1939–1946
11. Donnelly A, Blagg BS (2008) Novobiocin and additional inhibitors of the Hsp90 C-terminal nucleotide-binding pocket. Curr Med Chem 15:2702–2717
12. Thulasiraman V, Matts RL (1998) Luciferase renaturation assays of chaperones and chaperone antagonists. Methods Mol Biol 102:129–141
13. Thulasiraman V, Yun BG, Uma S, Gu Y, Scroggins BT, Matts RL (2002) Differential inhibition of Hsc70 activities by two Hsc70-binding peptides. Biochemistry 41:3742–3753
14. Uma S, Thulasiraman V, Matts RL (1999) Dual role for Hsc70 in the biogenesis and regulation of the heme-regulated kinase of the alpha subunit of eukaryotic translation initiation factor 2. Mol Cell Biol 19:5861–5871
15. Jackson RJ, Hunt T (1983) Preparation and use of nuclease-treated rabbit reticulocyte lysates for the translation of eukaryotic messenger RNA. Methods Enzymol 96:50–74
16. Matts RL, Hurst R (1992) The relationship between protein synthesis and heat shock proteins levels in rabbit reticulocyte lysates. J Biol Chem 267:18168–18174

17. Matts RL, Schatz JR, Hurst R, Kagen R (1991) Toxic heavy metal ions activate the heme-regulated eukaryotic initiation factor-2 alpha kinase by inhibiting the capacity of hemin-supplemented reticulocyte lysates to reduce disulfide bonds. J Biol Chem 266:12695–12702
18. Merrick WC (1983) Translation of exogenous mRNAs in reticulocyte lysates. Methods Enzymol 101:606–615
19. Schumacher RJ, Hurst R, Sullivan WP, McMahon NJ, Toft DO, Matts RL (1994) ATP-dependent chaperoning activity of reticulocyte lysate. J Biol Chem 269:9493–9499
20. Matts RL, Manjarrez JR (2009) Assays for identification of Hsp90 inhibitors and biochemical methods for discriminating their mechanism of action. Curr Top Med Chem 9:1462–1478

Chapter 8

Primary Colorectal Cells Culture as a Translational Research Model

Sheah Lin Lee, Nina Claire Dempsey-Hibbert, Dale Vimalachandran, Terence David Wardle, Paul A. Sutton, and John H.H. Williams

Abstract

Preclinical studies are an essential stage for any pharmacological agent hoping to make its way into clinical trials. An ideal preclinical model that can accurately predict clinical response does not exist and the best that the scientific community have at the moment is to select the most relevant study model pertaining to the disease of interest from those available, which includes: cell lines, animal models, and even in-silico methodology. Currently, there is a huge gap between preclinical and clinical trial results, indicating that there is much room for improvement in developing a better model to bridge the translational gap.

Key words Primary, Human, Colorectal, Carcinoma, Cells, Translational, Research model, Study , Hsp90 inhibitors

1 Introduction

Due to its involvement in tumorigenesis, the molecular chaperone HSPC1 (also known as Hsp90α) has garnered considerable interest as a pharmacological target in the last decade. Many preclinical studies have shown that HSPC1 inhibitors are effective either as single agents or in combination with other chemotherapeutic agents, leading to the progression of several HSPC1 inhibitors into clinical trials [1]. HSPC1 inhibitors have been tested in numerous Phase I and II clinical trials for various solid and non-solid tumors. However, positive clinical results have been few and far between. So far, two groups of patients showed positive results from trials with HSPC1 inhibitors—those with HER2 positive breast cancer or non-small cell lung carcinoma with ALK rearrangement [2, 3]. Despite the disappointing clinical trial results thus far, HSPC1 is still a very attractive target in cancer due to its ubiquitous role in chaperoning tumor-associated kinase activities, combined

Stuart K. Calderwood and Thomas L. Prince (eds.), *Chaperones: Methods and Protocols*, Methods in Molecular Biology, vol. 1709, https://doi.org/10.1007/978-1-4939-7477-1_8,

with its acceptable side effects profile. There are currently 19 phase I and II clinical trials involving HSPC1 inhibitors [4].

Finding a relevant in-vivo tumor model has been a challenge for preclinical studies testing the efficacy of anti-tumor activity. In-vitro cell-line culture provides researchers with a study model that is easily accessible, and has predictable growth and cell longevity. Cell lines have major drawbacks however: the effect of tumor micro-environment cannot be realistically studied and the genetic and epigenetic heterogeneity is not representative of a tumor [5]. Animal xenografts using either cell lines or primary tumors are also widely employed models in preclinical studies. The clinical situation can be better mimicked, especially for xeno-transplantable tumor, with predictive clinical outcome, taken directly from a fresh surgical sample [6, 7]. Although a superior study model, establishing a xenograft model is time and labor extensive and requires an animal facility. In addition, animals used in these tumor models are immunocompromised and thus lack the immunomodulation axis between host and tumor. Finally, most importantly, they are not human.

Colorectal cancer is an extremely heterogenous cancer with an estimated mutation incidence to be in the range 49–111 per tumor [8]. Since the publication of the landmark paper by Wood et al. (2007), it has been increasingly recognized that each tumor has a unique genomic profile, making the search for a preclinical model that accounts for this heterogeneity ever more important.

We propose here an alternative translation research model for the study of colorectal cancer that is relatively easy to set up and offers a varied, heterogenous population that has a closer resemblance to in-vivo tumor gene expression. Samples are checked for viability (Fig. 1) and for E-Cadherin expression (Fig. 2). Individual

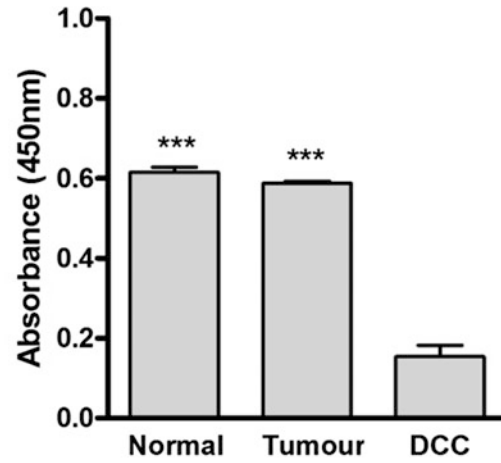

Fig. 1 MTS-based viability assay for colorectal tumor cells

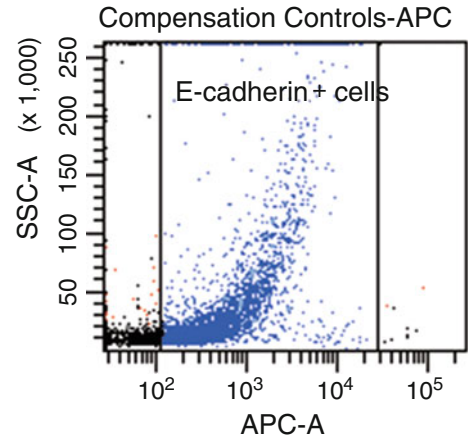

Fig. 2 E cadhedrin levels assayed by antibody staining and flow cytometry

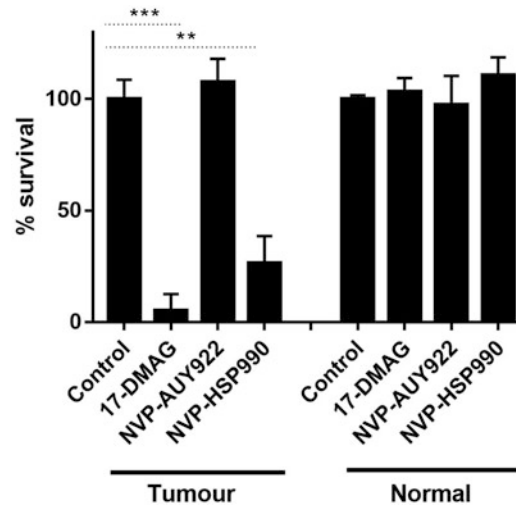

Fig. 3 Selective sensitivity to HSPC1 inhibitors of colorectal cells compared with normal mucosal cells

patient samples can be tested for sensitivity to agents targeting HSPC1, and in the example shown, the normal cells are not affected by HSPC1 inhibition, whereas the tumor cells are killed by DMAG and NVP-HSP990, but not NVP-AUY922 (Fig. 3). This ex-vivo human colorectal cell culture method is applicable to both normal and cancerous mucosal cells, making it an essential model system for testing anti-tumor agents. In the case of heat shock protein studies, comparisons of the effects of HSPC1 inhibitors between normal and cancer cells can be made using this model, which make it a highly desirable system.

2 Materials

2.1 Primary Cell Culture

1. 15 ml centrifuge tube.
2. 50 ml centrifuge tube.
3. Sterile cell strainer (40 μM nylon mesh).
4. 96-well cell culture cluster 3595.
5. Sterile disposable scalpel.
6. Forceps.
7. Hank's Balance Salt Solution (HBSS). *Gibco Life Technologies*. Cat no: 14,060–040.
8. Antibiotic Antimycotic Solution. Sigma-Aldrich. Cat no: A5955.
9. Minimal Essential Medium Eagle with L-Glutamine (EMEM). Lonza. Cat no: BE12-611F.
10. Trypsin Versene EDTA. Lonza. Cat no: BE-17-161E.
11. 10× Red Cell Lysis Buffer. *Dissolve ammonia chloride (8.02 g), sodium bicarbonate (0.84 g) and EDTA disodium (0.37 g) in 50 ml of distilled water. Store at 4 °C.*

2.2 Cell Viability Assay

1. Minimal Essential Medium Eagle with L-Glutamine (EMEM). Lonza. Cat no: BE12-611F.
2. MTS working solution. *1 ml of PES solution (0.0092 g in 10 ml of DPBS) added to 20 ml of MTS solution (0.042 g of MTS powder diluted in 21 ml of DPBS), pH adjusted to 6.5. Store in −20 °C.*
3. Methylated spirit Industrial 70%. Fisher scientific. Cat no: 11482874.

2.3 Flow Cytometry

1. 96-well V-bottom plate.
2. Trypsin Versene EDTA. Lonza. Cat no: BE-17-161E.
3. Dulbecco's Phosphate-Buffered Saline (DPBS). Cat no: BE1513F.
4. APC anti-human CD324 (E-cadherin). Biolegend. Cat no: 324108.
5. Wash Buffer. *5% of FBS in DPBS. Made up fresh each time.*
6. 4% Paraformaldehyde (PFA). *Dilute PFA (2 g) and 5 M NaOH (100 μl) in 40 ml of PBS and heat at 56 °C until PFA is dissolved. Adjust to pH 7.4 and made up final volume of 50 ml with PBS. Store at 4 °C.*

2.4 Equipment

1. Universal High Speed Centrifuge Z323K. HERMLE-LaborTechnik.

2. Roller mixer SRT1. Stuart.
3. Synergy TM HT Multi-Detection Microplate Reader. BioTek.
4. BD FACSCantoTM Flow Cytometer. BD Biosciences.

3 Methods

3.1 Primary Cell Culture

All the colorectal cell samples were obtained from Countess of Chester Hospital, United Kingdom, from the year of 2013 to 2014. Ethical approval was granted by National Research Ethics Service (NRES) Committee North West—Chester (REC reference: 12/NW/0011).

1. From each patient, the surgeon collects four 5 × 5 × 5 mm pieces of normal and cancerous cells from the mucosal surface immediately after surgical resection. Normal cells should be collected at the surgical resection margin furthest away from the tumor, whereas cancerous cells are to be collected from the visible tumor (*see* **Notes 1** and **2**).

   HINT: care must be taken to preserve the surgical resection margin.

2. Submerge specimens immediately in 2 ml of HBSS and transport to the laboratory within 30 min.
3. Transfer specimens onto a petri dish and wash three to five times with 10% antibiotic in EMEM. Immerse specimens in an antibiotics solution for 2 min between each wash (Fig. 4).
4. Further dissect each piece of specimen into smaller pieces of 1 mm × 1 mm × 1 mm and transfer them into a 15 ml

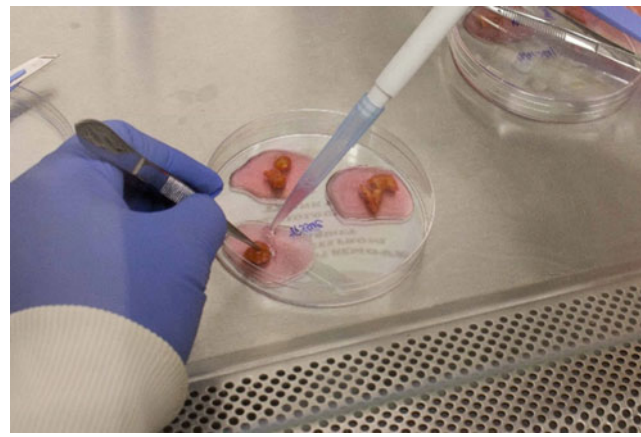

Fig. 4 Washing the human colorectal tumor samples in EMEM

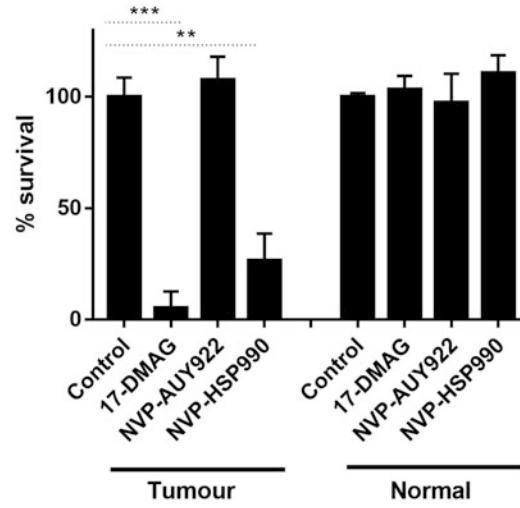

Fig. 5 Passing the tumor trypsin digests through a cell strainer to remove undigested materials

centrifuge tube. Submerge specimens in 10% antibiotics in EMEM at all time.

HINT: keep specimens wet at all stages.

5. Centrifuge specimens at 500 × *g* for 5 min.
6. Discard the supernatant and resuspend specimens in 3 ml of Trypsin EDTA.
7. Incubate specimen for 100 min at room temperature on a roller mixer, agitating the sample every 10–15 min.
8. Centrifuge specimens at 500 × *g* for 5 min.
9. Discard the supernatant (Trypsin EDTA) and resuspend specimens in 10% antibiotics diluted in EMEM.
10. Pass the specimens through a cell strainer to remove remaining undigested materials.

    HINT: Place cell strainer over a 50 ml centrifuge tube (Fig. 5).

11. Collect the single-cell suspension in a 15 ml test tube and centrifuge at 500 × *g* for 5 min.
12. Remove the supernatant and resuspend the cells in 1% antibiotics in EMEM.

Note: If traces of red blood cells were observed, remove the supernatant and resuspend the cells in a lysing solution (prepared as above) for 6 min at room temperature. Centrifuge the specimen at 500 × *g* for 5 min after the lysing process and follow **step 12**.

13. The cells are now ready to be plated at a density of 30,000 cells/well in a 96-well plate and culture at 37 °C in an atmosphere of 95% air and 5% carbon dioxide for 48 h.

3.2 Cell Viability Assay

1. Create dead cell control by submerging the cells in 10% Industrial Methylated Spirit for 2 h.
2. Gently pipette culture media off and add 100 μl EMEM to each well.
3. Add 20 μl of MTS working solution to each well and mix gently.
4. Incubate the cells at 37 °C for 1 h before analyzing on a microplate reader at absorbance of each well at 450 nm.
5. Cell viability analysis in normal and tumor cell as shown in Fig. 3, compared to dead cell control (DCC) (*see* **Note 3**).

3.3 Flow Cytometry

1. Gently pipette culture media off cells and add 100 μl of Trypsin EDTA to each well for 1 min at room temperature.
2. Remove Trypsin EDTA and add another 100 μl of Trypsin EDTA to each well for another 5 min at 37 °C.
3. Add 200 μl of DPBS to each well and mix well. Transfer the cells to a 96-well V-bottom plate.
4. Centrifuge the plate at 500 × *g* for 5 min. Remove the supernatant.
5. Add 100 μl of wash buffer to each well and incubate for 15 min at room temperature.
6. Centrifuge the plate at 500 × *g* for 5 min. Remove the supernatant.
7. Add 4 μl of APC anti-human CD324 (E-cadherin) to each well and incubate at 4 °C for 45 min.
8. Add 100 μl of wash buffer to each well.
9. Centrifuge the plate at 500 × *g* for 5 min. Remove the supernatant.
10. Add 100 μl of 4% PFA. Mix well and incubate at room temperature for 10 min.
11. Add 100 μl of DPBS to each well.
12. Centrifuge the plate at 500 × *g* for 5 min. Remove the supernatant.
13. Add 100 μl of DPBS to each well. Store at 4 °C until analysis.
14. E-cadherin analysis on a tumor sample as shown in Fig. 4.

4 Notes

1. The viability of the cells improves if they are removed from the surgical specimen as soon as possible following resection. Reduced viability is mostly likely due to ischaemic insult to tumor cells once the blood supply to tissues is compromised. While awaiting transport to the lab, the samples should be completely submerged in HBSS and kept submerged at all time. For optimal results, all the samples should be processed on the same day instead of leaving overnight in the laboratory.
2. Microbial overgrowth is an important complication in primary colorectal cell culture. Therefore, the combination and concentration of antibiotics will affect the final result.
   (a) The antibiotic antimycotic solution used in this method contains penicillin, streptomycin, and amphotericin B. This is different from the method described by Failli et al. [9], who used penicillin, streptomycin, gentamicin, amphotericin B, and metronidazole. The reason for using a different combination of antibiotics is due to known inhibition of HSPA1A activity by gentamicin [10]. As HSPA1A, a cytoprotective protein, is believed to confer resistance to HSPC1 inhibitor, gentamicin was avoided.
   (b) This method used 10% antibiotics solution (penicillin 1000 IU/ml, streptomycin 1 mg/ml, amphotericin B 2.5 μg/ml) to wash and suspend the specimens during the disaggregation process and 1% antibiotics for primary cell culture (48 h). In this series, the infection rate was only 9.5% (2/21 samples), showing that a low concentration of antibiotics is sufficient anti-microbial therapy for most samples. However, it is essential to wash specimens thoroughly before dissection.
3. As tumor cells are not selected in this method, other cells, especially immune cells present in the tumor microenvironment, can also be present in the cell culture. Therefore, it is vital to confirm that epithelial cells are present in abundance by using an epithelial cell marker prior to further experiment. In this method, E-cadherin was used to select colorectal epithelial-derived cells. However, there are advantages of having immune cells present in the culture, allowing for investigations of tumor-associated immune cells in the samples.

References

1. Hong DS et al (2013) Targeting the molecular chaperone heat shock protein 90 (HSP90): lessons learned and future directions. Cancer Treat Rev 39(4):375–387
2. Modi S et al (2011) HSP90 Inhibition is effective in breast cancer: a phase II trial of tanespimycin (17-AAG) plus trastuzumab in patients with HER2-positive metastatic breast cancer

progressing on trastuzumab. Clin Cancer Res 17(15):5132–5139

3. Socinski MA et al (2013) A multicenter phase II study of ganetespib monotherapy in patients with genotypically defined advanced non-small cell lung cancer. Clin Cancer Res 19 (11):3068–3077
4. National Cancer Institute. *Clinical Trials Search Results*. 2016 [cited 2016 11 December]
5. Young M, Ordonez L, Clarke AR (2013) What are the best routes to effectively model human colorectal cancer? Mol Oncol 7(2):178–189
6. Fichtner I et al (2008) Establishment of patient-derived non–small cell lung cancer Xenografts as models for the identification of predictive biomarkers. Clin Cancer Res 14 (20):6456
7. Fichtner I et al (2004) Anticancer drug response and expression of molecular markers in early-passage xenotransplanted colon carcinomas. Eur J Cancer 40(2):298–307
8. Wood LD et al (2007) The genomic landscapes of human breast and colorectal cancers. Science 318(5853):1108–1113
9. Failli A et al (2009) The challenge of culturing human colorectal tumor cells: establishment of a cell culture model by the comparison of different methodological approaches. Tumori 95 (3):343–347
10. Yamamoto S et al (2010) Gentamicin inhibits HSP70-assisted protein folding by interfering with substrate recognition. FEBS Lett 584 (4):645–651

Chapter 9

Cell Death and Survival Assays

Alexander E. Kabakov and Vladimir L. Gabai

Abstract

Heat shock proteins are well-known protectors from cell death. Cell death (in particular, apoptosis and necrosis) is accompanied by certain hallmarks manifested as specific alterations in cellular membranes, cytoplasm, nucleus, and mitochondria. Some of those hallmarks are easily detectable in situ and, therefore, they can be applied for the assessment of dying or dead cells. In turn, there are also signs of viable cells that include such features as normal functioning of their membranes and organelles, ability to proliferate, etc. This chapter describes several convenient methods for quantification of dead (apoptotic and necrotic) cells as well as methods for assessment of viable cells. We describe in detail methods of annexin V/propidium iodide (PI) staining, TUNEL assay, Hoechst/PI staining, caspase activation, MTS tetrazolium, lactate dehydrogenase (LDH) release, colony formation, and senescence assays, with the principles, advantages, and drawbacks of each technique.

Key words Apoptosis, Necrosis, Annexin V, TUNEL, Caspase, Colony formation assay, Tetrazolium assay, LDH release assay, Senescence

1 Introduction

It is generally accepted that heat shock proteins (HSPs) are "cell-death determinants" that affect molecular pathways resulting in cell survival or death. Consequently, up- or downregulation of the HSP expression or activities may determine the outcome of pathophysiological insults or some cytotoxic treatments by either promoting or preventing cell death (*see* [1–3] for review).

Researchers working in the field of cellular stress and HSPs often need to quantify the cell death/survival under stressful conditions. Furthermore, many pharmacologists and oncologists want to test the efficacy of tumor cell killing by chemotherapy or radiotherapy, and human tumors with the enhanced HSP expression are known to be more resistant to anticancer drugs and radiation exposure [4, 5]. The present chapter describes several popular assays for quantification of cell death/survival in multiple samples. This material may be especially useful as a set of practical

Stuart K. Calderwood and Thomas L. Prince (eds.), *Chaperones: Methods and Protocols*, Methods in Molecular Biology, vol. 1709, https://doi.org/10.1007/978-1-4939-7477-1_9,

recommendations for performing cell death/survival tests in terms of the HSP-related basic studies or medical applications.

Recently, new forms of cell death have been described, such as programmed necrosis (necroptosis), pyroptosis, mitotic catastrophe, autophagic cell death, etc. [6]. Although assays for these forms of cell demise are out of scope of this chapter, described here methods for quantification of basic cell viability (MTS and clonogenic assays) can be applied to them as well.

2 Materials

2.1 Annexin V and Propidium Iodide Assay

1. Dulbecco's phosphate-buffered saline (PBS, pH 7.4).
2. FITC-annexin V.
3. Binding buffer 10×: 0.1 M HEPES/NaOH, pH 7.4; 1.4 M NaCl; 25 mM $CaCl_2$.
4. 50 μg/ml Propidium Iodide 10× (PI).
5. Tubes for a fluorescence-activated cell sorter (FACS).

2.2 TUNEL Assay

1. 4% paraformaldehide.
2. 70% ice-cold ethanol.
3. TdT reaction buffer (5×); 1 M potassium or sodium cacodylate, 125 mM Tris–HCl, pH 6.6, 1.25 mg/ml BSA (store at −20 °C).
4. F-dUTP final concentration—2 mM.
5. Terminal deoxynucleotidyl Transferase (TdT).
6. Propidium Iodide (PI) 10× (50 μg/ml).
7. 24-Well plastic tissue culture plates.
8. Fluorescent microscope.

2.3 Hoechst 3342 and Propidium Iodide Assay

1. Hoechst 33342 100× stock solution in PBS (100 μg/ml).
2. Propidium iodide (PI) 100× stock solution in PBS (500 μg/ml).
3. Fluorescent microscope.

2.4 Caspase 3 Immunodetection Assay

1. Phosphate-buffered saline (PBS) with pH 7.2–7.4.
2. PBS containing 0.05% Tween-20 (PBS-T).
3. Lysis buffer: 50 mM Tris–HCl, pH 7.2, 250 mM NaCl, 0.1% NP-40, 2 mM EDTA, 10% glycerol.
4. Laemmli sample buffer.
5. Polyacrylamide and sodium dodecylsulfate (SDS).
6. Protein molecular mass standards for SDS-electrophoresis.

7. Nitrocellulose or polyvinylidene difluoride (PVDF) membranes adsorbing polypeptides.
8. Transfer buffer: 25 mM Tris, 190 mM Glycine, 20% methanol, pH 8.3.
9. Kits with "primary" antibodies recognizing either the procaspase-3 fragments or the PARP fragment(s) in Western Blotting and with respective "secondary" antibodies conjugated with horseradish peroxidase.
10. Appropriate reagents and equipment for vertical electrophoresis in slabs, electro-transfer, ECL-development of blots, films, or imaging devices.

2.5 MTS Assay

1. MTS /PMS ready-to-use solution can be purchased as CellTiter 96 Aqueous One Solution Cell Proliferation Assay (Promega). This solution can be stored long term for at −20 °C, protected from light, and thawed immediately before use. For frequent use, the solution may be stored at 4 °C, protected from light, for up to 6 weeks.
2. 96-well tissue culture plates.
3. Tissue culture incubator with a 5% CO_2 atmosphere.
4. 96-well plate reader capable of monitoring absorbance at 490 nm.

2.6 LDH Release Assay

1. Substrate mix, assay buffer, lysis solution, and stop solution are components of CytoTox 96® Non-Radioactive Cytotoxicity Assay (Promega).
2. 96-well plates.
3. Centrifuge with adaptor for 96-well plates.

2.7 Senescence Assay

1. Dulbecco's phosphate-buffered saline (PBS, pH 7.4).
2. Fixative, staining, X-gal, Solutions A and B are component of senescence beta-galactosidase staining kit (Cell Signaling).
3. Fixative Solution**:** Dilute the 10× Fixative Solution to a 1× solution with distilled water. You will need 1 ml of the 1× solution per 35 mm well.
4. Staining Solution**:** Redissolve the 10× Staining Solution by heating to 37 °C with agitation. Dilute the 10× staining solution to a 1× solution with distilled water. You will need 930 µl of the 1× Staining Solution per 35 mm well.
5. X-Gal: IMPORTANT**:** Always use *polypropylene* plastic or glass to make and store X-gal. Do not use polystyrene. Dissolve 20 mg of X-gal in 1 ml DMF to prepare a 20 mg/ml stock solution. Excess X-gal solution can be stored in −20 °C in a light-resistant container for up to 1 month.

6. β-Galactosidase Staining Solution: For each 35 mm well to be stained, combine the following in a polypropylene container: 930 μl 1× Staining Solution (*see* **item 3**), 10 μl 100× Solution A, 10 μl 100× Solution B, and 50 μl 20 mg/ml X-gal stock solution (*see* **item 4**).
7. Dimethylformamide.
8. 35 mm cell culture plates.
9. Polypropylene tubes.
10. Dry incubator *without* CO_2.

2.8 Clonogenic Assay

1. Dulbecco's phosphate-buffered saline (DPBS, pH 7.4), Trypsin-EDTA (0.05%), Crystal Violet, Ethanol (190 Proof).
2. Prepare 0.5% Crystal Violet solution in 70% ethanol (v/v). Use gloves during preparation to avoid staining or hands. This solution is stable for at least a month at room temperature.

3 Methods

3.1 Determination of Fractions of Apoptotic and Necrotic Cells by Staining with Labeled Annexin V and Propidium Iodide (PI)

Annexin V conjugated to a fluorescent label (e.g., FITC) or biotin is used to determine the fraction of cells within a population that are undergoing apoptosis. This method is based on the property of cells to lose membrane asymmetry at the early stage of apoptosis. In apoptotizing cells, the membrane phospholipid phosphatidylserine (PS) is translocated from the inner leaflet of the plasma membrane to the outer leaflet, thus exposing PS at the cell surface [7, 8]. Annexin V is a 35–36 kDa Ca^{2+}-dependent phospholipids-binding protein that has a high affinity to PS; therefore, this feature can be exploited for identifying apoptotic cells with exposed PS [8, 9] (*see* **Note 1**).

Importantly, the loss of membrane integrity which accompanies necrotic cell death would lead to total accessibility of membrane PS for binding to annexin V; thus, staining with fluorochrome-labeled annexin V is usually used in combination with a vital dye. Propidium iodide (PI) is a standard red-fluorescent probe enabling distinguishing viable cells from the dead ones. Viable cells with the intact plasma membrane exclude PI, whereas the membranes of dead (necrotic) cells are permeable to PI and such "cell corpses" become stained by red. The PI intercalates into the major groove of double-stranded DNA (and double-stranded RNA) and produces a highly fluorescent adduct with excitation at 488 nm and with a broad emission peaked around 600 nm. The excitation of PI at 488 nm facilitates its use with benchtop cytometers. (PI can also be excited in the UV range (351–364 nm from an argon laser) which should be taken into account when performing multicolor analysis on the multi-beam

cell sorters.) The red fluorescence of PI is well combined with the green fluorescence of FITC-annexin V in routine double-label FACS analysis of cell death. If some of the cells are stained with FITC-annexin V while being negative for PI, they undergo apoptosis. In turn, the cells positive for both FITC-annexin V and PI undergo necrosis (virtually, they are already dead). Finally, the cells negative for both PI and FITC-annexin V are considered alive (i.e., no measurable apoptosis or necrosis at the moment). An example of the FACS analysis is shown in Fig. 1.

1. Harvest cells, wash twice in PBS (4 °C), and resuspend at a concentration of 1×10^6 cells/ml in the 1× binding buffer.
2. Aliquot the cells (100 μl) into FACS tubes and add 5 μl FITC-Annexin V and/or 10 μl PI.
3. Mix gently and incubate for 15 min at room temperature in the dark.
4. Add 400 μl of the binding buffer to each tube and analyze immediately by flow cytometry on FACS.

Recommended samples for measurements and controls to set up compensation and quadrants:

1. Cells + FITC-annexin V.
2. Cells + PI.
3. Cells + annexin V + PI.

3.2 Visualization of Apoptotic Cells by TUNEL Assay

Terminal Transferase dUTP Nick End Labeling (TUNEL) assay is a method for in situ detection of DNA degradation in apoptotic cells because one of the hallmarks of late phases of apoptosis is the fragmentation of nuclear chromatin, which leads to an appearance of a multitude of 3′-hydroxil ends within broken DNA strands [12]. This can be used to identify apoptotic cells by labeling the nuclear DNA breaks with biotin- or fluorescein-tagged deoxyuridine triphosphate nucleotides (F-dUTP) [13]. The enzyme terminal deoxynucleotidyl transferase (TdT) catalyzes a template-independent addition of deoxyribonucleoside triphosphates to the 3′-hydroxil ends of double- or single-stranded DNA. As the apoptotic pathway generates numerous DNA breaks with exposed 3′-hydroxil ends, the TdT reaction serves to label these nuclear DNA break sites with F-dUTP. The labeled (apoptotic) cells are visualized on a fluorescent microscope as cells with heterogeneously stained (green) nuclei. The TUNEL technique reveals only apoptotic cells, while total cell numbers in each viewed preparation are also required to calculate a percentage of apoptosis. PI staining can be used for this purpose: after routine fixing and permeabilizing steps followed by the PI treatment, all cells are rendered red (PI-positive) and well visible in any microscope field taken for analysis (*see* **Note 2**).

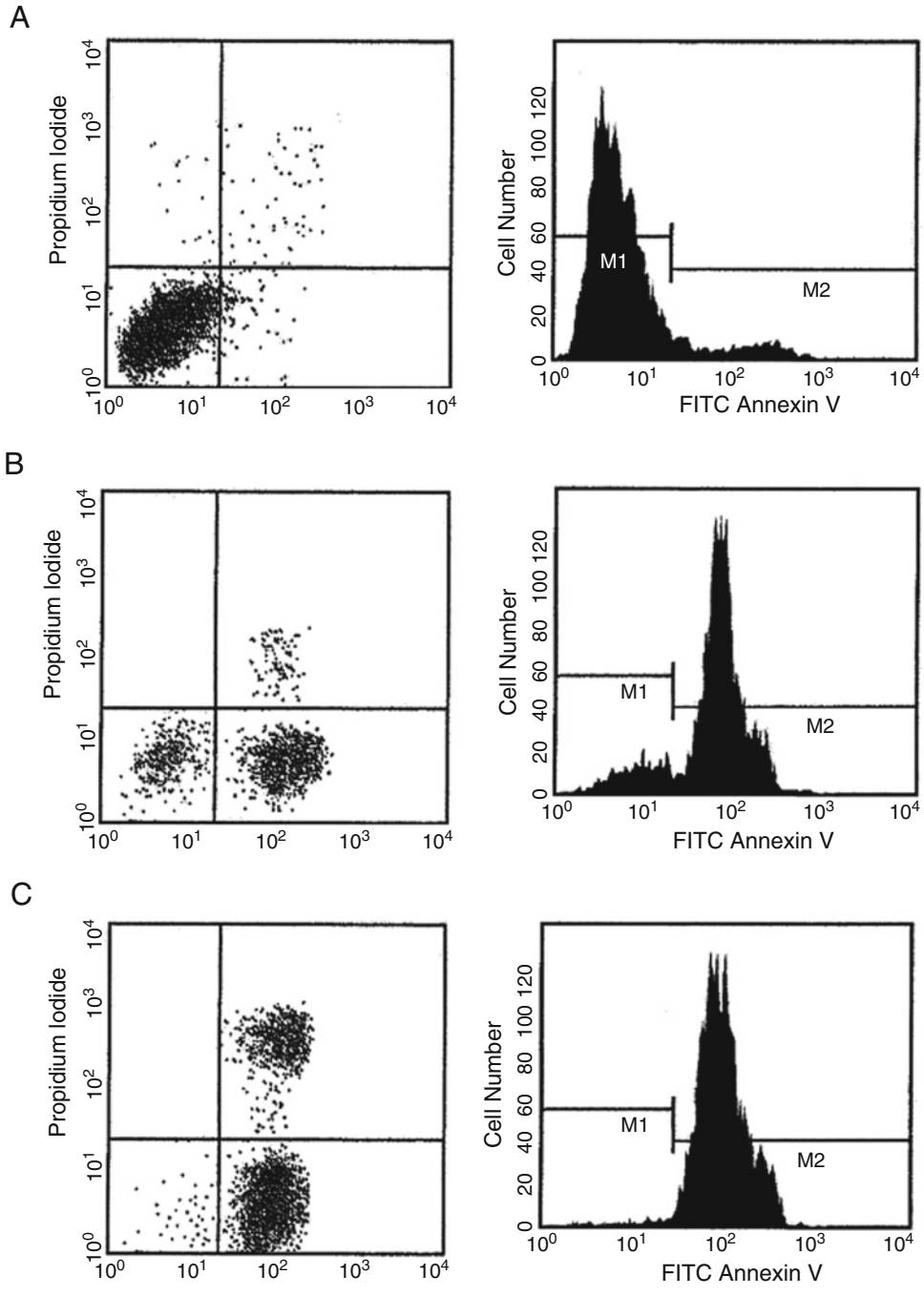

Fig. 1 Flow cytometric analyses of the cell death determination with FITC-annexinV and propidium iodide (PI). This figure demonstrates how this method was used to compare cancer cell death following treatment with 10 nM taxol (a cytostatic and apoptosis-inducing anticancer agent) or co-treatment with 10 nM taxol and 100 nM 17AAG (an inhibitor of the HSP90 chaperone activity). Since 17AAG is able to sensitize malignant cells to chemo-radiotherapy (*see* [4, 5, 26] for review), it was expected that this HSP90 inhibitor will enhance the cytotoxic effect of taxol on leukemic HL-60 cells. In fact, while 100 nM 17AAG was low-toxic for these cells

Instead of (or in addition to) F-dUTP, the deoxythymidine analog 5-bromo-2′-deoxyuridine 5-triphosphate (BrdUTP) can also be used as a substrate in the TdT reaction to label the DNA break sites. Once incorporated into the nuclear DNA ends, BrdU can be detected with an anti-BrdU antibody and standard immunofluorescence techniques. As compared with a use of F-dUTP alone, an approach with BrdUTP/anti-BrdU yields an enhancement of fluorescence thanks to the additional (antibody conjugate-conferred) labeling.

Non-apoptotic cells do not incorporate much of the F-dUTP or BrdUTP labels owing to the absence of large amounts of the exposed 3′-hydroxil ends in their nuclear DNA. If determination of necrotic cells is also required in the same cell preparation, pre-staining with PI is possible before the fixing step. The TUNEL assay is performed on fixed bio-material, so that this method is equally applicable for both tissue sections and cell culture samples. However, the TUNEL procedure for staining of tissue sections requires more controls and additional treatments (*see* Ref. [13]).

1. Grow cultures of adherent cells in 24-well plastic plates (or onto coverslips placed into such plates) and treat them by an apoptosis-inducing stimulus.
2. Wash the adherent cells twice with PBS.
3. Fix the cells by the addition of 5 ml of 4% paraformaldehyde and incubate on ice for 15 min.
4. Again wash the cells twice in PBS.
5. Permeabilize the cells by addition of ice-cold ethanol (70%) for at least 4 h on ice. (In the fixed state, the cells may be stored for several weeks in 70% ethanol at −20 °C.)
6. Wash fixed cell preparations in PBS and add 100 µl of TdT reaction solution: 20 µl TdT reaction buffer, 2 mM F-dUTP, 20 U TdT, 19 µl $CoCl_2$ (10 mM), 67 µl H_2O.

Fig. 1 (continued) (data not shown), the increased cytotoxicity in the case of co-treatment (10 nM taxol + 100 nM 17AAG) as compared with the effect of 10 nM taxol alone is clearly seen in (**b**) and (**c**). Leukemic HL-60 cells were either untreated (**a**) or incubated with 10 nM taxol (**b**), or with 10 nM taxol + 100 nM 17AAG (**c**). After 20 h incubation with the drug(s), the cells were stained with FITC-annexin V/PI and analyzed by flow cytometry. About 99% of the untreated cells (**a**) were FITC-annexin V- and PI-negative, thus indicating that they are viable and not undergoing apoptosis or necrosis. A major part of the cells treated with taxol alone (**b**) was undergoing apoptosis (FITC-annexin V-positive) and the minor cell fraction has already died (PI-positive), while many cells remained still viable. In the case of co-treatment taxol + 17AAG (**c**), the enhancement of cytotoxicity is seen: almost no viable cells remained and there is a considerably increased fraction of the already dead (PI-positive) cells. The *left panels* show a distribution of the stained cell subpopulations, while the *right panels* show the intensity of FITC fluorescence per cell

7. Incubate the cells for 40 min at 37 °C with occasional shaking (or at room temperature overnight).
8. Wash with PBS.
9. Add 1 ml of PI-staining solution, incubate for at least 30 min at room temperature in the dark.
10. Analyze on a microscope for FITC/PI fluorescence with appropriate controls.

3.3 Detection of Apoptotic and Necrotic Cells by Staining with Hoechst 33342 and PI

Apoptotizing cells exhibit characteristic morphology of their nuclei that are due to the apoptotic pathway-induced alterations in chromatin and nuclear matrix [12]. This morphology of the apoptotic nuclei seems hard to detect by light microscopy, but it is clearly seen on a fluorescent microscope after staining of cell samples with a chromatin-targeting fluorescent probe (e.g., Hoechst, acridine orange, etc.). In particular, Hoechst 33342 is a well-known fluorescent probe that brightly stains chromatin in cell nuclei; therefore, this blue-fluorescence-dye enables revealing the apoptosis-related alterations in the chromatin state. Among the morphological signs of apoptosis there are such typical as condensation (clumping) and/or fragmentation of chromatin within the nuclear compartment, and shrinking or fragmentation of the whole nucleus. All these patterns are easily recognized in a fluorescent microscope as abnormalities in the nucleus size or shape, heterogeneous staining of the nucleus with an appearance of extremely bright zones and/or unusual dark zones, formation of a brightly stained rim adjacent to the nuclear envelope, splitting the nucleus body, etc. In contrast, the most of non-apoptotic cells have normal morphology of their nuclei which are homogenously stained with Hoechst 33342 (*see*, for example, Fig. 2).

It seems very convenient to use double-label staining with Hoechst 33342 and PI because blue fluorescence of the former and red fluorescence of the latter are nicely combined and enable detecting both the fraction of apoptotic cells and the fraction of necrotic (PI-positive) cells within the same cell preparation. Overall, this is a relatively simple method, especially as compared with the annexin V staining or the TUNEL assay (*see* **Note 3**).

1. Add Hoechst 33342 (final concentration—1 μg/ml) and PI (final concentration—5 μg/ml) to the cells and incubate for 30 min in the dark at 37 °C.
2. View and photograph (as digitized color images) the stained cell preparations in a fluorescent microscope displaying Hoechst 33342/PI fluorescence.
3. Upon analyzing each stained preparation, count all cells with apoptotic nuclei and all PI-positive (necrotic) cells within 10–20 occasionally chosen microscopic fields.

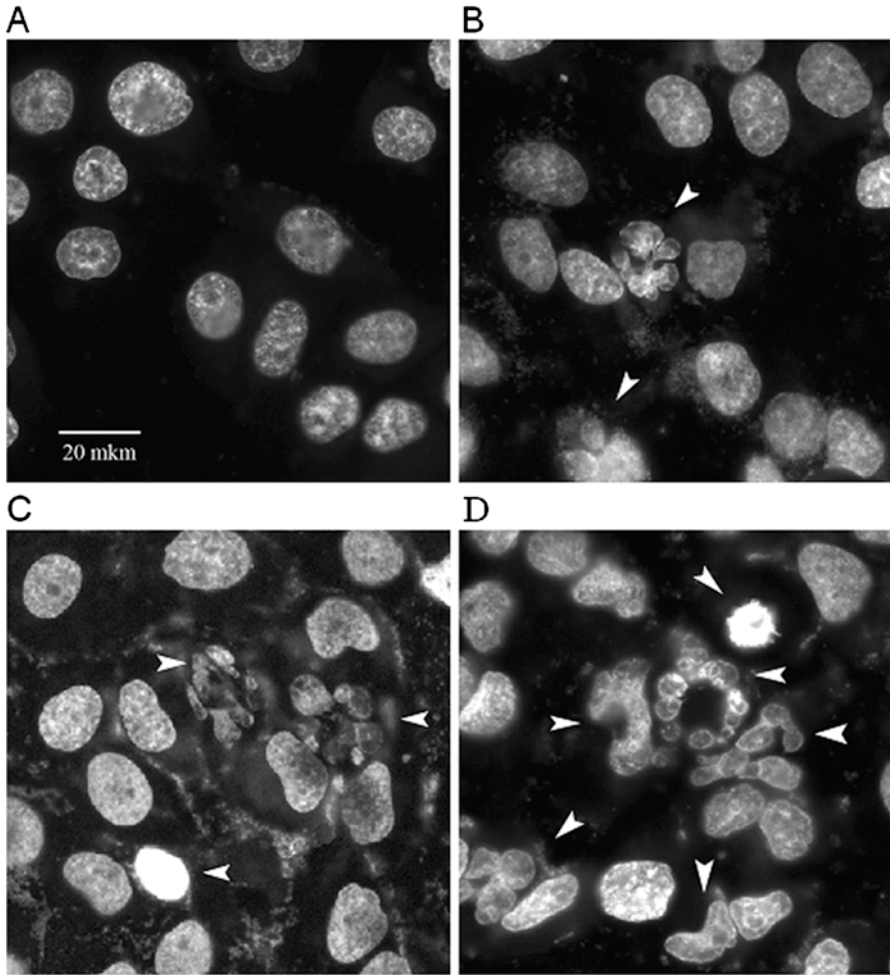

Fig. 2 Visualization of apoptotic nuclei in culture cell preparations by staining with Hoechst 33342. This figure illustrates how the staining with Hoechst 33342 was employed on an in vitro model of tumor cell thermosensitization. HeLa cells derive from a cervical tumor and are known to be thermoresistant [25]. To overcome their thermoresistance we used an approach with joint inhibition of both the chaperone activity of constitutively expressed HSP90 and the de novo induction of HSPs that occurs in the treated cells. The HSP90 chaperone activity and the de novo HSP induction were inhibited by simultaneously treating the cells with 200 nM 17AAG [26] and 40 nM triptolide [27] respectively. An evidence for either inhibitory action came from the results of immunoblotting (not shown). The treated cells and control samples were stained with Hoechst 33342 (1 μg/ml) and photographed on a fluorescent microscope. As compared with untreated control (**a**) or effects of hyperthermia (43 °C for 60 min) alone (**b**), or effect of the combined hyperthermia + triptolide (**c**), the cell sample exposed to all the three treatments (hyperthermia + 17AAG + triptolide) displays the greater number of apoptotic nuclei (**d**) thus confirming the fact of thermosensitization. Adherent HeLa cells were untreated (**a**) or subjected to hyperthermia (43 °C for 60 min) (**b**), or double treatment: 200 nM 17AAG + hyperthermia (**c**), or triple treatment: 200 nM 17AAG + 40 nM triptolide + hyperthermia (**d**). 24 h after the treatments, the non-fixed cells were incubated with Hoechst 33342 (1 μg/ml) for 30 min and then analyzed on a fluorescent microscope. The *arrows* denote typical apoptotic nuclei with fragmented chromatin or abnormal shape, or abnormal brightness. One can see the thermosensitizing effect of the triple treatment (**d**) when a conjunction of hyperthermia with simultaneous inhibition of the HSP90 chaperone activity (by 17AAG) and HSP induction (by triptolide) enhances apoptosis

3.4 Immunodetection of the "Lethal" Activation of Caspase-3

Caspases are known as a family of ubiquitous cysteine proteases playing a key role in the mechanism of caspase-dependent apoptosis [15]. Different caspases are activated and act in early and late stages of apoptosis; in particular, caspase-3 is an executive enzyme whose activation finalizes the apoptotic signal leading to ultimate cleavage of a set of certain intracellular proteins and thus resulting in cell death. It is generally accepted that the caspase-3 activation is a lethal event for the affected cell; thus determination of caspase-3 activity can assess the apoptotic death intensity in cells or tissues.

There are convenient and simple methods to detect active caspase-3 in biosamples using specific antibodies: such immunodetection allows revealing either products of the site-specific cleavage of pro-caspase-3 or products of the caspase-3-executed proteolysis of one of its relevant substrates, poly (ADP-ribose) polymerase (PARP). In unaffected cells, procaspase-3 exists in an inactive form with apparent MW (molecular weight) of 32 kDa. During apoptotic execution this pro-enzyme splits at aspartate residues into its large (apparent MW 17 kDa) and small (apparent MW 12 kDa) fragments that form a hetero-tetramer possessing the proteolytic activity [16]. Both these fragments can easily be detected by Western Blotting with respective antibodies (*see* Fig. 3a and protocols below). Furthermore, active caspase-3 begins to quickly split its protein substrates including PARP, a DNA repair-assisting enzyme with MW of 116 kDa. As a result of the caspase-3-executed cleavage, PARP divides into the two characteristic fragments with apparent MW of 85 and 25 kDa; presence of these PARP fragments is considered a hallmark of caspase-dependent apoptosis [17]. Similarly to the situation with cleavage of procaspase-3, the PARP fragments are easily immunodetected in Western Blotting (*see* Fig. 3b, and the protocols below) and this simple method enables assessing the levels of apoptosis in many samples of cells or tissues. Using polyacrylamide gels with appropriate density gradients (e.g., 6–22%) it is possible to obtain blots with the well-separated fragments of both procaspase-3 and PARP from one gel slab. Furthermore, the same blot can be probed with other antibodies of interest.

At present, several companies offer various kits with antibodies specifically recognizing both fragment(s) of procaspase-3 and PARP as well as the respective "secondary" antibodies conjugated to peroxidase and reagents for development of immunoreactive protein bands onto blots with the enhanced chemiluminiscence (ECL) technique. Such commercially available products can be used for comparative evaluation of the apoptotic cell death by immunoblotting of cell lysates or tissue extracts (*see* below). There are also convenient modern devices for the advanced development of antibody-treated blots that allow us to digitize and quantify images of the relevant fragments of procaspase-3 and/or PARP developed with the ECL; in these cases, it seems possible to

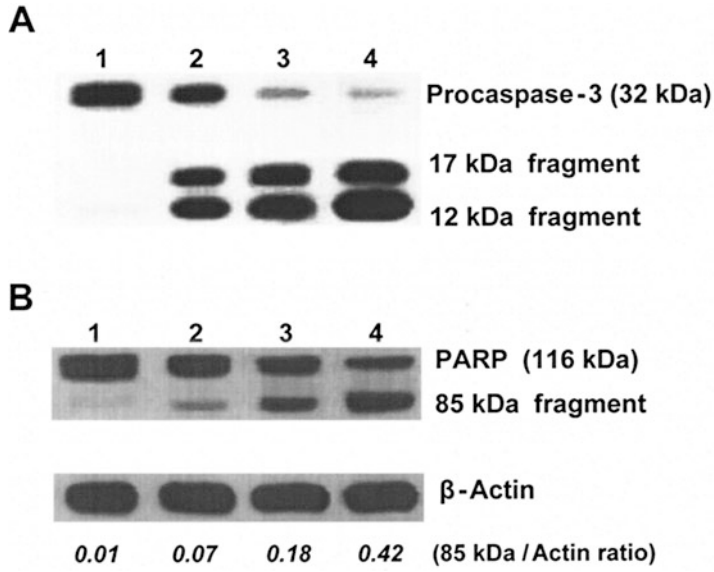

Fig. 3 Track-images in the ECL-developed blots showing how the detection of the active form of caspase-3 (**a**) and/or one of products of its activation—the 85 kDa fragment of PARP (**b**) can help to assess the level of apoptosis in treated tumor cell populations. Jurkat (human lymphoma) cells were cultured under normal conditions as control (*lanes 1*) or exposed to a low dose (3 Gy) of γ-photons (*lanes 2*). Some cell samples were subjected to hyperthermia (43 ° C for 1 h) before the radiation exposure (*lanes 3*) and in other samples, the cells underwent the same pre-irradiation hyperthermia in the presence of 40 μM quercetin, an inhibitor of the HSP induction (*lanes 4*). 24 h after the irradiation, the cells were lysed, fractioned in SDS-electrophoresis, and explored in Western Blotting with antibodies to procaspase-3, PARP, and β-actin. The ECL-developed images of the protein bands were analyzed on a double-dimension scanner and quantified on the basis of their area and darkness. It is clearly seen how the pretreatments enhance apoptosis in the irradiated cells: the small (17 and 12 kDa) fragments of procaspase-3 become upregulated in the cell samples experienced hyperthermia or (with the stronger effect) hyperthermia in the presence of quercetin as compared with the cell samples merely irradiated. The same can be said regarding the PARP cleavage: the disappearance of the intact PARP band and emergence of the 85 kDa fragment indicate the enhancement of apoptosis as a result of the radiosensitizing action of hyperthermia (*lanes 3*), especially when the heat-induced upregulation of anti-apoptotic HSPs is blocked by quercetin (*lanes 4*). The actin bands were developed for control of protein loading and also for relative evaluation of the apoptosis levels. The numbers at the bottom of actin blot represent the 85 kDa PARP fragment/actin band ratio calculated for each sample and these data reflect the apoptotic cell fractions in it

quantitatively assess the apoptosis level/dynamics because the area/intensity of either developed fragment band will positively correlate with amounts of apoptotizing cells within cell populations taken for analysis (*see* Fig. 3 as an example).

In addition, there is a method for immunostaining of apoptotic cells in situ using specific polyclonal antibodies to the large (17 kDa) fragments of procaspase-3, the so-called Cleaved Caspase-3 (Asp175) Antibody (Cell Signaling). Similarly, antibody specifically interacting with the 85 kDa C-terminal fragment of PARP can stain apoptotic cells in tissue sections (*Anti-PARP p85*

Fragment pAb, Promega). Such immunostaining based on in situ revealing cells with active caspase-3 can be used in combination with the TUNEL staining (*see* above) for more reliable quantification of apoptotic cells (*see* **Note 4**).

1. After washing the harvested cells or tissue homogenates three times with PBS, re-suspend them in 5–10× volumes of the ice-cold lysing buffer with appropriate protease inhibitors. Incubate it at +4 °C with rotating for 30 min, then sonicate for 10 s.
2. Centrifuge the tubes with lysates at 12,000 × *g* for 10 min at 4 °C and then transfer the supernatants to other tubes. Determine the protein concentration in the supernatants and add the ice-cold lysing buffer to make solutions with protein concentration approximately 8 μg/μl.
3. Mix the solutions with equal volumes of Laemmli sample buffer.
4. Boil the samples for 3 min and then centrifugate. Load 10 μl of each sample per lane in a 1 mm thick SDS-polyacrylamide gel and perform electrophoresis under Laemmli conditions.
5. Using a semi-dry system for electro-transfer, blot the separated proteins from the gels onto nitrocellulose or PVDF membranes (*see* the manufacturer's manual for the precise transfer procedure).
6. To block the residual protein-binding activity pre-incubate the membranes with PBS containing 1–3% fat-free milk for 2 h at room temperature or overnight at +4 °C.
7. Incubate the membranes with "primary" antibodies diluted in PBS containing 1% fat-free milk for 1 h at room temperature or overnight at +4 °C (the antibody concentration will depend on conditions).
8. Wash the membranes with PBS-T (5 min × three times) and then incubate the membranes with respective "secondary" antibodies conjugated to peroxidase and diluted (1: 5000–10,000) in PBS containing 1% fat-free milk for 1 h at room temperature.
9. Wash the membranes with PBS-T (5 min × three times); then wipe the excess buffer from the membranes and incubate the membrane with the mixture of ECL reagents for 1 min.
10. Remove the extra reagents from the membranes by dabbing with paper towel, seal it in plastic wraps, and expose it to an X-ray film in a dark room for 1–15 min.
11. Develop the film according to recommended procedures to obtain the protein band tracks (conditions for the exposure and development may vary). Alternatively use an imaging device to obtain a digital image.

3.5 Assay of Cell Viability by MTS Tetrazolium Compound

There are several widely used assays based on ability of live, but not dead cells to reduce tetrazolium compounds; it leads to the formation of colored formazan products which can be measured by a spectrophotometer. Here, we describe assay based on MTS [3-(4,5-dimethylthiazol-2-yl)-5-(3-carboxymethoxyphenyl)-2-(4-sulfophenyl)-2H-tetrazolium, inner salt], which in the presence of electron coupling reagent phenazinemethosulfate (PMS) is reduced by cells into formazan product. The main advantage of this assay compared to other similar assays (e.g., widely used MTT assay) is that the MTS/PMS colored formazan product is soluble in a standard tissue culture medium and can be measured directly in a 96-well assay plate without additional processing (i.e., solubilization of insoluble formazan product as in the MTT assay). This advantage is especially important when it is necessary to perform fast screen of toxicity of a large number of compounds, or monitor cell viability in a real time. Tetrazolium compounds including MTS are believed to be reduced mainly by mitochondrial electron transport chain; therefore, these assays actually measure metabolic activity of cells, not death per se. Because of this, the tetrazolium-based assay can be used in long-term experiments to assess cell proliferation along with viability (*see* Notes below). However, when used in short-term experiments (less than 24 h incubation with compounds), these assays can be employed for the determination of cell viability since the dead cells have damaged mitochondria and cannot reduce tetrazolium compounds (*see* **Note 5**).

This protocol is for the measurement of cell viability of attached cells in 96-well plates, but the assay can be used for suspension cultures and in larger or smaller size of plates.

1. Seed the cells in a 96-well plate to achieve approximately 50% confluency before the addition of tested compounds. Leave some wells empty (without cells, only with medium) as a blank control.
2. Incubate the cells with compounds of interest for certain time (up to 24 h, *see* Notes below).
3. At the end of incubation, add 1/10 volume of MTS/PMS One Solution Reagent (e.g., 20 μL to 200 μL of medium) to all wells including blank control.
4. Incubate the plates at 37 °C in humidified, 5% CO_2 atmosphere for 1–4 h to allow color development. Check color formation starting from 1 h. The time of incubation strongly depends on cell line used and should be adjusted experimentally.
5. Record the absorbance at 490 nm using a 96-well plate reader.
6. Calculate cell viability using absorbance in control (untreated) cells as 100%, and absorbance in blank wells without cells as 0%.

3.6 LDH Release Assay

This method is based on a property of dead cells to release its cytosolic glycolytic enzyme lactate dehydrogenase (LDH) into the medium due to plasma membrane permeabilization as a result of cell death. Released LDH in culture supernatants is measured with a 30 min coupled enzymatic assay, which results in the conversion of a tetrazolium salt into a red formazan product. The amount of color formed is proportional to the number of dead cells, and absorbance data are collected using a standard 96-well plate reader. There are several advantages of the assay. First, it can be applied to large-scale screening of cytotoxic compounds which is time-consuming with microscopic assays (trypan blue, eosin, propidium iodide). Second, compared with the MTS assay, this method can quantify only really dead (necrotic, or late apoptotic) cells rather than cells stopping to proliferate (e.g., senescent cells), or early apoptotic cells which keep their plasma membrane intact. Third, this assay may be used as an alternative to radioactive (^{51}Cr) cell cytotoxicity assay broadly employed in immunological studies, but this is out scope of this chapter.

1. Incubate the cells in a 96-well plate with studied compounds (*see* **Note 6**).
2. One hour prior supernatant harvest, add Lysis solution (10×) to assess maximum LDH release.
3. Collect supernatants after centrifugation at 250 × *g* for 5 min.
4. Transfer 50 μl of the supernatant from each well of the assay plate to the corresponding well of a flat-bottom plate using a multichannel pipette.
5. Reconstitute Substrate Mix using Assay Buffer. Add 50 μl of the reconstituted Substrate Mix to each well of the plate using the multichannel pipette. Cover the plate and incubate at room temperature, protected from light, for 30 min. Substrate mix can be stored at −20 ° C for 6–8 weeks.
6. Add 50 μl of the Stop Solution to each well of the plate and record absorbance at 490 nm.
7. Determine % cell death (cytotoxicity) using the formula:
   % cell death = Experimental LDH release (OD490)/Maximum LDH release (OD490).

3.7 Senescence Assay

Although senescence is not considered per se as a form of cell death, it is important for the assessment of the effect of anticancer treatment. Cancer cells, although able to divide indefinitely, can nevertheless undergo senescence upon exposure to certain anticancer drugs and radiation therapy. In fact, it seems that activation of the senescence program and consequent permanent growth arrest significantly contributes to the loss of the clonogenic capacity of tumor cells and probably to tumor regression after anticancer

therapy [18]. Interestingly, knockdown of inducible Hsp70 even in the absence of cytotoxic insults can cause senescence rather than apoptosis or necrosis in various tumor cells, whereas normal cells are resistant to this [19, 20].

There are several manifestations of senescence which can be assessed, but the most popular assay is β-galactosidase assay. It was found that during replicative senescence both in vitro and in vivo cells started to express acid β-galactosidase, but such an expression was absent in quiescent or terminally differentiated cells [21]; later this assay was adapted for broad range of cells and treatments. To assess β-galactosidase activity, the cells first are fixed with formaldehyde/glutaraldehyde, and incubated with a solution of X-gal (5-bromo-4-chloro-3-indolyl β-D-galactoside) at pH 6.0 and a mix of potassium ferrocyanide and potassium ferricyanide to maintain proper redox conditions. Although all these components are commercially available, we routinely use a prepared kit (senescence β-galactosidase staining kit) from Cell Signaling (*see* **Note 7**).

1. Remove growth media from the cells.
2. Rinse the plate once with 1× PBS (2 ml for 35 mm well plate).
3. Add 1 ml of 1× Fixative Solution to each 35 mm well. Allow the cells to fix for 10–15 min at room temperature.
4. Rinse the plate two times with 1× PBS.
5. Add 1 ml of the β-Galactosidase Staining Solution to each 35 mm. Important: Seal the plate with parafilm to prevent evaporation. Evaporation can cause crystals to form.
6. Incubate the plate at 37 °C at least overnight in a dry incubator (no CO_2). Note: The presence of CO_2 can cause changes to the pH which may affect staining results.
7. While the β-galactosidase is still on the plate, check the cells under a bright-field microscope (200× total magnification) for the development of blue color.
8. Count the cells in several random fields to have total number of at least 200 cells. Calculate fraction (percentage) of blue-stained (senescent cells).

3.8 Clonogenic Assay

It now appears that apoptosis is the major form of cell demise mainly in lymphoid cells, whereas in epithelial cells and fibroblasts clinically relevant doses of genotoxic drugs or radiation do not cause significant apoptosis, necrosis, or authophagic cell death. Instead, they may cause either growth arrest leading to DNA repair and cell survival, or, if DNA repair is unsuccessful, it leads to mitotic catastrophe or premature senescence (*see* Refs. [18, 22, 23] for review). Numerous in vitro studies clearly demonstrated that mitotic catastrophe and/or senescence rather than apoptosis are the main cause of elimination of epithelial tumor cells of different

origin [23, 24]. As a combined measure of different modes of cell death the most reliable method is apparently a clonogenic assay, since it measures the ability of a cell to divide and form a colony. Therefore, this assay is basically independent of the way how the cells are killed (e.g., by apoptosis, necrosis, autophagic cell death, mitotic catastrophe, or some other mechanism), and senescent cells cannot form colonies as well. Invented more than five decades ago, this assay is still a "gold standard" for the evaluation of cell sensitivity to radiation and various anticancer drugs, and there is a good correlation between clonogenic ability of cells in vitro and tumor response in vivo. Of note, however, that only fraction of cells (usually around 10–40%) of untreated tumor population can form colonies, i.e., divide indefinitely, but obviously this dividing cell subpopulation (which may be related to stem cells capacity) is the most important for tumor growth and its sensitivity to drugs and radiation (*see* **Note 8**).

Although the clonogenic assay may be adapted for suspension culture, here we will describe its most common application for attached cells.

1. Wash control and treated cells in DPBS, add Trypsin-EDTA (0.2–0.25 ml per 35 mm plate), and incubate at 37 °C for several min completely detach cells.
2. Add growth medium to the plates and resuspend the cells using pipetting to have final volume of 1 ml.
3. Count cell number using hemocytometer, or some other cell counting device.

   Place different dilutions of cells on 60 mm plates. For most cell lines, it should be between 200 and 1000 cells plated in control (without treatments). If you expect that your treatment significantly reduces number of surviving cells, you should plate a larger number of treated cells (starting from 10-fold up to 1000-fold). The main idea is that number of forming colonies should not be too high (it will be difficult to count), or too low (it will increase error). Optimal number of colonies per 60 mm plate should be 20–100 depending on cell line.
4. Incubate the plates with cells under their optimal conditions of growth for 6–14 days checking size of colonies in control (untreated cells) starting from day 6. When colonies will reach size of more than 50 cells (i.e., cells divide more than six times, $2^6 = 64$), remove the medium and stain formed colonies with Crystal Violet Solution for 5 min. Remove the staining solution with an aspirator and wash several times with DPBS to remove background staining.
5. Count colonies in control and treated cells manually or making pictures and using special software programs. Only colonies

containing more than 50 cells (i.e., relatively large) should be counted.

Calculate cell survival by taking into account number of seeded cells and initial clonogenic ability of control cells. For example, if in control 200 cells give 40 colonies (colony-forming units, CFU) and after treatment 400 cells give 10 CFU, cell survival (or survival fraction) after treatment will be 10/400: 40/200 = 0.125, or 12.5%.

4 Notes

1. The described method of FITC-annexin V staining followed by flow cytometric analysis is suitable mainly for non-adherent cell types (e.g., leukocytes/lymphocytes, suspension cell cultures, etc.). This is absolutely inapplicable for tissue sections and this is not a routine procedure for adherent cell types (e.g., HeLa, NIH 3T3, etc.) because specific membrane damage may occur during EDTA/trypsin treatments, cell detachment, and harvesting. Nonetheless, techniques that adapt the annexin V staining for flow cytometry on adherent cell types have also been reported [10, 11]. Another point of concern is that Ca^{2+} ions in an incubation medium can promote cell-to-cell sticking and aggregation, thus complicating performance of flow cytometric analysis. Herein, periodical vortexing and/or gentle resuspending by pipettes of each cell sample can minimize the problem of cell aggregation.
2. The exact incubation times for fixation, permeabilization, and TdT reaction for the TUNEL assay may vary depending on cell type; in some cases, it may be necessary to empirically optimize all these parameters for certain types of cells and applications. Also, remains of apoptotic cells are sometimes phagocytosed by neighboring (viable) cells [14] which, being viable prior to the fixation/staining procedure, afterward seem TUNEL-positive through TdT/dUTP targeting to the phagocytosed apoptotic nuclear fragments; such "false apoptotic" cells can, however, be identified by the presence of their own full-size and TUNEL-negative nuclei.
3. Sometimes, mitotic cells stained with Hoechst 33342 may resemble the apoptotic cells, therefore some experience needed to distinguish them. Also, a vast variety of patterns of the apoptotic nuclei complicate the use of standard image-analyzing software, while visual analysis of many samples is rather hard physically and may be biased. Finally, the cells with the high activity of drug-efflux pumps (e.g., overexpressing *MDR1* gene) are also poorly stained.

4. (a) A described "lethal" caspase-3 activation is not an attribute of all types of cell death. In particular, this method is inapplicable for the caspase-independent apoptosis, necrotic cell death, necroptosis, etc.

   (b) Sometimes, the short (17 and 12 kDa) fragments of procaspase-3 are poorly detected in Western Blotting because they, being more mobile, already go through the membrane into the Transfer buffer, whereas the longer (32 kDa) molecules of intact procaspase-3 are yet adsorbed onto the membrane. In such a situation, it is possible to "catch" the short fragments onto the second strip of the membrane placed immediately behind the first one. Besides, using of gradient gels (4–20%) can attenuate this problem by equalizing the rate of transferring for short and long polypeptides.

   (c) To be sure to recognize the relevant fragments, it is recommended to use positive control (e.g., lysates of Jurkat or HL60 cells previously exposed to any apoptosis inducers). Likewise, for better control of the protein load it is recommended to perform Western Blotting of the same samples (or reblot the membranes) with an antibody to β-actin (*see* Fig. 3b) or tubulin, or glyceraldehyde 3-phosphate dehydrogenase.

5. (a) MTS assay, although convenient, cannot discriminate between apoptosis, necrosis, or other forms of cell death. It works as cytotoxicity assay only for short-term incubations with compounds of interest. If used for longer time periods (more than 24 h), cytostatic, rather than cytotoxic effects of compounds, would lead to decreased formazan formation compared with control just because of decreased cell number due. For instance, if the cells multiply once every 24 h, after 72 h incubation cell number in control will increase eight-times (2^3); therefore, eight-times lower reading in treated cells would not mean that 7/8 of population of them are dead—they just stopped dividing (e.g., due to quiescence or senescence, *see* **Note 7** below). This decrease in formazan formation, however, is often considered in the literature as a loss of cell viability, which is basically incorrect.

   (b) Optimal absorbance in control (untreated) cells should be in the range 0.3–1.0 OD; therefore, cell number and incubation time should be adjusted accordingly.

   (c) Since the MTS assay measures metabolic activity of cells, some compounds (e.g., mitochondrial inhibitors) may interfere with the assay (decreasing or increasing formazan formation) without affecting actual cell viability.

(d) As with all the colorimetric assays, it may not be suitable for assessing toxicity of some colored compounds which absorb in the same wavelength (around 490 nm) as formazan. If the absorption of the compounds at this wavelength is not very high, such interference can be partially avoided by including additional wells containing only compounds + MTS/PMS (without cells) and using them as blank control.

6. (a) Two main factors in cell cultivation media can contribute to background absorbance: phenol red from media and LDH from animal serum. To correct for these factors, separate wells containing medium without cells should be included. Another option is to use phenol red—free medium and lower concentration of serum (e.g., 5%) which usually does not affect cell viability.

   (b) To assess sensitivity and linearity of the assay, LDH from the kit can be used as a positive control by making its serial dilution. If experimental OD490 values are above linear range of plate reader, shorter incubation time and/or lower cell numbers are recommended.

7. (a) Due to variations in water pH, be sure that the β-Galactosidase Staining Solution has a final pH of 6.0+/−0.1. pH differences can affect staining: a low pH can result in false positives and high pH can result in false negatives. If necessary, use HCl or NaOH to adjust pH.

   (b) Intensity of staining depends on cell density—it is lower at low density and higher at high density.

   (c) Time of staining is also important—it may vary from 16 to 48 h. It is also depends on size of plates; therefore, 35 mm plates are recommended. All these parameters should be adjusted for each cell culture, but basically under same conditions the assay is reproducible enough.

8. Although the clonogenic assay is the most sensitive and reliable method for assessing cell death/survival, it has some limitations. By definition it cannot be used for nondividing (differentiated) cells (e.g., lymphocytes, hepatocytes, cardiomyocytes, etc.) since these cells cannot form colonies at all. Some proliferating cell lines also may have poor colony-forming ability (less than 5–10%) which also makes these cell lines less convenient for this assay. It is also labor and time consuming since it takes at least 1–2 weeks to obtain results. Clonogenic ability of cell lines may differ significantly, so it may be necessary to adjust concentration of seeded cells to achieve statistically reliable results. Some cells are poorly attached and need fixation (e.g., by 4% paraformaldehyde for 10 min) before staining. Precise counting of cells before plating is critical for the assay. Especially clamping of cells before counting should be avoided by intense pipetting and vortexing.

References

1. Garrido C, Schmitt E, Cande C, Vahsen N, Parcellier A, Kroemer G (2003) HSP27 and HSP70: potentially oncogenic apoptosis inhibitors. Cell Cycle 2(6):579–584
2. Beere HM (2005) Death versus survival: functional interaction between the apoptotic and stress-inducible heat shock protein pathways. J Clin Invest 115(10):2633–2639
3. Yamashima T (2012) Hsp70.1 and related lysosomal factors for necrotic neuronal death. J Neurochem 120(4):477–494. https://doi.org/10.1111/j.1471-4159.2011.07596.x
4. Calderwood SK, Khaleque MA, Sawyer DB, Ciocca DR (2006) Heat shock proteins in cancer: chaperones of tumorigenesis. Trends Biochem Sci 31(3):164–172
5. O'Callaghan-Sunol C, Gabai VL (2007) Involvement of heat shock proteins in protection of tumor cells from genotoxic stresses. In: Calderwood S, Sherman MY, Ciocca DR (eds) Heat shock proteins in cancer, 1st edn. Springer, New York, pp 169–190
6. Galluzzi L, Vitale I, Abrams JM, Alnemri ES, Baehrecke EH, Blagosklonny MV, Dawson TM, Dawson VL, El-Deiry WS, Fulda S, Gottlieb E, Green DR, Hengartner MO, Kepp O, Knight RA, Kumar S, Lipton SA, Lu X, Madeo F, Malorni W, Mehlen P, Nunez G, Peter ME, Piacentini M, Rubinsztein DC, Shi Y, Simon HU, Vandenabeele P, White E, Yuan J, Zhivotovsky B, Melino G, Kroemer G (2012) Molecular definitions of cell death subroutines: recommendations of the Nomenclature Committee on Cell Death 2012. Cell Death Differ 19(1):107–120
7. Raynal P, Pollard HB (1994) Annexins: the problem of assessing the biological role for a gene family of multifunctional calcium- and phospholipid-binding proteins. Biochim Biophys Acta 1197(1):63–93. https://doi.org/10.1016/0304-4157(94)90019-1
8. Martin SJ, Reutelingsperger CP, McGahon AJ, Rader JA, van Schie RC, LaFace DM, Green DR (1995) Early redistribution of plasma membrane phosphatidylserine is a general feature of apoptosis regardless of the initiating stimulus: inhibition by overexpression of Bcl-2 and Abl. J Exp Med 182 (5):1545–1556. https://doi.org/10.1084/jem.182.5.1545
9. Vermes I, Haanen C, Steffens-Nakken H, Reutellingsperger C (1995) A novel assay for apoptosis flow cytometric detection of phosphatidylserine expression on early apoptotic cells using fluorescein labelled Annexin V. J Immunol Methods 184(1):39–51. https://doi.org/10.1016/0022-1759(95)00072-I
10. Casciola-Rosen L, Rosen A, Petri M, Schlissel M (1996) Surface blebs on apoptotic cells are sites of enhanced procoagulant activity: implications for coagulation events and antigenic spread in systemic lupus erythematosus. Proc Natl Acad Sci U S A 93(4):1624–1629
11. van Engeland M, Ramaekers FCS, Schutte B, Reutelingsperger CPM (1996) A novel assay to measure loss of plasma membrane asymmetry during apoptosis of adherent cells in culture. Cytometry 24(2):131–139. https://doi.org/10.1002/(sici)1097-0320(19960601)24:2<131::aid-cyto5>3.0.co;2-m
12. Samejima K, Earnshaw WC (2005) Trashing the genome: the role of nucleases during apoptosis. Nat Rev Mol Cell Biol 6(9):677–688
13. Gavrieli Y, Sherman Y, Ben-Sasson SA (1992) Identification of programmed cell death in situ via specific labeling of nuclear DNA fragmentation. J Cell Biol 119(3):493–501. https://doi.org/10.1083/jcb.119.3.493
14. Lauber K, Blumenthal SG, Waibel M, Wesselborg S (2004) Clearance of apoptotic cells. Mol Cell 14(3):277–287. https://doi.org/10.1016/s1097-2765(04)00237-0
15. Thornberry NA, Lazebnik Y (1998) Caspases: enemies within. Science 281 (5381):1312–1316. https://doi.org/10.1126/science.281.5381.1312
16. Nicholson DW, Ali A, Thornberry NA, Vaillancourt JP, Ding CK, Gallant M, Gareau Y, Griffin PR, Labelle M, Lazebnik YA, Munday NA, Raju SM, Smulson ME, Yamin T-T, Yu VL, Miller DK (1995) Identification and inhibition of the ICE/CED-3 protease necessary for mammalian apoptosis. Nature 376(6535):37–43
17. Fernandes-Alnemri T, Litwack G, Alnemri ES (1994) CPP32, a novel human apoptotic protein with homology to Caenorhabditis elegans cell death protein Ced-3 and mammalian interleukin-1 beta-converting enzyme. J Biol Chem 269(49):30761–30764
18. Roninson IB (2003) Tumor cell senescence in cancer treatment. Cancer Res 63 (11):2705–2715
19. Yaglom JA, Gabai VL, Sherman MY (2007) High levels of heat shock protein Hsp72 in cancer cells suppress default senescence pathways. Cancer Res 67(5):2373–2381. https://doi.org/10.1158/0008-5472.CAN-06-3796
20. Meng L, Hunt C, Yaglom JA, Gabai VL, Sherman MY (2011) Heat shock protein Hsp72 plays

an essential role in Her2-induced mammary tumorigenesis. Oncogene 30(25):2836–2845

21. Dimri G, Lee X, Basile G, Acosta M, Scott G, Roskelley C, Medrano E, Linskens M, Rubelj I, Pereira-Smith O, Peacocke M, Campisi J (1995) A biomarker that identifies senescent human cells in culture and in aging skin in vivo. Proc Natl Acad Sci U S A 92(20):9363–9367
22. Roninson IB (2002) Tumor senescence as a determinant of drug response in vivo. Drug Resist Updates 5(5):204–208
23. Roninson IB, Broude EV, Chang B-D (2001) If not apoptosis, then what? Treatment-induced senescence and mitotic catastrophe in tumor cells. Drug Resist Updates 4(5):303–313
24. Schmitt CA (2007) Cellular senescence and cancer treatment. Biochim Biophys Acta 1775 (1):5–20
25. Rossi A, Ciafrè S, Balsamo M, Pierimarchi P, Santoro MG (2006) Targeting the heat shock factor 1 by RNA interference: a potent tool to enhance hyperthermochemotherapy efficacy in cervical cancer. Cancer Res 66 (15):7678–7685. https://doi.org/10.1158/0008-5472.can-05-4282
26. Kabakov AE, Kudryavtsev VA, Gabai VL (2010) Hsp90 inhibitors as promising agents for radiotherapy. J Mol Med (Berl) 88(3):241–247. https://doi.org/10.1007/s00109-009-0562-0
27. Westerheide SD, Kawahara TLA, Orton K, Morimoto RI (2006) Triptolide, an inhibitor of the human heat shock response that enhances stress-induced cell death. J Biol Chem 281(14):9616–9622. https://doi.org/10.1074/jbc.M512044200

Chapter 10

Detecting the Potential Pharmacological Synergy of Drug Combination by Viability Assays In Vitro

Benjamin K. Gibbs and Carole Sourbier

Abstract

Heat shock protein 90 (HSP90) is a molecular chaperone necessary for the folding and proper function of multiple "client" proteins. HSP90 is involved in numerous biological processes and is critical to maintain proteostasis and to protect the cells from potentially harmful environmental stresses such as heat. However, in cancer, the role of HSP90, and other molecular chaperones, is corrupted as many of HSP90 clients are kinases and transcription factors whose aberrant activation or mutation drives tumor growth. Thus, developing a polytherapy, or combination therapy, that includes an HSP90 inhibitor in addition to targeting an oncogene or oncogenic pathway is an appealing therapeutic approach. This protocol will provide detailed methods on how to assess the potential synergy of polytherapy by viability assays in vitro.

Key words Polytherapy, Viability assays, Synergy, Methods

1 Introduction

Heat shock proteins (HSP) are highly abundant proteins and account for about 2% of the whole proteome. HSP90 is the most common HSP and while it is already highly expressed in unstressed conditions, its expression can double under environmental stress. HSP90 supports the stability and activity of numerous signal transducers in normal cells as well as during evolution and in diseases [1, 2]. In cancer, HSP90 stabilizes the structure and function of proteins in many oncogenic pathways, including transmembrane tyrosine kinases, mutated signaling proteins, fusion proteins, and steroid receptors [2–4]. Additionally, the tumor microenvironment (e.g., acidic pH, hypoxia) stresses the proteome of tumor cells increasing their dependence on HSP90 [3]. Thus, HSP90 is a promising target in cancer. Since HSP90 inhibitors target multiple signaling pathways at once, combining a targeted agent with an HSP90 inhibitor may have a synergistic effect and hypothetically may decrease the likelihood of development of resistance. In the clinic, HSP90 inhibitors have been used successfully in HER2(+)

Stuart K. Calderwood and Thomas L. Prince (eds.), *Chaperones: Methods and Protocols*, Methods in Molecular Biology, vol. 1709, https://doi.org/10.1007/978-1-4939-7477-1_10,

breast cancer in combination with the HER2 blocking antibody trastuzumab [5]. In a preclinical study, HSP90 inhibition was shown to be synergistic with the Met inhibitor crizotinib in vitro and in vivo in crizotinib-responsive and resistant Met-driven tumors [6].

In order to identify the optimal polytherapy in vitro, a quantitative evaluation of the combination of different agents is necessary. Indeed, a polytherapy could be synergistic, additive, or antagonistic. A synergistic combination means the compounds enhance each other's efficacy by more than the addition of their respective single-agent effect. An additive effect means that the response of each agent neither masks nor enhances the other agent's performance. Finally, if the combination is antagonistic, it means that the polytherapy is less effective than the individual single agents. The Chou-Talalay method quantitatively evaluates polytherapies by treating the combinations as single agents and assigns a combination index (CI), with $CI < 1$ being synergism, $CI > 1$ being antagonism, and $CI = 1$ being additive [7]. Alterations in the dose needed to achieve the EC_{50} also help determine efficacy and potential synergism. The following methods will describe how to perform a drug screening in vitro and how to analyze the outcomes of a polytherapy.

2 Materials

1. Dulbecco's Modified Eagle's Medium supplemented with 1 mM sodium pyruvate, 4.5 g/L glucose, and 0.584 g/L L-glutamine completed with 10% Fetal Bovine Serum; or any complete media used to usually propagate the cell line of interest.
2. Trypsin-EDTA or any cell dissociation reagents.
3. Black or white wall 96-well plates, TC-treated, flat optically clear bottom, sterile. Black plates are preferred for fluorescent assays and white plates for luminescence assay.
4. Dimethylsulfoxide (DMSO) and/or other vehicles.
5. Drug A (e.g., 10 mM HSP90 inhibitor in DMSO).
6. Drug B (e.g., 10 mM other agent in DMSO).
7. Set of single-channel micropipettes with disposable sterile tips.
8. Multi-channel pipet with disposable sterile tips (20–200 μL).
9. Sterile 15 mL and 50 mL conical tubes.
10. Sterile 1.5 mL Eppendorf tubes.
11. Sterile 50 mL reservoirs (*see* **Note 1**).
12. CellTiter-Glo® Luminescent Cell Viability Assay (Promega).

13. CyQUANT® Cell Proliferation Assay Kit (ThermoFisher Scientific).
14. Hemocytometer or automatic cell counter.
15. Plate reader (luminescence and/or fluorescence).

3 Methods

3.1 Determining the Optimal Plating Density

1. Prepare a single-cell suspension and count cells.
2. Make 2 mL of cells at 200,000 cells/mL and 150,000 cells/mL. Make twofold serial dilution of these cells so that there are concentrations of 200,000, 150,000, 100,000, 75,000, 50,000, 37,500, 25,000, 18,750, 12,500, 9375, 6250, and 4688 cells/mL.
3. Add 100 μL of complete media to the outer wells and five replicates of each concentration in the inner wells (Fig. 1).
4. Place the plate in an incubator (37 °C, 5% CO_2) for 72 h (this incubation time is variable as it should reflect the viability assay you will perform).
5. Determine cell viability with CyQUANT® Cell Proliferation Assay Kit or CellTiter-Glo® Luminescent Cell Viability Assay according to modified manufacturer's protocol noted below in the cell viability assay Subheading 3.3 (*see* **Note 2**).
6. Analyze cell viability data. For viability screening, the cells should be in log phase growth (usually reaching about 90% confluence). Therefore, the optimal plating density is the one just before the cell viability signal begins to plateau as described in analysis section below (Fig. 2).

3.2 Drug Screening

1. Prepare a single-cell suspension at the previously determined cell density in complete media.

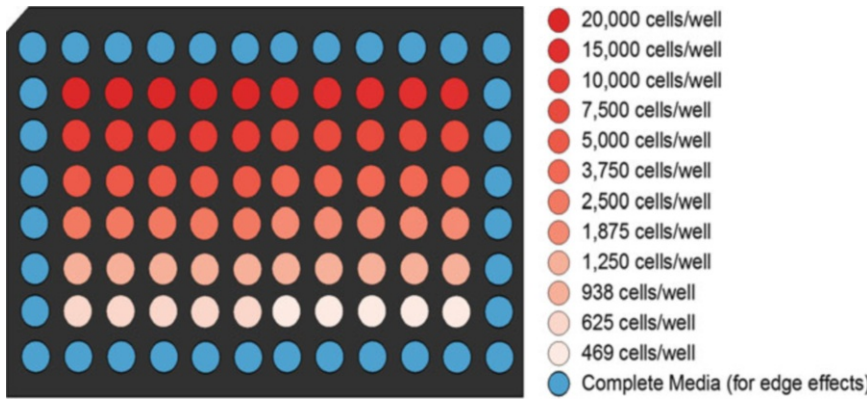

Fig. 1 Plate map of determination of cell density

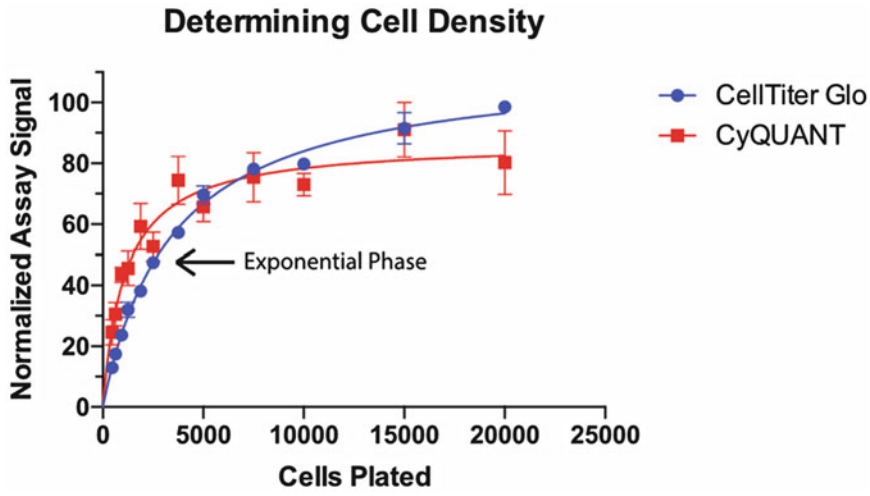

Fig. 2 Signal from different densities plated of UOK161. In these examples, we used UOK161, a VHL-deficient clear cell renal cell carcinoma. We determined 2500 cells per well to be an appropriate density of cells for UOK161

2. Plate inner wells with 100 μL of the cell suspension and fill outer wells with 100 μL of complete media. Incubate for 24 h at 37 °C, 5% CO_2 (*see* **Note 3**).
3. Prepare the different treatments (single agents and combination) in sterile 1.5 mL Eppendorf tubes. For the single agents: each well will require 100 μL of complete media containing five different drug dilutions to reach concentrations of 10 μM, 1 μM, 100 nM, 10 nM, and 1 nM, and a vehicle control. Treatments are performed in triplicates so for one plate, it is recommended to prepare at least 350–400 μL per concentration. Figure 3 shows how to prepare serial dilutions.
4. Gently aspirate the media (*see* **Note 4**) and treat the cells in triplicates with 100 μL of complete media containing the five different drug dilutions prepared as indicated above.
5. Add 100 μL Drug A serial concentrations (e.g., ganetespib) to upper left quadrant, 100 μL Drug B serial concentrations (e.g., everolimus) to upper right quadrant, 100 μL of Drug A + B serial concentrations to the lower left quadrant. Finally, in the lower right quadrant add 100 μL of vehicle A in 5 wells, 100 μL of vehicle B in 5 wells, and 100 μL of vehicles A + B in the remaining 5 wells (Fig. 4).
6. Incubate for an additional 48 h at 37 °C, 5% CO_2 prior to assessing cell viability as indicated in the next section.

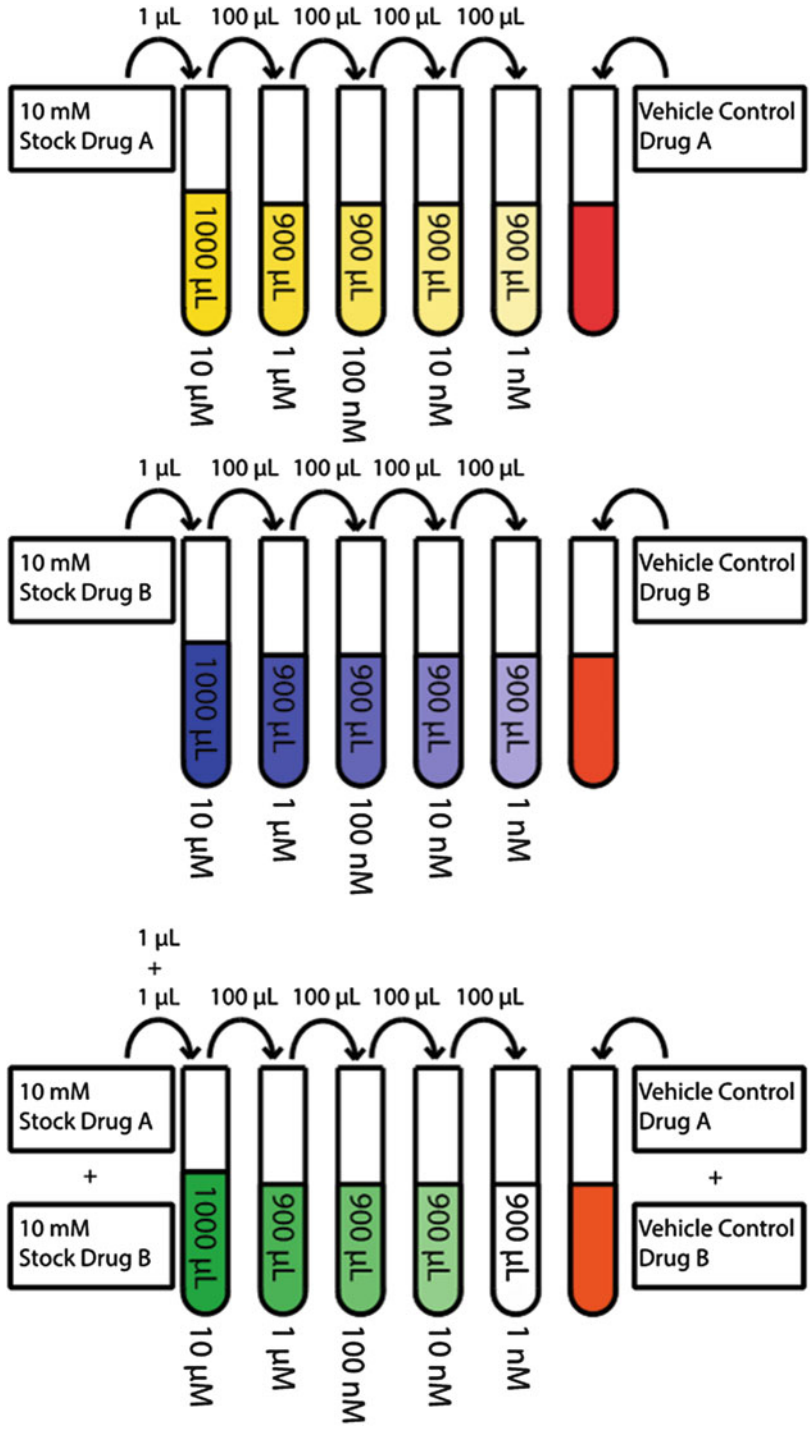

Fig. 3 Example of preparing drug treatments by serial dilution

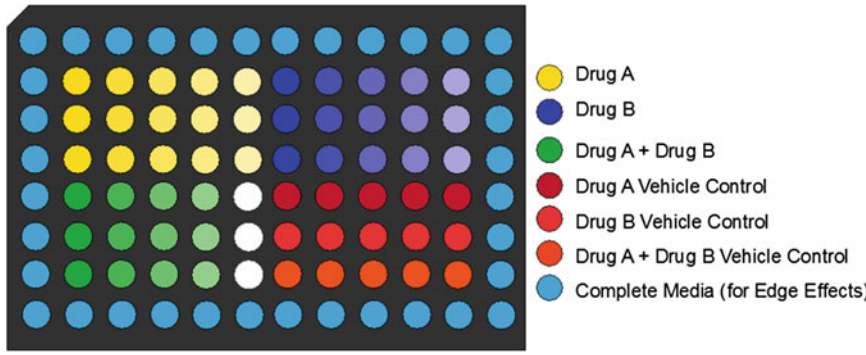

Fig. 4 Plate map for treating cells

3.3 Cell Viability Assays

Many methods of evaluating growth/viability can be used for drug screening. We favor two endpoint methods, CyQUANT® Cell Proliferation Assay Kit (ThermoFisher Scientific) and CellTiter-Glo® Luminescent Cell Viability Assay (Promega).

3.3.1 The CyQUANT Assay

The CyQUANT assay is a quick and sensitive fluorescent assay using a dye that enhances when it binds to nucleic acids. The fluorescent intensity is linear to nucleic acid content, a surrogate marker of cell abundance (*see* **Note 5**).

1. Remove media from the 96-well plate by flicking over a sink.
2. Wash by adding 100 μL 1x PBS to each well and flicking to remove PBS.
3. Place in a −80 °C freezer overnight to disrupt cell membranes.
4. Dilute 500 μL of 20× CyQUANT lysis buffer with 9.5 mL water per plate. Add 25 μL CyQUANT GR Dye.
5. Add 100 μL of CyQUANT GR Dye/lysis buffer to each well and incubate for 5 min protected from light.
6. Read 96-well plate on a fluorescence microplate reader equipped with fluorescein filter set (480/520 nm excitation/emission).

3.3.2 The CellTiter-Glo Assay

The CellTiter-Glo assay uses a luciferase reporter that reacts with cellular ATP. The rate of this reaction is directly proportional to the concentration of ATP and hence the luminescence is proportional to metabolically active cells. This is the only method mentioned that does not require removal of cell media and hence is most accurate representation of cell proliferation (*see* **Note 6**).

1. Thaw out CellTiter-Glo Buffer and lyophilized CellTiter-Glo Substrate to room temperature.
2. Add 10 mL of buffer to substrate to make CellTiter-Glo Reagent. Mix by inverting for a minute.

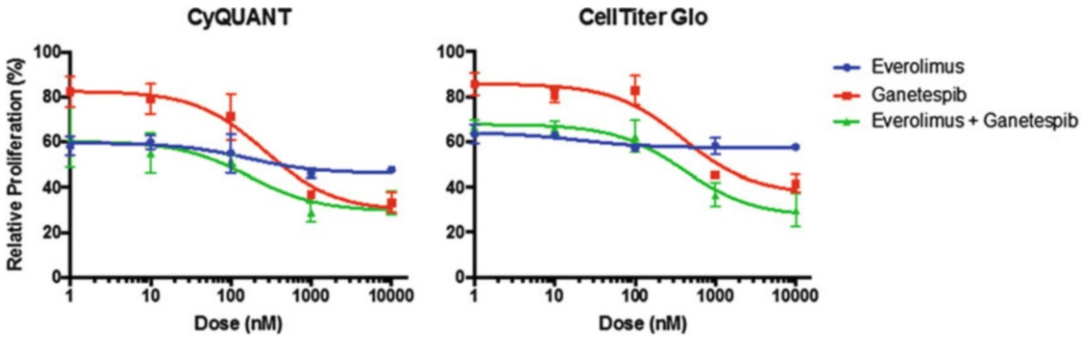

Fig. 5 Dose-response graph of everolimus, ganetespib or everolimus, and ganetespib determined by CyQUANT® Cell Proliferation Assay Kit or CellTiter-Glo® Luminescent Cell Viability Assay. The CyQUANT Cell Proliferation Assay Kit tends to have greater variability. Additionally, The CellTiter Glo kit can tend to have higher signal due to the ability to assay loose and detached cells since cell media is not removed

3. Equilibrate the 96-well plate to room temperature.
4. Add 100 μL of CellTiter-Glo Reagent directly to the 100 μL of media.
5. Mix contents on orbital shaker for 2 min to facilitate cell lysis.
6. Equilibrate for 10 min at ambient conditions.
7. Record luminescence on a plate reader.

3.3.3 Graphing the Data with GraphPad Prism

1. Remove background from the plate by subtracting the average of the values obtained in the complete media only wells.
2. Transform each well on the plate in percent of signal of the corresponding vehicle wells (divide the signal by the average vehicle well signal and multiply by 100).
3. Create a dose-response curve using the XY plot function. Transform data by clicking "analyze" and going to "transform." Transform X by using "X = log(X)" feature. Go to "analyze" and select "nonlinear regression (curve fit)," then under "Classic Equations from Prior Versions of Prism" use "Sigmodal dose-response." Change X axis to antilog with log minor ticks (Fig. 5).

3.3.4 Analysis of Synergy

To determine CI values and EC50 use the publicly available CompuSyn software (http://www.combosyn.com/).

1. Enter data for Drug A alone and Drug B alone (each dose for each effect).
2. Enter data for combination of Drug A and Drug B at a constant ratio. For ease, we favor equimolar. $(IC_{50})_1/(IC_{50})_2$ is also commonly used.
3. Generate the report. Find the CI values for each concentration evaluated in the report (Tables 1 and 2).

Table 1
Median Combination index determined by CyQUANT® Cell Proliferation Assay Kit or CellTiter-Glo® Luminescent Cell Viability Assay

	Median CI (CyQUANT)	Median CI (CellTiter Glo)
10,000	0.20216	0.68518
1000	0.06750	0.02876
100	14369.2	0.74183
10	180.709	0.02631
1	245.865	310.475

Table 2
Determination of dose needed to decrease cell proliferation by 50%

	ED50 by CyQUANT (nM)	ED50 by CellTiter Glo (nM)
Everolimus	79,480,000	958.462
Ganetespib	2885.12	817.784
Combination	308.868	70.0128

4 Notes

1. Sterile 12-column partitioned reservoirs can facilitate the treatment step.
2. Determination of the optimal plating density can also be performed visually by selecting the cell number that reaches about 90% confluency at the end of the incubation time.
3. Most cell lines require several hours to settle appropriately and start growing. A wait of 18–24 h' incubation is usually sufficient before treating the cells; however, some cell lines might require a shorter or longer lag time.
4. In case aspiration of the media to exchange with complete media containing the different drugs/controls is unwanted or technically challenging, 100 μL of media containing 2× concentrations could be directly added. This will not change the following steps using CyQuant. However, for CellTiterGlo assay, the ratio media:reagent to have an optimal signal is 1:1 so 100 μL of media would need to be removed prior to adding 100 μL of the luciferin solution (which can be a source of variability).

5. Some compounds may be fluorescent and hence should not be used with the CyQUANT assay as they may interfere with the reading.
6. A very popular method of cytotoxicity assay is the MTT assay (or the MTS assay). NADH-dependent oxidoreductase enzymes reduce the 3-(4,5-dimethylthiazol-2-yl)-2,5-diphenyltetrazolium bromide (MTT) into a purple insoluble formazan. The salt is dissolved in DMSO and the concentration is determined by evaluating absorbance [8]. Since we commonly work with the cells that have metabolic dysfunction, we avoid this method. However, it may have value for some applications and should be treated as a potential option.

Acknowledgments

This research was supported by the Intramural Research Program of the National Cancer Institute, NIH.

References

1. Taipale M, Jarosz DF, Lindquist S (2010) HSP90 At the hub of protein homeostasis: emerging mechanistic insights. Nat Rev Mol Cell Biol 11(7):515–528
2. Trepel J, Mollapour M, Giaccone G, Neckers L (2010) Targeting the dynamic HSP90 complex in cancer. Nat Rev Cancer 10(8):537–549
3. Neckers L, Workman P (2012) Hsp90 Molecular chaperone inhibitors: are we there yet? Clin Cancer Res 18(1):64–76
4. Kamal A, Boehm MF, Burrows FJ (2004) Therapeutic and diagnostic implications of Hsp90 activation. Trends Mol Med 10(6):283–290
5. Modi S, Stopeck A, Linden H, Solit D, Chandarlapaty S, Rosen N et al (2011) HSP90 Inhibition is effective in breast cancer: a phase II trial of tanespimycin (17-AAG) plus trastuzumab in patients with HER2-positive metastatic breast cancer progressing on trastuzumab. Clin Cancer Res 17(15):5132–5139
6. Miyajima N, Tsutsumi S, Sourbier C, Beebe K, Mollapour M, Rivas C et al (2013) The HSP90 inhibitor ganetespib synergizes with the MET kinase inhibitor crizotinib in both crizotinib-sensitive and -resistant MET-driven tumor models. Cancer Res 73(23):7022–7033
7. Chou TC (2010) Drug combination studies and their synergy quantification using the Chou-Talalay method. Cancer Res 70(2):440–446
8. Mosmann T (1983) Rapid colorimetric assay for cellular growth and survival: application to proliferation and cytotoxicity assays. J Immunol Methods 65(1–2):55–63

Chapter 11

Proteomic Profiling of Hsp90 Inhibitors

Sudhakar Voruganti, Jake T. Kline, Maurie J. Balch, Janet Rogers, Robert L. Matts, and Steven D. Hartson

Abstract

Mass spectrometry assays demonstrate that Hsp90 inhibitors alter the expression of approximately one-quarter of the assayable proteome in mammalian cells. These changes are extraordinarily robust and reproducible, making "proteomics profiling" the gold standard for validating the effects of new Hsp90 inhibitors on cultured cells. Proteomics assays can also suggest novel hypotheses regarding drug mechanisms. To assist investigators in adopting this approach, this Chapter provides detailed protocols for conducting simple proteomics assays of Hsp90 inhibition. The protocols present a robust label-free approach that utilizes pre-fractionation of protein samples by SDS-PAGE, thereby providing reasonably good penetration into the proteome while addressing common issues with sample quality. The actual programming and operation of liquid chromatography-tandem mass spectrometers is not covered, but expectations for achievable performance are discussed, as are alternative approaches, common challenges, and software for data analysis.

Key words Hsp90 inhibitor, Proteomics, Tandem mass spectrometry, Gel-LC, Protocol, Techniques, T cell, RIPA, Cancer, MaxQuant, Perseus, Differential protein expression, Fusion mass spectrometer, LC-MS/MS

1 Introduction

Mass spectrometry assays (LC-MS/MS) offer a remarkable and complex profile of protein expression in cells treated with Hsp90 inhibitors [1–8]. Results from these assays show that Hsp90 inhibition can alter the expression of ca. 25% of the cellular proteome. Many of these alterations reflect the induction of the heat shock response, a well-known effect of inhibitors that bind to Hsp90's N-terminal ATP binding pocket. Other alterations include the depletion of probable Hsp90 "client" proteins, likely reflecting a direct role for Hsp90 in their folding. Yet other inhibitor responses are less readily ascribed to these two phenomena.

This "proteomics profile" of Hsp90 inhibition is extraordinarily robust. The profile includes several large changes in the expression of readily detected proteins, such that even the simplest

Stuart K. Calderwood and Thomas L. Prince (eds.), *Chaperones: Methods and Protocols*, Methods in Molecular Biology, vol. 1709, https://doi.org/10.1007/978-1-4939-7477-1_11,

proteomics assay can identify and quantify nearly 100 changes in protein expression caused by Hsp90 inhibition (e.g., [6]). Deep proteome mining can extend the profile even further, documenting 1000 or more Hsp90 inhibitor-induced changes [3, 5, 7]. When changes induced by different Hsp90 inhibitors are compared in the same cell line, *R*-squared values can easily exceed 0.9 [6, 7]. - Inhibitor-induced changes in protein expression are also conserved across different cell lines [3, 7]. However, some proteins show cell-line-specific responses to Hsp90 inhibition, suggesting plasticity in Hsp90 dependencies that might one day shape decisions about the clinical deployment of Hsp90 inhibitors [3, 7].

Proteomics profiling has the potential to supplant traditional in vivo assays of Hsp90 inhibition. Traditionally, the efficacy and mechanism of putative Hsp90 inhibitors has been validated by Western blot assays directed against a small handful of proteins (e.g., [9–13]), and Western blots remain the tool of choice when asking a priori questions about specific proteins. This reflects the superior sensitivity and readily availability of the Western blot technique. However, arguments regarding putative Hsp90 inhibitors are much stronger when supported by a proteomics profile whose depth and breadth are orders of magnitude larger than the typical Western blot series. Moreover, proteomics assays can lead to novel hypotheses regarding Hsp90 function and the anti-cancer activities of Hsp90 inhibitors.

To assist investigators who might wish to adopt this approach, this Chapter provides detailed protocols for conducting proteomics assays of Hsp90 inhibition. The Chapter assumes theoretical knowledge of proteomics and quantitative mass spectrometry [14]. We provide practical guidance that proceeds from the treatment of cultures with inhibitor through the extraction of proteins and their preparation for LC-MS/MS, and we conclude with brief recommendations regarding methods for analyzing and comparing proteomics profiles. In the accompanying Notes, we discuss instrument capabilities, expectations, common challenges, and briefly touch upon best practices and alternative approaches.

For this Chapter, we present a label-free proteomics strategy coupled with pre-fractionation of protein samples by SDS-PAGE [7, 15, 16]. This choice is based upon clear preferences that we have observed among investigators undertaking their initial proteomics projects. The Gel-LC approach provides reasonably good penetration into the proteome while addressing common mass spectrometry issues such as contamination with detergents and other polymers, inaccurate protein quantifications, and samples that contain an overabundance of a single protein. Moreover, Gel-LC is easy to master, effective, reproducible, flexible, and requires no special equipment or expertise. The primary disadvantage of this approach is that it is labor-intensive, and does not provide the deep proteome

coverage that can be obtained with specialized techniques and instruments for peptide pre-fractionation and UPLC-MS (reviewed in [17]).

The robustness of the proteomics profile of Hsp90 inhibition makes simple label-free assays adequate for questions regarding conserved drug mechanisms. Nonetheless, the workflow presented also readily accommodates the pursuit of deeper assays using stable-isotope labeling with amino acids in cell culture (SILAC, [7, 18]). In contrast, the protocol provided here is not recommended for investigators wishing to use covalent chemical-isotope labels (e.g., iTRAQ, TMT, dimethyl labeling), and those investigators are instead directed to an orthogonal chromatography approach [16, 19].

The protocols provided here do not address important initial assays of cell survival and cell death, for which readers are directed to the accompanying chapter by Dr. Vladimir Gabai. Nor do we address configuring and operating LC-MS/MS instrumentation. Instead, we strive here to enable Hsp90 investigators who are new to proteomics techniques to collaborate productively with scientists who specialize in the discipline of LC-MS/MS.

2 Materials

2.1 Equipment

1. Clinical swinging bucket centrifuge with 50-ml rotor.
2. Clinical swinging bucket centrifuge with 10-ml rotor.
3. Tube rocker (one at 4 °C, and one at RT—or move it between steps).
4. Refrigerated microcentrifuge.
5. Apparti and buffers for SDS-PAGE.
6. Glass plates.
7. Razor blades (new).
8. Jurkat E6.1 cells (pedigreed).
9. Laminar flow hood (optional).
10. Centrifugal evaporator (e.g., Thermo SpeedVac).
11. High capacity solid phase extraction pipet tips (SPE tips).
12. LC-MS/MS system.
13. Software and computing resources for identifying peptides and quantifying proteins.

2.2 Reagents

1. 200× Hsp90 inhibitor stocks (TOXIC): 17-AAG, STA-9090, or AUY922. *See* Planning and Notes, below. Store at −80 °C.
2. RPMI: Traditional RPMI 1640 media supplemented with 10% heat-inactivated FBS, 2 mM glutamine, 100 U/ml penicillin, 100 μg/ml streptomycin. Store at 4 °C.

3. Incomplete RIPA: 25 mM Tris–HCl pH 7.6, 150 mM NaCl, 1% NP-40, 1% sodium deoxycholate, 0.1% SDS. Store at 4 °C.
4. Complete RIPA: Incomplete RIPA (above), supplemented with 2 mM sodium vanadate, 10 mM sodium fluoride, 0.1 mg/ml PMSF, 1× commercial protease inhibitor cocktail. Make fresh immediately before cell lysis, and hold on ice.
5. 50× Sodium Vanadate Stock: 100 mM sodium orthovanadate, 100 mM HEPES, no adjustment of pH. Aliquot into one-use vials, and store at −20 °C.
6. 50× Sodium Fluoride Stock: 0.5 M sodium fluoride, dissolved in water. Prepare at least 2 weeks before use, and store at 4 °C in a glass container.
7. 100× PMSF (TOXIC): 10 mg/ml phenylmethylsulfonyl fluoride in isopropanol. Dissolve immediately before cell lysis, and add 1/100th volume to Incomplete RIPA. Do not store.
8. Protease inhibitor cocktail (stored and used per the manufacturer's recommendations).
9. 1×PBS: 8 g/L NaCl, 0.2 g/L KCl, 1.44 g/L Na_2HPO_4, 0.24 g/L KH_2PO_4. (Or dilute from a 10× stock.) Store at 4 °C.
10. 0.2× Coomassie R-250 Stain Solution: 0.04% Coomassie Blue R250, 50% methanol, 10% acetic acid. Store at RT.
11. Fast Destain: 25% isopropanol, 10% acetic acid. Store at RT.
12. Slow Destain: 10% acetic acid. Store at RT.
13. Gel Wash Solution: 25 mM ammonium bicarbonate, 50% acetonitrile. Make fresh; hold at RT.
14. 100% Acetonitrile. Store at RT in a flammables cabinet.
15. 25 mM ABC: 0.2% in water. Make fresh; hold on ice.
16. ABC Reducing Buffer: 0.2% ammonium bicarbonate, 2.9 mg/ml tris(2-carboxyethyl)phosphine. Make fresh; do not store.
17. IAA Alkylating Solution (TOXIC): 1.8 mg/ml iodoacetamide, 0.2% ammonium bicarbonate. Make fresh; do not store.
18. Trypsinolysis Solution: 8 μg/ml trypsin, 0.2% ammonium bicarbonate. Dissolve trypsin immediately before use; hold on ice.
19. 0.5% TFA: Store at RT for up to 1 week.
20. 0.1% TFA: Store at RT for up to 1 week.
21. 70/0.1 Solution: 70% acetonitrile, 0.1% trifluoracetic acid. Store at RT for up to 1 week.

Table 1
Amounts and storage

Reagent	Volume needed	Notes
1×PBS	12 ml/culture condition	Can be made in advance and stored
0.5% TFA	1.4 ml/gel fraction	Can be made in advance and stored
0.1% TFA	50 ml	Can be made in advance and stored
70/0.1 solution	50 ml	Can be made in advance and stored
0.2× Coomassie R-250 stain solution	100–200 ml/gel	Can be made in advance and stored
Fast Destain	100–200 ml/gel	Can be made in advance and stored
Slow Destain	100–200 ml/gel	Can be made in advance and stored
Incomplete/complete RIPA	0.35 ml/culture condition	Chill this volume of incomplete RIPA on ice for Subheading 3.4
Gel wash solution	3.5 ml/gel fraction	Make fresh right before Subheading 3.6
25 mM ABC	1.3 ml/gel fraction	Make fresh right before Subheading 3.6
ABC reducing buffer	1.2 ml/gel fraction	Make fresh right before Subheading 3.6
IAA alkylating solution	0.6 ml/gel fraction	Make fresh right before Subheading 3.6
Trypsinolysis solution	0.3 ml/gel fraction	Make fresh right before Subheading 3.6

2.3 Reagent Notes

See Table 1.

3 Methods

3.1 Outline

See Table 2.

3.2 Plan the Experiment (See Note 1)

1. Optimize the dosage of Hsp90 inhibitor based upon inhibition of cell proliferation, cell viability, depletion of known clients, apoptosis markers, or other responses suited to the study goals (*see* **Note 2**).
2. Based upon the dose effects observed, prepare a 200× drug stock, aliquot into one-use vials, store at −80 °C (*see* **Note 3**).
3. Calculate the amount of protein needed for the experiment, and the cell culture volumes needed to yield this amount of protein (*see* **Note 4**).
4. Label three identical sets of 1.5 ml microfuge tubes with a name that reflects the original culture or PAGE lane number, and the name of the gel fraction (below). These names will become file names in the LC-MS workflow, so keep the nomenclature simple, and avoid characters that might be disallowed

Table 2
Workflow time costs

Subheading	Time required
3.2: Planning and solution making	Varies
3.3: Cell staging and treatment	3 days
3.4: Cell harvest and lysis	1 day
3.5: PAGE fractionation	2 days
3.6: Digest gel fractions	1 day
3.7: Extract peptides	1 day
3.8: Concentrate peptides	1/2 day
3.9: Solid phase extraction	0.5–2 days, depending upon number of samples
3.10: LC-MS/MS	Varies (ca. 0.5 days per biological sample using 100-min gradients)
3.11: Data analysis	Varies (often underestimated)

Table 3
Reagents and volumes

Reagent	Volume needed	Notes
1×PBS	12 ml/culture condition	Can be made in advance and stored
0.5% TFA	1.4 ml/gel fraction	Can be made in advance and stored
0.1% TFA	50 ml	Can be made in advance and stored
70/0.1 solution	50 ml	Can be made in advance and stored
0.2× Coomassie R-250 stain solution	100–200 ml/gel	Can be made in advance and stored
Fast Destain	100–200 ml/gel	Can be made in advance and stored
Slow Destain	100–200 ml/gel	Can be made in advance and stored
Incomplete/complete RIPA	0.35 ml/culture condition	Chill this volume of incomplete RIPA on ice for Subheading 3.4
Gel wash solution	3.5 ml/gel fraction	Make fresh right before Subheading 3.6
25 mM ABC	1.3 ml/gel fraction	Make fresh right before Subheading 3.6
ABC reducing buffer	1.2 ml/gel fraction	Make fresh right before Subheading 3.6
IAA alkylating solution	0.6 ml/gel fraction	Make fresh right before Subheading 3.6
Trypsinolysis solution	0.3 ml/gel fraction	Make fresh right before Subheading 3.6

by the MS software (only use numerals, letters, and underlines).

5. Calculate the volumes of buffers and solutions needed (below). Prepare the reagents that can be made in advance, and

pre-calculate the recipes those that must be made fresh. The volumes cited include a 15% excess for handling losses (*see* Table 3).

3.3 Stage the Cell Cultures, and Treat with Hsp90 Inhibitor (See Note 5)

1. Culture Jurkat cells in 25 ml of Complete RPMI in a T-75 flask at 37 °C in a 5% CO_2 incubator without agitation, until cell density approaches 8×10^5 cells/ml.
2. When cultures reach target density, directly dilute 3.2 ml of the culture into 21.8 ml of fresh pre-warmed Complete RPMI media (i.e., dilute to 1×10^5 cells/ml in fresh media), gently mix by swirling the upright flask, return the diluted culture to the incubator, and incubate for 24 h prior to drug treatment.
3. The next day, apply 125 μl of Hsp90 inhibitor (or drug vehicle control) to each 25 ml culture, and mix by using a 25 ml pipet to gently draw the whole culture volume up and down in the pipet three times.
4. Return the flasks to the incubator, and culture for 24 h.

3.4 Cell Harvest and Lysis

1. Place the required amount of Incomplete RIPA buffer on ice, warm 1×PBS to room temperature, and thaw the protease inhibitors and phosphatase inhibitors needed to prepare Complete RIPA. Preweigh the PMSF into an appropriate tube, and pour an aliquot of 100% isoproponal into a labeled beaker.
2. Using a 25 ml pipet, gently transfer each cell culture to a disposable 50 ml conical-bottom centrifuge tube, and centrifuge at RT for 3 min at 800 × *g* in a swinging bucket rotor (*see* **Note 6**).
3. Pipet 0.5 ml of 1×PBS to the cell pellet, very gently mix by flicking the bottom of the tube with your fingernail, then add another 10 ml of 1×PBS and mix by gentle inversion.
4. Pipet the mixed cell suspension into a disposable 15 ml conical-bottom centrifuge tube, centrifuge at RT for 3 min at 800 × *g* in a swinging bucket rotor, draw off the majority of the 1×PBS, re-pack the cells by centrifuging for 1 min at 800 × *g*, and then use a gel-loading pipet tip to withdraw the last of the 1×PBS wash (*see* **Note 7**).
5. Make Complete RIPA Buffer by adding protease inhibitors and phosphatase inhibitors to the chilled aliquot of Incomplete RIPA Buffer (*see* **Note 8**).
6. Pipet 350 μl of chilled Complete RIPA Buffer onto the cell pellet, vortex vigorously for 5 s, transfer this lysis mixture to a 1.5 ml microfuge tube, and then vigorously vortex the microfuge tube for 5 s.
7. Place the microfuge tube containing the lysis mixture on a rocker at 4 °C, and rock for 30 min.

8. Vortex the lysis tubes for 5 s, then centrifuge at 4 °C for 10 min at 12,000 × *g* in a fixed-angle microfuge rotor.
9. Without disturbing the debris pellet in the bottom of the tube, collect 300 μl of lysate supernatant, and transfer it to clean prechilled 1.5 ml microfuge tube.
10. Vortex the clarified lysate for 3 s, then split the lysate equally among three prechilled microcentrifuge tubes (*see* **Note 9**).
11. Freeze all the three tubes at −80 °C, and store for less than 1 month.

3.5 Fractionation and Visualization by SDS-PAGE (See Note 10)

1. Use one of the aliquots frozen in **step 11** in Subheading 3.4 (above) to assay the protein concentration in each lysate (*see* **Note 11**).
2. Mix 150 μg of each lysate with an appropriate volume of SDS Sample Buffer to yield a final SDS Sample Buffer concentration of 1–2× (*see* **Note 12**).
3. Load 150 μg of lysate into one lane of an SDS-PAGE gel. Using electrophoresis buffer that contains SDS, electrophorese the samples until the bromophenol blue dye front migrates 6 cm into the separating gel (*see* **Note 13**).
4. Stain for 5 min with 0.2× Coomassie R-250 Stain Solution, briefly rinse twice with Fast Destain, and then destain overnight with Slow Destain. Image the destained gel, and print two copies of the image (*see* **Note 14**).
5. Under a laminar flow hood and while wearing gloves, lay the destained gel on a clean glass plate, and use a new razor blade to cut off the right and left edges of the gel so that the new right-most edge and the new left-most edge are approximately the one-half the width of the spaces between the lanes (*see* **Note 15**).
6. Cut the gel horizontally, creating 4–8 ribbons of acrylamide 0.7–1.5 cm wide across the breadth of all the lanes. For large format gels, eight ribbons are recommended. Use prominent proteins as guides so that each ribbon slice is perfectly horizontal, and the cuts are perfectly uniform across the sample lanes. Record this "cut map" on your printed image of the gel (*see* **Note 16**).
7. Now cut the gel vertically between the first and second sample lanes, thus freeing the gel segments of the first lane from the rest of the gel.
8. Use the razor blade to transfer the top gel segment from the first lane onto a separate glass plate. Carefully cut the segment into 1.0-mm × 1.0-mm cubes, then use the razor blade to scoop the cubes into the corresponding labeled microfuge tube (*see* **Note 17**).

9. Repeat this cubing process for the other gel segments from the first lane, placing the cubes from each gel segment into a separate tube.
10. After all of the gel segments from the first lane have been cubed, inspect the remaining gel ribbons for drying, and pipet clean water onto the surface of the gel as needed to keep it wetted.
11. Switch out the used glass plate with clean glass plate (or move to a clean region of the previous plate), and repeat this process for the next lane of the gel.
12. Repeat the process for each gel lane until the whole gel has been cubed and tubed.
13. Store tubes at 4 °C overnight.

3.6 Digestion of Gel Fractions

1. Make fresh Gel Wash Solution, and hold it at RT (*see* **Note 18**).
2. Pipet 1.0 ml of Gel Wash Solution into each tube of gel cubes, rock at RT for 1 h. Adjust the rocker angles and tube positions to ensure that the gel cubes and solutions are moving freely and mixing well during rocking.
3. Shake down each microfuge tube to dislodge the gel cubes from the tube cap, push a pipet tip though the cube slurry and hold it lightly against the bottom of the tube, aspirate out all of the wash buffer, and discard the wash supernatant (*see* **Note 19**).
4. Repeat the wash three times in total, or as necessary to remove all or nearly all of the blue color, then withdraw the final wash solution (*see* **Note 19**).
5. Pipet 1.0 ml of 100% ACN into each sample, vortex briefly, incubate for 20 min, shake down gel cubes, then remove and discard the 100% ACN supernatant (*see* **Note 20**).
6. Air-dry the gel cubes at RT for 30 min.
7. Prepare fresh ABC Reducing Buffer (*see* **Note 21**).
8. Fill each microfuge tube with 1.0 ml of ABC Reducing Buffer, rock for 1 h at RT, then remove and discard the ABC Reducing Buffer supernatant.
9. Prepare fresh IAA Alkylating Solution (HAZARD) (*see* **Note 21**).
10. Pipet 0.5 ml of IAA Alkylating Solution to each tube, vortex briefly, incubate for 1 h in the dark at RT, then remove and discard the alkylating solution as hazardous waste.
11. Rinse the gel cubes with 1.0 ml of 25 mM of fresh ABC for 1 min, then remove and discard the rinse solution.

12. Pipet 1.0 ml of 100% ACN to each tube, incubate for 20 min to dehydrate and shrink the gel cubes, remove and discard the ACN, then air-dry for 30 min (*see* **Note 20**).
13. Place the tubes containing the dehydrated gel cubes on ice.
14. Prepare fresh Trypsinolysis Solution, and hold it on ice (*see* **Note 22**).
15. Pipet ca. 300 µl of Trypsinolysis Solution into each tube of gel cubes, and incubate on ice for 45 min. Inspect at 30 and 45 min to make sure that the gel cubes remain fully submerged while swelling, and add additional Trypsinolysis Solution if necessary.
16. After the gel cubes are fully swelled with Trypsinolysis Solution, push a pipet tip through the gel cube slurry to the bottom of the tube, remove all of the unabsorbed Trypsinolysis Solution, and discard it (*see* **Note 23**).
17. Add just enough chilled 25 mM ABC to barely cover the gel pieces. Some cubes should protrude slightly from the surface of the liquid.
18. Incubate overnight at 37 °C (*see* **Note 24**).

3.7 Extraction of Digested Peptides

1. Move the digestion tubes to RT, pipet 400 µl of 0.5% TFA into each sample tube, vortex briefly, shake the gel cubes down into the bottom of their tubes, and incubate on the benchtop for 2 h (*see* **Note 25**).
2. Vortex each tube for 5 s, shake down, push a pipet tip to the bottom of the tube, and transfer all of the extract supernatants containing the peptides into clean labeled microfuge tubes. Each digestion tube will need an individual peptide-collection tube.
3. Extract the gel cubes again with 400 µl of fresh 0.5% TFA for 2 h at RT, then collect the supernatant and pool it with the first extract.
4. Extract the gel cubes a third time with 400 µl of 0.5% TFA, and pool this third extract with the two previous extracts.
5. Store the peptide extracts overnight at minus 80 °C.
6. Discard the tubes containing residual gel material, or store briefly for troubleshooting.

3.8 Concentration of Peptide Extracts

1. Wipe out the centrifugal evaporator thoroughly, removing all dust and lint from the inner surfaces of the chamber (*see* **Note 26**).
2. Place the still-frozen extract tubes into the centrifugal evaporator, and centrifuge under vacuum without heating until the volume is just reduced to apparent dryness (but not longer, because over-drying will reduce sensitivity).

3. Inspect the dried tubes for fragments of acrylamide debris and/or excess salt. If the bottom of the tube contains more than 1 µl of solids, perform the Solid Phase Extraction procedure below. Else, simply return the dried tubes to minus 80 °C until LC-MS/MS.

3.9 Purification of Peptides by Solid Phase Extraction (See Note 27)

1. Dissolve the dried peptide extracts in 200 µl of 0.1% TFA for 20 min at RT, then vortex briefly.
2. Using 1.5 ml microcentrifuge tubes, prepare two reservoirs:

   Reservoir A, containing 1 ml of 70/0.01 Solvent.

   Reservoir B, containing 1 ml of 0.1% TFA.
3. Set a pipettor to 200 µl, mount an SPE tip, place the aperture of the SPE tip 1 cm deep inside Reservoir A. Keeping the tip in this position, wet the tip by pipetting 70/0.1 Solvent up and down through the tip ten times. On the tenth wetting stroke, eject the wetting solution, but hold the pipettor plunger down after the ejection stroke. Keep holding the plunger down while proceeding to the next step. Throughout the rest of this protocol, it is essential to not draw air into the SPE tip.
4. With the pipet plunger still held down, place the wetted SPE tip 1 cm deep inside Reservoir B. Keep it in this position, and pipet 0.1% TFA up and down through the tip ten times to equilibrate the tip. On the tenth equilibration stroke, eject the equilibration solution, but hold the ejection stroke down. Keep holding the plunger down while proceeding to the next step.
5. Use the technique above to bind the peptides. Holding the tip near the bottom of the dissolved peptide sample tube, bind the peptides to the SPE matrix by pipetting up and down ten times. On the tenth binding stroke, eject the pipet solution back into the mother tube, then hold the ejection stroke down and proceed to the next step.
6. Use the techniques above to wash the SPE-bound peptides: place the SPE tip 1 cm deep in Reservoir B, and wash the bound peptides by pipetting 0.1% TFA up and down three times. On the third wash stroke, eject the wash solution, but hold the ejection stroke down, and proceed to the next step.
7. *Now change your technique to elute the peptides.* With the pipet plunger still held down, draw up 200 µl of 70/0.1 Solvent from Reservoir A, BUT THEN STOP; *do not eject the liquid*. Instead, now dispense the solvent-filled SPE tip into a clean labeled receiver tube. Then, hold the tip near the bottom of the receiver tube, and complete the elution by pipetting the peptide eluate up and down four more times through the SPE tip, ejecting the final stroke back into the receiver tube.

8. Replace the solvent reservoirs, and repeat for all of the other samples in the experiment.
9. Freeze the eluates at −80 °C.
10. Dry the frozen eluates in an unheated centrifugal concentrator until just barely dry by eye, then 5 min more, and store at −80 °C for up to 1 month.

3.10 Liquid Chromatography and Mass Spectrometry (See Note 28)

1. Visit with your LC-MS/MS collaborator to discuss the LC-MS/MS method.
2. Dissolve each sample in 25 μl of 0.1% formic acid for 20 min at RT, vortex well, pool any fractions that will be analyzed as a single LC-MS/MS injection, and inject ca. 25% of each gel fraction onto the LC-MS/MS (*see* **Note 10**).

3.11 Data Analysis

1. Search the data using an appropriate sequence database (containing a representative proteome, potential contaminants, and decoy sequences). Use search settings that match the theoretical accuracy of your mass spectrometer. The output from your proteomics search software must support protein quantification (*see* **Note 29**).
2. Conduct *T*-tests for statistically significant changes in protein expression in treated vs. untreated cells. For each protein, calculate the ratio of protein expression in treated vs. untreated cells, and transform that ratio to log2. Create a volcano plot, wherein the log2(ratio treated/untreated) is graphed on the x axis, while the log10(*T*-test *p*-value) is graphed on the y axis. Study the distribution of ratios and *p*-values, to visualize appropriate *p*-value and fold-change cutoff thresholds for "significant" changes in protein expression. Validate the *T*-test thresholds further by applying Benjamini–-Hochberg and/or random-permutations multiple tests corrections. Decide on a final strategy for selecting and defending your chosen *T*-test *p*-value threshold for "significance" (*see* **Note 30**).
3. Perform other testing, data visualization, data comparisons, and bioinformatic analyses as might be appropriate to the project goals.

4 Notes

1. At risk of sounding pedantic, the investigator should spend significant time and effort defining the study's goals and needs before making large LC-MS/MS investments. A proteomics project may spend several months queued for LC-MS/MS time, and large projects can require weeks, even months, to

complete the actual LC-MS/MS work. Moreover, LC-MS/MS projects can incur significant costs for instrument recharges. As such, "getting it right the first time" can be paramount, and questions like those posed below merit careful consideration before beginning. How many biological replicates will be necessary to support the statistical testing? Typically three independent replicates are obligatory, but five full replicates are considerably better. If validating a novel compound as an Hsp90 inhibitor, will parallel assays be required using flagship Hsp90 inhibitors? If not, what approach will be used to quantify similarities between the novel proteomics profile vs. those previously described? Is the cell/tissue model appropriate for the study's goals? Is enrichment for a specific sub-proteome needed (e.g., phosphopeptides, a specific organelle, etc.)? Reproducibility in label-free assays is strongest when LC-MS/MS assays are performed back-to-back: is this commitment justified at this point of the project, or would preliminary LC-MS/MS experiments be worthwhile to address unanswered questions, to test key assumptions, or to validate the sample preparations? How deeply into the proteome does the study need to probe? For the MS instrument available, is this depth readily achievable, or will orthogonal fractions of each sample be required, perhaps warranting an isotope coding strategy (e.g., SILAC, dimethyl labeling, iTRAQ, TMT, *see* [20]). Will the study encompass a very large number of samples, such that a multiplexed isotope tagging strategy might be justified to maximize the productivity of the MS instrument? Are the protein targets of the study predefined, such that a "targeted proteomics" approach might be preferred over a "shotgun" approach [21]? What software and personnel are available to analyze the raw instrument data, and to conduct the bioinformatic studies that typically follow the identification of a set of differentially expressed proteins? Answers to these questions have the potential to redirect the project toward profoundly different proteomics approaches, and investigators are strongly urged to thoroughly discuss their project with their mass spectrometry collaborator before beginning.

2. While "how much drug" seems simple at first glance, the question is actually quite subtle. The range and intensity of cellular responses to Hsp90 inhibition is dose-dependent. Classic Hsp90 inhibitors give a robust proteomics profile at dosages that are sub-apoptotic. Very high doses of some compounds can quickly drive some cell lines into advanced stages of apoptosis, complicating efforts to ascribe a given cellular response directly to Hsp90 inhibition. Moreover, the effective dosage of an Hsp90 inhibitor can vary among cell lines, growth rates, confluence, serum, and other factors. To balance these

complexities, the investigator should first characterize the status of their inhibitor-dosed cells, i.e., using assays such as those described in the accompanying chapter by Dr. Vladimir Gabai.

3. DMSO can be used to prepare very concentrated inhibitor stocks, thus minimizing the amount of drug vehicle applied to cell cultures. DMSO concentrations in treated culture media should not exceed 0.5%. Special attention is called to the ability of DMSO to readily deliver drugs across the skin barrier and through thin glove materials, and to the experimental nature of Hsp90 inhibitors, which should be considered to be teratogens and carcinogens. DMSO stocks of Hsp90 inhibitors should be considered to a significant laboratory hazard, even though the volumes used are quite small.

   Hsp90 inhibitors stocks can decay even when stored at −80 °C. This decay is certainly accelerated by freeze-thaw cycles. Caution is urged with regards the vitality of a given stored drug stock, and parallel assays to confirm drug potency are recommended.

4. How many flasks? One T75 flask of Jurkat cells containing 25 ml of untreated media and cultured as described will yield ca. 4×10^5 cells/ml, from which 1–2 mg of protein can be isolated. For attached cells, we might obtain 4–6 mg of protein from a single T75 flask. However, even moderate dosages of Hsp90 inhibitors are cytostatic in Jurkat cells, reducing yield by 50%. Compounds that are actively cytotoxic will reduce protein yields even further. For the protocols described here, 150 μg of lysate is needed for the LC-MS/MS work, but additional lysate is invaluable to facilitate parallel Western blot characterizations of apoptosis and client depletion.

5. We find that the EC_{50} of Hsp90 inhibition varies depending upon the status of the cell culture being assayed. For maximum reproducibility, investigators should utilize a standardized protocol for seeding the cell cultures used for the dose determinations (above), and use this same protocol for the planned proteomics assays. In our hands, Jurkat cell growth begins to plateau as cell density approaches 1×10^6 cells/ml. Although higher densities are achievable, investigators are advised to work slightly below this density to avoid growth plateaus. Similarly, investigators working with attached cell lines should probably not allow cultures to become confluent. Additionally, we find it prudent to routinely monitor the doubling rates of the maintenance cultures; Jurkat cells should double every 20–24 h, and failure to do so indicates an underlying problem with media, contamination, CO_2, temperature, technique, etc. Any changes in media or serum lot will require re-validation of the inhibitor's efficacy.

6. Jurkat cells treated with Hsp90 inhibitor are very fragile, and must be handled more gently than normal cells. To accommodate this, gentle minimal washing of the cells is recommended.
7. Excess 1×PBS wash buffer will result in lysates that are more dilute than the targets recommended below, but will not otherwise compromise the samples.
8. RIPA Buffer is a detergent-based cell-lysis buffer originally developed for radioimmunoprecipitation assays (hence the acronym). However, RIPA buffer disrupts Hsp90's interactions with clients [22], thus RIPA must not be used for Hsp90 interactomics. Dogmatically, RIPA solubilizes all cellular membranes, thus providing access to the majority of the mammalian proteome. Nuclear proteins are well represented in RIPA lysates, but we have not encountered DNA viscosity issues when lysing Jurkat cells. The diversity and depth of the proteome yield may be enhanced further by non-traditional lysis strategies [17], but we find it more convenient to prepare traditional RIPA lysates so that protein concentrations can be quantified confidently, and to support parallel Western blot assays. We find commercial RIPA preparations to be more stable and easier to use than homemade formulations. Some RIPA recipes contain phosphate, chelators, and reducing agent; we recommend omitting chelators and reducing agents in order to avoid interferences with downstream protein quantifications. Investigators might also choose to omit the phosphatase inhibitors recommended here, but the protease inhibitors are strongly recommended. Detergents can grossly compromise LC-MS/MS assays, but the detergents in the RIPA recipe provided here are readily removed by TCA/acetone precipitation. However, protein recoveries from TCA/acetone precipitations may be as low as 15%. In contrast to RIPA, CHAPS detergent cannot be removed by TCA/acetone precipitation, but the gel-based protocols described here will remove CHAPS handily. Nonetheless, we prefer to avoid lysis buffers containing CHAPS (e.g., MPER® from Thermo), to maintain flexibility among choices for subsequent LC-MS/MS approaches.

   PMSF is added to RIPA buffer immediately before lysis in order to inhibit serine proteases, but PMSF is also a potent inhibitor of acetylcholinesterase, making PMSF a toxicant that should be handled with great care. PMSF is degraded by even trace amounts of water, and thus should only be dissolved immediately prior to cell lysis.
9. Three aliquots of lysate are recommended to avoid freeze-thaw cycles, while supporting other goals such as protein quantitation (below) and Western blotting. With care, insights gained

from one aliquot (e.g., concentration) will extrapolate robustly to the other aliquots.

10. The SDS-PAGE Gel-LC technique addresses the most common issues encountered when preparing samples for LC-MS/MS, and also provides an orthogonal fractionation that increases LC-MS/MS coverage of a complex proteome. Orthogonality is achieved by separating proteins from each other by MW in the PAGE dimension, thus generating unique fractions of the proteome. Subsequently, the peptides from each individual PAGE fraction are separated via C18 peptide chromatography eluting directly into ion source of the mass spectrometer. Alternative strategies for orthogonal separations are available, and the investigator's attention is drawn to their prevalence in the literature. Orthogonal pre-fractionation can take the investigator 2–5 times deeper into an experimental proteome than might be achieved by analyzing the proteome using a single LC-MS/MS injection (often termed a "one-shot" or "single-shot" approach). Expectations for depth of penetration are discussed in the concluding remarks below.

    The Gel-LC approach described here generates orthogonal PAGE fractions, but is also useful when orthogonal separation is not required. That is, peptides isolated from the gel fractions described in this approach can be pooled in various ways to reduce the actual number of LC-MS/MS runs performed.

11. LC-MS/MS comparisons of two or more proteomes will be strongest if nearly identical amounts of protein are analyzed. Thus, much like Western blotting, accurate quantification of the cell lysates is important. Because RIPA interferes significantly with the Bradford assay, we recommend using the BCA assay to quantify RIPA lysates. Additionally, we routinely validate our spectrophotometric assays of lysate concentrations by running 20 μg of each lysate side-by-side on a single analytical PAGE gel, staining it with Coomassie blue, and inspecting it by eye for equivalency. Alternatively, PVDF membranes destined for Western blotting can be stained using 0.2× Coomassie R250 Stain, and destained in Fast destain, dried, imaged, and then re-wetted for subsequent use by Western blotting. Some imperfections in quantification can be addressed by *post hoc* data normalization, but grotesque errors in lysate equivalencies should be corrected, if feasible, prior to making large LC-MS/MS investments.

12. The amount of cell lysate recommended for Gel-LC is quite high relative to typical PAGE assays. Indeed, by most measures the lanes will be grossly overloaded, in order to provide the desired protein yields for subsequent analyses. This will cause band distortions and lane flaring. These effects are expected;

the gels are serving a preparative, not analytical, purpose here, and perfect protein banding is neither expected nor needed.

Loading hundreds of micrograms of protein into a single PAGE well requires high starting concentrations of cell lysates and/or the use of gels with very voluminous wells. It may be necessary to concentrate the samples prior to gel loading, e.g., spin concentrators or TCA/acetone precipitation (but *see* **Note 8**, above).

13. We utilize commercial gradient mini-gels (4–20% acrylamide) and/or larger-format hand-cast linear PAGE gels (10%). In both the cases, the SDS-PAGE separation should be minimal, running the dye front ca. 6 cm into the separating gel.

14. The very high sample loads recommended here require an offsetting reduction in staining. If the gel is inadvertently over-stained, it can difficult or impossible to subsequently remove the Coomassie stain from the samples. The optimally stained gel is just dark enough to confidently visualize the major bands.

    Miniscule amounts of protein will diffuse out of PAGE gels during the first few minutes of staining, subsequently contaminating all the surfaces of the PAGE gel. This is seldom an issue in the preparative gels used for Gel-LC here, but the phenomenon is worth noting with regards hyper-abundant proteins, negative control lanes, and assays such as immunadsorptions; do not load "input lysate" onto the same gels with an immunoadsorption.

15. A laminar flow hood is not essential; a clean bench area will suffice. However, the glass plates must be immaculately clean and soap-free; a tiny trace of lab detergent can devastate an LC-MS/MS sample. Use labware-grade detergents, rinse copiously with hot water, and then with deionized water.

16. The number of gel segments excised for each lane can be varied to meet project goals and resources, but the volume of gel cubes placed into each microcentrifuge tube must not exceed 150 µl of apparent tube volume. We recommend cutting a mini-gel into four segments, whereas larger gel formats require eight segments in order to fit each segment into its own tube. Investigators are cautioned; however, the more gel segments used, the harder it is to maintain quantitative reproducibility.

    When planning and executing the gel dissection, if high-abundance proteins/bands are apparent (i.e., IgG, BSA, RuBisCo), excise them from less populated regions of the gel, and run them on the LC-MS/MS separately from low-abundance fractions.

17. A common mistake is to dice or mince the gels. If the gel cubes are too small, they will shrink during dehydration to produce

acrylamide pieces that will be aspirated into the pipet tip during the washing steps. This leads to sample loss, and compromises quantitative rigor.

18. Ammonium bicarbonate (ABC) is used throughout this protocol to buffer the trypsinolysis of the gel cubes. ABC does not require acid/base adjustment to generate the appropriate pH (ca. 8.5), but bicarbonate is volatile, and thus ABC solutions must be made fresh the same day that they are used.

    Some brands of pipet tip can shed significant polymeric residue ("mold release agent") from the manufacturing process, esp. 1-ml "blue" tips. Validate your tips by LC-MS/MS, or use tips recommended by your MS collaborator.

19. If the gel was over-stained, destaining may be prohibitively slow, or even impossible. In this case, it may be necessary to cycle between Gel Wash Solution and 100% acetonitrile in attempts to drive the destaining process.

    For all the steps that call for removing solvent or sample from the gel cubes (e.g., **step 3** in Subheading 3.6), push the pipet tip through the cube slurry, and hold it just tightly enough to the bottom of the tube so that there is not enough space to accidentally aspirate a gel cube.

20. Recall that 100% ACN will dehydrate the gel pieces, and they will shrink considerably, and may shrink to sizes so small that they can be accidentally aspirated up into the pipet tips.

21. In this protocol, disulfide bonds are reduced and Cys residues alkylated by the sequential actions of TCEP and IAA, respectively. IAA is a potent toxin, and should be handled with care. Although IAA primarily alkylates Cys, IAA will slowly alkylate other residues, and excessive concentrations or prolonged incubations exacerbate this artifact. IAA should not be used if the project might ask questions about ubiquitinylation, because the mass of IAA-Lysine di-alkylation artifacts is identical to that of the Gly-Gly isopeptide stubs produced by trysinolysis of ubiquitinylated peptides. For ubiquitin studies, use an alternative alkylation reagent.

22. The rehydration/trypsin infiltration step should be performed on ice to minimize trypsin autolysis. If desired, trypsinolysis can be enhanced by using Trypsin/Lys-C enzyme mixes and commercial MS-compatible detergent supplements, perhaps improving rates of protein identification, accuracy of protein quantitation, and analytical reproducibility. At minimum, use high-quality methylated trypsin ("sequencing grade" or "MS-grade").

23. Excess unabsorbed trypsin will lead to exaggerated amounts of trypsin autolysis peptide; hence, the goal here is to remove all of the unabsorbed trypsin.

24. Many protocols recommend shorter incubations for the trypsin digestions, but the work preceding the trypsin infiltration typically takes most of a day, making overnight digestions more convenient.
25. The volumes of extraction solvent and the incubation times used here are much greater than those traditionally used to extract gel bands or 2-D spots. This reflects the need to efficiently extract peptides from large volumes of acrylamide.
26. The vacuum concentrator must be approved for organic solvents and corrosives.
27. When large gel volumes are processed, Protocol 3.8 may yield samples that contain large amounts of salt and/or acrylamide debris. In this case, a solid phase extraction step (Protocol 3.9) is necessary to prevent samples from clogging the capillary lines and columns used in nanospray LC-MS/MS. Anecdotal evidence suggests that raw acrylamide extracts can foul electrospray tips prematurely, and that SPE can prolong tip performance. If a decision is made to perform solid phase extraction, all of the samples in an experiment should be handled in the same way: either do SPE for all the samples, or for none of them.

    This protocol uses commercial C18 material prepared as a monolithic matrix in the end of a pipet tip, and having a peptide-binding capacity of 50–100 μg. Manufacturers typically supply their own protocol, but the "universal" protocol provided here minimizes the number of solutions required. Solutions for SPE should be made up using MS-grade solvents. New users tend to make two mistakes. The first is that they become habituated to pipetting "up and down" during the protocol. As a result, in **step 7** in Subheading 3.9 they draw the eluting 70/0.1 Solvent up into the tip and then immediately eject it back into the solvent reservoir, thus losing the sample.

    A second common mistake is less problematic: drawing air into the tip at some point during the equilibration steps. In this case, the tip can be rescued simply by repeating the whole wetting and equilibration protocol—*if the peptides have not yet been bound to the tip.*

    When the de-salted peptides are re-concentrated by vacuum centrifugation, samples can become re-contaminated with particulates (dust or lint), or if placed into low-quality tubes or vials. Thus, the vacuum concentrator should be kept scrupulously clean. Tubes and vials should be of the highest quality, should be stored in closed containers, and kept capped when feasible.
28. It is beyond the scope of this Protocols article to attempt an exhaustive analysis of the range of the LC-MS/MS approaches

that can be used to probe the Hsp90-dependent proteome; investigators are instead directed to broad reviews of the mass spectrometry discipline [14, 17] and to recent deep proteomics assays of Hsp90 inhibition [2, 3, 5, 7]. Nonetheless, some basic suggestions follow in the hopes that they will facilitate a conversation between the Hsp90 investigator and their mass spectrometry collaborator.

Most proteomics studies are performed using capillary columns with an inner diameter of 75 μm. Typically, a 75 μm column can be loaded with up to 1.0–2.0 μg of peptide sample; fewer proteins will be identified and quantified if less sample is injected. Although this protocol begins with 150 μg of protein, the actual peptide yields are much lower. We recommend LC-MS/MS sample injections that represent 20–25% of the total material recovered from each gel fraction. Ideally, this will yield a heavy column load that causes minor tailing of the major peaks. On Thermo Q Exactive or Fusion instruments, this amount of Jurkat lysate corresponds to peptide ion intensities that approach 1×10^9 in the Base Peak Chromatogram view. Less diverse samples (i.e., dominated by an abundant protein(s)) will overload the column chromatography at lower sample loads.

Other chromatography factors also determine the number of proteins identified and quantified. It is well established that protein discovery is improved by using longer columns, smaller C18 particles, and longer HPLC gradients. We currently use columns 40 cm long, packed with C18 particles 3 μm in diameter, and heated to 45 °C. Such columns generate ca. 3000 psi backpressure, allowing robust day-to-day performance using standard-pressure nano-HPLC systems. In contrast, columns packed with 40–50 cm of 2 μm C18 particles can generate truly impressive coverage of the mammalian proteome, but this requires nano-LC pumps, fittings, and columns capable of withstanding very high backpressures ("UPLC").

An additional factor is the acetonitrile gradient used to elute peptides from the C18 column. Longer gradient times facilitate more protein discoveries, but at the expense of monopolizing the LC-MS/MS system. Because the Hsp90 inhibitor profile is robust and readily apparent, we currently elute peptides over a 100 min period, during which time the acetonitrile composition increases from 0% to 40% acetonitrile. Where maximum coverage of the proteome is desired, however, gradients of up to 4 h might be employed. For even deeper proteome coverage, long gradients are combined with upstream orthogonal fractionations. Because complex orthogonal fractionations introduce technical variability, they are typically employed in conjunction with an isotopic labeling strategy. *See* the discussion of expectations below.

29. To analyze the impacts of Hsp90 inhibitors on the cellular proteome, we currently use the "label-free quantitation" (LFQ) algorithm within the MaxQuant application [23, 24]. MaxQuantLFQ values are normalized throughout the peptide population seen in the whole experiment, to correct for technical variation among samples. Moreover, LFQ statements of individual protein abundances derive equally from all of a protein's peptides. MaxQuant can be used to analyze raw data from high-resolution Thermo Orbitrap instruments, and has also recently been modified to accept data from a Bruker QTOF instrument [25]. MaxQuant output consists of a large number of tab-delimited text files that can be ported to other applications. MaxQuant can be freely downloaded at http://www.coxdocs.org/doku.php, and is supported by numerous online presentations and forums, and by a popular summer training course at the Max Planck Institute of Biochemistry.

    The files generated by modern mass spectrometer can be quite large, generating Gb of data per LC-MS/MS run. As such, the computational power needed for a large proteomics project can be significant, and warrants a separate discussion between the investigator, their proteomics collaborator, and their bioinformatics team. Similar considerations should be made with regards data management and archiving.

30. We currently use the Perseus application [26] for biostatistics and informatics. Perseus can open MaxQuant output directly, and can also open other tabular text files. Like MaxQuant, Perseus is supported by numerous online presentations and forums, and by the Max Planck Institute of Biochemistry training course. Special attention is called to the Benjamini–Hochberg tests and random permutations tests available in Perseus, and the need to use these tools (or some other approach) to validate the investigator's choice of a given *p*-value threshold as "significant" (*see* [27] for discussion). Perseus can be downloaded at http://www.coxdocs.org/doku.php.

    Expectations and Summary—We can obtain a total of 5000 primary protein quantifications from a single Jurkat sample (as measured values, without imputation, based upon a minimum of two peptide ratios) when 150 µg of Jurkat RIPA lysate is pre-fractionated into eight Gel-LC segments, each injected separately onto a 40 cm column containing 3-µm C18 particles developed using a 100-min gradient, and eluted into the nanospray ion source of an Orbitrap Fusion mass spectrometer. Four Gel-LC fractions (four injections) yield 4000 protein quantifications. Two-fractions will quantify ca. 2500 proteins, and we obtain comparable rates of protein quantification from "one shot" analyses of Jurkat RIPA lysates.

However, older-generation mass spectrometers yield lower rates of identification and quantification: when using a 2007-vintage OrbitrapXL mass spectrometer, we obtain ca. 3000 protein identifications when 100 μg of pooled SILAC lysates are fractioned into ten Gel-LC segments and separated on longer 220 min gradients (also *see* [7]).

The Gel-LC approach described here is a compromise between sensitivity, vs. simple techniques, widely available equipment, robustness performance, and shared usage of LC-MS/MS instruments. Alternatively, 4000–8000 proteins can routinely be quantified when the latest generation of mass spectrometers is coupled to advanced techniques for sample preparation, chromatography, and data analysis, and specialized efforts can generate even deeper coverage [17].

However, this increase in proteome depth is typically associated with offsetting costs: analyzing 15 orthogonal fractions on long C18 gradients might increase protein quantifications by 25–50%, but could require a sevenfold increase in LC-MS/MS instrument time (e.g., 2–3 days of LC-MS/MS per biological sample). In reply to this bottleneck, some groups have identified 4000–8000 proteins using high-efficiency "one-shot" LC-MS/MS approaches [28–32].

Thus, investigators wishing to profile the effects of Hsp90 inhibition face choices among options for sample preparation and LC-MS/MS. These choices will be guided by the specific goals of the project. Investigators pursuing novel deep mechanistic queries should weigh the benefits of the deep proteome coverage offered by emerging technologies. On the other hand, investigators wishing to simply and robustly validate an emerging Hsp90 inhibitor can confidently do so on the basis of 4000 easily obtained protein quantifications described here.

References

1. Che Y, Best OG, Zhong L, Kaufman KL, Mactier S, Raftery M, Graves LM, Mulligan SP, Christopherson RI (2013) Hsp90 inhibitor SNX-7081 dysregulates proteins involved with DNA repair and replication and the cell cycle in human chronic lymphocytic leukemia (CLL) cells. J Proteome Res 12(4):1710–1722. https://doi.org/10.1021/pr301055y
2. Fierro-Monti I, Echeverria P, Racle J, Hernandez C, Picard D, Quadroni M (2013) Dynamic impacts of the inhibition of the molecular chaperone Hsp90 on the T-cell proteome have implications for anti-cancer therapy. PLoS One 8(11):e80425. https://doi.org/10.1371/journal.pone.0080425
3. Jacobson C, Kopp N, Layer JV, Redd RA, Tschuri S, Haebe S, van Bodegom D, Bird L, Christie AL, Christodoulou A, Saur A, Tivey T, Zapf S, Bararia D, Zimber-Strobl U, Rodig SJ, Weigert O, Weinstock DM (2016) HSP90 inhibition overcomes ibrutinib resistance in mantle cell lymphoma. Blood. https://doi.org/10.1182/blood-2016-04-711176
4. Samant RS, Clarke PA, Workman P (2012) The expanding proteome of the molecular chaperone HSP90. Cell Cycle 11(7):1301–1308. https://doi.org/10.4161/cc.19722
5. Sharma K, Vabulas RM, Macek B, Pinkert S, Cox J, Mann M, Hartl FU (2012) Quantitative proteomics reveals that Hsp90 inhibition preferentially targets kinases and the DNA damage

response. Mol Cell Proteomics 11(3): M111.014654. https://doi.org/10.1074/mcp.M111.014654

6. Voruganti S, Lacroix JC, Rogers CN, Rogers J, Matts RL, Hartson SD (2013) The anticancer drug AUY922 generates a proteomics fingerprint that is highly conserved among structurally diverse Hsp90 inhibitors. J Proteome Res 12(8):3697–3706. https://doi.org/10.1021/pr400321x
7. Wu Z, Gholami AM, Kuster B (2012) Systematic identification of the HSP90 candidate regulated proteome. Mol Cell Proteomics 11 (6):M111.016675. https://doi.org/10.1074/mcp.M111.016675
8. Hartson SD, Matts RL (2012) Approaches for defining the Hsp90-dependent proteome. Biochim Biophys Acta 1823(3):656–667. https://doi.org/10.1016/j.bbamcr.2011.08.013
9. Whitesell L, Mimnaugh EG, De Costa B, Myers CE, Neckers LM (1994) Inhibition of heat shock protein HSP90-pp60v-src heteroprotein complex formation by benzoquinone ansamycins: essential role for stress proteins in oncogenic transformation. Proc Natl Acad Sci U S A 91(18):8324–8328
10. Schulte TW, Blagosklonny MV, Ingui C, Neckers L (1995) Disruption of the Raf-1-Hsp90 molecular complex results in destabilization of Raf-1 and loss of Raf-1-Ras association. J Biol Chem 270(41):24585–24588
11. Smith DF, Whitesell L, Nair SC, Chen S, Prapapanich V, Rimerman RA (1995) Progesterone receptor structure and function altered by geldanamycin, an hsp90-binding agent. Mol Cell Biol 15(12):6804–6812
12. Hartson SD, Barrett DJ, Burn P, Matts RL (1996) Hsp90-mediated folding of the lymphoid cell kinase p56lck. Biochemistry 35 (41):13451–13459. https://doi.org/10.1021/bi961332c
13. Schulte TW, Blagosklonny MV, Romanova L, Mushinski JF, Monia BP, Johnston JF, Nguyen P, Trepel J, Neckers LM (1996) Destabilization of Raf-1 by geldanamycin leads to disruption of the Raf-1-MEK-mitogen-activated protein kinase signalling pathway. Mol Cell Biol 16(10):5839–5845
14. Aebersold R, Mann M (2016) Mass-spectrometric exploration of proteome structure and function. Nature 537 (7620):347–355. https://doi.org/10.1038/nature19949
15. Blagoev B, Ong SE, Kratchmarova I, Mann M (2004) Temporal analysis of phosphotyrosine-dependent signaling networks by quantitative proteomics. Nat Biotechnol 22 (9):1139–1145. https://doi.org/10.1038/nbt1005
16. Hubner NC, Ren S, Mann M (2008) Peptide separation with immobilized pI strips is an attractive alternative to in-gel protein digestion for proteome analysis. Proteomics 8 (23–24):4862–4872. https://doi.org/10.1002/pmic.200800351
17. Richards AL, Merrill AE, Coon JJ (2015) Proteome sequencing goes deep. Curr Opin Chem Biol 24:11–17. https://doi.org/10.1016/j.cbpa.2014.10.017
18. Ong SE, Blagoev B, Kratchmarova I, Kristensen DB, Steen H, Pandey A, Mann M (2002) Stable isotope labeling by amino acids in cell culture, SILAC, as a simple and accurate approach to expression proteomics. Mol Cell Proteomics 1(5):376–386
19. Batth TS, Olsen JV (2016) Offline high pH reversed-phase peptide fractionation for deep phosphoproteome coverage. Methods Mol Biol 1355:179–192. https://doi.org/10.1007/978-1-4939-3049-4_12
20. Lau KW, Jones AR, Swainston N, Siepen JA, Hubbard SJ (2007) Capture and analysis of quantitative proteomic data. Proteomics 7 (16):2787–2799. https://doi.org/10.1002/pmic.200700127
21. Remily-Wood ER, Liu RZ, Xiang Y, Chen Y, Thomas CE, Rajyaguru N, Kaufman LM, Ochoa JE, Hazlehurst L, Pinilla-Ibarz J, Lancet J, Zhang G, Haura E, Shibata D, Yeatman T, Smalley KS, Dalton WS, Huang E, Scott E, Bloom GC, Eschrich SA, Koomen JM (2011) A database of reaction monitoring mass spectrometry assays for elucidating therapeutic response in cancer. Proteomics Clin Appl 5(7–8):383–396. https://doi.org/10.1002/prca.201000115
22. Hartson SD, Matts RL (1994) Association of Hsp90 with cellular Src-family kinases in a cell-free system correlates with altered kinase structure and function. Biochemistry 33 (30):8912–8920
23. Cox J, Hein MY, Luber CA, Paron I, Nagaraj N, Mann M (2014) Accurate proteome-wide label-free quantification by delayed normalization and maximal peptide ratio extraction, termed MaxLFQ. Mol Cell Proteomics 13(9):2513–2526. https://doi.org/10.1074/mcp.M113.031591
24. Cox J, Mann M (2008) MaxQuant enables high peptide identification rates, individualized p.p.b.-range mass accuracies and proteome-wide protein quantification. Nat Biotechnol 26(12):1367–1372. https://doi.org/10.1038/nbt.1511

25. Beck S, Michalski A, Raether O, Lubeck M, Kaspar S, Goedecke N, Baessmann C, Hornburg D, Meier F, Paron I, Kulak NA, Cox J, Mann M (2015) The impact II, a very high-resolution quadrupole time-of-flight instrument (QTOF) for deep shotgun proteomics. Mol Cell Proteomics 14(7):2014–2029. https://doi.org/10.1074/mcp.M114.047407
26. Tyanova S, Temu T, Sinitcyn P, Carlson A, Hein MY, Geiger T, Mann M, Cox J (2016) The Perseus computational platform for comprehensive analysis of (prote)omics data. Nat Methods 13(9):731–740. https://doi.org/10.1038/nmeth.3901
27. Diz AP, Carvajal-Rodriguez A, Skibinski DO (2011) Multiple hypothesis testing in proteomics: a strategy for experimental work. Mol Cell Proteomics 10(3):M110.004374. https://doi.org/10.1074/mcp.M110.004374
28. Coscia F, Watters KM, Curtis M, Eckert MA, Chiang CY, Tyanova S, Montag A, Lastra RR, Lengyel E, Mann M (2016) Integrative proteomic profiling of ovarian cancer cell lines reveals precursor cell associated proteins and functional status. Nat Commun 7:12645. https://doi.org/10.1038/ncomms12645
29. Cristobal A, Hennrich ML, Giansanti P, Goerdayal SS, Heck AJ, Mohammed S (2012) In-house construction of a UHPLC system enabling the identification of over 4000 protein groups in a single analysis. Analyst 137(15):3541–3548. https://doi.org/10.1039/c2an35445d
30. Hebert AS, Richards AL, Bailey DJ, Ulbrich A, Coughlin EE, Westphall MS, Coon JJ (2014) The one hour yeast proteome. Mol Cell Proteomics 13(1):339–347. https://doi.org/10.1074/mcp.M113.034769
31. Pirmoradian M, Budamgunta H, Chingin K, Zhang B, Astorga-Wells J, Zubarev RA (2013) Rapid and deep human proteome analysis by single-dimension shotgun proteomics. Mol Cell Proteomics 12(11):3330–3338. https://doi.org/10.1074/mcp.O113.028787
32. Sacco F, Silvestri A, Posca D, Pirro S, Gherardini PF, Castagnoli L, Mann M, Cesareni G (2016) Deep proteomics of breast cancer cells reveals that metformin rewires signaling networks away from a pro-growth state. Cell Syst 2(3):159–171. https://doi.org/10.1016/j.cels.2016.02.005

Chapter 12

Analysis of HspB1 (Hsp27) Oligomerization and Phosphorylation Patterns and Its Interaction with Specific Client Polypeptides

André-Patrick Arrigo

Abstract

Human HspB1 (also denoted as Hsp27) belongs to the family of small (or stress) proteins (sHsps). The family, which contains ten members including αA,B-crystallin polypeptides, is characterized by a conserved C-terminal α-crystallin domain and molecular weights ranging from 20 to 40 kDa. Here, procedures are described for analyzing the dynamic oligomerization and phosphorylation patterns of HspB1 in cells exposed to different environments. Changes in the structural organization of HspB1 can reprogram its interaction with specific partner/client polypeptides. Methods are presented to analyze these interactions using tissue culture cells genetically modified to express different levels of this protein. In addition, the laboratory approaches presented here could be used to test the nine other human sHsp members as well as sHsps from other species.

Key words Small stress proteins, Heat shock proteins, Hsp27/B1-oligomerization, Phosphorylation

Abbreviations

Hsp27/B1	Heat shock protein 27/B1
Hsps	heat shock proteins
sHsp	small stress proteins

1 Introduction

HspB1 synthesis is stimulated when the cells are exposed to sub-lethal stress conditions that alter the folding of proteins [1]. This leads to enhanced resistance of cells to heat shock and other injuries. HspB1 is also constitutively expressed in numerous human cells, particularly in pathological conditions [2]. In humans, HspB1 is part of a family of ten different proteins (denoted as HspB1 to HspB10) [3], plus an additional less conserved

Stuart K. Calderwood and Thomas L. Prince (eds.), *Chaperones: Methods and Protocols*, Methods in Molecular Biology, vol. 1709, https://doi.org/10.1007/978-1-4939-7477-1_12,

polypeptide (Hsp16.2). The different members of this family have in common a C-terminal α-crystallin domain (about 40% of the protein) found in αA,B-crystallin polypeptides from the vertebrate eye [1, 4, 5] (Fig. 1A). sHsps are also characterized by a flexible C-terminal tail and a less conserved N-terminal domain containing an hydrophobic WDPF motif. As a consequence of their particular amino acids sequence, an intriguing property of sHsps is their ability to oligomerize in a complex and often heterogeneous way [1, 6] (Fig. 1A). The phenomenon is controlled, at least in some sHsp (i.e., HspB1), by stress-mediated phosphorylation-sensitive interactions in their N-terminal part [7]. Tetramers assembled from dimers appear as the building blocks of sHsps polydispersed oligomeric complexes [8]. Oligomerization of sHsps is dynamic and, as shown in the case of HspB1, the phenomenon is linked to the physiology of the cell [1, 6, 9–13]. The rapid changes in the oligomerization/phosphorylation status of sHsps can therefore be considered a sensor of the physiological status of cells (*see* Fig. 1B). Several sHsps (HspB1, Hsp4, Hsp5, HspB8, and Hsp16.2) are molecular chaperones that share an ATP-independent holdase activity. In stress conditions that alter protein folding (i.e., heat shock), the holdase activity favors interaction with misfolded polypeptides and subsequently their storage in a refolding competent state [14–19]. The phenomenon attenuates and/or suppresses irreversible protein aggregation that could be deleterious to the cell (*see* Fig. 1B). HspB1 holdase activity modulates the dynamic ability of this protein to change its oligomerization profile in order to trap and store denatured polypeptides (Fig. 1b). This activity differs from the ATP-dependent foldase chaperones (Hsp70, Hsp90, and Hsp60) that refold misfolded polypeptides [20–22], such as those trapped within large HspB1 large oligomeric structures [23–25]. Trapped polypeptides can also end up being degraded, as for example in the case of irreversibly oxidized proteins.

Recently, intriguing observations, made both in stressed and in non-stressed cells, point to the fact that sHsps are involved in many different cellular mechanisms suggesting that they have a large number of functions in the cell. The apparent pleiotropic activity of sHsps probably results from their chaperone activity which allow them to bind and stabilize the folding of a large number of protein client targets. Consequently, they stimulate their activity and/or modulate their half-life [26–31]. For example, pro-caspase 3, which interacts with HspB1, shows a proteasome-dependent proteolytic degradation in HspB1 immunodepleted cells [27, 32]. In contrast, the phosphatase PTEN is stabilized by its interaction with HspB1; a phenomenon that modulates the PI3K-Akt survival pathway [33]. Alteration in sHsps chaperone activity can therefore deregulate cellular homeostasis. The phenomenon is similar to the already

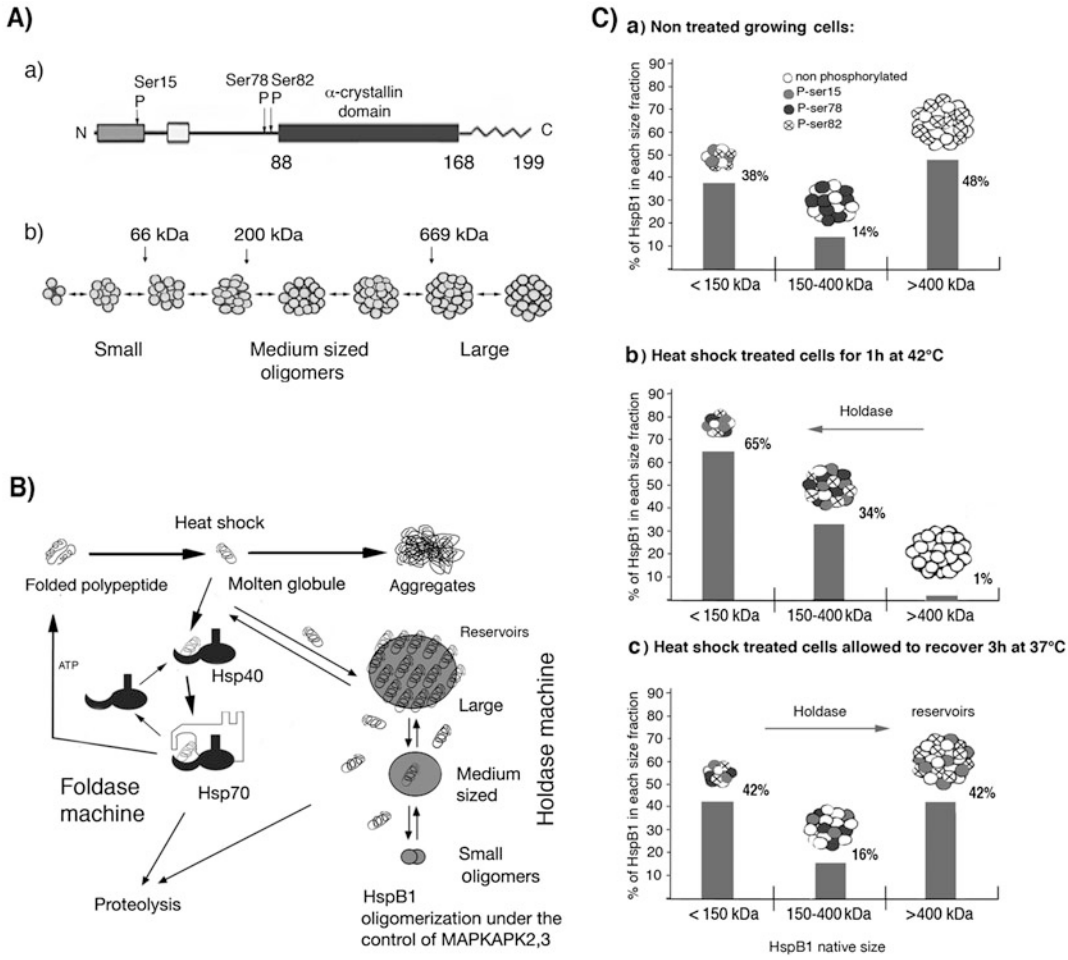

Fig. 1 (**A**) HspB1. (*a*) Organization of human HspB1 protein sequences. *Gray* box: N-terminal WD/EPF domain; light box:conserved region; *dark gray* box: alpha crystallin domain (aa 88–168); wave-like line: flexible C-terminal domain; P: phosphorylated serine residues. Amino acid number is indicated. (*b*) Oligomeric structure of HspB1 (from dimers to molecular masses larger than 700 kDa). Mosaic heterooligomers formed by different sHsps and/or their phosphorylated forms have been detected. (**B**) Exposure to stress alters the folding of polypeptides, which then accumulate as molten globules having the tendency to form deleterious aggregates. Molten globules are recognized by Hsp40 and are immediately refolded by ATP-dependent foldase chaperones (Hsp70), stored by HspB1 holdase chaperone to avoid their aggregation, or eliminated through proteolytic degradation. Rapid changes in HspB1 oligomerization and phosphorylation are observed during and after heat shock that probably reflect the capture and storage of the misfolded polypeptides. (**C**) Analysis of HspB1 oligomerization and phosphorylation in response to a heat stress of 1 h at 42 °C. The % of HspB1 displaying native molecular masses smaller than 150 kDa in the 150–400 kDa range and larger than 400 kDa is presented. Note that heat shock rapidly shifts HspB1 toward small oligomers. The phenomenon is transient, and 3 h after the heat shock HspB1 reforms large oligomers. However, the pattern of phosphorylation is drastically different from that observed in nontreated cells. This reflects changes in HspB1 holdase activity to better cope misfolded polypeptides

described "chaperone/client protein concept" mediated by Hsp90 [34, 35]. Future studies will let us know whether this is a fundamental property of chaperones or if it is restricted to some heat shock proteins. This property indirectly links constitutively expressed sHsps to numerous unrelated cellular functions and may explain the large number of effets associated with the expression of these proteins described in the current literature [31]. For example, HspB1 indirectly modulates mRNA translation by interacting with the initiation translation factor eIF4G [36]. HspB1 also stabilizes the cytoskeleton [37]. In cells exposed to oxidative [38] or apoptotic [39] conditions as well as in differentiating cells [40], the protective effects of HspB1 originate from its interaction with several crucial "client" regulators, as for example pro-caspase-3, cytochrome c, Daxx, GATA-1, PTEN, Ubiquitin, UBC-9, eIF4E, and Stat polypeptides [27]. The holdase activity may also be responsible for HspB1 and/or HspB5 direct or indirect effects toward Akt, Bax, Bcl-xs polypeptides and PKCα, Raf/MEK/ERK, Akt, Snail signaling pathways [41–44]. Other examples are HspB8 which, by interacting with Bag-3, indirectly modulates autophagy [45] and the well-known reciprocal holding of αB-crystallin (HspB5) and αA-crystallin (HspB4) in the lens eye. In differentiating muscle cells, HspB1 could also modulate the switch from the keratin MK5/MK14 network to the keratin MK1/MK10 network [46].

Does the holdase activity of HspB1 toward different clients depend or not on the formation of large oligomeric structures such as those trapping the heat shock-induced misfolded substrates (Fig. 1C)? The problem appears rather complex since the relationship between oligomerization, phosphorylation, and holdase activity was shown to be sHsp specific [10, 47, 48]. In that regard, our new observations revealed that, in response to different apoptotic inducers, the dynamic re-organization of HspB1 oligomerization/phosphorylation is an inducer-specific phenomenon which leads to the transient formation of new HspB1 structural platforms [13] that can interact with specific client polypeptides [27, 29, 31]. Another important property of sHps is their ability to interact and form complex mosaic oligomeric structures [29, 49–52]. For example, in the eye, HspB4 and HspB5 form a 3–1 unique large mosaic oligomer, called α-crystallin [53, 54]. In cells expressing several sHsps, complex and multiple combinatorial oligomeric structures are formed that may bear specific protein target recognition abilities [28–31]. Interactions between sHsps can also exclude some sHsp partners and therefore the recognition of distinct molecular targets. Only few of these complex structures have been characterized yet. Hence, small Hsps interaction networks are probably highly modulatable systems that can rapidly adapt to changes in cellular physiology [29, 31].

In this chapter, procedures are described for testing the oligomerization and phosphorylation patterns of HspB1 in response to change in the cellular environment. Methods to analyze its interaction with specific partner/client polypeptides are also reported using tissue culture cells genetically modified to express different levels of this protein. The procedures have been developed in my laboratory and could be used in any well-established cellular laboratory.

2 Materials

All reagents and materials used in the culture of tissue culture cells are sterile.

1. PBS medium: 137 mM NaCl, 2.7 mM KCl, 8 mM Na_2HPO_4, and 1.5 mM KH_2PO_4, pH 7.4.
2. Cell culture medium (HeLa cells): DMEM medium (Life Technologies, #41966052) containing 4.5 g/l glucose, 1 mM sodium pyruvate, L-glutamine supplemented with 5000 U/ml penicillin-streptomycin (Life Technologies, # 15070063), 250 μg/ml Fungizone (Life Technologies, # 15290026). 5–10% fetal calf serum (Life Technologies # 10270106) is added to cell culture medium. Fetal calf serum is kept at −70 °C. The cell culture medium is stored at 4 °C without serum and used within 5 weeks of supplementation. Medium containing serum is made fresh and used within 1 week of supplementation (storage at 4 °C). Geneticin G418 (Gibco BRL, # 11811049) must be present in the medium to select stably transfected clones. The culture medium is filtered in sterile conditions on 0.2 μm filters.
3. Trypsination buffer: PBS containing 0.05% Trypsin (Gibco BRL, # 35400027). The buffer is stored in aliquots at −20 °C.
4. Cell culture dishes (TPP, #93060) (Corning, # 430167).
5. Inverted photomicroscope equipped with phase-contrast equipment (i.e., TMS Nikon).
6. Trypan blue (Sigma-Aldrich, # T 0776).
7. Hemocytometer chamber.
8. TEM buffer (Tris–HCl pH 7.4, 20 mM; NaCl 20 mM; MgCl2 5 mM; EDTA 0.1 mM).
9. IPP 150 buffer (Tris–HCl PH 8; NaCl 150 mM; NP-40 0.05%).
10. IPP 300 buffer (Tris–HCl PH 8; NaCl 300 mM; NP-40 0.05%).

11. Monoclonal anti-human HspB1 (Stressgen, #H00027129-M01) antibody as well as polyclonal antibodies that specifically recognize HspB1 phosphorylated either at serine 15 (Stressgen #SPA-525), 78 (Stressgen #SPA-523), or 82 (Stressgen #SPA-524). Normal immunoglobulins (Santa Cruz Biotechnology, #sc-2025), secondary goat-anti mouse, or rabbit antibodies were provided by Santa Cruz Biotechnology (#sc-2031, sc-2030).
12. Recombinant human HspB1/27 (Stressgen, # SPP-715).
13. ECL kit from GE Healthcare (Amersham) (# RPN 2105).
14. Protein G-agarose (Sigma-Aldrich, #P7700).
15. Dithiothreitol (DTT) (Gibco, BRL, # 15508-013).
16. Triton X100 (Sigma-Aldrich # T 9284).
17. X-Omat AR films (Eastman Kodak Co, #1651454).
18. Cytochalasin D (Sigma-Aldrich, #C8273).
19. MG-132 (Sigma-Aldrich, #C2211).
20. Pre-swollen Sepharose 6B (Sigma-Aldrich, #6B100).
21. Gel filtration column (1 cm × 100 cm) (GE Healthcare Pharmacia, #28-4064-15).
22. Fraction collector (BioRad model 2110).
23. Peristaltic pump (BioRad model EP-1 Econo Pump).
24. Kit for Molecular Weights 29,000–700,000 for Gel Filtration Chromatography (Sigma-Aldrich, #MWND500).
25. Ampholines pH 3–10 and pH 5–7 (BioRad, #163-1113 and 163-1153).
26. Lipofectamine™ reagent (Invitrogen, #18324-020).
27. pCIneohsp27 sense and antisense cDNA vectors [55] were constructed using a EcoRI-EcoRI DNA fragment of plasmid psvhsp27 [56] that was inserted, in normal or reverse orientation, in the EcoRI sites of pCIneo vector (Promega, #E1841). The vectors bear a neomycin gene and the entire coding sequence of the human hspB1 gene placed in normal or reverse orientation downstream of the CMV promoter.
28. Mammalian vector Bluescript pKS vector plain or bearing wild-type human Hsp27/B1 gene (cDNApKS27wt), non-phosphorylatable mutant (three serine sites replaced by alanine, pKS2711-3A), or phospho-mimicry mutant (three serine sites replaced by aspartic acid, pKS2711-3D) were already described [9].
29. The pSuper RNAi system (Oligoengine, #VEC-pBS-0004; www.oligoengine.com) was used to direct intracellular synthesis of siRNA transcripts causing efficient and specific HspB1

gene silencing [57]. The mismatch, scramble, and HspB1 targetting pSuperneo vectors were prepared as previously described [38].

3 Methods

3.1 Cell Culture

When the cells reach 80–100% confluency proceed as follows:

1. Aspirate by pipetting the medium from the cell cultures.
2. Wash with PBS.
3. Add 1 ml of trypsin buffer to the culture dish. Let the dish stand for 2–3 min at 37 ° C and monitor under the microscope for the detachment of cells. Cell detachment can be accelerated by gently pipetting the buffer up and down.
4. Remove the trypsin buffer containing the detached cells from the dish and place it in a conical centrifuge tube. Rinse the dish with the complete culture medium and add it to the centrifuge tube. Serum is required to inhibit the action of trypsin.
5. Centrifuge the cell suspension at 1500 × *g* for 3 min and resuspend the cell pellet in 10 ml of complete culture medium. Count the cells and record for their viability using Trypan blue staining exclusion assay.

3.2 HspB1 Intracellular Distribution and Native Size

HspB1 is an oligomeric protein characterized by dynamic heterogeneous native sizes ranging between 50 and 700 kDa. In exponentially growing Hela cells, constitutively expressed HspB1 is recovered in two major oligomeric structures with native molecular masses comprised between 50 and 200 kDa (small oligomers) and 200 and 700 kDa (large oligomers) (*see* Fig. 1). Heat shock induces a phosphorylation-dependent dynamic redistribution of HspB1 structures toward small oligomers that bind polypeptides whose conformation is altered by heat shock. In cells recovering from heat shock, large HspB1 oligomers are recovered that store conformation altered proteins. Analysis of the oligomeric structures of HspB1 in the cells exposed to apoptotic inducers has revealed complex and inducer-specific changes in HspB1 oligomerization [13] that differed from those observed after heat shock, oxidative stress [58], or exposure to TNFα [59]. These changes may reflect putative interactions of HspB1 with key cellular regulators. To detect the dynamic changes in HspB1 distribution upon cell fractionation as well as its native size, cells expressing high loads of HspB1 have to be used, as for example HeLa cells that constitutively express 0.4 ng of HsB1 per μg of total cellular proteins. A fraction of HspB1 associates, in an F-actin integrity-dependent way, with non-ionic detergent sensitive structures, such as the plasma

membrane cytoskeleton compartment where actin nucleation occurs [60].

1. Expose cells, kept in a 37 °C incubator, to various stress inducers. Control non stressed cells are kept at 37 °C. Heat shock should be performed in a temperature-controlled water bath (+/− 0.1 °C) rather than in a cell culture incubator.

3.2.1 Cell Fractionation

1. Cells, washed in ice-cold PBS, pH 7.4, are lysed at 4 °C in a Dounce homogenizer in TEM lysis buffer in the absence or presence of 0.1% Triton X100.
2. Centrifuge the lysates at 10,000 × *g* for 10 min. Add SDS sample buffer (1× or 5×) to the resulting pellets and supernatants to obtain samples that have similar volumes. Boil immediately the samples which can then be stored at −20 °C.
3. Process for SDS-PAGE and immunoblot analysis using appropriate antibodies (*see* below **Note 1**). The presence of HspB1 in the pellet fraction and its absence when the cells are lyzed in the presence of Triton reflects its association with detergent-sensitive structures.
4. The F-actin integrity-dependent association can be tested by incubating the cells for 1 h with 0.5 μM of the F-actin disrupting agent cytochalasin D before they are lyzed.

3.2.2 Native Size Analysis

To detect changes in HspB1 native size in response to various stress, proceed as follows:

1. Prepare a Sepharose 6B gel filtration column (1 cm × 100 cm) equilibrated in TEM according to the manufacturer's procedures (void volume: 2000 kDa). The column should be kept in the cold room. Always keep some TEM at the top of the column to avoid it to dry. Changes in temperature will ruin the column (bubble formation).
2. Set the peristaltic pump to obtain a column flow of about 2.5 ml/5 min. Wash the column with at least one volume column of TEM. Set the fraction collector so that each fraction contains about 2.5 ml.
3. Calibrate the column using prestained molecular mass markers (Kit for Molecular Weights 29,000–700,000 for Gel Filtration Chromatography). The kit contains blue dextran (>2,000,000 Da), thyroglobulin (669,000 Da), Apoferritin (440,000 Da), β-amylase (200,000 Da), and carbonic anhydrase (29,000 Da). To calibrate the column, remove the TEM solution at the top of the column and load 1 ml of the kit preparation solution. Once the 1 ml solution has penetrated inside the sepharose, the column is developed in TEM. Fractions of 2.5 ml are collected and the optical density is

determined using a visible spectrophotometer. Note the fractions containing the different stained markers and their corresponding molecular masses.

4. 10^7 cells (in case of HeLa) are lyzed in 1 ml of TEM containing 0.1% Triton X100. Centrifugate the lyzate in the cold at 10,000 × *g* for 10 min and collect the supernatant sample.
5. Remove the TEM solution at the top of the column. Load the 1 ml supernatant sample on the top of the pre-equilibrated Sepharose 6B gel filtration column. Loading a larger volume of sample could alter the separating power of the column.
6. Once 1 ml of the sample has penetrated inside the sepharose, the column is developed in TEM. Fractions of 2.5 ml are collected and kept at 4 °C.
7. 50 µl of each column fraction is collected and mixed with 10 µl of 5×SDS sample buffer and boil immediately. No protein precipitation is required if 10^7 HeLa cells are analyzed per column run (*see* **Note 2**). Gel electrophoresis and immunoblots using HspB1 antibody are performed as already described [59] and revealed with the ECL kit from Amersham (*see* **Note 1** and Subheading 2). The detection in the different column fractions of phosphorylated HspB1 (*see* Subheading 3.5, **step 2**) or other polypeptides of interest can easily be performed by probing the immunoblots with specific antibodies. Interaction of HspB1 with other sHsps and formation of mosaic oligomeric structures has been described [29, 49–52]. It is therefore important to test the column fraction with antibodies recognizing other sHsps.
8. Autoradiographs from the immunoblot experiments are recorded onto X-Omat LS films (Eastman Kodak). Films are scanned (4990 Epson film scanner) and analyzed with ImageJ software™ (NIH, Bethesda). The duration of the exposure should be calculated so as to be in the linear response of the film.

3.3 Immunoprecipitation, Interaction with Partners or Client Proteins

The detection, in the above-described column fractions, of polypeptides that share the oligomeric profile of HspB1 can result in an interaction with this chaperone and can be tested by immunoprecipitation. For example, in growing HeLa cells client polypeptide like pro-caspase-3 interacts with HspB1 small oligomers while HDAC6 interacts only with the large ones suggesting that different phosphorylation/oligomerization organizations of HspB1 are required for their respective binding [27, 28]. In the case of pro-caspase-3, interaction with HspB1 enhances its stability. In contrast, when the level of HspB1 is artificially decreased (*see* Subheading 3.6) pro-caspase-3 is degraded through an ubiquitin-proteasome process. As described before, HspB1 can also interact

with other sHsps and form mosaic oligomeric structures [29]. It is therefore important to test the column fractions described in Subheading 3.2.2 with antibodies recognizing other sHsps or other putatively interesting polypeptides.

1. Perform immunoblots analysis of the column fractions using antibodies against polypeptides that have the potential to interact with HspB1. Check for common oligomeric structures and define the column fractions that should be analyzed. Several adjacent fractions can be pooled. The fractions should always be kept at 4 °C. Freezing may alter protein-protein interactions.
2. Collect a 100 µl aliquot of the pooled fractions and add 25 µl of 5× SDS sample buffer and immediately boil the sample (which can be denoted total non depleted sample). Collect at least 1 ml of the pooled fractions in two different tubes. One tube will receive 5 µl of non-immune antibody (normal immunoglobulins) and the other 5 µl of immune anti-HspB1 monoclonal antibody (*see* Subheading 2). Let it sit on ice for 3 h. Add 50 µl of a 1:1 slurry (made of water and protein G-agarose beads) to both the tubes. Attach the tubes to a rotating wheel in the cold room. After 3 h, collect the tubes and spin down the protein-G agarose beads (500 *g* × 5 min). In both the tubes (non-immune and immune) collect the supernatant and the pellet. Collect a 100 µl aliquot of the supernatant and add 25 µl of 5× SDS sample buffer and immediately boil the sample (which can be denoted as total depleted sample). Resuspend the agarose beads in 1 ml of IPP 150 buffer and repeat the washing of the beads at least three times. Resuspend the sepharose beads in 50 µl of 1× SDS buffer and boil. Spin the beads and collect the sample buffer on the top of the beads. Protein G-Agarose beads can be recycled.
3. Analyze the samples in SDS-PAGE and transfer the gel to the nitrocellulose membrane. Probe the immunoblot with anti-HspB1 antiserum and secondary antibody and reveal with ECL (*see* Subheading 2). Note the decreased signal of HspB1 in the total depleted sample compared to the original total non-depleted sample. If HspB1 is not detectable in the total depleted sample, the immunoprecipitation was quantitative (the antibody was able to immunoprecipitate all the HspB1 molecules present in the sample). Verify that HspB1 is indeed immunoprecipitated by anti-HspB1 antibody and not by the non-immune immunoglobins. In case the level of nonspecific protein bands is too high, repeat the experiment and include more stringent washes using IPP 300 buffer.
4. Probe a similar immunoblot blot (or the same one) with an antibody directed against a polypeptide sharing HspB1

oligomeric property (both the antibodies can be used simultaneously, *see* **Note 3**). In the total depleted fraction, check for a decrease in the level of the targeted polypeptide. Compare the percentage of decreased signal to that observed in the case of HspB1. A complete immunodepletion of the targeted polypeptide suggests that it forms a 1:1 complex with HspB1. Check for the presence of the polypeptide in the immunoprecipitated fraction (*see* **Note 4**).

5. Repeat the experiment but in this case the antibody directed against the interacting polypeptide is used to perform the immunoprecipitation. The resulting immunoblots are then probed with anti-HspB1 antibody.
6. Protein client. Once the interaction of HspB1 with a polypeptide has been detected repeat the experiments using the cells transfected with a DNA vector encoding an RNAi targeting HspB1 (*see* below Subheading 3.6, **step 2**). A direct analysis of cell lysates (without the sizing column step) can be performed. Check for the reduced level of expression of HspB1 that should not be observed in control cells transfected with DNA vectors encoding non-functional RNAi (scramble or mismatch) (*see* Subheading 3.6, **step 2**). A concomitant decrease in the level of the protein client means that it is protected against degradation by its interaction with HspB1 (chaperone activity). The effect can be reversed if the cells are pretreated with a proteasome inhibitor as MG-132 (0.1–0.5 μM for 24 h) before being analyzed.

3.4 Dimer Formation

Human HspB1, but not αB-crystallin (HspB5), contains a single cysteine (position 137 in HspB1) that is suceptible to oxidation (or even S-thiolation) and can promote dimer formation.

1. To detect the dimeric form of HspB1 in immunoblots, lysates of cells exposed to oxidative stress must be analyzed, as previously described [38, 61], under nonreducing conditions using SDS sample buffer devoid of dithiothreitol.
2. Analysis of cells transfected with HspB1 C137A dominant negative mutant (*see* Subheading 3.7, **step 2**) can be performed to visualize the aberrant oligomerization of HspB1 when its unique cysteine residue is mutated [61].

3.5 Isoforms Composition, Phosphorylation

3.5.1 Isoforms Composition

HspB1 phosphorylation is MAPKAP Kinase 2/3-dependent and occurs on three serine sites (Ser 15, 78, and 82). At least three isoforms of HspB1 can be resolved in 2-D immunoblots. The acidic end is to the right. The “a” and more basic isoform represents the unphosphorylated form of the protein. The “b” and “c” isoforms are representative of Hsp27 phosphorylated at one or two sites,

respectively. A minor isoform b' is detectable between the "a and b" isoforms. Its nature is still not known.

1. First dimension of the 2-d gels should be prepared using an ampholine mixture made of 20% ampholines pH 3–10 and 80% ampholines pH 5–7. The gel should be run as previously described [62].
2. Following the second SDS-PAGE dimension and transfer on nitrocellulose membrane, HspB1 isoforms are detected in immunoblots using antibodies that recognize HspB1 or its phosphorylated forms (*see* Subheading 2).

3.5.2 Direct Analysis of HspB1 Level of Phosphorylation

Immunoblot analysis of HspB1 phosphorylation at the different serine sites is performed by probing immunoblots with antibodies specific for HspB1 phosphorylation at either serine 15, serine 78, or serine 82 (*see* Subheading 2).

3.6 Modulation of HspB1 Level of Expression

Assessing the consequences of changes in HspB1 level of expression is an approach to increase our knowledge of the impact of this protein on cell physiology. This is also an easy way to detect client proteins stabilized by the holdase activity of HspB1 (*see* Subheading 3.3, **step 6**). Indeed, a decreased level of HspB1 can enhance the degradation of specific client polypeptides, such as caspase-3 [32].

1. Overexpression. Cells that do not (or weakly) constitutively express HspB1 are better used in this approach. Unfortunately, most human cells (except some lymphocytes such as HL-60 cells) constitutively express HspB1. Consequently, murine NIH 3T3 and L929 fibroblasts can be used that are devoid of murine HspB1 expression in the absence of heat shock. Transfection of these cells can be achieved using Lipofectamine™ reagent procedure (Subheading 2) as already described [55].
2. Underexpression. Cells constitutively expressing high loads of HspB1 such as HeLa, T47D, 16-HBE, and BO2 can be used to assess the consequences of a decreased level of HspB1. Transfection of cells can be achieved using the lipofectamine procedure [55, 63] using the pCIneohsp27 antisense cDNA vector (*see* Subheading 2). In the HeLa cells, this procedure decreases the HspB1 level by at least 40% [55]. A limitation of this approach is that HspB1 antisense RNA could potentially inhibit the expression of other sequence-related members of the sHsp family.

To overcome the problem, an RNAi approach that specifically targets the mRNA encoding HspB1 can be used. In separate culture dishes, cells are transfected with 10 μg of either HspB1-, Scramble-, or Mismatch-pSuperneo DNA vectors using the Lipofectamine™ reagents (*see* Subheading 2) according to the

manufacturer's instructions. Two to three days after transfection, perform immunoblot analysis to determine the efficiency of the siRNA-induced silencing. In HeLa cells the level of HspB1 should be reduced by at least 80%. Stable cell lines for siRNA expression can be established using neomycin selection [27, 64].

3.7 Expression of HspB1 Dominant-Negative Mutants Devoid of Holdase Activity

1. Phosphorylation mutants of HspB1. Effects of phosphorylation on HspB1 function are tested following cell transfection with previously described pKS27wt (wild-type Hsp27), pKS2711-3A (non-phosphorylatable mutant: 3 serine sites replaced by alanine), or pKS2711-3D (phospho-mimicry mutant: 3 serine sites replaced by aspartic acid) vector [9] (*see* Subheading 2). Expression of the Ser to Asp mutant shifts HspB1 toward small oligomeric structures and abolishes HspB1 holdase and protective activity [9, 10].
2. The C137A dominant-negative mutant (*see* Subheading 3.3, **step 6**) knocks out the holdase activity of HspB1. The complex formed by the mutant protein and endogenous wild-type HspB1 is an aberrant and non-functional oligomeric structure [61].

4 Notes

1. The level of HspB1 present in the different cell lines can be estimated by comparing the immunoblot signals to that of serial dilutions of the purified recombinant protein. Autoradiography must be performed within the range of proportionality of the film.
2. To avoid the time-consuming step of protein precipitation of the fractions eluting from the sizing column, the starting material should be at least 10^7 cells expressing about 4 ng of HspB1 per μg of total proteins (as for example HeLa cells).
3. Probing the same blot will work only if the client polypeptide has a gel migration different from that of HspB1.
4. This approach can give you an estimation of the cellular percentage of the client polypeptide that interacts with HspB1.

References

1. Arrigo A-P, Landry J (1994) Expression and function of the low-molecular-weight heat shock proteins. In: Morimoto RI, Tissieres A, Georgopoulos C (eds) The biology of heat shock proteins and molecular chaperones. Cold Spring Harbor Laboratory Press, Cold Spring Harbor, NY, pp 335–373
2. Arrigo AP (2012) Pathology-dependent effects linked to small heat shock proteins expression. Scientifica 2012:185641. doi:10.6064/2012/185641
3. Kappe G, Franck E, Verschuure P, Boelens WC, Leunissen JA et al (2003) The human genome encodes 10 alpha-crystallin-related small heat shock proteins: HspB1-10. Cell Stress Chaperones 8:53–61
4. Ingolia TD, Craig EA (1982) Four small heat shock proteins are related to each other and to

mammalian a-crystallin. Proc Natl Acad Sci U S A 79:2360–2364

5. de Jong WW, Caspers GJ, Leunissen JA (1998) Genealogy of the alpha-crystallin--small heat-shock protein superfamily. Int J Biol Macromol 22:151–162
6. Arrigo A-P, Suhan JP, Welch WJ (1988) Dynamic changes in the structure and intracellular locale of the mammalian low-molecular-weight heat shock protein. Mol Cell Biol 8:5059–5071
7. Lambert H, Charette SJ, Bernier AF, Guimond A, Landry J (1999) HSP27 Multimerization mediated by phosphorylation-sensitive intermolecular interactions at the amino terminus. J Biol Chem 274:9378–9385
8. Ehrnsperger M, Lilie H, Gaestel M, Buchner J (1999) The dynamics of hsp25 quaternary structure. Structure and function of different oligomeric species. J Biol Chem 274:14867–14874
9. Mehlen P, Hickey E, Weber L, Arrigo A-P (1997) Large unphosphorylated aggregates as the active form of hsp27 which controls intracellular reactive oxygen species and glutathione levels and generates a protection against TNFα in NIH-3T3-ras cells. Biochem Biophys Res Comm 241:187–192
10. Rogalla T, Ehrnsperger M, Preville X, Kotlyarov A, Lutsch G et al (1999) Regulation of Hsp27 oligomerization, chaperone function, and protective activity against oxidative stress/tumor necrosis factor alpha by phosphorylation. J Biol Chem 274:18947–18956
11. Garrido C (2002) Size matters: of the small HSP27 and its large oligomers. Cell Death Differ 9:483–485
12. Arrigo AP (2007) The cellular "networking" of mammalian Hsp27 and its functions in the control of protein folding, redox state and apoptosis. Adv Exp Med Biol 594:14–26
13. Paul C, Simon S, Gibert B, Virot S, Manero F et al (2010) Dynamic processes that reflect anti-apoptotic strategies set up by HspB1 (Hsp27). Exp Cell Res 316:1535–1552
14. Horwitz J, Huang Q-L, Ding L-L (1992) Alpha-crystallin can function as a molecular chaperone. Proc Natl Acad Sci U S A 89:10449–10453
15. Jakob U, Gaestel M, Engels K, Buchner J (1993) Small heat shock proteins are molecular chaperones. J Biol Chem 268:1517–1520
16. Ganea E (2001) Chaperone-like activity of alpha-crystallin and other small heat shock proteins. Curr Protein Pept Sci 2:205–225
17. Carra S, Sivilotti M, Chavez Zobel AT, Lambert H, Landry J (2005) HspB8, A small heat shock protein mutated in human neuromuscular disorders, has in vivo chaperone activity in cultured cells. Hum Mol Genet 14:1659–1669
18. Bellyei S, Szigeti A, Pozsgai E, Boronkai A, Gomori E et al (2007) Preventing apoptotic cell death by a novel small heat shock protein. Eur J Cell Biol 86:161–171
19. Markossian KA, Yudin IK, Kurganov BI (2009) Mechanism of suppression of protein aggregation by alpha-Crystallin. Int J Mol Sci 10:1314–1345
20. Freeman BC, Morimoto RI (1996) The human cytosolic molecular chaperones hsp90, hsp70 (hsc70) and hdj-1 have distinct roles in recognition of a non-native protein and protein refolding. EMBO J 15:2969–2979
21. Bukau B, Horwich AL (1998) The Hsp70 and Hsp60 chaperone machines. Cell 92:351–366
22. Buchner J (1999) Hsp90 & Co. - a holding for folding. Trends Biochem Sci 24:136–141
23. Lee GJ, Roseman AM, Saibil HR, Vierling E (1997) A small heat shock protein stably binds heat-denatured model substrates and can maintain a substrate in a folding-competent state. EMBO J 16:659–671
24. Ehrnsperger M, Graber S, Gaestel M, Buchner J (1997) Binding of non-native protein to Hsp25 during heat shock creates a reservoir of folding intermediates for reactivation. EMBO J 16:221–229
25. Lee GJ, Vierling E (2000) A small heat shock protein cooperates with heat shock protein 70 systems to reactivate a heat-denatured protein. Plant Physiol 122:189–198
26. Arrigo AP, Gibert B (2012) HspB1 Dynamic phospho-oligomeric structure dependent interactome as cancer therapeutic target. Curr Mol Med 12:1151–1163
27. Gibert B, Eckel B, Fasquelle L, Moulin M, Bouhallier F et al (2012) Knock down of heat shock protein 27 (HspB1) induces degradation of several putative client proteins. PLoS One 7: e29719
28. Arrigo AP, Gibert B (2013) Protein interactomes of three stress inducible small heat shock proteins: HspB1, HspB5 and HspB8. Int J Hyperth 29:409–422
29. Arrigo AP (2013) Human small heat shock proteins: protein interactomes of homo- and hetero-oligomeric complexes: an update. FEBS Lett 587:1959–1969
30. Arrigo AP, Gibert B (2014) HspB1, HspB5 And HspB4 in human cancers: potent oncogenic role of some of their client proteins. Cancers (Basel) 6:333–365

31. Arrigo AP, Ducarouge B, Lavial F, Gibert B (2015) Immense cellular implications associated to small stress proteins expression: impacts on human pathologies. In: Tanguay RM, Hightower LE (eds) The big book on small heat shock proteins, heat shock proteins 8 ©. Springer International Publishing, Switzerland, pp 27–83
32. Pandey P, Farber R, Nakazawa A, Kumar S, Bharti A et al (2000) Hsp27 Functions as a negative regulator of cytochrome c-dependent activation of procaspase-3. Oncogene 19:1975–1981
33. Cayado-Gutierrez N, Moncalero VL, Rosales EM, Beron W, Salvatierra EE et al (2012) Downregulation of Hsp27 (HSPB1) in MCF-7 human breast cancer cells induces upregulation of PTEN. Cell Stress Chaperones 18:243–249
34. Neckers L, Mimnaugh E, Schulte TW (1999) Hsp90 As an anti-cancer target. Drug Resist Updat 2:165–172
35. Georgakis GV, Younes A (2005) Heat-shock protein 90 inhibitors in cancer therapy: 17AAG and beyond. Future Oncol 1:273–281
36. Cuesta R, Laroia G, Schneider RJ (2000) Chaperone Hsp27 inhibits translation during heat shock by binding eIF4G and facilitating dissociation of cap-initiation complexes. Genes Dev 14:1460–1470
37. Nicholl ID, Quinlan RA (1994) Chaperone activity of alpha-Crystallins modulates intermediate filament assembly. EMBO J 13:945–953
38. Arrigo AP, Firdaus WJ, Mellier G, Moulin M, Paul C et al (2005) Cytotoxic effects induced by oxidative stress in cultured mammalian cells and protection provided by Hsp27 expression. Methods 35:126–138
39. Bruey JM, Ducasse C, Bonniaud P, Ravagnan L, Susin SA et al (2000) Hsp27 Negatively regulates cell death by interacting with cytochrome c. Nat Cell Biol 2:645–652
40. Arrigo AP (2005) In search of the molecular mechanism by which small stress proteins counteract apoptosis during cellular differentiation. J Cell Biochem 94:241–246
41. Mao YW, Liu JP, Xiang H, Li DW (2004) Human alphaA- and alphaB-crystallins bind to Bax and Bcl-X(S) to sequester their translocation during staurosporine-induced apoptosis. Cell Death Differ 11:512–526
42. Liu JP, Schlosser R, Ma WY, Dong Z, Feng H et al (2004) Human alphaA- and alphaB-crystallins prevent UVA-induced apoptosis through regulation of PKCalpha, RAF/-MEK/ERK and AKT signaling pathways. Exp Eye Res 79:393–403
43. Rane MJ, Pan Y, Singh S, Powell DW, Wu R et al (2003) Heat shock protein 27 controls apoptosis by regulating Akt activation. J Biol Chem 278:27828–27835
44. Wettstein G, Bellaye PS, Kolb M, Hammann A, Crestani B et al (2013) Inhibition of HSP27 blocks fibrosis development and EMT features by promoting snail degradation. FASEB J 27:1549–1560
45. Carra S (2009) The stress-inducible HspB8-Bag3 complex induces the eIF2alpha kinase pathway: implications for protein quality control and viral factory degradation? Autophagy 5:428–429
46. Duverger O, Paslaru L, Morange M (2004) HSP25 Is involved in two steps of the differentiation of PAM212 keratinocytes. J Biol Chem 279:10252–10260
47. Koteiche HA, McHaourab HS (2003) Mechanism of chaperone function in small heat-shock proteins. Phosphorylation-induced activation of two-mode binding in alphaB-crystallin. J Biol Chem 278:10361–10367
48. Aquilina JA, Benesch JL, Ding LL, Yaron O, Horwitz J et al (2004) Phosphorylation of alphaB-crystallin alters chaperone function through loss of dimeric substructure. J Biol Chem 279:28675–28680
49. Zantema A, Vries MV-D, Maasdam D, Bol S, Avd E (1992) Heat shock protein 27 and aB-cristallin can form a complex, which dissociates by heat shock. J Biol Chem 267:12936–12941
50. Bukach OV, Glukhova AE, Seit-Nebi AS, Gusev NB (2009) Heterooligomeric complexes formed by human small heat shock proteins HspB1 (Hsp27) and HspB6 (Hsp20). Biochim Biophys Acta 1794:486–495
51. Mymrikov EV, Seit-Nebi AS, Gusev NB (2011) Large potentials of small heat shock proteins. Physiol Rev 91:1123–1159
52. Mymrikov EV, Seit-Nebi AS, Gusev NB (2012) Heterooligomeric complexes of human small heat shock proteins. Cell Stress Chaperones 17:157–169
53. Sun TX, Liang JJ (1998) Intermolecular exchange and stabilization of recombinant human alphaA- and alphaB-crystallin. J Biol Chem 273:286–290
54. Saha S, Das KP (2004) Relationship between chaperone activity and oligomeric size of recombinant human alphaA- and alphaB-crystallin: a tryptic digestion study. Proteins 57:610–617
55. Paul C, Manero F, Gonin S, Kretz-Remy C, Virot S et al (2002) Hsp27 As a negative

regulator of cytochrome C release. Mol Cell Biol 22:816–834

56. Mehlen P, Préville X, Chareyron P, Briolay J, Klemenz R et al (1995) Constitutive expression of human hsp27, drosophila hsp27, or human alpha B-crystallin confers resistance to TNF- and oxidative stress-induced cytotoxicity in stably transfected murine L929 fibroblasts. J Immunol 154:363–374
57. Brummelkamp TR, Bernards R, Agami R (2002) A system for stable expression of short interfering RNAs in mammalian cells. Science 296:550–553.
58. Simon S, Dimitrova V, Gibert B, Virot S, Mounier N et al (2013) Analysis of the dominant effects mediated by wild type or R120G mutant of alphaB-crystallin (HspB5) towards Hsp27 (HspB1). PLoS One 8:e70545
59. Mehlen P, Mehlen A, Guillet D, Préville X, Arrigo A-P (1995) Tumor necrosis factor-a induces changes in the phosphorylation, cellular localization, and oligomerization of human hsp27, a stress protein that confers cellular resistance to this cytokine. J Cell Biochem 58:248–259
60. Pichon S, Bryckaert M, Berrou E (2004) Control of actin dynamics by p38 MAP kinase - Hsp27 distribution in the lamellipodium of smooth muscle cells. J Cell Sci 117:2569–2577
61. Diaz-Latoud C, Buache E, Javouhey E, Arrigo AP (2005) Substitution of the unique cysteine residue of murine hsp25 interferes with the protective activity of this stress protein through inhibition of dimer formation. Antioxid Redox Signal 7:436–445
62. Arrigo A-P, Welch W (1987) Characterization and purification of the small 28,000-dalton mammalian heat shock protein. J Biol Chem 262:15359–15369
63. Merendino AM, Paul C, Vignola AM, Costa MA, Melis M et al (2002) Heat shock protein-27 protects human bronchial epithelial cells against oxidative stress-mediated apoptosis: possible implication in asthma. Cell Stress Chaperones 7:269–280
64. Gibert B, Eckel B, Gonin V, Goldschneider D, Fombonne J et al (2012) Targeting heat shock protein 27 (HspB1) interferes with bone metastasis and tumour formation in vivo. Br J Cancer 107:63–70

Chapter 13

Nucleotide Exchange Factors for Hsp70 Chaperones

Heike Rampelt, Matthias P. Mayer, and Bernd Bukau

Abstract

The ATPase cycle of Hsp70 chaperones controls their transient association with substrates and thus governs their function in protein folding. Nucleotide exchange factors (NEFs) accelerate ADP release from Hsp70, which results in rebinding of ATP and release of the substrate, thereby regulating the lifetime of the Hsp70-substrate complex. This chapter describes several methods suitable to study NEFs of Hsp70 chaperones. On the one hand, steady-state ATPase assays provide information on how the NEF influences progression of the Hsp70 through the entire ATPase cycle. On the other hand, nucleotide release can be measured directly using labeled nucleotides, which enables identification and further characterization of NEFs.

Key words Nucleotide exchange factor, Hsp70, GrpE, Bag1, HspBP1, Hsp110, Steady-state ATPase, Nucleotide release, Stopped flow

1 Introduction

Hsp70 chaperones accomplish their role as folding helpers in a variety of cellular processes by associating with substrates in a manner controlled by cycles of ATP hydrolysis and ADP-to-ATP exchange [1]. Thus, analyzing the ATPase cycle of Hsp70s in molecular detail is crucial for our understanding of Hsp70-assisted protein folding. Hsp70 proteins consist of an N-terminal nucleotide-binding domain (NBD) allosterically coupled to a C-terminal substrate-binding domain (SBD). The NBD of Hsp70s consists of two lobes that form a deep cleft. The nucleotide is bound at the bottom of this cleft such that it interacts with all four subdomains that form the two lobes. The SBD consists of a β-sandwich subdomain, which encloses extended stretches of polypeptides with upward protruding loops, and an α-helical subdomain forming in the closed conformation a lid over the substrate-binding crevice. ATP binding to the NBD induces a conformational change in the SBD leading to the dissociation of the α-helical lid domain and a docking of the β-sandwich subdomain onto the NBD, resulting in a low affinity for substrates with high association and dissociation

Stuart K. Calderwood and Thomas L. Prince (eds.), *Chaperones: Methods and Protocols*, Methods in Molecular Biology, vol. 1709, https://doi.org/10.1007/978-1-4939-7477-1_13,

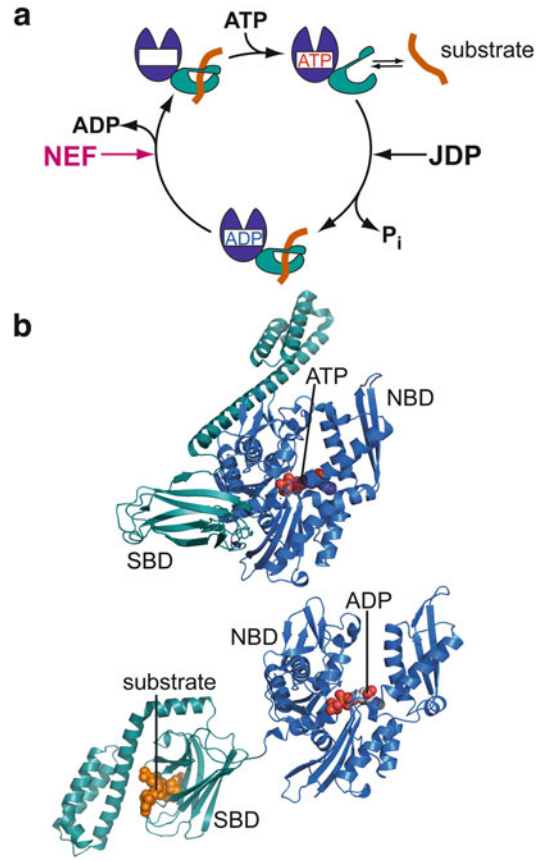

Fig. 1 Hsp70 cycle and structure. (**a**), The ATPase cycle of Hsp70 chaperones. (**b**), Cartoon representation of Hsp70 in the ATP bound open conformation (upper panel, PDB ID 4B9Q, [2]) and ADP bound closed conformation (lower panel, PDB ID 2KHO, [38]). NBD in *blue*; SBD in teal; substrate in *orange*, space filling representation

rates (Fig. 1) [2, 3]. Hydrolysis of ATP to ADP converts the SBD to the high-affinity state, which is characterized by low substrate association and dissociation rates. Cycling of the Hsp70 chaperone through these states is facilitated by the action of co-chaperones and by association with chaperone substrates. On the one hand, J-domain proteins deliver substrates to the chaperone or are located at cellular sites where Hsp70 substrates emerge, like the ribosome or translocation pores, and stimulate in synergism with the substrate ATP hydrolysis to facilitate substrate binding. On the other hand, the release of ADP is accelerated by nucleotide exchange factors (NEFs), whose interaction with the Hsp70 NBD enables ATP rebinding and concomitant substrate release (Fig. 1).

So far, five unrelated classes of NEFs have been structurally characterized [4–12]. Although each of these NEF classes possesses a unique structure and interacts with Hsp70 in a distinct fashion,

they can be placed into two groups according to their mode of action. Four NEF classes stimulate ADP release by tilting out subdomain IIB of the Hsp70 NBD which results in an opening of the nucleotide binding cleft: The prokaryotic/organellar GrpE; the eukaryotic Bag-1 type and Bag-2; and finally the eukaryotic Hsp110 and Grp170 proteins, which are divergent members of the Hsp70 family themselves. In contrast to these NEF classes, eukaryotic HspBP1-like NEFs displace ADP by wrapping around subdomain IIB of the Hsp70 NBD resulting in a massive destabilization of subdomains IA and IB.

Two complementary approaches lend themselves to study how co-chaperones affect the Hsp70 ATPase cycle: One can assess how co-chaperones affect the rate-limiting step of the Hsp70 ATPase cycle by studying steady-state kinetics, or alternatively, an individual step of the cycle, for instance ADP release, can be monitored in isolation.

2 Materials

2.1 Steady-State ATPase Assay

1. HKM buffer: 25 mM Hepes/KOH pH 7.6, 50 mM KCl, 5 mM $MgCl_2$ (*see* **Note 1**).
2. NADH 30 mM stock solution.
3. ATP 20 mM stock solution: Adjust the pH to 7.
4. Phosphoenolpyruvate (PEP) 50 mM stock solution.
5. Pyruvate kinase/lactate dehydrogenase mix: commercially available (Sigma Inc.).
6. Proteins: Hsp70, J-domain protein, NEF (*see* **Notes 2** and **3**).

2.2 Release of Radiolabeled Nucleotide

1. HKM buffer: 25 mM Hepes/KOH pH 7.6, 50 mM KCl, 5 mM $MgCl_2$ (*see* **Note 1**).
2. ATP 100 mM and 0.1 mM stock solutions: Adjust the pH to 7.
3. ADP 100 mM stock solution: Adjust the pH to 7.
4. [α-^{32}P]-ATP 3000 Ci/mmole.
5. 1 mg/ml BSA.
6. 3.6% (v/v) acetic acid/400 mM LiCl.
7. Proteins: Hsp70, NEF (*see* **Notes 2** and **3**).

2.3 Nucleotide Release by Stopped-Flow Instrumentation

1. HKM buffer: 25 mM Hepes/KOH pH 7.6, 50 mM KCl, 5 mM $MgCl_2$ (*see* **Note 1**).
2. N_8-(4-N′-methylanthraniloylaminobutyl)-8 amino- adenosine 5′-di/triphosphate (MABA-ADP/ATP) 100 mM stock solution, adjusted to pH 7.
3. ATP 100 mM stock solution: Adjust the pH to 7.
4. Proteins: Hsp70, NEF (*see* **Notes 2** and **3**).

3 Methods

3.1 NEF Effects on Hsp70 Steady-State ATPase Activity

In the ATPase cycle of an Hsp70 chaperone whose ATP hydrolysis is maximally stimulated by the concerted action of a J-domain protein and a substrate, ADP release becomes the rate-limiting step. Therefore, in the presence of a stimulatory J-domain protein, the addition of a NEF will increase Hsp70's ATPase rate in a steady-state assay. However, differences among J-domain proteins must be taken into account. The bacterial DnaJ, when present at equimolar concentration relative to DnaK, is sufficient for maximal stimulation of ATP hydrolysis (13-fold to a stimulated rate of ca. 0.01 s^{-1} in the absence of GrpE and 190-fold to a rate of 0.14 s^{-1} in the presence of GrpE [13, 14]). This is because under the artificial in vitro conditions DnaJ serves as both J-domain protein and substrate [15]. A similar situation is found for the yeast Ssa1/Ydj1 system [16]. In contrast, many other eukaryotic J-domain proteins on their own only marginally (two- to eightfold) stimulate their partner Hsp70 to hydrolyze ATP in the absence of a chaperone substrate [17, 18]. This presumably reflects that these J-domain proteins are not serving as substrate [19].

In contrast, in a single-turnover ATPase assay, many NEFs inhibit ATP hydrolysis because they can displace not only ADP from Hsp70, but also ATP prior to hydrolysis. Two examples are the bacterial NEF GrpE [20] and the yeast Hsp110 protein Sse1 [21]. This property can also become apparent under steady-state conditions (both in ATPase and substrate refolding assays), if the ratio of NEF to Hsp70 is too high [18, 20, 22, 23].

The most convenient method to determine the steady-state ATPase activity is a coupled enzymatic test, where pyruvate kinase and lactate dehydrogenase convert ADP produced by Hsp70, along with phosphoenolpyruvate and NADH into ATP, lactate and NAD^+ [24]. Consumption of NADH is monitored as a decrease in absorption at 340 nm (*see* **Note 4**).

1. Prepare a master mix containing phosphoenolpyruvate (PEP) and NADH, the pyruvate kinase/lactate dehydrogenase (PK/LDH) mix, and $MgCl_2$. The final concentrations in the assay should be 0.25 mM NADH; 0.4–1 mM PEP depending on the ATP hydrolysis rate of the Hsp70; 5 mM $MgCl_2$; dilute out the commercially available PK/LDH mix 1:100.
2. Dispense the master mix into a microtiter plate and add Hsp70 chaperone and co-chaperones as required. Hsp70 concentrations are typically around 1–3 μM. Monitor background ATP hydrolysis with a reaction lacking Hsp70 and co-chaperones. Also control for ATP hydrolysis by co-chaperones or contaminating ATPases by assaying all co-chaperone concentrations in the absence of Hsp70. It is also advisable to construct an

ATPase-deficient mutant of Hsp70 like the K71M-mutant of bovine Hsc70 [25] and purify this variant protein using the same protocol to determine the contamination level by co-purifying ATPases.

3. Start the reaction by the addition of different concentrations of ATP, e.g., 0.25–2 mM ATP.
4. Measure the decrease in A_{340} as a function of time, fit the data to a linear equation using a suitable software package, and calculate the amount of ADP produced by the Hsp70. Determine the k_{cat} [s^{-1}] of the hydrolysis reactions at increasing ATP concentrations, fitting the data to the Michaelis Menten equation (*see* ref. 26).

3.2 Determination of Nucleotide Exchange Using Radiolabeled Nucleotide

In a single turnover assay, nucleotide dissociation is monitored directly, which allows precisely defining the action of a potential NEF. The two methods outlined below similarly monitor the dissociation of labeled ADP or ATP from Hsp70 upon addition of excess unlabeled nucleotide and NEF. Either radiolabeled nucleotide (this chapter) or a fluorescent nucleotide analog (Subheading 3.3) may be used.

To assess the release of radiolabeled nucleotide, complexes of Hsp70 with [α-^{32}P]-ATP are incubated with excess unlabeled nucleotide in the absence or presence of a NEF. A rapid gel filtration step then separates dissociated from Hsp70-bound nucleotide and the radioactivity in the protein peak is measured by scintillation counting. Additionally, non-dissociated nucleotide may be analyzed by thin layer chromatography (TLC) [13, 23].

1. To form Hsp70-nucleotide complexes, prepare per reaction and per time point 5 μl samples each containing 5 μM of the Hsp70 chaperone with 5 μM ATP including 400 Bq of [α-^{32}P]-ATP and incubate for 2 min on ice. In order to obtain Hsp70-[α-^{32}P]-ADP complexes by ATP hydrolysis, the incubation is performed for 30 min at 30 °C.
2. Pre-warm the reaction at 30 °C and add 5 μl of pre-warmed buffer containing 20–100 mM cold ATP with or without a NEF at a 2–4-fold stoichiometric excess to the Hsp70.
3. At different time points, rapidly add 40 μl of ice-cold buffer to the sample and immediately load it onto a G-50 Nick gel filtration column (GE Healthcare) to separate Hsp70-nucleotide complexes from unbound labeled nucleotide. Before use, the column should be prepared in the following manner: Equilibrate the column with HKM buffer, then load 1 ml of 1 mg/ml BSA onto the column and elute with three column volumes of HKM buffer. This measure decreases non-specific interactions of the Hsp70 with the column material. Collect fractions of two drops in scintillation vials and determine the radioactivity of the fractions.

4. Calculate the amount of protein-associated radioactivity per total radioactivity for each time point and plot the decrease of bound nucleotide over time. In order to obtain basal and stimulated apparent release rates, fit a single-exponential decay function to the data.
5. To analyze release of ATP and ADP separately, pool protein fractions from the gel filtration column and spot the eluate onto a TLC-plate that has been prepared in the following manner: Spot 2 μl of a 5 mM ADP + 5 mM ATP solution on each start position of the TLC-plate. The unlabeled nucleotides serve as a carrier in the chromatographic separation of radiolabeled ATP and ADP.
6. Develop the TLC-plate in a running buffer of 10% (v/v) acetic acid/400 mM LiCl, dry the plate, and expose it to a phosphoimager screen.
7. Quantitate amounts of radioactive ADP and ATP using suitable software and fit exponential equations to the data.

3.3 Determination of Nucleotide Release Rates by Stopped-Flow Instrumentation

NEF-mediated stimulation of ADP release from an Hsp70 chaperone can be determined directly and elegantly using stopped flow instrumentation. This instrumentation is ideally suited for monitoring fast dissociation kinetics with half times of seconds to milliseconds since the instrument's dead time is approximately 1 ms. In principle, rapid mixing of two solutions starts the reaction whose progression is monitored as changes in fluorescence emission. The fluorescent ADP-analog MABA-ADP (N_8-(4-N′-methylanthraniloylaminobutyl)-8-aminoadenosine 5′-diphosphate) [27] is ideally suited to analyze nucleotide release from Hsp70 chaperones. Other fluorescent ADP analogs with linkage of the fluorescent dye to different positions of the nucleotide are not suitable for Hsp70s. Earlier studies have established that the fluorescent group in both MABA-ADP and MABA-ATP does not affect the affinity of the nucleotide analogs to DnaK [27] and, by extension, to other Hsp70 chaperones. However, when analyzing a different combination of nucleotide analog and ATPases, the equivalence of the fluorophore-labeled and unlabeled nucleotide needs to be established. To this end, the K_D of the nucleotide analog should be determined, and additionally, a competition experiment can be performed where the nucleotide analog is displaced by titrating in unlabeled nucleotide (see ref. 27). In the following the experimental setup for measuring MABA-ADP dissociation is described.

After pre-incubating the Hsp70 chaperone with MABA-ADP, the sample is mixed with either excess (≥100-fold) unlabeled nucleotide alone, or with excess nucleotide and different concentrations of the potential NEF, to determine basal and stimulated ADP release rates, respectively. Since protein-bound MABA-ADP exhibits a higher fluorescence than the free molecule (e.g., twofold

increase in fluorescence for DnaK-bound MABA-ADP [28]), its dissociation from the Hsp70 chaperone translates into a decreased fluorescence (*see* **Note 5**).

1. Equilibrate the stopped-flow instrument in assay buffer at the assay temperature. We employ a fluorescence excitation wavelength of 360 nm and a 420 nm cut-off filter for the detection of emission [27]. Use filtrated buffer and water throughout.
2. Pre-incubate the Hsp70 chaperone with MABA-ADP at assay temperature. We commonly use 0.5 μM of Hsp70 and nucleotide each, however, the concentrations may require adjusting in case the affinity of the Hsp70 for ADP is too low to allow for accurate measurement or the fluorescence increase upon binding is lower than for DnaK.
3. Pre-incubate solutions with excess unlabeled nucleotide (e.g., 250 μM ATP) +/− different concentrations of NEF. If the NEF of interest possesses a nucleotide binding domain itself, a potential role of nucleotide binding for its activity can be assayed by varying the nucleotide or changing its concentration in this step (*see* **Notes 6** and **7**).
4. Load the Hsp70-MABA-ADP sample and the chase solution (excess unlabeled nucleotide) into the two reservoir syringes of the stopped flow instrument.
5. Make a test measurement to collect the necessary information for setting the measurement parameters like the reaction time (record the reaction for 10× the reaction half time).
6. Perform multiple measurements for every reaction. Average and fit the data to a single-exponential equation to obtain apparent off-rates for basal and stimulated nucleotide release.

4 Notes

1. It is vital that the buffers used in Hsp70 experiments contain KCl. The Hsp70 NBD requires the presence of two potassium ions, which coordinate the bound nucleotide; ATP hydrolysis is minimal in the absence of potassium ions. Sodium ions cannot replace potassium due to their significantly smaller ionic radius, resulting in a fivefold reduction of the ATPase rate, altered nucleotide association and dissociation kinetics, and altered allostery [29, 30].
2. Since the steady-state ATPase assay also measures ATP hydrolysis by contaminating ATPases, the protein preparations should be highly pure. This applies especially to Hsp70 proteins due to their low intrinsic ATPase rates.

3. Hsp70s are generally purified using several chromatography steps [31, 32] because N- and C-terminal tags have been shown to influence the steady-state ATPase activity. However, an N-terminal His-tag has been used for the purification of the endoplasmic reticulum Hsp70 BiP/Grp78 and subsequently cleaved with thrombin to give the authentic N-terminus [33]. Similarly, an N-terminal fusion to SUMO was employed to purify the yeast Hsp70 chaperones Ssa1 [34].
   For purification procedures for the *E. coli* NEF GrpE and the human Bag1, refer to [20] and [35], respectively. HspBP1 and FES1 were purified using an N-terminal His-tag [23]. The Hsp110 proteins were purified with a TEV cleavable N-terminal Histag or as an N-terminal fusion to SUMO [34, 36].
4. Performing the steady-state ATPase assay in the presence of inorganic phosphate (e.g., 10 mM) enhances the stimulatory effect of NEFs because dissociation of ADP*P_i proceeds more slowly under these circumstances. This is due to the ordered product-release mechanism of Hsp70s where inorganic phosphate is released before the ADP [26].
5. Dissociation of MABA-ATP from an Hsp70 chaperone can be monitored in a manner similar to that of MABA-ADP, however, due to hydrolysis of the ATP, a double-mixing experiment has to be performed. In this case, Hsp70 protein is mixed in the stopped-flow apparatus with a MABA-ATP solution, and after an incubation time of, e.g., 30 s, the resulting solution is mixed with chase nucleotide and NEF and nucleotide release is measured.
6. As mentioned earlier, the NEFs from the Hsp110 and Grp170 protein families belong to the Hsp70 superfamily and thus bind and hydrolyze ATP themselves. The nucleotide requirements of these proteins for their NEF activity can be assessed in the stopped-flow nucleotide release assay by varying the chase nucleotide: You may pre-incubate the NEF with either ATP or ADP at differing concentrations. While the nature of the chase nucleotide does not have an influence on the nucleotide dissociation step, it may affect the activity of the NEF.
7. Similarly, the rate of ATP hydrolysis by these Hsp70-like NEFs may be stimulated upon interaction with their partner Hsp70 chaperone, as has been demonstrated for the yeast Grp170 protein Lhs1 [37]. To account for such a contribution to the total ATP hydrolysis measured in a steady-state assay, control measurements with the NEF and an Hsp70 mutant deficient in either nucleotide binding or ATP hydrolysis should be performed.

References

1. Mayer MP, Bukau B (2005) Hsp70 chaperones: cellular functions and molecular mechanism. Cell Mol Life Sci 62:670–684
2. Kityk R, Kopp J, Sinning I, Mayer MP (2012) Structure and dynamics of the ATP-bound open conformation of Hsp70 chaperones. Mol Cell 48:863–874
3. Qi R, Sarbeng EB, Liu Q, Le KQ, Xu X, Xu H, Yang J, Wong JL, Vorvis C, Hendrickson WA, Zhou L, Liu Q (2013) Allosteric opening of the polypeptide-binding site when an Hsp70 binds ATP. Nat Struct Mol Biol 20:900–907
4. Harrison CJ, Hayer-Hartl M, Di Liberto M, Hartl F, Kuriyan J (1997) Crystal structure of the nucleotide exchange factor GrpE bound to the ATPase domain of the molecular chaperone DnaK. Science 276:431–435
5. Sondermann H, Scheufler C, Schneider C, Höhfeld J, Hartl FU, Moarefi I (2001) Structure of a bag/Hsc70 complex: convergent functional evolution of Hsp70 nucleotide exchange factors. Science 291:1553–1557
6. Shomura Y, Dragovic Z, Chang H-C, Tzvetkov N, Young JC, Brodsky JL, Guerriero V, Hartl FU, Bracher A (2005) Regulation of Hsp70 function by HspBP1: structural analysis reveals an alternate mechanism for Hsp70 nucleotide exchange. Mol Cell 17:367–379
7. Polier S, Dragovic Z, Hartl FU, Bracher A (2008) Structural basis for the cooperation of Hsp70 and Hsp110 chaperones in protein folding. Cell 133:1068–1079
8. Schuermann JP, Jiang J, Cuellar J, Llorca O, Wang L, Gimenez LE, Jin S, Taylor AB, Demeler B, Morano KA, Hart PJ, Valpuesta JM, Lafer EM, Sousa R (2008) Structure of the Hsp110:Hsc70 nucleotide exchange machine. Mol Cell 31:232–243
9. Andréasson C, Fiaux J, Rampelt H, Druffel-Augustin S, Bukau B (2008) Insights into the structural dynamics of the Hsp110-Hsp70 interaction reveal the mechanism for nucleotide exchange activity. Proc Natl Acad Sci 105:16519–16524
10. Xu Z, Page RC, Gomes MM, Kohli E, Nix JC, Herr AB, Patterson C, Misra S (2008) Structural basis of nucleotide exchange and client binding by the Hsp70 cochaperone Bag2. Nat Struct Mol Biol 15:1309–1317
11. Briknarová K, Takayama S, Brive L (2001) Structural analysis of BAG1 cochaperone and its interactions with Hsc70 heat shock protein. Nat Struct Mol Biol 8(4):349
12. Briknarová K, Takayama S, Homma S, Baker K, Cabezas E, Hoyt DW, Li Z, Satterthwait AC, Ely KR (2002) BAG4/SODD protein contains a short BAG domain. J Biol Chem 277:31172–31178
13. Liberek K, Marszalek J, Ang D, Georgopoulos C (1991) Escherichia coli DnaJ and GrpE heat shock proteins jointly stimulate ATPase activity of DnaK. Proc Natl Aca Sci U S A 88 (7):2874–2878
14. McCarty JS, Buchberger A, Reinstein J, Bukau B (1995) The role of ATP in the functional cycle of the DnaK chaperone system. J Mol Biol 249:126–137
15. Laufen T, Mayer MP, Beisel C, Klostermeier D, Mogk A, Reinstein J, Bukau B (1999) Mechanism of regulation of hsp70 chaperones by DnaJ cochaperones. Proc Natl Acad Sci U S A 96:5452–5457
16. Cyr DM, Douglas MG (1994) Differential regulation of Hsp70 subfamilies by the eukaryotic DnaJ homologue YDJ1. J Biol Chem 269:9798–9804
17. Jiang RF, Greener T, Barouch W, Greene L, Eisenberg E (1997) Interaction of auxilin with the molecular chaperone, Hsc70. J Biol Chem 272:6141–6145
18. Gässler CS, Wiederkehr T, Brehmer D, Bukau B, Mayer MP (2001) Bag-1M accelerates nucleotide release for human Hsc70 and Hsp70 and can act concentration-dependent as positive and negative cofactor. J Biol Chem 276:32538–32544
19. Barouch W, Prasad K, Greene L, Eisenberg E (1997) Auxilin-induced interaction of the molecular chaperone Hsc70 with clathrin baskets. Biochemistry 36:4303–4308
20. Packschies L, Theyssen H, Buchberger A, Bukau B, Goody RS, Reinstein J (1997) GrpE accelerates nucleotide exchange of the molecular chaperone DnaK with an associative displacement mechanism. Biochemistry 36:3417–3422
21. Raviol H, Sadlish H, Rodriguez F, Mayer MP, Bukau B (2006) Chaperone network in the yeast cytosol: Hsp110 is revealed as an Hsp70 nucleotide exchange factor. EMBO J 25:2510–2518
22. Raynes DA, Guerriero V (1998) Inhibition of Hsp70 ATPase activity and protein renaturation by a novel Hsp70-binding protein. J Biol Chem 273:32883–32888
23. Kabani M, Beckerich J-M, Brodsky JL (2002) Nucleotide exchange factor for the yeast

Hsp70 molecular chaperone Ssa1p. Mol Cell Biol 22:4677–4689

24. Ali JA, Jackson AP, Howells AJ, Maxwell A (1993) The 43-kilodalton N-terminal fragment of the DNA gyrase B protein hydrolyzes ATP and binds coumarin drugs. Biochemistry 32:2717–2724
25. O'Brien MC, Flaherty KM, McKay DB (1996) Lysine 71 of the chaperone protein Hsc70 is essential for ATP hydrolysis. J Biol Chem 271:15874–15878
26. Ha JH, McKay DB (1994) ATPase kinetics of recombinant bovine 70 kDa heat shock cognate protein and its amino-terminal ATPase domain. Biochemistry 33:14625–14635
27. Theyssen H, Schuster HP, Packschies L, Bukau B, Reinstein J (1996) The second step of ATP binding to DnaK induces peptide release. J Mol Biol 263:657–670
28. Leskovar A, Reinstein J (2008) Photophysical properties of popular fluorescent adenosine nucleotide analogs used in enzyme mechanism probing. Arch Biochem Biophys 473:16–24
29. O'Brien MC, McKay DB (1995) How potassium affects the activity of the molecular chaperone Hsc70. I. Potassium is required for optimal ATPase activity. J Biol Chem 270:2247–2250
30. Wilbanks SM, McKay DB (1995) How potassium affects the activity of the molecular chaperone Hsc70. II. Potassium binds specifically in the ATPase active site. J Biol Chem 270:2251–2257
31. O'Brien MC, McKay DB (1993) Threonine 204 of the chaperone protein Hsc70 influences the structure of the active site, but is not essential for ATP hydrolysis. J Biol Chem 268:24323–24329
32. Buchberger A, Valencia A, McMacken R, Sander C, Bukau B (1994) The chaperone function of DnaK requires the coupling of ATPase activity with substrate binding through residue E171. EMBO J 13:1687–1695
33. Wei J, Hendershot LM (1995) Characterization of the nucleotide binding properties and ATPase activity of recombinant hamster BiP purified from bacteria. J Biol Chem 270:26670–26676
34. Andréasson C, Fiaux J, Rampelt H, Mayer MP, Bukau B (2008) Hsp110 is a nucleotide-activated exchange factor for Hsp70. J Biol Chem 283:8877–8884
35. Höhfeld J, Jentsch S (1997) GrpE-like regulation of the hsc70 chaperone by the anti-apoptotic protein BAG-1. EMBO J 16:6209–6216
36. Dragovic Z, Broadley SA, Shomura Y, Bracher A, Hartl FU (2006) Molecular chaperones of the Hsp110 family act as nucleotide exchange factors of Hsp70s. EMBO J 25:2519–2528
37. Steel GJ, Fullerton DM, Tyson JR, Stirling CJ (2004) Coordinated activation of Hsp70 chaperones. Science 303:98–101
38. Bertelsen EB, Chang L, Gestwicki JE, Zuiderweg ERP (2009) Solution conformation of wild-type E. Coli Hsp70 (DnaK) chaperone complexed with ADP and substrate. Proc Natl Acad Sci 106:8471–8476

Chapter 14

Determination of Hsp90 Activity Through Activation of Glucocorticoid Receptors in Yeast

Michael Reidy

Abstract

Heat shock protein 90 (Hsp90) is an essential regulator of cellular function through activation of so-called client proteins. Hsp90 is currently a target for potential anti-cancer therapeutics. Assaying for defects in Hsp90 using budding yeast (*Saccharomyces cerevisiae*) is possible and efficient due to the high conservation between the human and yeast Hsp90 systems. Here, we present a method for the determination of Hsp90 activity indirectly through the activation of exogenously expressed glucocorticoid receptor, a natural client protein of Hsp90.

Key words Hsp90, *Saccharomyces cerevisiae*, Glucocorticoid receptor

1 Introduction

Hsp90 is a highly conserved molecular chaperone that influences many different cellular processes by modulating the activity of so-called client protein substrates. In eukaryotes, Hsp90 is essential and abundant, even under optimal growth conditions. Importantly, Hsp90 itself is regulated by a cohort of co-chaperone proteins, which serve to guide Hsp90 through its cycle of ATP hydrolysis-driven binding and release of clients (reviewed in [1]).

Client binding and release is accompanied by conformational changes in Hsp90 dimers. The open conformation of Hsp90 is a homodimer making contact in the C-terminal domain. This conformation is stabilized by co-chaperones such as Hop (*Homo sapiens*)/Sti1 (*Saccharomyces cerevisiae*). Clients are brought to the middle domain of open Hsp90 dimers by the Hsp70/Hsp40 system. Hsp90 dimers then close and twist, facilitated by co-chaperones such as Aha1 and p23 (human)/Sba1 (yeast). The closed form of Hsp90 brings the N-terminal ATPase domains together, which is required for ATP hydrolysis. Upon ATP hydrolysis the N-termini open and the client protein is released. The

Stuart K. Calderwood and Thomas L. Prince (eds.), *Chaperones: Methods and Protocols*, Methods in Molecular Biology, vol. 1709, https://doi.org/10.1007/978-1-4939-7477-1_14,

molecule is thus reset for another cycle. The regulation of the Hsp90 reaction cycle is reviewed in greater detail in reference [2].

The yeast and human Hsp90 systems are highly conserved. Human co-chaperones complement their yeast counterparts. The high degree of conservation combined with the ease of genetic manipulations and diversity of biochemical assays available in the yeast system make it a valuable model organism for studying Hsp90 function. This is especially important since Hsp90 has become an attractive target for anti-cancer therapies, since some types of cancer cells are hypersensitive to Hsp90 inhibition.

While Hsp90 is known to have hundreds of clients, only a few of the pathways that rely on Hsp90 activity have been well characterized. One of these pathways is the mammalian glucocorticoid receptor (GR) pathway. GR is a modular cytosolic protein that contains domains that bind glucocorticosteroid hormones and DNA. In the absence of hormone, GR is bound to Hsp90 in complexes that also contain other co-chaperones. In this state GR is inactive. In the presence of hormone, GR is activated by Hsp90 and released, whereupon it moves to the nucleus and binds to specific GR-responsive elements (GREs) in the promoters of anti-inflammatory genes, upregulating their transcription [3, 4].

Even though yeast does not have a pathway comparable to GR, the level of conservation between the human and yeast Hsp90 systems is such that mammalian GR expressed exogenously in hormone-treated yeast efficiently activates the expression of GRE-driven reporter genes such as β-galactosidase (LacZ) [5–7]. Here, we present a detailed method for the analysis of Hsp90 activity in response to mutation or inhibition of Hsp90 or Hsp90 co-chaperones by quantification of GR activation in yeast. The protocol presented here is a slight modification of that found in reference [8].

In order to determine GR activation, a measure of Hsp90 activity, two plasmids must first be introduced into the yeast strains to be tested: the GR expression plasmid and the GR activity reporter plasmid. We present a method for transforming yeast cells with both plasmids with high efficiency in a single reaction. The transformed yeast carrying the GR and GR reporter plasmids are then grown in the presence of hormone, and the amount of LacZ activity is determined using a standard permeabilized yeast cell assay. The amount of LacZ activity, expressed in Miller units, is directly correlated to the amount of GR activation in response to hormone. Since GR activation is dependent upon the ability of the Hsp90 chaperone system, the affect of a particular treatment or mutation on the Hsp90 system can be measured relative to the proper controls.

2 Materials

2.1 Yeast Transformation

1. Appropriate yeast strain(s). The strain(s) should be auxotrophic for both uracil and tryptophan (*see* **Note 1**).
2. Appropriate liquid yeast growth media (*see* **Note 2**).
3. 14 mL round-bottom culture tubes, sterile.
4. Culture tube roller in 30 °C incubator.
5. 50 mL Erlenmeyer flasks, capped and autoclaved.
6. Shaking incubator.
7. Rat glucocorticoid receptor (GR) plasmid pG/N795 (Addgene cat. #1284). This plasmid expresses the rat GR open reading frame under the control of the strong constitutive *GPD* promoter and contains the 2 μ origin for high copy maintenance in yeast and the *TRP1* selectable marker.
8. GR reporter plasmid pUCΔSS-26X. This plasmid expresses LacZ under the control of a GR responsive promoter and contains the *URA3* selectable marker [8].
9. Sterile water.
10. Sonicated salmon sperm DNA (Agilent #201190). Before the first use, boil salmon sperm in a water bath for 10 min and then immediately submerge into ice (*see* **Note 3**).
11. Lithium acetate stock solution, 1 M: dissolve 5.1 g lithium acetate dihydrate in water to make up to 50 mL, then filter sterilize. Lithium acetate stock solution is good for up to 2 months when stored at room temperature.
12. PEG stock solution: 50% polyethylene glycol 3350 w/v in sterile water. Dissolve 25 g in 20 mL sterile water in a 50 mL Falcon tube. Shake vigorously to dissolve. Centrifuge briefly to remove air bubbles and adjust volume to 50 mL with sterile water. Mix well (*see* **Note 4**).
13. 10× TE: 100 mM Tris–HCl pH 8.0, 10 mM EDTA pH 8.0.
14. 1.5 mL flip-cap tubes, autoclaved.
15. Vortex mixer.
16. 42 °C water bath.
17. –Ura–Trp selective plates: 2% glucose, 0.7% yeast nitrogen base, 2% agar, −Ura–Trp dropout mix (*see* **Note 5**).

2.2 GR Activity Assay

1. Yeast strains harboring pG/N795 and pUCΔSS-26X plasmids.
2. 14 mL round-bottom culture tubes.
3. Selective liquid growth media: 2% glucose, 0.7% yeast nitrogen base, with appropriate nutrients for selection (*see* **Note 6**).
4. Culture tube roller in 30 °C incubator.

5. Deoxycorticosterone acetate (DOC) solution, 10 mM: dissolve 37 mg of DOC in 10 mL 95% ethanol. Protect from light and store at −20 °C.
6. Z-buffer: dissolve 0.375 g KCl, 8.05 g $Na_2HPO_4{\cdot}7H_2O$, 2.75 g $NaH_2PO_4{\cdot}H_2O$, 0.125 g $MgSO_4$ in 400 mL water. Adjust pH to 7.0, if necessary. Adjust volume to 500 mL and filter sterilize. Store at room temperature for up to 6 months (*see* **Note 7**).
7. 10% sodium dodecyl sulfate (SDS): dissolve 1 g SDS in 9 mL water then adjust final volume to 10 mL.
8. Chloroform ($CHCl_3$).
9. β-mercaptoethanol (βME).
10. Vortex mixer.
11. *o*-nitrophenyl-β-D-galactoside (ONPG) solution, 1 mg/mL: dissolve 50 mg of ONPG in 50 mL Z-buffer + βME (*see* Subheading 3.2, **step 3**). Be sure ONPG is fully dissolved—crushing crystals with a glass rod helps greatly. Prepare fresh on the day of the experiment. ONPG stock solutions older than 1 day should not be used.
12. Stop solution, 1 M Na_2CO_3: dissolve 2.6 g Na_2CO_3 in 20 mL water. Adjust final volume to 25 mL. Prepare fresh on the day of the experiment.
13. 2.0 mL round-bottom flip-cap tubes, autoclaved.
14. Spectrophotometer capable of determining absorbance at 600 nm and 450 nm.

3 Methods

3.1 Yeast Transformation

All the steps are performed at room temperature unless otherwise noted.

Day 1:

1. Inoculate 3 mL of the appropriate growth medium in 14 mL round-bottom culture tubes with the yeast strains to be transformed. Incubate overnight, with rolling, at 30 °C or appropriate temperature.

Day 2:

2. Prepare the following solutions:
   (a) LiAc/TE: add 1 mL lithium acetate stock solution and 1 mL 10× TE to 8 mL sterile water. Mix well.
   (b) LiAc/TE/PEG: add 1 mL lithium acetate stock solution, 1 mL 10× TE to 8 mL 50% PEG stock solution. Mix well; the solution will be very viscous.

3. Dilute 1 mL of overnight cultures with 9 mL fresh media in a sterile 50 mL Erlenmyer flask and incubate at 30 °C with shaking for 4 h. (*see* **Note 8**).
4. Harvest cells via centrifugation at 1000 × *g* for 1 min. Decant media.
5. Wash the cells with 10 mL sterile water. Centrifuge at 1000 × *g* for 1 min. Decant water.
6. Suspend the washed yeast cells in 1 mL of LiAc/TE solution. Incubate at room temperature for 5–10 min (*see* **Note 9**).
7. For each transformation reaction: In a separate, sterile 1.5 mL flip-cap tube, combine 50 µL cells from **step 6**, 5 µL boiled salmon sperm DNA, and 1 µg each of plasmids pG/N795 and pUCΔSS-26X. Mix via vortexing briefly at medium speed.
8. Add 350 µL LiAc/TE/PEG solution. Mix well by vortexing at high speed for 10–20 s (*see* **Note 10**).
9. Incubate the tubes in a 42 °C water bath for 30 min.
10. Centrifuge at 10,000 × *g* for 1 min.
11. Carefully remove the supernatant with the pipette and discard. Do not disturb the cell pellet. Remove as much of the solution as possible (*see* **Note 11**).
12. Suspend cells in 300 µL sterile water.
13. Spread 100–200 µL cells onto –Ura–Trp selection plate. Allow sufficient time for the water to soak into the media and then invert the plate (*see* **Note 12**).
14. Incubate at 30 °C for 3–5 days. Colonies should be visible starting on the third day after plating. Once colonies have reached 1–2 mm in diameter, the plates can be stored at room temperature for up to 2 weeks, or at 4 °C for up to 4 weeks, inverted. Discard plates after 1 month.

3.2 GR Activity Assay

All the steps are performed at room temperature unless otherwise noted.

Day 1

1. For each strain to be tested, inoculate 3 mL of appropriate –Ura, –Trp media in 14 mL round-bottom culture tubes with a single colony from the fresh GR/reporter plasmid transformation plate, ideally less than 1 week old. Do not use plates older than 2–3 weeks. Do this with three individual colonies for each strain to be tested. These will serve as independent biological replicates (*see* **Note 13**).
2. Incubate at 30 °C with rolling overnight.

Day 2

3. Prepare the following solutions fresh:

(a) Z-buffer + βME: to a 50 mL aliquot of Z-buffer, add βME to 50 mM.

(b) 0.01% SDS: add 1 μL of 10% SDS to 999 μL sterile water.

(c) ONPG solution (*see* Subheading 2.2, **step 11**).

(d) Stop solution (*see* Subheading 2.2, **step 12**).

4. In the morning, dilute 0.3 mL of cultures with 2.7 mL of fresh media in new 14 mL round-bottom culture tubes.
5. Add 3 μL of DOC stock solution to each. Include a wild-type strain with no DOC as a negative control and spectrophotometer blank.
6. Incubate at 30 °C with rolling for 4–6 h (*see* **Note 14**).
7. Measure and record the OD_{600} of all cultures (*see* **Note 15**).
8. Transfer 1 mL of each culture to a 2.0 mL round-bottom flip-cap tube (*see* **Note 16**).
9. Centrifuge at 10,000 × *g* for 1 min.
10. Carefully decant media by pouring. Be careful not to disturb cell pellet (*see* **Note 17**).
11. Resuspend the cells from **step 8** in 150 μL Z-buffer + βME (*see* **Note 18**).
12. Add 50 μL $CHCl_3$.
13. Add 20 μL 0.01% SDS.
14. Close the lid tightly and vortex for 1 min at high speed (*see* **Note 19**).
15. Add 700 μL ONPG solution.
16. Close the lid, mix well by inverting the tubes several times, and incubate for at least 10 min in a 30 °C water bath. Yellow color should be readily observable. Record the total time of the incubation, as this value is needed for the LacZ activity calculation (*see* **Note 20**).
17. Stop the reaction by adding 500 μL Stop solution. Close the lid and mix well by inversion (*see* **Note 21**).
18. Centrifuge at 10,000 × *g* for 30 s.
19. Transfer 500 μL of the supernatant to a spectrophotometer cuvette, being sure not to disturb the cell debris and chloroform layer at the bottom of the tube. Measure and record the absorbance at 450 nm. Use the reaction from the cells that were not treated with DOC as the blank.

3.3 Determination of GR Activity

1. Calculate Miller units of each sample using the following formula: Miller U = $(1000^{*}A_{450})/(t^{*}V^{*}OD_{600})$, where A_{450} is the absorbance at 450 nm of the stopped reaction, t is the time of the reaction in minutes, V is the volume of the culture used

in the reaction, and OD_{600} is the optical density of the culture used in the assay.

2. Calculate the average and standard deviation of the three biological replicates (individual GR/reporter plasmid transformants) for each sample.
3. Determine sample activity relative to the wild-type strain or other appropriate control. This calculation allows for more accurate comparison from experiment to experiment.

4 Notes

1. In order for this protocol to work, the strains to be tested must be both uracil and tryptophan auxotrophs. Specifically they must have null, non-reverting mutations in both the *URA3* and *TRP1* genes. Generally, this assay is used to test the effect of mutations in Hsp90 or Hsp90 co-chaperones on GR activation. This protocol assumes that such mutant strains are already in hand. For a method on plasmid shuffling in Hsp90-deleted strains, *see* [9]. Always include an isogenic wild-type strain as a positive control.
2. Use a liquid growth media that selects for any plasmids that may be in the strain. Strains that are deleted for both chromosomal Hsp90 genes and have an Hsp90 allele on a plasmid, but no other plasmids, do not require selectable growth conditions since Hsp90 is an essential gene.
3. Salmon sperm DNA performs a "carrier" role and greatly increases transformation efficiency. In order to achieve maximum transformation efficiency, it is essential that before the first use the salmon sperm DNA is boiled and then immediately moved to ice. Once boiled, salmon sperm DNA can be stored at −20 °C. It is not necessary to boil for subsequent uses. However, any drops in subsequent transformation efficiency can usually be remedied by additional boiling/ice cycles.
4. The PEG stock solution is very viscous. Use sterile water to dissolve PEG instead of filter sterilizing.
5. There are several forms of yeast nitrogen base (YNB) available. Use YNB that contains ammonium sulfate but lacks amino acids. In addition to lacking uracil and tryptophan, omit other appropriate nutrients in order to select for other plasmids that may be present in your strain. Prepare plates in advance to give them time to dry enough to readily take up the suspended cell solution.
6. Generally, the media used in this step is the same as used for the transformation, but in a liquid form.

7. Z-buffer lacking βME is stable at room temperature for up to 6 months. In this protocol, βME is added to an aliquot of Z-buffer immediately before use.
8. Highest transformation efficiencies are attained using cells that are in the logarithmic phase of growth. A simple way to check whether the cells are in log-phase growth is to estimate the percentage of yeast cells with buds via light microscopy. Most cells in a log-phase culture should contain buds, whereas most cells from the overnight (i.e., stationary phase) culture will be unbudded. Cells from the overnight culture may be used, but expect lower transformation efficiency.
9. Typically, one should have 0.5–1.0 OD_{600} units of cells per transformation reaction. Thus, the OD_{600} of the cells suspended in LiAc/TE should be 10–20. This protocol assumes the overnight culture had an OD_{600} of ~10, which is typical of cells grown overnight in rich, i.e., non-selective, media. If the overnight culture was grown in selective media, the final OD_{600} was probably 3–5, so adjust the final volume of cells in LiAc/TE accordingly.
10. The LiAc/TE/PEG solution is quite viscous. Be careful when pipetting to minimize transfer errors. Using a repeater pipette helps reduce pipetting errors. If using cells from an overnight culture, or if your strain does not transform well, addition of 1 μL of βME to the transformation mixture may improve efficiency.
11. Some residual LiAc/TE/PEG solution in the tube does not greatly impact transformation efficiency. However, excess residual LiAc/TE/PEG solution will affect efficiency. It is not necessary to wash the cells at this step, but washing may be advised if removing the LiAc/TE/PEG solution is problematic.
12. Yeast plates should be incubated and stored inverted, i.e., lid side down, in order to prevent any condensation that forms on the lid from spilling onto the media.
13. It is crucial that a wild-type control be included in each experiment. Importantly, we have found that assaying cells that have been freshly transformed with the GR and GR reporter plasmids gives the most reliable data. Prolonged subculturing of GR and GR reporter plasmid-carrying strains results in increased cell-to-cell variability in GR activation, probably due to accumulating differences in plasmid segregation at mitosis. Therefore, transformation of wild-type controls with the GR and GR reporter plasmids should be done fresh for each experiment. Individual transformant colonies represent independent biological replicates.

14. The duration of the hormone-incubation step is strain dependent. Typically, 4–6 h. of incubation results in one or two cell doublings and works well for our strains. The researcher should empirically determine the optimal length of hormone incubation for their strains and then use this condition consistently from experiment to experiment, in order to accurately compare results across experiments.
15. An accurate measurement of cell density is key for the determination of GR activation and controls for variability in yeast strain growth rates.
16. More or less volume of the culture may be used in the assay, depending on the strain growth rate. The volume of culture used is factored into the GR activation calculation, so if using a volume other than 1 mL, be sure to make note of this and adjust calculations accordingly. In general, it is suggested to have a comparable amount of cells in each reaction, to minimize errors due to loss of cells during manipulations.
17. In general, we have found that washing the cells may result in cell loss that contributes to variability and increased experimental error. We have found that omitting the wash step has no effect on LacZ activity. Excess media that may be stuck to the sides of the tube can be removed by carefully wicking it away with a KimWipe, but be sure not to disturb the cell pellet. Any detriment that may be caused by residual media is outweighed by the potential loss of cells that can occur from washing.
18. We have found that use of a repeater pipette for this and subsequent steps increases efficiency and decreases experimental error.
19. Thorough vortexing is crucial for the permeabilization of the cells. Be sure to use tubes that have lids that seal tightly to avoid spilling chloroform.
20. Factors that may influence LacZ reaction time include age of DOC and ONPG reagents. Temperature also greatly influences the reaction. Reactions may be incubated at 37 °C, as long as this is duly noted and consistently maintained from experiment to experiment. It is possible, but not necessary, to calculate rates of LacZ activity, rather than end points, by removing aliquots during the incubation step and immediately stopping with an appropriate amount of Stop solution.
21. The stopped reactions are moderately stable for up to 2 days at room temperature, if protected from light. However, we recommend measuring the Absorbance at 450 nm as soon as possible after stopping the reaction.

Acknowledgment

This work was supported by the Intramural Research Program of the National Institute of Diabetes, Digestive and Kidney Diseases (NIDDK).

References

1. Prodromou C (2016) Mechanisms of Hsp90 regulation. Biochem J 473(16):2439–2452. https://doi.org/10.1042/BCJ20160005
2. Pearl LH (2016) Review: the HSP90 molecular chaperone-an enigmatic ATPase. Biopolymers 105(8):594–607. https://doi.org/10.1002/bip.22835
3. Grad I, Picard D (2007) The glucocorticoid responses are shaped by molecular chaperones. Mol Cell Endocrinol 275(1–2):2–12. https://doi.org/10.1016/j.mce.2007.05.018
4. Pratt WB, Morishima Y, Murphy M, Harrell M (2006) Chaperoning of glucocorticoid receptors. Handb Exp Pharmacol 172:111–138
5. Picard D, Khursheed B, Garabedian MJ, Fortin MG, Lindquist S, Yamamoto KR (1990) Reduced levels of hsp90 compromise steroid receptor action in vivo. Nature 348 (6297):166–168. https://doi.org/10.1038/348166a0
6. Chang HC, Lindquist S (1994) Conservation of Hsp90 macromolecular complexes in *Saccharomyces cerevisiae*. J Biol Chem 269 (40):24983–24988
7. Nathan DF, Lindquist S (1995) Mutational analysis of Hsp90 function: interactions with a steroid receptor and a protein kinase. Mol Cell Biol 15(7):3917–3925
8. Louvion JF, Warth R, Picard D (1996) Two eukaryote-specific regions of Hsp82 are dispensable for its viability and signal transduction functions in yeast. Proc Natl Acad Sci U S A 93 (24):13937–13942
9. Genest O, Reidy M, Street TO, Hoskins JR, Camberg JL, Agard DA, Masison DC, Wickner S (2013) Uncovering a region of heat shock protein 90 important for client binding in *E. coli* and chaperone function in yeast. Mol Cell 49(3):464–473. https://doi.org/10.1016/j.molcel.2012.11.017

Chapter 15

Bacterial Hsp90 ATPase Assays

Joel R. Hoskins, Sue Wickner, and Shannon M. Doyle

Abstract

Bacterial Hsp90 is an ATP-dependent molecular chaperone involved in protein remodeling and activation. The *E. coli* Hsp90, $Hsp90_{Ec}$, collaborates in protein remodeling with another ATP-dependent chaperone, DnaK, the *E. coli* Hsp70. Both $Hsp90_{Ec}$ and DnaK hydrolyze ATP and client (substrate) proteins stimulate the hydrolysis. Additionally, ATP hydrolysis by the combination of $Hsp90_{Ec}$ and DnaK is synergistically stimulated in the presence of client (substrate). Here, we describe two steady-state ATPase assays used to monitor ATP hydrolysis by $Hsp90_{Ec}$ and DnaK as well as the synergistic stimulation of ATP hydrolysis by the combination of $Hsp90_{Ec}$ and DnaK in the presence of a client (substrate). The first assay is a spectrophotometric assay based on enzyme-coupled reactions that utilize the ADP formed during ATP hydrolysis to oxidize NADH. The second assay is a more sensitive method that directly quantifies the radioactive inorganic phosphate released following the hydrolysis of [γ-^{33}P] ATP or [γ-^{32}P] ATP.

Key words Hsp90, Hsp70, DnaK, ATP hydrolysis, Steady-state ATPase

1 Introduction

Hsp90 is a widely conserved and ubiquitous molecular chaperone that participates in ATP-dependent protein remodeling and activation in both eukaryotes and prokaryotes, an activity that requires the Hsp70 chaperone system [1–3]. Additionally, in eukaryotes the ATPase activity and the chaperone cycle of Hsp90 are regulated by a myriad of co-chaperones [1, 2]. In contrast to eukaryotic Hsp90, bacterial Hsp90 functions independently of Hsp90 cochaperones [4, 5].

Hsp90 is a functional homodimer, and each monomer is comprised of three domains: an N-terminal ATPase domain [6, 7], a middle domain that is involved in client binding [6, 8–10], and a C-terminal dimerization domain that also contains residues that interact with client [2, 8]. Hsp90 undergoes large-scale conformational changes upon ATP binding and hydrolysis, and these motions are coupled with the processes of client binding, remodeling, and release [6, 7, 10–12]. Apo Hsp90 in the solution exists as "V-shaped" dimers linked through the C-terminal domain

Stuart K. Calderwood and Thomas L. Prince (eds.), *Chaperones: Methods and Protocols*, Methods in Molecular Biology, vol. 1709, https://doi.org/10.1007/978-1-4939-7477-1_15,

[13]. However, ATP binding leads to closing of the ATP lid on the ATP-binding site, dimerization of the N-terminal domains, and compaction of the molecule [11–14]. ATP hydrolysis and ADP release trigger the dissociation of the N-domains and the return of apo Hsp90 to the "V-shaped" dimers [11–14]. Eukaryotic Hsp90 cochaperones including Aha1/Hch1, Hop/Sti1, Cdc37, and p23/Sba1 regulate the cycle of ATP binding and hydrolysis as well as imparting client protein specificity [1, 2, 12].

The Hsp70 chaperone system collaborates with Hsp90 in protein remodeling and activation [1, 3, 4]. Eukaryotic Hsp70 and its bacterial homolog, DnaK, are highly conserved, ATP-dependent molecular chaperones [15–17]. Hsp70 has both an N-terminal ATP-binding domain and a C-terminal substrate-binding domain, which are connected via a flexible linker [17]. Like Hsp90, Hsp70 undergoes large conformational changes upon ATP-binding, hydrolysis, and release [17]. Moreover, Hsp70 acts in conjunction with two cochaperones, Hsp40 (J-domain protein) and a nucleotide exchange factor (NEF). The Hsp40 cochaperone targets clients for recognition by Hsp70 and stimulates ATP hydrolysis by Hsp70, while the NEF triggers nucleotide exchange by Hsp70 [15, 18, 19].

In *E. coli*, $Hsp90_{Ec}$ acts in conjunction with DnaK and an *E. coli* J-domain protein, DnaJ or CbpA. GrpE, the *E. coli* NEF, stimulates protein reactivation, but is not essential [4, 5]. Homologs of eukaryotic Hsp90 cochaperones have not been identified in bacteria [1]. Instead, $Hsp90_{Ec}$ and DnaK directly interact, both in vivo and in vitro [4, 5], and this interaction is essential for collaboration in client remodeling and a synergistic stimulation of ATP hydrolysis [20]. Additionally, client binding and ATP hydrolysis by both chaperones is required for client remodeling and synergy in ATPase activity [20].

Two alternative methods for monitoring the ATPase activity of $Hsp90_{Ec}$, DnaK and the combination of the two chaperones are described here. One is an enzyme-coupled spectrophotometric assay that is performed in a microtiter plate. For each mole of ATP hydrolyzed, 1 mol of ADP is produced. The ADP produced is converted to ATP by pyruvate kinase (PK) in an enzymatic reaction requiring phosphoenolpyruvate (PEP) and producing pyruvate. Pyruvate is then reduced to lactate by L-lactate dehydrogenase (LDH) in an enzymatic reaction that is coupled to the oxidation of NADH to NAD+. Thus for each mole of ATP hydrolyzed, 1 mol of NADH is oxidized. The assay monitors the decrease in optical density at the NADH absorbance maxima, 340 nm, as a function of time. This decrease in NADH is directly proportional to the rate of ATP hydrolysis. The constant regeneration of ATP allows monitoring the ATP hydrolysis rate as long as PEP and NADH are present.

A second more sensitive method to measure ATP hydrolysis by $Hsp90_{Ec}$ is also described. In this method, radioactive inorganic phosphate, either $^{33}P_i$ or $^{32}P_i$, produced by hydrolysis of [γ-^{33}P] ATP or [γ-^{32}P] ATP is monitored following the formation of a phosphomolybdate complex and organic extraction.

2 Materials

All the solutions are prepared using ultrapure H_2O and analytical grade reagents from common sources (unless specifically indicated).

2.1 Enzyme-Coupled Spectrophotometric ATPase Assay

1. HKE buffer: 25 mM Hepes, pH 7.5, 50 mM KCl, and 0.1 mM EDTA (final concentrations in 100 μL reaction mixtures). A concentrated buffer (5× or 10×) can be prepared and used for accuracy and simplification. Store the concentrated buffer at room temperature. ATPase reactions are supplemented with DTT (2 mM final) during reaction assembly.
2. NADH (nicotinamide adenine dinucleotide), 25 mM stock solution in HKE buffer. NADH concentration can be determined by measuring A_{340} in a spectrophotometer. The extinction coefficient of NADH is 6.22×10^3/M/cm. Store frozen (−20 °C) in ~100 μL aliquots.
3. ATP, 100 mM stock solution. To 100 mg of ATP add 1 mL ultrapure H_2O. Adjust the pH to 7.5 using 1 M Tris base. Make a 1:1000 dilution (1 μL ATP + 999 μL ultrapure H_2O) and read the absorbance at 260 nm. The extinction coefficient of ATP is 15.4×10^3/M/cm. A 1:1000 dilution of 100 mM ATP has an absorbance of 1.54. Adjust the volume with ultrapure H_2O as needed to obtain a concentration of 100 mM.
4. Phosphoenolpyruvate (PEP), 100 mM stock solution in HKE buffer. Store frozen (−20 °C) in ~100 μL aliquots.
5. Pyruvate kinase/lactate dehydrogenase (PK/LDH) mix, commercially available (Sigma: P0294).
6. $MgCl_2$, 1 M stock solution in ultrapure H_2O. Store at room temperature.
7. DTT, 1 M stock in ultrapure H_2O. Store frozen (−20 °C).
8. Proteins: DnaK, $Hsp90_{Ec}$, ribosomal protein L2 (client protein).
9. Geldanamycin (Sigma), 30 mM stock solution in DMSO. $Hsp90_{Ec}$ is inhibited by 10–30 μM geldanamycin (*see* **Note 1**).

2.2 ATPase Assay Using Radioactive ATP

1. HKE buffer: 25 mM Hepes, pH 7.5, 50 mM KCl, and 0.1 mM EDTA (final concentrations in 50 μL reaction mixtures). A concentrated buffer (5× or 10×) can be prepared and used

for accuracy and simplification. Store the concentrated buffer at room temperature. ATPase reactions are supplemented with DTT (2 mM final), Triton X-100 (0.005% final), and $MgCl_2$ (10 mM final) during reaction assembly.

2. ATP, 100 mM stock solution (*see* Subheading 2.1, **item 3**).
3. [γ-^{33}P] ATP (Perkin Elmer: NEG302H) or [γ-^{32}P] ATP (Perkin Elmer: NEG002A). Make an ~0.1 μCi/μL stock solution (typically a 1:100 dilution into ultrapure H_2O). Freeze in aliquots at −20 °C.
4. $MgCl_2$, 1 M stock solution in ultrapure H_2O. Store at room temperature.
5. DTT, 1 M stock in ultrapure H_2O. Store frozen (−20 °C).
6. Triton X-100, 10% solution (Thermo Scientific: 28314).
7. Tungstosilicic (silicotungstic) acid solution, 20 mM stock solution in 10 mM $MgSO_4$. For 50 mL, solubilize 0.12 g $MgSO_4$ in ultrapure H_2O. Use 2.88 g silicotungstic acid and solubilize in the prepared 50 mL of 10 mM $MgSO_4$. Store at 4 °C.
8. KH_2PO_4, 2 mM stock solution. For 50 mL, solubilize 13.6 mg KH_2PO_4 in ultrapure H_2O. Store at 4 °C.
9. Ammonium molybdate solution, 5% stock solution (w/v) in 2 M H_2SO_4. For 50 mL, dilute stock H_2SO_4 to 2 M and then solubilize 2.5 g ammonium molybdate. Store at 4 °C.
10. Isobutanol:toluene solution, 1:1 (v/v). Store at room temperature in a sealed glass container.
11. Proteins: DnaK, $Hsp90_{Ec}$, L2.
12. Scintillation fluid for organic solvents (e.g., Eccoscint A).
13. Geldanamycin (Sigma), 30 mM stock solution in DMSO. $Hsp90_{Ec}$ is inhibited by 10–30 μM geldanamycin (*see* **Note 1**).

3 Methods

3.1 Enzyme-Coupled Spectrophotometric ATPase Assay

With the assay conditions described here, $Hsp90_{Ec}$ hydrolyzes ATP at a rate of ~0.1 nmol/min and the rate is stimulated ~fourfold in the presence of L2 (client protein) [8, 20]. DnaK hydrolyzes ATP at a rate of ~0.1 nmol/min and is only slightly stimulated by L2 [20]. When the three proteins are combined, an ~twofold stimulation above the additive values is observed [20]. The ATPase activity can be measured readily using a steady-state ATPase assay in a 96-well plate. In an enzyme-coupled reaction, ADP produced by the chaperones is regenerated to ATP by a reaction that is coupled with the conversion of NADH to NAD^+ [21, 22] (Fig. 1). The absorbance of NADH at 340 nm is monitored to measure the

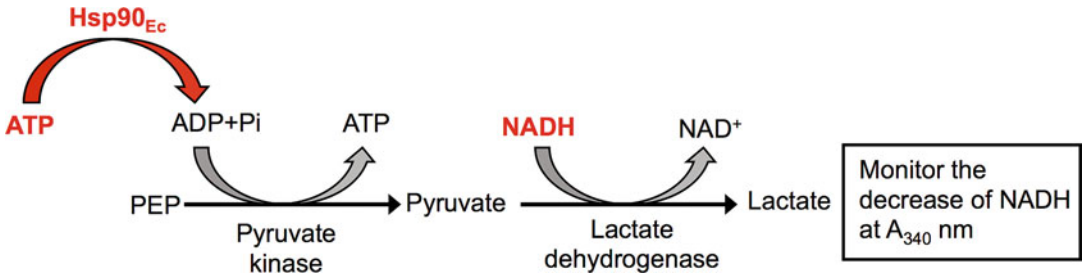

Fig. 1 Enzyme-coupled spectrophotometric ATPase assay. ADP produced by $Hsp90_{Ec}$, DnaK, or the combination of chaperones with or without L2 is regenerated to ATP by a reaction that is coupled with the conversion of NADH to NAD^+ [21, 22]. The decrease in NADH concentration is monitored

decrease in NADH concentration, which is quantitatively proportional to the rate of ATP hydrolysis.

1. Equilibrate a black, clear-bottom 96-well plate at 37 °C in a plate reader capable of monitoring A_{340} over time at 37 °C (*see* **Note 2**).
2. Prepare a 10× mixture of PEP, PK/LDH, NADH, $MgCl_2$, and ATP. The final concentrations of the components in 100 μL reactions are 1 mM PEP, 1:100 dilution of the PK/LDH mix, 0.5 mM NADH, 10 mM $MgCl_2$, and 2 mM ATP (*see* **Note 3**). Aliquot 12 μL of the 10× mix into individual PCR tubes. These mixtures will be used in **step 4** (*see* **Note 4**).
3. In individual 1.5 mL microcentrifuge tubes, assemble the chaperone mixtures (90 μL) containing HKE buffer, DTT, DnaK or $Hsp90_{Ec}$ or both together in the presence or absence of L2 (*see* **Note 5**). The final concentrations in 100 μL mixtures are 25 mM Hepes, pH 7.5, 50 mM KCl, 0.1 mM EDTA, and 2 mM DTT. The proteins are typically used at equilmolar ratios of DnaK monomer:$Hsp90_{Ec}$ dimer:L2 monomer at a concentration of 1 μM (*see* **Note 6**). Transfer the chaperone mixtures into wells of the 96-well plate.
4. Using a multichannel pipette, start the reactions by transferring 10 μL of the 10× mix of PEP, PK/LDH, NADH, $MgCl_2$, and ATP into the wells of the 96-well plate that contain the chaperone mixture. A multichannel pipette is used for this step to ensure that all the reactions have the same start time (*see* **Note 4**). Mix the reactions in the plate using a plate mixer or use the mixing function of the plate reader.
5. Measure the decrease in NADH absorbance at 340 nm as a function of time in a plate reader at 37 °C.
6. Fit the data to a linear equation using appropriate software (*see* **Note 7**). Calculate the amount of NADH (nmol) converted to NAD+ (nmol) in each reaction by comparing the slope to that of a previously determined NADH standard (*see* **Note 8**).

The amount of NADH (nmol) converted to NAD+ (nmol) is quantitatively proportional to the amount of ADP generated and can be used to determine the rate of ATP hydrolysis.

3.2 ATPase Assay Using Radioactive ATP

Alternatively, $Hsp90_{Ec}$ ATPase can be monitored by measuring the production of inorganic phosphate, $^{33}P_i$ or $^{32}P_i$, from the hydrolysis of [γ-^{33}P] ATP or [γ-^{32}P] ATP [23]. Free P_i, in the form of a phosphomolybdate complex, is quantitatively recovered by organic extraction.

1. Prepare a 10× mixture of 40 mM ATP and [γ-^{33}P] ATP (or [γ-^{32}P] ATP), such that after dilution each 50 μL reaction will contain 4 mM ATP and 0.1 μCi [γ-^{33}P] ATP (1 μL of 0.1 μCi/μL stock solution). The reactions will be started by the addition of 5 μL of this mixture in **step 3** below.
2. In individual 1.5 mL microcentrifuge tubes, assemble the chaperone mixtures (45 μL) containing HKE buffer, DTT, Triton X-100, $MgCl_2$, DnaK or $Hsp90_{Ec}$ or both together in the presence or absence of L2 (*see* **Note 5**). The final concentrations in 50 μL mixtures are 25 mM Hepes, pH 7.5, 50 mM KCl, 0.1 mM EDTA, 2 mM DTT, 0.005% Triton X-100, and 10 mM $MgCl_2$. The proteins are typically used at equilmolar ratios of DnaK monomer:$Hsp90_{Ec}$ dimer:L2 monomer at a concentration of 1 μM (*see* **Note 6**).
3. Start the reactions by adding 5 μL of the ATP mixture to each reaction mixture. Incubate mixtures at 25 °C for various times (*see* **Note 9**). To determine the total input radioactivity, add 1 μL of the 0.1 μCi [γ-^{33}P] ATP solution to 49 μL HKE buffer and transfer 50 μL into 10 mL scintillation fluid in a scintillation vial and determine radioactivity with the experimental samples.
4. Following incubation, add 100 μL 20 mM silicotungstic acid solution to each reaction and vortex gently. Next add 200 μL 2 mM KH_2PO_4 to each reaction. Then add 100 μL 5% ammonium molybdate solution to each reaction and vortex gently. Incubate the reactions for 1 min at 37 °C.
5. Add 450 μL of the isobutanol:toluene mixture to each reaction. Vortex each tube vigorously for 15 s (*see* **Note 10**). Let the tubes sit for 1 min at room temperature to allow phase separation.
6. Remove 100 μL of the top organic layer and add to 10 mL scintillation fluid in scintillation vials. Measure radioactivity in a liquid scintillation counter (*see* **Note 11**). Use the input radioactivity control to determine the fraction of $^{33}P_i$ or $^{32}P_i$ in each sample and calculate the amount of ATP hydrolyzed (*see* **Note 12**).

4 Notes

1. To determine if $Hsp90_{Ec}$ is contaminated with nonspecific ATPase activity, geldanamycin can be used. It specifically inhibits ATP hydrolysis by $Hsp90_{Ec}$ [4, 24].
2. The preincubation step allows the reactions to reach 37 °C faster and reduces the lag in hydrolysis that can make monitoring the linear phase of the reaction more difficult.
3. The NADH concentration indicated, 0.5 mM, is a starting suggestion and can be adjusted to accommodate various ATP hydrolysis rates.
4. The 10× mixture (12 μL) is added into PCR tubes (preferably strips) prior to the addition to the 96-well plate. In order for all the reaction mixtures to have the same starting time point, a multichannel pipette is used to remove 10 μL of the 10× mix from the PCR tubes and make the addition into the 96-well plate.
5. For background subtraction, carry out a reaction with buffer alone and buffer with L2 only. *See* **Note 1** for information about controls for ATPase contamination in $Hsp90_{Ec}$ samples.
6. These conditions have been optimized to monitor the synergy between $Hsp90_{Ec}$ and DnaK. Different ratios and concentrations of $Hsp90_{Ec}$, DnaK, and L2 may be used.
7. When fitting the data, usually only a portion of the data can be used for the linear fit. There is often a short lag at the start of the reaction, followed by a linear portion and then a plateau when NADH is exhausted. For the fit, only use data in the linear portion of the curve.
8. The NADH standard curve is determined by preparing NADH standards in duplicate as follows: (1) Transfer 3 μL of a 25 mM NADH solution into 297 μL HKE buffer to obtain 25 nmol NADH/100 μL. (2) Using150 μL of this dilution, make five twofold serial dilutions into 150 μL HKE buffer to make solutions of 12.5, 6.25, 3.13, 1.56, and 0.78 nmol NADH/100 μL. Transfer 100 μL of each concentration of NADH and HKE buffer alone into separate wells of a black, clear bottom 96-well plate. Measure absorbance at 340 nm using a plate reader. Plot A_{340} as a function of NADH (nmol) in Prism or another data analysis program. Fit the data using linear regression analysis and use the resulting linear equation to calculate the rate of NADH (nmol) converted to NAD^+ (nmol) from the experimental data.
9. This assay can be used as an end-point reaction from which the rate of ATP hydrolysis per minute can be calculated. However, it is important to determine that hydrolysis for each protein is

in a linear range by measuring the amount of ATP hydrolyzed after various times of incubation and adjusting the end-point incubation time as necessary.

10. Caution should be used when opening and closing microfuge tubes during this assay. Any defect in the lid can cause leaking upon vortexing the organic solution.
11. To accurately calculate the amount of radioactive P_i in the organic layer, determine the final volume of the organic layer. Perform a mock reaction using 50 μL of HKE buffer in place of a reaction mixture (**step 1**, Subheading 3.2) and follow **steps 2–5** as described (Subheading 3.2). Remove and determine the volume of the organic layer. This volume is necessary to calculate the amount of total P_i found in the organic layer as only 100 μL (~25%) is monitored by scintillation counting.
12. Convert cpm in each reaction mixture to nmol ATP hydrolyzed min^{-1}. Make sure to take into account the fraction of the organic layer counted, the reaction time in minutes, and the specific activity (cpm/nm) of ATP in the reaction, accounting for both the labeled and unlabeled ATP.

Acknowledgment

This work was supported by the Intramural Research Program of the NIH, NCI, Center for Cancer Research.

References

1. Johnson JL (2012) Evolution and function of diverse Hsp90 homologs and cochaperone proteins. Biochim Biophys Acta, Mol Cell Res 1823:607–613
2. Röhl A, Rohrberg J, Buchner J (2013) The chaperone Hsp90: changing partners for demanding clients. Trends Biochem Sci 38:253–262
3. Li J, Soroka J, Buchner J (2012) The Hsp90 chaperone machinery: conformational dynamics and regulation by co-chaperones. Biochim Biophys Acta, Mol Cell Res 1823:624–635
4. Genest O, Hoskins JR, Camberg JL, Doyle SM, Wickner S (2011) Heat shock protein 90 from Escherichia coli collaborates with the DnaK chaperone system in client protein remodeling. Proc Natl Acad Sci U S A 108:8206–8211
5. Nakamoto H, Fujita K, Ohtaki A, Watanabe S, Narumi S, Maruyama T, Suenaga E, Misono TS, Kumar PKR, Goloubinoff P, Yoshikawa H (2014) Physical interaction between bacterial heat shock protein (Hsp) 90 and Hsp70 chaperones mediates their cooperative action to refold denatured proteins. J Biol Chem 289:6110–6119
6. Prodromou C (2012) The 'active life' of Hsp90 complexes. Biochim Biophys Acta, Mol Cell Res 1823:614–623
7. Prodromou C, Morgan RML (2016) "Tuning" the ATPase activity of Hsp90. Adv Biochem Health Dis 14:469–490
8. Genest O, Reidy M, Street TO, Hoskins JR, Camberg JL, Agard DA, Masison DC, Wickner S (2013) Uncovering a region of heat shock protein 90 important for client binding in E. coli and chaperone function in yeast. Mol Cell 49:464–473
9. Karagöz GE, Rüdiger SGD (2015) Hsp90 interaction with clients. Trends Biochem Sci 40:117–125
10. Southworth DR, Agard DA (2008) Species-dependent ensembles of conserved conformational states define the Hsp90 chaperone ATPase cycle. Mol Cell 32:631–640
11. Graf C, Stankiewicz M, Kramer G, Mayer MP (2009) Spatially and kinetically resolved

changes in the conformational dynamics of the Hsp90 chaperone machine. EMBO J 28:602–613

12. Taipale M, Jarosz DF, Lindquist S (2010) HSP90 at the hub of protein homeostasis: emerging mechanistic insights. Nat Rev Mol Cell Biol 11:515–528
13. Shiau AK, Harris SF, Southworth DR, Agard DA (2006) Structural analysis of E. Coli hsp90 reveals dramatic nucleotide-dependent conformational rearrangements. Cell 127:329–340
14. Ali MMU, Roe SM, Vaughan CK, Meyer P, Panaretou B, Piper PW, Prodromou C, Pearl LH (2006) Crystal structure of an Hsp90-nucleotide-p23/Sba1 closed chaperone complex. Nature 440:1013–1017
15. Balchin D, Hayer-Hartl M, Hartl FU (2016) In vivo aspects of protein folding and quality control. Science 353:aac4354
16. Clerico EM, Tilitsky JM, Meng W, Gierasch LM (2015) How Hsp70 molecular machines interact with their substrates to mediate diverse physiological functions. J Mol Biol 427:1575–1588
17. Mayer MP (2013) Hsp70 chaperone dynamics and molecular mechanism. Trends Biochem Sci 38:507–514
18. Alderson TR, Kim JH, Markley JL (2016) Dynamical structures of Hsp70 and Hsp70-Hsp40 complexes. Structure 24:1014–1030
19. Zuiderweg ERP, Bertelsen EB, Rousaki A, Mayer MP, Gestwicki JE, Ahmad A (2013) Allostery in the Hsp70 chaperone proteins. Top Curr Chem 328:99–153
20. Genest O, Hoskins JR, Kravats AN, Doyle SM, Wickner S (2015) Hsp70 and Hsp90 of E. coli directly interact for collaboration in protein remodeling. J Mol Biol 427:3877–3889
21. Ali JA, Jackson AP, Howells AJ, Maxwell A (1993) The 43-kilodalton N-terminal fragment of the DNA gyrase B protein hydrolyzes ATP and binds coumarin drugs. Biochemistry 32:2717–2724
22. Sehgal P, Olesen C, Moller JV (2016) ATPase activity measurements by an enzyme-coupled spectrophotometric assay. Methods Mol Biol 1377:105–109
23. Shacter E (1984) Organic extraction of Pi with isobutanol/toluene. Anal Biochem 138:416–420
24. Prodromou C, Roe SM, O'Brien R, Ladbury JE, Piper PW, Pearl LH (1997) Identification and structural characterization of the ATP/ADP-binding site in the Hsp90 molecular chaperone. Cell 90:65–75

Chapter 16

Detecting Posttranslational Modifications of Hsp90

Rebecca A. Sager, Mark R. Woodford, Len Neckers, and Mehdi Mollapour

Abstract

The molecular chaperone Heat Shock Protein 90 (Hsp90) is essential in eukaryotes. Hsp90 chaperones proteins that are important determinants of multistep carcinogenesis. The chaperone function of Hsp90 is linked to its ability to bind and hydrolyze ATP. Co-chaperones as well as posttranslational modifications (phosphorylation, SUMOylation, and ubiquitination) are important for its stability and regulation of the ATPase activity. Both mammalian and yeast cells can be used to express and purify Hsp90 and also detect its posttranslational modifications by immunoblotting.

Key words Heat shock protein 90 (Hsp90), Molecular chaperones, Posttranslational modification, Phosphorylation, SUMOylation, Ubiquitination

1 Introduction

Heat Shock Protein 90 (Hsp90) is an essential molecular chaperone in eukaryotes [1, 2]. Its cellular functions have been most clearly identified in mammalian cells, Drosophilia, and baker's yeast *Saccharomyces cerevisiae* [3]. Hsp90 creates and maintains the functional conformation of a subset of proteins [4–6]. These targets (or "clients") are key components of signal transduction pathways and numerous transcription factors. Hsp90 and a discrete set of co-chaperone proteins "hold" these clients in a state from which they can respond to activating signals [7].

Hsp90 chaperone activity depends on ATP binding and hydrolysis [8–10]. This is coupled to a conformational cycle involving the opening and closing of a dimeric "molecular clamp" via transient association of Hsp90's N-terminal domain [11, 12]. The N-domain also binds the antitumor antibiotics geldanamycin and radicicol, both Hsp90 inhibitors [13–17].

Hsp90 ATPase activity is also regulated by co-chaperones. For example, Hop^{Sti1} [18–20], $p50^{Cdc37}$ [21–23], and $p23^{Sba1}$ [24, 25] have an inhibitory effect on the ATPase cycle of Hsp90, while Aha1 [26–30] and Cpr6 [31, 32] have an activating effect.

Stuart K. Calderwood and Thomas L. Prince (eds.), *Chaperones: Methods and Protocols*, Methods in Molecular Biology, vol. 1709, https://doi.org/10.1007/978-1-4939-7477-1_16,

Hsp90 is posttranslationally modified (PTMs) by phosphorylation, acetylation, *S*-nitrosylation, ubiquitination, and SUMOylation [33–36]. These PTMs, in concert with co-chaperones, fine-tune Hsp90 chaperone function, which ultimately leads to chaperoning of kinase and non-kinase client proteins of Hsp90 [37, 38]. The most extensively studied Hsp90 PTM is phosphorylation [39–49]. Early work has shown that cells treated with the serine/threonine phosphatase inhibitor, okadaic acid, demonstrate Hsp90 hyperphosphorylation and decreased association of the chaperone with $pp60^{v\text{-}Src}$, suggesting a link between Hsp90 phosphorylation and chaperoning of its target proteins [50, 51]. Subsequent study has shown that c-Src directly phosphorylates Tyr300 of Hsp90 under basal conditions, reducing its ability to chaperone client proteins [48].

Recent work has shown that Hsp90 is also subject to SUMOylation, which is an addition of a small ubiquitin-like modifier to a lysine residue. This modification affects cellular localization or function of a protein rather than signal for its degradation like ubiquitination. SUMOylation of Lys191 in human Hsp90α (Lys178 in yeast) promotes its binding to the co-chaperone Aha1 and also increases cells' sensitivity to Hsp90 inhibitors [33].

Lack of PTM-specific antibodies has made it difficult to study PTMs of Hsp90. There is currently only one phospho-Hsp90α antibody (Cell Signaling) available for detecting the phosphorylation of Hsp90α-Thr5/7 [52]. Also *HSP90* gene knockouts are lethal in mammalian systems; therefore, any PTM Hsp90 mutant must be investigated in a background of highly expressed native mammalian Hsp90 proteins.

Simple baker's yeast, *Saccharomyces cerevisiae*, is a well-established and valuable tool for studying various aspects of conserved protein chaperone machinery. The yeast system has provided us with a powerful tool to study Hsp90 phosphorylation, since it readily allows plasmid exchange whereby any introduced Hsp90 gene—provided it is partially functional—can provide 100% of the Hsp90 of the cell (Fig. 1). Such genetic modifications are simply not achievable in cultured mammalian cells. This plasmid exchange (Fig. 1) was used to isolate temperature-sensitive (*ts*) Hsp90 mutants.

This chapter describes the isolation and identification of yeast Hsp90 phosphorylation using immunoblotting procedures. Using the yeast system it is possible to show that Hsp90 is constitutively phosphorylated on serine and threonine residues. However, Hsp90 threonine phosphorylation is lost upon either heat shock stress or treatment with the Hsp90 inhibitor GA (Fig. 2).

This chapter also describes the isolation and analysis of the human (h)Hsp90-N-domain from mammalian cells. This is achieved by introducing a PreScission protease cleavage site between the N-domain and adjacent charged linker region of

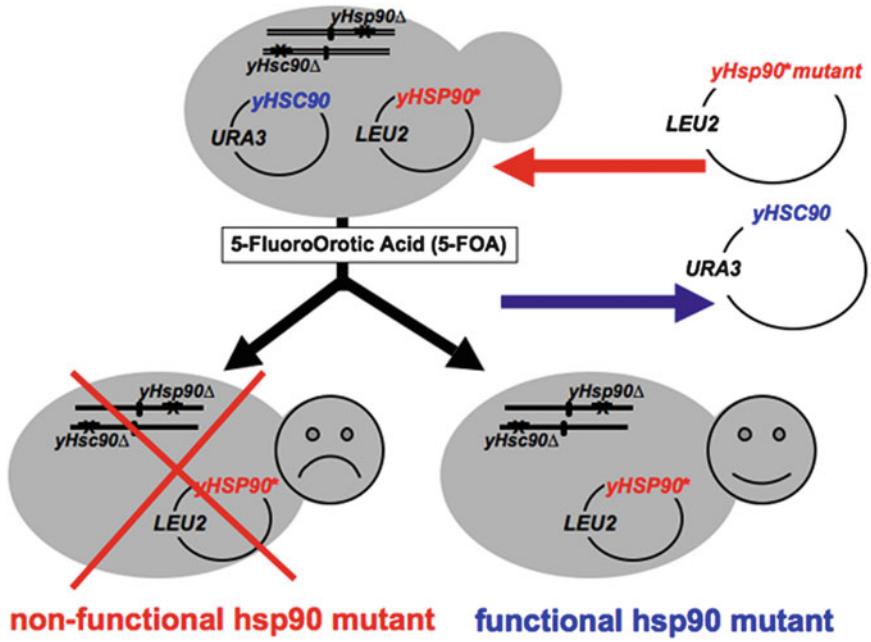

Fig. 1 With plasmid shuffling, a mutant *hsp90* gene can be made to provide all the Hsp90 of the yeast cell (yHsp90 = Hsp82 and yHsc90 = Hsc82). This involves introducing the mutation into yHsp90 on Leu2 plasmid and then introducing it into haploid yeast cells (yHsp90Δ, yHsp90Δ). Growth of these cells on 5-fluoroorotic acid (5-FOA) will "cure" the yeast cells of the wild-type yHsc90 therefore creating *hsp90* mutant

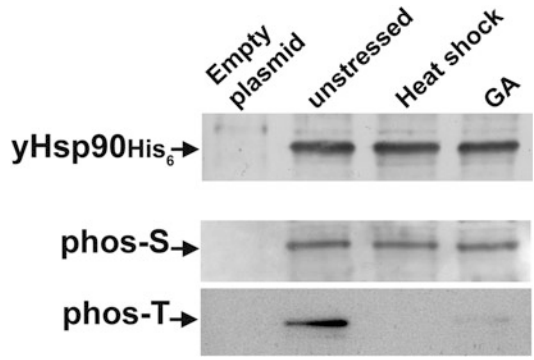

Fig. 2 Yeast Hsp90 phosphorylation on serine (phos-S) and threonine (p-T) residues. yHsp90-His_6 was purified from yeast cells that were heat shocked at 39 °C for 40 min or treated with 100 μM GA for 1 h. Wild-type cells containing the empty plasmid were used as negative control

hHsp90α, allowing isolation of the N-domain. Separation of the N-domain containing either wild-type or non-SUMOylated hHsp90α-K191R mutant from the full-length Hsp90 protein allows for better detection of SUMOylated Hsp90 by immunoblotting (Fig. 3).

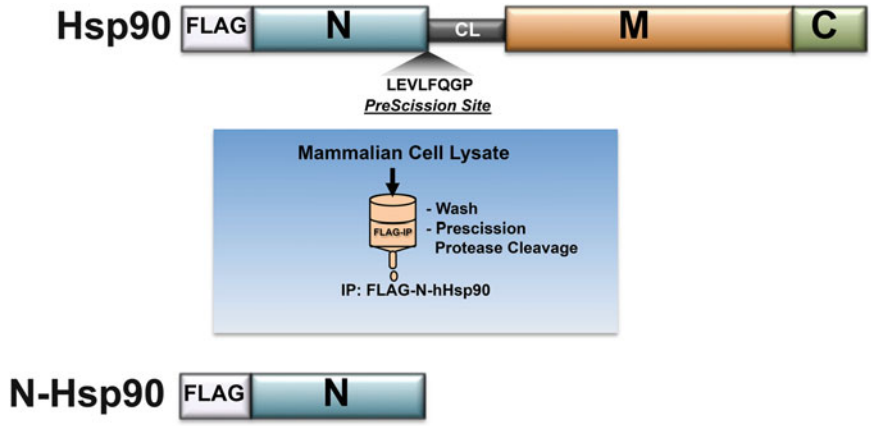

Fig. 3 Schematic representation of Hsp90-FLAG showing the amino (N-), charged linker (CL), middle (M-), and carboxy (C-) domains. Mammalian lysate with the Hsp90-FLAG will be attached to anti-FLAG agarose and Hsp90 N-domain can be isolated by PreScission protease digestion

2 Materials

1. YPD (2% (wt/vol) Bacto peptone, 1% (wt/vol) yeast extract, 2% (wt/vol) glucose, 20 mg/L adenine).
2. Yeast protein extraction buffer (yEB): 50 mM Tris–HCI, pH 6.8, 100 mM NaCl, 50 mM $MgCl_2$. One tablet of complete EDTA-free protease inhibitor cocktail (Roche) and one tablet of PhosphoSTOP (Roche) are added to 50 mL mEB.
3. 425–600 μm glass beads (acid washed) (Sigma).
4. Dulbecco's Modified Eagle's Medium—high glucose (DMEM; Sigma) supplemented with 10% fetal bovine serum (FBS).
5. Mammalian protein extraction buffer (mEB): 0.1% NP-40, 20 mM Tris–HCl, pH 7.4, 100 mM NaCl, 1 mM $MgCl_2$, 20 mM Na_2MoO_4. One tablet of complete EDTA-free protease inhibitor cocktail (Roche) and one tablet of PhosphoSTOP (Roche) are added to 50 mL mEB. (For the detection of SUMO, mEB should also contain 20 mM *N*-ethylmaleimide (NEM), *see* **Note 8**).
6. *Trans*IT-2020 transfection reagent (Mirus).
7. Bio-Rad Protein Assay Dye solution (Bio-Rad).
8. Ni-NTA agarose (Qiagen).
9. Imidazole (Sigma).
10. Anti-FLAG M2 Affinity Gel agarose (Sigma).
11. PreScission protease (GE Healthcare).

12. PreScission protease cleavage buffer: 50 mM Tris–HCl, 150 mM NaCl, 1 mM EDTA, 1 mM DTT (pH 7.0).
13. SDS-PAGE sample buffer (2×): 125 mM Tris–HCI pH 6.8, 20% glycerol, 2% SDS, 10% 2-mercaptoethanol, 0.01% bromophenol blue, stable at −20 °C. Aliquot and avoid freeze-thaw cycles.
14. Protran BA85, 0.45 μm Nitrocellulose membrane (Whatman).
15. Ponceau S solution (Sigma).
16. Tris-buffered saline (TBS): 150 mM NaCl, 25 mM Tris-Base. Adjust pH to 7.4 using HCI. Sterile filter and incubate at 4 °C.
17. Albumin, bovine serum (minimum purity 98%).
18. Dried skimmed milk.
19. Phospho-serine antibody (Sigma).
20. Phospho-threonine antibody (Sigma).
21. Phospho-tyrosine antibody (4G10; Millipore).
22. Acetylated lysine antibody (Cell Signaling).
23. Ubiquitin antibody (Santa Cruz).
24. SUMO-1 or SUMO-2/3 antibody (Cell Signaling).
25. 6×–His antibody (Invitrogen).
26. FLAG epitope antibody (ThermoScientific).
27. Anti-secondary mouse and/or rabbit antibody; ECL™ anti-mouse or anti-rabbit IgG, Horseradish Peroxidase-linked whole antibody (GE Healthcare).
28. ELC plus Western Blotting Detection System (GE Healthcare).
29. X-ray film, X-ray cassette, and X-ray film developing machine.

3 Methods

3.1 Extraction of Total Yeast Protein

1. Grow PP30 cells [8] expressing His_6 linked at the N domain of Hsp82 (yHsp90) on 150 mL YPD overnight a 28 °C.
2. Harvest and wash cells 2–3 times in ice-cold deionized water (dH_2O).
3. Transfer the cell pellet into a screw cap 2 mL tube.
4. Pellet the cells and remove the supernatant (*see* **Note 1**).
5. Add equal volume of cell pellets, ice-cold glass beads.
6. Add half the volume of pellet/glass beads, yEB.
7. Bead beat the cells using the mini-beadbeater (BioSpec Products, Inc.) for 30 s.
8. Incubate the cells on ice for 30 s.

9. Repeat **steps** (**7** and **8**), 10–12 times.
10. Centrifuge the tubes at (10,000 × *g*) for 10 min at 4 °C (*see* **Note 2**).
11. Transfer the supernatants into fresh 1.5 mL micro-centrifuge tubes.
12. Centrifuge the tubes at (10,000 × *g*) for 10 min at 4 °C (*see* **Note 2**).
13. Transfer the supernatants (soluble protein) into fresh 1.5 mL micro-centrifuge tubes.
14. Determine protein concentrations using Bio-Rad Protein Assay solution (Bio-Rad).
15. Transfer 40 μL of Ni-NTA Agarose slurry into a 1.5 mL micro-centrifuge tube (*see* **Note 3**).
16. Add 1.0 mL of yEB to the Ni-NTA Agarose and spin at 10,000 × *g* for 1 min at 4 °C.
17. Remove the supernatant and add 1.0 mL of yEB to the Ni-NTA Agarose (*see* **Note 4**).
18. Repeat **step** (**16**, **17**) four times.
19. Resuspend the Ni-NTA Agarose in 30 μM imidazole in yEB and incubate at 4 °C for 30 min (*see* **Note 5**).
20. Repeat **step 16–17** twice and remove the supernatant.
21. Add 1 mg of total protein to the Ni-NTA Agarose in a total volume of 600 μL.
22. Incubate the total proteins/Ni-NTA Agarose at 4 °C for 2 h (*see* **Note 6**).
23. Centrifuge the tubes at (1000 × *g*) for 1 min at 4 °C.
24. Gently remove the supernatant (*see* **Note 7**).
25. Add 1 mL of yEB to the Ni-NTA Agarose.
26. Repeat (23–25) five times.
27. Wash the Ni-NTA agarose with 30 μM imidazole in yEB.
28. Wash the Ni-NTA agarose with yEB once.
29. Centrifuge the micro-centrifuge tube at 15,000 × *g* for 1 min at 4 °C.
30. Remove as much supernatant as possible.
31. Add 40 μL of the protein sample buffer.
32. Boil the samples for 3–5 min.
33. Proceed to Subheading 3.3 for Western blotting and PTM detection.

3.2 Extraction of Total Protein from HEK293 Cells and Immunoprecipitation (IP) of hHsp90

1. Transfect HEK293 cells (~40% confluent in a 10 cm dish; growing in DMEM +10% FBS) with 2 μg hHSP90-FLAG using *Trans*IT-2020 reagent (Mirus) and incubate overnight at 37 °C, 5%CO_2.
2. Place the plates on ice and aspirate media. Wash 2× with cold PBS. Remove all remaining PBS from the plate.
3. Add 200 μL cold mEB to the plate. Scrape the cells and transfer to a 1.5 mL micro-centrifuge tube on ice (*see* **Note 8**).
4. Sonicate the lysate for 15 s. Incubate on ice for 15 s. Repeat ten times.
5. Centrifuge the tubes at (10,000 × *g*) for 8 min at 4 °C (*see* **Note 2**).
6. Transfer supernatants (soluble protein) into fresh 1.5 mL micro-centrifuge tubes.
7. Determine protein concentrations using Bio-Rad Protein Assay solution (Bio-Rad).
8. Transfer 50 μL anti-FLAG M2 Affinity Gel agarose (Sigma) into a 1.5 mL micro-centrifuge tube.
9. Add 500 μL mEB to the anti-FLAG agarose and spin at 10,000 × *g* for 1 min. Remove the supernatant (*see* **Note 4**).
10. Repeat **step 9** four times.
11. Add 1 mg of total protein to the anti-FLAG agarose in a total volume of 500 μL.
12. Incubate the total protein/anti-FLAG agarose at 4 °C for 2 h on a rotator (*see* **Note 6**).
13. Centrifuge the tubes at 1000 × *g* for 1 min.
14. Gently remove the supernatant (*see* **Note 7**).
15. Add 500 μL mEB to the anti-FLAG agarose.
16. Repeat (**steps 13–15**) five times.
17. Add 500 μL mEB to the anti-FLAG agarose.
18. Centrifuge at 15,000 × *g* for 1 min.
19. Remove as much supernatant as possible (*see* **Note 9** for optional PreScission protease cleavage, Fig. 3).
20. Add 40 μL of the protein sample buffer.
21. Boil the samples for 3–5 min.
22. Proceed to Subheading 3.3 for Western blotting and PTM detection.

3.3 Western Blotting and Detection of Hsp90 PTMs

1. Centrifuge the samples at 1000 × *g* and load the supernatant onto a 7.5% SDS-PAGE Tris-HCI gel (*see* **Note 10**).
2. Transfer the proteins from SDS-PAGE gel onto ProtranBA85, 0.45 μm nitrocellulose membrane (Whatman) (*see* **Note 11**).

3. Examine the quality and efficiency of the transfer by staining the membrane with Ponceau S solution (Sigma) for 2 min (*see* **Note 12**).
4. Wash the membrane with dH_2O.
5. Incubate the membrane in 5% milk in TBS-T for 15–20 min at room temperature.
6. Wash the membrane with 1× TBS-T for 5 min at room temperature.
7. Repeat (38) three times.
8. Incubate the membrane with primary antibody (*see* Table 1).
9. Wash the membrane three times with 1× TBS-T for 5 min at room temperature.
10. Incubate the membrane with 1:2000 dilution of secondary anti-mouse or anti-rabbit antibody in 5% milk-TBS-T for 1 h at room temperature.
11. Wash the membrane three times with 1× TBS-T for 5 min at room temperature.
12. Remove 1× TBS-T and then apply ECL plus (GE Healthcare) to nitrocellulose membrane for 2–3 min.
13. Drain nitrocellulose membrane of excess developing solution (do not let dry).

Table 1
Primary antibodies for Hsp90 post-translational modifications detection by Western blot

PTM	Antibody	Manufacturer	Dilution	Diluent	Time and temperature	Species
Phosphorylation	Phospho-serine (PSR-45)	Sigma (cat no. P5747)	1:500–1:1000	1 % BSA in TBS-T	o/n 4 °C	Mouse
	Phospho-threonine (PTR-8)	Sigma (cat no. P6623)	1:500–1:1000	1 % BSA in TBS-T	o/n 4 °C	Mouse
	Phospho-tyrosine (4G10)	Millipore (cat no. 05-321)				Mouse
Acetylation	Acetylated lysine	Cell Signaling (#9441)				Rabbit
Ubiquitination	Ubiquitin (P4D1)	Santa Cruz (sc-8017)	1:500–1:2000	5 % milk in TBS-T	o/n 4 °C	Mouse
SUMOylation	SUMO-1 (2A12)	Cell Signaling (#5718)				Mouse
	SUMO-2/3 (18H8)	Cell Signaling (#4971)				Rabbit

14. Wrap the blot in saran wrap.
15. Place the blot in the X-ray film cassette (*see* **Note 13**).
16. Expose the blots to X-ray films by placing X-ray film directly against the western blot at different lengths of time.

4 Notes

1. The cell pellet must be kept on ice.
2. At this stage, Bio-Rad Protein Assay solution (Bio-Rad) should be prepared.
3. Ni-NTA Agarose is precharged with Ni2+ ions and appears blue in color. It is provided as a 50% slurry in 30% ethanol.
4. Do not disturb the Ni-NTA or anti-FLAG Agarose pellet.
5. Imidazole at low concentrations is commonly used in the binding and wash buffer to minimize binding of unwanted host cell proteins.
6. Use Eppendorf Thermomixer R to gently mix total proteins/Ni-NTA Agarose solution.
7. Avoid disturbing the Ni-NTA or anti-FLAG Agarose.
8. For the detection of SUMO, mEB should always contain 20 mM *N*-ethylmaleimide (NEM).
9. PreScission protease cleavage: incubate hHsp90α-FLAG bound to anti-FLAG agarose with 2 units of PreScission Protease in 50 mM Tris–HCl, 150 mM NaCl, 1 mM EDTA, 1 mM DTT (pH 7.0) at 10 °C for 16 h.
10. Criteron precast gels from Bio-Rad are suitable for this purpose.
11. The high MW setting on the Bio-Rad Trans-Blot Turbo transfer system is suitable for this purpose.
12. Prepare 5% dry milk (LabScientific Inc.) in 1× TBS-T (0.1% Tween-20, Sigma) buffer before examining the membrane.
13. This procedure must be performed in the dark.

References

1. Prodromou C (2016) Mechanisms of Hsp90 regulation. Biochem J 473:2439–2452
2. Rohl A, Rohrberg J, Buchner J (2013) The chaperone Hsp90: changing partners for demanding clients. Trends Biochem Sci 38:253–262
3. Taipale M, Jarosz DF, Lindquist S (2010) HSP90 at the hub of protein homeostasis: emerging mechanistic insights. Nat Rev Mol Cell Biol 11:515–528
4. Karagoz GE, Rudiger SG (2015) Hsp90 interaction with clients. Trends Biochem Sci 40:117–125
5. Oroz J, Kim JH, Chang BJ, Zweckstetter M (2017) Mechanistic basis for the recognition of a misfolded protein by the molecular chaperone Hsp90. Nat Struct Mol Biol 24:407

6. Zierer BK, Rubbelke M, Tippel F et al (2016) Importance of cycle timing for the function of the molecular chaperone Hsp90. Nat Struct Mol Biol 23:1020–1028
7. Verba KA, Wang RY, Arakawa A et al (2016) Atomic structure of Hsp90-Cdc37-Cdk4 reveals that Hsp90 traps and stabilizes an unfolded kinase. Science 352:1542–1547
8. Panaretou B, Prodromou C, Roe SM et al (1998) ATP binding and hydrolysis are essential to the function of the Hsp90 molecular chaperone in vivo. EMBO J 17:4829–4836
9. Obermann WM, Sondermann H, Russo AA, Pavletich NP, Hartl FU (1998) In vivo function of Hsp90 is dependent on ATP binding and ATP hydrolysis. J Cell Biol 143:901–910
10. Grenert JP, Johnson BD, Toft DO (1999) The importance of ATP binding and hydrolysis by hsp90 in formation and function of protein heterocomplexes. J Biol Chem 274:17525–17533
11. Prodromou C, Roe SM, O'Brien R, Ladbury JE, Piper PW, Pearl LH (1997) Identification and structural characterization of the ATP/ADP-binding site in the Hsp90 molecular chaperone. Cell 90:65–75
12. Grenert JP, Sullivan WP, Fadden P et al (1997) The amino-terminal domain of heat shock protein 90 (hsp90) that binds geldanamycin is an ATP/ADP switch domain that regulates hsp90 conformation. J Biol Chem 272:23843–23850
13. Stebbins CE, Russo AA, Schneider C, Rosen N, Hartl FU, Pavletich NP (1997) Crystal structure of an Hsp90-geldanamycin complex: targeting of a protein chaperone by an antitumor agent. Cell 89:239–250
14. Roe SM, Prodromou C, O'Brien R, Ladbury JE, Piper PW, Pearl LH (1999) Structural basis for inhibition of the Hsp90 molecular chaperone by the antitumor antibiotics radicicol and geldanamycin. J Med Chem 42:260–266
15. Workman P, Burrows F, Neckers L, Rosen N (2007) Drugging the cancer chaperone HSP90: combinatorial therapeutic exploitation of oncogene addiction and tumor stress. Ann N Y Acad Sci 1113:202–216
16. Neckers L, Trepel JB (2014) Stressing the development of small molecules targeting HSP90. Clin Cancer Res 20:275–277
17. Neckers L, Workman P (2012) Hsp90 molecular chaperone inhibitors: are we there yet? Clin Cancer Res 18:64–76
18. Schmid AB, Lagleder S, Grawert MA et al (2012) The architecture of functional modules in the Hsp90 co-chaperone Sti1/hop. EMBO J 31:1506–1517
19. Richter K, Muschler P, Hainzl O, Reinstein J, Buchner J (2003) Sti1 is a non-competitive inhibitor of the Hsp90 ATPase. Binding prevents the N-terminal dimerization reaction during the atpase cycle. J Biol Chem 278:10328–10333
20. Song Y, Masison DC (2005) Independent regulation of Hsp70 and Hsp90 chaperones by Hsp70/Hsp90-organizing protein Sti1 (Hop1). J Biol Chem 280:34178–34185
21. Lee P, Shabbir A, Cardozo C, Caplan AJ (2004) Sti1 and Cdc37 can stabilize Hsp90 in chaperone complexes with a protein kinase. Mol Biol Cell 15:1785–1792
22. MacLean M, Picard D (2003) Cdc37 goes beyond Hsp90 and kinases. Cell Stress Chaperones 8:114–119
23. Vaughan CK, Mollapour M, Smith JR et al (2008) Hsp90-dependent activation of protein kinases is regulated by chaperone-targeted dephosphorylation of Cdc37. Mol Cell 31:886–895
24. McLaughlin SH, Sobott F, Yao ZP et al (2006) The co-chaperone p23 arrests the Hsp90 ATPase cycle to trap client proteins. J Mol Biol 356:746–758
25. Picard D (2006) Intracellular dynamics of the Hsp90 co-chaperone p23 is dictated by Hsp90. Exp Cell Res 312:198–204
26. Lotz GP, Lin H, Harst A, Obermann WM (2003) Aha1 binds to the middle domain of Hsp90, contributes to client protein activation, and stimulates the ATPase activity of the molecular chaperone. J Biol Chem 278:17228–17235
27. Meyer P, Prodromou C, Liao C et al (2004) Structural basis for recruitment of the ATPase activator Aha1 to the Hsp90 chaperone machinery. EMBO J 23:511–519
28. Panaretou B, Siligardi G, Meyer P et al (2002) Activation of the ATPase activity of hsp90 by the stress-regulated cochaperone aha1. Mol Cell 10:1307–1318
29. Wolmarans A, Lee B, Spyracopoulos L, LaPointe P (2016) The mechanism of Hsp90 ATPase stimulation by Aha1. Sci Rep 6:33179
30. Retzlaff M, Hagn F, Mitschke L et al (2010) Asymmetric activation of the hsp90 dimer by its cochaperone aha1. Mol Cell 37:344–354
31. Johnson JL, Halas A, Flom G (2007) Nucleotide-dependent interaction of Saccharomyces cerevisiae Hsp90 with the cochaperone proteins Sti1, Cpr6, and Sba1. Mol Cell Biol 27:768–776
32. Mayr C, Richter K, Lilie H, Buchner J (2000) Cpr6 and Cpr7, two closely related Hsp90-

associated immunophilins from Saccharomyces cerevisiae, differ in their functional properties. J Biol Chem 275:34140–34146

33. Mollapour M, Bourboulia D, Beebe K et al (2014) Asymmetric Hsp90 N domain SUMOylation recruits Aha1 and ATP-competitive inhibitors. Mol Cell 53:317–329
34. Woodford MR, Dunn D, Miller JB, Jamal S, Neckers L, Mollapour M (2016) Impact of posttranslational modifications on the anticancer activity of Hsp90 inhibitors. Adv Cancer Res 129:31–50
35. Mollapour M, Neckers L (2012) Post-translational modifications of Hsp90 and their contributions to chaperone regulation. Biochim Biophys Acta 1823:648–655
36. Preuss KD, Pfreundschuh M, Weigert M, Fadle N, Regitz E, Kubuschok B (2015) Sumoylated HSP90 is a dominantly inherited plasma cell dyscrasias risk factor. J Clin Invest 125:316–323
37. Soroka J, Wandinger SK, Mausbacher N et al (2012) Conformational switching of the molecular chaperone Hsp90 via regulated phosphorylation. Mol Cell 45:517–528
38. Xu W, Mollapour M, Prodromou C et al (2012) Dynamic tyrosine phosphorylation modulates cycling of the HSP90-P50 (CDC37)-AHA1 chaperone machine. Mol Cell 47:434–443
39. Nguyen MT, Kniess RA, Daturpalli S et al (2017) Isoform-specific phosphorylation in human Hsp90beta affects interaction with clients and the Cochaperone Cdc37. J Mol Biol 429:732–752
40. Woodford MR, Truman AW, Dunn DM et al (2016) Mps1 mediated phosphorylation of Hsp90 confers renal cell carcinoma sensitivity and selectivity to Hsp90 inhibitors. Cell Rep 14:872–884
41. Muller P, Ruckova E, Halada P et al (2012) C-terminal phosphorylation of Hsp70 and Hsp90 regulates alternate binding to co-chaperones CHIP and HOP to determine cellular protein folding/degradation balances. Oncogene 32:3101
42. Scroggins BT, Neckers L (2007) Post-translational modification of heat shock protein 90: impact on chaperone function. Expert Opin Drug Discov 2:1403–1414
43. Garnier C, Lafitte D, Jorgensen TJ, Jensen ON, Briand C, Peyrot V (2001) Phosphorylation and oligomerization states of native pig brain HSP90 studied by mass spectrometry. Eur J Biochem 268:2402–2407
44. Zhao YG, Gilmore R, Leone G, Coffey MC, Weber B, Lee PW (2001) Hsp90 phosphorylation is linked to its chaperoning function. Assembly of the reovirus cell attachment protein. J Biol Chem 276:32822–32827
45. Fontana J, Fulton D, Chen Y et al (2002) Domain mapping studies reveal that the M domain of hsp90 serves as a molecular scaffold to regulate Akt-dependent phosphorylation of endothelial nitric oxide synthase and NO release. Circ Res 90:866–873
46. Adinolfi E, Kim M, Young MT, Di Virgilio F, Surprenant A (2003) Tyrosine phosphorylation of HSP90 within the P2X7 receptor complex negatively regulates P2X7 receptors. J Biol Chem 278:37344–37351
47. Wang C, Chen J (2003) Phosphorylation and hsp90 binding mediate heat shock stabilization of p53. J Biol Chem 278:2066–2071
48. Duval M, Le Boeuf F, Huot J, Gratton JP (2007) Src-mediated phosphorylation of Hsp90 in response to vascular endothelial growth factor (VEGF) is required for VEGF receptor-2 signaling to endothelial NO synthase. Mol Biol Cell 18:4659–4668
49. Miyata Y, Yahara I (1992) The 90-kDa heat shock protein, HSP90, binds and protects casein kinase II from self-aggregation and enhances its kinase activity. J Biol Chem 267:7042–7047
50. Mimnaugh EG, Worland PJ, Whitesell L, Neckers LM (1995) Possible role for serine/threonine phosphorylation in the regulation of the heteroprotein complex between the hsp90 stress protein and the pp60v-src tyrosine kinase. J Biol Chem 270:28654–28659
51. Ogiso H, Kagi N, Matsumoto E et al (2004) Phosphorylation analysis of 90 kDa heat shock protein within the cytosolic arylhydrocarbon receptor complex. Biochemistry 43:15510–15519
52. Solier S, Kohn KW, Scroggins B et al (2012) Feature article: heat shock protein 90alpha (HSP90alpha), a substrate and chaperone of DNA-PK necessary for the apoptotic response. Proc Natl Acad Sci U S A 109:12866–12872

Chapter 17

Chromatin Immunoprecipitation (ChIP) of Heat Shock Protein 90 (Hsp90)

Aneliya Yoveva and Ritwick Sawarkar

Abstract

Chromatin immunoprecipitation followed by sequencing (ChIP-seq) is a widely used technique for genome-wide mapping of protein-DNA interactions and epigenetic marks in vivo. Recent studies have suggested an important role of heat shock protein 90 (Hsp90) at chromatin. This molecular chaperone assists other proteins to acquire their mature and functional conformation and helps in the assembly of many complexes. In this chapter, we provide specific details on how to perform Hsp90 ChIP-seq from Drosophila Schneider (S2) cells. Briefly, the cells are simultaneously lyzed and reversibly cross-linked to stabilize protein–DNA interactions. Chromatin is prepared from isolated nuclei and sheared by sonication. Hsp90-bound loci are immunoprecipitated and the corresponding DNA fragments are purified and sequenced. The described approach revealed that Hsp90 binds close to the transcriptional start site of around one-third of all Drosophila coding genes and characterized the role of the chaperone at chromatin.

Key words ChIP-Seq, Drosophila Schneider (S2) Cells, Hsp90

1 Introduction

Heat shock protein 90 (Hsp90) is a specialized molecular chaperone that facilitates complex formation, stability, and activity of many protein kinases and transcription factors. Predominantly localized and characterized in cellular cytosol Hsp90 has a well-established role in proteostasis, cell signaling, and carcinogenesis [1]. It has emerged as a promising target in cancer therapeutics with thirteen Hsp90 inhibitors undergoing clinical evaluation [2].

Recent reports suggest an important function of Hsp90 in nuclear events [3]. Nuclear Hsp90 has been found to regulate the function of both transcription factors and the general transcription machinery, thus contributing to regulation of gene expression [4]. One of the first examples of Hsp90 regulating transcription factor function was shown in studies of steroid hormone receptors [5, 6] where it modulates their assembly, disassembly, and activity [7]. In addition to hormone receptors, Hsp90 physically interacts

Stuart K. Calderwood and Thomas L. Prince (eds.), *Chaperones: Methods and Protocols*, Methods in Molecular Biology, vol. 1709, https://doi.org/10.1007/978-1-4939-7477-1_17,

and affects the activity of a variety of TFs, such as p53, c-myc, STAT3, NF-kB, HSF1 [4]. Another intriguing role for Hsp90 in the nucleus appears to be its interaction with the general transcription machinery. It not only mediates Pol II assembly in the cytoplasm and nuclear import of the fully assembled holoenzyme [8] but regulates Pol II pausing via stabilization of the negative elongation factor complex [9]. In addition, the chaperone is known to affect the packaging of DNA into chromatin and thus contributes to epigenetic regulation of gene expression [10]. It induces chromatin accessibility changes through interactions with chromatin-modifying/remodeling complexes that could either activate (SMYD3, trithorax/MLL, RSC complex) [11–13] or repress (EZH2) [14] gene expression.

Thus several studies link Hsp90 to transcription regulation at different levels. A comprehensive characterization of the nuclear clients of Hsp90 and the mechanism by which the chaperone controls gene expression is needed. Such efforts would enhance our understanding of the nuclear functions of Hsp90, traditionally considered to be a cytosolic chaperone. An important question remains largely unclear: does Hsp90 modulate the nuclear translocation and consequent activity of soluble, non-DNA-bound forms of clients or does Hsp90 directly interact with chromatin-bound forms? Further studies employing genome-wide occupancy analysis will be required to reveal Hsp90-bound chromatin loci to clearly understand its role at chromatin.

Identification of genome-wide occupancy of transcription factors, components of the basal transcription machinery, and modified histones has been critical in understanding the mechanisms of transcriptional regulation. Several widely used methods contribute to the study of how proteins interact with chromatin, and some of the popular techniques are detailed below:

- Chromatin Immunoprecipitation [15]—it has become an indispensable tool for studying gene regulation and epigenetic mechanisms. The first step involves reversible cross-linking of cells in their growth media in order to stabilize protein–DNA interactions. Following chromatin preparation and sonication, DNA fragments bound to protein of interest are enriched using an antigen-specific antibody. It allows the genome-wide localization of not only transcription (co)/factors but specific post-translational modifications of proteins such as histones for example. The major issues here originate from the cross-linking and immunoprecipitation steps. Cross-linking is very likely to mask some of the antigen epitopes and thus prevent antibody binding. The choice of a specific ChIP-grade antibody of a very good quality is critical.

  The following three approaches offer an important advantage over ChIP—they allow mapping the binding site of proteins for

which a good ChIP-seq-grade antibody is not available, as is the case with many chaperones. However, all of them have a significant disadvantage—they do not allow specific mapping of post-translationally modified proteins.

- Chemical affinity capture followed by sequencing (Chem-seq) [16]—this recent technique relies on small chemical compounds binding with a high affinity to the protein of interest to enrich it from cross-linked or uncross-linked chromatin. The small size of chemical components makes antigen recognition easier and is not that much hampered by the cross-linking of protein-DNA complexes. It is the first method that allows researchers to directly determine the location of cellular factors targeted by small molecules throughout the genome. The successful outcome of the protocol however relies on the existence of a chemical that binds to an antigen with a high specificity and efficiency. Therefore, it has been applied to a limited number of proteins. The increasing number of highly specific and potent Hsp90 inhibitors could soon allow the genome-wide Hsp90 localization through Chem-seq [17].
- Biotin-mediated ChIP (BioChIP) [18]—it involves endogenous expression of critical chromatin/DNA binding factors tagged with biotin. This allows their affinity capture by streptavidin. Biotin-streptavidin interaction is highly specific and one of the strongest non-covalent interactions in nature. These features significantly reduce the nonspecific binding background and favor a highly efficient target pull-down. A major disadvantage here is the need of recombinant biotin-tagged protein expression which is more time-consuming, elaborate and could introduce artifacts.
- DNA adenine methyltransferase identification (DamID) [19]—this alternative method involves expression of the DNA-binding protein of interest as a fusion protein with DNA methyltransferase. This enzyme mediates in vivo DNA adenosine methylation in the region of the binding site. By using methylation-sensitive restriction enzymes to enrich methylated DNA, this technique allows an identification of protein-bound DNA independent of immunoprecipitation.

In the following protocol, we focus on ChIP and provide specific details on how to identify Hsp90-bound chromatin loci in Drosophila Schneider (S2) cells. It could also be applied to other cell types and (co)chaperones such as p23 [13].

2 Materials

2.1 Reagents

Prepare all the solutions with molecular biology grade water (Milli-Q™) and supplement them with protease inhibitors.

2.2 Cells Preparation and Cross-Linking

1. Protease inhibitors at a final concentration of: 3 μg/mL aprotinin, 10 μg/mL leupeptin, 1 μg/mL pepstatin, 0.1 mM PMSF.
2. Methanol-free formaldehyde 16% (Thermo Scientific, Prod. Nr. 28906).
3. 10× cell lysis buffer: 50 mM HEPES, 50 mM NaCl, 10 mM EDTA, 5 mM EGTA.
4. Glycine 1 M.
5. Wash buffer: 50 mM Tris, pH 8.0, 15 mM NaCl, 0.5 mM EGTA, 60 mM KCl.

2.3 Chromatin Extraction and Sonication

1. Sonication buffer: 10 mM Tris, pH 8.0, 1 mM EDTA, 0.5 mM EGTA.

2.4 Chromatin Quality Check

1. RNase A 10 mg/mL (DNase and protease free; AppliChem, Prod. Nr. A3832).
2. Proteinase K 20 mg/mL (Sigma Aldrich, Prod. Nr. P2308).
3. TE buffer: 1 mM EDTA pH 8.0, 10 mM Tris–HCl pH 8.0.
4. Phenol–chloroform–isoamyl alcohol 25:24:1 (ROTH, Prod. Nr. A156.3).
5. Glycogen 5 mg/mL (Roche, Prod. Nr. 13741729).
6. 100% Ethanol.
7. EB buffer: 10 mM Tris–Cl, pH 8.5.
8. 1× TAE buffer: 40 mM Tris–acetate, 1 mM EDTA, pH 8.0.
9. 2% agarose gel in TAE buffer.
10. GelRed Nucleic Acid Gel Stain, 10,000× in water.
11. 100 bp DNA ladder.
12. DNA loading dye.
13. High Sensitivity DNA Kit (Agilent).

2.5 Immunoprecipitation

1. ChIP dilution buffer: 10 mM Tris, pH 8.0, 1 mM EDTA, 1% Triton X-100, 0.1% sodium deoxycholate, 0.1% SDS, 140 mM NaCl.
2. Specific antibody against a protein of interest (anti-Hsp90 polyclonal serum used in this case).

3. Protein A-Dynabeads (Novex by Life technologies, Prod. Nr. 10002D).
4. LiCl buffer: 10 mM Tris, 250 mM LiCl, 1 mM EDTA, 0.5% NP-40, 0.5% sodium deoxycholate.
5. Elution buffer: 1% SDS, 100 mM NaHCO3.

2.6 Equipment

1. End-over-end rotator.
2. Refrigerated tabletop centrifuge.
3. Protein Low Binding tubes.
4. DNA Low Binding tubes.
5. BioRuptor (Diagenode).
6. Magnetic rack.
7. Thermomixer.
8. Laboratory heating oven.
9. Vortex mixer.
10. Qubit fluorometer.
11. Agarose gel electrophoresis equipment.
12. UV-transilluminator.
13. 2100 Bioanalyzer.

3 Methods

3.1 Cells Preparation and Cross-Linking

1. Use 50×10^6 exponentially growing cells per reaction in 10 mL of growth media. Add 10× cell lysis buffer and Triton X-100 directly in the media to reach 1× and 0.5% final concentration, respectively.
2. Immediately add formaldehyde to a final concentration of 1% to facilitate cells cross-linking (*see* **Notes 1** and **2**).
3. Incubate for 15 min with end-over-end rotation at room temperature (*see* **Note 3**).
4. Stop the cross-linking reaction by adding glycine to a final concentration of 100 mM. Incubate for 5 min with end-over-end rotation at room temperature.
5. Spin down the isolated and cross-linked nuclei at $750 \times g$ for 5 min at 4 °C and discard the cross-linking solution (*see* **Note 4**).
6. Wash twice with ice cold wash buffer (*see* **Note 5**).

3.2 Chromatin Extraction and Sonication

All the following procedures should be performed at 4 °C with ice-cold buffers containing protease inhibitors.

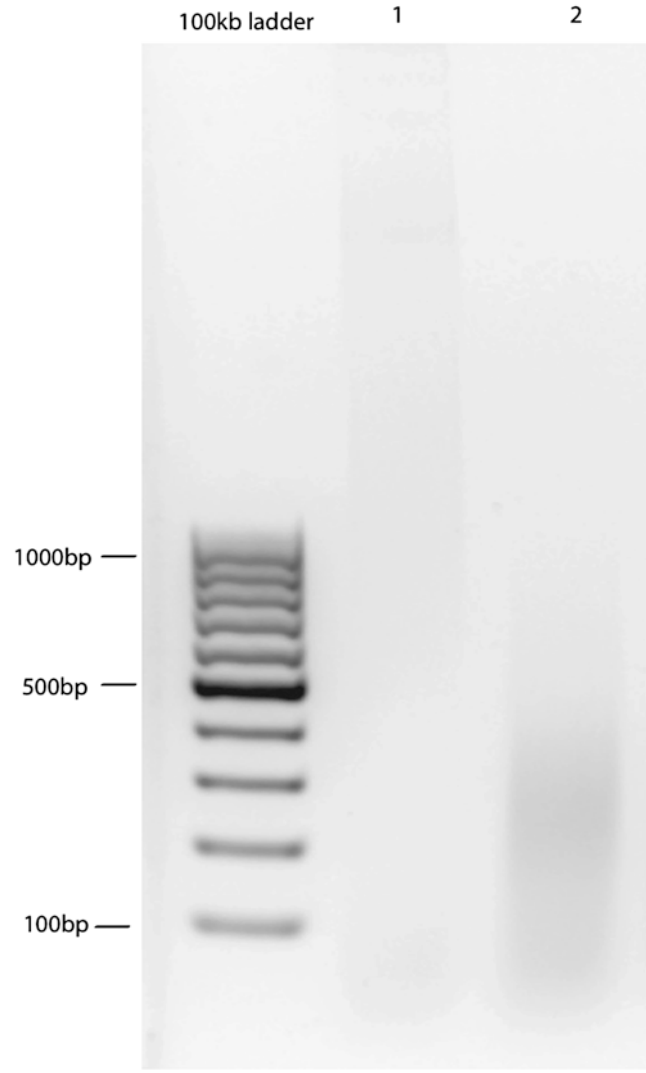

Fig. 1 Not sonicated (1) and sonicated (2) chromatin from Drosophila S2 cells

1. Resuspend the nuclei pellet thoroughly in 200 μL of sonication buffer and transfer to a protein low binding tube (*see* **Notes 6** and **7**).
2. Sonicate with Bioruptor (Diagenode) in cold water with the following settings: 30 cycles with intervals of 30 s ON/OFF at maximum power. The optimal size range of the acquired DNA fragments for ChIP-seq analysis should be between 200 and 600 base pairs appearing as a smear (Fig. 1) (*see* **Note 8**).
3. Spin down the sonicated material at 16,000 × *g* for 10 min (*see* **Notes 9** and **10**).

4. Transfer the supernatant to a fresh protein low binding tube (*see* **Note 11**).

3.3 Chromatin Quality Check

For optimal results confirm sonication efficiency and chromatin yield prior to IP. The following steps could be skipped once the protocol is optimized.

1. Take a 20 μL aliquot (1%) of the sheared chromatin. Add 1 μL of RNase A and 1 μL of proteinase K and incubate for 30 min at 37 °C.
2. Reverse cross-link overnight in a 65 °C oven (*see* **Note 12).**
3. Bring the volume of both IP and Input samples to 400 μL with TE buffer.
4. Add an equal volume of Phenol–chloroform–isoamyl alcohol (25:24:1) mixture and vortex (*see* **Note 13)**.
5. Incubate at room temperature for 1 min.
6. Spin down at 20,000 × *g* for 10 min at 4 °C.
7. Transfer the nucleic-acid-containing aqueous upper phase to a DNA low binding tube. Add sodium chloride and glycogen to 200 mM and 50 μg/mL final concentration, respectively (*see* **Note 14).**
8. Incubate the mixture for 2 h at −20 °C for 1 h at −80 °C (*see* **Note 15**).
9. Spin down at 20,000 × *g* for 10 min at 4 °C. Discard the supernatant.
10. Wash with 1 mL of 80% EtOH (precooled at −20 °C).
11. Spin down at 20,000 × *g* for 10 min at 4 °C. Discard the supernatant.
12. Air-dry the pellet around 5 min.
13. Resuspend in 20 μL of EB buffer.
14. Measure DNA amount by Qubit following the manufacturer's protocol—expected yield around 1 μg of DNA per 1×10^6 cells).
15. Assess chromatin shearing efficiency either on a 2% agarose gel or on Bioanalyzer 2100 using High Sensitivity DNA chip according to the manufacturer's protocol. The optimal size range of DNA for ChIP-seq analysis should be between 200 and 600 base pairs (Fig. 1).

3.4 Immuno-precipitation

1. Use 20–50 μg of chromatin for ChIP-seq and 5–10 μg for qPCR per reaction—one for the specific antibody (IP) and one for an appropriate negative control (mock-IP; pre-immunization serum or IgA/IgG antibody could be used) (*see* **Note 16)**.
2. Dilute it 1:10 in ChIP dilution buffer.

3. Take a 5% aliquot as input DNA. Freeze at −20 °C until needed.
4. Add 5 μg of Hsp90 or control antibody to the IP and mock-IP reactions, respectively (*see* **Note 17**).
5. Incubate overnight at 4 °C with end-over-end rotation.
6. Prepare 25 μL of Protein A-Dynabeads per reaction. Wash in ChIP dilution buffer (*see* **Note 18**).
7. Capture the antigen-antibody complexes by adding 25 μL of Protein A-Dynabeads per reaction and incubate for 4 h.
8. Separate the beads on a magnetic rack and discard the supernatant.
9. Transfer the beads in ChIP dilution buffer to a new tube.
10. Wash the beads five times per 5 min with 1 mL of ChIP dilution buffer.
11. Wash once per 5 min with 1 mL of LiCl buffer.
12. Wash twice per 5 min with 1 mL of TE buffer.
13. Elute by adding 50 μL of Elution buffer and incubating in a thermomixer at 65 °C for 15 min under vigorous shaking (1400 rpm) (*see* **Note 19**).

At this point, thaw the input DNA and process along with the IP samples.

14. Reverse cross-link overnight at 65 °C in a laboratory oven (*see* **Note 20**).
15. Add 200 μL of TE buffer and 8 μL of RNaseA. Incubate for 2 h at 37 °C in a thermomixer.
16. Add 4 μL of Proteinase K, mix and incubate overnight at 55 °C in a laboratory oven.
17. Purify the DNA using Phenol–chloroform–isoamyl alcohol (25:24:1) as previously described (Subheading 3.3, **steps 4–12**). DNA purification kits are not recommended due to loss of material and size selection.
18. Resuspend the DNA pellet in 50 μL of EB buffer and transfer to a fresh tube—expected yield around 15–30 ng per 50×10^6 cells.

IP DNA can then be sent for next-generation sequencing [20] (*see* **Note 21**).

4 Notes

1. Always use methanol-free formaldehyde for optimal and reproducible results (methanol reduces the fixing power of

formaldehyde). Ampoule-sealed solutions are highly recommended as they are well protected from both air oxidation and light. Formaldehyde is highly toxic and has to be handled carefully under a fume hood.

2. Simultaneous cell lysis and cross-linking achieved at this step generates isolated cross-linked nuclei—a much purer substrate for subsequent steps than whole cells. That initial cellular fractionation improves significantly the chromatin shearing process. A recently published protocol [21] offers an alternative—cross-linking of cells in growing media followed by ultrasound-based nuclear extraction. Nuclei isolation prior to chromatin preparation offers an additional advantage for proteins that are highly abundant in the cytosol (like Hsp90). By eliminating the cytosolic pool the efficiency of chromatin-bound Hsp90 pull-down is increased.
3. Cross- linking is a time- and temperature-dependent process. It should not exceed 15 min performed at room temperature. Extended cross-linking could lead to poor results due to reduced sonication efficiency, reduced antibody accessibility to antigen and epitope masking.
4. Discard formaldehyde-containing solution according to the institutional safety rules.
5. **Pause point**: cross-linked nuclei/cells could be snap frozen in liquid nitrogen and stored at −80 °C for at least 1 month.
6. Avoid foaming since it dramatically reduces cross-linking efficiency. If foaming occurs, centrifuge for 3 min at 20,000 × *g*. Resuspend the material gently leaving no foam bubbles.
7. Use non-siliconized protein low binding tubes to prevent proteins sticking to tube walls and thus protein loss.
8. One could use alternative sonication devices—Branson tip sonicator or Covaris ultrasonicator, for example. Sonication conditions however must be carefully optimized depending upon the specific sonicator to ensure the optimal quality of sheared chromatin. The optimal size range of the acquired DNA fragments for ChIP-seq analysis should be between 200 and 600 base pairs (Fig. 1). DNA fragments out of the range may not be sequenced later on.
9. Proper sonication will generate a clear solution. Turbidity could indicate insufficient sonication.
10. A minimal pellet should be visible at this point. If a larger pellet appears, the sonication did not work properly.
11. **Pause point**: sheared chromatin could be stored at 4 °C for up to 1 week.

12. Use a laboratory oven for longer thermal incubations to prevent sample condensation on the cap of the tube and ensure uniform heating.
13. Phenol–chloroform is highly toxic and should be handled under the fume hood. Avoid inhalation and skin contact. Wear protective clothing and gloves.
14. Glycogen increases the quantitative recovery of DNA.
15. **Pause point**: incubation at −20 °C or −80 °C could also be done overnight.
16. An isotype matched control immunoglobulin (a negative control) is necessary to determine the nonspecific DNA enrichment (background).
17. The choice of antibody is crucial. To test whether an antibody is ChIP-grade, follow the ChIP protocol until the IP washes are done. At this point boil the beads in 1× SDS loading buffer for 30 min (a longer boiling time is necessary to reverse cross-link) and perform a western blot.
    The amount of antibody per IP and the incubation time depend mainly on the affinity properties of the antibody and the abundance of the protein of interest. Test each new antibody to determine optimal conditions.
18. Protein A/G agarose beads could also be used but magnetic beads give a lower background, do not require blocking and are easier to handle.
19. Always use fresh Elution buffer. **Pause point**: the eluted material could be frozen at −20 °C and stored for up to a week.
20. Do not reverse cross-link for more than 18 h.
21. **Pause point**: the DNA could be stored frozen at −80 °C and stored for at least 1 month.

References

1. Verma S, Goyal S, Jamal S, Singh A, Grover A (2016) Hsp90: friends, clients and natural foes. Biochimie 127:227–240
2. Katerina S, Evangelia P (2014) HSP90 inhibitors: current development and potential in cancer therapy. Recent Pat Anticancer Drug Discov 9(1):1–20
3. Calderwood SK, Neckers L (2016) Chapter four – Hsp90 in cancer: transcriptional roles in the nucleus. In: Jennifer I, Luke W (eds) Advances in cancer research, vol 129. Academic Press, San Diego, Calif, pp 89–106
4. Sawarkar R, Paro R (2013) Hsp90@chromatin. Nucleus: an emerging hub of a networker. Trends Cell Biol 23(4):193–201
5. Pratt WB, Toft DO (1997) Steroid receptor interactions with heat shock protein and Immunophilin chaperones. Endocr Rev 18 (3):306–360
6. Bennesch MA, Segala G, Wider D, Picard D (2016) LSD1 engages a corepressor complex for the activation of the estrogen receptor α by estrogen and cAMP. Nucleic Acids Res 44 (18):8655–8670
7. Freeman BC, Yamamoto KR (2002) Disassembly of transcriptional regulatory complexes by molecular chaperones. Science 296 (5576):2232–2235
8. Boulon S et al (2010) HSP90 and its R2TP/Prefoldin-like Cochaperone are involved in the

cytoplasmic assembly of RNA polymerase II. Mol Cell 39(6):912–924

9. Sawarkar R, Sievers C, Paro R (2012) Hsp90 globally targets paused RNA polymerase to regulate gene expression in response to environmental stimuli. Cell 149(4):807–818
10. Isaacs JS (2016) Chapter five – Hsp90 as a "chaperone" of the epigenome: insights and opportunities for cancer therapy. In: Jennifer I, Luke W (eds) Advances in cancer research, vol 129. Academic Press, San Diego, pp 107–140
11. Brown MA et al (2015) C-terminal domain of SMYD3 serves as a unique HSP90-regulated motif in oncogenesis. Oncotarget 6 (6):4005–4019
12. Tariq M, Nussbaumer U, Chen Y, Beisel C, Paro R (2009) Trithorax requires Hsp90 for maintenance of active chromatin at sites of gene expression. Proc Natl Acad Sci U S A 106(4):1157–1162
13. Echtenkamp Frank J et al (2016) Hsp90 and p23 molecular chaperones control chromatin architecture by maintaining the functional pool of the RSC chromatin remodeler. Mol Cell 64:888–899
14. Fiskus W et al (2009) Panobinostat treatment depletes EZH2 and DNMT1 levels and enhances decitabine mediated de-repression of JunB and loss of survival of human acute leukemia cells. Cancer Biol Ther 8(10):939–950
15. Park PJ (2009) ChIP-seq: advantages and challenges of a maturing technology. Nat Rev Genet 10(10):669–680
16. Anders L et al (2014) Genome-wide determination of drug localization. Nat Biotechnol 32 (1):92–96
17. Moulick K et al (2011) Affinity-based proteomics reveal cancer-specific networks coordinated by Hsp90. Nat Chem Biol 7 (11):818–826
18. Baubec T, Ivánek R, Lienert F, Schübeler D (2013) Methylation-dependent and -independent genomic targeting principles of the MBD protein family. Cell 153(2):480–492
19. Bv S, Henikoff S (2000) Identification of in vivo DNA targets of chromatin proteins using tethered dam methyltransferase. Nat Biotechnol 18(4):424–428
20. Bardet AF, He Q, Zeitlinger J, Stark A (2012) A computational pipeline for comparative ChIP-seq analyses. Nat Protoc 7(1):45–61
21. Arrigoni L et al (2016) Standardizing chromatin research: a simple and universal method for ChIP-seq. Nucleic Acids Res 44(7):e67–e67

Chapter 18

A Workflow Guide to RNA-seq Analysis of Chaperone Function and Beyond

Benjamin J. Lang, Kristina M. Holton, Jianlin Gong, and Stuart K. Calderwood

Abstract

RNA sequencing (RNA-seq) is a powerful method of transcript analysis that allows for the sequence identification and quantification of cellular transcripts. RNA-seq has many applications including differential gene expression (DE) analysis, gene fusion detection, allele-specific expression, isoform and splice variant quantification, and identification of novel genes. These applications can be used for downstream systems biology analyses such as gene ontology analysis to provide insights into cellular processes altered between biological conditions. Given the wide range of signaling pathways subject to chaperone activity as well as numerous chaperone functions in RNA metabolism, RNA-seq may provide a valuable tool for the study of chaperone proteins in biology and disease. This chapter outlines an example RNA-seq workflow to determine differentially expressed (DE) genes between two or more sample conditions and provides some considerations for RNA-seq experimental design.

Key words RNA-seq, RNA sample collection, cDNA library construction, Differential gene expression, edgeR, Gene ontology, GOseq, Chaperones, Heat shock proteins

1 Introduction

RNA-seq is a versatile method of transcript analysis that utilizes sequenced RNA-derived cDNA libraries to assess gene expression. In the past decade, its use has expanded dramatically (Fig. 1). This has been facilitated by decreasing costs of next-generation sequencing, the availability of commercial kits for library construction, and continued refinement of methods for downstream analysis. In addition to these factors, the increasing utilization of RNA-seq has been driven by advantages it provides over previous transcriptomic methods such as tiling microarrays and cDNA Sanger sequencing, reviewed in [1, 2]. Features of RNA-seq include its wide quantitative range, high sequencing accuracy, conduciveness

Benjamin J. Lang and Kristina M. Holton contributed equally to this work.

Stuart K. Calderwood and Thomas L. Prince (eds.), *Chaperones: Methods and Protocols*, Methods in Molecular Biology, vol. 1709, https://doi.org/10.1007/978-1-4939-7477-1_18,

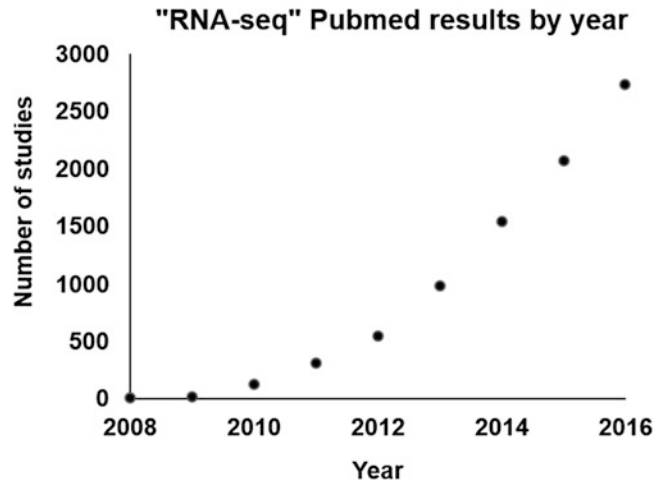

Fig. 1 A Pubmed search using term "RNA-seq" returned the displayed number of studies by year. Since 2008 the number of studies utilizing RNA-seq has rapidly increased

to high-throughput applications, adaptability to large genomes and detection of lowly expressed genes, low background noise and that it is not completely dependent upon the existence of an annotated genome. Unlike RT-qPCR, RNA-seq allows for transcript quantification across the entire gene body simultaneously and therefore has a greater capacity to distinguish between splice variants and isoforms.

Beyond their proteostatic functions, several studies have demonstrated chaperones to have various regulatory activities in transcription and mRNA metabolism. These have included roles for HSP90 members in RNA polymerase II complex assembly, facilitation of transcriptional pausing, mRNA splicing, and catalytic activity of the RNA-induced silencing complex (RISC) [3–6]. In addition, HSP70 family members bind to and mediate mRNA stability and decay [7–12], of note, these properties can be distinct between HSP paralogs and regulated by co-chaperones [13, 14]. These studies indicate a broad potential for chaperones to have significant impact upon transcriptomic profiles; however, few are yet to assess chaperone functions at a transcriptomic level. Given its above-mentioned advantages, RNA-seq is likely to be highly beneficial for future studies of RNA-chaperone functional relationships.

The RNA-seq workflow begins with the experimental conditions from which RNA samples are collected, followed by total RNA extraction, construction of cDNA libraries, sequencing of cDNA libraries, and subsequent bioinformatic analyses (Fig. 2). These general steps are somewhat universal for studies using RNA-seq; however, the parameters and method within each step

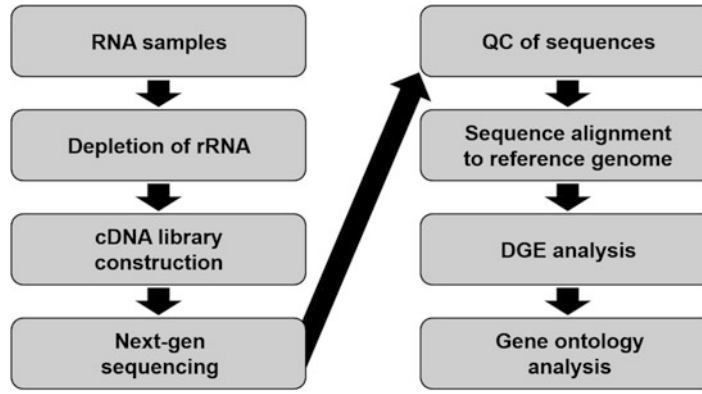

Fig. 2 A generalized workflow for an RNA-seq protocol examining differential gene expression (DE), and the topics of this chapter

are typically selected for the chosen application. This is reflected by the large variation in published RNA-seq protocols [15]. Bioinformatic analysis of RNA-seq data typically involves performing sequence quality control, alignment of sequences to a reference genome, generation of gene feature count data, followed by various assessments of gene transcript abundance, or identification including DE analysis, refinement of gene models, splice variant analysis, isoform expression quantification, gene fusion detection, and allele-specific expression. This chapter is intended to provide an RNA-seq workflow protocol for differential gene expression analysis of coding genes. Investigators may adapt the protocol to their chosen application and we provide some guidance for making such changes.

2 Materials

2.1 Samples

1. Samples for RNA extraction from cell culture or animal-derived tissue.

2.2 Tissue Harvest and RNA Isolation

1. Qiagen QIAshredder cat. no. 79654.
2. Qiagen RNeasy® mini kit cat. no. 217004.
3. β-mercaptoethanol.
4. RNAse-free microcentrifuge tubes.
5. RNase-away Molecular BioProducts cat. no. 7002.
6. DNase I Qiagen cat. no. 79254.
7. Cell culture plates.
8. 70% ethanol.

2.3 Assessment of the Concentration, Purity, and Integrity of the RNA Sample

1. Agilent® bioanalyzer with Expert 2100 software.
2. Agilent® RNA 6000 Nano microfluidic chips.
3. Reagents and consumables for Agilent RNA 6000 Nano microfluidic chip.

This instrumentation and service can commonly be accessed at core facilities.

2.4 cDNA Library Construction (Service Often Available at Next-Generation Sequencing Facility)

1. Solid-Phase Reversible Immobilization (SPRI) nucleotide-binding paramagnetic beads, e.g., Agencourt® AMPure® XP (Beckman Coulter cat no. A63880) or KAPA Pure Beads (KAPA Biosystems).
2. Illumina® TruSeq index adapters.
3. Thermocycler.
4. Magnetic rack.
5. Low-adhesion, RNAse-free, DNAse-free, 1.5 mL microcentrifuge tubes.
6. Low-adhesion, RNAse-free, DNAse-free, PCR tubes sized for thermocycler to be used.
7. Agilent® bioanalyzer tapestation.
8. Filtered pipette tips.
9. KAPA® Stranded RNA-Seq with RiboErase cat. no. KK8483.

2.5 Next-Generation Sequencing

1. Illumina® HiSeq 2500 sequencer.

2.6 Sequence Processing and Analysis

1. High performance computer cluster with UNIX command line.
2. Programs for;
   - Assessing read quality; FastqQC.
   - Trimming/filtering reads; Flexbar [16], Trimmomatic [17].
   - Read alignment; TopHat2/Bowtie 2 [18], HISAT [19], STAR [19].
   - Assigning read counts to annotated genes; samtools, htseq count [20].
3. R version 3.X.X, Bioconductor software packages [21], edgeR [22], GOseq [23], ggplot2 [24].

3 Methods

3.1 Experimental Design

1. Determine the number of samples needed for each condition. *See* Subheading 4.1 for further guidance on choosing number of biological replicates.

2. Determine the sequencing platform to be used. For this protocol an Illumina® HiSeq 2500 sequencer platform is used.
3. Decide how the cDNA libraries will be constructed, stranded, or un-stranded. This protocol uses the KAPA stranded RNA-Seq with RiboErase kit.
4. Determine the minimum read depth needed and the cost *See* Subheading 4.1.

3.2 RNA Collection from Cell Culture

1. Prepare experimental samples ready for RNA collection.
2. Clean working area and pipettes with ethanol and RNase away.
3. Remove media from culture dishes as much as possible. Note that the maximum number of animal cells recommended for the use of the RNeasy® Plus Mini kit protocol is 1×10^7.
4. Following the RNeasy® Plus Mini Handbook, use RLT buffer with β-mercaptoethanol to lyse the cells and collect cell lysate in a new RNase-free microcentrifuge tube.
5. Homogenize the sample by passing it through a QIAshredder column.
6. Continue the protocol with inclusion of the optional DNase I digestion step.
7. Continue to Subheading 3.3 of this protocol, RNA integrity analysis or store at −80 °C.

Note that RNeasy® mini kit buffers RLT and RW1 should not be mixed with bleach.

3.3 RNA Extraction from Mouse Tissue

1. Sacrifice mice per ethical protocol.
2. Excise the tissue of interest from the mouse.
3. Mince up to 30 mg of tissue to small pieces (1–3 mm) with scissors, and transfer into a round-bottom tube with appropriate volume of cell lysis buffer RLT with β-mercaptoethanol per RNeasy® Plus Mini Handbook.
4. Homogenize the sample by passing it through a QIAshredder column.
5. Continue the protocol with inclusion of the optional DNase I digestion step.
6. Continue to Subheading 3.3 of this protocol, RNA integrity analysis or store at −80 °C.

Note that RNeasy® mini kit buffers RLT and RW1 should not be mixed with bleach.

3.4 Assess the Concentration and Integrity of the RNA Sample

1. Quantify the concentration of RNA by absorbance spectrophotometry.
2. Assess RNA integrity using Agilent bioanalyzer. Submit 2–4 μL of RNA sample to core facility for analysis or if instrument is

available in-house, perform analysis per the manufacturer's directions.

3. Proceed with protocol if sample RNA is sufficiently intact (*see* Subheading 4.3.

3.5 Stranded cDNA Library Construction Using KAPA Stranded RNA-Seq Kit with RiboErase for Illumina® Platforms

Follow the manufacturer's protocol to complete these steps of cDNA library construction for RNA-seq using the Illumina® platform;

1. rRNA depletion to enrich for coding genes.
2. Fragmentation of RNA.
3. Reverse transcription of fragmented RNA to produce 1st strand cDNA.
4. Second strand synthesis, second strand marked with dUTP.
5. Ligation of dAMP to 3′ ends of dscDNA strands.
6. Ligation of indexed adaptors to each sample dscDNA.
7. PCR amplification of cDNA libraries.
   Note that numerous SPRI purifications are involved throughout the above steps and are dependent upon the protocol used. When using Agencourt ® AMPure ® XP or KAPA Pure Beads®, it is essential the RNA/DNA-binding steps are performed at room temperature for the RNA/DNA to associate with the beads. RNA/cDNA/Bead solutions that are not equilibrated to room-temperature will result in sample loss.

3.6 Next-Generation Sequencing

1. Perform library quality control and quantification of cDNA libraries.
2. Pool/ multiplex the cDNA libraries at equal proportions to create master pool mix.
3. Run the cDNA library pool on an Illumina® HiSeq 2500 sequencer flow cell or platform of choice.

3.7 Sequence Processing and Analysis

1. Export FASTQ files to remote directory—these are the raw sequence files containing the sequences or "reads" for each indexed sample.
2. Perform quality control upon ".fastq" files (raw reads) to remove low-quality reads and to remove or "trim" the indexed adaptors from the reads.
3. Align reads to reference genome using alignment software, e.g., tophat2 [18], STAR [25], HISAT2 [19].
4. Generate a counts matrix using "htseq count" to count the number of reads aligning to each annotated gene [20].
5. Compare gene-wise expression (differential gene expression "DE") across samples or conditions using EdgeR [22].

6. Assess changes in cellular or biological processes between conditions through gene ontology analysis using GOseq [23].
7. Representation of data.

4 Notes

1. Experimental design
   Immediate RNA-seq experimental design decisions include the number of biological replicates for each condition, whether the cDNA libraries will be stranded or un-stranded, whether the sequencing run will be paired end (PE) or single end (SE), read depth, read length, and cost. Choosing the most cost and statistically effective combination of these parameters can be challenging as there is no current standard; however, recent studies have provided direction on how each of these parameters should be prioritized according to the experimental application [26–29].

   One starting point is determining how many biological replicates the experiment will entail. Biological replicates are essential for encapsulating the biological variation within replicates and between conditions in the statistical analysis [29, 30]. For DE analysis, the investigator may perform a power analysis to predict the number of replicates needed based upon desired power, biological coefficient of variation (BCV), and effect size. This can be a challenge if the BCV for the model is not known. If a costly experiment is planned, it may pay to perform a pilot study to approximate the BCV for power analysis. A typical biological coefficient of variation (BCV) for animal tissue-derived samples is 0.2–0.6 and therefore may require more replicates to achieve a given power and effect size than samples derived from cell lines (BCV closer to 0.1). A study by Schurch et al., recommended 6 replicates to be the minimum for each condition, and at least 12 replicates for each condition if all DE genes are to be determined [28]. Next-generation sequencing (NGS) was shown to be highly reproducible; therefore, prioritizing biological replication over technical replication will benefit DE analysis [31].

   Increasing the number of sequence reads attributed to each biological sample, or "read depth," increases DE power up to a point of saturation [32]. A limiting factor for this parameter is commonly the cost of additional sequencing lanes and flow cells, and it is therefore balanced across an optimal number of biological replicates, the relationship of which was examined by Liu et al., [26]. For example, the Illumina HiSeq 2500 platform yields approximately 180 M reads per sequencing lane, if the cDNA library from one biological sample is applied to one

flow cell lane, the read depth would be approximately 180 M reads. For DE analysis of coding genes, allocating a pooled library of 10–12 cDNA libraries to one flow cell lane will yield approximately 18–15 million reads per sample, respectively. According to the findings by Liu et al., aiming for 10–20 million reads per sample is the most cost-efficient distribution of reads to gain maximum statistical power for DE RNA-seq [26].

Strand-marked or "stranded" cDNA libraries provide additional mapping information over un-stranded cDNA libraries. In contrast to un-stranded libraries, stranded cDNA libraries allow the RNA template strand to be recognized. This is an important distinction in regions where overlapping gene features exist on opposing DNA strands or when the anti-sense strand is also transcribed [33]. Levin et al. assessed different methods of strand marking protocols for RNA-seq and concluded dUTP marking of the second strand with paired-end sequencing to be a preferred method using the Illumina platform [33]. Opting for paired-end (PE) sequencing is generally considered a cost-effective choice to yield greater information from the RNA-seq experiment. PE RNA-seq improves read mapping to features and is also beneficial for splice variant analysis. For the DE analysis, 50 nt sequence cycles/read length is sufficient to assign reads to gene features, with very few genes mapping to multiple features [34]. Longer read lengths will significantly increase the cost and provide greater benefit for other applications.

As much as possible, the handling of RNA samples and processing of all cDNA libraries should be kept as consistent as possible throughout the protocol. Differences in sample processing can influence gene calls downstream and lead to batch effects in the data. Factors in an RNA-seq experiment that may contribute to a batch effect include: experiment date, isolation date, sample storage, sample age, sample gender, isolation area, isolation kit, researcher, and lab [27]. It is best practice to construct all cDNA libraries in concert and to sequence the samples as normalizedpooled cDNA libraries on the same flow cell lane if possible, or equal numbers of each condition spread across multiple flow cell lanes.

2. RNA collection
Careful RNA isolation, handling, and storage are critical for generating valid RNA-seq data. If using a commercial column-based extraction method, the column should be treated with DNase to reduce the chance of genomic contamination of the library preparations. Care should also be taken to prevent any buffer residue on the outside of the column reaching the final elution and thereby avoiding unwanted impurities entering the

sample. RNAses are ubiquitous and steps to protect the RNA sample from RNases such as using clean gloves, and wiping the working area and pipettes with RNAse solution are measures that can counter RNase contamination. Progressing through the RNA extraction protocol as promptly as possible as well as swift storage at −80 °C are also measures the investigator can take to limit sample degradation. We recommend either completing the RNA extraction protocol in its entirety once the sample is lyzed or if commercial RNA preservation reagents are used, then to closely follow the recommendations for their use. Repeated freeze-thaw cycles can lead to reduced RNA integrity and should be avoided.

3. RNA integrity analysis
   Prior to the construction of cDNA libraries for sequencing, it is important to assess the RNA integrity of each sample. This step not only provides confidence going forward through the workflow, but can save a great deal of time and downstream heartache where poor sample quality leads to misleading or no results. Currently, the best method to determine RNA integrity within a sample is to use the Agilent Bioanalyzer system for RNA integrity number (RIN) analysis. The RIN is an arbitrary number derived from an algorithm that uses the fluorescent spectra generated by running an RNA sample through the Agilent Bioanalyzer microcapillary electrophoresis system [35, 36]. Up to 12 samples can be run on one chip at a time and the analysis simultaneously determines RNA concentration in the sample. An example of the fluorescent spectra generated is shown in Fig. 3, where large peaks can be observed in samples with high integrity that correspond to 18S and 28S ribosomal RNA (Fig. 3a), which are absent in degraded samples (Fig. 3b). The algorithm used to generate the RIN number encompasses multiple features of RNA degradation that provides a more robust and reproducible method of determining RNA integrity than assessments based upon the 18S:28S ratio alone [35, 36].

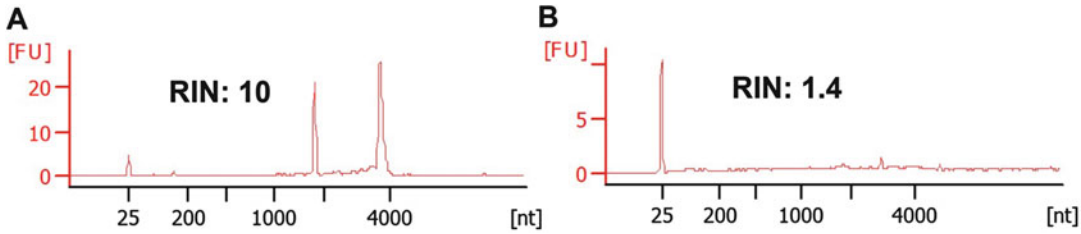

Fig. 3 Agilent Bioanalyzer analysis of RNA integrity. (**a**) An example fluorescence spectra generated by the Agilent Bioanalyzer from an intact RNA sample with RIN value of 10 with distinct peaks corresponding to 18S and 28S rRNA (**b**) A degraded RNA sample of low RIN value showing absence of fluorescent signal corresponding to 18S and 28S rRNA and high level of small RNA molecules

4. cDNA library construction
   (a) Ribosomal RNA (rRNA) makes up 80–90% of total RNA and for the DE analysis of coding genes, enrichment of non-rRNA is commonly employed to ensure that rRNA does not consume most sequence reads [29]. One method to enrich for coding genes is selection of polyA-mRNAs using poly-dT beads or poly-dT primers for reverse transcription [29]. This is a highly effective method of reducing downstream reads being allocated to rRNAs, however be aware that the poly-dT-based library construction can bias representation of 3′ reads [1, 37]. A common alternative to polyA-based enrichment is rRNA-depletion followed by random hexamer-primed reverse transcription, which too is subject to some bias, however to a lesser degree [38]. The KAPA stranded RNA-seq with RiboErase kit used in this protocol depletes rRNA by hybridizing rRNA-complementary DNA oligonucleotides to rRNA and degradation of RNA:DNA hybrids by RNase H while sparing the non-hybridized non-rRNA RNA molecules. The starting volume of total RNA used for the rRNA-depletion stage of the KAPA stranded RNA-seq with RiboErase protocol is 10 μL. Use the same mass of starting RNA across the samples, the amount that remains post-rRNA reduction will vary with variations in the proportion of rRNA across the samples; however, it is not necessary to requantify the rRNA-depleted RNA as variations in rRNA-depleted RNA input will be compensated for downstream when the cDNA libraries are pooled based upon cDNA concentration prior to sequencing.
   (b) For fragmentation of RNA, the KAPA stranded RNA-seq Kit with RiboErase kit uses heat treatment in the presence of magnesium. Varying the time and heat treatment will result in fragments of dependent length. For RNA-seq analysis of coding gene expression, we have typically used 6 min at 94 °C as designated by the kit's protocol to achieve fragments of approximately 200–300 bp. Optimal fragment length can be application-dependent and may also influence how many sequencing cycles one chooses. For example, some sequencing redundancy will occur if 100 bp fragments are generated and more than 50 sequencing cycles PE are used at the sequencing stage as the same sequence information will be duplicated.
   (c) If using a strand-specific protocol such as the KAPA stranded RNA-seq Kit with RiboErase kit, it is important to be aware that the second strand marked with dUTP will not be amplified at the latter PCR stage (3.4.7). The

complement of the coding gene-region will therefore be amplified and sequenced. When using the sequence alignment software, be sure to designate the strandedness of the cDNA libraries. This also applies for counting reads to gene features at stage (Htseq count- 3.6.4) where the --stranded = reverse option needs to be designated.

(d) A unique indexed adapter is ligated to the cDNA libraries of each biological sample. The KAPA stranded RNA-seq Kit with RiboErase kit provides a guide to how much adapter should be included in each ligation reaction and is proportionate to the amount of input RNA. The indexed adaptors serve two purposes. First, the ends of the adaptors allow for the cDNA libraries to bind the sequencing flow cell. Second, a unique 6-nucleotide sequence identifier or "index" allows for the cDNA libraries to be pooled together and run on the same flow cell lane as each sequence read is attributed to an individual biological sample based upon the unique index identifier. The adenylation of the 3′ ends of dscDNA allows for ligation of the adaptors at 3′ ends, the indexed adaptors are also ligated to the 5′ ends. The inclusion of adaptors at both the ends of dscDNA allows for paired-end sequencing (PE), where the final cDNA library fragments are sequenced from both directions. PE-sequencing is desirable as it allows for sequences to be located to the genome with greater confidence and allows quantification of alternatively spliced transcripts.

(e) PCR amplification of cDNA libraries is the final step of cDNA library construction. PCR primers complementary to the Illumina adaptors are added and the cDNA libraries are amplified by PCR for 8–16 cycles. The cycle number recommended by the KAPA protocol is dependent upon the amount of input RNA. The goal of this amplification stage is to increase the cDNA library yield while maintaining a representative distribution of the transcript-derived cDNA molecules. Molecules of cDNA representing transcripts in high abundance will be enriched more rapidly than cDNAs representing transcripts of low abundance and therefore choosing the optimum number of amplification cycles is a balance between increasing the cDNA library to a sufficient yield for sequencing while limiting over-amplification of highly abundant cDNAs. Over-amplification will lead to highly abundant cDNAs taking up a disproportionate number of binding sites on the flowcell and underrepresentation of lowly expressed transcripts. After the post-PCR purification stage, cDNA libraries should be stored at −20 °C.

5. Next-generation sequencing
   Once the cDNA libraries have been constructed it is important to quantify the cDNA concentration and assess the size distribution of each cDNA library. This is commonly achieved using the Agilent tapestation system to assess cDNA size distribution and by qPCR to determine cDNA library concentration [34]. The cDNA libraries are then normalized by concentration and combined or "pooled" to form a master/parent cDNA library that will be run on an Illumina flow cell lane. As described in **Note 1**, the sequencing parameters the investigator must choose are application-dependent. These parameters include whether the sequencing run is to be paired-end (PE) or single end (SE) and the number of sequencing cycles.
6. Sequence processing and analysis
   (a) Quality control of raw reads

   Quality control should always be performed as a first step to understanding the fastq sequence generated by RNA-seq. A fastq file is essentially a fasta (sequence) file, but with an added line, for the PHRED (quality) score, the scale of which depends on the sequencer generating it. Quality/degradation of input RNA, RNA library preparation, model and chemistry kit of the Next-Gen Sequencer, and length of sequence can all affect the consistency and quality of sequence throughout the read. The Java program FastQC generates an html report, including crucial graphical metrics like per base sequence quality, average quality per read, sequence duplication levels, and overrepresented sequence. With these metrics, a researcher can decide whether to trim their sequence to maximize alignment success based on a blunt end cutoff, or quality threshold. Sometimes barcodes or adapters have not been removed, and this should be addressed as well before proceeding with alignment. There are a myriad of trimming/grooming programs available, including Cutadapt/Trim Galore [39], FASTX-Toolkit, Skewer [40], PRINSEQ [41], Trimmomatic [17], to name a few. FastQC should be rerun on trimmed/groomed sequence for validation. For more advanced QC metrics and visualization, RSeQC contains an expansive collection of quality control tools and sequencing metrics, along with format conversion.

   (b) Alignment to reference genome
   TopHat2 with its underlying dependency on the Bowtie2 aligner was once the standard for Illumina sequencing alignment [18]. Taking an indexed genome along with an optional genome annotation file (GAF/GTF),

TopHat2 can discern reads that span splice junctions, and detect novel isoforms.

TopHat2 is a command line Unix tool, and as such, is best suited to run in a High Performance Compute (HPC) environment. It can distribute its computation over multiple processors to speed up alignment, which is a workflow very amenable to HPC. TopHat2 is now becoming deprecated, and replaced with HISAT2, by the same group at Johns Hopkins University [19]. The syntax for mismatches and multi-mappers is very similar, and HISAT2 is not plagued by many of the high memory requirements of other ultrafast aligners.

STAR aligner emerged as an ultrafast alignment alternative to TopHat2, equally capable of mapping reads across splice junctions and detecting novel isoforms [25]. STAR is a Unix tool with higher memory requirements, so is best in an HPC environment. STAR affords greater options and specificity as to mismatches, multi-mappers, and output format, and includes verbose alignment statistics.

(c) Differential expression analysis

The powerful R package edgeR is available through Bioconductor to perform DE analysis to derive a list of genes that statistically differ between conditions [22]. The edgeR package is able to derive meaningful biological signal from a low number of replicates, in terms of number of significant genes and precision, compared to other algorithms [28, 42].

The edgeR package performs DE analysis on raw counts data, as opposed to RPKM or FPKM, which have been shown to not effectively eliminate gene length bias [43]. Instead, by considering each gene and acknowledging that each gene length and therefore bias is the same between conditions, direct gene-wise comparisons can be made between conditions. Gene length can later be factored in during functional enrichment analysis, where the context of the DE genes is explored.

Lowly expressed genes (usually 5–10 counts per million (CPM)) are often considered to be noise, and are conditionally omitted out of the analysis, to prevent them from skewing the statistics. This thresholding can be set to a determined number of samples: all the genes in condition 1 must have a CPM > 5 to be considered, etc. Removing the lowly expressed genes shrinks the size of the input matrix to an easier-to-compute size.

While RPKM or FFKM normalization is not applied, the input data matrix still consists of varying library sizes

(total read counts per sample) that must be normalized to allow for even-footing comparison. Highly expressed genes may be dominating the total number of reads, and need to be compensated for. The edgeR package uses trimmed means of M normalization (TMM) [43]. TMM minimizes the log-fold changes between samples and derives a scaling factor. A scaling factor below one scales the counts up and the library size down, indicating that "a small number of high count genes are monopolizing the library size." [43]. Conversely, a scaling factor above one scales the counts down and the library size up. With the scaling factor, the counts data has a new, effective library size.

It is often useful to visualize how samples cluster using unsupervised methods. Multi-dimensional scaling (MDS) plots the leading log-fold change in the highest two dimensions. Ideally, samples from conditions will separate along the primary X-axis (Fig. 4). Hierarchical clustering on the top quartile varying genes, possibly in conjunction with a heatmap, can also identify any issues with sample consistency. Algorithms like surrogate vector analysis (SVA) [44] can be used to create a modified count to use in edgeR and correct for batch effects.

Like many popular R DE algorithms, edgeR DE is based on a Negative Binomial (NB) model. A NB model is an over-dispersed Poisson model, that is, it has a variation term. The variation is how much the genes in samples within a condition differ from their mean. The biological coefficient of variation (BCV) for an ideal model cell line is around 0.1, but is often as high as 0.6 for human samples, McCarthy et al. reported BCV of 0.4 to be typical of human samples [45]. The edgeR algorithm encapsulates the BCV in two ways: common and gene-wise. The common dispersion assumes that genes all have the same mean-variance relationship. This dispersion is further refined on a tag-wise (gene) level with empirical Bayesian shrinkage; genes more consistent between replicates are ranked higher [45].

The edgeR has two major implementations: "classic" and "generalized linear model" (GLM). The classic mode is for experiments with only two conditions (one factor), and uses quantile-adjusted conditional maximum likelihood (qCML) to determine if a gene differs between conditions. The common and tagwise dispersions work on pseudo counts conditioned on the effective library size. The actual DE is an exact test using the negative binomial distribution. The resultant p-values are then corrected to q-values for multiple testing errors with a

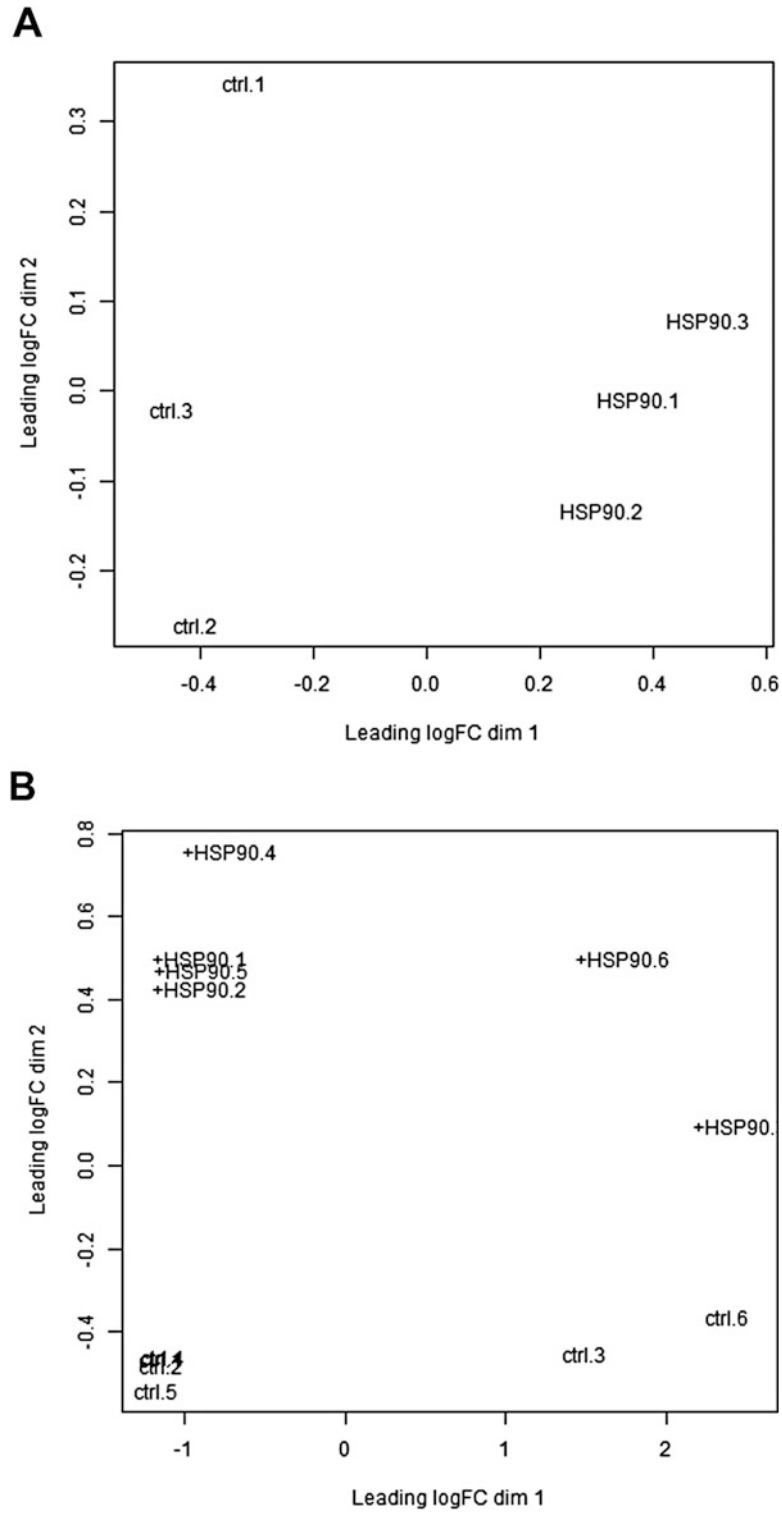

Fig. 4 Multi-dimensional scaling (MDS) plots are an informative visual representation of relatedness between samples. Ideally, samples will be separated across dimension 1 based upon the biological condition such as in (**a**). Where samples are not separated across dimension 1 based upon biological condition such as in (**b**) may be indicative of a batch effect heavily influencing the gene count data

false discovery rate, using Benjamini-Hochberg (BH) correction [46].

For multiple factor experimental designs, the GLM approach is more appropriate. The common and tagwise dispersion are estimated using Cox-Reid profile-adjusted likelihood (CR) by fitting generalized linear models to the design (experimental setup) matrix. The DE can be calculated between any pairwise factors using a GLM likelihood ratio test. P-values are corrected for multiple testing with BH to get resultant q-values. Some investigators choose to threshold q-values with a combination of log-fold change (logFC) to filter out only the statistically significant genes with the highest differential signal. Differentially expressed genes are most commonly represented as logFC to provide a scale upon which observed fold-changes can be represented.

(d) Gene ontology analysis using GOseq

Interrogating the biological context of a DE gene list is imperative to understanding what genes upregulated and downregulated do together. Gene Ontology (GO) is controlled vocabulary to describe a gene by three features: Biological Process (BP), Cellular Component (CC), and Molecular Function (MF). The Gene Ontology Consortium maintains a constantly updated catalog of ontology for many model organisms, and is manually curated and evidence-based [47]. By running variations of a Fisher's Exact Test against a DE list for each term's membership, a p-value and corrected q-value is derived, to determine if a GO term is significant in the dataset.

For RNA-seq data, the question of gene length is not addressed in the edgeR differential, as each gene is considered significant in isolate. But there is still a systemic bias of longer and more highly expressed transcripts being detected, and achieving greater statistical power, skewing the overall analysis [48]. To perform any sort of systems biology approach, like using GO terms, the gene length bias needs to be addressed [23].

The GOseq package in R was designed specifically to perform functional enrichment analysis of NGS data using GO terms, while addressing gene length bias and creating custom null distributions [23]. Using a Probability Weighting Function (PWF) against genes in the DE and not in the DE, the new probability that a gene is differentially expressed based on its transcript length is derived and the null distribution for each GO term is calculated. Only genes that were annotated in the analysis are included; this provides a statistical advantage over some

GO approaches, which use a "one background fits all" approach. The GOseq authors find that simple hypergeometric distribution as the null distribution is not sufficient to model the data appropriately. While resampling is preferred, this is computationally intensive. Instead, GOseq uses the Wallenius non-central hypergeometric distribution, which assumes that "all genes within in a category have the same probability of being chosen, but this probability is different from the probability of choosing genes outside this category" [23]. The resultant p-values are corrected for multiple testing using Benjamini- Hochberg FDR, and GO terms meeting the prespecified alpha are considered significant.

Because of the nature of GO terms, that is, they are organized in a Directed Acyclic Graph (DAG), where more specific, smaller membership terms belong to higher-level, larger membership terms, it is often difficult to tease out the exact context of the bigger picture. Tools like REVIGO (Reduce and Visualize Gene Ontology) take a list of significant GO terms as input and cluster-related terms, creating scatterplots, interactive graphs, and tag clouds [49]. The igraph tool, available in R, Python, and C/C_{++}, is another popular alternative to visualizing the networks from Gene Ontology [50].

(e) Representation of data

Data visualization plays a crucial role in conveying the results of an RNA-seq experiment. Beginning with the cursory glance at the alignment, Integrative Genomics Viewer (IGV) can display how reads map to the reference genome (Fig. 5) [52, 53]. Heatmaps with dendrograms provide a powerful visualization of a DE list, which is more manageable than the entire dataset. The heatmap.2 function in the R package gplots provides powerful functionality to create information-rich heatmaps with dendrograms. Some experimentalists use raw counts and adjust their color scaling. Another popular option is to calculate z-scores per gene, and graph these z-scores. Hierarchical clustering calculates the distance between samples and between genes. Samples of the same experimental factor should cluster together. Genes will cluster according to count or z-score in high-low blocks. Generic choices of clustering include Euclidean, Manhattan, and Pearson Correlation distance metrics. Branches can be cut as appropriate to denote sample or gene clusters.

7. Additional resources

Where institutional access to a high-performance computing cluster is not available, several commercial analysis services are available. These include the amazon cloud computing service

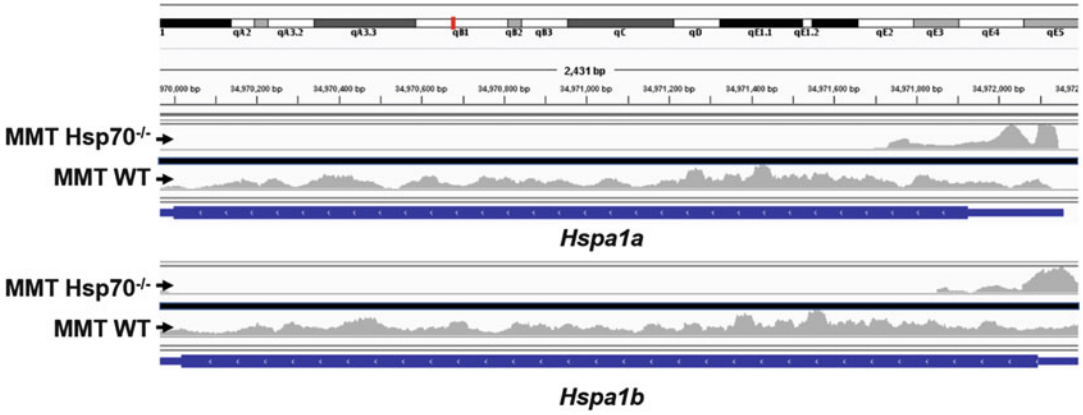

Fig. 5 Visualization of mapped reads using IGV**.** An example representation of read coverage across the mouse *Hspa1a* and *Hspa1b* genes in MMT Hsp70$^{-/-}$ and MMT WT mice [51]. Here, *Hspa1a* and *Hspa1b* coding regions have been largely deleted in the MMT Hsp70$^{-/-}$ sample, and however are still assigned read counts by htseq

which uses a UNIX command line and many of the steps outlined in this protocol could be adapted to using the amazon cloud, see Griffith et al., for reference [54]. The Xsede project is also openly available (https://www.xsede.org/) and provides computing resources to perform RNA-seq analysis. Online discussion forums such as biostars (https://www.biostars.org) and seqanswers (http://seqanswers.com/) are valuable tools to help navigate issues commonly faced when working through an RNA-seq workflow.

Acknowledgments

We thank Thiago De Borges (BIDMC, Harvard Medical School) for critical reading of this chapter.
Declaration of Interest: Kristina M Holton is currently a Campus Champion for the XSEDE project.

References

1. Wang Z, Gerstein M, Snyder M (2009) RNA-Seq: a revolutionary tool for transcriptomics. Nat Rev Genet 10(1):57–63
2. Weber AP (2015) Discovering new biology through sequencing of RNA. Plant Physiol 169(3):1524–1531
3. Boulon S et al (2010) HSP90 and its R2TP/Prefoldin-like cochaperone are involved in the cytoplasmic assembly of RNA polymerase II. Mol Cell 39(6):912–924
4. Iki T et al (2010) In vitro assembly of plant RNA-induced silencing complexes facilitated by molecular chaperone HSP90. Mol Cell 39(2):282–291
5. Sawarkar R, Sievers C, Paro R (2012) Hsp90 globally targets paused RNA polymerase to regulate gene expression in response to environmental stimuli. Cell 149(4):807–818
6. Ferraldeschi R et al (2016) Second-generation HSP90 inhibitor Onalespib blocks mRNA

splicing of androgen receptor variant 7 in prostate cancer cells. Cancer Res 76 (9):2731–2742
7. Duttagupta R et al (2003) A yeast homologue of Hsp70, Ssa1p, regulates turnover of the MFA2 transcript through its AU-rich 3′ untranslated region. Mol Cell Biol 23 (8):2623–2632
8. Henics T et al (1999) Mammalian Hsp70 and Hsp110 proteins bind to RNA motifs involved in mRNA stability. J Biol Chem 274 (24):17318–17324
9. Kishor A et al (2013) Hsp70 is a novel post-transcriptional regulator of gene expression that binds and stabilizes selected mRNAs containing AU-rich elements. Mol Cell Biol 33 (1):71–84
10. Laroia G et al (1999) Control of mRNA decay by heat shock-ubiquitin-proteasome pathway. Science 284(5413):499–502
11. Marucci A et al (2009) The role of HSP70 on ENPP1 expression and insulin-receptor activation. J Mol Med (Berl) 87(2):139–144
12. Wilson GM et al (2001) Thermodynamics and kinetics of Hsp70 association with a + U-rich mRNA-destabilizing sequences. J Biol Chem 276(48):44450–44456
13. Matsui H, Asou H, Inaba T (2007) Cytokines direct the regulation of Bim mRNA stability by heat-shock cognate protein 70. Mol Cell 25 (1):99–112
14. Zimmer C, Gabain AV, Henics T (2001) Analysis of sequence-specific binding of RNA to Hsp70 and its various homologs indicates the involvement of N- and C-terminal interactions. RNA 7:1628–1637
15. Conesa A et al (2016) A survey of best practices for RNA-seq data analysis. Genome Biol 17:13
16. Dodt M et al (2012) Flexbar- flexible barcode and adapter processing for next-generation sequencing platforms. Biology 1(3):895–905
17. Bolger AM, Lohse M, Usadel B (2014) Trimmomatic: a flexible trimmer for Illumina sequence data. Bioinformatics 30 (15):2114–2120
18. Trapnell C, Pachter L, Salzberg SL (2009) TopHat: discovering splice junctions with RNA-Seq. Bioinformatics 25(9):1105–1111
19. Kim D, Langmead B, Salzberg SL (2015) HISAT: a fast spliced aligner with low memory requirements. Nat Methods 12:357–360
20. Anders S, Pyl PT, Huber W (2015) HTSeq--a python framework to work with high-throughput sequencing data. Bioinformatics 31(2):166–169
21. Gentleman R et al (2004) Bioconductor: open software development for computational biology and bioinformatics. Genome Biol 5:R80
22. Robinson MD, McCarthy DJ, Smyth GK (2010) edgeR: a Bioconductor package for differential expression analysis of digital gene expression data. Bioinformatics 26 (1):139–140
23. Young MD, Wakefield MJ, Smyth GK, Oshlack A (2010) Gene ontology analysis for RNA-seq: accounting for selection bias. Genome Biol 11: R14
24. Wickham H (2009) ggplot2: elegant graphics for data analysis. Springer-Verlag, New York
25. Dobin A et al (2013) STAR: ultrafast universal RNA-seq aligner. Bioinformatics 29(1):15–21
26. Liu Y, Zhou J, White KP (2014) RNA-seq differential expression studies: more sequence or more replication? Bioinformatics 30 (3):301–304
27. Fang Z, Cui X (2011) Design and validation issues in RNA-seq experiments. Brief Bioinform 12(3):280–287
28. Schurch NJ et al (2016) How many biological replicates are needed in an RNA-seq experiment and which differential expression tool should you use? RNA 22(6):839–851
29. Sims D et al (2014) Sequencing depth and coverage: key considerations in genomic analyses. Nat Rev Genet 15(2):121–132
30. Anders S, Reyes A, Huber W (2012) Detecting differential usage of exons from RNA-seq data. Genome Res 22(10):2008–2017
31. Marioni JC et al (2008) RNA-seq: an assessment of technical reproducibility and comparison with gene expression arrays. Genome Res 18(9):1509–1517
32. Tarazona S et al (2011) Differential expression in RNA-seq: a matter of depth. Genome Res 21 (12):2213–2223
33. Levin JZ et al (2010) Comprehensive comparative analysis of strand-specific RNA sequencing methods. Nat Methods 7(9):709–715
34. Korpelainen E et al (2015) In: Britton NF et al (eds) RNA-seq data analysis: a practical approach. Mathematical and computational biology series. Chapman & Hall/CRC Press, Boca Raton, FL
35. Schroeder A et al (2006) The RIN: an RNA integrity number for assigning integrity values to RNA measurements. BMC Mol Biol 7:3
36. Imbeaud S et al (2005) Towards standardization of RNA quality assessment using user-independent classifiers of microcapillary electrophoresis traces. Nucleic Acids Res 33(6):e56

37. Shanker S et al (2015) Evaluation of commercially available RNA amplification kits for RNA sequencing using very low input amounts of total RNA. J Biomol Tech 26(1):4–18
38. Hansen KD, Brenner SE, Dudoit S (2010) Biases in Illumina transcriptome sequencing caused by random hexamer priming. Nucleic Acids Res 38(12):e131
39. Martin M (2011) Cutadapt removes adapter sequences from high-throughput sequencing reads. EMBnet Journal 17(1):10–12
40. Jiang H et al (2014) Skewer: a fast and accurate adapter trimmer for next-generation sequencing paired-end reads. BMC Bioinformatics 15:182
41. Schmieder R, Edwards R (2011) Quality control and preprocessing of metagenomic datasets. Bioinformatics 27(6):863–864
42. Seyednasrollah F, Laiho A, Elo LL (2015) Comparison of software packages for detecting differential expression in RNA-seq studies. Brief Bioinform 16(1):59–70
43. Robinson MD, Oshlack A (2010) A scaling normalization method for differential expression analysis of RNA-seq data. Genome Biol 11 (3):R25
44. Leek JT, Storey JD (2007) Capturing heterogeneity in gene expression studies by surrogate variable analysis. PLoS Genet 3(9):e161
45. McCarthy DJ, Chen Y, Smyth GK (2012) Differential expression analysis of multifactor RNA-Seq experiments with respect to biological variation. Nucleic Acids Res 40 (10):4288–4297
46. Benjamini Y, Hochberg Y (1995) Controlling the false discovery rate: a practical and powerful approach to multiple testing. J R Stat Soc Series B Stat Methodol 57(1):289–300
47. Gene Ontology C (2015) Gene ontology consortium: going forward. Nucleic Acids Res 43 (D1):D1049–D1056
48. Oshlack A, Wakefield MJ (2009) Transcript length bias in RNA-seq data confounds systems biology. Biol Direct 4:14
49. Supek F et al (2011) REVIGO summarizes and visualizes long lists of gene ontology terms. PLoS One 6(7):e21800
50. Csardi G, Nepusz T (2006) The igraph software package for complex network research. Inter Journal Complex Systems:1695
51. Gong J et al (2015) Targeting the hsp70 gene delays mammary tumor initiation and inhibits tumor cell metastasis. Oncogene 34 (43):5460–5471
52. Robinson JT et al (2011) Integrative genomics viewer. Nat Biotechnol 29:24–26
53. Thorvaldsdottir H, Robinson JT, Mesirov JP (2013) Integrative genomics viewer (IGV): high-performance genomics data visualization and exploration. Brief Bioinform 14 (2):178–192
54. Griffith M et al (2015) Informatics for RNA sequencing: a web resource for analysis on the cloud. PLoS Comput Biol 11(8):e1004393

Chapter 19

Computational Modeling of the Hsp90 Interactions with Cochaperones and Small-Molecule Inhibitors

Gennady M. Verkhivker

Abstract

Allosteric interactions of the molecular chaperone Hsp90 with a diverse array of cochaperones and client proteins, such as protein kinases and transcription factors, allow for efficient molecular communication in signal transduction networks. Deregulation of pathways involving these proteins is commonly associated with cancer pathologies and allosteric inhibition of oncogenic clients by targeting Hsp90 provides a powerful therapeutic strategy in cancer research. We review several validated computational approaches and tools used in the studies of the Hsp90 interactions with proteins and small molecules. These methods include experimentally guided docking to predict Hs90-protein interactions, molecular and binding free energy simulations to analyze Hsp90 binding with small molecules, and structure-based network modeling to evaluate allosteric interactions and communications in the Hsp90 regulatory complexes. Through the lens of allosteric-centric view on Hsp90 function and regulation, we discuss newly emerging computational tools that link protein structure modeling with biophysical simulations and network-based systems biology approaches.

Key words Hsp90 chaperone, Cochaperones, Protein client interactions, Experimentally guided protein docking, Drug discovery, Small-molecule inhibitors, Protein-ligand interactions, Binding free energy simulations, Protein structure network analysis, Systems biology

1 Introduction

The molecular chaperone Hsp90 (90 kDa heat-shock protein) is required for managing conformational development, stability, and function of proteins in the crowded cellular environment [1–4]. Hsp90 plays a key role in regulating stability and activation mechanisms of a wide range of regulatory and signaling proteins, most notably protein kinases, and transcription factors that are critical for signal transduction, regulatory mechanisms, and immune response [5–9]. The diverse regulatory mechanisms of the Hsp90 machinery are enabled through cooperation with a cohort of cochaperones that tailor structural and functional plasticity of Hsp90 to facilitate evolutionary development and execute functions of client proteins [10–14]. Conformational changes of

Stuart K. Calderwood and Thomas L. Prince (eds.), *Chaperones: Methods and Protocols*, Methods in Molecular Biology, vol. 1709, https://doi.org/10.1007/978-1-4939-7477-1_19,

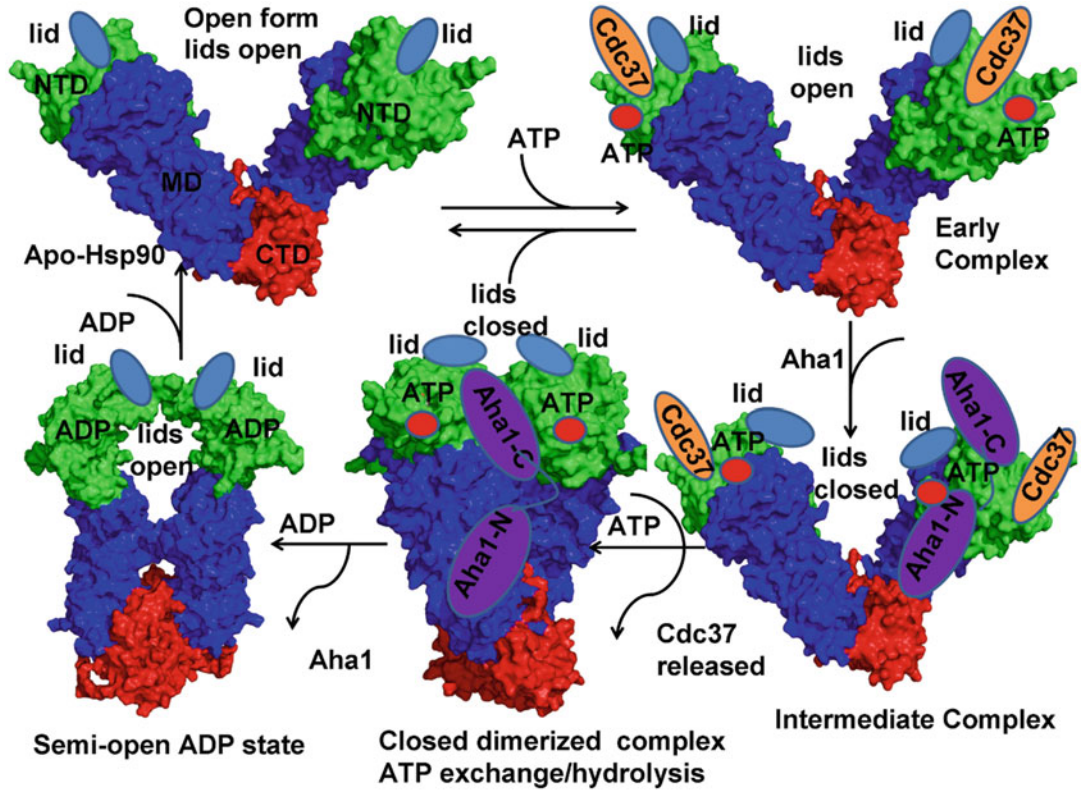

Fig. 1 The Hsp90-ATPase Chaperone Cycle. In the course of the Hsp90 functional cycle, ATP binding to the Hsp90-NTD of the apo Hsp90 in the open form induces a fast dynamic exchange between a nucleotide-free Hsp90 and an intermediate ATP-bound state in which the ATP lids and Hsp90-NTDs are still open. The kinase-specific cochaperone Cdc37 acts early in the chaperone cycle and binds to the Hsp90-NTDs inducing a partially contracted open form of Hsp90 and stabilizing the nucleotide-free chaperone conformation. Protein kinase clients are recruited to the Hsp90 system though the action of Cdc37. After ATP binding, Hsp90 reaches the next intermediate state in which the ATP lids are closed but the Hsp-90-NTDs are still open. Starting from Cdc37-Hsp90 complexes, ATP binding results in an open-closed equilibrium. The hydrolysis is inhibited by Cdc37. In an intermediate ATP-bound complex, with the ATP lids closed but the Hsp90-NTDs are still separated, the cochaperone Aha1 binds to the Hsp90-MD via its N-terminal domain and begins to compete with Cdc37 binding. ATP binding shifts the binding properties to favor the Aha1 binding, leading to the full displacement of Cdc37 from complexes. After nucleotide-induced conformational changes are established, the Hsp90-NTDs are dimerized leading to the formation of the closed intermediate state. Aha1 accelerates the ATPase cycle by facilitating dimerization process of the Hsp90-NTDs and the formation of a partially closed state with the dynamically associated ATP. Binding of p23 displaces Aha1 and stabilizes the completely closed ATP-bound Hsp90 dimer in a conformation committed for ATP hydrolysis. After ATP is hydrolyzed, p23 is released from the complex and the Hsp90-NTDs dissociate leading to the formation of the semi-open ADP-bound state. At the final state, ADP is released and Hsp90 comes back to the nucleotide-free open state

the Hsp90 chaperone are only weakly coupled to nucleotide binding and, in the absence of cochaperones and substrate proteins, the Hsp90-ATPase functional cycle is primarily determined by stochastic transitions between different functional forms of Hsp90 [15–19]. Central to the role of cochaperones is precisely

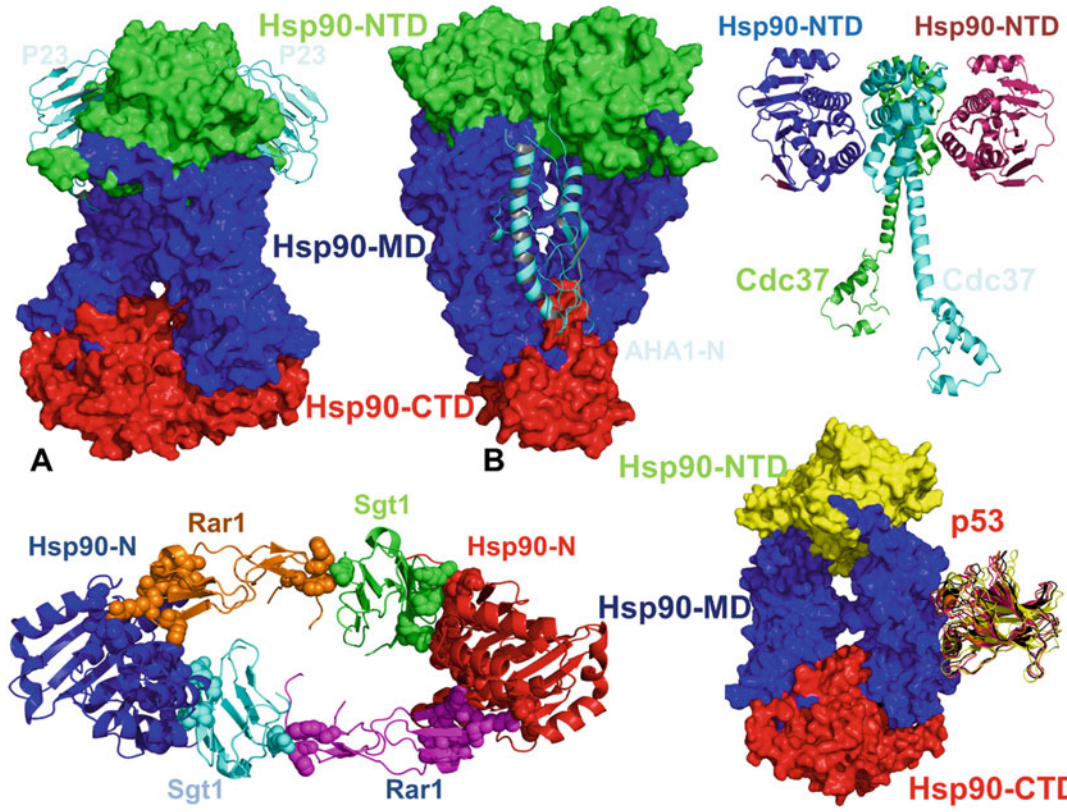

Fig. 2 Structures of the Hsp90-cochaperone Complexes. (**a**) The cocrystal structure of yeast Hsp90 bound to the AMP-PNP and two molecules of p23 (pdb id 2CG9). The Hsp90 dimer is shown in surface representation with the Hsp90-NTD in green, the Hsp90-MD in blue, and the Hsp90-CTD in red. The two p23 molecules are shown in cyan ribbons. (**b**) Structural mapping of the Hsp90-Aha1 interactions from the NMR experiments. The Hsp90 dimer is annotated as in (**a**) and the Aha1 molecule is shown in cyan ribbons. (**c**) The crystal structure of the human Cdc37 construct in the complex with the yeast Hsp90-NTD (pdb id 1US7). (**d**) The crystal structure of the HSP90-Sgt1-Rar1 complex (pdb id 2XCM) is a heterohexamer in a ring configuration with two copies of each component. The two Hsp90-NTD molecules are shown in blue and red ribbons; the two Sgt1-CS domains are presented in cyan and green ribbons; and the two Rar1-CHORD2 domains are depicted in orange and magenta ribbons respectively. (**e**). The NMR ensemble of solution structures of the p53-DBD (PDB ID 2FEJ). The Hsp90 dimer is shown in surface representation with the Hsp90-NTD in green, the Hsp90-MD in blue, and the Hsp90-CTD in red

orchestrated coupling of the Hsp90-ATPase cycling machine to requirements of client proteins, whereby stochastic conformational fluctuations of Hsp90 are modulated leading to a deterministic succession of specific chaperone states that guide timely recruitment, activation, and release of the protein clientele (Fig. 1). Functional classification of Hsp90 cochaperones into client recruiters (Sti1/Hop, Cdc37, Sgt1), remodelers of Hsp90 (Aha1, FKBP51/FKBP52), and late-acting cochaperones (p23) highlights distinctive functional roles and mechanisms of cochaperones that support client proteins through modulation of the Hsp90 conformational ensemble (Fig. 2) [25]. These cochaperones are involved in

regulating the rate of ATP hydrolysis (Aha1, Cdc37, p23), modulating conformational flexibility of Hsp90 (p23, Sgt1), and assisting in client-specific Hsp90 recognition (Sti1/Hop, Cdc37, Sgt1). Aha1 (Activator of Heat shock 90 kDa protein ATPase homolog 1) is a cochaperone which stimulates the ATPase activity. Cochaperones p23/Sba1p [20, 21], Sti1p/Hop [22], and Cdc37 [23] can arrest the Hsp90-ATPase cycle in a particular conformational state to recruit and support activities of specific protein clients. The client recruiter cochaperone Cdc37 functions as a highly specialized adaptor that can deliver kinase clients to the chaperone system and, in coordination with Hsp90, can promote and maintain stabilization of protein kinases during the maturation process. Hsp90 binding with cycle-accelerating cochaperones (Aha1, Cpr6) and cycle-inhibiting cochaperones (p23) can modulate the progression of the ATPase cycle by providing temporal control over conformational transitions required for proper loading and release of the substrate proteins [24]. Cochaperones Sgt1 and Rar1 are cooperatively integrated into the Hsp90 system to ensure proper folding and stabilization of immune sensing client proteins [25]. The interactions of Hsp90 with cochaperones and client proteins are dynamic and synergistic in nature, causing cooperative structural changes in the interacting partners and eliciting global conformational rearrangements of Hsp90 [26, 27].

There has been increasing evidence that allosteric interactions of the Hsp90 proteins can ultimately determine the regulatory mechanisms and cellular functions of signaling cascades that are under chaperone's control. The statistical model of allosteric regulation assumes the ensemble of pre-existing conformational states and communication pathways can be modulated by allosteric perturbations [28]. Integration of molecular docking, atomistic and coarse-grained simulations, and protein structure network analysis has provided a convenient platform for quantifying the regulatory principles underlying allosteric interactions of Hsp90 with cochaperones and client proteins. Computational studies have employed structural and dynamic approaches to quantifying mechanistic aspects of Hsp90 regulation. Our early studies have provided the first atomic resolution models of allosteric regulation in the Hsp90 chaperone and presented evidence of a cross-talk between the N- and C-terminal binding sites of Hsp90 [29, 30]. Atomistic molecular dynamics (MD) simulations and coarse-grained approaches have been used to systematically investigate functional dynamics and global motions of the Hsp90 chaperone [31]. Allosteric interactions of the Hsp90 with cochaperones and client proteins have been dissected in recent studies of the Hsp90 regulatory complexes with Aha1 and p23 cochaperones [32], Cdc37 and Sgt1 cochaperones [33], and p53 client protein [34] (Fig. 2). These studies integrated biochemical characterizations of Hsp90 interactions

with cochaperone and client proteins in experimentally guided reconstruction of binding interfaces for the Hsp90 complexes.

Protein docking approaches can integrate experimental data such as mutagenesis data and NMR chemical shift perturbations as experimental restrains to guide sampling of protein-protein complexes [35, 36]. A graph-based representation of protein structures provides a robust framework for the prediction of allosteric interactions and communications in protein systems through network modeling of residue interactions and protein-protein binding [37, 38]. Using this model, residue interaction networks could be described as weighted graphs and use common measures of node centrality to characterize the local connectivity of a particular node (degree) and global indices of node connectivity (closeness and betweenness). These network descriptors describe fundamental topological features of a biological system and can identify functional residues involved in ligand binding and protein interactions. MD simulations combined with the protein structure network analysis can characterize allosteric structural changes in the conformational populations [39]. Protein network approaches integrated dynamic contact maps of residue cross-correlations in the description of residue connectivity to characterize allosteric communications in protein systems [40]. Residue interaction networks could be often organized in partially overlapping local communities of interacting nodes in which the network connections are dense within communities, but between which they are sparser. We conducted a protein structure network analysis and community decomposition of the Hsp90 complexes and analyzed principal differences in the residue interaction networks [41]. According to these studies, allosteric regulation of the Hsp90 chaperone may be mediated by modules of structurally stable residues that display high centrality in the global interaction network. The network analysis has reproduced a number of structural and mutagenesis experiments, suggesting that the network parameters and centrality analysis could present a robust and simple tool for predicting hot spots of the Hsp90 activity. Computational studies of the Hsp90 interactions have argued for relevance of a synergistic approach that combines functional dynamics and protein structure network approaches as a robust tool for probing mechanisms of Hsp90 regulation by cochaperones and client proteins.

Since Hsp90 is responsible for folding of many proteins associated with malignant progression, inhibition of the Hsp90 protein folding machinery can produce a broad-spectrum antitumor activity and lower the risk of drug resistance due to a combinatorial blockade of multiple signaling pathways [42, 43]. Several natural compounds including Geldanamycin, Radicicol [44], Taxifolin [45], and Withaferin A (WA) [46] are effective inhibitors of Hsp90 and cause the depletion of multiple oncogenic client proteins by binding to the ATP binding site of the Hsp90 N-terminal

domain (Hsp90-NTD). Multiple chemical series of small-molecule inhibitors targeting the Hsp90-NTD have been developed by leveraging crystallographic information in combination with structure-based virtual screening and ligand docking [47, 48]. -Pharmacophore-based virtual screening and shape-based ligand similarity screening combined protein and ligand-centric strategies in the discovery of the Hsp90-NTD inhibitors [49, 50]. MD simulations combined with the binding free energy analysis using the molecular mechanics-generalized born surface area (MM/GBSA) method have been also explored in rationale design and optimization of binding activities of the Hsp90-NTD inhibitors [51–53]. Recent studies have demonstrated that the Hsp90 C-terminal domain (CTD) is important for the dimerization of the chaperone and contains a second nucleotide binding site [54, 55]. Molecular docking studies combined with MD simulations guided design of novel allosteric inhibitors targeting the Hsp90-CTD binding pocket [56–59]. By integrating biochemical and cell-based studies within experimentally guided modeling of the Hsp90 interactions, we have discovered a series of small molecules can bind the Hsp90-CTD binding site and exhibit activity in different tumor cell lines destabilizing binding various Hsp90 client kinases [60–63]. A comprehensive account of molecular modeling approaches used in the discovery of clinically relevant Hsp90 inhibitors has shown that structure-based docking, binding free energy simulations, and network-based approaches could significantly accelerate discovery process [64].

We review computational approaches and tools that can be employed in studies of the Hsp90 interactions with cochaperones, client proteins, and small-molecule inhibitors. These methods include protein docking, binding free energy simulations, and structure-based modeling of the residue interaction networks.

2 Methods

2.1 Experimentally Guided Protein Docking

Experimentally guided docking using HADDOCK methodology [35, 36] utilizes sets of experimental data such as mutagenesis data and NMR chemical shift as experimental restrains that guide sampling of protein-protein complexes (Fig. 3).

1. Structural and functional information is converted into a series of Ambiguous Interaction Restraints (AIR) determined by the selection of active and passive residues.
2. Definition and selection of active and passive residues forming the AIR templates are based on two primary sources of experimental information: structural topology of and functional effects of specific residues based biochemical and structural

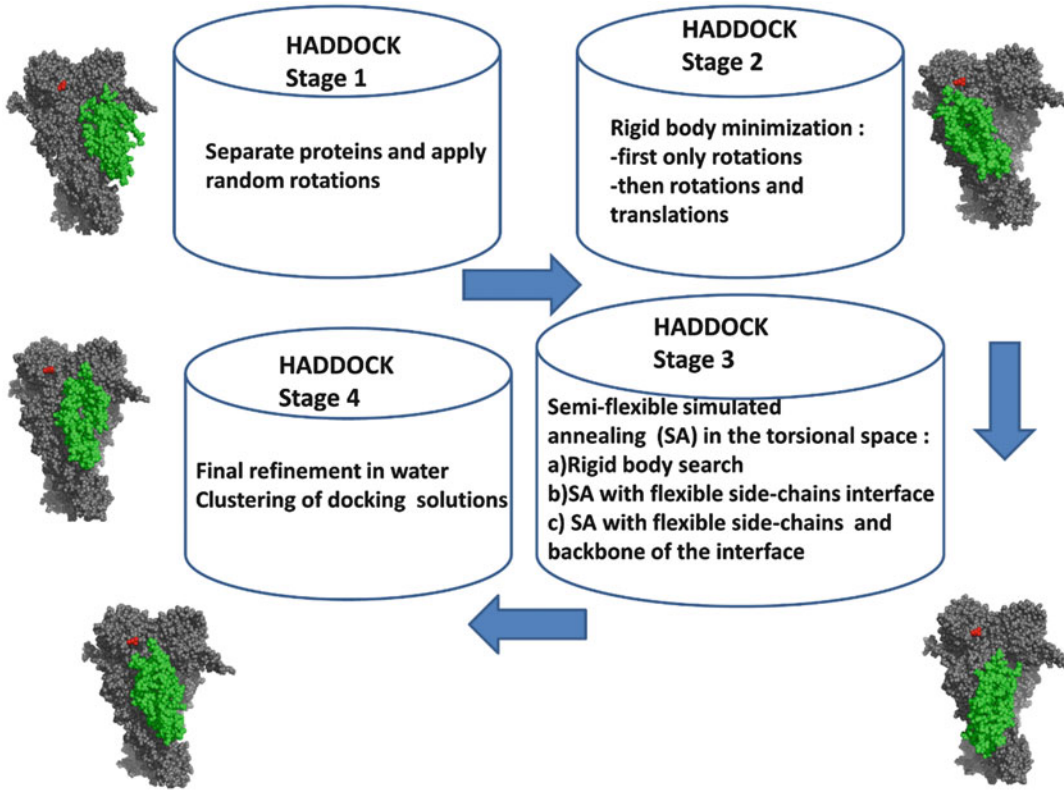

Fig. 3 An Overview of Experimentally Guided Docking using HADDOCK Approach**.** The cartoon outlines and summarizes the selections of active/passive residues and experimental restraints for HADDOCK simulations. The docking protocol consists of consecutive stages: (**a**) randomization of protein orientations; (**b**) rigid body energy minimization (EM); (**c**) semi-flexible simulated annealing in torsion angle space (TAD-SA), which consists of a rigid body MD search and first round of simulated annealing, followed by a second round semi-flexible simulated annealing during which side chains at the interface are free to move. A third round of semi-flexible simulated annealing is the next step of the search during which both side chains and backbone at the interface are free to move; (**d**) a final refinement in Cartesian space with explicit solvent concludes HADDOCK docking simulation

studies of chaperones and kinase clients. The active residues used in HADDOCK modeling are defined as those involved in the Hsp90-cochaperone-specific interactions. Passive residues are defined as residues within a 5A radius of active residues.

3. The docking protocol consists of several stages: randomization of orientations followed by rigid body energy minimization (EM); semi-flexible simulated annealing in torsion angle space, which consists of a rigid body MD search and first round of simulated annealing, followed by a second round semi-flexible simulated annealing during which side chains at the interface are free to move. A third round of semi-flexible simulated annealing is the next step of the search during which both side chains and backbone at the interface are free to move. A final refinement in

Cartesian space with explicit solvent concludes the run. In the course of each independent run, 2000 rigid-body structures are generated during the initial rigid body docking phase. A large number of independent runs (~5000) combined with the default number of randomly generated initial structures (~2000) in each of the conducted runs are expected to produce an adequate sampling of the conformational space for the Hsp90 complexes (Fig. 3).

4. Docked solutions are judged by the total intermolecular energy:

$$\text{HADDOCK Score} = E_{\text{vdw}} + E_{\text{elec}} + E_{\text{AIR}}$$

where E_{vdw} is the van der Waals energy, E_{elec} is the electrostatic energy, and $E_{\text{AIR is}}$ the restraint contribution respectively. The best 200 docked models are submitted to cycles of the semi-flexible simulated annealing and final water refinement. The structures are ranked with standard weights. After the water refinement stage, the total energy is calculated as the weighted sum of the contributing terms:

$$\text{HADDOCK Score} = 1.0E_{\text{vdw}} + 0.2E_{\text{elec}} + 0.1E_{\text{dist}} + 1.0E_{\text{solv}}$$

E_{solv} is the solvation energy. The nonbonded intermolecular interactions are calculated with an 8.5 Å cutoff using the OPLS parameters. The dielectric constant epsilon is set to 10 in the vacuum part of the protocol and to 1 for the explicit solvent refinement. The secondary structure elements are kept intact during the simulated annealing refinement through hydrogen bond and dihedral angle restraints. The cutoff distance of 10 Å and a minimum cluster size of 5 structures are used in clustering of docked poses. The best scored structures from each cluster can be reported and analyzed.

2.2 Protein Structure Modeling and Ligand-Protein Binding

Structure preparation of proteins and ligands for molecular simulations of ligand-protein binding and binding free energy computations consisted of several stages and included checking and correcting for errors, adding missing residues and atoms, filling valences with hydrogens, predicting pK values for titratable amino acids, assigning predefined partial charges and radii to all atoms, and generating force field parameter and topology files for MD simulations. We describe the main components and details of structure analysis and preparation.

2.2.1 Protein Structure Preparation

1. Protein crystal structures are obtained and downloaded from the Protein Data Bank [65].
2. Protein residues in the crystal structures are systematically inspected for missing residues and protons. Hydrogen atoms and missing residues are initially added and assigned according

to the WHATIF program web interface [66, 67]. Protonation states for titratable groups are initially determined using WHAT IF pKa calculations in aqueous solution at pH 7.0 [68, 69]. The initial assignments of protonation states are checked for consistency and subjected to a second round of refinement using *H++* approach (http://biophysics.cs.vt.edu/H++) [70, 71]. Using this approach, missing hydrogens are added to the studied protein structures based on predicted pKa of titratable groups. These calculations are based on the continuum solvent approach in the framework of the Poisson-Boltzmann (PB) model [72].

3. The unresolved structural segments and missing loops are modeled using loop prediction approaches ModLoop [73, 74] or ArchPRED [75]. The protein structures are then optimized using the 3Drefine method that is based on an atomic-level energy minimization using a composite physics and knowledge-based force fields [76].

2.2.2 Ligand Structure Preparation

1. The crystallographic coordinates of the ligand-protein complexes are used to extract the inhibitor conformation, followed by optimization of the inhibitor geometry with density functional theory at the B3LYP/6-31G level using the Gaussian 09 package. In this stage of structure preparation, a strategy of comprehensive and compatible parameterization for the protein and inhibitor atoms is applied that utilizes a set of CHARMM General Force Field (CGenFF)-compatible parameters [77–79]. The atomistic charge parameters for small-molecule inhibitors are initially probed using ParamChem approach by assigning parameters based on analogy with a set of CGenFF parameters [80]. The inhibitor parameters are then refined using the restrained electrostatic potential (RESP) charge fitting procedure [81–83] on the electrostatic potentials produced by single-point quantum mechanical calculations at the Hartree-Fock level with a 6-31G* basis set. The adopted protocol is consistent with the accepted best practices in the employment of CHARMM force field for simulations of protein-inhibitor complexes that include RESP fitting procedure or extracting charges directly from quantum mechanical calculations.

2. VMD plugin ffTK can be used to complete computation of partial atomic charges and parameters for small-molecule inhibitors [84]. This protocol is based on the CGenFF force field and parameterization strategy that allows for compatibility between CHARMM22 force field parameters for proteins and CGenFF parameters. Similar tools ANTECHAMBER [85] and ACPYPE [86] simplify the automatic generation of topology and parameters and *assignment of partial charges for small molecules* from quantum mechanical computations that may be used with the General Amber Force Field (GAFF) [87, 88] and OPLS force field [89].

2.2.3 Ligand-Protein Binding Free Energy Calculations

1. The binding free energy of the ligand-protein complexes is calculated using the MM-GBSA approach [90–92]. In this approach the binding free energy ΔG_{bind} is written as the sum of the gas phase contribution ΔG_{MM}, the solvation free energyΔG_{solv}, and an entropic contribution $-T\Delta S$.

$$\Delta G_{\text{bind}} = < \Delta G_{\text{MM}} > + < \Delta G_{\text{solv}} > - < T\Delta S > .$$

The brackets <> denote an average of these contributions calculated over the MD trajectories. The gas-phase contribution $<\Delta G_{\text{MM}}>$ to the binding free energy is the difference in the molecular mechanics energy of the complex and the isolated protein and ligand. These contributions are calculated according to the CHARMM or AMBER molecular mechanics force field. The solvation free energy ΔG_{solv} is the difference between the solvation energy of the complex and solvation free energies of the isolated protein and ligand. The solvation free energy of a molecule is given as the sum of nonpolar and polar contributions. The nonpolar contribution is computed using the solvent accessible surface area (SASA) model and given as $\Delta G_{solv}^{np} = \sigma^* SASA$ where the parameter σ=0.0072 kcal/ (mol*Å^2). The electrostatic contribution to the solvation free energy $\Delta G_{\text{solv}}^{\text{elec}}$ is calculated using the analytical generalized Born (GB) model. The entropy contribution consists of translationalΔS_{trans}, rotational ΔS_{rot} and vibrational ΔS_{vib}components.

2. Binding free energy is computed either from a single trajectory of the complex ("single-trajectory approach") or from separate trajectories of complex, receptor, and ligand ("three-trajectory approach"). In a "single trajectory" variation of the MM-GBSA approach, calculations are based on the MD simulations of the complexes followed by the separation of the individual snapshots into isolated protein and ligand conformations. This protocol is less rigorous but more efficient and robust by reducing cancellation errors associated with the differences in the intramolecular energies and yielding better convergence of binding free energies [90–92].
3. A workflow tool FEW [93] can facilitate setup and execution of ligand binding free energy calculations with AMBER for multiple ligands. FEW allows preparing implicit solvent molecular mechanics calculations according to the MM-PBSA and the MM-GBSA approach. Prerequisite for the setup of MM-GBSA calculations is the existence of MD trajectories in the MD simulation folders generated with the help of the MD setup functionality of the FEW workflows. We follow the setup of the MM-GBSA, 3-trajectory approach calculations using the FEW command file ana_am1_3trj_pb0_gb2.

```
@WAMM
#########################################################################
##########
# Command file for MM-PBSA / MM-GBSA calculations based on trajectories
# generated by molecular dynamics simulations previously.
#########################################################################
##########
# Location and features of input and output directories / file(s)
#
# lig_struct_path: Folder containing the ligand input file(s)
# output_path: Basis directory in which all setup and analysis folders will
#              be generated. The directory needs to be identical with the
#              'output_path' directory used for setup of the MD simulations.
lig_struct_path             /home/user/structs
output_path                 /home/user/

# Receptor features
# water_in_rec: Water present in receptor PDB structure
#               used for setup of MD simulations
water_in_rec                1

#########################################################################
##########
# General Parameters for MM-PBSA / MM-GBSA calculation setup
#
# mmpbsa_calc: Setup MM-PBSA / MM-GBSA calculations
# 1_or_3_traj: "1" or "3" trajectory approach
# charge_method: Charge method used for MD, either "resp" or "am1"
# additional_library: If an additional library file is required, e.g. for
#                     non-standard residues present in the receptor structure,
#                     this file must be specified here.
# additional_frcmod: If additional parameters are needed, e.g. for describing
#                    non-standard residues present in the receptor structure,
#                    a parameter file should be provided here.
# mmpbsa_pl: Path to mm_pbsa.pl script
mmpbsa_calc             1
1_or_3_traj             3
charge_method           am1
additional_library      /home/user/input_info/CA.lib
add_frcmod
mmpbsa_pl               $AMBERHOME/bin/mm_pbsa.pl
#########################################################################
#########
# Parameters for coordinate (snapshot) extraction
#
# extract_snapshots: Request coordinate (snapshot) extraction
# snap_extract_template: Template file for extraction of coordinates from
#                        trajectory, i.e. input-file for mm_pbsa.pl; only
#                        required if non-standard input-file shall be used.
# image_trajectories: If set to "1" solutes of the specified trajectories
#                     will be imaged to the origin before coordinates are
#                     extracted. Please regard that this may require a large
#                     amount of additional disc space.
# trajectory_files: Trajectory files to regard. The path will be determined
#                   automatically. Specify 'all' to regard all trajectories
```

```
#                files produced in MD. This ensures consistent snapshot
#                numbering. Subsets of snapshots will be generated according
#                to the parameters first_snapshot, last_snapshot, and
#                offset_snapshots. If only a subset of the available MD
#                trajectories shall be used, the individual files must be
#                specified as 'trajectory_files  <file_name>' providing
#                one entry per line.
# first_snapshot: First structure that shall be extracted from trajectory
# last_snapshot:  Last structure that shall be extracted from trajectory
# offset_snapshots:  Frequency of structure extraction
#
extract_snapshots          1
snap_extract_template
image_trajectories         1
#
trajectory_files           all
#
first_snapshot             1
last_snapshot              100
offset_snapshots           1
###############################################################################
##########
# MM-PBSA / MM-GBSA Analysis
# mmpbsa_template: Template file for MM-PBSA / MM-GBSA analysis - File used
#               as input-file for mm_pbsa.pl; only required if non-standard
#               file shall be used.
# PB: If not zero PB calculation will be performed
#    Options: "0" -> No PB
#             "1" -> PB with calculation of the non-polar part of the
#                  solvation free energy using the Method developed by
#                  Tan et al. (J. Phys. Chem. B, 2007, 111, 12263-12274).
#                  This method can only be run in combination with GB=1
#                  or GB=0.
#             "2" -> Hybrid model developed by H. Gohlke and A. Metz
#                  with IVCAP=5 and CUTCAP=50
#             "3" -> PB with MS=1 and Parse radii
#             "4" -> PB with MS=1 and mbondi radii. This method can only
#                  be combined with GB=1 or GB=0.
# GB: If not zero GB calculation will be performed
#    Options: "0" -> No GB
#             "1", "2", "5" -> GB analysis according to 'igb' (see manual)
#
# decomposition: If larger 0 energy decomposition of specified type is
#              performed. Options: 1-4 - See Amber manual for decomposition
#              type options. Decomposition only works with PB=4 and GB=1.
#              SASA is calculated by the ICOSA method.
# no_of_rec_residues: Number of residues in the receptor structure
#
# total_no_of_intervals: Total number of intervals to analyze.
#                    The total_no_of_intervals needs to be consistent with
#                    the number of 'first_PB_snapshot', 'last_PB_snapshot',
#                    and 'offset_PB_snapshots' definitions below. Setting
#                    total_no_of_intervals to a value larger than 1, is
#                    usually only necessary if snapshots with different
#                    offsets shall be analyzed.
```

```
# first_PB_snapshot: Structure to start analysis with
# last_PB_snapshot: Last structure to regard in analysis
# offset_PB_snapshots: Specification of offset between structures that shall
#                      be regarded in the MM-PBSA calculation
#
# mmpbsa_batch_template: Batch script template for MM-PBSA calculation
# mmpbsa_batch_path: Optional, path to regard as basis path for batch script
#                    setup, in case it differs from <output path>.
#
# mmpbsa_sander_exe: Optional, Sander executable can be defined here if not
#                    the default executable in $AMBERHOME/bin shall be
#                    used for carrying out the MM-PB(GB)SA calculations.
# parallel_mmpbsa_calc: No. of processors to use for parallel run
mmpbsa_template
PB                      0
GB                      2
#
decomposition           0
no_of_rec_residues      290
#
total_no_of_intervals   1
first_PB_snapshot       51
last_PB_snapshot        100
offset_PB_snapshots     1
#
mmpbsa_batch_template   /home/user/input_info/MMPBSA.sge
mmpbsa_batch_path       /home/user/
#
mmpbsa_sander_exe
parallel_mmpbsa_calc    1
```

4. When you have ensured thaont the path of the basic input/output directory is specified correctly in the command file, setup of the MM-GBSA calculations by FEW can be invoked by.

```
$FEW/FEW.pl MMGBSA /home/user/cfiles/mmpbsa_am1_3trj_pb0_gb2
```

After the successful completion of the FEW run, a new folder called calc_a_3t exists in the basic input/output directory. This calc_a_3t folder, which is named after the procedure employed (a = am1 and 3t = 3-trajectory approach), contains a sub-folder for each ligand in which the topologies without water (topo), the extracted snapshots (snapshots), and the input-files for the MM-GBSA calculation (s51_100_1) are located.

5. To start the MM-GBSA calculations execute the qsub_s51_100_1_pb0_gb2.sh script located in the calc_a_3t folder.

```
/home/user/calc_a_3t/qsub_s51_100_1_pb0_gb2.sh
```

The result files of the calculations appear in the folder.

```
/home/user/calc_a_3t/<ligand name>/s51_100_1/pb0_gb2
```

2.3 Protein Structure Network Analysis

Protein structure network that is also often referred to as Residue Interaction Network (RIN), or protein structure graph (PSG) can be constructed and analyzed using web based tools GraProStr [94] and NAPS [95].

2.3.1 Residue Interaction Network Construction

1. A graph representation of proteins can be used in the protein structure network analysis, where amino acid residues are considered nodes and edges correspond to the nonbonding residue-residue interactions (Fig. 4). An amino acid residue represented by the C_β atom is considered node in the network and an edge is constructed if the distance between the C_β atoms is within the lower and upper thresholds defined by the user (default upper threshold = 7 Å; lower threshold = 0 Å).
2. The pair of residues with the interaction strength I_{ij} greater than a user-defined cutoff ($I_{\min}$) are connected by edges and produce a protein structure network graph for a given interaction strength $I_{\min}$. The strength of interaction between two amino acid side chains is evaluated as

$$I_{ij} = \frac{n_{ij}}{\sqrt{(N_i \times N_j)}} \times 100$$

where n_{ij} is the number of distinct atom pairs between the side chains of amino acid residues i and j that lie within a distance of 4.5 Å. N_i and N_j are the normalization factors for residues i and j respectively [72, 76]. The number of interaction pairs including main chain and side chain made by residue type i with all its surrounding residues in a protein k is evaluated. A pair of residues can be connected if $I_{\min} > 3.0\%$.

3. A weighted network representation of the protein structure described in [37–40] can be adopted. This model incorporates both the non-covalent connectivity of side chains and residue cross-correlation fluctuation matrix in the construction of network graphs. The weight w_{ij} is defined according to [40] as $w_{ij} = -\log(|C_{ij}|)$ where C_{ij} is the element of the covariance matrix measuring the cross-correlation between fluctuations of residues i and j obtained from MD simulations.

2.3.2 Residue Interaction Network Parameters

1. The analysis of the interaction networks can be done in GraProStr and NAPS web portals by computing network parameters such as hubs, cliques, and communities (Fig. 4). If the total number of edges incident on the node (called the degree of a node) is at least 4 the node is identified as a hub. The k-cliques are complete subgraphs of size k in which each node is connected to every other node. A k-clique is defined as a set of k nodes that are represented by the protein residues in which each node is connected to all the other nodes. A k-clique

community is determined by the Clique Percolation Method [96, 97] as a subgraph containing k-cliques that can be reached from each other through a series of adjacent k-cliques.

2. The shortest paths between two residues are determined using the Floyd–Warshall algorithm [98] that compares all possible paths through the graph between each pair of residue nodes. At the first step, the distance between connected residues is considered to be one, and the shortest path is identified as the path in which the two distant residues are connected by the smallest number of intermediate residues.

2.3.3 Residue Centrality Analysis

All the topological measures can be computed using python scripts in a graph library package Networkx (http://networkx.github.io/). NetworkX is a Python software package for the creation, manipulation, and study of complex networks [99].

1. Residue centrality analysis is based on computations of the shortest paths between residue nodes. The length of a path $L(n_i, n_j)$between distant nodes n_i and $n_j$is estimated the sum of the edge weights between the consecutive nodes (n_k, n_l) along the path:

$$L(n_i, n_j) = \sum_{kl} w(n_k, n_l)$$

2. The betweenness of residue i is defined to be the sum of the fraction of shortest paths between all pairs of residues that pass through residue i:

$$C_b(n_i) = \sum_{j<k}^{N} \frac{g_{jk}(i)}{g_{jk}}$$

where g_{jk} denotes the number of shortest geodesics paths connecting j and k, and $g_{jk}(i)$ is the number of shortest paths between residues j and k passing through the node n_i. Residues with high occurrence in the shortest paths connecting all residue pairs have higher betweenness values. Computation of betweenness centrality is implemented a NetworkX function `betweenness_centrality` (G, $k = None$, $normalized = True$, $weight = None$, $endpoints = False$, $seed = None$)

3. The closeness of residue i is defined as the inverse of the average shortest path (geodesic distance) from residue i to all other residues in the network. Residues with shorter geodesic distances to the remaining residues typically have higher closeness values. Closeness centrality quantitatively measures information transition from a given node to other accessible nodes in the network.

Computation of closeness centrality is implemented as one of the NetworkX functions closeness centrality (G, $u = None$, $distance = None$, $normalized = True$).

2.3.4 Community Analysis of Residue Interaction Networks

We use the Girvan–Newman algorithm that extends the definition of node/residue betweenness to the case of edges, defining the "edge betweenness" of an edge as the number of shortest paths between pairs of nodes that run along this edge [100]. If there is more than one shortest path between a pair of nodes, each path is assigned equal weight such that the total weight of all of the paths is equal to unity. If a network contains communities or groups that are only loosely connected by a few intermodular edges, then all shortest paths between different communities must go along one of these few edges. The algorithm for community detection includes the following steps: (a) the betweenness of all the existing edges in the network is calculated first; (b) the edge with the highest betweenness is removed; (c) the betweenness of all the edges affected by the removal is recalculated; (d) steps b and c are repeated until no edges remain. Girvan-Newman algorithm for computing communities is implemented as one of the NetworkX functions girvan_newman(G, $most\_valuable\_edge = None$) that can be used in the protein structure analysis.

3 Notes

1. During structure preparation for HADDOCK simulations, missing atoms will be automatically generated by HADDOCK when generating the topologies and PDB files of the molecules in the begin directory. In case of missing residues, chain breaks will be introduced.
2. HADDOCK docking with an ensemble of structures may also include single-point mutants provided that the PDB file of the mutant is edited and the mutated residue is renamed to the proper amino acid name.
3. In HADDOCK program, active and passive residues have to be defined by the users based on their own interpretation of the experimental data, especially in the case of NMR titration data. One way to interpret the significance of the shift is to calculate the average perturbation and to consider that all perturbations higher than the average are significant.
4. In HADDOCK definition of active and passive residues the accessibility cutoff is not a hard limit. The identity of the residues at the Hsp90 interfaces with cochaperones and client proteins (Fig. 2) should be analyzed prior to docking to include residues with lower accessibility as they may correspond to functional groups.

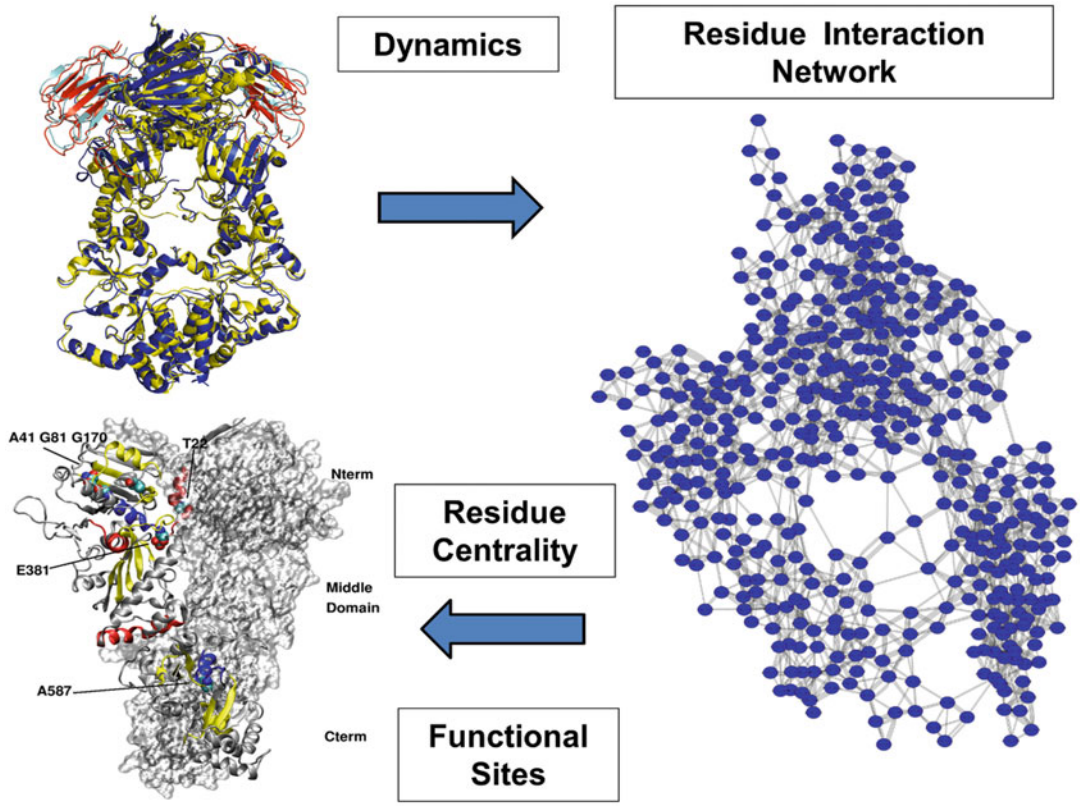

Fig. 4 Computational Modeling of the Hsp90 Interactions**.** Atomistic simulations of the Hsp90 structures and interactions can be synergistically integrated with the protein structure network analysis. The residue centrality and community analysis of the interaction networks can infer functional sites implicated in Hsp90 regulation and binding with the interacting proteins and small molecules

5. To guarantee a sufficient sampling of the Hsp90-protein interactions, the number of structures generated at the rigid-body stage (it0) should be between 5000 and 10,000
6. The validity of the MM-GBSA approach is rested on rigor of the free energy decomposition into additive contributions originating from different groups of atoms and various types of interactions. The free energy errors resulting from non-additivity effects can be progressively minimized in the limit of a small perturbation step. MM-GBSA binding free energy computations require a sufficiently large number of intermediate snapshots that can produce a reliable characterization of binding free energies.

References

1. Pearl LH, Prodromou C (2001) Structure, function, and mechanism of the Hsp90 molecular chaperone. Adv Protein Chem 59:157–186
2. Lindquist SL (2005) HSP90 and the chaperoning of cancer. Nat Rev Cancer 5:761–772
3. Prodromou C (2016) Mechanisms of Hsp90 regulation. Biochem J 473:2439–2452

4. Pearl LH (2016) Review: the HSP90 molecular chaperone-an enigmatic ATPase. Biopolymers 105:594–607
5. McClellan AJ, Xia Y, Deutschbauer AM, Davis RW, Gerstein M, Frydman J (2007) Diverse cellular functions of the Hsp90 molecular chaperone uncovered using systems approaches. Cell 131:121–135
6. Zhao R, Houry WA (2007) Molecular interaction network of the Hsp90 chaperone system. Adv Exp Med Biol 594:27–36
7. Pearl LH (2005) Hsp90 and Cdc37 -- a chaperone cancer conspiracy. Curr Opin Genet Dev 15:55–61
8. Taipale M, Jarosz DF, Lindquist S (2010) Hsp90 at the hub of protein homeostasis: emerging mechanistic insights. Nat Rev Mol Cell Biol 11:515–528
9. Taipale M, Krykbaeva I, Koeva M, Kayatekin C, Westover KD, Karras GI et al (2012) Quantitative analysis of HSP90-client interactions reveals principles of substrate recognition. Cell 150:987–1001
10. Prodromou C (2012) The 'active life' of Hsp90 complexes. Biochim Biophys Acta 1823:614–623
11. Li J, Soroka J, Buchner J (2012) The Hsp90 chaperone machinery: conformational dynamics and regulation by cochaperones. Biochim Biophys Acta 1823:624–635
12. Röhl A, Rohrberg J, Buchner J (2013) The chaperone Hsp90: changing partners for demanding clients. Trends Biochem Sci 38:253–262
13. Verma S, Goyal S, Jamal S, Singh A, Grover A (2016) Hsp90: friends, clients and natural foes. Biochimie 127:227–240
14. Theodoraki MA, Caplan AJ (2012) Quality control and fate determination of Hsp90 client proteins. Biochim Biophys Acta 1823:683–688
15. Graf C, Stankiewicz M, Kramer G, Mayer MP (2009) Spatially and kinetically resolved changes in the conformational dynamics of the Hsp90 chaperone machine. EMBO J 28:602–613
16. Mickler M, Hessling M, Ratzke C, Buchner J, Hugel T (2009) The large conformational changes of Hsp90 are only weakly coupled to ATP hydrolysis. Nat Struct Mol Biol 16:281–286
17. Hessling M, Richter K, Buchner J (2009) Dissection of the ATP-induced conformational cycle of the molecular chaperone Hsp90. Nat Struct Mol Biol 16:287–293
18. Ratzke C, Nguyen MN, Mayer MP, Hugel T (2012) From a ratchet mechanism to random fluctuations evolution of Hsp90's mechanochemical cycle. J Mol Biol 423:462–471
19. Ratzke C, Berkemeier F, Hugel T (2012) Heat shock protein 90's mechanochemical cycle is dominated by thermal fluctuations. Proc Natl Acad Sci U S A 109:161–166
20. Richter K, Walter S, Buchner J (2004) The co-chaperone Sba1 connects the ATPase reaction of Hsp90 to the progression of the chaperone cycle. J Mol Biol 342:1403–1413
21. McLaughlin SH, Sobott F, Yao ZP, Zhang W, Nielsen PR, Grossmann JG et al (2006) The co-chaperone p23 arrests the Hsp90 ATPase cycle to trap client proteins. J Mol Biol 356:746–758
22. Lee CT, Graf C, Mayer FJ, Richter SM, Mayer MP (2012) Dynamics of the regulation of Hsp90 by the co-chaperone Sti1. EMBO J 31:1518–1528
23. Mandal AK, Lee P, Chen JA, Nillegoda N, Heller A, DiStasio S et al (2007) Cdc37 has distinct roles in protein kinase quality control that protect nascent chains from degradation and promote posttranslational maturation. J Cell Biol 176:319–328
24. Li J, Richter K, Reinstein J, Buchner J (2013) Integration of the accelerator Aha1 in the Hsp90 cochaperone cycle. Nat Struct Mol Biol 20:326–331
25. Kadota Y, Shirasu K, Guerois R (2010) NLR sensors meet at the SGT1-HSP90 crossroad. Trends Biochem Sci 35:199–207
26. Southworth DR, Agard DA (2011) Client-loading conformation of the Hsp90 molecular chaperone revealed in the cryo-EM structure of the human Hsp90:hop complex. Mol Cell 42:771–781
27. Genest O, Reidy M, Street TO, Hoskins JR, Camberg JL, Agard DA et al (2013) Uncovering a region of heat shock protein 90 important for client binding in *E. coli* and chaperone function in yeast. Mol Cell 49:464–473
28. Tsai CJ, Sol AD, Nussinov R (2009) Protein allostery, signal transmission and dynamics: a classification scheme of allosteric mechanisms. Mol BioSyst 5:207–216
29. Colombo G, Morra G, Meli M, Verkhivker G (2008) Understanding ligand-based modulation of the Hsp90 molecular chaperone dynamics at atomic resolution. Proc Natl Acad Sci U S A 105:7976–7981
30. Morra G, Verkhivker G, Colombo G (2009) Modeling signal propagation mechanisms and ligand-based conformational dynamics of the Hsp90 molecular chaperone full length dimer. PLoS Comput Biol 5:e1000323

31. Dixit A, Verkhivker GM (2012) Probing molecular mechanisms of the Hsp90 chaperone: biophysical modeling identifies key regulators of functional dynamics. PLoS One 7: e37605
32. Blacklock K, Verkhivker G (2013) Differential modulation of functional dynamics and allosteric interactions in the Hsp90-cochaperone complexes with p23 and Aha1: a computational study. PLoS One 8:e71936
33. Blacklock K, Verkhivker G (2014) Allosteric regulation of the Hsp90 dynamics and stability by client recruiter cochaperones: protein structure network modeling. PLoS One 9: e86547
34. Blacklock K, Verkhivker G (2013) Experimentally guided structural modeling and dynamics analysis of Hsp90-p53 interactions: allosteric regulation of the Hsp90 chaperone by a client protein. J Chem Inf Model 53:2962–29784
35. Dominguez C, Boelens R, Bonvin AM (2003) HADDOCK: a protein-protein docking approach based on biochemical or biophysical information. J Am Chem Soc 125:1731–1737
36. de Vries SJ, van Dijk M, Bonvin AM (2010) The HADDOCK web server for data-driven biomolecular docking. Nat Protoc 5:883–897
37. Brinda KV, Vishveshwara S (2005) A network representation of protein structures: implications for protein stability. Biophys J 89:4159–4170
38. Vijayabaskar MS, Vishveshwara S (2010) Interaction energy based protein structure networks. Biophys J 99:3704–3715
39. Bhattacharyya M, Vishveshwara S (2011) Probing the allosteric mechanism in pyrrolysyl-tRNA synthetase using energy-weighted network formalism. Biochemistry 50:6225–6236
40. Sethi A, Eargle J, Black AA, Luthey-Schulten Z (2009) Dynamical networks in tRNA:protein complexes. Proc Natl Acad Sci U S A 106:6620–6625
41. Blacklock K, Verkhivker GM (2014) Computational modeling of allosteric regulation in the hsp90 chaperones: a statistical ensemble analysis of protein structure networks and allosteric communications. PLoS Comput Biol 10:e1003679
42. Neckers L, Workman P (2012) Hsp90 molecular chaperone inhibitors: are we there yet? Clin Cancer Res 18:64–76
43. Butler LM, Ferraldeschi R, Armstrong HK, Centenera MM, Workman P (2015) Maximizing the therapeutic potential of HSP90 inhibitors. Mol Cancer Res 13:1445–1451
44. Roe SM, Prodromou C, O'Brien R, Ladbury JE, Piper PW, Pearl LH (1999) Structural basis for inhibition of the Hsp90 molecular chaperone by the antitumor antibiotics radicicol and geldanamycin. J Med Chem 42:260–266
45. Verma S, Singh A, Mishra A (2012) Dual inhibition of chaperoning process by taxifolin: molecular dynamics simulation study. J Mol Graph Model 37:27–38
46. Mohan R, Hammers HJ, Bargagna-Mohan P, Zhan XH, Herbstritt CJ, Ruiz A et al (2004) Withaferin A is a potent inhibitor of angiogenesis. Angiogenesis 7:115–122
47. Barta TE, Veal JM, Rice JW, Partridge JM, Fadden RP, Ma W et al (2008) Discovery of benzamide tetrahydro-4H-carbazol-4-ones as novel small molecule inhibitors of Hsp90. Bioorg Med Chem Lett 18:3517–3521
48. Kung PP, Funk L, Meng J, Collins M, Zhou JZ, Johnson MC et al (2008) Dihydroxylphenyl amides as inhibitors of the Hsp90 molecular chaperone. Bioorg Med Chem Lett 18:6273–6278
49. Hong TJ, Park H, Kim YJ, Jeong JH, Hahn JS (2009) Identification of new Hsp90 inhibitors by structure-based virtual screening. Bioorg Med Chem Lett 19:4839–4842
50. Lauria A, Abbate I, Gentile C, Angileri F, Martorana A, Almerico AM (2013) Synthesis and biological activities of a new class of heat shock protein 90 inhibitors, designed by energy-based pharmacophore virtual screening. J Med Chem 56:3424–3428
51. Zhang T, Hamza A, Cao X, Wang B, Yu S, Zhan CG et al (2008) A novel Hsp90 inhibitor to disrupt Hsp90/Cdc37 complex against pancreatic cancer cells. Mol Cancer Ther 7:162–170
52. Tomaselli S, Meli M, Plescia J, Zetta L, Altieri DC, Colombo G, Ragona L (2010) Combined in silico and experimental approach for drug design: the binding mode of peptidic and non-peptidic inhibitors to hsp90 N-terminal domain. Chem Biol Drug Des 76:382–391
53. Yi CH, Chen JZ, Shi SH, GD H, Zhang QG (2010) A computational analysis of pyrazole-based inhibitors binding to Hsp90 using molecular dynamics simulation and the MM-GBSA method. Mol Simul 36:454–460
54. Marcu MG, Chadli A, Bouhouche I, Catelli M (2000) Neckers LM (2000) the heat shock protein 90 antagonist novobiocin interacts

with a previously unrecognized ATP-binding domain in the carboxyl terminus of the chaperone. J Biol Chem 275:37181–37186

55. Garnier C, Lafitte D, Tsvetkov PO, Barbier P, Leclerc-Devin J, Millot JM et al (2002) Binding of ATP to heat shock protein 90: evidence for an ATP-binding site in the C-terminal domain. J Biol Chem 277:12208–12214
56. Sgobba M, Forestiero R, Degliesposti G, Rastelli G (2010) Exploring the binding site of C-terminal hsp90 inhibitors. J Chem Inf Model 50:1522–1528
57. Moroni E, Zhao H, Blagg BS, Colombo G (2014) Exploiting conformational dynamics in drug discovery: design of C-terminal inhibitors of Hsp90 with improved activities. J Chem Inf Model 54:195–208
58. Zhao H, Garg G, Zhao J, Moroni E, Girgis A, Franco LS et al (2015) Design, synthesis and biological evaluation of biphenylamide derivatives as Hsp90 C-terminal inhibitors. Eur J Med Chem 89:442–466
59. Sattin S, Tao J, Vettoretti G, Moroni E, Pennati M, Lopergolo A et al (2015) Activation of Hsp90 enzymatic activity and conformational dynamics through rationally designed allosteric ligands. Chemistry 21:13598–13608
60. Morra G, Neves MA, Plescia CJ, Tsustsumi S, Neckers L, Verkhivker G et al (2010) Dynamics-based discovery of allosteric inhibitors: selection of new ligands for the C-terminal domain of Hsp90. J Chem Theory Comput 6:2978–2989
61. Matts RL, Brandt GE, Lu Y, Dixit A, Mollapour M, Wang S et al (2011) A systematic protocol for the characterization of Hsp90 modulators. Bioorg Med Chem 19:684–692
62. Matts RL, Dixit A, Peterson LB, Sun L, Voruganti S, Kalyanaraman P et al (2011) Elucidation of the Hsp90 C-terminal inhibitor binding site. ACS Chem Biol 6:800–807
63. Roy SS, Kapoor M (2016) In silico identification and computational analysis of the nucleotide binding site in the C-terminal domain of Hsp90. J Mol Graph Model 70:253–274
64. Kumalo HM, Bhakat S, Soliman ME (2015) Heat-shock protein 90 (Hsp90) as anticancer target for drug discovery: an ample computational perspective. Chem Biol Drug Des 86:1131–1160
65. Berman HM, Westbrook J, Feng Z, Gilliland G, Bhat TN, Weissig H et al (2000) The Protein Data Bank. Nucleic Acids Res 28:235–242
66. Hooft RW, Sander C, Vriend G (1996) Positioning hydrogen atoms by optimizing hydrogen-bond networks in protein structures. Proteins 26:363–376
67. Hekkelman ML, Te Beek TA, Pettifer SR, Thorne D, Attwood TK, Vriend G (2010) WIWS: a protein structure bioinformatics web service collection. Nucleic Acids Res 38: W719–W723
68. Nielsen JE, Andersen KV, Honig B, Hooft RW, Klebe G, Vriend G et al (1999) Improving macromolecular electrostatics calculations. Protein Eng 12:657–662
69. Nielsen JE, Vriend G (2001) Optimizing the hydrogen-bond network in Poisson-Boltzmann equation-based pK (a) calculations. Proteins 43:403–412
70. Gordon JC, Myers JB, Folta T, Shoja V, Heath LS, Onufriev A (2005) H++: a server for estimating pKas and adding missing hydrogens to macromolecules. Nucleic Acids Res 33:W368–W371
71. Anandakrishnan R, Aguilar B, Onufriev AV (2012) H++ 3.0: automating pK prediction and the preparation of biomolecular structures for atomistic molecular modeling and simulations. Nucleic Acids Res 40: W537–W541
72. Bashford D, Karplus M (1990) pKa's of ionizable groups in proteins: atomic detail from a continuum electrostatic model. Biochemistry 29:10219–10225
73. Fiser A, Do RK, Sali A (2000) Modeling of loops in protein structures. Protein Sci 9:1753–1773
74. Fiser A, Sali A (2003) ModLoop: automated modeling of loops in protein structures. Bioinformatics 19:2500–2501
75. Fernandez-Fuentes N, Zhai J, Fiser A (2006) ArchPRED: a template based loop structure prediction server. Nucleic Acids Res 34: W173–W176
76. Bhattacharya D, Cheng J (2013) 3Drefine: consistent protein structure refinement by optimizing hydrogen bonding network and atomic-level energy minimization. Proteins 81:119–131
77. Vanommeslaeghe K, Hatcher E, Acharya C, Kundu S, Zhong S, Shim J et al (2010) CHARMM general force field: a force field for drug-like molecules compatible with the CHARMM all-atom additive biological force fields. J Comput Chem 31:671–690
78. Vanommeslaeghe K, AD MK Jr (2012) Automation of the CHARMM general force field (CGenFF) I: bond perception and atom typing. J Chem Inf Model 52:3144–3154

79. Vanommeslaeghe K, Raman EP, AD MK Jr (2012) Automation of the CHARMM general force field (CGenFF) II: assignment of bonded parameters and partial atomic charges. J Chem Inf Model 52:3155–3168
80. Zoete V, Cuendet MA, Grosdidier A, Michielin O (2011) SwissParam: a fast force field generation tool for small organic molecules. J Comput Chem 32:2359–2368
81. Bayly CI, Cieplak P, Cornell WD, Kollman PA (1993) A well-behaved electrostatic potential based method using charge restraints for determining atom-centered charges: the RESP model. J Phys Chem 97:10269–10280
82. Cornell WD, Cieplak P, Bayly CI, Kollman PA (1993) Application of RESP charges to calculate conformational energies, hydrogen bond energies and free energies of solvation. J Am Chem Soc 115:9620–9631
83. Cieplak P, Cornell WD, Bayly CI, Kollman PA (1995) Application of the multimolecule and multiconformational RESP methodology to biopolymers: charge derivation for DNA, RNA and proteins. J Comput Chem 16:1357–1377
84. Mayne CG, Saam J, Schulten K, Tajkhorshid E, Gumbart JC (2013) Rapid parameterization of small molecules using the force field toolkit. J Comput Chem 34:2757–2770
85. Wang J, Wang W, Kollman PA, Case DA (2006) Automatic atom type and bond type perception in molecular mechanical calculations. J Mol Graph Model 25:247–260
86. Sousa da Silva AW, Vranken WF (2012) ACPYPE - AnteChamber PYthon parser interface. BMC Res Notes 5:367
87. Wang J, Wolf RM, Caldwell JW, Kollman PA, Case DA (2004) Development and testing of a general amber force field. J Comput Chem 25:1157–1174
88. Debiec KT, Cerutti DS, Baker LR, Gronenborn AM, Case DA, Chong LT (2016) Further along the road less traveled: AMBER ff15ipq, an original protein force field built on a self-consistent physical model. J Chem Theory Comput 12:3926–3947
89. Harder E, Damm W, Maple J, Wu C, Reboul M, Xiang JY et al (2016) OPLS3: a force field providing broad coverage of drug-like small molecules and proteins. J Chem Theory Comput 12:281–296
90. Kollman PA, Massova I, Reyes C, Kuhn B, Huo S, Chong L et al (2000) Calculating structures and free energies of complex molecules: combining molecular mechanics and continuum models. Acc Chem Res 33:889–897
91. Hou T, Wang J, Li Y, Wang W (2011) Assessing the performance of the MM/PBSA and MM/GBSA methods. 1. The accuracy of binding free energy calculations based on molecular dynamics simulations. J Chem Inf Model 51:69–82
92. Sun H, Li Y, Tian S, Xu L, Hou T (2014) Assessing the performance of MM/PBSA and MM/GBSA methods. 4. Accuracies of MM/PBSA and MM/GBSA methodologies evaluated by various simulation protocols using PDBbind data set. Phys Chem Chem Phys 16:16719–16729
93. Homeyer N, Gohlke H (2013) FEW: a workflow tool for free energy calculations of ligand binding. J Comput Chem 34:965–973
94. Vijayabaskar MS, Niranjan V, Vishveshwara S (2011) GraProStr—graphs of protein structures: a tool for constructing the graphs and generating graph parameters for protein structures. Open Bioinform J 5:53–58
95. Chakrabarty B, Parekh N (2016) NAPS: network analysis of protein structures. Nucleic Acids Res 44:W375–W382
96. Palla G, Derényi I, Farkas I, Vicsek T (2005) Uncovering the overlapping community structure of complex networks in nature and society. Nature 435:814–818
97. Adamcsek B, Palla G, Farkas IJ, Derényi I, Vicsek T (2006) CFinder: locating cliques and overlapping modules in biological networks. Bioinformatics 22:1021–1023
98. Floyd RW (1962) Algorithm 97: shortest path. Commun ACM 5:345
99. Hagberg A, Schult D, Swart P (2008) Exploring network structure, dynamics, and function using NetworkX, p 11–15. In: 7th python in science conference (SciPy 2008). Pasadena
100. Girvan M, Newman ME (2002) Community structure in social and biological networks. Proc Natl Acad Sci U S A 99:7821–7826

Chapter 20

Computational Analysis of the Chaperone Interaction Networks

Ashwani Kumar, Kamran Rizzolo, Sandra Zilles, Mohan Babu, and Walid A. Houry

Abstract

We provide computational protocols to identify chaperone interacting proteins using a combination of both physical (protein–protein) and genetic (gene–gene or epistatic) interaction data derived from the published large-scale proteomic and genomic studies for the budding yeast *Saccharomyces cerevisiae*. Using these datasets, we discuss bioinformatic analyses that can be employed to build comprehensive high-fidelity chaperone interaction networks. Given that many proteins typically function as complexes in the cell, we highlight various step-wise approaches for combining both the genetic and physical interaction datasets to decipher intra- and inter-connections for distinct chaperone- and non-chaperone-containing complexes in the network. Together, these informatics procedures will aid in identifying protein complexes with distinctive functional specializations in the cell that yield a very broad and diverse set of interactions. The described procedures can also be leveraged to datasets from other eukaryotes, including humans.

Key words Chaperone network, Functional enrichment, Genetic interactions, Physical interactions, Protein complexes

1 Introduction

Molecular chaperones are key players of cellular protein folding and assembly [1, 2]. Chaperone proteins are found in all cellular compartments and are involved in numerous physiological processes. Typically, chaperones are grouped into families depending on sequence similarity and function. The major chaperone families in the budding yeast *Saccharomyces cerevisiae* are 2 Hsp90s, 14 Hsp70s, 22 Hsp40s, 8 CCTs, 1 Hsp60, 1 Hsp10, 6 prefoldins, 5 ATPases associated with diverse cellular activities (AAA+), 7 small heat-shock proteins (sHsps), and 1 calnexin (total of 67 chaperones). Additionally, the Hsp70 and Hsp90 chaperones function with 4 and 11

Ashwani Kumar and Kamran Rizzolo are Co-first authors.
Mohan Babu and Walid A. Houry are co-corresponding authors.

Stuart K. Calderwood and Thomas L. Prince (eds.), *Chaperones: Methods and Protocols*, Methods in Molecular Biology, vol. 1709, https://doi.org/10.1007/978-1-4939-7477-1_20,

partner proteins termed cochaperones, respectively [3]. Despite many mechanistic and functional studies on both chaperones and cochaperones (CCos), the spectrum of cellular substrates and cellular functions they mediate remains largely incomplete. Hence, to obtain a better view of the division of labor among molecular chaperones in the cell, it is necessary to study them at a global systems level.

The use of proteomic methods has become a key tool to study phenotypes in cells by mapping physical (protein–protein) and genetic (gene–gene or epistatic) interaction networks. Typically, experiments to map physical interactions involve three essential steps: (1) separation and isolation of proteins; (2) the acquisition of sequence information for protein identification; and (3) database utilization for downstream analysis [4]. While protein–protein interactions (PPIs) can be mapped using various proteomic approaches in many model organisms such as human and yeast [5–7], the most standard techniques used to perform large-scale, systematic measurements of PPIs involves precision-based mass-spectrometry (MS) methods [8]. For instance, PPIs can be obtained by affinity purifying the endogenously tagged bait protein and then identifying co-purifying interactors by tandem MS/MS.

On the other hand, large-scale genetic interaction (GI) data have also been used to unmask gene and protein organization in the cell. Most insights into genetic interaction networks have been gained from the work done in the budding yeast [9], Gram-negative bacteria [10, 11], Gram-positive bacteria [12, 13], and other species [14–16]. To study GIs in yeast, double mutant strains are systematically created by mating a resistance-marked "query" deletion mutant strain against an array of single-gene deletion mutants typically marked with kanamycin using synthetic genetic analysis (SGA) technology [9, 17]. Such methodology allows for a quantitative assessment of the relative fitness of a double-mutant meiotic progeny using the GI scores, which are further categorized into aggravating (negative or synthetic lethal) or alleviating (positive or buffering) GIs. Aggravating interactions occur when the double-mutant fitness is lower than the expected for the two single mutants and may reflect compensatory pathways. The most extreme type of aggravating GIs is referred to as "synthetic lethal" where the double-mutant (compared to single mutants) does not grow at all. In contrast, alleviating interactions occur when the double-mutant fitness is greater than that expected for the two single mutants. For instance, this scenario can occur when genes function in the same nonessential pathway or complex. Both types of GIs from the network can be organized in a two-dimensional hierarchical clustering, where clusters are formed from the query genes according to the overlap of their interactions with the array genes. Sets of genes either with similar GI scores (positive or negative) or those functioning within the same pathway

(or subunits within a complex) tend to cluster together. Furthermore, the GI profile similarity provides a potential biological function for an uncharacterized gene based on its GI profile similarity with known genes.

Using the PPI and GI frameworks, our group published in 2005 a comprehensive physical and genetic analysis of the Hsp90 chaperone interaction network, showing a broad role of the chaperones in many distinct cellular pathways [18, 19]. Subsequently, in 2009, we published a yeast chaperone physical interaction atlas for 63 chaperones [20], which allowed us to uncover a clear distinction between chaperones that are promiscuous and chaperones that are functionally specific. The analysis indicated the presence of cellular hot spots of chaperone interactions in the cell. Recent efforts by our groups have also concentrated on building a comprehensive chaperone and cochaperone (CCo) interaction network using a combination of PPI and GI data. The integration applicability of various data types in network biology can provide a multidimensional approach to the study of proteomics [21]. This is very useful for CCos given that they are typically promiscuous in their interactions. The use of both physical and genetic data types provides information on inter- and intra- CCo complex interactions that would otherwise be missed by using one single approach.

In this chapter, we provide detailed computational protocols and source codes to build a comprehensive interaction network based on PPI and GI data. Most of our work has concentrated on chaperones and their cochaperones, but the described algorithms can be applied to networks with proteins involved in any other functions.

2 Methods

The protocols provided demonstrate various computational methods to determine functional relationships among genes and proteins. We also describe approaches to integrating similar (e.g., protein interactions from different studies) as well as different (e.g., proteomic and genomic) biological data. Various sources of protein interactome and computational tools are provided below along with relevant analyses. The algorithms have been provided in R code (https://www.r-project.org), which is a language for statistical computing and graphics.

2.1 Construction of the Chaperone Genetic Interaction (GI) Network

SGA-based large-scale screening is the most widely used approach to identifying genetic interactions (i.e., epistatic relationships) between genes. Briefly, a GI between two genes is estimated by comparing the growth fitness defects of the strains having single-gene deletion mutants versus strains with both genes deleted. The process of construction and quantification of growth fitness

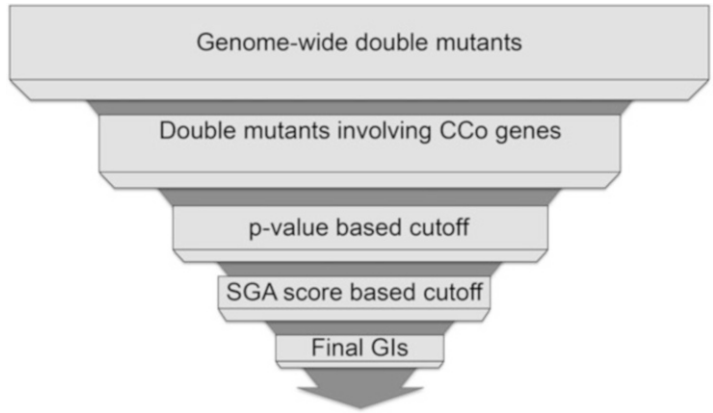

Fig. 1 A flowchart summarizing the construction of CCo GI network extracted from the genome-wide double mutant growth fitness data

of all three mutants (two single and one double) pertaining to two genes is described in [22]. The SGA score for a gene pair is calculated using the following multiplicative model [23].

$$\text{SGA Score} = W_{AQ} - (W_A \times W_Q).$$

where W_{AQ}, W_A, and W_Q are the double, single array, and single query mutant growth fitness values, respectively. A statistical confidence measure (*p*-value) is assigned to each interaction based on a combination of the observed variation of each double mutant across four experimental replicates and estimates of the background lognormal error distributions for the corresponding query and array mutants [22]. The two criteria of, for example, SGA scores $\geq |0.08|$ and *p*-value <0.05 are used to evaluate the strength of a GI. Such GIs are then combined to construct a GI network. In the case of multiple testing (gene pair tested multiple times in different batches) or reciprocal redundancy (gene pair tested as both array-query as well as query-array), the SGA score for that pair with best *p*-value is selected. A succinct schematic description of the GI network construction is shown in Fig. 1.

2.2 Quantifying CCo Interaction Densities

CCos help thousands of substrate proteins fold, assemble, and traffic appropriately. Consequently, CCos are expected to have, on average, a higher number of GIs in comparison to the rest of the yeast genes. To confirm this supposition, we can compare the GI density distribution of CCos with that of all other genes in the whole-genome network [22].

```
#R script to generate density distribution of the GIs of CCos
versus rest of the genes.
# Importing the input file
data <- read.table(file.choose(),header=T,sep="\t")
# Importing the required R libraries
```

```
library(ggplot2)
library(reshape2)
attach(data)
data.m <- melt(data)
p <- ggplot(aes(x=value, colour=variable), data=data.m)
p + geom_density() +
theme_bw() + theme(panel.grid.major = element_blank(),
panel.grid.minor = element_blank(), axis.text.x =
element_text(angle=0),legend.position = c(0.8, 0.8)) +
scale_x_continuous(breaks = round(seq(0, 1000, by = 100),1),
name="Number of interactions", expand = c(0, 0)) +
scale_y_continuous(breaks = seq(0,0.0035,0.0005), limits=c
(0,0.004), name="Density", expand = c(0, 0)) +
labs(colour = "Genes") + annotate(geom="text", x=400,
y=0.0015, label="italic(P) < 0.02", parse=TRUE, color-
="black") +
# To add lines to represent the average number of GIs of two
gene sets. For example, 160 and 80 for CCos and all other
genes, respectively.
geom_vline(xintercept = 80, size = 0.5, colour = "black",
linetype = "dashed") + geom_vline(xintercept = 160, size =
0.5, colour = "black",linetype = "dashed")
```

2.3 Analysis of GI Network

2.3.1 Clustering of GI Profiles

Two genes are considered to have similar GI profiles when their set of positive and negative GIs are significantly alike. Two genes with similar profiles can, therefore, be considered functionally associated [22]. A very powerful way to organize genes according to their GI profiles is by applying two-dimensional (2-D) hierarchical clustering. Conceivably, genes pertaining to same pathways and/or complexes are more likely to cluster together. 2-D hierarchical clustering can be performed by using a standalone tool called Cluster 3.0 which can be downloaded from http://bonsai.hgc.jp/~mdehoon/software/cluster/software.htm. A detailed manual explaining how to use Cluster 3.0 is also provided. Obtained images can then be visualized in the form of a heatmap using the Java TreeView tool (http://jtreeview.sourceforge.net/). The strength of this approach lies in the functional prediction of genes for which little or no information is available in the literature (also known as orphan genes). If a well-annotated gene is clustered together with an orphan gene through the guilt-by-association principle [24], it can be proposed that those two genes have similar molecular functions.

2.3.2 Bioprocess Enrichment in the GI Network

A bioprocess represents a group of genes that delineate a series of events achieved by one or more coordinated assemblies of molecular functions. The following analysis can be performed to determine

bioprocesses that are significantly enriched for GIs in the GI network indicating their importance. If NETn is the number of genes in the GI network whereas BPn is the number of genes in a bioprocess, we calculate four numbers:

1. The number of observed interactions for genes in a bioprocess G ($\mathrm{BPint}_{\mathrm{obs}}$)

$$|\{(u,v)\in E(G) \mid u\in V(BP)\vee \ v\in V(BP)\}|$$

here, u and v are two of the all (V) genes in the BP and E represents the edges (interactions) in the network.

2. The maximum possible number of interactions for genes in a bioprocess G ($\mathrm{BPint}_{\mathrm{max}}$)

$$BPn(NETn-BPn)+BPn(BPn-1)/2$$

3. The number of actually observed interactions in the GI network G ($\mathrm{NETint}_{\mathrm{obs}}$)

$$|\{(u,v)\in E(G) \mid u\in V(G)\vee \ v\in V(G)\}|$$

4. The maximum possible number of interactions in the GI network G ($\mathrm{NETint}_{\mathrm{max}}$)

$$NETn(NETn-1)/2$$

```
#R script to calculate enrichment
#Typically, large-scale GI studies involve genes from many
bioprocesses. Assuming that there is an input file containing
BPint_obs, BPint_max, NETint_obs and NETint_max values for each
bioprocess separated by tab delimiters.
# Importing the input file
data <- read.table(file.choose(),header=T,sep="\t")
# Function to calculate hypergeometric distribution based
p-values
data.P <- phyper(data$BPint_obs, data$BPint_max, data$NETint_obs -
data$BPint_max, data$NETint_max, lower.tail = FALSE)
# Function to calculate corrected p-values, i.e., false dis-
cover rate (FDR)
data.FDR <- p.adjust(data.P, "fdr")
# Joining the p- and FDR values to the input file
data.P.FDR <- cbind(data, data.P, data.FDR)
# Exporting the calculated values
write.table(data.P.FDR, "Data-P_FDR.txt", sep="\t")
```

In general, a bioprocess with p-value (or FDR) < 0.05 is accepted as enriched.

Table 1
contingency table

	GIs involving BP_1	GIs not involving BP_1
GIs involving BP_2	A	C
GIs not involving BP_2	B	D

Where,
A = Number of GIs between BP_1 and BP_2 genes
B = Number of GIs between BP_1 and non- BP_2 genes
C = Number of GIs between BP_2 and non- BP_1 genes
D = Number of GIs that do not involve BP_1 or BP_2 genes

2.3.3 Bioprocess Crosstalk in the GI Network

Significance of the observed GIs between two bioprocesses can be evaluated using Fisher's Exact test. For that, we make a contingency Table 1:

```
#Assuming that there is an input file containing BP1, BP2, A, B, C and D values for each bioprocess pair separated by tab delimiters, the R script to calculate bioprocess pair enrichment (p-value) is

data <- read.table(file.choose(),header=T,sep="\t")
get_fisher <- function(data){
  mat <- matrix(as.numeric(data[c(3:6)]),nrow=2, ncol=2)
  f <- fisher.test(as.table(mat), alternative="greater")
  return(c(df[1],  f$p.value))
}
P.values   <-  apply(df, 1,  get_fisher)
```

As described above, *p*-value corrections can be performed on the obtained *p*-values. Generally, a bioprocess pair with *p*-value (or FDR) < 0.05 is accepted as enriched. Similarly, we can compute crosstalk enrichment between CCo families.

2.3.4 Building the CCo GI Profile Correlation Similarity Network

The GI profile of a given gene is composed of the list of positive and negative GIs involving that gene across the whole genome. A strong correlation in the GI profile of two genes should indicate high similarity in the pattern of their genetic interactions with other genes in the genome, suggesting similar molecular function or pathway/complex [22]. This property can be used to assess the connectivity between CCos in the cell by building a GI profile correlation similarity network. The mathematical formula to calculate the Pearson correlation coefficient (r) is

$$r = \frac{n\sum xy - (\sum x)(\sum y)}{\sqrt{n(\sum x^2) - (\sum x)^2}\sqrt{n(\sum y^2) - (\sum y)^2}}$$

where n is the number of pairs of data points in the GI profiles, x and y, of two genes. Assuming that we have a list of GIs as three column file (Gene1, Gene2, and SGA score), the following R script can be used to (1) generate the SGA score matrix and then (2) calculate Pearson correlation coefficient values for each gene pair in the matrix.

```
data <- read.table(file.choose(),header=T,sep="\t")
data.mat <- acast(data, Gene1~Gene2, value.var="Score")
 PCC <- cor(data.mat)
write.table(PCC, file="Output-matrix.txt")
```

Similar to GI scores, GI profile correlation can be used to generate the epistatic network. A threshold on the significance of the GI profile correlation scores can be set either by using statistical means such as null distribution-based p-values. The GI profile correlation similarity network can be visualized using the Spatial Analysis of Functional Enrichment (SAFE) tool which is described in detail elsewhere [25]. Briefly, SAFE highlights regions that are densely connected with a particular attribute such as Gene Ontology (GO) or cellular bioprocesses.

2.3.5 Finding Positive and Negative GI Hubs

Hub genes in the network are genes with high number of GIs [26], and are typically central to the network's architecture because of their essential role in the cellular processes. Their functions become even more vital in the differential (or dynamic) network when two static GI networks screened under two different conditions are compared. In a given static network, the number of direct connections a node i (gene or protein) has is referred to as its connectivity degree. When a network is represented as an adjacency matrix M, the degree of gene i is calculated by

$$\sum_{j=1}^{NETn} M(i,j)$$

where $M(i, j)$ is an index representing ith row and jth column of the matrix M. NETn is the number of genes in the network or number of columns in the matrix M. High number of interactions of a gene in the GI network is expected to have an important role. Consequently, CCos with wider role in the network are likely to be hubs. On the other hand, genes interacting with many CCos, especially a particular chaperone family, could be predicted to have close functional association with them. Furthermore, a

dominant type of GI (positive or negative) could further help in deciphering the nature of the potential associations.

Assuming that we have a list of GIs as three column files (Gene1, Gene2, and SGA score), the following R script can be used to calculate the number of positive and negative interactions of each gene in the network.

```
# Read GI file containing gene names and GI score (Gene1,
Gene2, and Score delimited by tab)
data <- read.table(file.choose(),header=T,sep="\t")
#Separating positive and negative GIs
data.neg <- subset(data, data$Score < 0, select = c(Gene1,
Gene2))
data.pos <- subset(data, data$Score > 0, select = c(Gene,
Gene2))


#Importing igraph library to do graph based calculations
library(igraph)
#Generating graph for positive and negative GIs, respectively
g.pos <- graph_from_data_frame(data.pos, directed=F)
g.neg <- graph_from_data_frame(data.neg, directed=F)
# Converting gene degree values into a dataframe
g.pos.degree <- as.data.frame(degree(g.pos))
g.neg.degree <- as.data.frame(degree(g.neg))
library(data.table)
#Use gene names as first column of the dataframe
setDT(g.pos.degree, keep.rownames = TRUE)
setDT(g.neg.degree, keep.rownames = TRUE)
#Assign desired names to the columns in the dataframe
setnames(g.pos.degree, 1, "Genes")
setnames(g.pos.degree, 2, "Degree")
setnames(g.neg.degree, 1, "Genes")
setnames(g.neg.degree, 2, "Degree")
#Merge 2 dataframes with respect to gene names
g.pos.neg.degree <- (merge(g.pos.degree, g.neg.degree, by.
x="Genes", by.y="Genes", sort=F, all =T))
#Assign desired names to the columns in the dataframe
setnames(g.pos.neg.degree, 2, "PositiveDegree")
setnames(g.pos.neg.degree, 3, "NegativeDegree")
#Replace "NA" value with 0
g.pos.neg.degree[is.na(g.pos.neg.degree)] <- 0
#Export the results
write.table(g.pos.neg.degree,"CHap-net-degree-alle-aggr.txt",
sep="\t", row.names = FALSE, quote = FALSE)
```

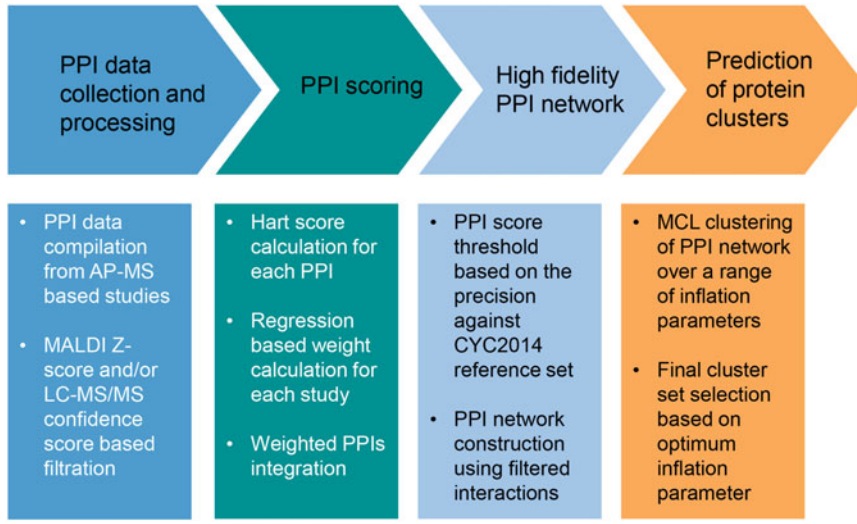

Fig. 2 A computational framework to integrate PPIs obtained from multiple high-throughput studies to construct a high-fidelity PPI network

2.4 Construction of PPI Network from Multiple High-Throughput Studies

Ideally, the integration of PPIs from several high-throughput studies should be performed because it broadens the coverage of the chaperone interactome (Fig. 2). To illustrate the chaperone-based PPI network construction, we can use the following large-scale proteomic studies, where interactions can be restricted to a bait (or target) CCo protein: Gavin et al. [5], Krogan et al. [27], Wodak et al. [28], Babu et al. [29], and Gong et al. [20]. These studies utilized MALDI-TOF (Matrix-assisted Laser Desorption/Ionization Time of Flight) MS and/or tandem liquid chromatography (LC-MS/MS) based confidence probability scores [30] for protein identification. Briefly, the confidence scores are calculated as the probability of a prey protein (or peptide), suggesting the likelihood of its appearance in the purifications pertaining to a bait. Gold standard literature reference set of PPIs from BioGRID (https://thebiogrid.org/) can be used to calculate an optimum probability score as a threshold at a high precision value. Specific thresholds of these two (typically, Z-score ≥ 1 for MALDI-TOF/MS, LC-MS/MS and confidence score $> 70\%$) scores can be used to discard low confidence PPI detections [27, 31].

In order to make use of the compiled PPI datasets, an appropriate relative weighting must be performed as the different datasets may have different scoring methods, which can lead to a scoring bias. In the case of chaperone PPIs, the purification enrichment (PE) and the hypergeometric Hart interaction scores [32, 33] are computed and compared by selecting the method that yields the highest number of CCos. In the case of the Hart score, an integrated PPI score can be computed by summing the relative

weights from each dataset as follows: Gavin_Hart × γ1 + Babu_-Hart × γ2 + Krogan_Hart × γ3 + Gong_Hart × γ4, where γ is the weight of an individual dataset obtained by applying logistic regression. The γ value varies according to the influence of each dataset on the overall precision of the PPI scoring.

To determine an optimum threshold of the Hart score, PPIs can be compared to a high-confidence experimentally validated set of protein complexes from a CYC2014 gold standard reference set [34]. An individual dataset can increase or decrease the overall precision and, therefore, its γ value can be fine-tuned to obtain a score cutoff, where coverage of interactions is maximized while maintaining a high precision value. We find the Hart scoring method to be a better predictor of CCo PPIs.

2.5 Prediction of Protein Complexes Using Clustering Algorithm

Since densely connected regions of a PPI network suggest that associated proteins are likely to have a similar function [28], clustering methods have been used to identify and predict protein complexes and functional modules [35]. The Markov clustering method (MCL) can be used [36] to identify the macromolecular assemblies within the CCo PPI network. The resulting clusters can be benchmarked based on the overall cluster properties such as the number of clusters, average cluster size, intra- and inter-cluster functional diversity as measured by Shannon index of gene ontology (GO) terms in biological process and molecular function [37], as well as CYC2014 [34] complex coverage through precision and homogeneity metric [38]. Based on the minimization of intra-cluster average functional diversity and coverage of known CYC2014 complex members, an inflation parameter can be chosen to generate the finalized PPI clustering. An MCL clustering algorithm tool can be downloaded from http://micans.org/mcl/ and can be run from command line. An example of the application of this tool is shown below:

```
mcl <-|InputFile> --abc -o OutputFile
```

When running this program, the inflation value is usually chosen in the range of 1.2–5.0.

2.5.1 Quality Assessment of Predicted Protein Complexes

A substantial overlap of a predicted cluster with one or more high-confidence literature-curated protein complexes (CYC2014) is a measure of high quality [27]. Here, we provide a detailed explanation on how to do this analysis. Assuming that there are c predicted clusters ($C_1 \ldots C_c$) and m CYC2014 complexes ($CYC_1 \ldots CYC_m$), we construct a $m \times c$ matrix A (also called confusion matrix) where rows represent the number of common proteins in each of the CYC_i complexes in CYC2014 with the C_j clusters and columns representing the number of common proteins in each of the C_j clusters with that of CYC2014 complexes.

$$A = \begin{pmatrix} p_{11} & p_{12} & \cdots & p_{1c} \\ \vdots & \vdots & \ddots & \vdots \\ p_{m1} & p_{m2} & \cdots & p_{mc} \end{pmatrix} = \left(p_{ij}\right) \in \mathbb{N}^{m \times c}$$

where p_{ij} represents an index of the matrix A.

The following four quantities are then computed:

1. S_i is the sensitivity that quantifies the extent by which a CYC2014 complex CYC_i aggregated within the same predicted cluster.

$$S_i = \max_j\left(p_{ij}\right) / \sum_{j=1}^{c} p_{ij}$$

2. H_i^{CYC} is the homogeneity that quantifies the extent by which a CYC2014 complex is distributed among predicted clusters.

$$H_i^{\text{CYC}} = \sum_{j=1}^{c} \left(p_{ij} / \sum_{j=1}^{c} p_{ij}\right) \cdot \left(p_{ij} / \sum_{i=1}^{m} p_{ij}\right)$$

3. Positive predicted value, PPV_j, of a predicted cluster determines the maximum portion of it being part of a CYC2014 complex

$$\text{PPV}_j = \max_i\left(p_{ij}\right) / \sum_{i=1}^{m} p_{ij}$$

4. H_j^C is the homogeneity of a predicted cluster calculating the extent to which it is distributed among CYC2014 complexes.

$$H_j^C = \sum_{i=1}^{m} \left(p_{ij} / \sum_{i=1}^{m} p_{ij}\right) \cdot \left(p_{ij} / \sum_{j=1}^{c} p_{ij}\right)$$

These four quantities are then used to calculate overall agreement between CYC2014 complexes and predicted clusters represented by $\text{Precision}_{\text{total}}$ and $\text{Homogeneity}_{\text{total}}$ which are defined as:

$$\text{Precision}_{\text{total}} = \text{sqrt}(S_{\text{mean}} \times PPV_{\text{mean}})$$
$$\text{Homogeneity}_{\text{total}} = \text{sqrt}\left(H_{\text{mean}}^{\text{CYC}} \times H_{\text{mean}}^{C}\right)$$

Here, S_{mean} and PPV_{mean} are the averages of S_i and PPV_j values across the columns and rows, respectively. $H_{\text{mean}}^{\text{CYC}}$ and H_{mean}^{C} are the averages of all the H_i^{CYC} and H_j^C values, respectively. Below is an R script to calculate the overall precision and homogeneity as described above.

```
#Read an input file containing a matrix in which each cell
represents the overlapping proteins between a literature
complex (rows) and predicted MCL cluster (columns)

data <- (read.table("mat.txt",sep="\t", header=T, row.names=1))

#Function to calculate Precision_total and Homogeneity_total

Preci.homog <- function (D){
M <- as.matrix(D, nrow = 1, ncol = 1, byrow = FALSE, dimnames
= NULL, row.names = 1)

HCmean <- mean(colSums(t(apply(M, 1, function(i) i/sum(i)))
*apply(M, 2, function(i) i/sum(i))))

HMmean <- mean(rowSums(t(apply(M, 1, function(i) i/sum(i)))
*apply(M, 2, function(i) i/sum(i))))

Smean <- mean(apply(M,1,max)/(rowSums(M)))

PPVmean <- mean(apply(M,2,max)/(colSums(M)))

Precision.tot <- sqrt(Smean*PPVmean)

Homogeneity.tot <- sqrt(HMmean*HCmean)

newlist <- list("Precision_total" = Precision.tot, "Homoge-
neity_total" = Homogeneity.tot)

return(newlist)
}

#Calling the function for input matrix
Preci.homog(data)
```

2.6 Building a Combined Physical-Genetic Interaction Network

Deciphering the functional relationships among proteins is essential to comprehend all facets of cell biology. Typically, proteins in the cellular environment work as complexes and are part of a multidimensional proteome [21]. In Subheading 2.3.1, we described an elegant approach to predict protein complexes or pathways by applying hierarchical clustering to the GI profiles. Experimentally identified or predicted protein complexes on their own would not exhibit connections with each other. An auxiliary course to fill in this knowledge gap is to use GI information to investigate association between already known or predicted protein complexes [39]. Furthermore, these techniques help in the prediction of new members of complexes since a gene holding high GI profile correlation with most of the complex members is likely to be

another component of the complex. To establish functional connections between protein complexes, the GI profile similarity network can be overlaid onto the predicted MCL clusters obtained from the physical PPIs. This data integration is essential as the PPI network cannot establish genetic (or epistatic) connections between complexes. Hence, integrating GI with PPI provides an additional layer of information to the network.

By using the average GI profile similarity scores between genes (proteins) of two clusters as a connectivity score, a quantitative inter-complex connection can be established (Fig. 3). At the intra-complex level, proteins are connected using their respective GI profile similarity metrics. Only positive correlations among genes within the same complex are considered to be meaningful in this analysis.

3 Concluding Remarks

Our stepwise strategy provides a computational framework for capturing PPI and GI data on CCos. Given their promiscuous and typically transient folding functions in the cell, most CCo interactions tend to be difficult to obtain using affinity purification

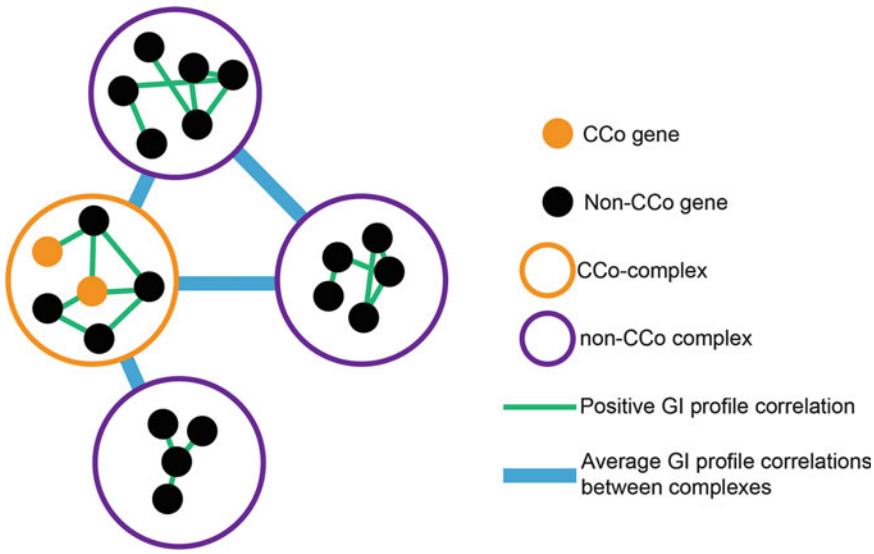

Fig. 3 Schematic overview of mapping GI profile correlations onto predicted protein clusters. Functional relationships between predicted protein clusters are obtained by averaging the GI profile correlation scores among their (gene) members. Similarly, positive GI profile correlation scores are used to enhance the envisaged functional connections within a cluster

(AP)/MS methods. Furthermore, some CCo genes, like Hsp90, are pleiotropic and are considered prototypical capacitors of genetic variation in many organisms [40–42]. This complicates their interaction study using GI data since pleiotropic genes tend to have many GIs with different genes from multiple pathways. Therefore, even though pleiotropic genes often are hubs in the GI network, they seldom show functional enrichment with specific pathways/processes. Hence, by combining both the GI and the PPI data, a global CCo functional pattern can be elucidated where complexes containing specialized CCos have more inter-complex connections compared to complexes containing functionally general CCos.

The computational approaches described here can generate a comprehensive and high-fidelity CCo network that exposes the global functional role of CCos in protein homeostasis. This can serve as a powerful resource for anyone studying CCo interactions from any organism as we recently did for yeast CCos [43].

Acknowledgements

K.R. was supported by a Canadian Institutes of Health Research (CIHR) Training Program in Protein Folding and Interaction Dynamics: Principles and Diseases fellowship and by a University of Toronto Fellowship in the Department of Biochemistry. M.B. holds a CIHR New Investigator award (MSH-130178). This work was funded by CIHR grants MOP-125952, RSN-124512, 132191, and FDN-154318 and MOP-132191 to M.B. and by MOP-93778, MOP-81256, and MOP-130374 to W.A.H.

References

1. Saibil H (2013) Chaperone machines for protein folding, unfolding and disaggregation. Nat Rev Mol Cell Biol 14:630–642
2. Balchin D, Hayer-Hartl M, Hartl FU (2016) In vivo aspects of protein folding and quality control. Science 353:aac4354
3. Finka A, Mattoo RU, Goloubinoff P (2016) Experimental milestones in the discovery of molecular chaperones as polypeptide unfolding enzymes. Annu Rev Biochem 85:715–742
4. Graves PR, Haystead TA (2002) Molecular biologist's guide to proteomics. Microbiol Mol Biol Rev 66:39–63
5. Gavin AC, Bosche M, Krause R, Grandi P, Marzioch M, Bauer A, Schultz J, Rick JM, Michon AM, Cruciat CM, Remor M, Hofert C, Schelder M, Brajenovic M, Ruffner H, Merino A, Klein K, Hudak M, Dickson D, Rudi T, Gnau V, Bauch A, Bastuck S, Huhse B, Leutwein C, Heurtier MA, Copley RR, Edelmann A, Querfurth E, Rybin V, Drewes G, Raida M, Bouwmeester T, Bork P, Seraphin B, Kuster B, Neubauer G, Superti-Furga G (2002) Functional organization of the yeast proteome by systematic analysis of protein complexes. Nature 415:141–147
6. Perez-Riverol Y, Alpi E, Wang R, Hermjakob H, Vizcaino JA (2015) Making proteomics data accessible and reusable: current state of proteomics databases and repositories. Proteomics 15:930–949
7. Martens L, Vizcaino JA (2017) A golden age for working with public proteomics data. Trends Biochem Sci 42:333–341
8. Aebersold R, Mann M (2016) Mass-spectrometric exploration of proteome structure and function. Nature 537:347–355

9. Boone C, Bussey H, Andrews BJ (2007) Exploring genetic interactions and networks with yeast. Nat Rev Genet 8:437–449
10. Babu M, Arnold R, Bundalovic-Torma C, Gagarinova A, Wong KS, Kumar A, Stewart G, Samanfar B, Aoki H, Wagih O, Vlasblom J, Phanse S, Lad K, Yeou Hsiung YA, Graham C, Jin K, Brown E, Golshani A, Kim P, Moreno-Hagelsieb G, Greenblatt J, Houry WA, Parkinson J, Emili A (2014) Quantitative genome-wide genetic interaction screens reveal global epistatic relationships of protein complexes in Escherichia Coli. PLoS Genet 10:e1004120
11. Kumar A, Beloglazova N, Bundalovic-Torma C, Phanse S, Deineko V, Gagarinova A, Musso G, Vlasblom J, Lemak S, Hooshyar M, Minic Z, Wagih O, Mosca R, Aloy P, Golshani A, Parkinson J, Emili A, Yakunin AF, Babu M (2016) Conditional epistatic interaction maps reveal global functional rewiring of genome integrity pathways in Escherichia Coli. Cell Rep 14:648–661
12. Peters JM, Colavin A, Shi H, Czarny TL, Larson MH, Wong S, Hawkins JS, CH L, Koo BM, Marta E, Shiver AL, Whitehead EH, Weissman JS, Brown ED, Qi LS, Huang KC, Gross CA (2016) A comprehensive, CRISPR-based functional analysis of essential genes in bacteria. Cell 165:1493–1506
13. Koo BM, Kritikos G, Farelli JD, Todor H, Tong K, Kimsey H, Wapinski I, Galardini M, Cabal A, Peters JM, Hachmann AB, Rudner DZ, Allen KN, Typas A, Gross CA (2017) Construction and analysis of two genome-scale deletion libraries for Bacillus subtilis. Cell Syst 4:291–305. e297
14. Lehner B, Crombie C, Tischler J, Fortunato A, Fraser AG (2006) Systematic mapping of genetic interactions in Caenorhabditis elegans identifies common modifiers of diverse signaling pathways. Nat Genet 38:896–903
15. Yu J, Pacifico S, Liu G, Finley RL Jr (2008) DroID: the drosophila interactions database, a comprehensive resource for annotated gene and protein interactions. BMC Genomics 9:461
16. Fischer B, Sandmann T, Horn T, Billmann M, Chaudhary V, Huber W, Boutros M (2015) A map of directional genetic interactions in a metazoan cell. eLife 4:e05464
17. Tong AH, Lesage G, Bader GD, Ding H, Xu H, Xin X, Young J, Berriz GF, Brost RL, Chang M, Chen Y, Cheng X, Chua G, Friesen H, Goldberg DS, Haynes J, Humphries C, He G, Hussein S, Ke L, Krogan N, Li Z, Levinson JN, Lu H, Menard P, Munyana C, Parsons AB, Ryan O, Tonikian R, Roberts T, Sdicu AM, Shapiro J, Sheikh B, Suter B, Wong SL, Zhang LV, Zhu H, Burd CG, Munro S, Sander C, Rine J, Greenblatt J, Peter M, Bretscher A, Bell G, Roth FP, Brown GW, Andrews B, Bussey H, Boone C (2004) Global mapping of the yeast genetic interaction network. Science 303:808–813
18. Zhao R, Davey M, Hsu YC, Kaplanek P, Tong A, Parsons AB, Krogan N, Cagney G, Mai D, Greenblatt J, Boone C, Emili A, Houry WA (2005) Navigating the chaperone network: an integrative map of physical and genetic interactions mediated by the hsp90 chaperone. Cell 120:715–727
19. Zhao R, Houry WA (2007) Molecular interaction network of the Hsp90 chaperone system. Adv Exp Med Biol 594:27–36
20. Gong Y, Kakihara Y, Krogan N, Greenblatt J, Emili A, Zhang Z, Houry WA (2009) An atlas of chaperone-protein interactions in Saccharomyces cerevisiae: implications to protein folding pathways in the cell. Mol Syst Biol 5:275
21. Larance M, Lamond AI (2015) Multidimensional proteomics for cell biology. Nat Rev Mol Cell Biol 16:269–280
22. Costanzo M, VanderSluis B, Koch EN, Baryshnikova A, Pons C, Tan G, Wang W, Usaj M, Hanchard J, Lee SD, Pelechano V, Styles EB, Billmann M, van Leeuwen J, van Dyk N, Lin ZY, Kuzmin E, Nelson J, Piotrowski JS, Srikumar T, Bahr S, Chen Y, Deshpande R, Kurat CF, Li SC, Li Z, Usaj MM, Okada H, Pascoe N, San Luis BJ, Sharifpoor S, Shuteriqi E, Simpkins SW, Snider J, Suresh HG, Tan Y, Zhu H, Malod-Dognin N, Janjic V, Przulj N, Troyanskaya OG, Stagljar I, Xia T, Ohya Y, Gingras AC, Raught B, Boutros M, Steinmetz LM, Moore CL, Rosebrock AP, Caudy AA, Myers CL, Andrews B, Boone C (2016) A global genetic interaction network maps a wiring diagram of cellular function. Science 353:aaf1420
23. Baryshnikova A, Costanzo M, Kim Y, Ding H, Koh J, Toufighi K, Youn JY, Ou J, San Luis BJ, Bandyopadhyay S, Hibbs M, Hess D, Gingras AC, Bader GD, Troyanskaya OG, Brown GW, Andrews B, Boone C, Myers CL (2010) Quantitative analysis of fitness and genetic interactions in yeast on a genome scale. Nat Methods 7:1017–1024
24. Oliver S (2000) Guilt-by-association goes global. Nature 403:601–603
25. Baryshnikova A (2016) Systematic functional annotation and visualization of biological networks. Cell Syst 2:412–421

26. Boucher B, Jenna S (2013) Genetic interaction networks: better understand to better predict. Front Genet 4:290
27. Krogan NJ, Cagney G, Yu H, Zhong G, Guo X, Ignatchenko A, Li J, Pu S, Datta N, Tikuisis AP, Punna T, Peregrin-Alvarez JM, Shales M, Zhang X, Davey M, Robinson MD, Paccanaro A, Bray JE, Sheung A, Beattie B, Richards DP, Canadien V, Lalev A, Mena F, Wong P, Starostine A, Canete MM, Vlasblom J, Wu S, Orsi C, Collins SR, Chandran S, Haw R, Rilstone JJ, Gandi K, Thompson NJ, Musso G, St Onge P, Ghanny S, Lam MH, Butland G, Altaf-Ul AM, Kanaya S, Shilatifard A, O'Shea E, Weissman JS, Ingles CJ, Hughes TR, Parkinson J, Gerstein M, Wodak SJ, Emili A, Greenblatt JF (2006) Global landscape of protein complexes in the yeast Saccharomyces cerevisiae. Nature 440:637–643
28. Wodak SJ, Pu S, Vlasblom J, Seraphin B (2009) Challenges and rewards of interaction proteomics. Mol Cell Proteomics 8:3–18
29. Babu M, Vlasblom J, Pu S, Guo X, Graham C, Bean BD, Burston HE, Vizeacoumar FJ, Snider J, Phanse S, Fong V, Tam YY, Davey M, Hnatshak O, Bajaj N, Chandran S, Punna T, Christopolous C, Wong V, Yu A, Zhong G, Li J, Stagljar I, Conibear E, Wodak SJ, Emili A, Greenblatt JF (2012) Interaction landscape of membrane-protein complexes in Saccharomyces cerevisiae. Nature 489:585–589
30. Babu M, Krogan NJ, Awrey DE, Emili A, Greenblatt JF (2009) Systematic characterization of the protein interaction network and protein complexes in Saccharomyces cerevisiae using tandem affinity purification and mass spectrometry. Methods Mol Biol 548:187–207
31. Babu M, Kagan O, Guo H, Greenblatt J, Emili A (2012) Identification of protein complexes in Escherichia coli using sequential peptide affinity purification in combination with tandem mass spectrometry. J Vis Exp 69:e4057
32. Hart GT, Lee I, Marcotte ER (2007) A high-accuracy consensus map of yeast protein complexes reveals modular nature of gene essentiality. BMC Bioinformatics 8:236
33. Zhang B, Park BH, Karpinets T, Samatova NF (2008) From pull-down data to protein interaction networks and complexes with biological relevance. Bioinformatics 24:979–986
34. Pu S, Wong J, Turner B, Cho E, Wodak SJ (2009) Up-to-date catalogues of yeast protein complexes. Nucleic Acids Res 37:825–831
35. Wang J, Li M, Deng Y, Pan Y (2010) Recent advances in clustering methods for protein interaction networks. BMC Genomics 11 (Suppl 3):S10
36. Enright AJ, Van Dongen S, Ouzounis CA (2002) An efficient algorithm for large-scale detection of protein families. Nucleic Acids Res 30:1575–1584
37. Loganantharaj R, Cheepala S, Clifford J (2006) Metric for measuring the effectiveness of clustering of DNA microarray expression. BMC Bioinformatics 7(Suppl 2):S5
38. Pu S, Vlasblom J, Emili A, Greenblatt J, Wodak SJ (2007) Identifying functional modules in the physical interactome of Saccharomyces cerevisiae. Proteomics 7:944–960
39. Collins SR, Miller KM, Maas NL, Roguev A, Fillingham J, Chu CS, Schuldiner M, Gebbia M, Recht J, Shales M, Ding H, Xu H, Han J, Ingvarsdottir K, Cheng B, Andrews B, Boone C, Berger SL, Hieter P, Zhang Z, Brown GW, Ingles CJ, Emili A, Allis CD, Toczyski DP, Weissman JS, Greenblatt JF, Krogan NJ (2007) Functional dissection of protein complexes involved in yeast chromosome biology using a genetic interaction map. Nature 446:806–810
40. Rutherford SL, Lindquist S (1998) Hsp90 as a capacitor for morphological evolution. Nature 396:336–342
41. Queitsch C, Sangster TA, Lindquist S (2002) Hsp90 as a capacitor of phenotypic variation. Nature 417:618–624
42. Karras GI, Yi S, Sahni N, Fischer M, Xie J, Vidal M, D'Andrea AD, Whitesell L, Lindquist S (2017) HSP90 shapes the consequences of human genetic variation. Cell 168:856–866
43. Rizzolo K, Huen J, Kumar A, Phanse S, Vlasblom J, Kakihara Y, Zeineddine HA, Minic Z, Snider J, Wang W, Pons C, Seraphim TV, Boczek EE, Alberti S, Costanzo M, Myers CL, Stagljar I, Boone C, Babu M, Houry WA (2017) Features of the chaperone cellular network revealed through systematic interaction mapping. Cell Rep 20:2735–2748

Chapter 21

Immunohistochemistry of Human Hsp60 in Health and Disease: From Autoimmunity to Cancer

Francesco Cappello, Everly Conway de Macario, Francesca Rappa, Giovanni Zummo, and Alberto J.L. Macario

Abstract

Hsp60 (also called Cpn60) is a chaperonin with essential functions for cell physiology and survival. Additionally, its involvement in the pathogenesis of a variety of diseases (e.g., some autoimmune disorders and cancer) is becoming evident with new research. For example, the distribution and levels of Hsp60 in cells and tissues have been found altered in many pathologic conditions, and the significance of these alterations is being investigated in a number of laboratories. The aim of this ongoing research is to determine the meaning of these Hsp60 alterations with regard to pathogenetic mechanisms, diagnosis, classification of lesions, and assessing prognosis and response to treatment.

Hsp60 occurs in the mitochondria, i.e., its typical residence according to classic knowledge, and also in other locales, such as the cytosol, the cell membrane, the intercellular space, and biological fluids (e.g., blood and cerebrospinal fluid). Detection and quantitative determinations in all these locations are becoming essential components of laboratory pathology in clinics and research. Consequently, immunohistochemistry targeting Hsp60 is also becoming essential for pathologists and researchers interested in disorders involving this chaperonin.

In this chapter, we summarize some recent discoveries on the participation of Hsp60 in the pathogenesis of human diseases, and describe in detail how to perform immunohistochemical reactions for detecting the chaperonin, determining its location, and measuring its quantitative levels.

Key words Hsp60, Chaperonin Hsp60, Hsp60 immunohistochemistry, Hsp60 immunostaining, Hsp60 in tissues, Hsp60 locations, Hsp60 in cancer, Hsp60 and autoimmunity, Molecular mimicry, Hsp60 antibodies

1 Introduction

Hsp60 is a chaperonin conserved in evolution, typically described as a mitochondrial molecule (named Cpn60) related to bacterial GroEL that works together with Hsp10 (evolutionarily related to bacterial GroES) in assisting the correct folding of other mitochondrial proteins [1, 2]. However, we now know that in mammalian cells up to 40% of cellular Hsp60 occurs in extra-mitochondrial sites

Stuart K. Calderwood and Thomas L. Prince (eds.), *Chaperones: Methods and Protocols*, Methods in Molecular Biology, vol. 1709, https://doi.org/10.1007/978-1-4939-7477-1_21,

(e.g., cytosol and cell membrane) in normal and pathological tissues [3–5].

A number of in vivo studies have revealed that the levels of cytosolic Hsp60 gradually increase or decrease during the carcinogenetic steps that go from normal tissue through dysplasia to carcinoma in various organs [4, 6–9]. These data stimulated the use of Hsp60 as a biomarker for assessing diagnosis and prognosis of pre-neoplastic and neoplastic lesions [4, 8, 10].

In addition, the presence of Hsp60 on the cell membrane (mHsp60) has been noted in normal [11], stressed [12], and tumor [13, 14] cells and was thought to be associated with membrane transport and signaling [15–17]. An increase in mHsp60 levels (which may be accompanied by Hsp60 release into circulation) is considered a danger signal for the immune system since it can lead to the activation of innate and/or adaptive immune responses [18–21].

Interestingly, mHsp60 occurs on the cell surface of certain tumors [14], associated with p21ras protein [22] and/or alpha-3-beta-1 integrin, the latter involved in the adhesion of metastatic breast-cancer cells to lymph nodes and bone tissue [23]. This chaperonin favors cell proliferation through its ability to survive to apoptotic stimuli in different types of tumors [24]. It has also been shown that mHsp60 plays a role in the metastatization of pancreatic carcinoma [13] and that it occurs on the surface of oral tumor cells, participating in the mechanism of the tumor-cell lysis induced by gammadelta-T lymphocytes [25]. In vitro experiments have demonstrated that photodynamic therapy induces an increase of mHsp60 which may be taken to indicate that Hsp60 could be used as target antigen in anticancer immunotherapy [26–29].

Other than with carcinogenesis, Hsp60 has been associated with several diseases [30], particularly those with autoimmune components [31, 32] like atherosclerosis [33–38], systemic autoimmune vasculitis [39–41], degenerative joint diseases [42–44], autoimmune glomerulonephritis [45, 46], juvenile dermatomyositis [47], cutaneus disease [48, 49], and neurological disorders including epilepsy [50]. In some of these diseases, molecular mimicry of human and microbial Hsp60 has been postulated as the pathogenic mechanism [51, 52]. For instance, Hsp60 from eukaryotes shares about 50% identical amino acids with prokaryotic (e.g., bacterial pathogens) counterparts [51, 53]. This high similarity in primary structure implies common antigenic sites, which would react with cross-reactive antibodies [51, 54]. Exogenous Hsp60 from a microbe elicits an immune response in humans that although directed primarily against the microbial molecule will also recognize the endogenous chaperonin [55]. Thus, Hsp60 provides a link between infection and development of autoimmune diseases [51], as postulated for arthritis [56], multiple sclerosis

[57], mialgic encephalomyelitis [58], diabetes [59], myasthenia gravis [60], and inflammatory bowel diseases [51, 61].

The findings summarized above and the identification of the chaperonopathies as an important group of newly recognized disorders [30, 62] have stimulated interest in Hsp60 in physicians, including oncologists, immunologists, and pathologists, who study this molecule to learn about its presence and degree of expression in human tissues and to correlate their findings with disease onset and progression, and response to treatment [63].

In this chapter, we describe methods to perform immunohistochemistry for Hsp60 in normal and pathological human tissues, in order to detect and localize the chaperonin and to assess its levels.

Although molecular techniques (e.g., PCR) are nowadays gaining in importance not only in research but also in diagnostics (e.g., in surgical pathology), immunohistochemistry still represents the "gold standard," the reference technique in many laboratories for protein identification in situ. This is because of the potential of immunohistochemistry to identify, localize, and assess the quantity of a protein while at the same time providing information on the cell type (normal, tumoral, epithelial, stromal, etc.) in which the protein (e.g., Hsp60) is expressed, and the characteristics (e.g., normal or pathologic) of the structures in the vicinity. Thus, immunohistochemistry provides a range of information not only on the protein itself but also on its surroundings. The methods we describe are applicable to a large variety of tissues and proteins, such as Hsp60 and also other Hsp-chaperones by just substituting the pertinent specific antibodies.

Essentially, the methodology we will describe is based on the principle that if Hsp60 is present in a histological section fixed onto a glass slide it will react with anti-Hsp60 antibody (i.e., the primary antibody). To make visible this reaction, a biothinylated secondary antibody directed against the primary antibody serves as a bridge for a signal-emitting compound, such as the enzyme peroxidase. The latter is linked to streptavidine, which has high affinity for the biotin in the secondary antibody and, therefore, it will bind to the complex primary/biotinylated secondary antibody when the complex is bound to the histological section because the ligand for the primary antibody, i.e., Hsp60, is present in the tissue. The following step consists of revealing and assessing the signal. If the sign-emitting molecule is an enzyme such as peroxidase, its presence will be revealed by adding an enzyme substrate that, upon enzymatic action, yields a compound that produces a colored precipitate (the visible signal) in the tissue, exactly on the spot in which Hsp60 is located. In a simplistic way it can be said that if there is no signal, the conclusion is that Hsp60 is not present in the tissue tested. On the contrary, if there is signal, the conclusion is that the bigger the signal the more Hsp60 occurs in the tissue. However, controls must

be run with every test to rule out false positive and false negative results, as will be explained later.

2 Materials (*See* also Notes 1–15 for Important Details)

1. Ten staining jars.
2. One staining humid tray.
3. Hydrophobic marker pen (PAP pen).
4. Xylene (stored at 23 °C).
5. Alcohol, both absolute and 96°, and distilled water (all stored at 23 °C).
6. Aqueous 3% H_2O_2 (stored at 4 °C).
7. Dulbecco's phosphate-buffered saline (PBS) (stored at 23 °C).
8. 10% Bovine Serum Albumin (BSA), or ready-to-use protein blocking solution, serum-free (both stored at 4 °C).
9. Primary antibody for Hsp60 (stored as indicated by the supplier) to be diluted in the diluent provided with the antibodies, or a similar commercially available alternative (both stored at 4 °C). Make a fresh dilution, following the directions in the antibody instructions-datasheet; this dilution is stable at 4 °C for variable periods of times (few hours to few days), depending on the antibody.
10. Ready-to-use biotinylated secondary antibodies diluted in PBS (stored at 4 °C).
11. Ready-to-use streptavidin-peroxidase complex diluted in PBS (stored at 4 °C).
12. Ready-to-use chromogen (i.e., aminoethilcarbazole or diaminobenzidine). These reagents must be used with caution since they are highly toxic and light sensitive, and must always be manipulated wearing protective gloves. Store at 4 °C in the dark.
13. Sodium hypochlorite.
14. Ready-to-use aqueous haematoxylin (stored at 4 °C).
15. Ready-to-use aqueous mounting medium (stored at 23 °C).

3 Methods

Immunohistochemical procedure to demonstrate the presence of Hsp60 on formalin-fixed paraffin-embedded histological sections on glass slides. All the steps are carried out at 23 °C. **Steps 1–4, 8, 11, 13, 15, 18, 19**, and **20** are to be done in appropriate staining jars. **Steps 6, 7, 9, 10**, **12, 14**, and **16** have to be performed in a humid

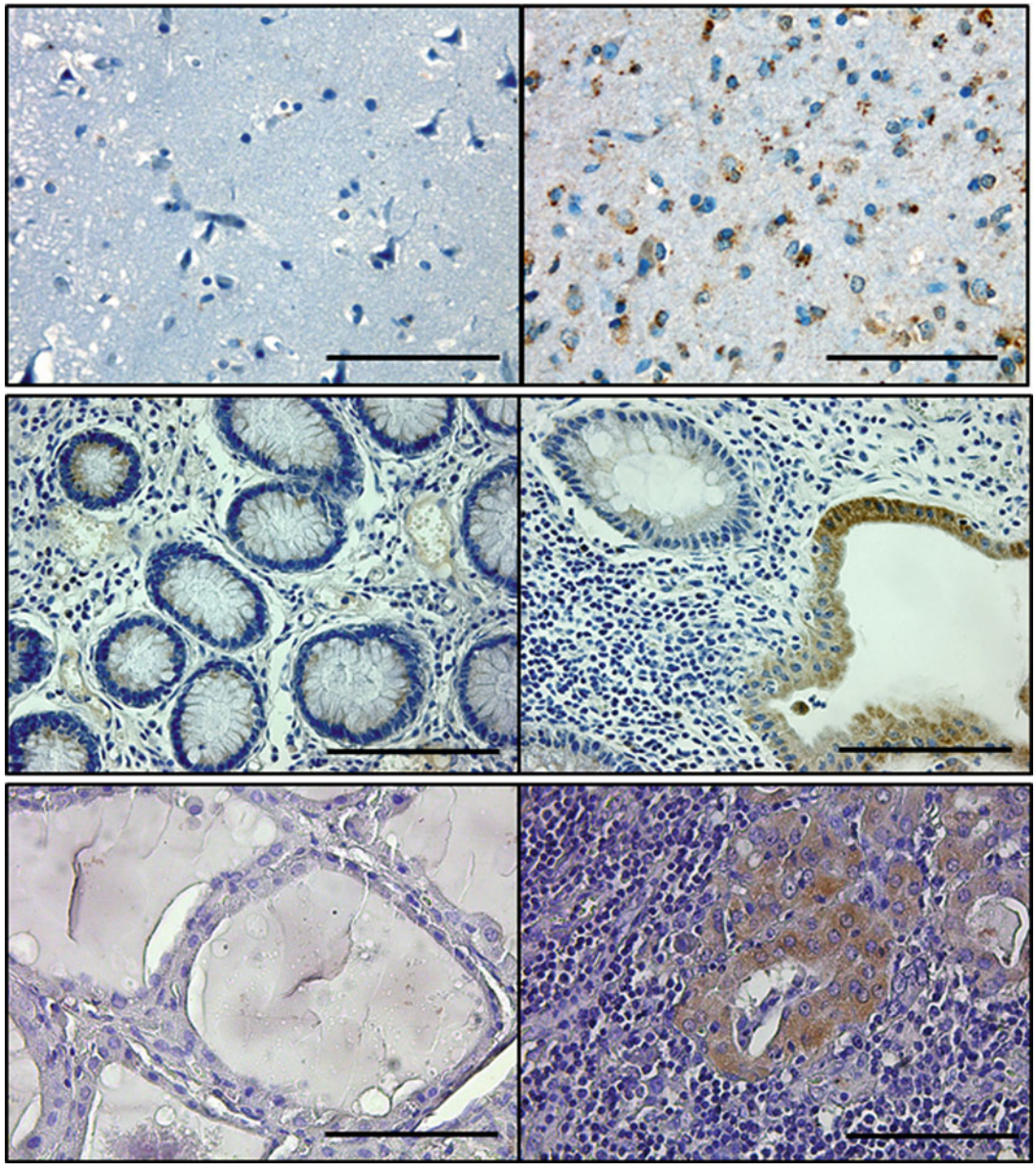

Fig. 1 Representative images of immunostaining for Hsp60. The three panels on the *right* show intense positivity for Hsp60 (*brown*) in contrast with the almost absence of reaction on the control tissues on the left as follows: normal brain (*top panel*), normal colonic mucosa (*central panel*), and thyroid goiter (*bottom panel*). On the right, intense cytoplasmic positivity for Hsp60 in samples from astrocytoma (top panel), epithelial cells of chronically inflamed mucosa from Crohn's disease (central panel), and oncocytic metaplasia area of Hashimoto Thyroiditis (*bottom panel*). Magnification 400×; *scale bar*: 100 μm

staining tray (put a sheet of wet laboratory paper on the bottom of the tray) protected with a cover to transform the tray into a closed chamber. "Slide" in what follows means glass slide with a histological thin section onto it (Fig. 1) (Attention: Please, *see* **Notes 1–15** for important details).

1. Remove wax from the slides ("dewaxing" procedure) by immersing them in xylene for 10 min, twice.
2. Clear with absolute alcohol for 5 min, once.
3. Dehydrate slides passing them through a series of alcohols, from 96° through 80°/70°/50° to 30°, one time, 5 min for each alcohol.
4. Place the slides in distilled water for 5 min to remove excess alcohol.
5. Blot away (with absorbent paper) excess water from the slides: first allow water to drain and then gently dry the slide with appropriate absorbent paper. Encircle the histological section on the slide with the PAP pen to make it visible throughout the steps that follow.
6. Place the slides horizontally in the humid tray on the wet paper at the bottom or, better still, place the slides on glass rods placed parallel to each other like rails separated by the distance necessary to provide support at each end of the slides.
7. Apply on the top of the section a drop of aqueous 3% H_2O_2 for 10 min (to block the tissue's endogenous peroxidase).
8. Rinse the slides with fresh PBS for 5 min. Drain excess PBS and dry the slides as above (**step 5**).
9. Apply 10% BSA (or protein-blocking serum-free solution) for 10 min.
10. Do not rinse the slides with PBS but, after blotting excess of blocking solution, apply directly diluted Hsp60 primary antibody onto the section. Simultaneously, apply normal serum to the negative control section in the negative control slide. Likewise, in the positive control slide, apply a primary antibody known to give a positive reaction in the tissue under examination (for example, antibody anti-cytokeratins will give a positive reaction in colon cancer specimens). Keep all the reagents on the slides for 1 h in the humid tray now closed with a cover, so it becomes a humid chamber (evaporation must be avoided at all costs!).
11. Rinse the slides twice with PBS, each for 5 min. Drain PBS and dry the slides (*see* **step 5**).
12. Apply biotinylated secondary antibody to all sections for 15 min (in the humid chamber).
13. Rinse the slides twice with PBS, each for 5 min. Drain PBS and dry the slides (*see* **step 5**).

14. Apply streptavidin peroxidase complex to all the sections for 15 min (in the humid chamber).
15. Rinse the slides twice with PBS, each for 5 min. Drain PBS and dry the slides (as above).
16. Apply chromogen for 9 min (or as indicated in the instructions-datasheet provided by the supplier), in the humid chamber.
17. Rinse off chromogen from the slides into the staining tray and add into the tray 5–10 drops of sodium hypochlorite to inactivate the chromogen.
18. Rinse the slides twice with fresh water, each for 5 min. Drain water and dry the slides (*see* above).
19. Apply hematoxylin for 1–2 min for counterstaining.
20. Rinse the slides twice with fresh water, each for 5 min. Drain water and dry the slides (see above).
21. Mount coverslips with an aqueous mounting medium.
22. Examine the slides microscopically: positive stain (presence of Hsp60) appears brown or red (depending on the chromogen: red for aminoethilcarbazole or dark brown for diaminobenzidine).
23. A common light microscope equipped with 4×, 10×, 20×, and 40× objectives and 10× eyepieces is suitable to the examination of the stained slides. The magnifications obtained by combining these objectives with 10× eyepieces are 40-, 100-, 200-, and 400-fold, respectively, each providing complementary information in a way that the final result, after examining the section at all these magnifications, is a complete set of immunohistochemical information. The lowest magnification provides a panoramic view of the section and the general characteristics of the reaction (e.g., highly localized or generalized and, if localized, in only one or few spots as opposed to many spots). As the magnification increases, more details of the cells positive and negative for Hsp60 become evident. It also becomes possible to tell whether the positive reaction (indicating presence of Hsp60) is located, for example, in the epithelium but not in the connective tissue or, when there is a tumor, it is possible to determine where the positivity occurs, namely in the tumor or in the surrounding normal tissue. At the highest magnification it is possible to ascertain whether the positivity is in the cell nucleus, or in the cytoplasm, or in the membrane.

4 Notes

1. Perform the same immunostaining in two serial sections, to compare them. If immunopositivity differs in the two series, technical problems are likely and the procedure must be repeated with new slides.
2. Before the start, mark with a pencil the side and part of the slide in which the histological section lies, to be sure throughout the procedure of the location of the section. Also, enumerate the slides to be tested, using Arabic numbers.
3. It is better to prepare the antibody dilution as a first step, before starting dewaxing the slides. Keep the diluted antibody at 4 °C, ready for use.
4. Dewax and rehydrate sections under a chemical hood, to avoid personal exposure to xylene and alcohols vapors (*see* Subheading 3, **step 1**).
5. Make alcohol dilutions frequently, so they do not become altered due to evaporation and hydration and to minimize these problems keep the alcohols in sealed bottles (*see* Subheading 3, **step 2**).
6. After rinsing the slides with PBS carefully drain excess PBS and dry (*see* Subheading 3, **step 5**) outside the PAP pen circle (*see* Subheading 3, **step 5**) but keep wet the section inside the circle. It helps to use a small square of adsorbent paper (2 cm each side) to dry the slides.
7. Verify using a spirit bubble level that the staining tray is perfectly horizontal, to avoid that the reagent solutions cover the section unevenly: the reagent solutions must cover the section completely and evenly (*see* Subheading 3, **step 6**).
8. Make sure that each reagent (i.e., aqueous 3% H_2O_2, primary antibody dilution, biotinylated secondary antibody, streptavidin, and chromogen) added on the slide covers the histological section completely; the section must never be dry (*see* Subheading 3, **steps 7**, **10**, **12**, **14**, and **16**).
9. PBS solution should be made fresh the same day of use, or at most 1 day before. Check the pH (it must be 7.2–7.4) (*see* Subheading 3, **steps 8**, **11**, **13**, and **15**).
10. Many antibodies need antigen retrieval to improve the demonstration of antigens. It consists of a pretreatment with an antigen retrieval solution that breaks the protein cross-links formed by formalin fixation and thereby uncovers hidden antigenic sites. Some antibodies for Hsp60 do not need antigen retrieval before staining; we strongly suggest buying this kind of antibodies, since antigen retrieval may alter integrity of the

section and thus alter the quality of the results (*see* Subheading 3, **step 10**).

11. Calculate a final volume of 20–100 μL of diluted antibody solution for each section, depending on its size (*see* Subheading 3, **step 10**).
12. Some chromogens are not sold "ready-to-use" but they consist of two components that must be mixed a few minutes before use. The mixing procedure is quite simple and it can be done during the step (15 min) of streptavidin incubation (*see* Subheading 3, **step 16**).
13. Make sure to wear good quality gloves without wholes of any size when handling chromogen and sodium hypochlorite (*see* Subheading 3, **steps 16** and **17**).
14. For mounting the coverslip, put it on the bench, put a little drop of aqueous mounting medium over it, and put the slide with the immunostaining over the drop. Wait a few seconds until the drop spreads toward the borders of the slide, thus covering all the section. Blot away excess of liquid with a small square of adsorbent paper (*see* Subheading 3, **step 21**).
15. Microscopic examination (*see* Subheading 3, **steps 22** and **23**) to analyze the reaction on the histological section must be preceded by an evaluation at various magnifications of the reaction quality. Here, the pathologist's experience plays a deciding role. One must learn how to detect false positives, for example. If the negative control slide is positive, it is very likely that the reaction in the experimental slides produced false positives. Clues in this regard are given by looking at the cells that are known beforehand that they do not contain the antigen one is looking for and, if these cells are positive, the conclusions are that the reaction did not go well and produced false positives, and that the test must be repeated. On the contrary, if the positive control slide does not show the expected positivity in terms of intensity and distribution, it is highly likely that the reaction in the experimental slides will show a false negativity. In the experimental slides, if the cells that should have been positive are not, the conclusion is that the test produced false negatives, which is often confirmed by a general lack of reaction in all the areas. The test should be repeated. Obviously, the preceding guidelines are not always applicable in their entirety, but at least some of them always are, and these should be the tenets for a complete evaluation of slide and reaction quality and, when this is satisfactory, the examination of the slide and the recording of results can be done with confidence.

Acknowledgments

A.J.L.M. and E.C. de M. were partially supported by IMET; A.J.L.M. and F.C. were partially supported by IEMEST. This work was done under the umbrella of the agreement between the Euro-Mediterranean Institute of Science and Technology (IEMEST; Italy) and the Institute of Marine and Environmental Technology (IMET; USA) signed March 2012 (this is IMET contribution number IMET 17-195). In this work were used instruments provided by the Euro-Mediterranean Institute of Science and Technology, and funded by the Italian National Operational Programme for Research and Competitiveness 2007–2013 grant (Project code: PONa3_00210, European Regional Development Fund).

References

1. Levy-Rimler G, Bell RE, Ben-Tal N, Azem A (2002) Type I chaperonins: not all are created equal. FEBS Lett 529:1–5
2. Hansen JJ, Bross P, Westergaard M, Nielsen MN, Eiberg H, Borglum AD, Mogensen J, Kristiansen K, Bolund L, Gregersen N (2003) Genomic structure of the human mitochondrial chaperonin genes: HSP60 and HSP10 are localised head to head on chromosome 2 separated by a bidirectional promoter. Hum Genet 112:71–77
3. Soltys BJ, Gupta RS (1999) Mitochondrial proteins at unexpected cellular locations: export of proteins from mitochondria from an evolutionary perspective. Int Rev Cytol 194:133–196
4. Cappello F, Conway de Macario E, Marasà L, Zummo G, Macario AJL (2008) Hsp60 expression, new locations, functions and perspectives for cancer diagnosis and therapy. Cancer Biol Ther 7:801–809
5. Macario AJL, Conway de Macario E (2008/2009) The chaperoning system: physiology and pathology. In: Gerbino A, Crescimanno G, Zummo G (eds) Experimental medicine reviews, vol 2/3. Plumelia, Bagheria, Italy, pp 9–21
6. Cappello F, Bellafiore M, Palma A, David S, Marciano V, Bartolotta T, Sciume C, Modica G, Farina F, Zummo G, Bucchieri F (2003) 60 kDa chaperonin (HSP60) is overexpressed during colorectal carcinogenesis. Eur J Histochem 47:105–110
7. Rappa F, Farina F, Zummo G, David S, Campanella C, Carini F, Tomasello G, Damiani P, Cappello F, Conway de Macario E, Macario AJL (2012) HSP-molecular chaperones in cancer biogenesis and tumor therapy: an overview. Anticancer Res 32:5139–5150
8. Campanella C, Rappa F, Sciumè C, Marino Gammazza A, Barone R, Bucchieri F, David S, Curcurù G, Caruso Bavisotto C, Pitruzzella A, Geraci G, Modica G, Farina F, Zummo G, Fais S, Conway de Macario E, Macario AJL, Cappello F (2015) Heat shock protein 60 levels in tissue and circulating exosomes in human large bowel cancer before and after ablative surgery. Cancer 121:3230–3239
9. Rappa F, Unti E, Baiamonte P, Cappello F, Scibetta N (2013) Different immunohistochemical levels of Hsp60 and Hsp70 in a subset of brain tumors and putative role of Hsp60 in neuroepithelial tumorigenesis. Eur J Histochem 57:e20
10. Hamelin C, Cornut E, Poirier F, Pons S, Beaulieu C, Charrier JP, Haïdous H, Cotte E, Lambert C, Piard F, Ataman-Önal Y, Choquet-Kastylevsky G (2011) Identification and verification of heat shock protein 60 as a potential serum marker for colorectal cancer. FEBS J 278:4845–4859
11. Soltys BJ, Gupta RS (1997) Cell surface localization of the 60 kDa heat shock chaperonin protein (hsp60) in mammalian cells. Cell Biol Int 21:315–320
12. Lin L, Kim SC, Wang Y, Gupta S, Davis B et al (2007) HSP60 in heart failure: abnormal distribution and role in cardiac myocyte apoptosis. Am J Physiol Heart Circ Physiol 293: H2238–H2247
13. Piselli P, Vendetti S, Vismara D, Cicconi R, Poccia F et al (2000) Different expression of CD44, ICAM-1, and HSP60 on primary

tumor and metastases of a human pancreatic carcinoma growing in scid mice. Anticancer Res 20:825–831

14. Shin BK, Wang H, Yim AM, Le Naour F, Brichory F et al (2003) Global profiling of the cell surface proteome of cancer cells uncovers an abundance of proteins with chaperone function. J Biol Chem 278:7607–7616
15. Dziewanowska K, Carson AR, Patti JM, Deobold CF, Bayles KW et al (2000) Staphylococcal fibronectin binding protein interacts with heat shock protein 60 and integrins: role in internalization by epithelial cells. Infect Immun 68:6321–6328
16. Merendino AM, Bucchieri F, Campanella C, Marcianò V, Ribbene A et al (2010) Hsp60 is actively secreted by human tumor cells. PLoS One 5:e9247
17. Campanella C, Bucchieri F, Merendino AM, Fucarino A, Burgio G et al (2012) The odyssey of Hsp60 from tumor cells to other destinations includes plasma membrane-associated stages and Golgi and exosomal protein-trafficking modalities. PLoS One e42008:7
18. Osterloh A, Meier-Stiegen F, Veit A, Fleischer B, von Bonin A et al (2004) Lipopolysaccharide-free heat shock protein 60 activates T cells. J Biol Chem 279:47906–47911
19. Chen W, Syldath U, Bellmann K, Burkart V, Kolb H (1999) Human 60- kDa heat shock protein: a danger signal to the innate immune system. J Immunol 162:3212
20. Marino Gammazza A, Rizzo M, Citarrella R, Rappa F, Campanella C et al (2014) Elevated blood Hsp60, its structural similarities and cross-reactivity with thyroid molecules, and its presence on the plasma membrane of oncocytes point to the chaperonin as an immunopathogenic factor in Hashimoto's thyroiditis. Cell Stress Chaperones 19:343–353
21. Quintana FJ, Cohen IR (2011) The HSP60 immune system network. Trends Immunol 32:89–95
22. Ikawa S, Weinberg RA (1992) An interaction between p21ras and heat shock protein hsp60, a chaperonin. Proc Natl Acad Sci U S A 89:2012–2016
23. Barazi HO, Zhou L, Templeton NS, Krutzsch HC, Roberts DD (2002) Identification of heat shock protein 60 as a molecular mediator of alpha 3 beta 1 integrin activation. Cancer Res 62:1541–1548
24. Ghosh JC, Dohi T, Kang BH, Altieri DC (2008) Hsp60 regulation of tumor cell apoptosis. J Biol Chem 283:5188–5194
25. Laad AD, Thomas ML, Fakih AR, Chiplunkar SV (1999) Human gamma delta T cells recognize heat shock protein-60 on oral tumor cells. Int J Cancer 80:709–714
26. Hanlon JG, Adams K, Rainbow AJ, Gupta RS, Singh G (2001) Induction of Hsp60 by Photofrin-mediated photodynamic therapy. J Photochem Photobiol B 64:55–61
27. Jalili A, Makowski M, Switaj T, Nowis D, Wilczynski GM et al (2004) Effective photoimmunotherapy of murine colon carcinoma induced by the combination of photodynamic therapy and dendritic cells. Clin Cancer Res 10:4498–4508
28. Korbelik M, Sun J, Cecic I (2005) Photodynamic therapy-induced cell surface expression and release of heat shock proteins: relevance for tumor response. Cancer Res 65:1018–1026
29. Pace A, Barone G, Lauria A, Martorana A, Piccionello AP et al (2013) Hsp60, a novel target for antitumor therapy: structure-function features and prospective drugs design. Curr Pharm Des 19:2757–2764
30. Macario AJL, Conway de Macario E (2004) The pathology of anti-stress mechanisms: a new frontier. Stress 7:243–249
31. Landstein D, Ulmansky R, Naparstek Y ((2015)) HSP60: a double edge sword in autoimmunity. Oncotarget 6:32299–32300
32. Raska M, Weigl E (2005) Heat shock proteins in autoimmune diseases. Biomed Pap Med Fac Univ Palacky Olomouc Czech Repub 149:243–249
33. Xu Q, Schett G, Perschinka H, Mayr M, Egger G et al (2000) Serum soluble heat shock protein 60 is elevated in subjects with atherosclerosis in a general population. Circulation 102:14–20
34. Rizzo M, Macario AJL, Conway de Macario E, Gouni-Berthold I, Berthold HK et al (2011) Heat shock protein-60 and risk for cardiovascular disease. Curr Pharm Des 17:3662–3668
35. Wick G, Jakic B, Buszko M, Wick MC, Grundtman C (2014) The role of heat shock proteins in atherosclerosis. Nat Rev Cardiol 11:516–529
36. Almanzar G, Öllinger R, Leuenberger J, Onestingel E, Rantner B et al (2012) Autoreactive HSP60 epitope-specific T-cells in early human atherosclerotic lesions. J Autoimmun 39:441–450
37. Grundtman C, Kreutmayer SB, Almanzar G, Wick MC, Wick G (2011) Heat shock protein 60 and immune inflammatory responses in atherosclerosis. Arterioscler Thromb Vasc Biol 31:960–968

38. Matsuura E, Kobayashi K, Matsunami Y, Shen L, Quan N et al (2009) Autoimmunity, infectious immunity, and atherosclerosis. J Clin Immunol 29:714–721
39. Alard JE, Dueymes M, Youinou P, Jamin C (2008) HSP60 and anti-HSP60 antibodies in vasculitis: they are two of a kind. Clin Rev Allergy Immunol 35:66–71
40. Rauch J, Dieudé M, Subang R, Levine JS (2010) The dual role of innate immunity in the antiphospholipid syndrome. Lupus 19:347–353
41. Choi B, Choi M, Park C, Lee EK, Kang DH et al (2015) Cytosolic Hsp60 orchestrates the survival and inflammatory responses of vascular smooth muscle cells in injured aortic vessels. Cardiovasc Res 106:498–508
42. Krenn V, Vollmers HP, von Landenberg P, Schmausser B, Rupp M (1996) Immortalized B lymphocytes from rheumatoid synovial tissue show specificity for bacterial HSP60. Virchows Arch 427:511–518
43. Vercoulen Y, van Teijlingen NH, de Kleer IM, Kamphuis S, Albani S et al (2009) Heat shock protein 60 reactive T cells in juvenile idiopathic arthritis: what is new? Arthritis Res Ther 11:231
44. Huang MN, Yu H, Moudgil KD (2010) The involvement of heat-shock proteins in the pathogenesis of autoimmune arthritis: a critical appraisal. Semin Arthritis Rheum 40:164–175
45. Lang A, Benke D, Eitner F, Engel D, Ehrlich S et al (2005) Heat shock protein 60 is released in immune-mediated glomerulonephritis and aggravates disease: in vivo evidence for an immunologic danger signal. J Am Soc Nephrol 16:383–391
46. Slot MC, Theunissen R, van Paassen P, Damoiseaux JG, Cohen Tervaert JW (2006) Evaluation of antibodies against human HSP60 in patients with MPO-ANCA associated glomerulonephritis: a cohort study. J Autoimmune Dis 5:3–4
47. Elst EF, Klein M, de Jager W, Kamphuis S, Wedderburn LR et al (2008) Hsp60 in inflamed muscle tissue is the target of regulatory autoreactive T cells in patients with juvenile dermatomyositis. Arthritis Rheum 58:547–555
48. Kasperkiewicz M, Tukaj S, Gembicki AJ, Silló P, Görög A et al (2014) Evidence for a role of autoantibodies to heat shock protein 60, 70, and 90 in patients with dermatitis herpetiformis. Cell Stress Chaperones 19:837–843
49. Seung NR, Park EJ, Kim CW, Kim KH, Kim KJ et al (2007) Comparison of expression of heat-shock protein 60, toll-like receptors 2 and 4, and T-cell receptor gammadelta in plaque and guttate psoriasis. J Cutan Pathol 34:903–911
50. Marino Gammazza A, Colangeli R, Orban G, Pierucci M, Di Gennaro G, Lo Bello M, D'Aniello A, Bucchieri F, Pomara C, Valentino M, Muscat R, Benigno A, Zummo G, Conway de Macario E, Cappello F, Di Giovanni G, Macario AJL (2015) Hsp60 response in exper- imental and human temporal lobe epilepsy. Sci Rep 5:9434
51. Tomasello G, Rodolico V, Zerilli M, Martorana A, Bucchieri F et al (2011) Changes in immunohistochemical levels and subcellular localization after therapy and correlation and colocalization with CD68 suggest a pathogenetic role of Hsp60 in ulcerative colitis. Appl Immunohistochem Mol Morphol 19:552–561
52. Cappello F, Conway de Macario E, Di Felice V, Zummo G, Macario AJL (2009) Chlamydia trachomatis infection and anti-Hsp60 immunity: the two sides of the coin. PLoS Pathog 5:e1000552
53. Karlin S, Brocchieri L (2000) Heat shock protein 60 sequence comparisons: duplications, lateral transfer, and mitochondrial evolution. Proc Natl Acad Sci U S A 97:11348–11353
54. Zügel U, Kaufmann SH (1999) Role of heat shock proteins in protection from and pathogenesis of infectious diseases. Clin Microbiol Rev 12:19–39
55. Pockley AG (2003) Heat shock proteins as regulators of the immune response. Lancet 362:469–476
56. Res PC, Schaar CG, Breedveld FC, van Eden W, van Embden JD et al (1988) Synovial fluid T cell reactivity against 65kDa heat shock protein of mycobacteria in early chronic arthritis. Lancet 2:478–480
57. Georgopoulos C, Mc Farland H (1993) Heat shock proteins in multiple sclerosis and other autoimmune diseases. Immunol Today 14:373–375
58. Elfaitouri A, Herrmann B, Bölin-Wiener A, Wang Y, Gottfries CG et al (2013) Epitopes of microbial and human heat shock protein 60 and their recognition in myalgic encephalomyelitis. PLoS One 8:e8115
59. Child D, Smith C, Williams C (1993) Heat shock protein and the double insult theory for the development of insulin-dependent diabetes. J R Soc Med 86:217–219
60. Gammazza AM, Bucchieri F, Grimaldi LM, Benigno A, Conway de Macario E et al (2012) The molecular anatomy of human Hsp60 and its similarity with that of bacterial

orthologs and acetylcholine receptor reveal a potential pathogenetic role of anti-chaperonin immunity in myasthenia gravis. Cell Mol Neurobiol 32:943–947

61. Rodolico V, Tomasello G, Zerilli M, Martorana A, Pitruzzella A et al (2010) Hsp60 and Hsp10 increase in colon mucosa of Crohn's disease and ulcerative colitis. Cell Stress Chaperones 15:877–884
62. Macario AJL, Conway de Macario E (2005) Sick chaperones, cellular stress and disease. N Engl J Med 353:1489–1501
63. Cappello F, Marino Gammazza A, Palumbo Piccionello A, Campanella C, Pace A et al (2014) Hsp60 chaperonopathies and chaperonotherapy:targets and agents. Expert Opin Ther Targets 18:185–208

Chapter 22

Immunohistochemical and Flow Cytometric Analysis of Intracellular and Membrane-Bound Hsp70, as a Putative Biomarker of Glioblastoma Multiforme, Using the cmHsp70.1 Monoclonal Antibody

Stefan Stangl, Gemma A. Foulds, Helena Fellinger, Geoffrey J. Pilkington, A. Graham Pockley, and Gabriele Multhoff

Abstract

The major stress-inducible 70 kDa heat shock (stress) protein 70 (Hsp70) is frequently overexpressed in highly aggressive tumor cells and thus might serve as a tumor-specific biomarker of aggressive disease. We have previously shown that, in contrast to normal cells, tumor cells present Hsp70 on their plasma membrane. In order to elucidate the role of intracellular and membrane-bound Hsp70 as a potential tumor biomarker in glioblastoma multiforme, herein, we describe protocols for the staining of cytosolic Hsp70 in tumor formalin fixed paraffin-embedded (FFPE) sections using immunohistochemistry, and for plasma membrane-bound Hsp70 by multi-parametric flow cytometry using the cmHsp70.1 monoclonal antibody (mAb).

Key words Intracellular and membrane-bound heat shock protein 70 (Hsp70), Glioblastoma multiforme, Formalin fixed paraffin-embedded (FFPE) sections, Immunohistochemistry, Flow cytometry, Hsp70 antibody epitope

1 Introduction

Although great progress in the treatment of many cancers has been achieved, glioblastoma multiforme (GBM) remains a debilitating and life-threatening disease. Comprising nearly 75% of all the cases, glioblastoma is the most frequent primary malignant tumor of the central nervous system (CNS) and continues to be associated with very poor long-term survival and the worst prognosis of all glial brain tumors (gliomas). Despite improvements in the treatment of glioblastoma using advanced neurosurgical techniques and radiation therapy, there remains no effective cure for this tumor [1]. The average life-expectancy after diagnosis is less than 1 year, and fewer than 10% of patients survive longer than 5 years after diagnosis, even

Stuart K. Calderwood and Thomas L. Prince (eds.), *Chaperones: Methods and Protocols*, Methods in Molecular Biology, vol. 1709, https://doi.org/10.1007/978-1-4939-7477-1_22,

after total tumor resection [1–3]. Administration of the alkylating chemotherapeutic agent Temozolomide (TMZ) only increases median survival rates to approximately 15 months [4–11]. Death from glioblastoma is due to a rapid, aggressive local infiltration of glioblastoma cells in the brain. Moreover, a high genetic tumor heterogeneity can mediate resistance to radio(chemo)therapy. An inherent or acquired resistance to radio(chemo)therapy drastically reduces life expectancy. It is therefore essential to have reliable tumor biomarkers that can identify patients who are likely to acquire resistance to TMZ at an early time point.

The major stress-inducible 70 kDa heat shock (stress) protein Hsp70 is frequently overexpressed in the cytosol for a large variety of different tumor cells and elevated cytosolic Hsp70 levels are often associated with therapy resistance. Therefore, we propose Hsp70 as a potential biomarker of disease in GBM.

Using a unique monoclonal antibody (mAb, cmHsp70.1), the Multhoff laboratory made the seminal discovery that, in addition to its cytosolic localization, Hsp70 is also selectively expressed on the plasma membrane of tumor cells (but not normal tissue) [12–14]. The same laboratory also showed that the expression density of membrane Hsp70 on a broad profile of cancer cell lines is further increased in vitro by standard treatments such as radio (chemo)therapy [15, 16] where it also can confer therapy resistance. Furthermore, membrane Hsp70 is more highly expressed on metastatic disease than its corresponding primary tumor [17], and its expression is associated with an unfavorable prognosis and a reduced overall survival for some tumors [18]. An ongoing screening program of over 1500 patients with various solid tumors in the Multhoff laboratory reveals that more than 50% of all the patients have membrane Hsp70 positive tumors, as identified by flow cytometric analysis of isolated viable tumor cells using the cmHsp70.1 mAb.

These findings indicate that membrane-bound Hsp70 might act as a universal, selective tumor-specific marker of "aggressive" disease. Therefore, it is of importance that, apart from cytosolic Hsp70 levels also the membrane status of Hsp70 should be determined to describe a tumor. Furthermore, membrane-bound Hsp70 also could act as a tumor-specific therapeutic target which enables the development of new approaches for the treatment of GBM such as cell-based therapies. A number of preclinical studies have shown the capacity of ex vivo activated (low-dose IL-2 plus a 14-mer Hsp70-derived peptide, IL-2/TKD) activated NK cells to target a range of cancer cell types expressing the membrane form of Hsp70 [12, 13, 19–24]. Studies have also demonstrated that this cytotoxic effect is manifested by the release and uptake of granzyme B into target cells via membrane Hsp70 [25]. The clinical safety and tolerability of IL-2/TKD activated NK cells has been demonstrated in a Phase I clinical trial [26], and its efficacy for the treatment of patients with

non-small cell lung carcinoma after radiochemotherapy is currently being assessed in a multi-center Phase II clinical trial [27].

We have also previously reported that recombinant human granzyme B binds to membrane Hsp70 on cancer cells and that its subsequent uptake, which results in the selective killing of membrane Hsp70 expressing cells and tumors, occurs via an Hsp70-mediated endocytosis process that is independent of perforin [17, 28]. Taken together, these findings make membrane Hsp70 an excellent and broadly-applicable molecule on which to develop a portfolio of new immunotherapeutics based on ex vivo IL-2/TKD activated NK cells [21, 22, 24, 26, 27, 29], human recombinant granzyme B [17, 25, 28], or Hsp70-targeting antibodies. The membrane-Hsp70-specific antibody (cmHsp70.1) itself can induce antibody-dependent cellular cytotoxicity (ADCC) [14], or can be used for a targeted delivery of therapeutics in the form of antibody-drug conjugates (ADCs) or as a therapeutic "cargo" delivered by nanoparticles.

Membrane Hsp70 has also been used as a basis for the development of innovative imaging platforms for tumor detection and outcome monitoring which employ the cmHsp70.1 monoclonal antibody or a 14-mer tumor penetrating peptide (TPP) [15, 30–32].

Given the established association between membrane Hsp70 expression and disease aggressiveness, and the portfolio of theranostic approaches that are being developed to target tumors expressing membrane Hsp70, techniques for determining the membrane Hsp70 expression by human glioblastoma tissue, and cell lines derived from primary glioblastomas have been established using the cmHsp70.1 mAb. These immunohistochemical and flow cytometry-based approaches are described herein.

2 Materials

2.1 Patient-Derived Glioblastoma Multiforme Cell Lines

The human, low passage glioblastoma (UP007, UP029, and SEBTA027) and brain metastatic lung carcinoma (SEBTA028) cell lines were established in culture at the University of Portsmouth from biopsy tissue obtained at Kings College Hospital London under ethics permission, 11/SC/0048. All the cell lines were cultured in the DMEM growth medium supplemented with 10% v/v fetal bovine serum (FBS).

1. **UP-007** was derived obtained from a 71 year old treatment naive male de novo GBM patient with wild-type IDH1.
2. **UP-029** was derived from a 66 year old treatment naive female de novo GBM patient with wild-type IDH1 and IDH2.

3. **SEBTA-027** was derived from a 59 year old female with recurrent GBM in the right parieto-occipital region, with sarcomatous elements, grade IV, wild-type IDH1, unmethylated MGMT, and a 40% Ki67 labeling in dex and who had previously received radiotherapy and Temozolomide chemotherapy.
4. **SEBTA-028** was derived from a 52 year old male with brain metastatic lung carcinoma in the right temporal-occipital-parietal region.

2.2 Patient- and Preclinical Model-Derived Paraffin-Embedded Tissue

The diagnosis of glioblastoma multiforme was based on hematoloxylin/eosin staining of FFPE sections (2 μm) of two patients with glioblastoma multiforme WHO stage IV. Additionally, sections (2 μm) of orthotopically implanted GL261 mouse glioblastoma were used for the analysis. Ethical approval for access to patient tissue was obtained from the local ethical committee of the Technische Universität München, and informed consent was provided.

2.3 cmHsp70.1 Anti-Hsp70 Monoclonal Antibody (mAb)

The cmHsp70.1 monoclonal antibody (mAb, multimmune GmbH, Munich, Germany), which selectively binds to membrane Hsp70 on tumor cells, was generated by immunization of mice with the 14-mer peptide TKDNNLLGRFELSG, termed "TKD," comprising amino acids 450–461 ($aa_{450–461}$) in the C terminus of the inducible Hsp70. Since the human and murine "TKD" sequences only differ in one amino acid (T**K**DNNLLGRFELSG; mouse T**R**DNNLLGRFELSG) [33], and the minimal antibody epitope (NNLLGRF) is identical among different species [14], the human cmHsp70.1 mAb shows cross-reactivity for human, mouse, canine, and feline tumors.

The "TKD" sequence that is exposed to the extracellular milieu of tumors resides in the C-terminally localized oligomerization domain which is part of the substrate binding domain of the Hsp70 molecule [34]. In contrast to other commercially available Hsp70 antibodies, the cmHsp70.1 mAb uniquely identifies the membrane form of Hsp70 on viable human and mouse tumor cells not only in vitro but also in vivo in tumor-bearing mice [30].

In contrast to the cmHsp70.1 mAb, other commercially available mouse antibodies directed against Hsp70 fail to stain the surface of viable tumor cells.

2.4 Immunohistochemistry (IHC)

2.4.1 Deparaffinization Reagents

1. Xylene.
2. Ethanol absolute 100% v/v.
3. Ethanol 96% v/v.
4. Ethanol 70% v/v.
5. Ethanol 50% v/v.
6. $H_2O_{dd.}$

2.4.2 Target Retrieval and Staining Reagents

1. Target retrieval solution: $1\times/H_2O_{dd}$, $0.5\times$ H_2O_{dd} (DAKO cat #: S1699).
2. Peroxidase blocking solution: 3% v/v H_2O_2/0.1% w/v sodium azide/Phosphate-buffered saline (PBS).
3. Protein blocking solution: 5% v/v rabbit serum/antibody diluent (DAKO REAL antibody diluent, cat #: S2022).
4. Phosphate-buffered saline (PBS).
5. Murine IgG1 anti-Hsp70 monoclonal antibody cmHsp70.1: working solution 1: 500 in antibody diluent (multimmune GmbH, Munich).
6. Horseradish peroxidase (HRP)-conjugated rabbit anti-mouse polyclonal antibody: DAKO EnVision + system HRP-conjugated rabbit anti-mouse polyclonal antibody.
7. DAB (3,3′-diaminobenzidine): DAKO liquid DAB+ Substrate and Chromogen System.

2.5 Flow Cytometry

1. Cells of interest.
2. Fc receptor (FcR)-blocking immunoglobulin (Ig; e.g., normal rat IgG) solution, 200 μg/ml or specific Fc blocking reagents that are suitable for use in the species of interest.
3. Carboxyfluorescein or FITC-conjugated cmHsp70.1 IgG1 murine anti-Hsp70 monoclonal antibody (multimmune GmbH).
4. Carboxyfluorescein or FITC-conjugated IgG1 murine monoclonal antibody to Hsp70 (clone C92F3A, StressMarq Biosciences Inc. *see* Subheading 4).
5. Appropriately conjugated murine immunoglobulin (Ig) isotype controls.
6. Phosphate-buffered saline (PBS) supplemented with 0.1% w/v sodium azide (NaN_3) and bovine serum albumin (BSA) (PAB; *see* recipe below).
7. Nuclear/membrane integrity (viability) staining compound dissolved in PBS: 200 μg/ml PI [alternative options include 250 μg/ml 7-AAD, 250 μg/ml TO-PRO-3 (Molecular Probes), or 200 μg/ml PY(G)]—*see* Subheading 4.

2.5.1 PBS, pH 7.2, Supplemented with Sodium Azide (NaN_3) and Fetal Bovine Serum (FBS)

1. Dulbecco's PBS, Ca^{2+}- and Mg^{2+}-free (e.g., Life Technologies), containing:
2. 0.1% (w/v) sodium azide.
3. 10% (w/v) fetal bovine serum (FBS).
4. Adjust pH to 7.2 using 1 N NaOH or 1 N HCl.
5. Filter solution through 0.22 μm membrane.
6. Store up to 1 month at 4 °C.

7. EDTA (1 mM) can be added to reduce cellular aggregation.

CAUTION: Always keep cells and reagents at 4 °C. Be extremely careful when handling sodium azide.

3 Methods

3.1 Immunohistochemistry (IHC)

IHC must be performed on formalin-fixed, paraffin-embedded (FFPE) tissue sections (2 μm) using a rabbit anti-mouse polyclonal antibody staining kit (DAKO). In brief, tissue sections were boiled by microwaving for 30 min in target retrieval buffer (DAKO) to unmask the epitope. Between each of the following incubation steps, sections were washed in PBS (Sigma). Nonspecific binding must be blocked in a protein blocking solution for 60 min. Slides must be incubated overnight at 4 °C with cmHsp70.1 mAb (multimmune GmbH) or with a corresponding IgG control (Sigma). After washing, the sections are incubated with the HRP-conjugated anti-mouse polyclonal antibody, followed by the DAB chromogen reaction to detect the binding of the primary antibody. Nuclei are counterstained with hematoxylin and sections embedded in embedding medium.

3.1.1 Rehydration

1. Xylene I & II	2 × 15 min
2. Ethanol absolute I & II	2 × 10 min
3. Ethanol 96%	2 × 5 min
4. Ethanol 70%	1 × 5 min
5. Ethanol 50%	1 × 5 min
6. H_2O_{dd}	1 × 5 min

3.1.2 Target Retrieval and Staining

1. Target retrieval solution	1 × 30 min boiling (microwave)
2. Cooling down period	1 × 10 min in target retrieval solution
3. H_2O_{dd}	1 × 2 min
4. Marking of the section with a hydrophobic pen	
5. Peroxidase blocking solution	1 × 30 min
6. H_2O_{dd}	3 × 5 min
7. Protein blocking solution	1 × 60 min

(continued)

8. PBS	2 × 5 min
9. cmHsp70.1 mAb (1:500)	Overnight (4 °C)
10. PBS	2 × 5 min
11. Envision + System HRP Labelled anti-mouse polymer	1 × 30 min (RT)
12. PBS	1 × 5 min
13. Dab	1 × 4 min
14. H_2O_{dd}	1 × 5 min
15. Counterstain with hematoxylin	1 × 30 s
16. Rinse with warm tab water	1 × 5 min

3.1.3 Dehydration and Embedding

1. Ethanol 50%	1 × 5 min
2. Ethanol 70%	1 × 5 min
3. Ethanol 96% II & II	2 × 5 min
4. Ethanol absolute III & IV	2 × 5 min
5. Xylene III & IV	2 × 10 min
6. Embedding (Eukitt)	

CAUTION: Keep the time of the chromogen reaction exactly at 4 min and use sections of the same thickness (2 μm) in order to be able to compare staining intensities of different experiments. Always run reference sections with a defined staining intensity as an internal control.

3.1.4 Scoring Criteria of IHC Using cmHsp70.1 mAb

The staining intensity must be analyzed semi-quantitatively within the tumor area. The staining intensity of tumor cells is graded into different scores: normal (+), intermediate (++), strong (+++). Normal tissues are graded as weak (+/−). The localization of the staining (cytosolic, nuclear) as well as the percentage of positively stained cells must be considered. The scoring must be performed by at least two independent researchers.

3.2 Flow Cytometry

1. Prepare single-cell suspensions of tumor cells in ice-cold PBS supplemented with 10% (v/v) FBS (PBS/FBS).
2. Dispense 1×10^5 cells into microcentrifuge tubes.
3. Pellet the cells by centrifugation for 5 min at 500 × *g*, 4 °C.

4. Remove the supernatant by vacuum aspiration.
5. Add 4 μl ice-cold cmHsp70.1 mAb (1 μg/μl) to the pellet containing approximately 50 μl PBS/FBS, resuspend and vortex the tubes slightly.
6. Incubate the tubes for 30 min on ice and wash in ice-cold PBS/FBS.
7. Resuspend the cell pellet in 300 μl PBS/FBS.
8. Add 3 μl PI to tube (*Alternatively, add 4 μl 7-AAD, 4 μl TO-PRO-3, or 5 μl PY(G)*.
9. Incubate th cells on ice for 5 min.
10. Analyze the cells using a flow cytometer immediately thereafter.
11. Keep samples on ice during analysis.
12. Prolonged periods before analyzing them are generally not recommended.

4 Notes

4.1 Immunohistochemistry (IHC) Scoring

Every nucleated human cell type expresses the stress-inducible Hsp70 at low levels in the cytosol, whereas the membrane-bound form of Hsp70 appears to be restricted to tumor cells. Given that the cmHsp70.1 antibody can stain both, the membrane-bound and cytosolic forms of Hsp70 and that approximately 70%–90% of the total Hsp70 is residing intracellularly, it is nearly impossible to distinguish between the membrane-bound and cytosolic localizations of Hsp70 by IHC. Therefore, membrane-bound Hsp70 must be determined by flow cytometry of viable cells with intact plasma membranes, whereas cytosolic Hsp70 can be determined by IHC. It is well known that highly aggressive tumor cells show a higher expression density and a different subcellular localization of Hsp70 compared to normal cells. Therefore, the intensity and the subcellular distribution (cytosol, membrane, nucleus) of Hsp70 can be considered tumor-specific characteristics. Since no human cell type is completely negative for cytosolic Hsp70, different Hsp70 staining intensities rather than Hsp70 negative and Hsp70 positive phenotypes can be distinguished. For a comparable scoring of different staining intensities in different IHC staining procedures, it is key to run control sections (tumor and normal tissue sections) as a reference. The thickness of the sections must be exactly 2 μm to be able to correctly score different staining intensities. Apart from the staining intensity, many glioblastomas show a heterogeneous staining pattern within the tumor tissue. Therefore, it is also necessary to determine the percentage of the field which shows a certain staining intensity. Finally, the subcellular distribution of the Hsp70

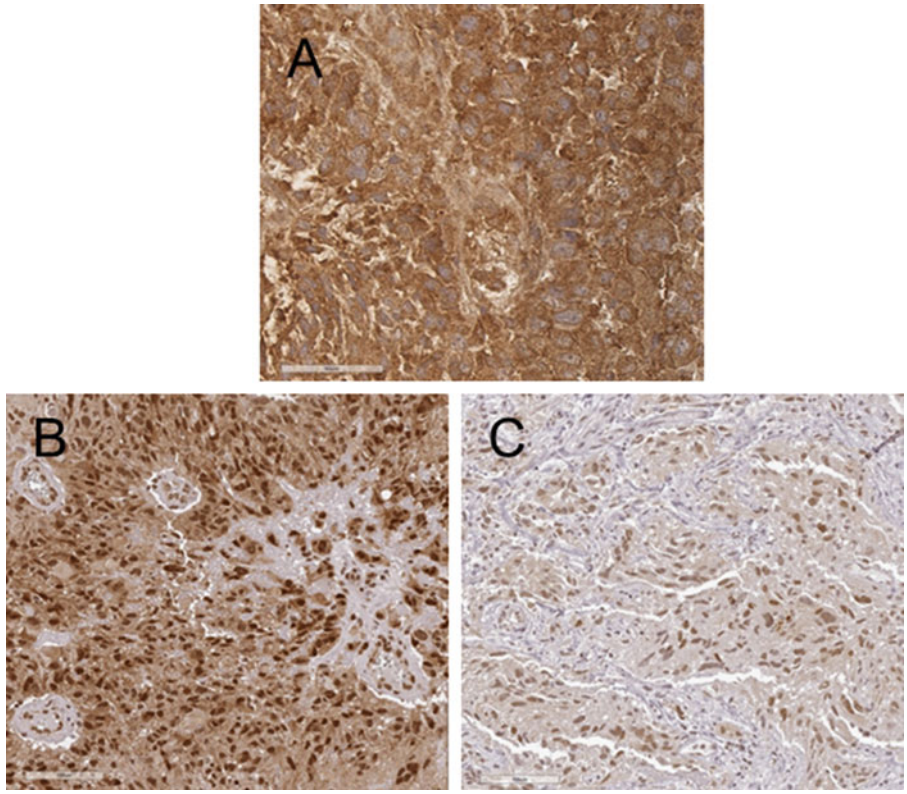

Fig. 1 Representative immunohistochemical (IHC) staining patterns of sections (2 μm) of GL261 mouse glioblastoma (**a**), human glioblastoma multiforme WHO grade IV (**b**, **c**) with cmHsp70.1 mAb. Staining intensity scores are as follows: A: +++, B: +++, C: +. Panel A shows a typical cytosolic staining pattern, panels B and C show representative examples of a cytosolic and nuclear staining pattern

staining also needs to be considered. Figure 1 provides a typical example of strong and weak staining intensity in the nucleus and the cytosol in the tumor of a single patient with GBM.

4.2 Flow Cytometry

The inclusion of the IgG1 murine monoclonal antibody to Hsp70 (clone C92F3A, StressMarq Biosciences Inc) in the staining protocol is essential to determine the amount of Hsp70 which is bound to receptors such as TLRs or scavenger receptors on the cell surface of tumor cells. This antibody does not stain the confirmation of lipid bound Hsp70 in the plasma membrane of tumor cells.

Although cell viability should routinely be assessed in all flow cytometric analyses, as nonviable cells and debris can nonspecifically take up and bind probes and antibodies and so must be excluded from phenotypic analysis, it is particularly essential for the specific analysis of membrane Hsp70 expression by flow cytometry, as cells

having a compromised cell membrane will be highly positive for intracellular Hsp70 expression. Nonviable cells might also exhibit a higher level of autofluorescence and/ or release DNA which can promote cell clumping and aggregation. Cell aggregation can be inhibited by including a small amount of DNAse in the staining solution, and nonviable cells can be excluded from the analysis using viability stains.

The viability of cultured cells can be quite low, however cell death during sample processing can be minimized by performing all cell preparations and staining procedures (including wash steps) at 4 °C or on ice and in the presence of bovine serum albumin (BSA) or heat-inactivated fetal bovine serum (FBS). Cells should be analyzed in a flow cytometer as soon as possible. **Cells should not be fixed when analyzing the expression of membrane Hsp70.**

The best method for excluding dead cells from data analysis is to use a vital DNA dye in all the samples. Although some of the more common vital dyes used in multicolor analyses are propidium iodide (PI), 7-aminoactinomycin D (7-AAD), TO-PRO-3, and pyronin Y(G) [PY(G)], a range of options are now available from commercial suppliers. A note of caution is that dyes such as PI and 7-AAD can be taken up into viable cells over time, and so these stains should be added immediately prior to analysis.

The relatively broad emission spectrum of 7-AAD can result in spectral overlap into other detectors and require considerable compensation in large multi-parameter panels. It is also quite a "dim" fluorescent molecule.

The far-red viability dye DRAQ7™ (Biostatus Ltd., UK) can be used in similar settings to PI and 7-AAD. A particularly useful feature of DRAQ7™ is that its dual excitation characteristics allow multibeam excitation and the exclusion of dead (DRAQ7+) cells without "consuming" what could be a vital additional fluorescent channel. Figure 2 provides a panel of typical flow cytometry results of membrane Hsp70 expression in patient-derived cancer cell lines.

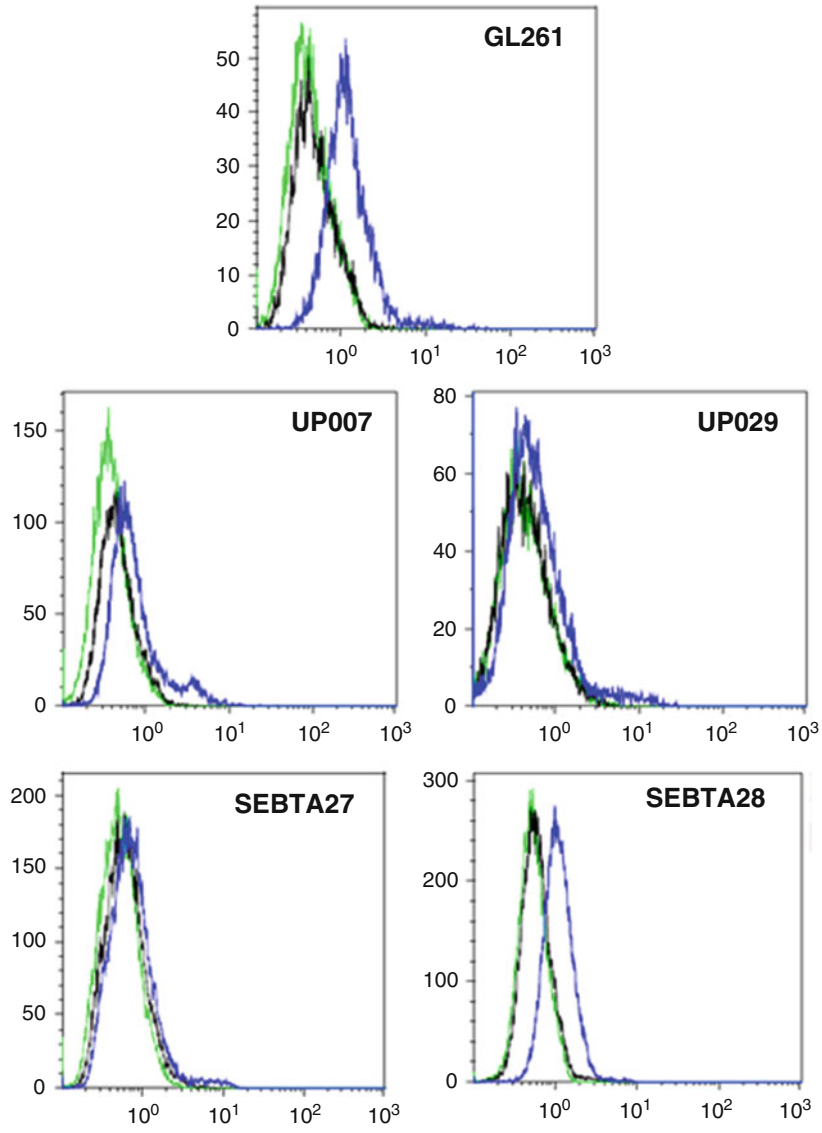

Fig. 2 Representative flow cytometric histograms illustrating membrane Hsp70 expression by a panel of patient-derived cell lines, as described in the main body of the text. GL261 tumors were induced via intracranial injection of methylcholanthrene followed by serial intracranial and subcutaneous transplantations of tumor fragments into syngeneic C57BL/6 mice. *Green*—unstained control; *black*—stained using the C92F3A clone mAb; *blue*—stained using the cmHsp70.1 clone mAb

Acknowledgments

Gabriele Multhoff is supported by grants of the Deutsche Forschungsgemeinschaft (SFB824/2; DFG INST95/980-1 FUGG, INST411/37-1 FUGG), the DFG Cluster of Excellence: Munich-Centre for Advanced Photonics (MAP), the Bundesministerium für Forschung und Technologie (BMBF Innovative Therapies,

01GU0823; Kompetenzverbund Strahlenforschung 02NUK038A), EU-CELLEUROPE (315963) and the German Cancer Consortium Radiation Oncology Group, Munich (DKTK-ROG).
The John van Geest Cancer Research Centre is supported by funding from the John and Lucille van Geest Foundation, Nottingham Trent University, the European Regional Development Fund (ERDF) via the Healthcare and Bioscience iNET, as delivered by Medilink East Midlands, UK and the Headcase Cancer Trust.
The University of Portsmouth Brain Tumour Research Centre is core funded by Brain Tumour Research.

References

1. Burton EC, Prados MD (2000) Malignant gliomas. Curr Treat Options in Oncol 1 (5):459–468
2. Nieder C, Grosu AL, Molls M (2000) A comparison of treatment results for recurrent malignant gliomas. Cancer Treat Rev 26 (6):397–409
3. Dazzi C, Cariello A, Giannini M, Del Duca M, Giovanis P, Fiorentini G, Leoni M, Rosti G, Turci D, Tienghi A, Vertogen B, Zumaglini F, De Giorgi U, Marangolo M (2000) A sequential chemo-radiotherapeutic treatment for patients with malignant gliomas: a phase II pilot study. Anticancer Res 20(1B):515–518
4. Barrié M, Couprie C, Dufour H, Figarella-Branger D, Muracciole X, Hoang-Xuan K, Braguer D, Martin PM, Peragut JC, Grisoli F, Chinot O (2005) Temozolomide in combination with BCNU before and after radiotherapy in patients with inoperable newly diagnosed glioblastoma multiforme. Ann Oncol: Off J Eur Soc Med Oncol/ESMO 16 (7):1177–1184
5. Combs SE, Gutwein S, Thilmann C, Debus J, Schulz-Ertner D (2005) Reirradiation of recurrent WHO grade III astrocytomas using fractionated stereotactic radiotherapy (FSRT). Strahlentherapie und Onkologie: Organ der Deutschen Rontgengesellschaft [et al] 181 (12):768–773
6. Combs SE, Thilmann C, Edler L, Debus J, Schulz-Ertner D (2005) Efficacy of fractionated stereotactic reirradiation in recurrent gliomas: long-term results in 172 patients treated in a single institution. J Clin Oncol: Off J Am Soc Clin Oncol 23(34):8863–8869
7. Combs SE, Wagner J, Bischof M, Welzel T, Wagner F, Debus J, Schulz-Ertner D (2008) Postoperative treatment of primary glioblastoma multiforme with radiation and concomitant temozolomide in elderly patients. Int J Radiat Oncol Biol Phys 70(4):987–992
8. Combs SE, Wagner J, Bischof M, Welzel T, Edler L, Rausch R, Wagner F, Zabel-du Bois A, Debus J, Schulz-Ertner D (2008) Radiochemotherapy in patients with primary glioblastoma comparing two temozolomide dose regimens. Int J Radiat Oncol Biol Phys 71(4):999–1005
9. Frenay M, Lebrun C, Lonjon M, Bondiau PY, Chatel M (2000) Up-front chemotherapy with fotemustine (F)/cisplatin (CDDP)/etoposide (VP16) regimen in the treatment of 33 - non-removable glioblastomas. Eur J Cancer 36(8):1026–1031
10. Stupp R, Mason WP, van den Bent MJ, Weller M, Fisher B, Taphoorn MJ, Belanger K, Brandes AA, Marosi C, Bogdahn U, Curschmann J, Janzer RC, Ludwin SK, Gorlia T, Allgeier A, Lacombe D, Cairncross JG, Eisenhauer E, Mirimanoff RO, European Organisation for R, Treatment of Cancer Brain T, Radiotherapy G, National Cancer Institute of Canada Clinical Trials G (2005) Radiotherapy plus concomitant and adjuvant temozolomide for glioblastoma. N Engl J Med 352(10):987–996
11. Stupp R, Hegi ME, Mason WP, van den Bent MJ, Taphoorn MJ, Janzer RC, Ludwin SK, Allgeier A, Fisher B, Belanger K, Hau P, Brandes AA, Gijtenbeek J, Marosi C, Vecht CJ, Mokhtari K, Wesseling P, Villa S, Eisenhauer E, Gorlia T, Weller M, Lacombe D, Cairncross JG, Mirimanoff RO (2009) Effects of radiotherapy with concomitant and adjuvant temozolomide versus radiotherapy alone on survival in glioblastoma in a randomised phase III study: 5-year analysis of the EORTC-NCIC trial. Lancet Oncol 10 (5):459–466

12. Multhoff G, Botzler C, Wiesnet M, Eissner G, Issels R (1995) CD3$^-$ large granular lymphocytes recognize a heat-inducible immunogenic determinant associated with the 72-kD heat shock protein on human sarcoma cells. Blood 86:1374–1382
13. Multhoff G, Botzler C, Wiesnet M, Muller E, Meier T, Wilmanns W, Issels RD (1995) A stress-inducible 72-kDa heat-shock protein (HSP72) is expressed on the surface of human tumor cells, but not on normal cells. Int J Cancer 61:272–279
14. Stangl S, Gehrmann M, Riegger J, Kuhs K, Riederer I, Sievert W, Hube K, Mocikat R, Dressel R, Kremmer E, Pockley AG, Friedrich L, Vigh L, Skerra A, Multhoff G (2011) Targeting membrane heat-shock protein 70 (Hsp70) on tumors by cmHsp70.1 antibody. Proc Natl Acad Sci U S A 108 (2):733–738
15. Gehrmann M, Stangl S, Foulds GA, Oellinger R, Breuninger S, Rad R, Pockley AG, Multhoff G (2014) Tumor imaging and targeting potential of an hsp70-derived 14-mer peptide. PLoS One 9(8):e105344
16. Gehrmann M, Pfister K, Hutzler P, Gastpar R, Margulis B, Multhoff G (2002) Effects of antineoplastic agents on cytoplasmic and membrane-bound heat shock protein 70 (Hsp70) levels. Biol Chem 383:1715–1725
17. Gehrmann M, Stangl S, Kirschner A, Foulds GA, Sievert W, Doss BT, Walch A, Pockley AG, Multhoff G (2012) Immunotherapeutic targeting of membrane hsp70-expressing tumors using recombinant human granzyme B. PLoS One 7(7):e41341
18. Pfister K, Radons J, Busch R, Tidball JG, Pfeifer M, Freitag L, Feldmann HJ, Milani V, Issels R, Multhoff G (2007) Patient survival by Hsp70 membrane phenotype: association with different routes of metastasis. Cancer 110:926–935
19. Multhoff G, Botzler C, Jennen L, Schmidt J, Ellwart J, Issels R (1997) Heat shock protein 72 on tumor cells: a recognition structure for natural killer cells. J Immunol 158:4341–4350
20. Multhoff G, Hightower LE (2011) Distinguishing integral and receptor-bound heat shock protein 70 (Hsp70) on the cell surface by Hsp70-specific antibodies. Cell Stress Chaperones 16(3):251–255
21. Multhoff G, Pfister K, Gehrmann M, Hantschel M, Gross C, Hafner M, Hiddemann W (2001) A 14-mer Hsp70 peptide stimulates natural killer (NK) cell activity. Cell Stress Chaperones 6(4):337–344
22. Multhoff G, Pfister K, Botzler C, Jordan A, Scholz R, Schmetzer H, Burgstahler R, Hiddemann W (2000) Adoptive transfer of human natural killer cells in mice with severe combined immunodeficiency inhibits growth of Hsp70-expressing tumors. Int J Cancer 88:791–797
23. Gross C, Hansch D, Gastpar R, Multhoff G (2003) Interaction of heat shock protein 70 peptide with NK cells involves the NK receptor CD94. Biol Chem 384:267–279
24. Gross C, Holler E, Stangl S, Dickinson A, Pockley AG, Asea AA, Mallappa N, Multhoff G (2008) An Hsp70 peptide initiates NK cell killing of leukemic blasts after stem cell transplantation. Leuk Res 32(4):527–534
25. Gross C, Koelch W, DeMaio A, Arispe N, Multhoff G (2003) Cell surface-bound heat shock protein 70 (Hsp70) mediates perforin-independent apoptosis by specific binding and uptake of granzyme B. J Biol Chem 278 (42):41173–41181
26. Krause SW, Gastpar R, Andreesen R, Gross C, Ullrich H, Thonigs G, Pfister K, Multhoff G (2004) Treatment of colon and lung cancer patients with ex vivo heat shock protein 70-peptide-activated, autologous natural killer cells: a clinical phase I trial. Clin Cancer Res 10:3699–3707
27. Specht HM, Ahrens N, Blankenstein C, Duell T, Fietkau R, Gaipl US, Gunther C, Gunther S, Habl G, Hautmann H, Hautmann M, Huber RM, Molls M, Offner R, Rodel C, Rodel F, Schutz M, Combs SE, Multhoff G (2015) Heat shock protein 70 (Hsp70) peptide activated natural killer (NK) cells for the treatment of patients with non-small cell lung cancer (NSCLC) after Radiochemotherapy (RCTx) - from preclinical studies to a clinical phase II trial. Front Immunol 6:162
28. Gehrmann M, Doss BT, Wagner M, Zettlitz KA, Kontermann RE, Foulds G, Pockley AG, Multhoff G (2011) A novel expression and purification system for the production of enzymatic and biologically active human granzyme B. J Immunol Methods 371(1–2):8–17
29. Milani V, Stangl S, Issels R, Gehrmann M, Wagner B, Hube K, Mayr D, Hiddemann W, Molls M, Multhoff G (2009) Anti-tumor activity of patient-derived NK cells after cell-based immunotherapy--a case report. J Transl Med 7:50
30. Stangl S, Gehrmann M, Dressel R, Alves F, Dullin C, Themelis G, Ntziachristos V, Staeblein E, Walch A, Winkelmann I, Multhoff G (2010) *In vivo* imaging of CT26 mouse tumors by using cmHsp70.1 monoclonal antibody. J Cell Mol Med 15(4):874–887

31. Stangl S, Varga J, Freysoldt B, Trajkovic-Arsic-M, Siveke JT, Greten FR, Ntziachristos V, Multhoff G (2014) Selective *in vivo* imaging of syngeneic, spontaneous, and xenograft tumors using a novel tumor cell-specific hsp70 peptide-based probe. Cancer Res 74 (23):6903–6912
32. Gehrmann MK, Kimm MA, Stangl S, Schmid TE, Noel PB, Rummeny EJ, Multhoff G (2015) Imaging of Hsp70-positive tumors with cmHsp70.1 antibody-conjugated gold nanoparticles. Int J Nanomedicine 10:5687–5700
33. Zhang H, Liu R, Huang W (2007) A 14-mer peptide from HSP70 protein is the critical epitope which enhances NK activity against tumor cells in vivo. Immunol Investig 36(3):233–246
34. Fouchaq B, Benaroudj N, Ebel C, Ladjimi MM (1999) Oligomerization of the 17-kDa peptide-binding domain of the molecular chaperone HSC70. Eur J Biochem 259 (1–2):379–384

Chapter 23

Detection and Analysis of Extracellular Hsp90 (eHsp90)

Stephanie Cortes, Alexander J. Baker-Williams, Mehdi Mollapour, and Dimitra Bourboulia

Abstract

Heat Shock Protein 90 (Hsp90) is a ubiquitous molecular chaperone that comprises about 1–3% of the total cellular protein. Over the last decade, Hsp90 has been detected and studied in the extracellular space (extracellular or eHsp90) of normal and neoplastic cells. Once outside the cell, eHsp90 has been shown to interact with extracellular client proteins and promote their stabilization and function. Cell conditioned media are routinely collected to detect and quantify eHsp90, and determine its interactions with extracellular clients. Finally, targeting specifically the eHsp90 with pharmacologic inhibitors or antibodies that are unable to cross the plasma membrane has been beneficial in inhibiting tumor cell motility and invasion.

Key words Extracellular Heat Shock Protein 90 (eHsp90), Clients, Co-chaperones

1 Introduction

The molecular chaperone Hsp90 is an essential and highly abundant protein in eukaryotes [1, 2]. The Hsp90 chaperone function is regulated by a complex interplay of mechanisms including adenosine triphosphate (ATP)-dependent Hsp90 conformational changes, posttranslational modifications, and interactions with cofactors or co-chaperones, all of which facilitate the optimal function of the chaperone and assist in folding, stabilization, and activation of "client" proteins [3, 4]. Two major isoforms of Hsp90, α and β, are constitutively expressed in the cytoplasm; however, only the Hsp90α is induced in response to cellular stressors.

Although Hsp90 has been considered a predominant cytosolic protein, recent studies have increasingly supported early findings by Eustace et al. that cells (normal and tumor) secrete Hsp90 to the extracellular space, where it could exist as free unbound protein or bound to the cell surface [5]. Following its release, Hsp90α can be detected on the cell surface and in the conditioned media of a variety of tumor cells including HT1080 fibrosarcoma cells and MDA-MD231 breast carcinoma cells [5–7]. Detection of

Stuart K. Calderwood and Thomas L. Prince (eds.), *Chaperones: Methods and Protocols*, Methods in Molecular Biology, vol. 1709, https://doi.org/10.1007/978-1-4939-7477-1_23,

extracellular Hsp90β has been less successful and occasionally studies have resulted in conflicting observations [5, 6, 8]. In contrast, osteosarcoma cells were shown to secrete Hsp90β, with Hsp90α being undetectable [9].

In cancer, increased levels of eHsp90 have been associated with migration, invasion, and metastasis of tumor cells [10, 11]. eHsp90, similarly to the intracellular form, interacts with extracellular client proteins, some found in free form, others cell surface bound [6, 12, 13]. Matrix metalloproteinases (MMP-2 and MMP-9) are secreted proteases shown to interact with eHsp90, and appear to rely on eHsp90 for their stability and activity [14, 15]. Increased expression and hyperactivity of MMPs is a hallmark of tumor development and progression since extensive, irreversible extracellular matrix proteolytic degradation provides a promigratory, proinvasive, and proangiogenic environment for tumor cells [16].

The development of small-molecule inhibitors or anti-eHsp90-specific antibodies that do not readily cross the plasma cell membrane has introduced a unique approach of targeting and inhibiting specifically the extracellular Hsp90 [17, 18]. The non-membrane permeable Hsp90 inhibitor biotinylated ganetespib (STA-12-7191) was recently shown to specifically bind to eHsp90, exhibiting low toxicity in cell viability assays and blocking wound healing and breast cancer cell migration [6]. Anti-eHsp90-specific antibodies have also been used to inhibit eHsp90 function, tumor cell invasion, and metastasis in in vivo human xenograft mouse models [17, 19].

This chapter describes a procedure for detecting, isolating, and characterizing cell secreted, extracellular unbound Hsp90. The protocol includes detailed steps including mammalian cell culture, protein isolation, western blot, and immunoprecipitation/co-immunoprecipitation (Fig. 1).

2 Materials

1. Protein Extraction Buffer (50 mL): 1 mL 1 M Tris pH 7.4, 50 μL 1 M $MgCl_2$, 1 mL 5 M NaCl, 2 mL 500 nM sodium molybdate, 500 μL NP40 IGEPAL (Sigma), 1 Phosphatase inhibitor tablet (Thermo Fisher), 1 Protease inhibitor tablet (Sigma), ~45 mL dH_2O.
2. 10× TBS (1 L): 24.2 g Trizma (Sigma), 80 g NaCl, 13 mL HCl, 1 L dH_2O.
3. 1× TBST (1×, 1 L): 900 mL dH_2O, 100 mL 10× TBS, 1 mL Tween 20 (working solution).

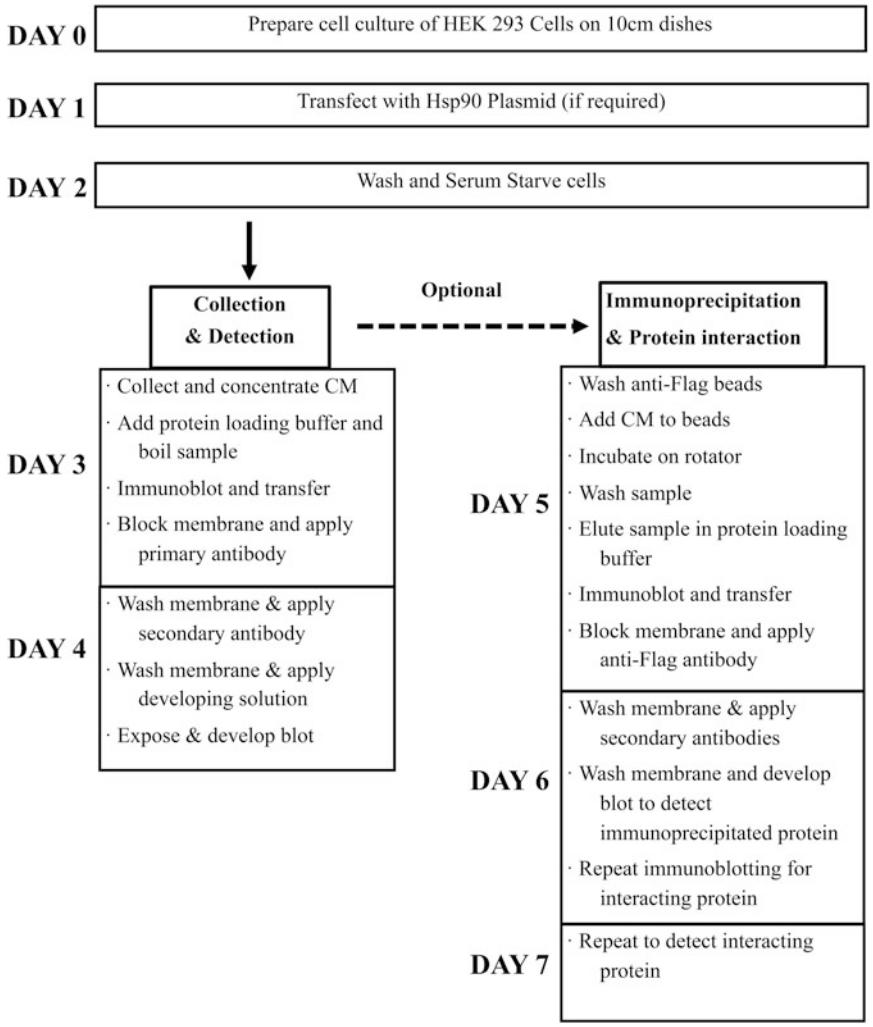

Fig. 1 Schematic representation of the experimental timeline. The experiment is completed in 4–7 days. *CM* cell-conditioned media

4. Protein Loading Buffer (5×, 15 mL): 4.7 mL 1 M Tris pH 6.8, 4.5 mL Glycerol, 1.5 g SDS, 0.75 mL 1% Bromophenol blue, 0.75 mL Beta-mercaptoethanol, ~4.3 mL dH_2O.
5. 10× Running Buffer: 121.2 g Trizma (Sigma), 576.8 g Glycine, 20 g SDS, 3.2 L dH_2O.
6. 10× Transfer Buffer: 800 mL 5× Transfer buffer (Bio-Rad), 800 mL Ethanol, 2.4 L dH_2O.
7. 4–20% Criterion™ Tris–HCl polyacrylamide gel (Bio-Rad).
8. Ponceau S solution (Sigma).
9. Dried skimmed milk.
10. Protran BA85, 0.45 μm Nitrocellulose membrane (Whatman).

11. Thermo Scientific™ Pierce™ ECL 2 Western Blotting Substrate (Thermo Scientific).
12. ECL2 or SuperSignal™ West Femto Maximum Sensitivity Substrate (Thermo Scientific).
13. Rabbit anti-Flag antibody, Cat# PA1-984B, (Thermo Scientific).
14. Rat anti-Hsp90 mAb (16F1), Cat# ADI-SPA-835F (Enzo Life Sciences).
15. Rabbit anti-MMP-2 (D8N9Y) mAb, Cat# 13132 (Cell Signaling Technology).
16. HRP-conjugated secondary antibodies (Santa Cruz, anti-rabbit Cat #sc-2004, anti-rat Cat# sc-2006).
17. X-ray film, X-ray cassette, and X-ray film developing machine.
18. Centrifugal concentrators (Amicon).
19. TransIT-2020 (Muris), transfection reagent for mammalian cells.
20. Dulbecco's Modified Eagle Medium (Sigma).
21. Fetal Bovine Serum (FBS) (Sigma).
22. Phosphate-Buffer Saline (PBS) cell culture grade (Sigma).
23. Hsp90α or β cloned in mammalian expressing vector with Flag tag.
24. Anti-Flag agarose beads (anti-Flag M2 Affinity Gel, Cat#A2220, SIGMA).

3 Methods

3.1 Cell Culture and Immunoblotting (See Note 1)

1. Culture human embryonic kidney (HEK293) cells on a 10 cm plate at 37 °C in a humidified atmosphere of 5% CO_2, in 10% FBS/DMEM culture media for 18 h.
2. Transfect cells using 6 μL of TransIT-2020, 600 μL serum-free DMEM, and plasmid DNA (ranging from 1 μg to 3 μg) per 10 mL complete media per 10 cm plate (*see* **Note 2**).
3. Incubate the cells overnight at 37 °C in a humidified atmosphere of 5% CO_2.
4. Next day remove media and wash the cells gently twice with 5 mL PBS.
5. Serum starve the cells for 24 h with serum-free DMEM (*see* **Note 3**).
6. Next day collect CM (avoiding disruption of attached cell monolayer) (*see* **Note 4**).
7. Centrifuge CM at 4 °C for 5 min at a speed of 94 × *g*.

8. Collect the supernatant. Transfer CM to centrifugal concentrators.
9. Concentrate CM 10× by centrifuging at 2900 × *g* for 5–15 min depending on CM volume (*see* **Note 5**).
10. Add protein loading buffer to sample in a 1:1 ratio.
11. Boil samples for 5 min.
12. Briefly centrifuge sample.
13. Load samples on 4–20% Criterion™ Tris–HCl polyacrylamide gel (Bio-Rad).
14. Run the sample at 200 V until bands are clearly separated in 1× running buffer.
15. Transfer gel onto nitrocellulose membrane.
16. Briefly wash membrane with 1× TBST.
17. Block membrane in 5% milk in 1× TBST for 1 h.
18. Wash membrane three times for 5 min each in 1× TBST.
19. Rock membrane overnight at 4 °C in antibody of interest (5% Milk in 1× TBST).
20. Use rabbit anti-Flag antibody, 1:2000 in 1× TBST 5% milk, incubation for 2 h at room temperature.
21. If endogenous Hsp90 is detected, use primary anti-Hsp90 antibody at 1:2000, overnight incubation at 4 °C.
22. Rabbit anti-MMP-2 antibody, 1:2000 in 1× TBST 5% milk, incubation overnight at 4 °C.
23. Wash membrane three times for 5 min each in 1× TBST.
24. Rock membrane with secondary antibody in 5% milk in 1× TBST for 1 h at room temperature.
25. Anti-rabbit antibody 1:4000 and anti-rat antibody 1:2000, both in 1× TBST 5% milk, incubation for 1 h at room temperature.
26. Wash membrane three times for 5 min each in 1× TBST.
27. Remove 1× TBST and apply developing solution (ECL-2 or SuperSignal™ West Femto Maximum Sensitivity Substrate) to membrane for 3–4 min 24. Remove excess of developing solution (*see* **Note 6**).
28. Place blot on X-ray film cassette.
29. Expose blot to X-ray films for different lengths of time.
30. Detect the Hsp90 protein at ~90 kDa.
31. Detect the MMP-2 protein at ~72 kDa (pro-MMP-2). Occasionally, a second or even a third band between 62 and 67 kDa may be present, corresponding to the intermediate and fully activated MMP-2 forms.

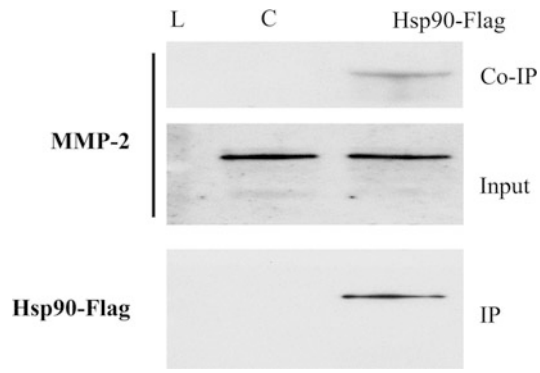

Fig. 2 Detection and immunoprecipitation of Hsp90 from the conditioned media of HEK293 cells. Hsp90-Flag was transfected and media collected for analysis. Immunoprecipitation (IP) of Hsp90 was followed by co-immunoprecipitation (co-IP) of MMP-2. Secreted MMP-2 levels are detected in the CM (input). *L* ladder, *C* control, *IP* immunoprecipitation, *co-IP* co-immunoprecipitation

3.2 Immuno-precpitation and Co-immuno-precipitation (See Note 1)

This protocol describes isolation of secreted Hsp90-Flag and determination of eHsp90-interacting proteins in co-immunoprecipitation experiments. Here, we determine interaction with extracellular protease MMP-2 (Fig. 2).

1. Following the transfection and immunoblotting protocols as described above in 3.1, Hsp90-Flag and MMP-2 expression are determined in CM.
2. Wash 50 μL/sample of anti-Flag beads with 500 μL of 0.1% protein extraction buffer for 30 s at 21,000 × *g*. Repeat this step three times and vortex samples in between washes.
3. Add adjusted volume of concentrated or non-concentrated CM to beads (based on the input levels of the interacting protein MMP-2).
4. Adjust the sample to final volume of 500 μL with 0.1% protein extraction buffer.
5. Rotate samples for 1 h at 4 °C.
6. Centrifuge at 4 °C for 30 s at 845 × *g*. Discard the supernatant and keep the beads pellet.
7. Wash beads twice with 500 μL of 0.1% protein extraction buffer for 30 s at 845 × *g*, and vortex in between washes.
8. Wash with 500 μL of 0.1% protein extraction buffer for 30 s at 21,000 × *g*. Remove the supernatant.
9. Elute protein from beads by adding 60–100 μL 5× protein loading buffer to the beads and heat for 5 min (*see* **Note 7**).
10. Centrifuge at 21,000 × *g* for 30 s. Collect the supernatant containing immunoprecipitated protein. Freeze samples at −80 °C or continue with immunoblot (*see* **Note 8**).

11. Load supernatant samples (5 μL) on 4–20% Criterion™ Tris–HCl polyacrylamide gel (Bio-Rad) to detect the immunoprecipitated Hsp90-Flag.
12. Run gel at 200 V until bands are clearly separated in 1× running buffer.
13. Transfer gel onto nitrocellulose membrane.
14. Wash membrane once with 1× TBST.
15. Block membrane in 5% milk in 1× TBST for 1 h.
16. Wash membrane three times for 5 min in 1× TBST.
17. Rock membrane for 1 h at room temperature with anti-flag antibody in 5% Milk in 1× TBST.
18. Wash membrane three times for 5 min in 1× TBST.
19. Incubate membrane with secondary antibody in 5% milk 1× TBST for 1 h at room temperature.
20. Wash membrane three times for 5 min in 1× TBST.
21. Remove 1× TBST and apply developing solution (ECL-2 or SuperSignal™ West Femto Maximum Sensitivity Substrate) to membrane for 3–4 min.
22. Remove excess developing solution.
23. Place blot on X-ray film cassette.
24. Expose blot to X-ray films for different lengths of time.
25. If inputs of Hsp90-Flag are equal proceed to co-immunoprecipitation.
26. Equalize or run equal volumes of immunoprecipitated samples in new gel and transfer as in **step 13**.
27. Wash blot three times for 5 min with 1× TBST.
28. Block blot for 30 min with 5% milk in 1× TBST.
29. Add anti-MMP-2 antibody (co-immunoprecipitated protein) and incubate overnight at 4 °C.
30. Repeat **steps 18–24**.

4 Notes

1. All the steps involving CM are performed on ice.
2. No need to transfect if endogenous, secreted Hsp90 is the protein of interest.
3. Treatment with drug or antibody should be completed following serum starvation for 24 h.

4. Cell extracts should also be collected if interested in intracellular signaling and to ensure drug/antibody did not pass through cell membrane.
5. If high levels of secreted Hsp90 are expected, no need to concentrate CM.
6. Use Femto if signal not strong enough to be seen with ECL 2.
7. Compete with FLAG peptide if heavy/light chain is close to protein of interest in immunoprecipitation (that applies to Flag-tagged proteins).
8. Store samples (CM, lysates, IPs) at −80 °C if not being used right away.

References

1. Rohl A, Rohrberg J, Buchner J (2013) The chaperone Hsp90: changing partners for demanding clients. Trends Biochem Sci 38:253–262
2. Taipale M, Jarosz DF, Lindquist S (2010) HSP90 at the hub of protein homeostasis: emerging mechanistic insights. Nat Rev Mol Cell Biol 11:515–528
3. Vartholomaiou E, Echeverria PC, Picard D (2016) Unusual suspects in the twilight zone between the Hsp90 interactome and carcinogenesis. Adv Cancer Res 129:1–30
4. Woodford MR, Dunn D, Miller JB, Jamal S, Neckers L, Mollapour M (2016) Impact of posttranslational modifications on the anticancer activity of Hsp90 inhibitors. Adv Cancer Res 129:31–50
5. Eustace BK, Sakurai T, Stewart JK et al (2004) Functional proteomic screens reveal an essential extracellular role for hsp90 alpha in cancer cell invasiveness. Nat Cell Biol 6:507–514
6. McCready J, Wong DS, Burlison JA, Ying W, Jay DG (2014) An impermeant ganetespib analog inhibits extracellular Hsp90-mediated cancer cell migration that involves lysyl oxidase 2-like protein. Cancers (Basel) 6:1031–1046
7. Tsutsumi S, Neckers L (2007) Extracellular heat shock protein 90: a role for a molecular chaperone in cell motility and cancer metastasis. Cancer Sci 98:1536–1539
8. Dong H, Zou M, Bhatia A et al (2016) Breast cancer MDA-MB-231 cells use secreted heat shock protein-90alpha (Hsp90alpha) to survive a hostile hypoxic environment. Sci Rep 6:20605
9. Suzuki S, Kulkarni AB (2010) Extracellular heat shock protein HSP90beta secreted by MG63 osteosarcoma cells inhibits activation of latent TGF-beta1. Biochem Biophys Res Commun 398:525–531
10. Li J, Soroka J, Buchner J (2012) The Hsp90 chaperone machinery: conformational dynamics and regulation by co-chaperones. Biochim Biophys Acta 1823:624–635
11. Wong DS, Jay DG (2016) Emerging roles of extracellular Hsp90 in cancer. Adv Cancer Res 129:141–163
12. Sidera K, Gaitanou M, Stellas D, Matsas R, Patsavoudi E (2008) A critical role for HSP90 in cancer cell invasion involves interaction with the extracellular domain of HER-2. J Biol Chem 283:2031–2041
13. Stellas D, El Hamidieh A, Patsavoudi E (2010) Monoclonal antibody 4C5 prevents activation of MMP2 and MMP9 by disrupting their interaction with extracellular HSP90 and inhibits formation of metastatic breast cancer cell deposits. BMC Cell Biol 11:51
14. Sims JD, McCready J, Jay DG (2011) Extracellular heat shock protein (Hsp)70 and Hsp90alpha assist in matrix metalloproteinase-2 activation and breast cancer cell migration and invasion. PLoS One 6:e18848
15. Song X, Wang X, Zhuo W et al (2010) The regulatory mechanism of extracellular Hsp90 {alpha} on matrix metalloproteinase-2-processing and tumor angiogenesis. J Biol Chem 285:40039–40049
16. Bourboulia D, Stetler-Stevenson WG (2010) Matrix metalloproteinases (MMPs) and tissue inhibitors of metalloproteinases (TIMPs): positive and negative regulators in tumor cell adhesion. Semin Cancer Biol 20:161–168
17. Stellas D, Karameris A, Patsavoudi E (2007) Monoclonal antibody 4C5 immunostains human melanomas and inhibits melanoma cell

invasion and metastasis. Clin Cancer Res 13:1831–1838

18. Tsutsumi S, Scroggins B, Koga F et al (2008) A small molecule cell-impermeant Hsp90 antagonist inhibits tumor cell motility and invasion. Oncogene 27:2478–2487

19. Wang X, Song X, Zhuo W et al (2009) The regulatory mechanism of Hsp90alpha secretion and its function in tumor malignancy. Proc Natl Acad Sci U S A 106:21288–21293

Chapter 24

Molecular Chaperone Receptors

Ayesha Murshid, Jimmy Theriault, Jianlin Gong, and Stuart K. Calderwood

Abstract

Extracellular heat shock proteins (HSP) play important roles in cell signaling and immunity. Many of these effects are mediated by surface receptors expressed on a wide range of cell types. We have investigated the nature of such proteins by cloning candidate receptors into cells (CHO-K1) with the rare property of being null for HSP binding. Using this approach we have discovered that Hsp70 binds avidly to at least two classes of receptors including: (1) c-type lectin receptors (CLR) and (2) scavenger receptors (SR). However, the structural nature of the receptor-ligand interactions is not clear at this time. Hsp70 can bind to LOX-1 (a member of both the CLR and SR), with the c-type lectin binding domain (CTLD) as well as the SR family members SREC-I and FEEL-1/CLEVER-1/STABILIN-1, which by contrast have arrays of EGF-like repeats in their extracellular domains. In this chapter we will discuss: (1) methods for discovery of HSP receptors, (2) approaches to the study of individual receptors in cells that contain multiple such receptors, and (3) methods for investigating HSP receptor function in vivo.

Key words Extracellular, Heat, Shock, Protein, Scavenger, Receptor, Immunity

1 Introduction

It is apparent that heat shock proteins (HSP) play significant signaling roles in the extracellular microenvironment [1, 2].HSP have been found in human serum particularly after disease or stress [3, 4]. The 70 kDa heat shock protein (Hsp70) has been shown to be released from cells after acute stress as well as being secreted after exposure to a number of stimuli [5, 6]. Extracellular HSPs may thus be able to play the role of danger signal (danger activated molecular pattern or DAMP) [7]. In this context, they may interact with pattern recognition receptors (PRR) such as Toll-like receptors (TLR) and activate pro-inflammatory signaling and transcription [8, 9]. Proteins including Hsp60, Hsp70, Grp 96 have been implicated as DAMPs [10, 11]. However, interpretation of such experiments however requires caution and careful control as some HSPs have the ability to bind to prokaryotic molecules that activate

Stuart K. Calderwood and Thomas L. Prince (eds.), *Chaperones: Methods and Protocols*, Methods in Molecular Biology, vol. 1709, https://doi.org/10.1007/978-1-4939-7477-1_24,

TLR signaling, such as lipopolysaccharides and the inflammatory properties of HSPs are influenced by tissue context [2, 12]. In addition, many members of the HSP family can participate in adaptive immunity by binding to antigenic peptides and transporting them into antigen-presenting cells (APC) [13, 14]. HSPs mediate the process of *antigen cross presentation* [15] by facilitating internalization of antigens and permitting their delivery to major histocompatability class I (MHC class I) molecules [16] as well as MHC Class II [17]. MHC I-peptide complexes can then stimulate cognate T cell receptors on T lymphocytes and initiate the activation of clones of such powerful immune effectors [16, 17]. HSP may thus play a versatile role in anti-tumor immunity by activating the innate and adaptive arms. HSP can additionally activate natural killer cells and lead to tumor cell killing and CD25+ immune regulatory T cells [18–20]. HSP can thus upregulate or downregulate immunity depending on context.

Many studies have suggested that HSP activate immunity by binding to receptors on the cell surface [21–29]. HSP binding is saturable and competed for by unlabeled ligand, properties of receptor-mediated signaling. However, this is where consensus seems to end and some controversy exists as to the most significant HSP receptors. We have attempted to address this issue by screening the various contenders for binding to Hsp70 and Hsp90.

2 Materials

2.1 Plasmids

pET23 *hsp90a* plasmid.

pDEST™10.

AC-to-BAC Baculovirus transfection kit.

pCDNA3.1 eukaryotic expression vector.

2.2 Cell Lines

Chinese Hamster Ovary-K1 cells (CHO-K1).

A375 human melanoma.

MISA human breast carcinoma cells.

Sf9 insect cells.

MC38 cells stably expressing the MUC1 tumor antigen.

B16 melanoma cells.

B16 melanoma cells stably expressing the MUC1 tumor antigen.

2.3 Mouse Systems and Primary Murine Cells

Wild type mice C57BL/6 and *tlr2*$^{-/-}$/*tlr4*$^{-/-}$ double knockouts.

Primary mouse bone marrow dendritic cells were prepared from C57BL/6 as in text.

Splenocytes and/or lymph node cells (LNC) were isolated from mice immunized with Hsp70.PC fusion vaccine as described [30].

2.4 Chromatography

Ni-NTA purification system (Quiagen).

10 mL Sephadex G-25 in PD10 column (Sigma-Aldrich).

5.0 mL ADP-agarose column (Sigma-Aldrich).

20 mL DEAE-cellulose anion exchange column (Pierce Chemicals).

2.5 Buffers and Reagents

Hypotonic Buffer: 10 mM $NaHCO_3$, 0.5 mM PMSF, pH 7.1.

Buffer D: 20 mM Tris-acetate, 20 mM NaCl, 15 mM b-mercaptoethanol, 3 mM $MgCl_2$, 0.5 mM PMSF, pH 7.5.

ADP–agaroseElution buffer: 3.0 mM ADP in buffer D.

FPLC buffer: 20 mM sodium mono and diphosphate, 20 mM NaCl, pH 7.0.

DEAE-cellulose elution buffer: 150 mM NaCl in FPLC buffer.

Hsp70 binding buffer (PFNC): 0.5% FBS, 0.05% NaN_3 and 1 mM $CaCl_2$.

Hanks' Buffered Saline Solution.

2.6 Antibodies

Anti-Hsp70 antibody (SPA-810, Assay Designs Inc.).

2.7 Chromophores

Alexa488 (Molecular Probes).

2.8 shRNA to SREC-I

MISSION™ shRNA plasmids (shRNA) were purchased (Sigma-Aldrich, St. Louis, MI) and the Lentivirus generation and transduction were performed according the manual of ViralPower™ Lentiviral Expression Systems (Invitrogen).

3 Screening for HSP Receptors

We have screened receptors for HSP binding in the context of cell surface expression, by expressing candidate receptors in cells null for Hsp70 binding. A number of primary and tissue culture cells were therefore screened for lack of capacity to bind to Hsp70. We screened both primary cells and established cell lines (Table 1). Maintenance of established cell lines is described previously [31]. Human Umbilical Vein Endothelial Cells (HUVEC) were maintained in Endothelial Basal Medium-2 (EBM-2) supplemented with Clonetics™ SingleQuot® (Cambrex/Biowittaker). Isolation of peritoneal macrophages was carried out as previously described [32]. Briefly, peritoneal macrophages were isolated from 6 to 10-week old C57BL/6 background mice. The mice

Table 1
Relative capacity for a range of different tissue culture cells to bind to Hsp70

Binding to Hsp70		
Cell type	**Species**	**Hsp70 binding**
THP1, monocyte	Human	+
RAW264.7, macrophage	Mouse	++
Primary macrophage	Mouse	++
Primary dendritic cell	Mouse	++
HEK293 embryonic kidney	Human	+
Vacular endothelial	Human	++
PC-3, prostate carcinoma	Human	+
HeLa, cervical carcinoma	Human	++
Hela S3 cervical carcinoma	Human	+
MCF7, mammary cancer	Human	+
IMR90, fibroblast	Human	–
K562, pluripotent leukemia	Human	–
A375, melanoma	Human	–
CHO K1, ovarian cells	Chinese hamster	–

were injected intraperitoneally with 3 mL of thioglycollate, and after 4 days peritoneal exudate cells were harvested by lavage with 10 mL of RPMI 1640 and cultured in RPMI 1640 medium supplemented with 10% heat-inactivated FBS and penicillin streptomycin. Bone marrow-derived dendritic cells (BMDCs) were generated from the femur and tibiae of C57BL/6 mice. The bone marrow was flushed out and cultured in RPMI 1640 supplemented with 10% heat inactivated fetal bovine serum (FBS) and 40 ng/mL GMCSF for 6 days. On day 3, a third of the media was replaced by fresh growth media.

3.1 Alexa 488-Labeled Purified HSP70 Preparation

Human melanoma cells A375-MEL or mouse MISA cells were used as starting material for the Hsp70 preparation because high endogenous HSC70 and/or HSP70 levels were detected in these cell types (J. Theriault & SK Calderwood, unpublished). In addition, for some experiments we used minced mouse liver as an abundant source for Hsp70. The Hsp70 purification protocol was based on previous studies [33]. Briefly, a 10 mL cell pellet of tumor cells or minced liver was homogenized in 40 mL hypotonic buffer by Dounce homogenization. The homogenate was then spun at

10,000 × *g* for 30 min and the supernatant was further treated for 60 min. at 100,000 × *g*. The sample buffer was changed to buffer D using a PD-10 desalting column (Amersham-Biosciences). The material was then applied directly to a 5 mL ADP-agarose column pre-equilibrated with buffer D. Hsp70 was eluted from the ADP-agarose column with 3 mM ADP in buffer D. The sample buffer was then changed to FPLC buffer with PD-10 column. The supernatant was applied to a DEAE anion exchange column equilibrated with FPLC buffer (Amersham-Biosciences). Hsp70 was eluted with the FPLC buffer containing 150 mM NaCl. Protein concentrations were determined by *Bradford* assay. Purified Hsp70 was then labeled with fluorophore Alexa 488 according to the manufacturer's instructions (Molecular Probes, USA). Intactness and purity of the labeled Hsp70 was checked by SDS-PAGE, Coumassie staining and the presence of Hsp70 in the preparation confirmed by Western blotting using a mouse monoclonal antibody specific for HSP70 (*see* **Note 1**).

3.2 Alexa 488-Labeled Purified Hsp90 Preparation

Hsp90 alpha DNA was prepared by PCR amplification from the pET23 plasmid and cloned into pDEST™10. Overexpression of Hsp90 alpha in Sf9 cells was achieved according to the BAC-to-BAC Transfection kit protocol of *Invitrogen*. Transfer vector was transformed into DH10BAC competent cells containing bacmid DNA. Later, colonies containing recombinant bacmid were identified and prepared. The bacmid DNA was then transfected into Sf9 cells using CellFECTIN (Invitrogen) to make recombinant baculovirus according to the manufacturer's protocol.

Sf9 cells were grown in Sf900II serum-free medium (Invitrogen) supplemented with 100 U/mL penicillin-streptomycin and 2 mM of L-glutamine in suspension cultures with continuous shaking at 150 rpm at 27 °C in a non-humidified environment. The insect cultures were infected in the log phase of growth with recombinant baculovirus. Cells were harvested for 48 h post infection, washed with Hank's buffered saline solution, and protein was purified using the Ni-NTA purification system according to the manufacturer's protocol (Invitrogen). AcTEV protease was used to cleave the 6× His tag from the fusion protein generated using pDEST™10 after purifying the recombinant protein on a nickel chelating resin. Purified Hsp90 was then labeled with Alexa 488 as above. Intactness and purity of the labeled Hsp90 was checked by SDS-PAGE, Coumassie Blue staining and the presence of Hsp90 in the preparation confirmed by immunoblot.

3.3 HSP Binding Assay

Cells were first screened by binding to Alexa 488-labeled HSP in vitro and analysis by flow cytometry (Table 1). 2×10^5 non-trypsinized cells were washed twice in PFNC buffer and incubated with 150 nM Alexa 488-labeled BSA (negative control), Hsp70 or Hsp90 for 30 min on ice with gentle shaking. The cells

were washed twice in PFNC buffer and Alexa 488-labeled protein binding was monitored by flow cytometry (Becton Dickinson) (*see* **Notes 2** and **3**).

Experiments utilizing flow cytometry were next confirmed by confocal fluorescence microscopy. Alexa Fluor conjugated BSA, Hsp70, or Hsp90 were prepared as above. Cells were labeled with ligand for 20–30 min on ice. Cells were later washed with ice-cold stripping buffer to remove unbound Hsp90.PC. Cells were then fixed with 4% para-formaldehyde and permeabilized with 0.1% TritonX-100. Fluorescence was then visualized using a Zeiss 510 confocal microscope (Carl Zeiss GmbH, Jena, Germany). Fluorophores were visualized using 488 nm excitation and a band pass 505–530 emission filter for Alexa 488. Images were taken using a 63 × numerical aperture (NA) 1.4 oil immersion objective lens.

3.4 To Assay Individual Receptors for HSP Binding, We Selected CHO-K1 Cells as Null for HSP Binding in the Wild-Type State

Cells were then transfected with expression plasmids for individual receptors following the protocol used for study of LOX-1.

2.5×10^5 CHO-K1 cells were transiently transfected with 5 μg of empty vector (pCDNA3) or pCDNA3 plasmids encoding Myc-tagged LOX-1, for 48 h using the Superfect transfection reagent according to the manufacturer's instructions (QIAGEN). Expression of recombinant proteins was analyzed after transfection by SDS-PAGE and immunoblot with the mouse monoclonal anti-Myc antibody (clone 9E10, Stratagene, USA). Cell lines were maintained by selection with neomycin and checked routinely for the expression of Myc-tagged product. In addition, we examined the cell surface location of the candidate receptors using antibodies to the extracellular domains of such proteins.

Using this approach, we have examined a number of candidate receptors. As previous studies had suggested a role for LOX-1 in immune responses to Hsp70, we began with the study of this protein and have confirmed that Hsp70 binds avidly to CHO--LOX-1 cells (Table 2) [24, 34]. LOX-1 has been assigned to at least two distinct protein families, the c-type lectins and the scavenger receptors (SR) [34, 35]. C-type lectin receptors (CLR) are a large family of receptors characterized by the possession of a common binding domain—the Ca^{++}-dependent carbohydrate binding motif (CTLD) [36, 37]. Binding to protein ligands can be inhibited by the use of hapten sugars that differ between different CLR family members. In the case of LOX-1, fucoidin is a hapten sugar that interacts with its CTLD domain and inhibits Hsp70 binding to LOX-I [24]. Scavenger receptors (SR) have been studied mostly in endothelial cells but are expressed in dendritic cells and macrophages also (J. Gong, A Murshid & SK Calderwood, in preparation). SR are a group of proteins that are clustered according to their function in cells—their ability to interact with chemically modified proteins in the extracellular fluid, as exemplified by binding oxidized low density lipoprotein and acetylated or maleylated

Table 2
Candidate cell surface receptors tested for binding to Hsp70 and Hsp90 and degree of association as indicate by symbol (+)

Candidate HSP receptors				
Receptor	**Type**	**Expressed in**	**Hsp70**	**Hsp90**
TLR2	Signaling	APC etc.	–	ND
TLR4	Signaling	APC etc.	–	ND
CD14	Signaling	APC etc.	–	ND
CD40	Signaling	APC	–	ND
CD91	Internalizing	Many	–	ND
LOX-1	Scavenger/CTL	Endo, APC	+	++
DC-SIGN	Scavenger/CTL	APC	–	ND
Dectin 1	Scavenger	APC	–	ND
CLEC-1	Scavenger	APC	–	ND
CLEC2	Scavenger	APC	–	ND
SREC-1	Scavenger	APC	++	++
FEEL-1	Scavenger	APC	++	++
NKG2A	CTL	NK	++	ND
NKG2C	CTL	NK	++	ND
NKG2D	CTL	NK, T cell	++	ND

Binding to receptors was assayed in CHO transfectants with two exceptions, which are DC-SIGN, which was in K-562 (also HSP binding null) and the TLR, which were in HEK293. Ability to compete with 25-fold XS cold HSP70 is indicated in last column

bovine serum albumin (BSA) [38–41]. Binding of HSP to SR can initially be screened by competition assay using known SR binding proteins such as maleylated BSA, oxidized LDL, acetylated LDL, apolipoprotein B, or polyanions such as polyinosine [24]. In this approach, one ligand is labeled (fluorescently for flow cytometry) and the other one remains unlabeled. The competition assay is done with a constant concentration of labeled HSP and varying concentration of unlabeled ligands such as mBSA, AcLDL. The basis for this interaction as well as HSP binding is nor well understood as the extracellular domains of individual SR are highly divergent [41].

We screened members of these receptor families and confirmed that Hsp70 binds to LOX-1 and as well as two other SR family members, SREC-I and FEEL-1/Stabilin1/CLEVER-1 when expressed in CHO-K1 (Table 2) [42–46]. Others have subsequently shown that another SR family member—scavenger receptor A can interact with HSP family members that however fail to

bind CD36, MARCO, and CLA-1 [24, 47]. Hsp70 also binds to other members of the CLR family such as NKG2D that are expressed in natural killer cells (Table 2) [42]. However, in our studies, Hsp70 failed to bind to a number of major CLR family members including Dectin-1, DC-SIGN, CLEC-1, and CLEC-2 (Table 2) [42]. Some studies also indicate a role for the LDL receptor-related protein (LRP) or CD91 in HSP binding. LRP/CD91 contains four clusters of binding repeats that mediate association with at least 30 different ligands including apolipoprotein E, $\alpha_2$macroblobulin, pro-urokinase, and others [48, 49]. Most ligands bind specifically to two of these clusters of binding repeats within domains II and IV [48]. However, we could not detect Hsp70 binding to either domain II or IV when expressed in CHO-K1 cells, and in addition, LRP null cells appeared to bind Hsp70 as well as wild-type cells (Table 2) [23, 42, 50]. Endocytosis of the molecular chaperone calreticulin was also not decreased in $CD91^{-/-}$ cells casting some doubt on CD91 as a universal endocytic receptor for HSPs [51]. By contrast scavenger receptor SRA has been shown to be required for a large proportion of gp96 and calreticulin uptake [22]. In the case of Hsp90, neither fucoidin (LOX-1 agonist) nor α_2-macroglobulin (LRP/CD91 agonist) was able to block representation of a peptide bound to Hsp90 [52]. Nonetheless, others have shown that inactivation of CD91 can lead to loss of antigen re-presentation ability in cells exposed to gp96/peptide complexes [53]. The large heat shock proteins Hsp110 and Grp170, which have potent immune properties, can bind to SRA and SREC-I and there is also some evidence for binding to LRP/CD91 [25]. There is additionally evidence indicating a possible role for LRP/CD91 in Hsp70 binding to macrophages [24]. Inhibition by $\alpha_2$macroblobulin competition has often been used as a criterion for HSP binding to LRP/CD91 [25]. In addition, our unpublished experiments indicate that levels of SREC-I and LOX-1 are very low in unstimulated murine macrophages in which CD91 may play a significant role. The usage of HSP receptors could thus vary with the nature of the chaperone ligand, immune cell type, and the activation state of the cell. Our studies in vivo indicate that TLR signaling is essential for SREC-I-expressing DC to traffic to afferent lymph nodes after vaccination with Hsp70 vaccine [30]. Hsp70 can itself induce SREC-I expression in TLR pathway proficient murine DC suggesting a feed-forward mechanism in which Hsp70 induces its own receptors (SR) and amplifies immune effects of Hsp70-peptide complexes [30]. There are also indications that Hsp70 activates signaling receptors such as TLR2, TLR4, and CD40 and may be involved in inducing inflammation and innate immunity [10, 11, 54]. However, using the CHO transfection system described above, we were unable to confirm direct binding of Hsp70 to these molecules (Table 2). At least in the case of TLR2, indirect

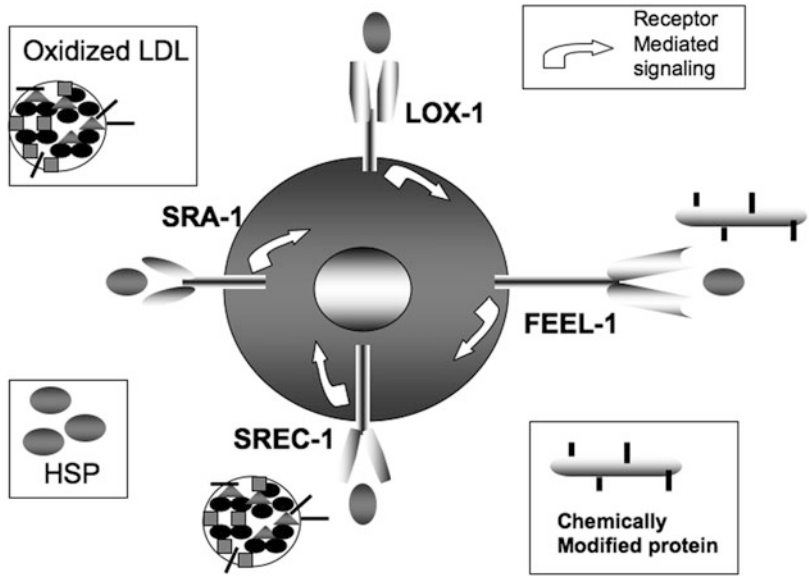

Fig. 1 Hsp70, oxidized LDL and chemically modified proteins each bind to scavenger receptors LOX-1, FEEL-1, SRECI and SRA-1

activation of this receptor downstream of both LOX-1 and SREC-I is observed after receptor binding to bacterial protein OMP1 [55].

Figure 1 shows a cartoon indicating that at least 4 HSP receptors exist and could potentially be co-expressed in a single cell. In addition, a range of other ligands can interact with such receptors. The existence of multiple receptors therefore complicates interpretation of experiments probing the function of extracellular HSP. This difficulty is exacerbated by the findings that, while SREC-I and LOX-1 have pro-immune functions, SRA-1 appears to be inhibitory to the immune response by inhibiting the activity of TLR4 [24, 30, 47, 56]. The receptors may thus have both additive and confounding effects.

With this plethora of receptors, the nature of the HSP-receptor interaction is still in some doubt. However, the crystal structure of ligand-bound LOX-1 has recently been determined. These studies indicate that the ligand (oxidized LDL) binding surface is hydrophobic except for a basic spine composed of arginine residues essential for ligand binding [57, 58]. These positively charged arginine residues together with the hydrophobic residues appear to confer the specificity of LOX-1 for negatively charged lipids and lipoproteins [57]. LOX-1 binds to its ligands as a homodimer with an intramolecular disulfide bond [58]. It is not clear to what degree the ligand-binding properties of SREC-I and FEEL-1/CLEVER1 resemble those of LOX-1 (Fig. 1). The extracellular domains of these two SR do not contain CTLD, but consist mostly of multiple EGF-like repeats [59]. These repeat domains have a length of approximately

40 amino acids and are characterized by conserved arrangement of six cysteine residues found in EGF itself [60, 61]. It has been shown that at least four tandem repeats of EGF-like regions are required for the FEEL-1 homolog FEEL-2 (STABILIN-2) to bind the acidic lipid phosphatidylserine [62]. It is apparent therefore that much is left to be learnt regarding the specificity and sequence requirements for HSP binding to these candidate receptors.

4 Studying HSP-SREC-I Interaction In Vivo

As we are currently have not developed SREC-I knockout mice, we took the approach of knocking down SREC-I in dendritic cells by shRNA. Our studies had indicated that in mice with TLR2/TLR4 knockdown, responses to Hsp70 vaccine (Hsp70-FC) were strongly inhibited [30, 63]. We utilized this finding to study the significance of SREC-I in responses to Hsp70 in vivo. To address this issue, we first determined whether the decreased immunity in TLR knockout cells could be reversed by adoptive transfer of wild-type DC (WT-DC) into $tlr2^{-/-}/tlr4^{-/-}$ mice [30]. Indeed, transfer of Hsp70-FC pulsed DC was able to induce immunity to tumors in naive WT mice and support tumor-specific cytotoxicity [30]. We next showed that immunization of $tlr2^{-/-}/tlr4^{-/-}$ mice with WT DC that had been pulsed with Hsp70-FC also increased the cytotoxic lymphocyte (CTL) activity and CTL frequency of such mice [30]. This implies that WT donor DC were able to compensate for the endogenous, inactive DC in $tlr2^{-/-}/tlr4^{-/-}$ mice. Groups of such knockout mice were next immunized with DC generated from WT mice that had been infected with SREC-I shRNA or control shRNA constructs and then pulsed with Hsp70-FC. SREC-I knockdown inhibited the ability of WT DC to compensate for TLR knockout indicating that this is a viable approach for studying SREC-I function in vivo. These experiments therefore suggested that SREC-I is essential for antigen presentation by DC exposed to Hsp70.PC. These findings were confirmed by assessing the frequency of antigen-specific T cells induced using an MHC-class-I/peptide tetramer (iTAg). The 8-mer peptide (SAPDTRPA) is a dominant epitope from MUC1 that binds to C57BL/6 MHC class I, H-$2K^b$ [64]. MUC1 is one of the most prominent tumor antigens present in the Hsp70-FC vaccine [30]. The MUC1-8 iTAg was used to identify and assess the tetramer-positive T cells. The numbers of MUC1-8 iTAg-positive T cells from $tlr2^{-/-}/tlr4^{-/-}$ immunized with SRECI knockdown DC were significantly decreased compared with those from mice transferred with DC infected with control virus. Immunization of $tlr2^{-/-}/tlr4^{-/-}$ mice either with Hsp70-FC pulsed DC after SREC-I knockdown or after infection with control virus resulted 1.45% and 3.51% CD8 T cells positive for MUC1-8 indicating that SRECI plays an important role in the induction of antigen-specific T cells by Hsp70-based vaccines.

4.1 shRNA Directed Against SRECI

MISSION™ shRNA plasmids (shRNA) were purchased (Sigma-Aldrich, St. Louis, MI) and the Lentivirus generation and transduction were performed according to the manual of ViralPower™ Lentiviral Expression Systems (Invitrogen). The effectiveness of shRNA for knockdown of murine SRECI (five clones: TRCN0000067873; TRCN0000067874; TRCN0000067875; TRCN0000067876; and TRCN0000067877) was examined Real-Time PCR and immunoblot. The most effective construct for mSREC-I mRNA knockdown (TRCN0000067875) was used. The Lentivirus (insert sequence was 5′–CCGCAGGTATGCACGCGT-3′ which does not target any mouse genes, but will activate RISC and the RNAi pathway in the cells) was used as negative control.

Three-day-old DC were collected, purified, placed in 96-well round-bottom plates with 1×10^6 cell per well for O/N culture in a medium containing GM-CSF. On the second day, half of the medium (100 μL) was removed and 100 μL Lenti-virus supernatant (1 virus: 1 DC) was added. After 20 h, 150 μL of medium from each well was replaced by fresh GM-CSF medium for additional culture. DC infected with SREC-I shRNA or control constructs or un-infected DC were collected for SREC1 expression and T cell stimulation assay. Significant SRECI knockdown at the protein level was achieved in 90–100 h.

5 Notes

1. *Purified HSP.* Most heat shock proteins are encoded by multigene families. This is particularly true for Hsp70 in which there are, depending on species, at least 12 closely related gene family members each of which may bind to cells with differing affinities [42]. This complication could be remedied by the use of recombinant proteins. However, if recombinant proteins are produced in *E. coli*, great care must be taken to remove contaminating PAMPs such as lipolysaccharides or peptidoglycans [12]. We have prepared recombinant HSPs using the baculovirus/sf9 system to avoid these problems. However, LPS in particular can be introduced into protein preparations from contaminated glassware and we have been very carefull to assay all the batches of HSP by the *limulus* assay.
2. HSP bind with only moderate affinity to the receptors uncovered so far and these are promiscuous in terms of binding partners. In most cases the structural basis for HSP-receptor binding is not known. Thus, much needs to be learned regarding HSP-receptor interaction. Future in vitro studies should address questions of three dimensional structure of HSP-receptor complexes and the exact affinities of the interactions [2].

3. Many cells express multiple HSP receptors and great care must be taken to isolate the properties of individual receptors. It seems likely that other as yet unknown receptors exist [2].

Acknowledgment

This work was supported by NIH research grants RO-1CA047407, R01CA119045 and RO-1CA094397.

References

1. Calderwood SK, Mambula SS, Gray PJ Jr, Theriault JR (2007) Extracellular heat shock proteins in cell signaling. FEBS Lett 581:3689–3694
2. Calderwood SK, Gong J, Murshid A (2016) Extracellular HSPs: the complicated roles of extracellular HSPs in immunity. Front Immunol 7:159
3. Pockley AG (2002) Heat shock proteins, inflammation, and cardiovascular disease. Circulation 105:1012–1017
4. Pockley AG, Shepherd J, Corton JM (1998) Detection of heat shock protein 70 (Hsp70) and anti-Hsp70 antibodies in the serum of normal individuals. Immunol Investig 27:367–377
5. Mambula SS, Calderwood SK (2006) Heat induced release of Hsp70 from prostate carcinoma cells involves both active secretion and passive release from necrotic cells. Int J Hyperthermia 22:575–585
6. Mambula SS, Calderwood SK (2006) Heat shock protein 70 is secreted from tumor cells by a nonclassical pathway involving lysosomal endosomes. J Immunol 177:7849–7857
7. Matzinger P (2002) The danger model: a renewed sense of self. Science 296:301–305
8. Vabulas RM, Ahmad-Nejad P, da Costa C et al (2001) Endocytosed HSP60s use toll-like receptor 2 (TLR2) and TLR4 to activate the toll/interleukin-1 receptor signaling pathway in innate immune cells. J Biol Chem 276:31332–31339
9. Vabulas RM, Ahmad-Nejad P, Ghose S, Kirschning CJ, Issels RD, Wagner H (2002) HSP70 as endogenous stimulus of the toll/interleukin-1 receptor signal pathway. J Biol Chem 277:15107–15112
10. Asea A, Rehli M, Kabingu E et al (2002) Novel signal transduction pathway utilized by extracellular HSP70: role of toll-like receptor (TLR) 2 and TLR4. J Biol Chem 277:15028–15034
11. Asea A, Kraeft SK, Kurt-Jones EA et al (2000) HSP70 stimulates cytokine production through a CD14-dependant pathway, demonstrating its dual role as a chaperone and cytokine. Nat Med 6:435–442
12. Henderson B, Calderwood SK, Coates AR et al (2009) Caught with their PAMPs down? The extracellular signalling actions of molecular chaperones are not due to microbial contaminants. Cell Stress Chaperones 15(2):123–141
13. Singh-Jasuja H, Toes RE, Spee P et al (2000) Cross-presentation of glycoprotein 96-associated antigens on major histocompatibility complex class I molecules requires receptor-mediated endocytosis. J Exp Med 191:1965–1974
14. Srivastava P (2002) Interaction of heat shock proteins with peptides and antigen presenting cells: chaperoning of the innate and adaptive immune responses. Annu Rev Immunol 20:395–425
15. Rock KL (2003) The ins and outs of cross-presentation. Nat Immunol 4:941–943
16. Murshid A, Gong J, Calderwood SK (2010) Heat shock protein 90 mediates efficient antigen cross presentation through the scavenger receptor expressed by endothelial cells-I. J Immunol 185:2903–2917
17. Murshid A, Gong J, Calderwood SK (2014) Hsp90-peptide complexes stimulate antigen presentation through the class II pathway after binding scavenger receptor SREC-I. Immunobiology 219:924–931
18. Multhoff G (2002) Activation of natural killer cells by heat shock protein 70. Int J Hyperth 18:576–585
19. Multhoff G, Hightower LE (1996) Cell surface expression of heat shock proteins and the immune response. Cell Stress Chaperones 1:167–176
20. van Eden W, van der Zee R, Prakken B (2005) Heat-shock proteins induce T-cell regulation

of chronic inflammation. Nat Rev Immunol 5:318–330

21. Berwin B, Delneste Y, Lovingood RV, Post SR, Pizzo SV (2004) SREC-I, a type F scavenger receptor, is an endocytic receptor for calreticulin. J Biol Chem 279:51250–51257
22. Berwin B, Hart JP, Rice S et al (2003) Scavenger receptor-A mediates gp96/GRP94 and calreticulin internalization by antigen-presenting cells. EMBO J 22:6127–6136
23. Binder RJ, Han DK, Srivastava PK (2000) CD91: a receptor for heat shock protein gp96. Nat Immunol 1:151–155
24. Delneste Y, Magistrelli G, Gauchat J et al (2002) Involvement of LOX-1 in dendritic cell-mediated antigen cross-presentation. Immunity 17:353–362
25. Facciponte JG, Wang XY, Subjeck JR (2007) Hsp110 and Grp170, members of the Hsp70 superfamily, bind to scavenger receptor-A and scavenger receptor expressed by endothelial cells-I. Eur J Immunol 37:2268–2279
26. Gross C, Hansch D, Gastpar R, Multhoff G (2003) Interaction of heat shock protein 70 peptide with NK cells involves the NK receptor CD94. Biol Chem 384:267–279
27. Kettner S, Kalthoff F, Graf P et al (2007) EWI-2/CD316 is an inducible receptor of HSPA8 on human dendritic cells. Mol Cell Biol 27:7718–7726
28. Sondermann H, Becker T, Mayhew M, Wieland F, Hartl FU (2000) Characterization of a receptor for heat shock protein 70 on macrophages and monocytes. Biol Chem 381:1165–1174
29. Whittall T, Wang Y, Younson J et al (2006) Interaction between the CCR5 chemokine receptors and microbial HSP70. Eur J Immunol 36:2304–2314
30. Gong J, Zhu B, Murshid A et al (2009) T cell activation by heat shock protein 70 vaccine requires TLR signaling and scavenger receptor expressed by endothelial Cells-1. J Immunol 183(5):3092–3098
31. Theriault JR, Mambula SS, Sawamura T, Stevenson MA, Calderwood SK (2005) Extracellular HSP70 binding to surface receptors present on antigen presenting cells and endothelial/epithelial cells. FEBS Lett 579:1951–1960
32. Mambula SS, Sau K, Henneke P, Golenbock DT, Levitz SM (2002) Toll-like receptor (TLR) signaling in response to Aspergillus fumigatus. J Biol Chem 277:39320–39326
33. Peng P, Menoret A, Srivastava PK (1997) Purification of immunogenic heat shock protein 70-peptide complexes by ADP-affinity chromatography. J Immunol Methods 204:13–21
34. Mehta JL, Chen J, Hermonat PL, Romeo F, Novelli G (2006) Lectin-like, oxidized low-density lipoprotein receptor-1 (LOX-1): a critical player in the development of atherosclerosis and related disorders. Cardiovasc Res 69:36–45
35. Chen M, Masaki T, Sawamura T (2002) LOX-1, the receptor for oxidized low-density lipoprotein identified from endothelial cells: implications in endothelial dysfunction and atherosclerosis. Pharmacol Ther 95:89–100
36. Zelensky AN, Gready JE (2005) The C-type lectin-like domain superfamily. FEBS J 272:6179–6217
37. Drickamer K (1999) C-type lectin-like domains. Curr Opin Struct Biol 9:585–590
38. Adachi H, Tsujimoto M (2006) Endothelial scavenger receptors. Prog Lipid Res 45:379–404
39. Rigotti A (2000) Scavenger receptors and atherosclerosis. Biol Res 33:97–103
40. van Berkel TJ, Out R, Hoekstra M, Kuiper J, Biessen E, van Eck M (2005) Scavenger receptors: friend or foe in atherosclerosis? Curr Opin Lipidol 16:525–535
41. Krieger M (1997) The other side of scavenger receptors: pattern recognition for host defense. Curr Opin Lipidol 8:275–280
42. Theriault JR, Adachi H, Calderwood SK (2006) Role of scavenger receptors in the binding and internalization of heat shock protein 70. J Immunol 177:8604–8611
43. Adachi H, Tsujimoto M (2002) Characterization of the human gene encoding the scavenger receptor expressed by endothelial cell and its regulation by a novel transcription factor, endothelial zinc finger protein-2. J Biol Chem 277:24014–24021
44. Politz O, Gratchev A, McCourt PA et al (2002) Stabilin-1 and -2 constitute a novel family of fasciclin-like hyaluronan receptor homologues. Biochem J 362:155–164
45. Murshid A, Borges TJ, Calderwood SK (2015) Emerging roles for scavenger receptor SREC-I in immunity. Cytokine 75:256–260
46. Murshid A, Borges TJ, Lang BJ, Calderwood SK (2016) The scavenger receptor SREC-I cooperates with toll-like receptors to trigger inflammatory innate immune responses. Front Immunol 7:226
47. Wang XY, Facciponte J, Chen X, Subjeck JR, Repasky EA (2007) Scavenger receptor-A negatively regulates antitumor immunity. Cancer Res 67:4996–5002

48. Herz J, Strickland DK (2001) LRP: a multifunctional scavenger and signaling receptor. J Clin Invest 108:779–784
49. Newton CS, Loukinova E, Mikhailenko I et al (2005) Platelet-derived growth factor receptor-beta (PDGFR-beta) activation promotes its association with the low density lipoprotein receptor-related protein (LRP). Evidence for co-receptor function. J Biol Chem 280:27872–27878
50. Obermoeller-McCormick LM, Li Y, Osaka H, FitzGerald DJ, Schwartz AL, Bu G (2001) Dissection of receptor folding and ligand-binding property with functional minireceptors of LDL receptor-related protein. J Cell Sci 114:899–908
51. Walters JJ, Berwin B (2005) Differential CD91 dependence for calreticulin and pseudomonas exotoxin-A endocytosis. Traffic 6:1173–1182
52. Kurotaki T, Tamura Y, Ueda G et al (2007) Efficient cross-presentation by heat shock protein 90-peptide complex-loaded dendritic cells via an endosomal pathway. J Immunol 179:1803–1813
53. Binder RJ, Srivastava PK (2005) Peptides chaperoned by heat-shock proteins are a necessary and sufficient source of antigen in the cross-priming of CD8+ T cells. Nat Immunol 6:593–599
54. Becker T, Hartl FU, Wieland F (2002) CD40, an extracellular receptor for binding and uptake of Hsp70-peptide complexes. J Cell Biol 158:1277–1285
55. Jeannin P, Bottazzi B, Sironi M et al (2005) Complexity and complementarity of outer membrane protein A recognition by cellular and humoral innate immunity receptors. Immunity 22:551–560
56. Kottke T, Pulido J, Thompson J et al (2009) Antitumor immunity can be uncoupled from autoimmunity following heat shock protein 70-mediated inflammatory killing of normal pancreas. Cancer Res 69(19):7767–7774
57. Sawamura T (2005) LOX-1 unlocked. Structure 13:834–835
58. Ohki I, Ishigaki T, Oyama T et al (2005) Crystal structure of human lectin-like, oxidized low-density lipoprotein receptor 1 ligand binding domain and its ligand recognition mode to OxLDL. Structure 13:905–917
59. Pluddemann A, Neyen C, Gordon S (2007) Macrophage scavenger receptors and host-derived ligands. Methods 43:207–217
60. Appella E, Weber IT, Blasi F (1988) Structure and function of epidermal growth factor-like regions in proteins. FEBS Lett 231:1–4
61. Shibata M, Ishii J, Koizumi H et al (2004) Type F scavenger receptor SREC-I interacts with advillin, a member of the gelsolin/villin family, and induces neurite-like outgrowth. J Biol Chem 279:40084–40090
62. Park SY, Kim SY, Jung MY, Bae DJ, Kim IS (2008) Epidermal growth factor-like domain repeat of stabilin-2 recognizes phosphatidylserine during cell corpse clearance. Mol Cell Biol 28:5288–5298
63. Enomoto Y, Bharti A, Khaleque AA et al (2006) Enhanced immunogenicity of heat shock protein 70 peptide complexes from dendritic cell-tumor fusion cells. J Immunol 177:5946–5955
64. Apostolopoulos V, Yu M, Corper AL et al (2002) Crystal structure of a non-canonical low-affinity peptide complexed with MHC class I: a new approach for vaccine design. J Mol Biol 318:1293–1305

Chapter 25

Creation of Recombinant Chaperone Vaccine Using Large Heat Shock Protein for Antigen-Targeted Cancer Immunotherapy

Chunqing Guo, John R. Subjeck, and Xiang-Yang Wang

Abstract

Large heat shock proteins (HSPs) or stress proteins, including Hsp110 and Grp170, are unique molecular chaperones with superior capability of shuttling tumor protein antigens into professional antigen-presenting cells, such as dendritic cells, for highly efficient cross-presentation and T cell priming. Reconstituted chaperone complexes of large HSP and tumor protein antigen have been demonstrated to generate a robust antigen-specific T lymphocyte response with therapeutic potency against multiple cancer types in preclinical models. Here, we describe the methods for preparing this recombinant chaperone complex vaccine and analyzing the vaccine-induced activation of antigen-specific T cells using in vitro and in vivo systems.

Key words Large heat shock protein, Hsp110, Grp170, Chaperone vaccine, Antigen cross-presentation, T cell activation

1 Introduction

Heat shock proteins (HSPs) are among the most abundant and ubiquitous intracellular proteins. As molecular chaperones, they are actively involved in almost every aspect of protein homeostasis, e.g., folding/refolding, assembly, translocation, and degradation [1]. The extensive studies have shown that certain tumor-derived HSPs can serve as effective cancer vaccines [2–4], which is believed to be due to the HSP-carried antigenic "fingerprint" of the tumor [5]. It has been well documented that exogenous HSPs are highly effective in directing associated antigens into antigen-presenting cells (APCs) though the interactions with surface endocytic receptors [6–9], resulting in cross-presentation of antigens on MHC class I molecules. In addition to promoting antigen processing and presentation, HSP interactions with certain signaling receptors, such as toll-like receptors, facilitate phenotypic and functional maturation of professional APCs, e.g., dendritic cells (DCs) or

Stuart K. Calderwood and Thomas L. Prince (eds.), *Chaperones: Methods and Protocols*, Methods in Molecular Biology, vol. 1709, https://doi.org/10.1007/978-1-4939-7477-1_25,

monocytes [10, 11]. Thus, the properties of HSPs as antigen carriers and as activators of innate immune cells enable these chaperone molecules to be utilized as immunostimulatory adjuvants for development of various immunotherapeutic approaches to treatment cancer or infectious diseases [12].

High molecular weight or large HSPs, called Hsp110 and Grp170, exhibit similar albeit distinct structural and functional features compared to other chaperone molecules [13, 14]. In light of their exceptional client protein-holding capacity and superior immunostimulatory activity [4, 15–17], we have created recombinant heat shock or chaperone vaccines by complexing clinically relevant tumor protein antigens to these large HSPs in vitro [18–20]. Since it has long been understood that HSPs chaperone full-length protein substrates, these generated complexes are believed to resemble natural intracellular HSP-substrate chaperone complexes. We have demonstrated that these recombinant chaperone vaccines exhibit strong antitumor activities in various preclinical tumor models [18–24]. Intriguingly, these large HSPs (e.g., Hsp110) are significantly more potent than complete Freund's adjuvant (CFA) as an adjuvant in promoting antitumor immunity [18], which may be attributed to their superior ability to facilitate cross-presentation of associated tumor protein antigen in the vaccine cargo by DCs [25]. This "chaperoning" approach that we have developed for creation of a targeted vaccine clearly provides several advantages over autologous tumor vaccines, including no requirement for a surgical tumor specimen, unlimited quantities of off-the-shelf vaccines with uniformity, broad applicability, and easy immunomonitoring using well-defined tumor antigens [14, 26].

Here, we describe the methods for preparing recombinant large HSPs and protein antigens using protein expression system involving baculovirus-insect cells, generating large HSP-protein antigen chaperone complexes by heat shock, and assessing this vaccine-stimulated activation of T cells using both in vitro and in vivo systems.

2 Materials

2.1 Preparation of Recombinant Large HSPs and Tumor Protein Antigen

1. BacPAK baculovirus expression system (Clontech).
2. Baculovirus rapid titer kit (Clontech).
3. Ni^{2+}-nitrilotriacetic acid (Ni-NTA)-agarose (Qiagen).
4. Lysis buffer: 20 mM Tris–HCl (pH 7.9), 0.5 M NaCl, 5 mM Imidazole (Sigma), 0.1% Nonidet P-40, and protease inhibitor cocktail tablets (Roche Molecular Biochemicals).
5. Binding buffer: 20 mM Tris–HCl (pH 7.9), 0.5 M NaCl, 5 mM Imidazole.

6. Wash buffer: 20 mM Tris–HCl (pH 7.9), 0.5 M NaCl, 20–50 mM Imidazole.
7. Elution buffer: 20 mM Tris–HCl (pH 7.0), 0.5 M NaCl, 300 mM Imidazole.

2.2 Chaperone Complex Formation In Vitro

1. Luciferase aggregation assay buffer: 25 mM HEPES (pH 7.9), 5 mM magnesium acetate, 50 mM KCl, and 5 mM β-mercaptoethanol.
2. Complexing buffer: Phosphate-buffered saline containing 20 mM HEPES, pH 7.2, 20 mM NaCl.
3. GelCode Blue Stain Reagent (Pierce).
4. BCA (bicinchoninic acid) protein assay kit (Pierce).
5. Enhanced chemiluminescence detection system (Amersham Pharmacia).

2.3 Measuring Antigen Cross-Presentation In Vitro Using BMDCs

1. Complete BMDC medium: RPMI-1640 medium containing 10% heat-inactivated fetal bovine serum (FBS), 10 mM HEPES (PH7.3, Invitrogen), 20 ng/ml GM-CSF (R&D system), 2 mM L-glutamine, 100 U/ml penicillin, and 100 μg/ml streptomycin and 50 μM β-ME (Sigma).
2. Red blood cell lysis buffer: 0.15 M NH_4Cl, 10 mM $KHCO_3$, 0.1 M Na_2EDTA, pH 7.2.
3. TruStain FcX™ (anti-mouse CD16/32) antibody (Clone 93, BioLegend).
4. FITC BrdU Flow kits (BD Pharmingen).
5. PerCP/Cy5.5 anti-mouse CD90.1 antibody (clone OX-7, BioLegend).
6. FACS staining buffer: PBS containing 0.1% (m/v) bovine serum albumin, 0.1% Na_3N.

2.4 Measuring the Immunogenicity of Chaperone Complex Vaccine In Vivo

2.4.1 The Enzyme-Linked ImmunoSpot (ELISPOT) Assay

1. Red blood cell lysis buffer: 0.15 M NH_4Cl, 10 mM $KHCO_3$, 0.1 M Na_2EDTA, pH 7.2.
2. RPMI-1640 complete medium containing 10% FBS, 2 mM L-glutamine, 100 U/ml penicillin, and 100 μg/ml streptomycin and 50 μM β-ME.
3. 96-well nitrocellulose-backed microtiter plates (Millipore).
4. Rat anti-mouse IFN-γ (clone R4-6A2, BD Pharmingen).
5. Wash solution: PBS containing 0.05% (v/v) Tween 20.
6. Biotinylated IFN-γ antibody (clone XMG1.2, BD Pharmingen).
7. Avidin-alkaline phosphatase D (Vector Laboratories).
8. 5-bromo-4-chloro-3-indolyl phosphatase/Nitro Blue Tetrazolium (BCIP/NBT) (Boehringer Mannheim).
9. Human $Gp100_{25–33}$ peptide (KVPRNQDWL, AnaSpec).

2.4.2 Intracellular IFN-γ Staining Assay

1. Human $Gp100_{25–33}$ peptide (KVPRNQDWL, AnaSpec).
2. FITC anti-mouse IFN-γ antibody (clone XMG1.2, BioLegend).
3. PE Rat anti-mouse CD8 antibody (clone 53–6.7, BioLegend).
4. FACS staining buffer: PBS containing 0.1% (m/v) bovine serum albumin, 0.1% Na_3N.
5. Intracellular Fixation & Permeabilization Buffer Set (eBiosciences).
6. Cell Stimulation Cocktail (plus protein transport inhibitors) (eBiosciences).

3 Methods

3.1 Preparation of Recombinant Large HSP and Tumor Protein Antigen

The baculovirus-insect cell expression system, which not only facilitates proper protein folding and posttranslational processing, but also greatly reduces endotoxin contamination, is used to generate recombinant large HSPs (i.e., Hsp110 and Grp170) and protein antigens (e.g., Gp100). The full-length cDNAs for large HSPs or targeted antigens are first subcloned into a baculovirus transfer vector (pBacPAK) containing the promoter for transcription as well as the sequences for homologous recombination and selection. The 6× histidine (His) affinity tag is introduced into the N-terminus or C-terminus of the proteins to facilitate protein binding to Ni^{2+}-NTA agarose for purification. The constructed plasmids are co-transfected along with replication-deficient baculovirus DNA into Sf21 insect cells for virus packaging.

The Bacfectin-DNA mixture is prepared by diluting transfer vector (0.5 μg) with linear viral DNA (0.1 μg) and the Bacfectin (4 μl) in 100 μl steriled nuclease-free water and then added dropwise to a 35 mm culture dish containing Sf21 cells while gently swirling the dish to mix (*see* **Note 1**). 1.5 ml of BacPak complete medium is then added after culture at 27 °C overnight. When the signs of infection, such as irregular shapes and increased volumes, appear (approximately 5 days post-transfection), culture supernatants are harvested for plaque assay. Freshly prepared sf21 cells in 35 mm dish are incubated with the serially diluted supernatant (10^{-2} ~ 10^{-12}) at room temperature for 1 h. After removing the virus inoculums, the pre-warmed 1% SeaPlaque agarose solution (FMC Bioproducts) is gently overlaid on the infected cell monolayer and BacPAK complete medium will be subsequently added on the solidified agarose (*see* **Note 2**). After culture in a humidified incubator for 5–7 days, the plates are stained with 0.03% neutral red solution (Sigma) in PBS and the well-isolated viral plaques are picked using sterile pasteur pipettes. Vortex of agarose plug in the medium will allow the viruses to diffuse out of the agarose plug. 0.1 ml of inoculum from each virus plaque will be amplified for

3–4 days using fresh sf21 cells until the cells appear grainy with irregularly shaped membranes. The supernatants are collected after centrifugation at 1000 × *g* for 5 min at room temperature (passage I virus stock). Expression of large HSPs and targeted antigen should be determined at this step using the infected remaining cells by SDS-PAGE and immunoblotting analysis. The positive recombinant virus plaques are further amplified (0.1 ml passage I stock into 1.5×10^7 cells/30 ml medium in a 150 mm plate) for 4–6 days to produce passage II virus stock. Several aliquots should be kept at −70 °C for long-term storage and the remainder kept at 4 °C as the working stock. The titration of virus should be performed using passage II virus so that subsequent infections can be optimized to produce the maximal yield of recombinant proteins. Virus titers can be determined using a baculovirus rapid titer Kit (Clontech) and calculated as follows: The titer of the virus stock (pfu/ml) = (average plaques per dish) × 10 × (dilution factor)$^{-1}$. Passage II virus stocks for large HSPs and protein antigens (e.g., Gp100) usually have a high titer of 5×10^7 pfu/ml.

Recombinant proteins are produced in large quantities by infecting insect cells growing in suspension using higher multiplicity of infection (MOI, ~5–10). Adding glucose (4.5 mg/ml) to culture media was seen in our hands to increase the glycosylation of certain glycoproteins such as Grp170 and Gp100. Three to four days after virus infection, a small aliquot of cells is subjected to SDS-PAGE to ensure protein expression before cells are collected for the scale-up of protein production. Cells are sonicated in lysis buffer (10^9 cells per 100 ml lysis buffer) and incubated for 30 min on ice. The supernatant of post-centrifugation at 10,000 × *g* for 1 h at 4 °C will be incubated with Ni^{2+}-NTA agarose beads under native conditions at 4 °C (volume ratio ~ 20:1) and the resins are packed onto columns the next day. The columns are washed first with ten-fold bed volume of binding buffer and subsequently with wash buffer to remove nonspecific protein binding (*see* **Note 3**). His-tagged recombinant proteins are eluted from column with 5–10 ml of elution buffer. The eluted proteins are dialyzed against phosphate-buffered saline (PBS) using Slide-A-Lyzer (Pierce) and concentrated with Centriplus (Milipore) or Vivaspin (Vivascience) ultrafiltration columns. The recovered proteins are quantified using BCA protein assay with bovine serum albumin as a standard. The estimated total protein yield is 1–2 mg per 10^9 cells.

3.2 Complex Formation of Large HSP and Tumor Protein Antigen

It is recommended that aggregation protection assays using luciferase as a reporter protein are performed to assess the chaperoning capability of recombinant large HSPs prior to the complex reconstitution [18, 27]. 150 nM luciferase and Hsp110 or Grp170 at a molar ratio of 1:1 are incubated in the aggregation assay buffer at 43 °C for 30 min, and protein aggregation is monitored by measuring the optical density at 320 nm using a spectrophotometer

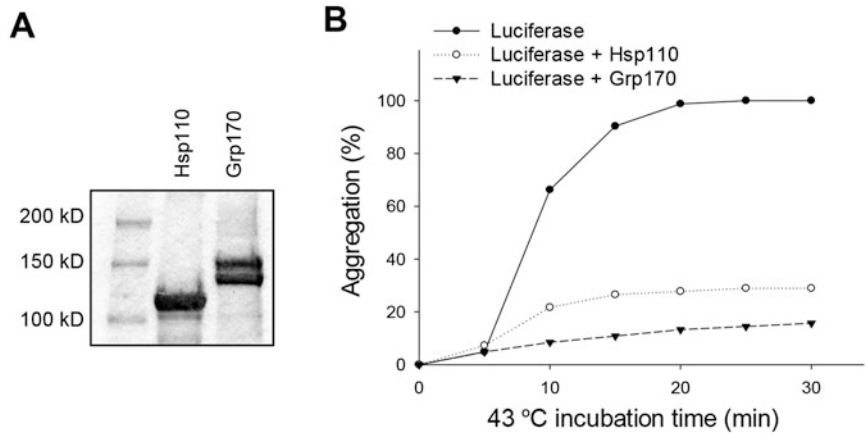

Fig. 1 In vitro chaperoning activity assay using luciferase as a reporter protein. (**a**). Purified Hsp110 and Grp170 were analyzed by SDS–PAGE and subsequent gel staining. (**b**). Luciferase was incubated in the presence or absence of Hsp110 or Grp170 at 43 °C. The optical density of reaction samples at 320 nm was monitored using a spectrophotometer. Aggregation of heated luciferase alone was set as 100%

that is connected to a water bath for temperature control. Hsp110 or grp170 should be able to protect 70–90% of luciferase from heat shock-induced denaturation (Fig. 1). For the generation of chaperone vaccines, recombinant large HSPs and targeted protein antigens (e.g., melanoma antigen Gp100) are incubated under heat shock conditions for 30 min, and then incubated at 37 °C for another 1 h. Since the "melting" temperatures differ for individual protein antigens, a pilot study should be carried out to determine the approximate temperature at which the protein starts to denature as indicated by aggregation and precipitation of the protein. The addition of Hsp110 or Grp170 to the protein antigen should then inhibit aggregation as a result of complex formation. While this model is generally applicable, there is an important caveat. There is an upper temperature limit of approximately 65 °C that can be used to induce aggregation since Hsp110 itself begins to aggregate at about 70 °C. While most proteins examined do aggregate in the available temperature range and therefore adhere to this simple model, not all do. Some proteins are simply thermostable and not suitable for complexing, e.g., ovalbumin. However, we have had experience with protein antigens, which were purified from bacterial inclusion bodies, that did not aggregate but readily complexed with Hsp110 at higher temperature as indicated by co-immunoprecipitation (e.g., the intracellular domain of HER-2/Neu [27]), yielding potent vaccines. Therefore, while a simple precipitation assay is an initial way to set parameters of complexing, failure of this assay should not be reason to abandon the antigen as not suitable. Most protein antigens that we have examined do aggregate in the available temperature range and

complex with Hsp110 or Grp170. In addition, the molar ratios of large HSPs and the antigen can be adjusted to achieve the maximal complexing efficiency, although a one-to-one molar ratio has been found to be effective in most instances.

The complex formation will be confirmed using immunoprecipitation assays as previously described [21]. Anti-Hsp110 (1:200) or Grp170 (1:100) antibodies are incubated with the complexes to pull down chaperone proteins. Normal rabbit sera are used as negative controls. The immune complexes are then precipitated by Protein-A Sepharose CL-4B (Amersham Pharmacia) and subjected to SDS-PAGE followed by either Gel-blue staining (Pierce) or immunoblotting analysis with antibodies against the targeted antigen (e.g., Gp100). Visualization of co-precipitated Hsp110 (or Grp170) and the protein antigen by Gel-blue staining also allows for an estimation of the molar ratio of complexing. This can be quantitated from a gel scan by adjusting for molecular weight differences and by assuming similar amino acid compositions. For example, Gp100 has a molecular weight of about 75 kDa, so a 1 to 1 molar ratio with Hsp110 would be seen as a ratio of about 0.70 based of Gel-blue band intensities. In practice, this ratio is closer to 0.60 indicating that most Hsp110 molecules are occupied with Gp100 protein antigens. However, simple visualization of both bands by Gel-blue staining appears to guarantee sufficient complexing to generate a significant immune response.

3.3 Measuring the Chaperone Complex-Facilitated Antigen Cross-Presentation In Vitro

In order to test the ability of large HSPs to enhance the cross-presentation of chaperoned protein antigen, mouse bone marrow-derived DCs (BMDCs) are prepared and used as APCs. The mouse tibiae and femurs will be removed and cut with scissors to expose the marrow cavity, and the bone marrow cells are flushed out from the bones using a 3 cc syringe (VWR) attached to a 27-G needle (Becton Dickinson) with ice-cold serum-free RPMI1640. Clusters within the marrow suspension should be disintegrated by vigorous pipetting, followed by the removal of red blood cells from the cell suspension using lysis buffer. Cells are washed and passed through a cell strainer (Becton Dickinson) to remove small pieces of bone and debris. Yields are routinely $5 \sim 7 \times 10^7$ mononuclear cells per mouse (two tibiae and two femurs) with a viability of >99%. Cells in complete BMDCs culture medium are seeded at 2×10^6 cells/well into 12-well plates (Corning) on day 0. The loosely adherent granulocytes should be carefully depleted on day 3 and replaced with fresh BMDC culture medium (*see* **Note 4**). On days 5 and 7 half of the culture supernatant is harvested and centrifuged. The cell pellet is resuspended in fresh medium and given back into the original wells. After 7 day cultures, the clustering adherent DCs will dislodge from the stromal cells and float in the culture medium. On day 9, the non- and semi-adherent cells are collected by gentle

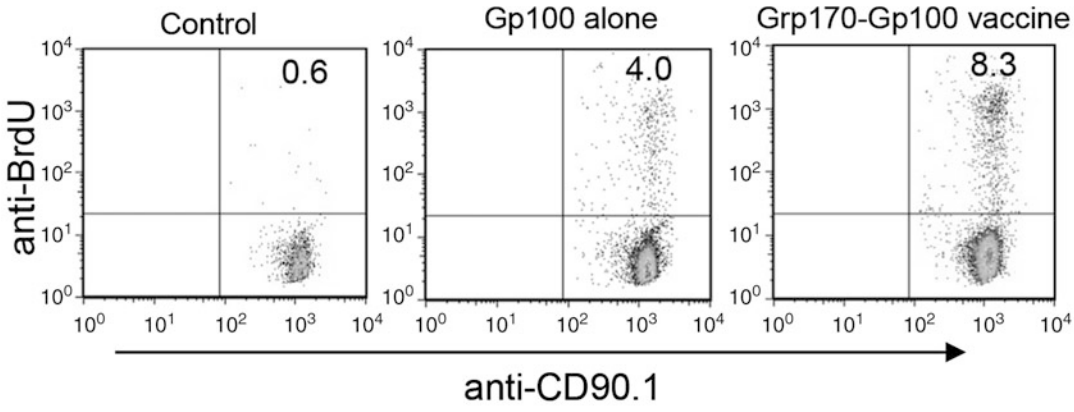

Fig. 2 Recombinant Grp170 promotes cross-presentation of Gp100 and activation of Gp100-specific T cells in vitro. Purified $CD90.1^+CD8^+$ Pmel T cells that recognize MHC I-restricted $Gp100_{25–33}$ peptide were cocultured with BMDCs pulsed with Gp100 or Grp170-Gp100 chaperone complexes at a molar ratio of 10:1 (T cells: DCs) for 72 h. BrdU (10 μM) was added at the beginning of the coculture. Cells were stained with anti-CD8, CD90.1 and BrdU antibodies conjugated with various fluorophores. $BrdU^+$ cells were analyzed using flow cytometry by gating in $CD8^+CD90.1^+$ cells

pipetting using a Pasteur pipet. The cells will be at least 80% of DCs as identified by surface marker CD11c, MHC class II, and B7.1/B7.2.

In vitro antigen-specific T cell proliferation assay will be used to measure large HSP-enhanced antigen cross-presentation. Bromodeoxyuridine (BrdU), a synthetic nucleoside that is an analogue of thymidine, can be incorporated into the newly synthesized DNA of dividing cells. Therefore, BrdU incorporation assay involving immunofluorescent staining of incorporated BrdU and flow cytometric analysis provides an alternative non-radioisotope-based method for assessing the complex-promoted T cell activation. The procedure described here is to determine the frequency of BrdU incorporating T cells following coculture with BMDCs that have been loaded with recombinant large HSP-protein antigen complexes (e.g., Grp170-Gp100). Alternatively, T cell activation may be evaluated by intracellular staining of IFN-γ and flow cytometry analysis that determines the frequency of antigen-specific T cells. The cytokines that indicate T cell activation (e.g., IFN-γ) may also be assessed using ELISA assays with commercially available kits according to the manufacturer's instructions.

BMDCs are incubated with recombinant Gp100 protein, Grp170-Gp100 protein complexes or left untreated in a 200 μl RPMI complete medium overnight at 37 °C. BMDCs are washed and seeded into 96-well U-bottom cell culture cluster as stimulators ($1–2 \times 10^4$/well). Gp100-specific $CD90.1^+$ CD8 T cells are purified from Pmel17 TCR transgenic mice (Jackson Laboratory) as responders using mouse CD8 cell recovery column kit (Cedarlane laboratories Limited) and cocultured with BMDCs at different

ratios in the 96-well plates. BrdU solution is added at a final concentration of 10 μM. After 72 h culture in a humidified 37 °C, 5% CO_2 incubator, the cells are washed and blocked with CD16/CD32 antibodies in FACS staining buffer, followed by staining using anti-CD8-PE and CD90.1-PerCP/Cy5.5 antibodies at 4 °C for 30 min. The cells are fixed, treated with DNase I (300μg/ml), and stained with FITC-conjugated anti-BrdU antibodies (BD Pharmingen). The cells are analyzed on a flow cytometer (e.g., BD FACS Calibur) for the frequency of $BrdU^+$ $CD90.1^+$ T-cells (Fig. 2).

3.4 Measuring the Chaperone Complex Induced T Cell Activation In Vivo

The most reliable readout for the immunogenicity of protein antigen-targeted chaperone complex vaccines is to determine their ability to generate functional T cell responses in vivo. Several T cell assays have been established, which include enzyme-linked immunosorbent spot (ELISPOT) assay, in vitro cytolytic assay, in vivo CTL killing assay, intracellular cytokine staining, ELISA assay, or MHC class I-peptide tetramer assay. Here, we will briefly discuss the ELISPOT assay, which measures the frequency of cytokine producing T cells in response to antigen stimulation on a single-cell level. The ELISPOT assay takes advantage of the relatively high concentration of the cytokines in the environment surrounding the cytokine-secreting cell, which can be captured and detected using high-affinity cytokine antibodies. A total of 25–30 μg of large HSP-protein antigen (e.g., Gp100) complexes is injected in a volume of 100 μl intradermally to naïve mice. Mice immunized with large HSP alone, protein antigen with or without heat shock treatment will serve as controls. One week later, a second vaccination is given to boost the immune responses. Spleen or draining lymph nodes are collected after an additional week and a single-cell suspension is prepared. Red blood cells are removed by lysis buffer. A 96-well, nitrocellulose-backed microtiter plates (Millipore) are precoated with 10 μg/ml rat anti-mouse IFN-γ in PBS overnight at 4 °C or 2 h at room temperature. Splenocytes, lymph node cells, or purified $CD8^+$ T cells purified using magnetic beads (Myltenyi Biotec) are plated at a concentration of $2–10 \times 10^5$ cells/well in RPMI1640 complete medium containing antigens (e.g., 20 μg/ml Gp100 protein or 1 μg/ml $Gp100_{25–32}$ peptide) on a level surface. Following culture in a humidified 37 °C, 5% CO_2 incubator for 24 h and extensive rinse with wash buffer, the plates are incubated sequentially with 5 μg/ml biotinylated IFN-γ antibody and 0.2 U/ml avidin-alkaline phosphatase D. Spots will be developed by adding 5-bromo-4-chloro-3-indolyl phosphatase/Nitro Blue Tetrazolium (BCIP/NBT) to each well and incubating at room temperature until color develops. The number of the spots are counted with a Zeiss ELISPOT reader and presented as the number of IFN-γ spots per 1×10^6 cells (*see* **Note 5**).

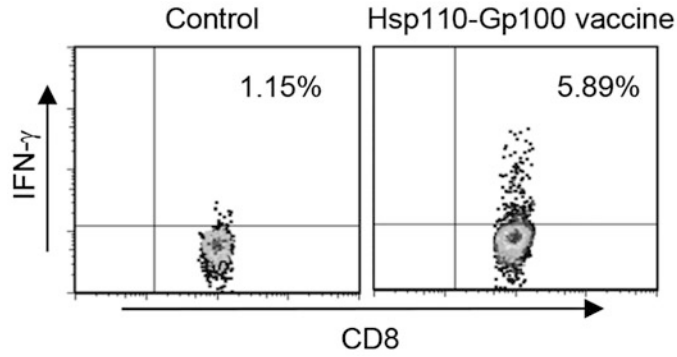

Fig. 3 Recombinant Hsp110-Gp100 chaperone vaccine induces activation of antigen-specific T cell response. C57BL/6 mice were immunized with Hsp110-Gp100 complex vaccine twice at weekly intervals. Lymph node cells were stimulated with $Gp100_{25–33}$ and subjected to intracellular staining for IFN-γ expression to determine the frequency of antigen-specific $CD8^+$ T cells after vaccination

The frequency of IFN-γ producing $CD8^+$ T cells in the spleens and lymph nodes of the Hsp110/Grp170-Gp100 complex-immunized mice may also be examined by intracellular IFN-γ staining and flow cytometry (Fig. 3). Cells prepared from spleen or lymph nodes are stimulated with human $Gp100_{25–33}$ peptide (1 μg/ml) and IL-2 (20 IU/ml) for 3 days in RPMI1640 complete medium. Cells are then stimulated in RPMI1640 complete medium containing Cell Stimulation Cocktail for 4 h followed by staining of cell surface markers (e.g., CD8). After the last wash, the cells are fixed in Fixation Buffer and incubated for 30 min at room temperature in the dark. Cells are washed with Permeabilization Buffer twice and resuspended in 100 μl Permeabilization Buffer (*see* **Note 6**). FITC-conjugated anti-mouse IFN-γ antibody is added and incubated for 30 min at room temperature in the dark. After wash with Permeabilization Buffer, the stained cells are resuspended in Flow Cytometry Staining Buffer and analyzed by flow cytometry to determine the frequency of IFN-γ^+CD8^+ T-cells.

To determine the therapeutic efficacy of the chaperone complex vaccine against transplanted tumor xenografts, B16 melanoma (ATCC) will be established subcutaneously in the flank area of C57BL/6 mice (The Jackson Laboratory). When tumor size reaches ~5–6 mm in diameter, mice will receive chaperone complex (30 μg Gp100 protein complexed with Hsp110 or Grp170 at 1 to 1 molar ratio), Gp100 protein alone (30 μg) or left untreated. The treatment will be performed every 3 days for a total of four doses. Tumor volumes are monitored by measuring perpendicular tumor diameters using an electronic digital caliper. Immune responses will be assayed using the procedures described above.

4 Notes

1. Given the inhibitory effect of FBS on the transfection, it is necessary to wash the insect cell once with BacPAK Grace basic medium (GIBCO) and replace the normal medium with serum-free medium before adding the Bacfectin-DNA mixture to the cells.
2. To achieve maximal protein expression, log phase Sf21 cells that are at least 98% viable should be used for infections. Both the quality of virus plaques and the level of protein production are highly dependent on the viability of the cells. In addition, sometimes a protein antigen can be engineered to improve solubility and expression, e.g., removal of a transmembrane domain as in the case of melanoma antigen Gp100.
3. Including a low concentration of imidazole in the lysis and wash buffers can help minimize nonspecific binding. Drying of the columns should be always avoided during washes, since this will result in the early elution of His-tagged proteins.
4. Male mice are preferred for the generation of DCs because of their larger bone size compared to female mice. We flush out the bone marrow cells using ice-cold serum-free RPMI 1640 instead of the complete medium, because FBS in the complete medium can generate a lot of foam during the repeated flushes that may be harmful to the cells. To increase the purity of DCs, the loosely adherent granulocytes should be removed thoroughly without disturbing the large clusters of DCs.
5. A diffuse darkening of the nitrocellulose membrane is commonly observed when too many cells per well are seeded. Inadequate removal of cells from the ELISPOT plates after antibody incubation may cause a high background. Washing the plate at least once with distilled water will help reduce the "noise".
6. 1 × Permeabilization Buffer for intracellular cytokine staining should be freshly prepared by diluting in ddH_2O. Recover the buffer to room temperature before staining will enhance the sensitivity of antibodies, especially for those samples in which IFN-γ expression is low.

Acknowledgments

This work was supported by National Institutes of Health Grants CA175033, CA154708, W81XWH-13-0455, and in part by

National Cancer Institute (NCI) Cancer Center Support Grant to VCU Massey Cancer Center P30CA16059. X-Y.W. is the Mary Anderson Harrison Distinguished Professor in the VCU Massey Cancer Center.

References

1. Welch WJ (1993) Heat shock proteins functioning as molecular chaperones: their roles in normal and stressed cells. Philos Trans R Soc Lond Ser B Biol Sci 339:327–333
2. Tamura Y, Peng P, Liu K, Daou M, Srivastava PK (1997) Immunotherapy of tumors with autologous tumor-derived heat shock protein preparations. Science 278:117–120
3. Graner M, Raymond A, Romney D, He L, Whitesell L, Katsanis E (2000) Immunoprotective activities of multiple chaperone proteins isolated from murine B-cell leukemia/lymphoma. Clin Cancer Res 6:909–915
4. Wang XY, Kazim L, Repasky EA, Subjeck JR (2001) Characterization of heat shock protein 110 and glucose-regulated protein 170 as cancer vaccines and the effect of fever-range hyperthermia on vaccine activity. J Immunol 166:490–497
5. Srivastava P (2002) Interaction of heat shock proteins with peptides and antigen presenting cells: chaperoning of the innate and adaptive immune responses. Annu Rev Immunol 20:395–425
6. Binder RJ, Han DK, Srivastava PK (2000) CD91: a receptor for heat shock protein gp96. Nat Immunol 1:151–155
7. Delneste Y, Magistrelli G, Gauchat J et al (2002) Involvement of LOX-1 in dendritic cell-mediated antigen cross-presentation. Immunity 17:353–362
8. Berwin B, Hart JP, Rice S et al (2003) Scavenger receptor-a mediates gp96/GRP94 and calreticulin internalization by antigen-presenting cells. EMBO J 22:6127–6136
9. Facciponte JG, Wang XY, Subjeck JR (2007) Hsp110 and Grp170, members of the Hsp70 superfamily, bind to scavenger receptor-a and scavenger receptor expressed by endothelial cells-I. Eur J Immunol 37:2268–2279
10. Asea A, Kraeft SK, Kurt-Jones EA et al (2000) HSP70 stimulates cytokine production through a CD14-dependant pathway, demonstrating its dual role as a chaperone and cytokine. Nat Med 6:435–442
11. Vabulas RM, Ahmad-Nejad P, Ghose S, Kirschning CJ, Issels RD, Wagner H (2002) HSP70 as endogenous stimulus of the toll/interleukin-1 receptor signal pathway. J Biol Chem 277:15107–15112
12. Wang XY, Facciponte JG, Subjeck JR (2006) Molecular chaperones and cancer immunotherapy. Handb Exp Pharmacol 172:305–329
13. Easton DP, Kaneko Y, Subjeck JR (2000) The hsp110 and Grp1 70 stress proteins: newly recognized relatives of the Hsp70s. Cell Stress Chaperones 5:276–290
14. Wang XY, Subjeck JR (2013) High molecular weight stress proteins: identification, cloning and utilisation in cancer immunotherapy. Int J Hyperth 29:364–375
15. Oh HJ, Chen X, Subjeck JR (1997) Hsp110 protects heat-denatured proteins and confers cellular thermoresistance. J Biol Chem 272:31636–31640
16. Park J, Easton DP, Chen X, MacDonald IJ, Wang XY, Subjeck JR (2003) The chaperoning properties of mouse grp170, a member of the third family of hsp70 related proteins. Biochemistry 42:14893–14902
17. Wang XY, Arnouk H, Chen X, Kazim L, Repasky EA, Subjeck JR (2006) Extracellular targeting of endoplasmic reticulum chaperone glucose-regulated protein 170 enhances tumor immunity to a poorly immunogenic melanoma. J Immunol 177:1543–1551
18. Wang XY, Chen X, Manjili MH, Repasky E, Henderson R, Subjeck JR (2003) Targeted immunotherapy using reconstituted chaperone complexes of heat shock protein 110 and melanoma-associated antigen gp100. Cancer Res 63:2553–2560
19. Park JE, Facciponte J, Chen X et al (2006) Chaperoning function of stress protein grp170, a member of the hsp70 superfamily, is responsible for its immunoadjuvant activity. Cancer Res 66:1161–1168
20. Wang XY, Sun X, Chen X et al (2010) Superior antitumor response induced by large stress protein chaperoned protein antigen compared with peptide antigen. J Immunol 184:6309–6319
21. Manjili MH, Henderson R, Wang XY et al (2002) Development of a recombinant HSP110-HER-2/neu vaccine using the chaperoning properties of HSP110. Cancer Res 62:1737–1742

22. Manjili MH, Wang XY, Chen X et al (2003) HSP110-HER2/neu chaperone complex vaccine induces protective immunity against spontaneous mammary tumors in HER-2/neu transgenic mice. J Immunol 171:4054–4061
23. Kim H, Sun X, Subjeck J, Wang X-Y (2007) Evaluation of renal cell carcinoma vaccines targeting carbonic anhydrase IX using heat shock protein 110. Cancer Immunol Immunother 56:1097–1105
24. Qian J, Yi H, Guo C et al (2011) CD204 suppresses large heat shock protein-facilitated priming of tumor antigen gp100-specific T cells and chaperone vaccine activity against mouse melanoma. J Immunol 187:2905–2914
25. Wang H, Yu X, Guo C et al (2013) Enhanced endoplasmic reticulum entry of tumor antigen is crucial for cross-presentation induced by dendritic cell–targeted vaccination. J Immunol 191:6010–6021
26. Guo C, Manjili MH, Subjeck JR, Sarkar D, Fisher PB, Wang XY (2013) Therapeutic cancer vaccines: past, present, and future. Adv Cancer Res 119:421–475
27. Oh HJ, Easton D, Murawski M, Kaneko Y, Subjeck JR (1999) The chaperoning activity of hsp110. Identification of functional domains by use of targeted deletions. J Biol Chem 274:15712–15718

Chapter 26

A Novel Heat Shock Protein 70-based Vaccine Prepared from DC-Tumor Fusion Cells

Desheng Weng, Stuart K. Calderwood, and Jianlin Gong

Abstract

We have developed an enhanced molecular chaperone-based vaccine through rapid isolation of Hsp70 peptide complexes after the fusion of tumor and dendritic cells (Hsp70.PC-F). In this approach, the tumor antigens are introduced into the antigen processing machinery of dendritic cells through the cell fusion process and thus we can obtain antigenic tumor peptides or their intermediates that have been processed by dendritic cells. Our results show that Hsp70.PC-F has increased immunogenicity compared to preparations from tumor cells alone and therefore constitutes an improved formulation of chaperone protein-based tumor vaccine.

Key words Heat shock proteins70 (Hsp70), Dendritic cells (DC), Cell fusion, Extraction of Hsp70 peptide complexes (Hsp70.PC), Tumor vaccine

1 Introduction

The heat shock proteins 70 (Hsp70) family is intrinsic to cellular life, permitting client proteins to perform essential enzymatic, signaling and structural functions within the tightly crowded milieu of the cell and working to avert the catastrophe of protein aggregation during stress [1–3]. There are at least 12 members of the human Hsp70 family, including proteins expressed in the cytoplasm, endoplasmic reticulum, and mitochondria [1, 4, 5]. For molecular chaperone function, Hsp70 family members are equipped with two major functional domains, including a carboxy-terminal region that binds peptides and denatured proteins and an N-terminal ATPase domain that controls the opening and closing of the peptide-binding domain [4, 6]. These two domains play important roles in the functions of Hsp70 in tumor immunity, mediating the acquisition of cellular antigens and their delivery to immune effector cells [7, 8]. Hsp70 expression becomes dysregulated in many types of cancer leading to elevated Hsp70 levels under non-stress conditions that protect emerging cancer cells from the apoptosis

Stuart K. Calderwood and Thomas L. Prince (eds.), *Chaperones: Methods and Protocols*, Methods in Molecular Biology, vol. 1709, https://doi.org/10.1007/978-1-4939-7477-1_26,

that accompanies many steps in transformation, but also create an opportunity for vaccine design [5, 9–12].

The molecular chaperone-based tumor vaccine was pioneered by Srivastava et al. who prepared autologous vaccines in mice and in human patients with the direct aim of targeting the unique antigens that characterize each individual neoplasm [13–17]. In this approach, Hsp70 peptide complexes (Hsp70.PC) are isolated from the patients' tumors by affinity chromatography using ATP-agarose and formulations of Hsp70 applied in a multi-dose regimen. The aim is for Hsp70.PC to facilitate antigen cross-presentation to the patient's T cells through host APC and for the unique mixture of peptides from the individual tumor to induce antitumor immunity. Despite immunologic and clinical responses obtained in a subset of patients with malignant tumors in the early phase I and/or II trials with molecular chaperone GP96.PC (vitespen) purified from patient-derived tumors [16–19], the randomized phase III trials, however, showed mixed results [20, 21].

We have attempted to produce an enhanced molecular chaperone-based vaccine through rapid isolation of Hsp70 peptide complexes from fusions of tumor and dendritic cells (Hsp70.PC-F). In our animal studies, Hsp70.PC-F vaccines show superior immunological properties such as enhanced induction of CTL against tumor cells and stimulation of DC maturation over counterparts from tumor cells [22, 23]. More importantly, immunization of mice with Hsp70.PC-F resulted in a T-cell-mediated immune response including significant increase of CD8 T cells and induction of effector and memory T cells able to break T cell unresponsiveness to a non-mutated tumor antigen and provide protection of mice against challenge with tumor cells. By contrast, the immune response to vaccination with Hsp70.PC derived from tumor cells alone is muted against such non-mutated tumor antigen. Hsp70.PC-F complexes differed from those derived from tumor cells in a number of key manners, most notably, enhanced association with immunologic peptides. In addition, the molecular chaperone Hsp90 was found to be associated with Hsp70.PC-F as indicated by co-immunoprecipitation, suggesting ability to carry an increased repertoire of antigenic peptides by the two chaperones. These experiments indicate that Hsp70.PC derived from DC-tumor fusion cells have increased their immunogenicity and therefore constitute an improved formulation of chaperone protein-based tumor vaccine.

The rationale for the extraction of Hsp70.PC from DC-tumor fusion cells is based on the observation that DC are the most potent antigen-presenting cells [24, 25]. The fusion of DC and tumor cells through chemical [26–43], physical [29, 44–53], or biological [54, 55] means creates a heterokaryon that combines DC-derived costimulatory molecules, efficient antigen-processing and -presentation machinery, and an abundance of tumor-derived antigens.

The DC and tumor cells become one hybrid cell sharing a unified cytoplasm. The integration of cytoplasm from DC and tumor cells renders the tumor antigens endogenous to the DC heterokaryon and, therefore, facilitates the entry of tumor antigens into the DC endogenous pathway of antigen-processing and -presentation machinery [32, 56, 57]. It is likely that the antigen-processing machinery from DC can sort or select the immunogenic peptides to be processed and presented and work much more efficiently than that from tumor cells, thus increasing the quality and quantity of the Hsp-associated complexes.

2 Materials

2.1 Isolation of Tumor Cells from Patient-Derived Solid Sample or Malignant Fluid

DNase (0.1 mg/ml, Sigma-Aldrich, Saint Louis, MO).

Collagenase (1 mg/ml, Worthington Biochemical Corporation, Lakewood, NJ).

Ca^{2+}/Mg^{2+}-free Hanks balanced salt solution (HBSS medium, Mediatech Inc., Manassas, VA).

A sterile 50 μm nylon mesher (Sigma-Aldrich, Saint Louis, MO).

Heat-inactivated human AB serum (Sigma-Aldrich, Saint Louis, MO).

RPMI 1640 medium (Mediatech, Manassas, VA).

L-Glutamine (2 mM, Mediatech, Manassas, VA).

Penicillin and Streptomycin (100 U/ml and 100 μg/ml) (Mediatech Inc., Manassas, VA).

2.2 Generation of DC from Human Peripheral Blood Monocytes

Ficoll density gradient centrifugation (Ficoll-Paque™ plus, GE healthcare Bio-Sciences AB, Sweden).

Granulocyte-macrophage colony-stimulating factor (hGM-CSF, 1000 U/ml) (Genzyme, Framingham, MA).

Interleukin-4 (hIL-4, 500 U/ml) (R&D Systems, Minneapolis, MN).

2.3 Preparation of DC-Tumor Fusions

Polyethylene glycol (PEG, 50% MW1450) (Sigma-Aldrich, Saint Louis, MO).

2.4 Preparation of Hsp70.PC Extraction from DC-Tumor Fusions

Tris–HCl (pH 7.4, 50 mM) (Boston Bioproduct, Ashland, MA).

NaCl (50 mM) (Sigma-Aldrich, Saint Louis, MO).

Nonidet P-40 (NP40, 1%, Sigma-Aldrich, Saint Louis, MO).

Protease inhibitor cocktail tablets, Complete Mini (Roche, Mannheim, Germany).

Sodium Orthovanadate ($NaVO_4$, 1 mM) (Boston Bioproduct, Ashland, MA).

Antibody against human Hsp70 (5C1A12, Developed by ProMab Biotechnologies, Inc., Albany, CA).

Dye Reagent Concentrate for protein assay (Bio-Rad, Hercules, CA).
Protein A Sepharose (GE Healthcare, Waukesha, WI).
Protein G Sepharose (GE Healthcare, Waukesha, WI).

2.5 Measurement of Levels of Endotoxin

Limulus amebocyte lysate (LAL kit, Cambrex Bio Science Inc., Walkersville, MD).

3 Methods

Cell fusion between DC and tumor cells can be achieved through chemical, physical, or biological means. In our laboratory, we use PEG to fuse DC and tumor cells. We have used the following protocol to prepare Hsp70.PC extracts from DC-tumor fusion cells (Fig. 1).

3.1 Generation of DC from Human Peripheral Blood Monocytes

DC can be generated from human peripheral blood monocytes (PBMC) derived from patients or from healthy donors. We usually use Ficoll to separate PBMC and culture these cells in medium containing hGM-CSF. The protocol is based on a previously described method [58–60] with modifications:

1. Peripheral blood mononuclear cells (PBMC) obtained from patients or leucopacks are transferred into 50 ml centrifuge tube and sedimented at low speed.
2. The serum on the top of tube is collected into a clear tube as serum for cell culture. The blood cells at the bottom of the tube are resuspended with RPMI 1640 medium without serum (1:2 dilution).
3. The blood cells are gently laid on the top of the tube containing a Ficoll density gradient.
4. Tubes are centrifuged at $699 \times g$ for 20 min at room temperature.
5. After Ficoll density gradient centrifugation, the cells in the interface layer are collected into another tube with RPMI 1640 and 2% serum.
6. Cells are washed twice with serum-free medium and the numbers of the cells are counted.
7. Culture 1×10^6 cells/ml in RPMI 1640 containing 5% human serum, 2 mM L-glutamine, 100 U/ml penicillin, and 100 μg/ml streptomycin for 1 h in a humidified CO_2 incubator.
8. After 1 h culture, gently wash and remove the non-adherent cells. The adherent fraction is cultured in RPMI/AIM-V (1:1) medium with 1% of human serum and 1000 U/ml hGM-CSF and 500 U/ml hIL-4 for 5 days.

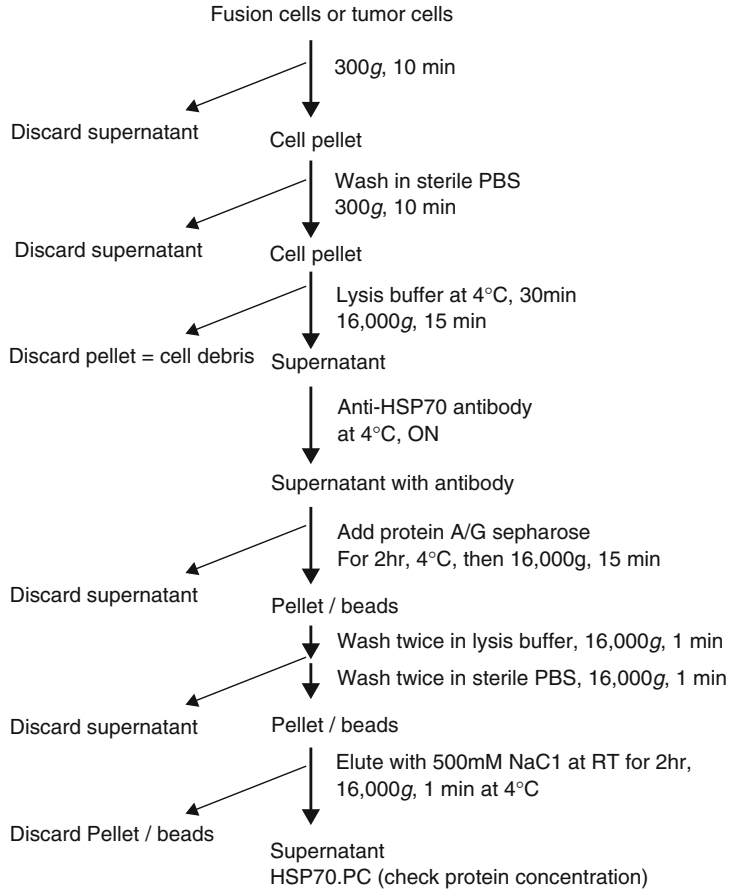

Fig. 1 Flow chart for Hsp70.PC purification

9. On day 3 of culture, cell clusters appear. Fresh medium with 1000 U/ml of hGM-CSF is added if the color of medium becomes yellow.
10. On day 5 of culture, the loosely adherent cell or cell clusters are collected by gently dislodging the cells by pipetting and then the cells are counted (most cells are immature DC).

3.2 Preparation of Tumor Cells

Tumor cells can be either freshly isolated from tumor samples or obtained from vials of frozen cell lines. The method described here is used to isolate and culture tumor cells from patient-derived breast or ovarian cancer sample under sterile condition.

1. The resected human tumor sample is weighted, minced to small pieces (1–3 mm) and digested in HBSS solution containing 1 mg/ml collagenase, 0.1 mg/ml DNase, 100 U/ml penicillin, and 100 μg/ml streptomycin.

2. The digested tumor tissue is then mashed through a sterile 50 μm nylon mesher under sterile conditions in a tissue culture hood.
3. Cells are washed twice with cold HBSS solution.
4. Single-tumor cell suspensions are obtained by passing through a cell strainer and the numbers of tumor cells counted.
5. Culture the tumor cells in high glucose DMEM medium containing 10% human serum and antibiotics. Remove the non-adherent dead cells.
6. Incubate the cells at 37 °C for 2–3 days. The cells are ready for fusion when they are in the logarithmic phase of growth.

3.3 Cell Fusion

1. The DC generated from PBMC are cultured in 1000 U/ml hGM-CSF medium for 5 days.
2. Tumor cells are maintained in DMEM supplemented with 10% heat-inactivated FCS, 2 mM L-glutamine, 100 U/ml penicillin, 100 μg/ml streptomycin.
3. The DC are mixed with tumor cells at a 10:1 ratio and the mixture is washed once with serum-free medium followed by low speed spin (500 rpm) to obtain cell pellets.
4. The mixed cell pellets are gently resuspended in pre-warmed 50% PEG solution (1 ml per 1–5 $\times 10^8$ cells) for 5 min at room temperature.
5. The PEG solution is diluted by slow addition and mixing of 1, 2, 4, 8, and 16 ml warm serum-free medium within 10 min.
6. The cell pellets obtained after centrifugation at 394 $\times g$ are resuspended in RPMI 1640 medium supplemented with 10% heat-inactivated FCS, 2 mM L-glutamine, 10 mM nonessential amino acids, 1 mM sodium pyruvate, 10% NCTC 109, 100 U/ml penicillin, 100 μg/ml streptomycin, and 500 U/ml hGM-CSF, and further cultured for 5 days.
7. After 5 days, DC-tumor fusion cells are loosely adherent to the culture dish, whereas tumor–tumor fusions and unfused tumor cells are attached firmly to the dish. The loosely adherent fusion cells are obtained first by the gentle pipetting.
8. The fusion efficiency is determined by dual expression of tumor antigens such as MUC1 and DC markers (MHC class II molecules or co-stimulatory molecules).

3.4 Extraction of Hsp70 Peptide Complexes (Hsp70.PC) from DC-Tumor Fusion Cell Products

1. DC-tumor fusion cells are collected and counted.
2. Resuspend the cell pellets with lysis buffer (50 mM Tris–HCl, pH 8.0, containing 50 mM NaCl, 1% Nonidet P-40, 1 mM PMSF) (1 ml lysis buffer for 2 $\times 10^7$ cells) on ice for 30 min.
3. Centrifuge the cell lysate at 9116 $\times g$ for 15 min at 4 °C.

4. After centrifuge, collect the supernatant into a clear tube.
5. Check protein concentration with standard procedure (Bio-Rad Bradford Protein Assay Kit):
   (a) Prepare dye reagent by diluting one part Dye Reagent Concentrate with four parts distilled, deionized water.
   (b) Prepare three to five dilutions of a protein standard, which is representative of the protein solution to be tested.
   (c) Pipette 100 μl of each standard and sample solutions into 5.0 ml of diluted dye reagent.
   (d) Incubate the test samples at room temperature for at least 5 min. Absorbance will increase over time. Samples should be incubated at room temperature for not more than 15 min.
   (e) Measure absorbance at 595 nm. Calculate the protein concentration based on the standard curve.
6. The lysates are clarified by centrifugation, and the aqueous phase is collected and incubated with mAb against human Hsp70 at a concentration of 1:100, rotating through overnight at 4 °C.
7. For protein analysis, the immunoprecipitates are dissolved in Laemmli SDS sample buffer (0.1 Tris-Cl, 4% SDS, 20% glycerol, 0.05% bromphenol blue, 5% 2-ME) and analyzed by immunoblotting.

   For Binding of the Immune Complex:
   (a) Mix Protein A Sepharose and Protein G Sepharose at a 1:1 ratio followed by wash with lysis buffer once.
   (b) Spin down at 13,000 rpm for 1 min at 4 °C, discard the supernatant, and resuspend the beads with 250 μl lysis buffer.
   (c) Pipette 100 μl A/G mixture beads into sample tubes and incubate for 2 h at 4 °C.
   (d) After incubation, spin down at 13,000 rpm for 1 min at 4 °C. Remove the supernatant.
   (e) Wash beads with 0.5 ml of lysis buffer for 5 min (rotate at 4 °C) followed by centrifugation at 13,000 rpm for 1 min at 4 °C.
   (f) Wash beads with 0.5 ml of sterile PBS for 5 min (rotate at 4 °C) followed by centrifugation at 13,000 rpm for 1 min at 4 °C.
8. After extensive wash with lysis buffer, the immunoprecipitates are eluted with sterile high salt elution buffer.
   (a) Elute the proteins with (500 mM NaCl, 100 μl) at RT for 2 h.

(b) Centrifuge at 13,000 rpm for 1 min at 4 °C.

(c) Collect the supernatant and measure the protein concentration by Bradford protein assay.

9. The Hsp70.PC preparations are checked by the limulus amebocyte lysate assay to ensure minimal contamination with endotoxins, aliquoted into 1.5 ml eppendorf tubes and stored at −80 °C.

4 Notes

The PEG solution is diluted by gradual addition and progressive mixing of 1, 2, 4, 8, and 16 ml warm serum-free medium. The cell pellets obtained after centrifugation at 1350 rpm are resuspended in the medium containing 10% heat-inactivated FCS and GM-CSF. The variable factor for cell fusion is the length of time the cells are exposed to PEG. We have found that there is some difference in the sensitivity of cells to PEG. It is desirable to perform a dose–response test to evaluate the conditions of PEG fusion for each type of tumor cell and to determine the optimal exposure time. Unlike electrofusion, DC–tumor fusion by PEG is an active and evolving process, and it is thus likely that the larger the initial contact surface between the cells, the faster the integration of these cells. Fusion efficiency is lowest immediately after the fusion process is initiated, and one-week culture results in more than a tenfold increase in efficiency (Gong J., unpublished data). In addition, short-term culture will give the fusion cells sufficient time to integrate and display the antigen in the context of MHC molecules.

For protein concentration measurement, Bradford dye reagent absorbance will increase over time. Samples should incubate at room temperature for at least 5 min, but no more than 15 min. After protein A/G sepharose binding with Hsp70 immunoglobulin, the beads should be gently mixed with lysis buffer to wash off nonspecific interactions. However, the use of vortex should be avoided since it may break the binding of sepharose beads and immunoglobulins. Background caused by actin contamination can be avoided by adding 10 mM ATP to lysis buffer. All the steps should be performed at 4 °C to reduce proteolysis and denaturation of antigens. This is especially important for the binding step which is typically incubated overnight (or at least 2 h) at 4 °C.

References

1. Lindquist S, Craig EA (1988) The heat shock proteins. Ann Rev Genet 22:631–637
2. Georgopolis C, Welch WJ (1993) Role of the major heat shock proteins as molecular chaperones. Ann Rev Cell Biol 9:601–634
3. Richter K, Haslbeck M, Buchner J (2010) The heat shock response: life on the verge of death. Mol Cell 40(2):253–266
4. Bukau B, Horwich AL (1998) The Hsp70 and Hsp60 chaperone machines. Cell 92 (3):351–366
5. Tang D et al (2005) Expression of heat shock proteins and HSP messenger ribonucleic acid in human prostate carcinoma in vitro and in tumors in vivo. Cell Stress Chaperones 10:46–58
6. Kityk R et al (2015) Pathways of allosteric regulation in Hsp70 chaperones. Nat Commun 6:8308
7. Noessner E et al (2002) Tumor-derived heat shock protein 70 peptide complexes are cross-presented by human dendritic cells. J Immunol 169(10):5424–5432
8. Srivastava PK, Amato RJ (2001) Heat shock proteins: the 'Swiss Army Knife' vaccines against cancers and infectious agents. Vaccine 19(17–19):2590–2597
9. Nylandsted J, Brand K, Jaattela M (2000) Heat shock protein 70 is required for the survival of cancer cells. Ann N Y Acad Sci 926:122–125
10. Cornford PA et al (2000) Heat shock protein expression independently predicts clinical outcome in prostate cancer. Cancer Res 60 (24):7099–7105
11. Clark PR, Menoret A (2001) The inducible Hsp70 as a marker of tumor immunogenicity. Cell Stress Chaperones 6(2):121–125
12. Calderwood SK, Gong J (2016) Heat shock proteins promote cancer: it's a protection racket. Trends Biochem Sci 41:311–323
13. Srivastava P (2002) Interaction of heat shock proteins with peptides and antigen presenting cells: chaperoning of the innate and adaptive immune responses. Annu Rev Immunol 20:395–425
14. Srivastava P (2003) Hypothesis: controlled necrosis as a tool for immunotherapy of human cancer. Cancer Immun 3:4
15. Srivastava PK (2000) Immunotherapy of human cancer: lessons from mice. Nat Immunol 1(5):363–366
16. Belli F et al (2002) Vaccination of metastatic melanoma patients with autologous tumor-derived heat shock protein gp96-peptide complexes: clinical and immunologic findings. J Clin Oncol 20(20):4169–4180
17. Mazzaferro V et al (2003) Vaccination with autologous tumor-derived heat-shock protein gp96 after liver resection for metastatic colorectal cancer. Clin Cancer Res 9(9):3235–3245
18. Parmiani G et al (2006) Heat shock proteins gp96 as immunogens in cancer patients. Int J Hyperth 22(3):223–227
19. Pilla L et al (2006) A phase II trial of vaccination with autologous, tumor-derived heat-shock protein peptide complexes Gp96, in combination with GM-CSF and interferon-alpha in metastatic melanoma patients. Cancer Immunol Immunother 55(8):958–968
20. Testori A et al (2008) Phase III comparison of vitespen, an autologous tumor-derived heat shock protein gp96 peptide complex vaccine, with physician's choice of treatment for stage IV melanoma: the C-100-21 Study Group. J Clin Oncol 26(6):955–962
21. Wood C et al (2008) An adjuvant autologous therapeutic vaccine (HSPPC-96; vitespen) versus observation alone for patients at high risk of recurrence after nephrectomy for renal cell carcinoma: a multicentre, open-label, randomised phase III trial. Lancet 372(9633):145–154
22. Enomoto Y et al (2006) Enhanced immunogenicity of heat shock protein 70 peptide complexes from dendritic cell-tumor fusion cells. J Immunol 177(9):5946–5955
23. Weng D et al (2013) Immunotherapy of radioresistant mammary tumors with early metastasis using molecular chaperone vaccines combined with ionizing radiation. J Immunol 191(2):755–763
24. Steinman RM (1991) The dendritic cell system and its role in immunogenicity. Annu Rev Immunol 9:271–296
25. Steinman RM (2001) Dendritic cells and the control of immunity: enhancing the efficiency of antigen presentation. Mt Sinai J Med 68 (3):106–166
26. Gong J et al (1997) Induction of antitumor activity by immunization with fusions of dendritic and carcinoma cells. Nat Med 3 (5):558–561
27. Gong J et al (2002) Immunization against murine multiple myeloma with fusions of dendritic and plasmacytoma cells is potentiated by interleukin 12. Blood 99(7):2512–2517
28. Liu Y et al (2002) Engineered fusion hybrid vaccine of IL-4 gene-modified myeloma and relative mature dendritic cells enhances antitumor immunity. Leuk Res 26(8):757–763

29. Lindner M, Schirrmacher V (2002) Tumour cell-dendritic cell fusion for cancer immunotherapy: comparison of therapeutic efficiency of polyethylen-glycol versus electro-fusion protocols. Eur J Clin Investig 32(3):207–217
30. Homma S et al (2001) Preventive antitumor activity against hepatocellular carcinoma (HCC) induced by immunization with fusions of dendritic cells and HCC cells in mice. J Gastroenterol 36(11):764–771
31. Cao X et al (1999) Therapy of established tumour with a hybrid cellular vaccine generated by using granulocyte-macrophage colony-stimulating factor genetically modified dendritic cells. Immunology 97(4):616–625
32. Wang J et al (1998) Eliciting T cell immunity against poorly immunogenic tumors by immunization with dendritic cell-tumor fusion vaccines. J Immunol 161(10):5516–5524
33. Hayashi T et al (2002) Immunogenicity and therapeutic efficacy of dendritic-tumor hybrid cells generated by electrofusion. Clin Immunol 104(1):14–20
34. Xia J et al (2003) Prevention of spontaneous breast carcinoma by prophylactic vaccination with dendritic/tumor fusion cells. J Immunol 170(4):1980–1986
35. Kao JY et al (2003) Tumor-derived TGF-beta reduces the efficacy of dendritic cell/tumor fusion vaccine. J Immunol 170(7):3806–3811
36. Takeda A et al (2003) Immature dendritic cell/tumor cell fusions induce potent antitumour immunity. Eur J Clin Investig 33(10):897–904
37. Zhang JK et al (2003) Antitumor immunopreventive and immunotherapeutic effect in mice induced by hybrid vaccine of dendritic cells and hepatocarcinoma in vivo. World J Gastroenterol 9(3):479–484
38. Li J et al (2001) Purified hybrid cells from dendritic cell and tumor cell fusions are superior activators of antitumor immunity. Cancer Immunol Immunother 50(9):456–462
39. Xia D, Chan T, Xiang J (2005) Dendritic cell/myeloma hybrid vaccine. Methods Mol Med 113:225–233
40. Homma S et al (2005) Cancer immunotherapy by fusions of dendritic and tumour cells and rh-IL-12. Eur J Clin Investig 35(4):279–286
41. Kao JY et al (2005) Superior efficacy of dendritic cell-tumor fusion vaccine compared with tumor lysate-pulsed dendritic cell vaccine in colon cancer. Immunol Lett 101(2):154–159
42. Ogawa F, Iinuma H, Okinaga K (2004) Dendritic cell vaccine therapy by immunization with fusion cells of interleukin-2 gene-transduced, spleen-derived dendritic cells and tumour cells. Scand J Immunol 59 (5):432–439
43. Akasaki Y et al (2001) Antitumor effect of immunizations with fusions of dendritic and glioma cells in a mouse brain tumor model. J Immunother 24(2):106–113
44. Scott-Taylor TH et al (2000) Human tumour and dendritic cell hybrids generated by electrofusion: potential for cancer vaccines. Biochim Biophys Acta 1500(3):265–279
45. Tanaka H et al (2002) Therapeutic immune response induced by electrofusion of dendritic and tumor cells. Cell Immunol 220(1):1–12
46. Siders WM et al (2003) Induction of specific antitumor immunity in the mouse with the electrofusion product of tumor cells and dendritic cells. Mol Ther 7(4):498–505
47. Jantscheff P et al (2002) Cell fusion: an approach to generating constitutively proliferating human tumor antigen-presenting cells. Cancer Immunol Immunother 51(7):367–375
48. Goddard RV et al (2003) In vitro dendritic cell-induced T cell responses to B cell chronic lymphocytic leukaemia enhanced by IL-15 and dendritic cell-B-CLL electrofusion hybrids. Clin Exp Immunol 131(1):82–89
49. Marten A et al (2003) Allogeneic dendritic cells fused with tumor cells: preclinical results and outcome of a clinical phase I/II trial in patients with metastatic renal cell carcinoma. Hum Gene Ther 14(5):483–494
50. Trevor KT et al (2004) Generation of dendritic cell-tumor cell hybrids by electrofusion for clinical vaccine application. Cancer Immunol Immunother 53(8):705–714
51. Suzuki T et al (2005) Vaccination of dendritic cells loaded with interleukin-12-secreting cancer cells augments in vivo antitumor immunity: characteristics of syngeneic and allogeneic antigen-presenting cell cancer hybrid cells. Clin Cancer Res 11(1):58–66
52. Trefzer U et al (2005) Tumour-dendritic hybrid cell vaccination for the treatment of patients with malignant melanoma: immunological effects and clinical results. Vaccine 23 (17–18):2367–2373
53. Shimizu K et al (2004) Comparative analysis of antigen loading strategies of dendritic cells for tumor immunotherapy. J Immunother 27 (4):265–272
54. Phan V et al (2003) A new genetic method to generate and isolate small, short-lived but highly potent dendritic cell-tumor cell hybrid vaccines. Nat Med 9(9):1215–1219
55. Hiraoka K et al (2004) Enhanced tumor-specific long-term immunity of hemagglutinating [correction of hemaggluttinating] virus of

Japan-mediated dendritic cell-tumor fused cell vaccination by coadministration with CpG oligodeoxynucleotides. J Immunol 173 (7):4297–4307

56. Koido S et al (2004) Dendritic cells fused with human cancer cells: morphology, antigen expression, and T cell stimulation. Clin Immunol 113(3):261–269
57. Galea-Lauri J et al (2002) Eliciting cytotoxic T lymphocytes against acute myeloid leukemia-derived antigens: evaluation of dendritic cell-leukemia cell hybrids and other antigen-loading strategies for dendritic cell-based vaccination. Cancer Immunol Immunother 51 (6):299–310
58. Gong J et al (2000) Fusions of human ovarian carcinoma cells with autologous or allogeneic dendritic cells induce antitumor immunity. J Immunol 165(3):1705–1711
59. Gong J et al (2000) Activation of antitumor cytotoxic T lymphocytes by fusions of human dendritic cells and breast carcinoma cells. Proc Natl Acad Sci U S A 97(6):2715–2718
60. Koido S et al (2005) Assessment of fusion cells from patient-derived ovarian carcinoma cells and dendritic cells as a vaccine for clinical use. Gynecol Oncol 99(2):462–471

Chapter 27

Hsp70: A Cancer Target Inside and Outside the Cell

Christophe Boudesco, Sebastien Cause, Gaëtan Jego, and Carmen Garrido

Abstract

Heat shock protein 70 (Hsp70) is the most ubiquitous stress-inducible chaperone. It accumulates in the cells in response to a wide variety of physiological and environmental insults including anticancer chemotherapy, thus allowing the cell to survive to lethal conditions. Intracellular Hsp70 is viewed as a cytoprotective protein. Indeed, this protein can inhibit key effectors of the apoptotic and autophagy machineries. In cancer cells, the expression of Hsp70 is abnormally high, and Hsp70 may participate in oncogenesis and in resistance to chemotherapy. In rodent models, Hsp70 overexpression increases tumor growth and metastatic potential. Depletion or inhibition of Hsp70 frequently reduces the size of the tumors and can even cause their complete involution. However, HSP70 is also found in the extra-cellular space where it may signal via membrane receptors or endosomes to alter gene transcription and cellular function. Overall, Hsp70 extracellular function is believed to be immnunogenic and the term chaperokine to define the extracellular chaperones such as Hsp70 has been advanced. In this chapter the knowledge to date, as well as some emerging paradigms about the intra- and extra-cellular functions of Hsp70, are presented. The strategies targeting Hsp70 that are being developed in cancer therapy will also be discussed.

Key words Hsp70, Apoptosis, Cancer, Anti-cancer therapy, Immunomodulator

Abbreviations

Hsp	Heat shock proteins
MDSC	Myeloid-derived suppressive cells
ROS	Reactive oxygen species
TLR	Toll-like receptor

Gaëtan Jego and Carmen Garrido contributed equally to this work.

Stuart K. Calderwood and Thomas L. Prince (eds.), *Chaperones: Methods and Protocols*, Methods in Molecular Biology, vol. 1709, https://doi.org/10.1007/978-1-4939-7477-1_27, © Springer Science+Business Media, LLC 2018

1 Introduction

The heat shock response is a universal mechanism induced by almost all cells and tissues after many different stresses, it is associated with an increase in the expression of a family of proteins called heat shock proteins (Hsps). Most Hsps have strong cytoprotective effects and behave as molecular chaperones for other cellular proteins [1]. Acute or chronic stress results in protein misfolding, protein aggregation, or disruption of regulatory complexes. The action of chaperones, through their properties in protein homeostasis, is thought to restore balance. Mammalian Hsps have been classified into five families according to their molecular size: Hsp100, Hsp90, Hsp70, Hsp60, and small Hsps (15–30 kDa) that includes Hsp27. Each family of Hsps is composed of members that are expressed either constitutively or regulated inductively, and that are targeted to different subcellular compartments. High molecular weight Hsps are ATP-dependent chaperones, while small Hsps act in an ATP-independent fashion. Chaperones are instrumental for signaling and protein traffic, even in the absence of stress. However, the need of Hsps increases after proteotoxic damage. Hsp70 is one of the most strongly and universally induced chaperones and has strong cytoprotective properties. Overexpressed Hsp70 prevents cell death triggered by various stimuli, including hyperthermia, oxidative stress, or cytotoxic drugs [2, 3]. Several among these stimuli induce Hsp70 overexpression themselves [4, 5], providing an example of how pro-apoptotic stimuli, delivered below a threshold level, can elicit protective responses.

Hsps have also been shown to play a role in cell differentiation. For instance, we and other groups have demonstrated that Hsp70 played a key role in erythroid differentiation. During red blood cells formation, Hsp70 accumulates within the nucleus of the erythroblast and directly associates with GATA-1 protecting this transcription factor required for erythropoiesis from its inactivation. As a result, erythroblats continue their differentiation process instead of dying by apoptosis [6]. We have demonstrated that defects in Hsp70 nuclear translocation are at the base of erythropoietic pathologies like Myelodisplatic syndromes or beta-thalassemia [7, 8].

Hsp70 basal levels are unusually high in malignant cells, and Hsp70 has been involved in oncogenesis and/or in chemotherapy resistance, presumably due to its capacity to disable cell death [9]. In this chapter, we will describe the different pathways through which Hsp70 modulates cancer cell death and the emerging strategies that are being developed for cancer therapy. The immunogenic function of extra-cellular Hsp70 will also be discussed.

2 Cytoprotective Functions of Hsp70

2.1 Hsp70 Is a Molecular Chaperone

Human cells contain several Hsp70 family members including stress-inducible Hsp70, constitutively expressed Hsc70, mitochondrial Hsp75, and GRP78, which is localized in the endoplasmic reticulum [10]. Hsp70 proteins function as ATP-dependent molecular chaperones. Under stressful conditions, elevated Hsp70 levels allow cells to cope with increased concentrations of unfolded or denatured proteins [11]. Some of the important house-keeping functions attributed to Hsp70 include: (1) import of proteins into cellular compartments; (2) folding of proteins in the cytosol, endoplasmic reticulum, and mitochondria; (3) degradation of unstable proteins; (4) dissolution of protein complexes; (5) control of regulatory proteins; (6) refolding of misfolded proteins; and (7) translocation of precursor proteins into mitochondria [12].

Hsp70 contains two distinct functional regions (Fig. 1): a peptide-binding domain (PBD) and the amino-terminal ATPase domain (ABD). The PBD, which includes a carboxyl-terminal chaperone EEVD motif, is responsible for substrate binding and refolding. The ABD, in turn, facilitates the release of the client protein after ATP hydrolysis. A conserved proline in the ATPase domain is essential to alternate Hsp70 conformations in response to ATP binding and hydrolysis [13]. Distinct co-chaperones bind to Hsp70 and regulate its chaperone function (Fig. 1). They can be classified into three groups. (A) The J-domain co-chaperones, like Hsp40, are a relatively large group that binds to the Hsp70 ABD and stimulate the low ATPase activity of this chaperone [14, 15]. (B) The nucleotide exchange factor co-chaperones catalyze the release of ADP, which is required for the completion of Hsp70 ATPase cycle. Members of this group are Bag-1, Bag-3, Hsp110, or HspBP1. Of note, in the context of tumors, Hsp70s role in the regulation of signaling has been reported to be mediated by Bag3 [16] whereas in the regulation of tumorigenesis, at least in colon cancer, Hsp110 seems to be the essential co-chaperone [17, 18]. C) The TPR domain co-chaperones (Hop, CHIP) bind to the C-terminal EEVD motif presented in both Hsp70 and Hsp90 [19]. They are essential for combinational assembly of Hsp70 and Hsp90 complexes. CHIP, which has an ubiquitin ligase activity, has been implied in the ubiquitination of at least some Hsp client proteins [19].

It must be noted that most of the information on human Hsp70 is derived from the *E. coli* Hsp70 homolog DnaK, although this bacterial homolog only shares ~50% amino acid sequence identity [20]. To get more insight into the structure of human Hsp70, we have produced the protein using a recently developed methodology, which allows the production of large quantities of pure, full-length, and fully active human Hsp70 [21]. After the

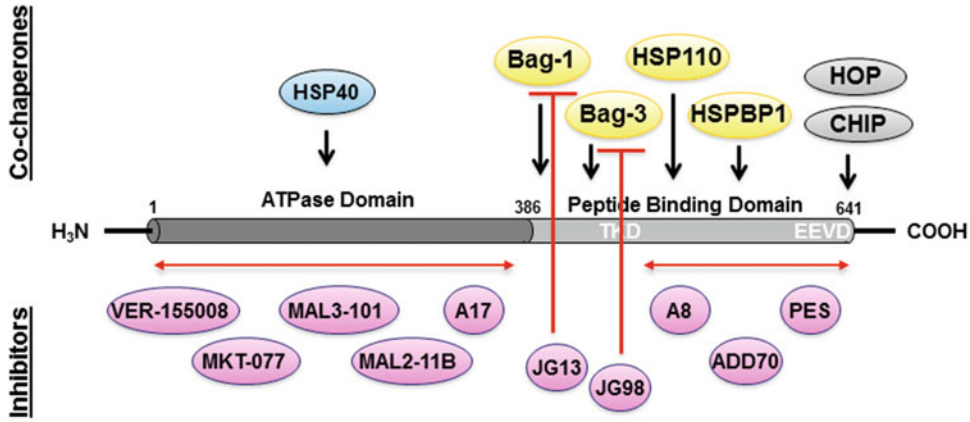

Fig. 1 Structure of Hsp70 with co-chaperones and sites of action of drugs discussed in the review. HSP70 contains two distinct functional regions: a Peptide Binding Domain (PBD) that includes a carboxyl-terminal EEVD motif or chaperone motif which is responsible for substrate binding and refolding, and the amino-terminal ATP binding domain or ATPase Domain (ABD), which facilitates the release of the client protein. Indicated are the main co-chaperones that regulate Hsp70 chaperone function. Below, the principal inhibitors of Hsp70 are listed (see the text)

analysis of the protein by multi-angle light scattering combined with bio-layer interferometry, we have shown that whereas human Hsp70 can form homodimers that involve the C-terminal domain, bacterial Hsp70 cannot [21].

2.2 Hsp70 Cytoprotective Function

Hsp70 is an evolutionarily conserved protein whose expression enhances the ability of cells to survive to a panel of lethal conditions. Gene ablation studies demonstrate that Hsp70 plays an important role in apoptosis. Cells lacking *hsp70.1* and *hsp70.3*, the two genes that code for inducible Hsp70, are highly sensitive to apoptosis induced by a wide range of lethal stimuli [22]. Ablation of the testis-specific isoform of Hsp70 (*hsp70.2*) results in germ cell apoptosis. In line with these results, overexpression of Hsp70 inhibits apoptosis and prevents caspase activation in many different cellular models upon a variety of cellular stresses, including accumulation of misfolded proteins, ROS, or DNA damage [23–25]. On the contrary, depletion of Hsp70, either by antisense constructions or siRNA strategies, increases the cells' sensitivity to apoptotic stimuli [26, 27]. In some cellular contexts, Hsp70 depletion is sufficient to trigger apoptosis through caspase-3 activation, in the absence of any additional stressful stimulus [27, 28].

2.2.1 Inhibition of Apoptosis

Hsp70 interacts with several targets in upstream signaling pathways. Growth factors, such as nerve growth factor or platelet-derived growth factor, induce cell survival by activating the Phosphatidylinositol 3-Kinase pathway (PI3-K). Activated PI3-K phosphorylates inositol lipids in the plasma membrane that attract the

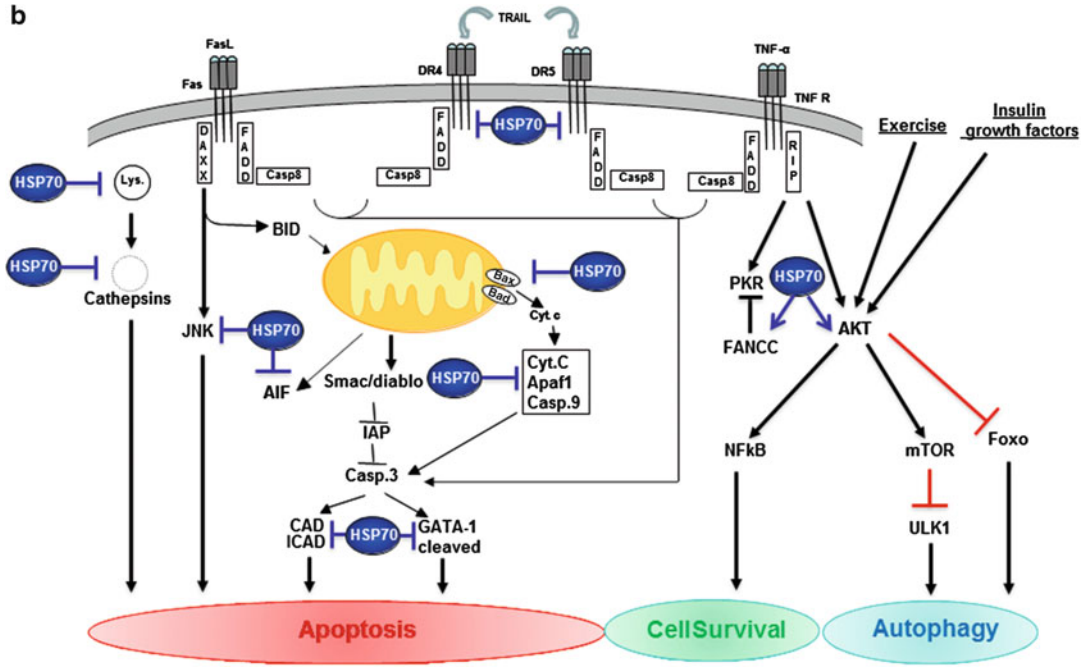

Fig. 2 Targets of Hsp70 in the apoptotic and cell survival pathways. HSP70 is a decisive negative regulator of the mitochondrial pathway of apoptosis that can block cell death at different levels. At a pre-mitochondrial stage by inhibiting stress inducing signals; at the mitochondrial stage, by preventing mitochondrial membrane permeabilization through the blockage of Bax translocation; and, finally, at the post-mitochondrial level by interacting with AIF and Apaf-1 or by protecting essential nuclear proteins from caspase-3 cleavage. Hsp70 also favors cell survival through Akt

serine/threonine kinase Akt/PKB, a protein that generates a survival signal in response to growth factor stimulation. Hsp70 binds and stabilizes Akt/PKB (Fig. 2) [29]. Interestingly, the endothelial-specific HspA12B, a distant member of Hsp70 family that is required for zebrafish vasculature development, is involved in endothelial cell migration and tube formation through sustaining Akt activity [30]. Thus, Hsp70 family members could play a role in both the control of cell survival and differentiation. Hsp70 also binds to non-phosphorylated Protein Kinase C (PKC) via the kinase's unphosphorylated carboxyl-terminus, priming the kinase for rephosphorylation and stabilizing the protein [29].

Hsp70 can inhibit stress-activated kinases such as apoptosis signal regulating kinase 1 (Ask1), e.g., Hsp70 downregulation facilitates H_2O_2-induced Ask1 activation and subsequent apoptosis in NIH3T3 cells [31]. Hsp70 also binds to c-Jun N-terminal Kinase (JNK), and prevents its activation independently of ATP [3, 24]. For example, MEF *hsp70.1*$^{-/-}$ resist to JNK-mediated apoptosis induced by hyperosmolarity whereas AEG3482, a promising novel compound, inhibits JNK activity through

increased expression of Hsp70 [32, 33]. Hsp70 also negatively interferes with p38 kinase activity [34].

The role of Hsp70 in regulating Nuclear Factor-κB (NF-κB) function is more controversial. It has been postulated that cytosolic Hsp70 could inhibit NF-κB while plasma membrane-associated Hsp70 could activate this transcription factor [35–38]. However, the stimuli that induce accumulation of cytosolic and membrane-bound Hsp70 are the same [39, 40].

Hsp70 has also been shown to affect some transcription factors involved in the expression of the Bcl-2 family. Bcl-2 and Bax are transcriptional targets of the tumor suppressor protein p53: the transcription of Bcl-2 is repressed by p53 whereas that of Bax is induced. As a consequence, p53 expression induces apoptosis in response to DNA damage [1]. Many tumor cells have a mutated p53 and either Hsp70 or Hsc70 could form stable complexes with this mutant protein. Hsp70 could also mask the nuclear localization sequence of p53, thus preventing its nuclear import [41].

At the mitochondrial level, Hsp70 coupled to Hsp40 blocks Bax translocation, thus preventing mitochondrial outer membrane permeabilization and inhibiting the release of cytochrome c and other mitochondrial apoptogenic molecules such as Apoptosis Inducing Factor (AIF) [42]. This Hsp70 function depends on both its chaperone and its ATP hydrolytic domains (Fig. 2) [43, 44].

Hsp70 also acts at the post-mitochondrial level. It has been found that Hsp70 inhibited apoptosis downstream of the release of cytochrome c and upstream of the activation of caspase-3. Indeed, Hsp70 has been demonstrated to bind directly to Apaf-1, thereby preventing the recruitment of procaspase-9 to the apoptosome [45]. The ATPase domain of Hsp70 was described to be necessary for this interaction [46]. One protein target of caspase-3 is the Caspase Activated DNAse (CAD), responsible for chromosomal DNA digestion during the final phases of apoptosis. The enzymatic activity and proper folding of CAD has been reported to be regulated by Hsp70, its co-chaperone Hsp40 and ICAD, the inhibitor of CAD. ICAD recognizes an intermediate folding state conferred by Hsp70-Hsp40 [47]. It has also been reported in TCR-stimulated T cells that Hsp70 binds CAD and enhances its activity [48]. Poly [ADP-ribose] polymerase (PARP), a nuclear protein involved in DNA repair, is an early target of caspase-3 and its inactivation by cleavage is necessary to prevent necrosis and inflammation during apoptosis. It has also been shown that Hsp70 interacts simultaneously with PARP1 and XRCC1, another DNA repair protein, in the nucleus of cells undergoing single-strand breaks after heat treatment [49]. These results suggest that Hsp70 could play a role in DNA integrity through its association with PARP1 to create the repair protein complex. Another final target of caspase-3 is the transcription factor GATA-1. We have

demonstrated in human primary erythroid precursors that Hsp70 can protect GATA-1 from caspase-3 cleavage. As a consequence, erythroid cells do not die by apoptosis but instead differentiate (Fig. 2) [6, 8]. Therefore, HSP70 by acting at a very late point in the apoptotic pathway can rescue cells from the dying.

2.2.2 Hsp70 and the Extrinsic Death Receptor Pathway

Hsp70 inhibits TNF-α-induced neuronal cell death during hypoxia [50]. Exposure of hematopoietic cells to TNF-α induces the activity of the pro-apoptotic double-stranded RNA-dependent Protein Kinase (PKR). An inhibitor of PKR is the Fanconi Anemia Complementation group C gene product (FANCC). Hsp70 interacts with the FANCC protein via its ATPase domain and, together with Hsp40, inhibits TNF-induced apoptosis through the ternary complex Hsp70, FANCC, and PKR [51, 52].

In human chronic myeloid leukemia cells, Hsp70 can mediate Bcr-Abl-induced resistance to TNFα-Related Apoptosis-Inducing Ligand (TRAIL)-induced apoptosis by preventing the formation of death-inducing signaling complexes involving the death receptors DR4 and DR5 (Fig. 2) [53]. The role of Hsp70 in Fas-mediated apoptosis is more controversial with opposite effects that depend on the cellular context. However, Hsp70 can block the cleavage of Bid by activated caspase-8 [54].

2.2.3 Hsp70 and Alternatives Apoptosis-Like Pathways

Upon activation of the intrinsic pathway, not only cytochrome c is released from the mitochondria. AIF and endonuclease G (EndoG), two mitochondria intermembrane proteins, translocate to the nucleus and trigger caspase-independent nuclear changes (Fig. 2) [55]. Hsp70 has been shown to prevent cell death in conditions in which caspase activation does not occur, either due to the addition of exogenous caspase inhibitors [56], or in cells in which Apaf-1 or caspase-9 were genetically inactivated [57], indicating that the cytochrome c/Apaf-1/caspase was not the sole pathway involved in the anti-apoptotic effect of Hsp70. Indeed, Hsp70 directly binds to AIF and inhibits AIF-induced chromatin condensation. Of note, endogenous levels of Hsp70 seem to be sufficiently high to control AIF-mediated apoptosis since down-regulation of Hsp70 by an anti-sense construct sensitized the cells to serum withdrawal and AIF [57]. This protective effect of Hsp70 might be physiologically relevant as AIF sequestration by Hsp70 reduces neonatal hypoxic/ischemic brain injury [58]. In addition, Hsp70 inhibits erythroblast apoptosis by blocking the nuclear import of AIF [59]. Hsp70 also associates with EndoG to prevent DNA fragmentation, but this association could involve AIF as a molecular bridge [60].

2.2.4 Hsp70 and Autophagy

Lysosomes also function as integrators of cell death signals in many different cell death scenarios [61, 62]. Lysosomal proteases, of which the most studied are the cathepsins, translocate from the

lysosomal lumen to the cytosol in response to a wide variety of apoptotic stimuli. Upon release to the cytosol, cathepsins can trigger mitochondrial outer membrane permeabilization [63, 64]. Hsp70 is found in the endolysosomal membranes of many tumors and stressed cells where it inhibits the release of lysosomal cathepsins into the cytosol [63, 65]. Lysosomes positive for Hsp70 display an increased size and resistance against chemical and physical membrane destabilization [63].

However, the interplay between HSP70 and lysosomes is in fact much more complex, as HSP70 also affects autophagic pathways. "Autophagy" usually refers to macroautophagy, a well-described cellular process by which the cell may degrade part of its cytoplasm in a random manner. In macroautophagy, double-membraned vesicles called autophagosomes form around a portion of the cytoplasm. These autophagosomes may then fuse with lysosomes or late endosomes and the content of the former is degraded by the enzymes contained in the latter. It is suspected that macroautophagy favors cell survival by facilitating the turnover of damaged proteins and organelles, and by providing ATP and amino acids recycled from the degraded autophagosome content. Multiple recent studies in various cancer types have shown that inhibiting autophagy using drugs such as chloroquine sensitizes cancer cells to chemotherapy or radiotherapy [66] in cells either starved or treated with rapamycin (known inducers of macroautophagy) [67]. HSP70 induces Akt phosphorylation/activation, which in turn activates mTOR, a negative regulator of macroautophagy (Fig. 2). The ATPase activity of HSP70 must be intact for this effect to take place. One would expect therefore that if HSP70 is inhibited that macroautophagy would increase. This is not however the case. Leu et al. reported that inhibition of Hsp70 by 2-phenylethynesulfonamide (PES, or pifithrin-μ, *see* Subheading "Targeting the Peptide-Binding Domain") resulted in an increase in LC3-II and autophagosomes. However, the content of these autophagosomes failed to be degraded. The study proposes an explanation for this through the fact that the cathepsins (and notably cathepsin L) contained in the lysosomes could not mature in the presence of PES [68]. All in all, this suggests that HSP70 has a negative effect on the first step of macroautophagy, through the mTor pathway, which prevents the formation of autophagosomes. Yet HSP70 seems important in the maturing of lysosomes needed for the degradation of the autophagosomes' content. Nevertheless, an off-target effect of PES should be investigated as other studies have shown that in the absence of HSP70, the lysosomal proteases are still effective, as they can diffuse to the cytosol and cause caspase-independent cell death [63]. In accordance with this result, we have shown that during monocytes differentiation, Hsp70

interacts with the transcription factor Spi1/PU1 and blocks its lysosomal degradation thereby assuring the viability of the differentiated macrophages [69].

2.2.5 In Conclusion, Hsp70 Can Be Considered as the Quintessential Inhibitor of Cell Death

Hsp70 is a strong cytoprotective protein that efficiently protects cells from different types of cell death (Fig. 2).

Does the effect of Hsp70 in cell death processes result from the chaperoning of the different proteins that interact with Hsp70? As indicated in Fig. 1, Hsp70 has two domains. The domain necessary for the chaperone function is the carboxyl-terminal domain. All the reports that studied the domain of interaction with Hsp70 indicate that the apoptotic partners of Hsp70 bind to the PBD of the protein. However, for some interaction/protective properties, the ATPase function of Hsp70 is needed but not for others. For instance, while the ATPase function seems necessary for Apaf-1 and AIF [44, 45], it is dispensable for JNK or GATA-1 binding/protection [8]. In erythroblasts, in which Hsp70 blocks apoptosis by protecting GATA-1 from caspase-3 cleavage, an Hsp70 mutant that only contains the PBD is as efficient as wild-type Hsp70 to ensure their protection [6]. Based on these data, we can hypothesize that Hsp70 might chaperone proteins in an ATP-dependent as well as ATP-independent manner.

What drives the interaction of Hsp70 with a given partner? It may be determined by its cellular localization. For example, the presence of Hsp70 in the lysosomal membrane is necessary for inhibiting the lysosomal death pathway. The migration of Hsp70 into the nucleus is essential to determine whether an erythroblast is going to die by apoptosis or to differentiate into a red blood cell [7]. In tumor cells, Hsp70 expression at the plasma membrane interferes with their clearance by the immune system. Membrane Hsp70 facilitates granzyme B penetration in a perforin-independent way and ensures cytotoxic T-lymphocytes killing through FasL/Fas [39, 70, 71].

3 Hsp70 and Cancer

3.1 Hsp70: Tumorigenicity and Cancer Cell Resistance

In normal cells, under non-stressed conditions, the expression of Hsp70 is usually very low. In contrast, high Hsp70 expression is a property of cancer cells and essential for the survival of many cancers. Hsp70 expression further increases after anti-cancer therapy and, due to Hsp70 strong cytoprotective properties, its cellular content has been inversely correlated with the response to the therapy. Clinical studies suggested Hsp70 as a bad prognosis factor. Increased expression of Hsp70 has been reported in high-grade malignant tumors such as endometrial cancer, osteosarcoma, and renal cell tumors [72]. Hsp70, along with PSA, are good tumor markers to identify patients with early stage prostate cancer [73]. Hsp70 is very abundant in chronic myeloid leukemia

characterized by Bcr-Abl expression [74]. This overexpression of Hsp70 is associated with resistance to imatinib, an effective chemotherapeutic agent used for its ability to block Bcr-Abl tyrosine kinase activity [75]. A relationship between Hsp70 and gastric cancer has also been reported through the effect of Helicobacter Pylori in Hsp70 expression [76]. Hsp70.2, a member of the Hsp70 family that is normally expressed only in spermatogenesis, is present at high levels in breast cancer and inhibits the onset of senescence [75]. High expression of Hsp70 in breast, endometrial, gastric cancer, or leukemia has been associated with metastasis, poor prognosis, and resistance to chemotherapy or radiation therapy [23, 77, 78]. Nuclear accumulation of Hsp70 has been defined as an objective marker for the presence of epithelial dysplasia and the presence of antibodies against Hsp70 in the serum has been described as a diagnostic marker in patients with hepatocellular carcinoma [79, 80]. More recently, the presence of circulating exosomes expressing Hsp70 has been presented as an interesting strategy to detect early metastasis [40, 81].

Studies in Bcr-Abl human leukemia cells show that Hsp70 is a promising therapeutic target for reversing cancer cell drug resistance probably because of its ability to inhibit apoptosis both upstream and downstream of the mitochondrial signaling [53, 74]. In experimental in vivo models, Hsp70 overexpression has been shown to increase the tumorigenicity of cancer cells (colon cancer, melanoma, myeloblastoma, and pancreatic adenocarcinoma), while Hsp70 downregulation or inhibition strongly decreases tumorigenicity [82, 83]. In this way, Hsp70 depletion or inhibitors have chemosensitizing properties and may even kill cancer cells (in the context of adenoviral infection) in the absence of additional stimuli [82]. The cytotoxic effect of Hsp70 down-modulation is particularly strong in transformed cells, yet undetectable in normal, non-transformed cell lines or primary cells [83]. The fact that depletion of Hsp70 selectively sensitizes or kills cancer cells has been rationalized by assuming that tumor cells have a strong need of chaperones (in particular Hsp70) for their survival, as compared to their normal counterparts, because they have to rewire their metabolism.

3.2 The Inhibition of Hsp70 in Cancer Therapy

Neutralizing Hsp70 is therefore an attractive strategy for anti-cancer therapy. However, in contrast to another Hsp, Hsp90, for which many specific inhibitors are available and some are in advanced clinical trials, there are not yet inhibitors of Hsp70 ready to enter the clinic. The main raison is that Hsp70, in contrast to Hsp90, is not an easily "druggable" protein. To block Hsp70, until quite recently, the authors used inhibitors of the heat shock response that act at the level of the heat shock transcription factor 1 (HSF1) and thereby block the transcription of all stress-inducible Hsps. These inhibitors include the flavonoid quercetin, the

diterpene triperoxide, triptolide [26, 84–88], and the benzo(a) pyrene, described to inhibit Hsp70 expression in endothelial cells [89]. Although it is true that these products by affecting HSF1 function block Hsp70, one of the heat shock proteins involved in the stress response, they remain rather unspecific. Another nonspecific inhibitor of Hsp70 is resveratrol, described to inhibit Hsp70 expression in K562 cells via downregulation of Akt kinase activity and upregulation of ERK1/2 kinase activity [90].

3.2.1 Specific Inhibitors of Hsp70

Targeting the Peptide-Binding Domain

Our group has demonstrated that the rationally designed decoy targets of Hsp70 derived from AIF can sensitize cancer cells to apoptosis induction by neutralizing the function of Hsp70. These AIF-derived peptides all carry the AIF region from aa 150 to aa 228, previously defined as required for binding Hsp70 on its PBD and lacking AIF's pro-apoptotic function [91]. These inhibitors, called ADD70 (for AIF-derived decoy for Hsp70), bind to and inhibit Hsp70 (Fig. 1). In vivo experiments, in a syngenic rat colon cancer cell model and in a mice model of melanoma (B16F10), showed that ADD70 decreased the size of the tumors in rats and induced an important growth delay of the mice tumors. In addition, ADD70 sensitizes both the rat colon cancer cells and mouse melanoma cells to the chemotherapeutic agent cisplatin [43].

More recently, we have selected peptide aptamers of 8–13 amino acids (E. coli thioredoxin was used as a scaffold) based on their ability to bind Hsp70 (Fig. 1). One of these, aptamer A8, binds to the PBD and more precisely to a domain of 14 amino acids that remain extracellular when Hsp70 is inserted into the membrane. A8 blocks several extracellular functions of Hsp70 and particularly its capacity to activate myeloid-derived suppressive cells. As a consequence, A8 has anti-tumorigenic effects in vivo which are associated with an increase in tumor-infiltrating cytotoxic $CD8^+$ T-cells (*see* Subheading 4.1) [40].

Concerning chemical molecules specifically inhibiting Hsp70, Leu et al. described a small-molecule inhibitor that interacts with the C-terminal domain of Hsp70 called 2-phenylethynesulfonamide (PES, Fig. 1). PES inhibits Hsp70 chaperone activity leading to the aggregation of misfolded proteins, and destabilization of lysosome membranes thus inducting an autophagic cell death [92]. However, other reports indicate that PES induces a clear apoptotic, caspase-dependent, cell death [92]. The ability of PES to induce an apoptotic or autophagic cell death could be cell-type dependent [93].

Targeting the Amino-terminal ATPase Domain (ABD)

By analogy with the Hsp90 inhibitors, compounds that displace ATP from Hsp70 are expected to be powerful tools. Williamson et al. designed and synthesized adenosine derived molecules based on the X-ray crystal structure of a commercially available ATP

analog. Although further studies are necessary to determine their specificity, some in vitro results are encouraging [94].

VER-155008 is an adenosine-derived compound that fits into the ATPase domain of Hsp70 (and Hsc70), thereby inhibiting the chaperone activity of these proteins (Fig. 1). This compound is probably the Hsp70 inhibitor that has gone farthest in its preclinical studies as it has even been tested in different cancer animal models including in canines [95], alone or in combination with Hsp90 inhibitors [96, 97].

A high-throughput screening for ATP turnover mediated by human Hsp70 allowed the identification of azure C, methylene blue, and myricetin as inhibitors of Hsp70. However, their specificity for inducible Hsp70 family has not been analyzed [98].

The ABD domain is also the site of action of MKT-077, a cationic rhodacyanine dye with selectivity toward cancer cells. MKT-077 localizes in the mitochondria where it interacts with mitochondrial Hsp70. This product has been tested in a phase I clinical trial as an anti-tumor agent but showed renal toxicity. However, combination of hsp90 inhibitors (17-AAG) and MKT-077 in a xenografted model of hepatocellular carcinoma showed anti-cancer effects [99]. More stable and promising analogues have been produced recently (*see* Subheading "Targeting Hsp70 Co-chaperones").

Screening for Hsp70 ATPase activity within a NCI drug collection allowed the identification of NSC 630668, a dihydropyrimidine. More interesting is the second generation compound MAL3-101, which inhibits Hsp70 ATPase activity and blocks proliferation of breast cancer and multiple myeloma cancer cells [100, 101]. Furthermore, a strong synergy was observed in combination with proteasome or HSP90 inhibitors. MAL2-11B was shown to inhibit the activity of a viral J-domain protein, T antigen, suggesting that it may be a new class of polyomavirus inhibitors [102]. The molecular mechanism of action of these molecules requires further study.

Our team has selected a peptide aptamer of 13 amino acids (aptamer A17) for its ability to specifically interact with Hsp70 ATP binding domain and to block Hsp70 ATPase activity. A17 inhibits Hsp70 chaperone activity, yet does not affect that of Hsc70 or Hsp90. In vivo, A17 has a strong anti-tumor effect and increases the sensitivity to apoptosis induction by anti-cancer drugs such as cisplatin [83].

Targeting Hsp70 Co-chaperones

An interesting way of inhibiting only certain functions of Hsp70 is to find molecules that specifically disrupt the interaction of Hsp70 with a particular co-chaperone. Although exploitation of this strategy in drug discovery has only just started, using an alphaScreen high-throughput approach, pyrimidotriazinediones were found to interfere with Hop/Hsp70 interaction. However, these

compounds were toxic for WST-1 cells in vitro [103]. It has been reported that drugs targeting Hip impair Hsp70 chaperone proteostasis and stimulate neurodegeneration [104]. Derivatives of MKT-077 (a rhodacyanine dye) have shown the ability to interfere with HSP70 co-chaperones. For instance, JG13 blocks the interaction of Hsp70 with Bag-1 interaction [105] whereas JG98 blocks Hsp70/Bag-3 interaction [106]. Although more studies are necessary, this later interaction seems to be a promising therapeutic target as Bag-3 is important for the pro-tumoral function of Hsp70 [16]. Concerning Hsp40 (DNAJ), an RNA sequencing study in hepatocellular fibro-lamellar carcinomas has demonstrated the interest of targeting it [107]. An RNA aptamer targeting the Hsp40 ATPase activity has been described [108].

We have shown that an essential co-chaperone to target, at least in colon cancer, is HSP110. We have demonstrated that colon cancers of the MSI type (microsatellite instability) all bear a dominant negative mutation that we have called HSP110DE9 [17]. This truncated protein binds to wild-type HSP110 at a 1:1 ratio, blocks the co-chaperone and thereby the whole Hsp70 chaperone network. As a consequence, the presence of HSP110DE9 is associated with an excellent prognosis (response to Folfox chemotherapy) as demonstrated in a multicentric study including more than 3000 colorectal cancer patients [109]. More recently, we have demonstrated that HSP110DE9 not only sensitizes colon cancer cells to the chemotherapy but also inhibits cancer cells proliferation [18] and the polarizing effect of wild-type HSP110 in macrophages toward a tolerant pro-tumoral phenotype [110]. Unfortunately, most colorectal cancers are not MSI and therefore do not express this endogenous HSP110 inhibitor that is HSP110DE9 (only about 10–15% of all colorectal cancers express HSP110DE9). An interesting strategy would be to render MSI-like a resistant colorectal tumor by introducing HSP110DE9 or a molecular mimic.

3.2.2 Combinational Therapies

The inhibition of Hsp70 is also considered an interesting strategy in combination with other drugs since most of these, including Hsp90 inhibitors, induce Hsp70 that can circumvent the drugs' tumor cell killing effect [22, 43]. And, as a matter of fact, in clinical trials testing Hsp90 inhibitors (most of which are geldanamycin derivatives such as 17-AAG), Hsp70 expression is used as a bio-marker.

This Hsp70 induction by Hsp90 inhibitors has not only been associated with the toxicity of the treatment but has also been related to calcium mobilization [111] and TGF-beta signaling [112]. Whatever the pathway leading to it, Hsp70 accumulation can reduce cell death induced by Hsp90 inhibitors and therefore decrease their anti-tumor efficacy. Indeed, many articles demonstrate the interest of combining Hsp90 and Hsp70 inhibitors. In

support of this, the depletion of Hsp70 by siRNA strongly increases cancer cells' sensitivity to 17-AAG [113] and Hsp70 inhibitor VER-155008 also potentiates the effect of 17-AAG in inducing apoptosis in colon carcinoma cells [114]. We obtained a similar increase in 17-AAG anti-cancer activity in colon cancer cells when using ADD70 to block Hsp70 [43]. Future studies will tell if such a combinational strategy gives the expected clinical results.

HDAC inhibitors are promising therapeutic tools as they induce hyperacetylation and inhibition of several molecular chaperones and co-chaperones [115]. However, similarly to Hsp90 inhibitors, they also induce hsp70 expression in cancer cells by disrupting the Hsp90–HDAC6–HSF1–p97 complex and activating HSF1-dependent gene transcription. HDAC inhibitors also provoke the hyperacetylation of Hsp70 thereby promoting autophagy, a cytoprotective mechanism induced by Hsp70 in cancer cells [116]. Therefore, a strong rationale exists for combing inhibitors of both HDAC and Hsp70.

4 Anticancer Therapeutic Approaches Based on Extracellular Hsp70

4.1 Extracellular Hsp70 Has an Immunological Function

Apart from the already discussed protective roles of Hsp70 within the cell, Hsp70 can also be extracellular (i.e., Hsp70 can be located in the extracellular space or on the plasma membrane) and play a role in the stimulation of the immune system and affect the tumor microenvironment. In humans, the presence of Hsp70 in the serum has been associated with stress or pathological conditions including cancer. Tumor cells were identified as a natural source of extracellular Hsp70. Previous studies identified a role for Hsp70 expressed at the cancer cell surface during tumor growth and metastatic spread [117]. An active release of Hsc70 from tumor cells was observed following treatment with interferon-γ [118]. In vitro, the members of the Hsp70 family have been detected in the medium of antigen-presenting cells (APCs). The immunogenic function of extracellular Hsps is mainly described through their role in chaperoning antigenic peptides. The word "chaperokine" has been evoked [119].

How Hsp70 is released into the extracellular environment is still a debated issue. When the cells overexpress Hsp70, a small fraction of the protein (around 10–15% depending on the cells) anchors into the membrane, exposing a 14 amino acid stretch of the PBD to the outside of the cell. Cytosolic Hsps do not contain leader peptides enabling membrane localization. One possibility is that cytosolic Hsps are transported to the plasma membrane in concert with other proteins possessing transmembrane domains. Another possibility for membrane anchorage might be a direct interaction of Hsps with lipid components. Hsp70 has been shown to associate with phosphatidylserine (PS) in PC12 tumor

cells [120] and to colocalize with PS in the outer membrane leaflet of hypoxic tumor cells [121]. Thus, it has been hypothesized that in stressed tumor cells translocation of Hsp70 to the outer membrane leaflet would be allowed by a mechanism associated with PS flipping.

Concerning the presence of Hsps in the extracellular medium, today there are two mechanisms reported by which Hsps may be released from cells: (1) a passive release mechanism that includes: necrotic cell death, severe blunt trauma, surgery and following infection with lytic viruses; (2) an active release mechanism that involves the non-classical protein release pathway in which Hsps are released from highly immunogenic exosomes and as free Hsp [122, 123]. De Maio's group has demonstrated in vitro, in HepG2 cells exposed to a heat shock, that Hsp70 was released into the extracellular environment associated in a membrane-associated form. Extracellular membranes containing Hsp70 strongly activated macrophages, much more than free recombinant Hsp70, as indicated by their ability to induce TNF-α production [124]. Interestingly, we have demonstrated that exosomes released by cancer cells but not those released by normal cells have HSP70 in their membrane. These HSP70-exosomes are able to activate myeloid-derived suppressive cells (MDSC) through the interaction of Hsp70 with the TLR2 receptor on the MDSC. As a consequence, the development of an efficient anticancer immune response is blocked. The release of HSP70-exosomes by the cancer cells is probably a mechanism of defense of the cancer cells to avoid its immune clearance [40, 71]. Interestingly, our previously described peptide aptamer A8 that binds to the 14 amino acids-extracellular portion of membrane anchored Hsp70 blocks the interaction between Hsp70 and TLR2. As a result, A8 treatment of animals bearing a tumor results in tumor regression associated with a strong intra tumoral infiltration by immune cells, notably CD8+ T-cells and cytotoxic macrophages (M1-like) [40].

Hsp70 has been shown to activate innate and adaptive immune reactions [125, 126]. Hsp70 chaperones antigenic peptides and channels them in a receptor-mediated manner into the major histocompatibility complex (MHC) class I presentation pathway of professional APCs, which then prime peptide-specific cytotoxic T-lymphocyte (CTL) [127]. Therefore, Hsp70 derived from tumors can be used as tumor-specific vaccines [128]. Hsp70 also elicits the release of pro-inflammatory cytokines from innate immune cells and increases the expression of co-stimulatory molecules [129, 130]. Furthermore, Hsp70 has been shown to activate the Natural Killer (NK) cell lytic machinery against tumors expressing Hsp70 at the cell surface [131]. These features have led to viewing Hsp70 as an endogenous adjuvant and immunological danger signal [132].

The members of the Hsp70 family together with those of the Hsp90 family were identified as key regulators of the host's immune system. In vivo, in animal models, Hsp-peptide complexes isolated from tumors developed an anti-tumor response while those isolated from normal tissues did not induce an anti-cancer immune response [133]. Therefore, the tumor-specific peptides chaperoned by Hsps were essential for their immunogenicity. Following cross-presentation of Hsp-chaperoned peptides on MHC class I molecules, a T cell response is initiated [134–139] The exogenously delivered antigenic peptides complexed to heat shock proteins, like Hsp70, are able to enter the endogenous Ag-processing pathway and prime CD8+ T cells for antigen production [140]. Hsps have been found to be important players in the process of cross-presentation of tumor-derived, antigenic peptides that are uptaken by the APCs [141, 142]. Hsp-chaperoned antigenic peptides derived from tumor cells are internalized in the APCs by endocytosis via "Hsp receptors" (i.e., CD91, CD40, TLR2/4 ± CD14, CD35, LOX-1, SR-A). Following uptake and processing, the peptides are presented to the MHC class I molecules and thus induce a CD8+ T cell response against cancer. Recombinant Hsp70 enhances tumor antigen cross-presentation by means of complex formation and augmenting antigen uptake. Innate immune activation by recombinant Hsp70 was not observed [143].

Hsp70-peptide complexes have also been described to enhance MHC class II restricted peptide presentation and CD4+ T cells activation [144]. Even in the absence of immunogenic antigens, Hsps can provide danger signals for the host's immune system [145]. In this aspect, it is believed that Hsp70-peptide complexes can suppress tumor growth via at least two pathways: one antigen-dependent and the other antigen-independent. The c-terminal domain of Hsp70 seems to be crucial in eliciting antigen-independent responses, including NK cell stimulation against tumor challenges [39, 146]. This can explain why, in experimental models, immunization with multiple Hsp70-fusion peptide complexes resulted in a better anti-tumor effect [147]. Hsp70 has been suggested to have cytokine-inducing effects. In APCs, it induces the release of pro-inflammatory cytokines like IL-1β, IL-6, or TNF-α [39]. In established melanomas, Hsp70 has been shown to act as a potent immune adjuvant inducing the production of TNF-α [148]. However, this role of Hsps in inducing cytokines production has been reported to be, at least in some cases, a consequence of LPS contaminations in the Hsp preparations [149, 150]. HSP70 levels could also impact its immunological effect, as supra-constitutive concentration of HSPs is often used to obtain a cytokine-inducing effect, whereas Hsp70 at physiological amounts shows a rather inhibitory effect [151].

4.2 Immuno-therapeutic Approaches Based on Hsp70

As mentioned before, some Hsps-based immunotherapeutical approaches against cancer exploit their carrier function for immunogenic peptides [152]. In experimental models of metastatic prostate cancer, Hsp70 is used as a potent adjuvant to induce cancer auto-immunity [153]. It has been shown that immunization with leukemic cells A20-derived Hsp70 induced the production of leukemia A20-specific antibodies which, in turn, induced complement-dependent cytotoxicity against A20 cells and enabled eradication of leukemia cells in mice [154]. Therapeutic vaccination with dendritic cells pulsed with tumor-derived Hsp70 induces immunity against B16 melanoma, which is increased in combination with COX-2 inhibitors [155]. CD8+ and CD4+ T cell epitopes, fused to the carboxyl-terminus of Hsc70, can enhance tumor immunity beyond the effect of the CD8+ epitope alone and eradicate tumors [156]. Fusion of HPV16 E7 to the C-terminus half of Hsp70 can induce potent antigen-specific CTL activity in experimental models [157]. Moreover, a recombinant N domain of Calreticulin/E7/C-terminal half of Hsp70, through synergistic effects, can generate both potent antitumoral immunity and anti-angiogenesis [157]. A small-molecule (apoptozole) inhibitor of Hsp70 ATPase activity enhances the immune response to protein antigens, i.e., production of antibodies and increase in the release of Th1 and Th2-type cytokines [158].

Unfortunately, so far the clinical results obtained using Hsp70 in protein vaccines in cancer therapy, although encouraging, are far from the conclusive results obtained in rodent models treated with Hsps-based vaccines [133].

Also exploiting the immunogenic properties of extracellular Hsp70, Multhoff's group has developed a different approach. NK cells, important effectors of the innate immune system, play a role in the anti-tumor immunity generated by chaperone-rich cells lysate vaccination [159]. Hsp70 is a triggering factor for NK cells [160]. Incubation of NK cells with cytokines plus soluble Hsp70 protein or TKD peptide (the extracellular 14 amino acids peptide of membrane Hsp70) enhances the cell surface density of NK cell activating receptors including CD94 [160]. Concomitantly, the cytolytic and migratory capacity of resting NK cells was found to be initiated [161]. Membrane-bound Hsp70 serves as a tumor-selective target structure, since Hsp70 is frequently presented on the plasma membrane of tumors and metastases but not in normal tissues. Incubation of peripheral blood lymphocytes with the TKD peptide plus IL-2 initiates the cytolytic and migratory capacity of NK cells toward membrane Hsp70 positive tumor cells in vitro and in a xenograft tumor mouse model [162]. A phase I clinical trial has been performed in patients with therapy-refractory, metastasized colorectal and non-small lung cell carcinoma with very encouraging results [163] and prompted the initiation in non-small lung cell carcinoma of a Phase II randomized clinical study in 2015

[131]. The advantage of this approach is the excellent safety profile and the unlimited availability of the synthetic Hsp70 peptide which stimulates NK cells, as compared with the complex Hsp-peptides/vaccines isolated from patients. Of note, a pilot study of injection of recombinant HSP70 in the tumor bed of patients with brain tumor has recently shown one complete clinical response and one partial response [164], encouraging the development of more clinical trials.

5 Concluding Remarks: Hsp70 in Cancer Theranostics

Hsp70 may have oncogene-like functions and likewise mediate "non-oncogene addiction" of stressed tumor cells that must adapt to hostile microenvironments, thereby becoming dependent on Hsp70 for their survival. Pro-survival functions of Hsp70 in cancer depend on its intra- or extra-cellular localization. Intracellular HSP70 has a well-described cytoprotective function through: (1) its chaperone role in newly synthesized proteins or misfolded proteins; (2) its strong anti-apoptotic properties; and (3) its role in autophagy and protein degradation. Extracellular Hsp70 can chaperone peptide antigens, act as a danger signal, and activate immunosuppressive cells. Inhibitors of extracellular Hsp70 (antibodies or aptamers that target membrane Hsp70) have been shown to restore the development of an efficient anticancer immune response. Therefore, the dual function of Hsp70 (protective, immunogenic) strongly increases the interest for this molecule in cancer therapy and, consequently, the search for inhibitors of Hsp70 has dramatically increased over the last years.

However, Hsp70 can also be a potential biomarker in cancer patients' follow up and for the diagnosis of early metastasis. Hsp70 is found in the extracellular medium either in a soluble form or in nanovesicles and notably exosomes, nanoparticles (diameter: ~50–100 nm) released into the extracellular environment via the endosomal vesicle pathway by fusion with the plasma membrane. Some authors but not others have reported an association of Hsp70 blood levels and bad prognosis in cancer. The reason for this discrepancy may be the low stability and very fast turnover of soluble Hsp70 in the blood. In contrast, the exosomes act as a carrier and protect Hsp70 from extracellular enzymes. Almost all cells secrete exosomes but we have demonstrated that only those secreted by cancer cells have Hsp70 on their membrane. We have called this subpopulation of tumour-derived nanoparticles *HSP70-exosomes*. We have patented an interferometry biolayer technique using the HSP70 peptide aptamer developed to selectively bind the extracellular domain of membrane-anchored HSP70 (PCT/EP2015/063186). Using this technology to capture HSP70-exosomes, we have provided a proof of that we can measure

HSP70-exosomes in human fluids and notably in blood and urine samples from cancer patients. Further, in a small cohort of cancer patients (breast, lung) we have demonstrated that HSP70-exosomes are abundant in cancer patients while hardly detectable in healthy volunteers [40]. Since one single cancer cell can secrete thousands of exosomes, this can be a very interesting approach to explore in the future for early cancer detection.

Toward a more individualized patients care, this approach to quantifying extracellular Hsp70 will also allow determining the population more susceptible to respond (in terms of Hsp expression) to a Hsp70-inhibition therapy. Since many chemotherapeutic drugs, to a bigger or lesser extent, induce an increase in Hsp70, measuring circulating levels of Hsp70 gives a rationale to determine which chemotherapies may benefit the most from their combination with a Hsp70-targeted therapy.

Acknowledgment

This work was supported by grants from the "Ligue Nationale Contre le Cancer". CG's group has the label de "La Ligue Contre le Cancer". The work was also supported by grants from the "Institut National du Cancer", the "Conseil Regional de Bourgogne", and the European Regional Development Fund (FEDER); and a French government grant managed by the French National Research Agency (ANR) under the program "Investissements d'Avenir" with reference ANR-11-LABX-0021-01-LipSTIC LabEx.

References

1. Goloudina AR, Demidov ON, Garrido C (2012) Inhibition of HSP70: a challenging anti-cancer strategy. Cancer Lett 325:117–124
2. Parcellier A, Gurbuxani S, Schmitt E, Solary E, Garrido C (2003) Heat shock proteins, cellular chaperones that modulate mitochondrial cell death pathways. Biochem Biophys Res Commun 304:505–512
3. Park HS, Lee JS, Huh SH, Seo JS, Choi EJ (2001) Hsp72 functions as a natural inhibitory protein of c-Jun N-terminal kinase. EMBO J 20:446–456
4. Garrido C, Gurbuxani S, Ravagnan L, Kroemer G (2001) Heat shock proteins: endogenous modulators of apoptotic cell death. Biochem Biophys Res Commun 286:433–442
5. Qian SB, McDonough H, Boellmann F, Cyr DM, Patterson C (2006) CHIP-mediated stress recovery by sequential ubiquitination of substrates and Hsp70. Nature 440:551–555
6. Ribeil JA, Zermati Y, Vandekerckhove J et al (2007) Hsp70 regulates erythropoiesis by preventing caspase-3-mediated cleavage of GATA-1. Nature 445:102–105
7. Frisan E, Vandekerckhove J, de Thonel A et al (2012) Defective nuclear localization of Hsp70 is associated with dyserythropoiesis and GATA-1 cleavage in myelodysplastic syndromes. Blood 119:1532–1542
8. Arlet JB, Ribeil JA, Guillem F et al (2014) HSP70 sequestration by free α-globin promotes ineffective erythropoiesis in β-thalassaemia. Nature 514:242–246
9. Jego G, Hazoume A, Seigneuric R, Garrido C (2013) Targeting heat shock proteins in cancer. Cancer Lett 332:275–285

10. Daugaard M, Rohde M, Jäättelä M (2007) The heat shock protein 70 family: Highly homologous proteins with overlapping and distinct functions. FEBS Lett 581:3702–3710
11. Zuiderweg ER, Hightower LE, Gestwicki JE (2017) The remarkable multivalency of the Hsp70 chaperones. Cell Stress Chaperones 22:173–189
12. Voos WA (2003) new connection: chaperones meet a mitochondrial receptor. Mol Cell 11:1–3
13. Vogel M, Bukau B, Mayer MP (2006) Allosteric regulation of Hsp70 chaperones by a proline switch. Mol Cell 21:359–367
14. Hennessy F, Nicoll WS, Zimmermann R, Cheetham ME, Blatch GL (2005) Not all J domains are created equal: implications for the specificity of Hsp40-Hsp70 interactions. Protein Sci 14:1697–1709
15. Young JC, Agashe VR, Siegers K, Hartl FU (2004) Pathways of chaperone-mediated protein folding in the cytosol. Nat Rev Mol Cell Biol 5:781–791
16. Colvin TA, Gabai VL, Gong J et al (2014) Hsp70-Bag3 interactions regulate cancer-related signaling networks. Cancer Res 74:4731–4740
17. Dorard C, de Thonel A, Collura A et al (2011) Expression of a mutant HSP110 sensitizes colorectal cancer cells to chemotherapy and improves disease prognosis. Nat Med 17:1283–1289
18. Berthenet K, Bokhari A, Lagrange A et al (2017) HSP110 promotes colorectal cancer growth through STAT3 activation. Oncogene 36:2328–2336
19. Bukau B, Weissman J, Horwich A (2006) Molecular chaperones and protein quality control. Cell 125:443–451
20. Angles F, Castanie-Cornet MP, Slama N et al (2017) Multilevel interaction of the DnaK/DnaJ(HSP70/HSP40) stress-responsive chaperone machine with the central metabolism. Sci Rep 7:41341
21. Marcion G, Seigneuric R, Chavanne E et al (2015) C-terminal amino acids are essential for human heat shock protein 70 dimerization. Cell Stress Chaperones 20:61–72
22. Schmitt E, Parcellier A, Gurbuxani S et al (2003) Chemosensitization by a non-apoptogenic heat shock protein 70-binding apoptosis-inducing factor mutant. Cancer Res 63:8233–8240
23. Garrido C, Brunet M, Didelot C, Zermati Y, Schmitt E, Kroemer G (2006) Heat shock proteins 27 and 70: anti-apoptotic proteins with tumorigenic properties. Cell Cycle 5:2592–2601
24. Mosser DD, Caron AW, Bourget L et al (2000) The chaperone function of hsp70 is required for protection against stress-induced apoptosis. Mol Cell Biol 20:7146–7159
25. Mosser DD, Morimoto RI (2004) Molecular chaperones and the stress of oncogenesis. Oncogene 23:2907–2918
26. Aghdassi A, Phillips P, Dudeja V et al (2007) Heat shock protein 70 increases tumorigenicity and inhibits apoptosis in pancreatic adenocarcinoma. Cancer Res 67:616–625
27. Gurbuxani S, Bruey JM, Fromentin A et al (2001) Selective depletion of inducible HSP70 enhances immunogenicity of rat colon cancer cells. Oncogene 20:7478–7485
28. Filomenko R, Poirson-Bichat F, Billerey C et al (2002) Atypical protein kinase C zeta as a target for chemosensitization of tumor cells. Cancer Res 62:1815–1821
29. Gao T, Newton AC (2002) The turn motif is a phosphorylation switch that regulates the binding of Hsp70 to protein kinase C. J Biol Chem 277:31585–31592
30. Hu G, Tang J, Zhang B et al (2006) A novel endothelial-specific heat shock protein HspA12B is required in both zebrafish development and endothelial functions in vitro. J Cell Sci 119:4117–4126
31. Park HS, Cho SG, Kim CK et al (2002) Heat shock protein hsp72 is a negative regulator of apoptosis signal-regulating kinase 1. Mol Cell Biol 22:7721–7730
32. Lee JS, Lee JJ, Seo JS (2005) HSP70 deficiency results in activation of c-Jun N-terminal Kinase, extracellular signal-regulated kinase, and caspase-3 in hyperosmolarity-induced apoptosis. J Biol Chem 280:6634–6641
33. Salehi AH, Morris SJ, Ho WC et al (2006) AEG3482 is an antiapoptotic compound that inhibits Jun kinase activity and cell death through induced expression of heat shock protein 70. Chem Biol 13:213–223
34. Gabai VL, Yaglom JA, Volloch V et al (2000) Hsp72-mediated suppression of c-Jun N-terminal kinase is implicated in development of tolerance to caspase-independent cell death. Mol Cell Biol 20:6826–6836
35. Asea A, Rehli M, Kabingu E et al (2002) Novel signal transduction pathway utilized by extracellular HSP70: role of toll-like receptor (TLR) 2 and TLR4. J Biol Chem 277:15028–15034
36. Mijatovic T, Mathieu V, Gaussin JF et al (2006) Cardenolide-induced lysosomal

membrane permeabilization demonstrates therapeutic benefits in experimental human non-small cell lung cancers. Neoplasia 8:402–412

37. Ran R, Lu A, Zhang L et al (2004) Hsp70 promotes TNF-mediated apoptosis by binding IKK gamma and impairing NF-kappa B survival signaling. Genes Dev 18:1466–1481
38. Feng X, Bonni S, Riabowol K (2006) HSP70 induction by ING proteins sensitizes cells to tumor necrosis factor alpha receptor-mediated apoptosis. Mol Cell Biol 26:9244–9255
39. Schmitt E, Gehrmann M, Brunet M, Multhoff G, Garrido C (2007) Intracellular and extracellular functions of heat shock proteins: repercussions in cancer therapy. J Leukoc Biol 81:15–27
40. Gobbo J, Marcion G, Cordonnier M, et al. Restoring anticancer immune response by targeting tumor-derived exosomes with a HSP70 peptide aptamer. J Natl Cancer Inst 2015;108(3)
41. Akakura S, Yoshida M, Yoneda Y, Horinouchi SA (2001) role for Hsc70 in regulating nucleocytoplasmic transport of a temperature-sensitive p53 (p53Val-135). J Biol Chem 276:14649–14657
42. Kondrikov D, Fulton D, Dong Z, Su Y (2015) Heat shock protein 70 prevents hyperoxia-induced disruption of lung endothelial barrier via caspase-dependent and AIF-dependent pathways. PLoS One 10: e0129343
43. Schmitt E, Maingret L, Puig PE et al (2006) Heat shock protein 70 neutralization exerts potent antitumor effects in animal models of colon cancer and melanoma. Cancer Res 66:4191–4197
44. Ruchalski K, Mao H, Li Z et al (2006) Distinct hsp70 domains mediate apoptosis-inducing factor release and nuclear accumulation. J Biol Chem 281:7873–7880
45. Beere HM, Wolf BB, Cain K et al (2000) Heat-shock protein 70 inhibits apoptosis by preventing recruitment of procaspase-9 to the Apaf-1 apoptosome. Nat Cell Biol 2:469–475
46. Pandey P, Saleh A, Nakazawa A et al (2000) Negative regulation of cytochrome c-mediated oligomerization of Apaf-1 and activation of procaspase-9 by heat shock protein 90. EMBO J 19:4310–4322
47. Sakahira H, Nagata S (2002) Co-translational folding of caspase-activated DNase with Hsp70, Hsp40, and inhibitor of caspase-activated DNase. J Biol Chem 277:3364–3370
48. Liu QL, Kishi H, Ohtsuka K, Muraguchi A (2003) Heat shock protein 70 binds caspase-activated DNase and enhances its activity in TCR-stimulated T cells. Blood 102:1788–1796
49. Kotoglou P, Kalaitzakis A, Vezyraki P et al (2009) Hsp70 translocates to the nuclei and nucleoli, binds to XRCC1 and PARP-1, and protects HeLa cells from single-strand DNA breaks. Cell Stress Chaperones 14:391–406
50. Goel G, Guo M, Ding J et al (2010) Combined effect of tumor necrosis factor (TNF)-alpha and heat shock protein (HSP)-70 in reducing apoptotic injury in hypoxia: a cell culture study. Neurosci Lett 483:162–166
51. Pang Q, Keeble W, Christianson TA, Faulkner GR, Bagby GC (2001) FANCC interacts with Hsp70 to protect hematopoietic cells from IFN-gamma/TNF-alpha-mediated cytotoxicity. EMBO J 20:4478–4489
52. Pang Q, Christianson TA, Keeble W, Koretsky T, Bagby GC (2002) The anti-apoptotic function of Hsp70 in the interferon-inducible double-stranded RNA-dependent protein kinase-mediated death signaling pathway requires the Fanconi anemia protein, FANCC. J Biol Chem 277:49638–49643
53. Guo F, Sigua C, Bali P et al (2005) Mechanistic role of heat shock protein 70 in Bcr-Abl-mediated resistance to apoptosis in human acute leukemia cells. Blood 105:1246–1255
54. Gabai VL, Mabuchi K, Mosser DD, Sherman MY (2002) Hsp72 and stress kinase c-jun N-terminal kinase regulate the bid-dependent pathway in tumor necrosis factor-induced apoptosis. Mol Cell Biol 22:3415–3424
55. Candé C, Vahsen N, Garrido C, Kroemer G (2004) Apoptosis-inducing factor (AIF): caspase-independent after all. Cell Death Differ 11:591–595
56. Creagh EM, Carmody RJ, Cotter TG (2000) Heat shock protein 70 inhibits caspase-dependent and -independent apoptosis in Jurkat T cells. Exp Cell Res 257:58–66
57. Ravagnan L, Gurbuxani S, Susin SA et al (2001) Heat-shock protein 70 antagonizes apoptosis-inducing factor. Nat Cell Biol 3:839–843
58. Matsumori Y, Hong SM, Aoyama K et al (2005) Hsp70 overexpression sequesters AIF and reduces neonatal hypoxic/ischemic brain injury. J Cereb Blood Flow Metab 25:899–910
59. Lui JC, Kong SK (2007) Heat shock protein 70 inhibits the nuclear import of apoptosis-

inducing factor to avoid DNA fragmentation in TF-1 cells during erythropoiesis. FEBS Lett 581:109–117

60. Kalinowska M, Garncarz W, Pietrowska M, Garrard WT, Widlak P (2005) Regulation of the human apoptotic DNase/RNase endonuclease G: involvement of Hsp70 and ATP. Apoptosis 10:821–830
61. Hernandez-Tiedra S, Fabrias G, Davila D et al (2016) Dihydroceramide accumulation mediates cytotoxic autophagy of cancer cells via autolysosome destabilization. Autophagy 12:2213–2229
62. Jäättelä M, Tschopp J (2003) Caspase-independent cell death in T lymphocytes. Nat Immunol 4:416–423
63. Nylandsted J, Gyrd-Hansen M, Danielewicz A et al (2004) Heat shock protein 70 promotes cell survival by inhibiting lysosomal membrane permeabilization. J Exp Med 200:425–435
64. Kirkegaard T, Roth AG, Petersen NH et al (2010) Hsp70 stabilizes lysosomes and reverts Niemann-Pick disease-associated lysosomal pathology. Nature 463:549–553
65. Bivik C, Rosdahl I, Ollinger K (2007) Hsp70 protects against UVB induced apoptosis by preventing release of cathepsins and cytochrome c in human melanocytes. Carcinogenesis 28:537–544
66. Yue Z, Friedman L, Komatsu M, Tanaka K (2009) The cellular pathways of neuronal autophagy and their implication in neurodegenerative diseases. Biochim Biophys Acta 1793:1496–1507
67. Dokladny K, Zuhl MN, Mandell M et al (2013) Regulatory coordination between two major intracellular homeostatic systems: heat shock response and autophagy. J Biol Chem 288:14959–14972
68. Leu JI, Pimkina J, Frank A, Murphy ME, George DL (2009) A small molecule inhibitor of inducible heat shock protein 70. Mol Cell 36:15–27
69. Jego G, Lanneau D, De Thonel A et al (2014) Dual regulation of SPI1/PU.1 transcription factor by heat shock factor 1 (HSF1) during macrophage differentiation of monocytes. Leukemia 28:1676–1686
70. Sashchenko LP, Dukhanina EA, Shatalov YV et al (2007) Cytotoxic T lymphocytes carrying a pattern recognition protein Tag7 can detect evasive, HLA-negative but Hsp70-exposing tumor cells, thereby ensuring FasL/Fas-mediated contact killing. Blood 110:1997–2004
71. Chalmin F, Ladoire S, Mignot G et al (2010) Membrane-associated Hsp72 from tumor-derived exosomes mediates STAT3-dependent immunosuppressive function of mouse and human myeloid-derived suppressor cells. J Clin Invest 120:457–471
72. Ciocca DR, Frayssinet P, Cuello-Carrión FD (2007) A pilot study with a therapeutic vaccine based on hydroxyapatite ceramic particles and self-antigens in cancer patients. Cell Stress Chaperones 12:33–43
73. Abe M, Manola JB, Oh WK et al (2004) Plasma levels of heat shock protein 70 in patients with prostate cancer: a potential biomarker for prostate cancer. Clin Prostate Cancer 3:49–53
74. Ray S, Lu Y, Kaufmann SH et al (2004) Genomic mechanisms of p210BCR-ABL signaling: induction of heat shock protein 70 through the GATA response element confers resistance to paclitaxel-induced apoptosis. J Biol Chem 279:35604–35615
75. Pocaly M, Lagarde V, Etienne G et al (2007) Overexpression of the heat-shock protein 70 is associated to imatinib resistance in chronic myeloid leukemia. Leukemia 21:93–101
76. Targosz A, Pierzchalski P, Krawiec A et al (2006) Helicobacter pylori inhibits expression of heat shock protein 70 (HSP70) in human epithelial cell line. Importance of Cag A protein. J Physiol Pharmacol 57:265–278
77. Brondani Da Rocha A, Regner A, Grivicich I et al (2004) Radioresistance is associated to increased Hsp70 content in human glioblastoma cell lines. Int J Oncol 25:777–785
78. Nylandsted J (2009) Extracellular heat shock protein 70: a potential prognostic marker for chronic myeloid leukemia. Leuk Res 33:205–206
79. Seoane JM, Varela-Centelles PI, Ramirez JR, Cameselle-Teijeiro J, Romero MA, Aguirre JM (2006) Heat shock proteins (HSP70 and HSP27) as markers of epithelial dysplasia in oral leukoplakia. Am J Dermatopathol 28:417–422
80. Takashima M, Kuramitsu Y, Yokoyama Y et al (2006) Proteomic analysis of autoantibodies in patients with hepatocellular carcinoma. Proteomics 6:3894–3900
81. Cordonnier M, Chanteloup G, Isambert N et al (2017) Exosomes in cancer theranostic: diamonds in the rough. Cell Adhes Migr 11:151–163
82. Nylandsted J, Wick W, Hirt UA et al (2002) Eradication of glioblastoma, and breast and

colon carcinoma xenografts by Hsp70 depletion. Cancer Res 62:7139–7142

83. Rérole AL, Gobbo J, De Thonel A et al (2011) Peptides and aptamers targeting HSP70: a novel approach for anticancer chemotherapy. Cancer Res 71:484–495
84. Westerheide SD, Kawahara TL, Orton K, Morimoto RI (2006) Triptolide, an inhibitor of the human heat shock response that enhances stress-induced cell death. J Biol Chem 281:9616–9622
85. Phillips PA, Dudeja V, McCarroll JA et al (2007) Triptolide induces pancreatic cancer cell death via inhibition of heat shock protein 70. Cancer Res 67:9407–9416
86. Bae JH, Kim JY, Kim MJ et al (2010) Quercetin enhances susceptibility to NK cell-mediated lysis of tumor cells through induction of NKG2D ligands and suppression of HSP70. J Immunother 33:391–401
87. Antonoff MB, Chugh R, Borja-Cacho D et al (2009) Triptolide therapy for neuroblastoma decreases cell viability in vitro and inhibits tumor growth in vivo. Surgery 146:282–290
88. Li M, Wang J, Jing J et al (2009) Synergistic promotion of breast cancer cells death by targeting molecular chaperone GRP78 and heat shock protein 70. J Cell Mol Med 13:4540–4550
89. Gong Z, Yang J, Yang M et al (2006) Benzo (a)pyrene inhibits expression of inducible heat shock protein 70 in vascular endothelial cells. Toxicol Lett 166:229–236
90. Banerjee Mustafi S, Chakraborty PK, Raha S (2010) Modulation of Akt and ERK1/2 pathways by resveratrol in chronic myelogenous leukemia (CML) cells results in the downregulation of Hsp70. PLoS One 5:e8719
91. Gurbuxani S, Schmitt E, Cande C et al (2003) Heat shock protein 70 binding inhibits the nuclear import of apoptosis-inducing factor. Oncogene 22:6669–6678
92. Steele AJ, Prentice AG, Hoffbrand AV et al (2009) 2-Phenylacetylenesulfonamide (PAS) induces p53-independent apoptotic killing of B-chronic lymphocytic leukemia (CLL) cells. Blood 114:1217–1225
93. Balaburski GM, Leu JI, Beeharry N et al (2013) A modified HSP70 inhibitor shows broad activity as an anticancer agent. Mol Cancer Res 11:219–229
94. Williamson DS, Borgognoni J, Clay A et al (2009) Novel adenosine-derived inhibitors of 70 kDa heat shock protein, discovered through structure-based design. J Med Chem 52:1510–1513
95. Asling J, Morrison J, Mutsaers AJ (2016) Targeting HSP70 and GRP78 in canine osteosarcoma cells in combination with doxorubicin chemotherapy. Cell Stress Chaperones 21:1065–1076
96. Cavanaugh A, Juengst B, Sheridan K, Danella JF, Williams H (2015) Combined inhibition of heat shock proteins 90 and 70 leads to simultaneous degradation of the oncogenic signaling proteins involved in muscle invasive bladder cancer. Oncotarget 6:39821–39838
97. Kim SH, Kang JG, Kim CS et al (2014) The hsp70 inhibitor VER155008 induces paraptosis requiring de novo protein synthesis in anaplastic thyroid carcinoma cells. Biochem Biophys Res Commun 454:36–41
98. Jinwal UK, Miyata Y, Koren J et al (2009) Chemical manipulation of hsp70 ATPase activity regulates tau stability. J Neurosci 29:12079–12088
99. Guo W, Yan L, Yang L et al (2014) Targeting GRP75 improves HSP90 inhibitor efficacy by enhancing p53-mediated apoptosis in hepatocellular carcinoma. PLoS One 9:e85766
100. Evans CG, Wisén S, Gestwicki JE (2006) Heat shock proteins 70 and 90 inhibit early stages of amyloid beta-(1-42) aggregation in vitro. J Biol Chem 281:33182–33191
101. Braunstein MJ, Scott SS, Scott CM et al (2011) Antimyeloma effects of the heat shock protein 70 molecular chaperone inhibitor MAL3-101. J Oncol 232037:2011
102. Wright CM, Seguin SP, Fewell SW et al (2009) Inhibition of Simian Virus 40 replication by targeting the molecular chaperone function and ATPase activity of T antigen. Virus Res 141:71–80
103. Yi F, Regan LA (2008) novel class of small molecule inhibitors of Hsp90. ACS Chem Biol 3:645–654
104. Roodveldt C, Bertoncini CW, Andersson A et al (2009) Chaperone proteostasis in Parkinson's disease: stabilization of the Hsp70/alpha-synuclein complex by Hip. EMBO J 28:3758–3770
105. Li X, Srinivasan SR, Connarn J, et al. (2013) Analogs of the allosteric heat shock protein 70 (Hsp70) inhibitor, MKT-077, as anticancer agents. ACS Med Chem Lett 4(11)
106. Li X, Colvin T, Rauch JN et al (2015) Validation of the Hsp70-Bag3 protein-protein interaction as a potential therapeutic target in cancer. Mol Cancer Ther 14:642–648
107. Simon EP, Freije CA, Farber BA et al (2015) Transcriptomic characterization of fibrolamellar hepatocellular carcinoma. Proc Natl Acad Sci U S A 112:E5916–E5925

108. Thirunavukarasu D, Shi H, An RNA (2015) aptamer specific to Hsp70-ATP conformation inhibits its ATPase activity independent of Hsp40. Nucleic Acid Ther 25:103–112
109. Collura A, Lagrange A, Svrcek M et al (2014) Patients with colorectal tumors with microsatellite instability and large deletions in HSP110 T17 have improved response to 5-fluorouracil-based chemotherapy. Gastroenterology 146:401–11e1
110. Berthenet K, Boudesco C, Collura A et al (2016) Extracellular HSP110 skews macrophage polarization in colorectal cancer. Oncoimmunology 5:e1170264
111. Chang YS, Lee LC, Sun FC, Chao CC, Fu HW, Lai YK (2006) Involvement of calcium in the differential induction of heat shock protein 70 by heat shock protein 90 inhibitors, geldanamycin and radicicol, in human non-small cell lung cancer H460 cells. J Cell Biochem 97:156–165
112. Yun CH, Yoon SY, Nguyen TT et al (2010) Geldanamycin inhibits TGF-beta signaling through induction of Hsp70. Arch Biochem Biophys 495:8–13
113. Powers MV, Clarke PA, Workman P (2009) Death by chaperone: HSP90, HSP70 or both? Cell Cycle 8:518–526
114. Massey AJ, Williamson DS, Browne H et al (2010) A novel, small molecule inhibitor of Hsc70/Hsp70 potentiates Hsp90 inhibitor induced apoptosis in HCT116 colon carcinoma cells. Cancer Chemother Pharmacol 66:535–545
115. Rao R, Fiskus W, Ganguly S, Kambhampati S, Bhalla KN (2012) HDAC inhibitors and chaperone function. Adv Cancer Res 116:239–262
116. Rao R, Fiskus W, Yang Y et al (2008) HDAC6 inhibition enhances 17-AAG-mediated abrogation of hsp90 chaperone function in human leukemia cells. Blood 112:1886–1893
117. Bausero MA, Page DT, Osinaga E, Asea A (2004) Surface expression of Hsp25 and Hsp72 differentially regulates tumor growth and metastasis. Tumour Biol 25:243–251
118. Bausero MA, Gastpar R, Multhoff G, Asea A (2005) Alternative mechanism by which IFN-gamma enhances tumor recognition: active release of heat shock protein 72. J Immunol 175:2900–2912
119. Asea A, Kabingu E, Stevenson MA, Calderwood SK (2000) HSP70 peptidembearing and peptide-negative preparations act as chaperokines. Cell Stress Chaperones 5:425–431
120. Arispe N, Doh M, Simakova O, Kurganov B, De Maio A (2004) Hsc70 and Hsp70 interact with phosphatidylserine on the surface of PC12 cells resulting in a decrease of viability. FASEB J 18:1636–1645
121. Schilling D, Gehrmann M, Steinem C et al (2009) Binding of heat shock protein 70 to extracellular phosphatidylserine promotes killing of normoxic and hypoxic tumor cells. FASEB J 23:2467–2477
122. Asea A (2007) Mechanisms of HSP72 release. J Biosci 32:579–584
123. Mambula SS, Calderwood SK (2006) Heat shock protein 70 is secreted from tumor cells by a nonclassical pathway involving lysosomal endosomes. J Immunol 177:7849–7857
124. Vega VL, Rodríguez-Silva M, Frey T et al (2008) Hsp70 translocates into the plasma membrane after stress and is released into the extracellular environment in a membrane-associated form that activates macrophages. J Immunol 180:4299–4307
125. Srivastava P (2002) Roles of heat-shock proteins in innate and adaptive immunity. Nat Rev Immunol 2:185–194
126. Nicchitta CV (2003) Re-evaluating the role of heat-shock protein-peptide interactions in tumour immunity. Nat Rev Immunol 3:427–432
127. Castellino F, Boucher PE, Eichelberg K et al (2000) Receptor-mediated uptake of antigen/heat shock protein complexes results in major histocompatibility complex class I antigen presentation via two distinct processing pathways. J Exp Med 191:1957–1964
128. Castelli C, Rivoltini L, Rodolfo M, Tazzari M, Belgiovine C, Allavena P (2015) Modulation of the myeloid compartment of the immune system by angiogenic- and kinase inhibitor-targeted anti-cancer therapies. Cancer Immunol Immunother 64:83–89
129. Asea A, Kraeft SK, Kurt-Jones EA et al (2000) HSP70 stimulates cytokine production through a CD14-dependant pathway, demonstrating its dual role as a chaperone and cytokine. Nat Med 6:435–442
130. Kuppner MC, Gastpar R, Gelwer S et al (2001) The role of heat shock protein (hsp70) in dendritic cell maturation: hsp70 induces the maturation of immature dendritic cells but reduces DC differentiation from monocyte precursors. Eur J Immunol 31:1602–1609
131. Specht HM, Ahrens N, Blankenstein C et al (2015) Heat shock protein 70 (Hsp70) peptide activated natural killer (NK) cells for the treatment of patients with non-small cell lung cancer (NSCLC) after radiochemotherapy

(RCTx)—from preclinical studies to a clinical phase II trial. Front Immunol 6:162

132. Todryk SM, Melcher AA, Dalgleish AG, Vile RG (2000) Heat shock proteins refine the danger theory. Immunology 99:334–337
133. Castelli C, Rivoltini L, Rini F et al (2004) Heat shock proteins: biological functions and clinical application as personalized vaccines for human cancer. Cancer Immunol Immunother 53:227–233
134. Liu J, Cao X (2016) Cellular and molecular regulation of innate inflammatory responses. Cell Mol Immunol 13:711–721
135. Basu S, Binder RJ, Ramalingam T, Srivastava PK (2001) CD91 is a common receptor for heat shock proteins gp96, hsp90, hsp70, and calreticulin. Immunity 14:303–313
136. Binder RJ, Vatner R, Srivastava P (2004) The heat-shock protein receptors: some answers and more questions. Tissue Antigens 64:442–451
137. Sondermann H, Becker T, Mayhew M, Wieland F, Hartl FU (2000) Characterization of a receptor for heat shock protein 70 on macrophages and monocytes. Biol Chem 381:1165–1174
138. Doody AD, Kovalchin JT, Mihalyo MA, Hagymasi AT, Drake CG, Adler AJ (2004) Glycoprotein 96 can chaperone both MHC class I- and class II-restricted epitopes for in vivo presentation, but selectively primes CD8+ T cell effector function. J Immunol 172:6087–6092
139. Singh-Jasuja H, Toes RE, Spee P et al (2000) Cross-presentation of glycoprotein 96-associated antigens on major histocompatibility complex class I molecules requires receptor-mediated endocytosis. J Exp Med 191:1965–1974
140. Flechtner JB, Cohane KP, Mehta S et al (2006) High-affinity interactions between peptides and heat shock protein 70 augment CD8+ T lymphocyte immune responses. J Immunol 177:1017–1027
141. Habich C, Baumgart K, Kolb H, Burkart V (2002) The receptor for heat shock protein 60 on macrophages is saturable, specific, and distinct from receptors for other heat shock proteins. J Immunol 168:569–576
142. Vabulas RM, Ahmad-Nejad P, da Costa C et al (2001) Endocytosed HSP60s use toll-like receptor 2 (TLR2) and TLR4 to activate the toll/interleukin-1 receptor signaling pathway in innate immune cells. J Biol Chem 276:31332–31339
143. Bendz H, Ruhland SC, Pandya MJ et al (2007) Human heat shock protein 70 enhances tumor antigen presentation through complex formation and intracellular antigen delivery without innate immune signaling. J Biol Chem 282:31688–31702
144. Haug M, Schepp CP, Kalbacher H, Dannecker GE, Holzer U (2007) 70-kDa heat shock proteins: specific interactions with HLA-DR molecules and their peptide fragments. Eur J Immunol 37:1053–1063
145. Matzinger P (2002) The danger model: a renewed sense of self. Science 296:301–305
146. Joly AL, Wettstein G, Mignot G, Ghiringhelli F, Garrido C (2010) Dual role of heat shock proteins as regulators of apoptosis and innate immunity. J Innate Immun 2:238–247
147. Zhang H, Huang W (2006) Fusion proteins of Hsp70 with tumor-associated antigen acting as a potent tumor vaccine and the C-terminal peptide-binding domain of Hsp70 being essential in inducing antigen-independent anti-tumor response in vivo. Cell Stress Chaperones 11:216–226
148. Sanchez-Perez L, Kottke T, Daniels GA et al (2006) Killing of normal melanocytes, combined with heat shock protein 70 and CD40L expression, cures large established melanomas. J Immunol 177:4168–4177
149. Gao B, Tsan MF (2003) Recombinant human heat shock protein 60 does not induce the release of tumor necrosis factor alpha from murine macrophages. J Biol Chem 278:22523–22529
150. Reed RC, Berwin B, Baker JP, Nicchitta CV (2003) GRP94/gp96 elicits ERK activation in murine macrophages. A role for endotoxin contamination in NF-kappa B activation and nitric oxide production. J Biol Chem 278:31853–31860
151. van Eden W, Spiering R, Broere F, van der Zee RA (2012) case of mistaken identity: HSPs are no DAMPs but DAMPERs. Cell Stress Chaperones 17:281–292
152. Janetzki S, Palla D, Rosenhauer V, Lochs H, Lewis JJ, Srivastava PK (2000) Immunization of cancer patients with autologous cancer-derived heat shock protein gp96 preparations: a pilot study. Int J Cancer 88:232–238
153. Kottke T, Sanchez-Perez L, Diaz RM et al (2007) Induction of hsp70-mediated Th17 autoimmunity can be exploited as immunotherapy for metastatic prostate cancer. Cancer Res 67:11970–11979
154. Jimbo J, Sato K, Hosoki T et al (2008) Induction of leukemia-specific antibodies by immunotherapy with leukemia-cell-derived heat shock protein 70. Cancer Sci 99:1427–1434

155. Toomey D, Conroy H, Jarnicki AG, Higgins SC, Sutton C, Mills KH (2008) Therapeutic vaccination with dendritic cells pulsed with tumor-derived Hsp70 and a COX-2 inhibitor induces protective immunity against B16 melanoma. Vaccine 26:3540–3549
156. Mizukami S, Kajiwara C, Ishikawa H, Katayama I, Yui K, Udono H (2008) Both CD4+ and CD8+ T cell epitopes fused to heat shock cognate protein 70 (hsc70) can function to eradicate tumors. Cancer Sci 99:1008–1015
157. Liu B, Ye D, Song X et al (2008) A novel therapeutic fusion protein vaccine by two different families of heat shock proteins linked with HPV16 E7 generates potent antitumor immunity and antiangiogenesis. Vaccine 26:1387–1396
158. Baek KH, Zhang H, Lee BR, Kwon YG, Ha SJ, Shin I (2015) A small molecule inhibitor for ATPase activity of Hsp70 and Hsc70 enhances the immune response to protein antigens. Sci Rep 5:17642
159. Zeng Y, Chen X, Larmonier N et al (2006) Natural killer cells play a key role in the antitumor immunity generated by chaperone-rich cell lysate vaccination. Int J Cancer 119:2624–2631
160. Gross C, Hansch D, Gastpar R, Multhoff G (2003) Interaction of heat shock protein 70 peptide with NK cells involves the NK receptor CD94. Biol Chem 384:267–279
161. Gastpar R, Gehrmann M, Bausero MA et al (2005) Heat shock protein 70 surface-positive tumor exosomes stimulate migratory and cytolytic activity of natural killer cells. Cancer Res 65:5238–5247
162. Stangl S, Wortmann A, Guertler U, Multhoff G (2006) Control of metastasized pancreatic carcinomas in SCID/beige mice with human IL-2/TKD-activated NK cells. J Immunol 176:6270–6276
163. Krause SW, Gastpar R, Andreesen R et al (2004) Treatment of colon and lung cancer patients with ex vivo heat shock protein 70-peptide-activated, autologous natural killer cells: a clinical phase i trial. Clin Cancer Res 10:3699–3707
164. Shevtsov MA, Kim AV, Samochernych KA et al (2014) Pilot study of intratumoral injection of recombinant heat shock protein 70 in the treatment of malignant brain tumors in children. Onco Targets Ther 7:1071–1081

Chapter 28

Evidence for Hsp90 Co-chaperones in Regulating Hsp90 Function and Promoting Client Protein Folding

Marc B. Cox and Jill L. Johnson

Abstract

Molecular chaperones are a diverse group of highly conserved proteins that transiently interact with partially folded polypeptide chains during normal cellular processes such as protein translation, translocation, and disassembly of protein complexes. Prior to folding or after denaturation, hydrophobic residues that are normally sequestered within a folded protein are exposed to the aqueous environment and are prone to aggregation or misfolding. Multiple classes of molecular chaperones, such as Hsp70s and Hsp40s, recognize and transiently bind polypeptides with exposed hydrophobic stretches in order to prevent misfolding. Other types of chaperones, such as Hsp90, have more specialized functions in that they appear to interact with only a subset of cellular proteins. This chapter focuses on the role of Hsp90 and partner co-chaperones in promoting the folding and activation of a diverse group of proteins with critical roles in cellular signaling and function.

Key words Hsp90, Hop, p23, Immunophilins, Co-chaperones

1 HSP90 Molecular Chaperone Machine

Hsp90 (heat shock protein, 90 kDA) refers to a family of homologous proteins. Yeast and mammalian cells contain two isoforms of cytosolic Hsp90. Higher eukaryotes also contain mitochondrial Trap-1 and Grp94 of the endoplasmic reticulum. The *E. coli* homolog is known as HtpG. Hsp90 contains three conserved domains: an N-terminal ATP-binding domain, a middle domain, and a carboxy-terminal domain. The ability of Hsp90 to bind and hydrolyze ATP is essential for its function. Although there are slight differences in structure and rates of ATP hydrolysis, a unified model for the conformational changes of cytosolic Hsp90, TRAP1, Grp94, and HtpG has emerged (reviewed in [1–4]). A simplified model is presented in Fig. 1. In the absence of nucleotide, Hsp90 is dimerized at the carboxy-terminus, resulting in an open conformation. Nucleotide binding induces the closing of a lid over bound nucleotide. The N-terminal domains then associate to

Stuart K. Calderwood and Thomas L. Prince (eds.), *Chaperones: Methods and Protocols*, Methods in Molecular Biology, vol. 1709, https://doi.org/10.1007/978-1-4939-7477-1_28,

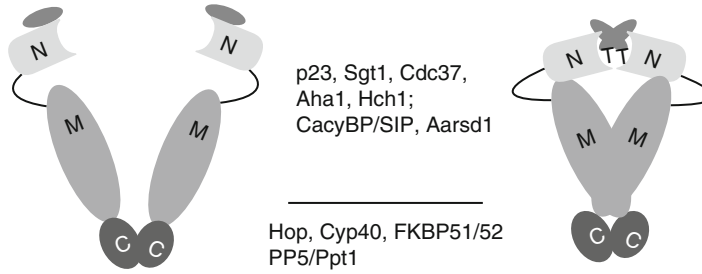

Fig. 1 Hsp90 ATPase cycle. In the absence of ATP (left), Hsp90 is dimerized at its C-terminus in the 'open' conformation. Upon ATP binding (right), the N-terminal domains undergo subsequent conformational changes that result in closing of a 'lid' over the bound nucleotide and additional dimerization of the amino-termini. Co-chaperones may be separated into those that bind the amino-terminal or middle domains (above the line) or those that bind the EEVD sequence at the carboxy-terminus of Hsp90 (below the line)

form the "closed" conformation, in which portions of the amino-terminal domain "cross-over" to associate with the other protomer. The Hsp90 dimer then forms a compact twisted structure that results in the association of a flexible loop from the middle domain with the nucleotide-binding pocket. This structure is capable of ATP hydrolysis. After hydrolysis, Hsp90 returns to the open conformation. Some forms of Hsp90 adopt the "closed" conformation even in the absence of nucleotide, suggesting that nucleotide shifts the equilibrium between distinct conformations rather than triggering specific conformational changes [5]. Asymmetric interactions with clients, co-chaperone proteins, and posttranslational modifications help drive the folding process [6–10].

Cytosolic Hsp90 complexes function as part of an ATP-dependent, ordered pathway in which clients are transferred from Hsp70 to Hsp90 [11–13]. HtpG directly interacts with Hsp70 and cooperates with Hsp70 to fold model clients such as denatured luciferase [14]. Grp94 and the Hsp70 Bip also sequentially interact with clients [15]. As discussed in more detail below, the cytosolic Hsp90 function is also dependent on dozens of co-chaperones. No co-chaperones for HtpG or TRAP1 are known, but two, Cnpy-3 and MZB1, have been described for GRP94 [16, 17]. For the purpose of this review, co-chaperones are proteins that have physical interaction with Hsp90 but cooperate with Hsp90 to fold clients rather than being clients themselves. Another useable test to distinguish whether a protein is a client or a co-chaperone is to test the effect of Hsp90 inhibitors. Many Hsp90 clients become unstable and are targeted for degradation by the proteasome upon Hsp90 inhibition (reviewed in [18]), while the levels of co-chaperones are unaffected.

2 HSP90 as a Global Cellular Regulator

The first two classes of Hsp90 clients identified through classical biochemical techniques were steroid hormone receptors (the progesterone receptor and glucocorticoid receptor) and the v-src kinase [19, 20]. Hsp90 interacts with the GR and PR in the absence of hormone, repressing transcriptional activity. Hsp90 also maintains the receptor in a conformation capable of high-affinity hormone binding. Once hormone binds, Hsp90 and associated co-chaperones are released and the receptors become active as transcription factors. Multiple protein kinases require Hsp90 for stability and become targets for degradation upon Hsp90 inhibition. Additional clients require Hsp90 for folding, activation, transport, or incorporation into multiprotein complexes [3, 21, 22].

High-throughput studies that measured the impact of genetic or pharmacological inhibition of Hsp90 indicate up to 10–15% of all proteins are directly or indirectly dependent on Hsp90 for function. Proteins of *S. cerevisiae* that physically interact with Hsp90 and/or display altered mRNA or protein level upon Hsp90 inhibition have been identified [23–27]. Studies in *C. albicans* suggest that the Hsp90 clientele, judged by proteins with altered regulation upon Hsp90 inhibitor, varies in a growth-state-dependent manner [28, 29]. Similar to those studies, human proteins affected by Hsp90 inhibition were identified [30]. Protein kinases, transcription factors, and E3 ligases are among the most prevalent types of Hsp90 clients [31]. Additional classes of Hsp90 clients include proteins with leucine-rich repeat domains or β-propeller domains [32], chromatin remodelers [33, 34], and additional proteins, such as telomerase [35] and iNOS [36]. Hsp90 is also needed for RNA-induced silencing complexes [37] (Table 1).

The list of known clients of TRAP1 and GRP94 is smaller. TRAP1 regulates the metabolic switch between respiration and glycolysis and loss of TRAP1 disrupts mitochondrial function [38, 39]. Gpr94 is required for a subset of secreted proteins or proteins expressed on the cell surface, such as immunoglobulins [15, 17], insulin-growth factor II [40], Toll-like receptors [16], and components of the Wnt signaling pathway [41]. Although loss of HtpG does not cause significant growth defects in *E. coli*, a few clients of bacterial HtpG have been identified, such as the ribosomal protein L2 [42] and other proteins [43, 44].

3 HSP90 Interaction with Clients

Hsp90 interacts with hundreds of clients that do not share any obvious sequence or structural homology. For a long time, it has been thought that clients interact with Hsp90 while in a nearly

Table 1
Representative list of Hsp90 client proteins[a]

Transcription factors	Ref. (and refs within)
Nuclear hormone receptors	
Progesterone, glucocorticoid, estrogen receptors	[45]
Heme-responsive transcription factor, Hap1	[218]
Aryl hydrocarbon receptor	[219]
Mutant p53	[220]
Heat shock factor, Hsf1	[219]
HIF1a	[221]
Protein kinases	
v-src	[19]
Raf, Ste11	[156]
PKR, dsRNA-dependent kinase	[161]
Wee1 kinase	[222]
ErbB2	[164]
Fes tyrosine kinase	[219]
AKT	[223]
Cdk4	[7]
Other	
Telomerase	[35]
Hepatitis B reverse transcriptase	[224]
matrix metalloproteinase 2 (MMP2)	[225]
iNOS	[36]
RSC chromatin remodeler	[33]
Rvb1 and Rvb2 helicases	[34]
RISC	[37]
Nod1	[226]

[a]A complete list of client proteins is maintained at http://www.picard.ch/downloads/Hsp90interactors.pdf

completely folded conformation, stabilizing client conformations in such a way to allow them to quickly respond to an activation signal, such as ligand binding or phosphorylation [45]. Two recent studies describe how protein instability could promote Hsp90 interaction. A key factor that dictates Hsp90 interaction with protein kinases was the intrinsic instability of the kinase [31]. Moreover, the cyro-electro microscopy structure of the Hsp90-Cdc37-Cdk4 kinase

complex demonstrates how Hsp90 stabilizes the kinase in an unfolded state [7].

Given the diversity of Hsp90 clients, it is possible that clients have different binding sites and/or that the client-binding site changes as Hsp90 undergoes conformational changes. A conserved client-binding site has been identified [7, 46], and there is some overlap between those sites and other recently identified client-binding sites [8, 10]. However, single-particle electron microscopy structure of an Hsp90-Cdc37-Cdk4 kinase complex [47] suggests additional sites may also be used. Other reviews and articles within discuss specifics of the Hsp90-client interaction in more detail [48, 49].

4 HSP90 Co-chaperones

Early studies found that Cdc37 is present in Hsp90-complexes with protein kinases [50], and that Hop, p23, and a set of tetratricopeptide repeat (TPR) containing proteins were present in complex with various steroid hormone receptors [51], although the composition varied in a receptor-dependent manner [52]. Since then many additional co-chaperones have been identified (a comprehensive list is maintained by Dr. Didier Picard (https://www.picard.ch/downloads)) [53]. Co-chaperones are variously characterized by the domains of Hsp90 with which they interact, their own biochemical functions or in the order in which they appear to interact with particular client proteins [3, 54]. Our intent is not to provide a comprehensive listing of all co-chaperones. Instead, we will focus on what is known about how the in vivo functions of a few co-chaperones, particularly with regard to client specific and/or the outcome of client folding (Tables 1 and 2). Importantly, co-chaperones frequently exhibit mutually exclusive binding to Hsp90, either by competing for the same binding site or because they stabilize conformations of Hsp90 that preclude interactions with other co-chaperones [45, 55, 56]. Further, some co-chaperones only interact with proteins with specific structural domains [32].

5 Co-chaperones with CS Domains (CHORD and Sgt1)

p23. p23 and its yeast homolog, Sba1, preferentially bind Hsp90 in the presence of ATP or non-hydrolyzable analogs. p23 inhibits the ATPase activity, stabilizing the closed conformation, which results in prolonged interaction of the client with Hsp90 [57–62]. p23 has molecular chaperone activity and is able to suppress the aggregation of citrate synthase [63, 64]. p23 is essential for development and mice lacking p23 die in an early embryonic stage [65]. Although

Table 2
Select Hsp90 cochaperones and their functions

Co-chaperone	Biochemical functions	Known client protein-Hsp90 complex interactions
p23 (Sba1)	Chaperone activity [64]; inhibits Hsp90 ATPase activity [58, 60]	Steroid hormone receptors, telomerase, Hepatitis B virus reverse transcriptase [45], RSC chromatin remodeler [33]
Sgt1 (Sgt1)	Adapter protein [71]	Kinetochore complex, NLR immune sensors [32, 74]
Cdc37	Adaptor, binds protein kinases [227]; inhibits Hsp90 ATPase activity [228]	Protein kinases [31, 227]
Aha1	Activates Hsp90 ATPase activity [80]	Mutant CFTR [90]
Hop (Sti1)	Inhibits Hsp90 ATPase activity; stimulates Hsp70 ATPase activity [100, 102]	Steroid hormone receptors [146], kinases [115]
Cyp40 (Cpr6/7)	Chaperone activity; PPIase activity [64, 130]	Steroid hormone receptors [146]
FKBP51/52	Chaperone activity; PPIase activity [119]	Steroid hormone receptors [146]
PP5 (Ppt1)	Dephosphorylates Hsp90, Cdc37 [78, 148]	Steroid hormone receptors [146], kinases [147]

not essential in yeast, Sba1 is required for optimal growth and activity of Hsp90 clients [66].

p23 is found in complex with Hsp90 and a range of client proteins including steroid hormone receptors, telomerase, duck hepatitis B reverse transcriptase [45], the RSC chromatin remodeler [33], and argonaute [32, 67]. High-throughput genomic and proteomic studies demonstrate that p23 has additional roles in ribosome biogenesis and cellular transport [68].

6 Sgt1

Although the structures of p23 and the CS domain of Sgt1 are similar, they exhibit distinct interactions with Hsp90 [69, 70]. Sgt1 does not modulate the ATPase activity of Hsp90 and may exhibit altered interactions with Hsp90 in the presence or absence of nucleotide [71, 72]. Like many other co-chaperones, Sgt1 contains a tetratricopeptide repeat (TPR) domain, which typically mediates interaction with the carboxy-terminus of Hsp90 [45]. However,

the TPR domain of Sgt1 is not required for Hsp90 interaction and is absent from Sgt1 orthologs in some species [73]. *SGT1* is essential in yeast, and Sgt1 appears to act early in the Hsp90 folding cycle, serving as an adaptor protein that helps to recruit client proteins to Hsp90 [71]. Sgt1 interacts with the CBF3 kinetochore complex, Polo kinase, plant R (resistance) proteins, and related Nod-like receptors (reviewed in [74]). In high-throughput studies, Sgt1 exhibited a strong preference for binding proteins with leucine-rich repeat domains [32].

7 CacyBP/SIP and Aarsd1

The CS domain is also found in additional co-chaperones 7. including Calcyclin Binding Protein/Siah-1 Interacting Protein (CacyBP/SIP) and Aarsd1 [75, 76]. CacyBP/SIAP binds Hsp90 and exhibits chaperones activity, but its overall function in the Hsp90 machinery remains unknown. AArsd1 is a muscle-specific co-chaperone in mammalian cells that interacts with the Hsp90 beta isoform during muscle differentiation. By replacing p23, it alters activity of the glucocorticoid receptor.

8 Cdc37

Cdc37 is essential in yeast and is required for the folding and stabilization of approximately 60% of protein kinases in yeast and mammalian cells [31, 77]. The Hsp90-Cdc37 interaction is regulated by phosphorylation of a conserved residue of Cdc37 [78]. Early structures showed that the middle domain of Cdc37 (also known as $p50^{cdc37}$) binds directly to the amino-terminal domain of Hsp90 and inhibits ATPase activity [79]. However, in the structure of an Hsp90-Cdc37-Cdk4 kinase complex [7], Cdc37 binds the middle domain of Hsp90. Thus, it is possible that Hsp90-Cdc37 contact sites change during the folding process. The structure of the Hsp90-Cdc37-Cdk4 kinase structure details how Cdc37 binds the unfolded kinase.

9 Aha1 and Hch1

Aha1 (activator of Hsp90 ATPase) dramatically stimulates the ATPase activity of Hsp90 [80, 81]. Hsp90 has a split ATPase domain, which requires association of the amino-terminal and middle domains for hydrolysis to occur. Aha1 stimulates ATP hydrolysis by promoting a conformational change that allows a catalytic loop of the middle domain to associate with the amino-terminus [9, 82, 83]. Hch1 is a fungal-specific co-chaperone that is

homologous to the first half of Aha1. Hch1 is also able to stimulate the ATPase activity of Hsp90, albeit weakly [80]. Hch1 and Aha1 appear to have differing in vivo functions [84–87]. The function of Hch1 appears to be replaced in higher eukaryotes by a posttranslational modification of Hsp90 [88].

Aha1 plays a critical role in the quality control process that leads to degradation of the mutant cystic fibrosis transmembrane conductance regulator (CFTR), an Hsp90 client [89, 90]. The CLC-1 chloride channel also interacts with Aha1 [91]. High-throughput studies identified additional proteins that interact with Aha1 [32, 92, 93]. This list includes ribosomal proteins, proteins required for transcription, translation, and DNA maintenance. The specific in vivo functions of Hch1 are largely unknown.

10 TPR-Containing Co-chaperones

A number of co-chaperones contain TPR domains and dynamically compete for a common-binding site at the carboxy-terminus of Hsp90, which contains the terminal sequence EEVD [45, 94]. Although there are two EEVD-binding sites, evidence suggests that a single Hop/Sti1 binds the Hsp90 dimer, and it is possible for two different TPR-containing proteins to bind simultaneously to help drive the folding cycle [95, 96]. Comparative studies examined the interaction of a variety of TPR-containing co-chaperones with both Hsp90 and cytosolic Hsp70, which also contains a carboxy-terminal EEVD sequence [94, 97–99].

11 Hop (Hsp70-Hsp90 Organizing Protein)

Sti1, the yeast homolog of Hop, binds Hsp90 in the absence of ATP and inhibits dimerization of the amino-terminal domain, resulting in reduced ATPase activity [100, 101]. Sti1 was also able to stimulate the ATPase activity of the Hsp70 Ssa1 [102]. Hop/Sti1 contains three TPR domains, one that preferentially binds Hsp70, one that binds Hsp90, and one that is able to weakly bind either Hsp70 or Hsp90 [94]. Simultaneous binding of Hop to Hsp70 and Hsp90 helps mediate transfer of client protein from Hsp70 to Hsp90 [13, 103]. Multiple studies have elucidated the dynamics and structure of the Hsp90-Hsp70-Hop/Sti1 complex formation [95, 104–107]. Similar to other co-chaperones, Hop/-Sti1 function and/or localization are regulated by phosphorylation [108, 109].

Hop interacts with a variety of Hsp90 clients [32, 110–112]. Hop also interacts with the prion protein [113]. A review of Hop/Sti1 functions is available [114]. Deletion of *STI1* from yeast results in slow growth at high and low temperatures, as

well as defects in Hsp90 clients such as heterologous steroid hormone receptors and kinases [115]. Knockdown of Hop/Sti1 levels has been linked to attention deficit disorders in mice [116] and decreased migration of cancer cells [117].

12 Immunophilins

Immunophilins are a group of proteins that bind immunosuppressant drugs such as FK506, rapamycin, or cyclosporin A [118]. Although they vary in size and domain structure, all the members of the immunophilin family have peptidyl-prolyl isomerase activity (PPIase activity). The immunosuppressant drugs bind the catalytic pocket and inhibit PPIase activity. Two types of immunophilins, Cyp40 (which binds cyclosporin A) and FKBP51/FKBP52 (which bind FK506), also contain TPR domains that mediate interaction with Hsp90 [45]. These two classes of immunophilins have dissimilar sequence and structures, yet both types of co-chaperones mediate the activity of known Hsp90 client proteins and have molecular chaperone activity that is independent of their PPIase activity [64, 119].

Compared to other tissues the immunophilins are most abundant in the nervous system where some family members may have a role in neuronal differentiation [120, 121]. In addition, the immunophilins are implicated as having PPIase-dependent roles in a variety of protein conformational disorders including Parkinson's disease and Alzheimer's disease (reviewed in [122]). The aggregation of partially misfolded proteins (e.g., abnormally phosphorylated Tau) is a hallmark of these diseases and some immunophilin family members regulate the conformational stability of these neuronal aggregates. Several immunophilin family members are also known to associate with and regulate microtubule assembly or disassembly in a PPIase-dependent manner [121, 123–125]. The immunophilins can also associate with steroid hormone receptor Hsp90 complexes and regulate receptor folding, hormone binding, and nuclear translocation (reviewed in [126, 127]. A slightly different collection of these TPR proteins co-purify with different steroid hormone receptors, indicating client specificity, but the basis for this selectivity is poorly understood [52]. The mechanism(s) by which the immunophilins regulate steroid hormone receptor activity is still unclear, but in all the cases examined the PPIase activity is not required for receptor regulation. In addition to these more characterized roles, immunophilin family members have been implicated in a wide variety of fundamental biological processes, signaling cascades, and disease states (reviewed in [126]).

13 Cyp40

Cyp40 associates with nuclear steroid hormone receptors, including the progesterone, estrogen, and glucocorticoid receptors [45]. Cyp40 contains an amino-terminal PPIase domain and a TPR domain separated by a small linker region. In *S. cerevisiae*, there are two homologs of Cyp40, Cpr6 and Cpr7, that have different in vivo functions [128, 129]. Purified Cpr6 had no effect on the ATPase activity of Hsp90 [100]. Cells lacking *CPR6* exhibit few discernible phenotypes, while loss of *CPR7* results in slow growth and defects in Hsp90 client protein activity. Cpr6 and Cpr7 exhibit different PPIase and molecular chaperone activities, but it is unclear how these activities affect Hsp90 client activity [130, 131]. The role of the PPIase domain remains unclear, but the TPR domain and/or the hydrophobic linker that separates the PPIase and TPR domains appear to be critical for molecular chaperone and Hsp90 client activity [132, 133].

14 FKBP51 and FKBP52

FKBP51 and FKBP52 are two related proteins that are found in complex with steroid hormone receptors. There are no FKBP homologs that contain TPR domains in yeast. Similar to CyP40, FKBP51 and FKBP52 contain a PPIase domain and a TPR domain, separated by a short linker. Despite their sequence similarities, FKBP52 and FKBP51 have distinct effects on steroid receptor activity. The presence of FKBP52 in steroid hormone receptor complexes results in higher hormone binding affinity. FKBP51 offsets the positive effects of FKBP52, suggesting that the ratio of the two proteins is important. The specific ability of FKBP52 to promote steroid hormone receptor activity is dependent on non-catalytic residues in the PPIase domain that may interact directly with the ligand-binding domain or indirectly through interaction with factors regulating through the ligand binding domain [134]. Consistent with a positive role in steroid hormone receptor function, mice lacking FKBP52 exhibit androgen, progesterone, and glucocorticoid receptor-related defects including androgen insensitivity in males, uterine defects and implantation failure in females, hepatic steatosis, increased susceptibility to high fat diet-induced hyperglycemia and hyperinsulinemia, and behavioral defects [135–143]. While mice lacking FKBP51 have no overt morphological defects, they have reduced sensitivity to pain presumably through defects in glucocorticoid receptor signaling in the spinal cord and they are more resilient to stress and depression [137, 144, 145]. The importance of FKBP51 in regulating glucocorticoid receptor is also highlighted in New World primates.

These primates overexpress FKBP51 relative to Old World primates, resulting in reduced GR hormone-binding affinity and glucocorticoid resistance. The overexpression of FKBP51 may be an adaption to higher circulating levels of glucocorticoids in New World Primates [146]. These studies emphasize that the type of TPR-containing co-chaperone bound to Hsp90 may have dramatic effects on client protein activity.

15 PP5

PP5 is a serine-threonine phosphatase that interacts with Hsp90 through its TPR domains. PP5 interacts with a wide range of proteins involved in signaling pathways, including ATM/ATR and the Rac GTPase (reviewed in [147]). Deletion of the yeast homolog, *PPT1*, results in Hsp90 client-specific defects [148]. Intriguingly, Ppt1 appears to be able to dephosphorylate both Hsp90 and Cdc37 [78, 148], indicating that Ppt1 may have a general role in regulating the activity of the Hsp90 molecular chaperone machine and other proteins [149].

16 Assays Used to Study the Role of HSP90 And Co-chaperones in Client Folding

Early analysis of the interaction of Hsp90 with client proteins focused on analysis of steroid hormone receptors and protein kinases, and those remain the most well-studied clients. A common theme of Hsp90 function is that folding or assembly is dynamic and requires sequential interactions with various components of the Hsp90 molecular chaperone machine. Most clients likely require Hsp70 and Hsp40. However, there is increasing evidence that clients interact with distinct sets of additional co-chaperones [32, 45, 150, 151]. In particular, different sets of clients appear to use Hop, Cdc37, or Sgt1 as adaptors to facilitate Hsp90 interaction.

17 Protein Kinases

Overexpression of the heterologous v-src kinase is toxic to the yeast *Saccharomyces cerevisiae*, but mutations in Hsp90 or co-chaperones, particularly Cdc37 and Ydj1, disrupt kinase level or activity reduce toxicity [152, 153]. The most commonly used construct is the one that expresses v-src under a galactose-regulated promoter [154, 155]. Ste11 is a mitogen-activated kinase homologous to mammalian Raf that exhibits reduced levels in cells expressing mutant forms of Hsp90 or co-chaperones [156, 157]. Overexpression of the Ste11 kinase domain (Ste11ΔN) is toxic, but not in cells

expressing mutant forms of Hsp90. A plasmid that constitutively expresses Ste11ΔN-K444R, which is inactive as a kinase, has been used to study interaction of Hsp90 and co-chaperones [158, 159]. An alternative approach measures the ability of Ste11 to activate downstream genes using *lacZ* fusions or rtPCR [160]. Reagents to study the mammalian dsRNA-dependent kinase PKR and the yeast kinase Gcn2 have also been developed for use in yeast [161, 162].

Hsp90 inhibitors result in reduced steady-state levels of mammalian Hsp90-dependent protein kinases and reduced Hsp90-kinase interaction [163]. Some kinases are more sensitive to Hsp90 inhibitors than others [164–166]. Many studies of Hsp90-kinase interaction use pull-down assays [167]. A sophisticated series of pull-down assays demonstrate how tyrosine phosphorylation mediates kinase folding through a cycle of posttranslational modifications of Hsp90 and Cdc37 [168]. That study showed that progression through the cycle required Cdc37 release and Aha1 interaction. More recently, the LUMIER assay, in which one protein is FLAG-tagged and the other is tagged with Renilla luciferase, was adapted to study Hsp90 interaction with client proteins [31]. This assay is able to provide quantitative analysis of the interaction of human kinases with Hsp90.

The instability of Hsp90-dependent protein kinases in the absence of Hsp90 makes analysis challenging, but the interaction of Hsp90 with two purified kinases has been analyzed. Hsp40, Hsp70, Cdc37, and Hsp90 were sufficient to restore Chk1 kinase activity. Although not required for kinase activity, the presence of Hop further enhanced activity [169]. Genetic evidence also suggests that the functions of Hop and Cdc37 at least partially overlap [160]. The structure of a cryo-EM complex of Hsp90-Cdc37-Cdk4 is now available [7]. In order to obtain the stable complex, the three proteins were co-expressed in Sf9 insect cells. Molybdate, which is known to stabilize Hsp90-client interactions, was used [170]. Consistent with proposed roles for Hsp70 and Hsp40 in loading kinase onto Hsp90, simply mixing purified Hsp90, Cdc37 and Cdk4 did not promote complex formation.

18 Steroid Hormone Receptors

Steroid hormone receptors are found in complex with Hsp90 and co-chaperones when hormone is not present. Glucocorticoid receptor and progesterone receptor stripped of Hsp90 and associated proteins are unable to bind hormone. The first experiments to identify Hsp90 and co-chaperones involved isolation of steroid hormone receptor complexes from vertebrate cell extracts in the absence of hormone [51, 171]. These progressed to in vitro assembly reactions of Hsp90 and other proteins onto resin-bound

receptor capable or hormone binding in rabbit reticulolysates [172–174]. A few years later the system was modified to enable addition of purified proteins (Hsp70, Hsp90, Hop, Hsp40, and p23) to resin-bound receptor to form the high affinity hormone-binding state [175–177]. These studies support a model that newly synthesized or misfolded receptor first interacts with Hsp40 and Hsp70. Hsp40 interacts directly with the progesterone receptor and is required to promote Hsp70 interaction. In contrast, Hsp70 appears to bind glucocorticoid receptor prior to Hsp40 [178, 179]. Subsequent interaction of Hop/Sti1 promotes Hsp90 interaction. Nucleotide-binding results in the formation of the ATP-bound closed form of Hsp90 and p23 interaction. It is in this "late complex" that the receptor is capable of high affinity hormone binding. Client dissociation occurs upon hormone binding and ATP hydrolysis.

The immunophilin component within the Hsp90-receptor complex is not required for receptors to reach hormone binding conformation in vitro and is not included in this model. Their relevance within these complexes and this model are discussed below.

The above studies were complicated by the fact that many client proteins are extremely unstable in the absence of Hsp90. The steroid hormone receptors are an example of a client protein that cannot be purified in full-length form without the presence of Hsp90. Expression and purification of the steroid hormone receptors in a bacterial system is not possible. The receptors can be stably expressed in insect cells and yeast cells solely because of the presence of Hsp90 and associated co-chaperones. Two recent studies used soluble glucocorticoid receptor ligand-binding domain (GRLBD) to study Hsp90 interaction using only purified proteins. Kirschke et al. monitored the interaction of Hsp70 and Hsp90 with GRLBD containing the F602S mutation, which increases solubility [12]. Consistent with earlier reports, they observed distinct roles for Hsp70, Hsp90, Hop, Hsp40, and p23 in order to bind hormone. However, their results found that isolated GRLBD was able to bind hormone, and that Hsp70 partially unfolded GRLBD prior to promoting Hsp90 interaction. In a separate study, Lorenz et al. used a different mutant of the GRLBD to gain new insights into interaction sites between GR and Hsp90 and how GR interaction affects Hsp90 conformation and ATPase activity [8].

Studies in yeast were the first to demonstrate a role for Hsp90 in steroid hormone maturation [20]. These studies use two plasmids: one that constitutively expresses the receptor (usually GR), and another that expresses beta-galactosidase under a glucocorticoid response element (GRE-*lacZ*). GR activation is dependent on hormone addition. Yeast expressing mutations in Hsp90 or containing deletions or mutations in genes encoding Ydj1 (an Hsp40), Sba1 (p23), or Sti1 (Hop) exhibit reduced or altered GR activity

[115, 180–182]. Similar studies with Hsp70 are complicated since Ssa, the Hsp70 that interacts with GR, is encoded by four different genes.

The traditional model suggests that after Hsp70 release and ATP-associated conformational changes in Hsp90, other co-chaperones such as p23 and immunophilins bind and stabilize the closed conformation of Hsp90. Based on the model, the TPR-containing Hop protein is exchanged for a TPR-containing immunophilin during this transition. However, recent evidence demonstrated that Hsp90 can accommodate both Hop and FKBP52 simultaneously suggesting the possibility of an additional transitional complex involving both Hop and an immunophilin [96, 183]. Thus, the exact mechanism by which the receptor transitions from "intermediate" Hsp70-based complexes to "late" Hsp90-based complexes is currently unclear. The "late" complex is actually a collection of complexes distinguished by which TPR containing proteins are bound at the carboxy-terminus of Hsp90. Studies with different steroid hormone receptors showed that different levels of Cyp40, PP5, FKBP51, and FKBP52 bind the receptors [52]. Thus, the composition of the late complex varies in a client-specific manner. However, there is not yet enough evidence about the composition of other "late" client complexes to know the extent of this variation. Upon activation ATP hydrolysis occurs and Hsp90 and co-chaperones are released from the client protein. However, it is also clear that some of the chaperone components have a direct regulatory role in the receptor signaling pathways. The Hsp90 complex silences steroid hormone receptor function until hormone binding occurs by blocking access to the receptor nuclear localization signal, blocking receptor dimerization, and blocking the association of transcriptional coactivators (reviewed in [184]). Additionally, the immunophilin FKBP52 can directly influence receptor hormone binding [139, 185, 186] and receptor translocation to the nucleus [187, 188]. While the immunophilin component within these "late" complexes is not considered necessary for receptors to reach the hormone binding conformation in vitro, the fact that FKBP52 increases the efficiency of hormone binding suggests that at least FKBP52 is required for hormone binding in vivo at low, physiologically relevant hormone concentrations.

Based on studies of the steroid hormone receptors it is generally assumed that the late stage complexes are relatively short lived. In the case of PR the mature conformation of the receptor lasts only several minutes [11], which correlates with the slow ATPase cycle of Hsp90 (reviewed in [2, 3]). After several minutes the complex dissociates and the receptor is cycled back into the chaperoning pathway. Thus, the receptor-folding pathway is a dynamic, ordered process that involves many transient interactions. In the absence of Hsp90 the receptors are unstable and degraded rapidly through the proteosomal degradation pathway [54].

Upon hormone binding the steroid hormone receptors are translocated to the nucleus, if not already within that compartment, where they dimerize, associate with hormone responsive enhancer elements on the DNA, and mediate gene transcription. The role of the late stage chaperones in these processes remains unclear. There is evidence that chaperones are involved in the nuclear translocation of GR including chaperone and co-chaperone interactions with dynein motor proteins and interactions with nuclear pore proteins [189, 190]. These findings suggest that the late stage complex is required at least until GR reaches the nuclear pore. However, whether or not the Hsp90 chaperone complex dissociates in the cytosol or travels into the nucleus with GR is debated. Given that some of the receptors (ER and PR) already exist largely within the nucleus [191, 192], one would assume that late stage complexes with these receptors are present in the nucleus. Given their presence in the nucleus it is plausible that the late stage chaperones could have a role in all the steps of the steroid hormone receptor signaling pathway including DNA binding and the regulation of gene transcription. Some evidence exists suggesting that Hsp90 and p23 can regulate the receptors at the level of gene transcription but the exact role of the late stage chaperones on the DNA remains unclear [193].

While the immunophilins associate with "late" complexes to regulate receptor activity, whether or not that regulation is through direct contacts with the receptor within the context of the larger complex is unknown. One approach that has been used is to immune-deplete Hsp90 from cell extracts prior to immuno-precipitation or immuno-precipitating client protein and stripping off the chaperones with high salt prior to the addition of the interacting co-chaperone. The latter approach was used to demonstrate a direct interaction between FKBP52 and GR [194] . The functional significance of this interaction remains unclear given the fact that FKBP52 regulation of GR requires FKBP52 interaction with Hsp90 [186]. Introducing mutations that abrogate co-chaperone interaction with Hsp90 could also be used to assess direct interactions. An FKBP52 mutant containing a single point mutation (K354A) in the TPR domain that abrogates binding to Hsp90 exists [186]. Interestingly, FKBP52 was recently shown to bind directly to β-catenin and promote β-catenin interaction with, and regulation of, the androgen receptor through the AR-binding function 3 (BF3) surface, and this functional synergy is independent of FKBP52 binding to Hsp90 given that it was unaffected by the FKBP52-K354A mutation [195]. The fact that this co-regulatory mechanism is specific to the androgen receptor suggests that FKBP52 may have multiple distinct roles in steroid hormone receptor signaling pathways, some of which are independent of Hsp90. This also presents the possibility that FKBP52 regulates receptors through direct and/or indirect interactions at

multiple sites on the receptors. Indeed, another study suggests that the helix 1–3 (H1–H3) loop in the GR hormone-binding domain is an FKBP51 and FKBP52 regulatory site [196], but whether or not they regulate this site through direct or indirect interaction is unknown.

19 RNA-Induced Silencing Complex (RISC)

RISC is the main complex involved in RNA interference. Hsp90 and a set of co-chaperones similar to those involved in steroid hormone receptor maturation have been found to be involved in loading RNA duplexes into Argonaute proteins in mammalian, drosophila, and plant cells [37, 67, 197]. Hsp90, Hsp70, hop, an Hsp40, Cyp40, p23 and Aha1 are among those proteins with described roles in the ATP-dependent assembly of RISC complexes.

20 Leucine-Rich Repeat Proteins

Sgt1 (suppressor of G2 allele of skp1) is an Hsp90 co-chaperone that exhibits specificity for proteins containing leucine-rich repeat protein-interaction domains [32, 198]. Sgt1 appears to enable Hsp90 to interact with a wide range of client proteins involved in the innate immune responses of animals and E3 ubiquitin ligases [74, 199]. Sgt1 and Hsp90 were identified in pull-down assays with the yeast kinetochore protein Skp1 [200]. Subsequent studies using purified components resulted in the model that Sgt1 directly binds Skp1 and delivers it to Hsp90. Sti1 may also function as part of these complexes since ternary complexes between Sgt1, Sti1 and Hsp90 have been observed [71]. A role for Hsp70 in Sgt1 complexes has also been established [201]. The crystal structure of the TPR domain of Sgt1 bound to Skp1 is available [199]. Further, the ability of Sgt1 to stabilize LRR domains has been used to enhance expression and solubility of NOD1 expression [202].

21 Co-chaperones as Drug Targets

Hsp90 has attracted considerable attention as a target for cancer chemotherapy because Hsp90 is required for the functions of proteins that influence multiple steps in cancer progression [203, 204]. Similar to Hsp90, some Hsp90 co-chaperones are overexpressed in tumor cells [205]. Small-molecule inhibitors that bind Hsp90, destabilize clients, and induce apoptosis have been used in clinical trials to treat a range of tumor types. Most Hsp90 inhibitors bind the ATPase domain of Hsp90, and thus

inhibit the wide range of Hsp90 functions. The most promising results with Hsp90 inhibitors in clinical trials are as part of combination therapies for breast cancer, lung cancer, and some leukemias [206–208]. Hsp90 inhibitors are also potential therapies to combat pathogenic fungi [209]. Inhibitors that target co-chaperones may also have clinical significance. The compound Y-632 disrupts Hop-Hsp90 function and has anti-tumor effects [210]. Similarly, two compounds, gedunin and ailanthone, which target p23 also exhibit anti-tumor activity [211, 212]. A compound that disrupts Cdc37-Hsp90 interaction did not reduce the activity of Hsp90-dependent kinases [213], likely due to the presence of direct Cdc37-kinase interactions [7]. Compounds that target other co-chaperones may have more specific effects. For example, an inhibitor of Aha1 might be used to alleviate the effects of cystic fibrosis [90]. In addition, specific immunophilin family members are promising therapeutic targets for the treatment of a variety of diseases including endocrine and behavioral disorders, neurodegeneration and cancer (reviewed in [126]). The immunosuppressive drug FK506 effectively reduces androgen-dependent prostate cancer cell growth presumably through disruption of FKBP52-regulated androgen receptor activity [214]. Thus, compounds that target FKBP52 and/or the mechanism by which FKBP52 regulates receptors, but lack immunosuppressive effects, might be used for the treatment of prostate cancer. Indeed, MJC13, a drug thought to target the AR BF3 surface, was shown to block FKBP52 and β-catenin interaction with, and regulation of, the androgen receptor [215, 216]. MJC13 prevents dissociation of the AR-Hsp90 complex upon hormone binding in an FKBP52-specific manner leading to reduced androgen-dependent gene expression, AR-dependent prostate cancer cell proliferation, and prostate tumor growth in a mouse xenograft model [215–217].

22 Remaining Questions About Co-chaperone Function

Many additional questions remain about how specific co-chaperones direct the function of Hsp90 to properly fold and activate the diverse array of client proteins. One of the main questions about co-chaperone function is why cytosolic Hsp90 requires co-chaperones whereas other forms of Hsp90 (TRAP1 and HtpG) do not. In addition, the co-chaperones encoded by diverse eukaryotic species vary, suggesting that each organism has a slightly different component of co-chaperones [73]. More work is required to determine whether the requirement for specific co-chaperones is due to how it regulates Hsp90 versus how co-chaperones directly affect client function. In most cases, the role of direct co-chaperone-client interaction is largely unknown. It is possible that a co-chaperone does not interact directly with client protein alone

but co-chaperone association with the Hsp90 complex could bring the co-chaperone into direct contact with the client protein. Identifying and characterizing direct client protein:co-chaperone interactions has traditionally been a challenging task. Hsp90 is one of the most abundant proteins in the cell. Thus, any system in which Hsp90 is present cannot determine direct interactions without the use of additional tools as one cannot be sure that the client:co-chaperone interaction observed is simply through both proteins associating with the Hsp90 complex.

Acknowledgments

M.B.C. is supported in part by NIH/NIGMS grant No. 1SC1GM084863 and Grant Number 5G12RR008124 (to the Border Biomedical Research Center/University of Texas at El Paso) from the National Center for Research Resources (NCRR/NIH). The contents of this publication are solely the responsibility of the authors and do not necessarily represent the official views of NCRR or NIH.

References

1. Kim YE et al (2013) Molecular chaperone functions in protein folding and proteostasis. Annu Rev Biochem 82:323–355
2. Neckers L, Mollapour M, Tsutsumi S (2009) The complex dance of the molecular chaperone Hsp90. Trends Biochem Sci 34 (5):223–226
3. Wandinger SK, Richter K, Buchner J (2008) The Hsp90 chaperone machinery. J Biol Chem 283(27):18473–18477
4. Dollins DE et al (2007) Structures of GRP94-nucleotide complexes reveal mechanistic differences between the hsp90 chaperones. Mol Cell 28(1):41–56
5. Southworth DR, Agard DA (2008) Species-dependent ensembles of conserved conformational states define the Hsp90 chaperone ATPase cycle. Mol Cell 32(5):631–640
6. Mayer MP, Le Breton L (2015) Hsp90: breaking the symmetry. Mol Cell 58(1):8–20
7. Verba KA et al (2016) Atomic structure of Hsp90-Cdc37-Cdk4 reveals that Hsp90 traps and stabilizes an unfolded kinase. Science 352(6293):1542–1547
8. Lorenz OR et al (2014) Modulation of the hsp90 chaperone cycle by a stringent client protein. Mol Cell 53(6):941–953
9. Retzlaff M et al (2010) Asymmetric activation of the hsp90 dimer by its cochaperone aha1. Mol Cell 37(3):344–354
10. Karagoz GE et al (2014) Hsp90-Tau complex reveals molecular basis for specificity in chaperone action. Cell 156(5):963–974
11. Smith DF (1993) Dynamics of heat shock protein 90-progesterone receptor binding and the disactivation loop model for steroid receptor complexes. Mol Endocrinol 7:1418–1429
12. Kirschke E et al (2014) Glucocorticoid receptor function regulated by coordinated action of the Hsp90 and Hsp70 chaperone cycles. Cell 157(7):1685–1697
13. Wegele H et al (2006) Substrate transfer from the chaperone Hsp70 to Hsp90. J Mol Biol 356(3):802–811
14. Genest O et al (2011) Heat shock protein 90 from Escherichia coli collaborates with the DnaK chaperone system in client protein remodeling. Proc Natl Acad Sci U S A 107:8206–8211
15. Melnick J, Dul JL, Argon Y (1994) Sequential interaction of the chaperones BiP and GRP94 with immunoglobulin chains in the endoplasmic reticulum. Nature 370(6488):373–375
16. Liu B et al (2010) Folding of Toll-like receptors by the HSP90 paralogue gp96 requires a substrate-specific cochaperone. Nat Commun 1:79
17. Rosenbaum M et al (2014) MZB1 is a GRP94 cochaperone that enables proper

immunoglobulin heavy chain biosynthesis upon ER stress. Genes Dev 28 (11):1165–1178

18. Theodoraki MA, Caplan AJ (2012) Quality control and fate determination of Hsp90 client proteins. Biochim Biophys Acta 1823 (3):683–688
19. Xu Y, Lindquist S (1993) Heat-shock protein hsp90 governs the activity of pp60v-src kinase. Proc Natl Acad Sci U S A 90:7074–7078
20. Picard D et al (1990) Reduced levels of hsp90 compromise steroid receptor action in vivo. Nature 348:166–168
21. Pearl LH, Prodromou C (2006) Structure and mechanism of the hsp90 molecular chaperone machinery. Annu Rev Biochem 75:271–294
22. Makhnevych T, Houry WA (2012) The role of Hsp90 in protein complex assembly. Biochim Biophys Acta 1823(3):674–682
23. Zhao R, Houry WA (2007) Molecular interaction network of the Hsp90 chaperone system. Adv Exp Med Biol 594:27–36
24. Franzosa EA et al (2011) Heterozygous yeast deletion collection screens reveal essential targets of Hsp90. PLoS One 6(11):e28211
25. McClellan AJ et al (2007) Diverse cellular functions of the hsp90 molecular chaperone uncovered using systems approaches. Cell 131 (1):121–135
26. Gopinath RK et al (2014) The Hsp90-dependent proteome is conserved and enriched for hub proteins with high levels of protein-protein connectivity. Genome Biol Evol 6(10):2851–2865
27. Millson SH et al (2005) A two-hybrid screen of the yeast proteome for Hsp90 interactors uncovers a novel Hsp90 chaperone requirement in the activity of a stress-activated mitogen-activated protein kinase, Slt2p (Mpk1p). Eukaryot Cell 4(5):849–860
28. Diezmann S, Leach MD, Cowen LE (2015) Functional divergence of Hsp90 genetic interactions in biofilm and planktonic cellular states. PLoS One 10(9):e0137947
29. Diezmann S et al (2012) Mapping the Hsp90 genetic interaction network in Candida albicans reveals environmental contingency and rewired circuitry. PLoS Genet 8(3):e1002562
30. Wu Z, Moghaddas Gholami A, Kuster B (2012) Systematic identification of the HSP90 candidate regulated proteome. Mol Cell Proteomics 11(6):M111 016675
31. Taipale M et al (2012) Quantitative analysis of HSP90-client interactions reveals principles of substrate recognition. Cell 150(5):987–1001
32. Taipale M et al (2014) A quantitative chaperone interaction network reveals the architecture of cellular protein homeostasis pathways. Cell 158(2):434–448
33. Echtenkamp FJ et al (2016) Hsp90 and p23 molecular chaperones control chromatin architecture by maintaining the functional pool of the RSC chromatin remodeler. Mol Cell 64(5):888–899
34. Zhao R et al (2008) Molecular chaperone Hsp90 stabilizes Pih1/Nop17 to maintain R2TP complex activity that regulates snoRNA accumulation. J Cell Biol 180(3):563–578
35. Holt SE et al (1999) Functional requirement of p23 and Hsp90 in telomerase complexes. Genes Dev 13(7):817–826
36. Ghosh A, Chawla-Sarkar M, Stuehr DJ (2011) Hsp90 interacts with inducible NO synthase client protein in its heme-free state and then drives heme insertion by an ATP-dependent process. FASEB J 25 (6):2049–2060
37. Iwasaki S et al (2010) Hsc70/Hsp90 chaperone machinery mediates ATP-dependent RISC loading of small RNA duplexes. Mol Cell 39(2):292–299
38. Lisanti S et al (2014) Deletion of the mitochondrial chaperone TRAP-1 uncovers global reprogramming of metabolic networks. Cell Rep 8(3):671–677
39. Yoshida S et al (2013) Molecular chaperone TRAP1 regulates a metabolic switch between mitochondrial respiration and aerobic glycolysis. Proc Natl Acad Sci U S A 110(17): E1604–E1612
40. Ostrovsky O, Ahmed NT, Argon Y (2009) The chaperone activity of GRP94 toward insulin-like growth factor II is necessary for the stress response to serum deprivation. Mol Biol Cell 20(6):1855–1864
41. Liu B et al (2013) Essential roles of grp94 in gut homeostasis via chaperoning canonical Wnt pathway. Proc Natl Acad Sci U S A 110 (17):6877–6882
42. Motojima-Miyazaki Y, Yoshida M, Motojima F (2010) Ribosomal protein L2 associates with E. coli HtpG and activates its ATPase activity. Biochem Biophys Res Commun 400 (2):241–245
43. Sato T et al (2010) HtpG, the prokaryotic homologue of Hsp90, stabilizes a phycobilisome protein in the cyanobacterium Synechococcus elongatus PCC 7942. Mol Microbiol 76(3):576–589
44. Saito M et al (2008) Interaction of the molecular chaperone HtpG with uroporphyrinogen decarboxylase in the cyanobacterium

Synechococcus elongatus PCC 7942. Biosci Biotechnol Biochem 72(5):1394–1397

45. Pratt WB, Toft DO (2003) Regulation of signaling protein function and trafficking by the hsp90/hsp70-based chaperone machinery. Exp Biol Med (Maywood) 228 (2):111–133
46. Genest O et al (2013) Uncovering a region of heat shock protein 90 important for client binding in E coli and chaperone function in yeast. Mol Cell 49(3):464–473
47. Vaughan CK et al (2006) Structure of an Hsp90-Cdc37-Cdk4 complex. Mol Cell 23 (5):697–707
48. Karagoz GE, Rudiger SG (2015) Hsp90 interaction with clients. Trends Biochem Sci 40(2):117–125
49. Street TO et al (2014) Elucidating the mechanism of substrate recognition by the bacterial Hsp90 molecular chaperone. J Mol Biol 426 (12):2393–2404
50. Stepanova L et al (1996) Mammalian p50Cdc37 is a protein kinase-targeting subunit of Hsp90 that binds and stabilizes Cdk4. Genes Dev 10:1491–1502
51. Smith DF, Faber LE, Toft DO (1990) Purification of unactivated progesterone receptor and identification of novel receptor-associated proteins. J Biol Chem 265(7):3996–4003
52. Riggs D et al (2004) Functional specificity of co-chaperone interactions with Hsp90 client proteins. Crit Rev Biochem Mol Biol 39 (5–6):279–295
53. Echeverria PC et al (2011) An interaction network predicted from public data as a discovery tool: application to the Hsp90 molecular chaperone machine. PLoS One 6(10): e26044
54. Pearl LH, Prodromou C, Workman P (2008) The Hsp90 molecular chaperone: an open and shut case for treatment. Biochem J 410 (3):439–453
55. Harst A, Lin H, Obermann WM (2005) Aha1 competes with Hop, p50 and p23 for binding to the molecular chaperone Hsp90 and contributes to kinase and hormone receptor activation. Biochem J 387(Pt 3):789–796
56. Siligardi G et al (2004) Co-chaperone regulation of conformational switching in the Hsp90 ATPase cycle. J Biol Chem 279 (50):51989–51998
57. Johnson JL, Toft DO (1995) Binding of p23 and hsp90 during assembly with the progesterone receptor. Mol Endocrinol 9 (6):670–678
58. McLaughlin SH et al (2006) The co-chaperone p23 arrests the Hsp90 ATPase cycle to trap client proteins. J Mol Biol 356 (3):746–758
59. Young JC, Hartl FU (2000) Polypeptide release by Hsp90 involves ATP hydrolysis and is enhanced by the co-chaperone p23. EMBO J 19(21):5930–5940
60. Richter K, Walter S, Buchner J (2004) The Co-chaperone Sba1 connects the ATPase reaction of Hsp90 to the progression of the chaperone cycle. J Mol Biol 342 (5):1403–1413
61. Ali MM et al (2006) Crystal structure of an Hsp90-nucleotide-p23/Sba1 closed chaperone complex. Nature 440(7087):1013–1017
62. Cox MB, Miller CA 3rd (2004) Cooperation of heat shock protein 90 and p23 in aryl hydrocarbon receptor signaling. Cell Stress Chaperones 9(1):4–20
63. Weikl T, Abelmann K, Buchner J (1999) An unstructured C-terminal region of the Hsp90 co-chaperone p23 is important for its chaperone function. J Mol Biol 293(3):685–691
64. Freeman BC, Toft DO, Morimoto RI (1996) Molecular chaperone machines: chaperone activities of the cyclophilin Cyp-40 and the steroid aporeceptor-associated protein p23. Science 274(5293):1718–1720
65. Grad I et al (2006) The Hsp90 cochaperone p23 is essential for perinatal survival. Mol Cell Biol 26(23):8976–8983
66. Fang Y et al (1998) SBA1 encodes a yeast hsp90 cochaperone that is homologous to vertebrate p23 proteins. Mol Cell Biol 18 (7):3727–3734
67. Pare JM, LaPointe P, Hobman TC (2013) Hsp90 cochaperones p23 and FKBP4 physically interact with hAgo2 and activate RNA interference-mediated silencing in mammalian cells. Mol Biol Cell 24(15):2303–2310
68. Echtenkamp FJ et al (2011) Global functional map of the p23 molecular chaperone reveals an extensive cellular network. Mol Cell 43 (2):229–241
69. Zhang M et al (2008) Structural and functional coupling of Hsp90- and Sgt1-centred multi-protein complexes. EMBO J 27 (20):2789–2798
70. Kadota Y et al (2008) Structural and functional analysis of SGT1-HSP90 core complex required for innate immunity in plants. EMBO Rep 9(12):1209–1215
71. Catlett MG, Kaplan KB (2006) Sgt1p is a unique co-chaperone that acts as a client-adaptor to link Hsp90 to Skp1p. J Biol Chem 281(44):33739–33748
72. Eckl JM et al (2014) Nematode Sgt1-homologue D1054.3 binds open and closed

conformations of Hsp90 via distinct binding sites. Biochemistry 53(15):2505–2514

73. Johnson JL, Brown C (2009) Plasticity of the Hsp90 chaperone machine in divergent eukaryotic organisms. Cell Stress Chaperones 14(1):83–94
74. Picard D (2008) A stress protein interface of innate immunity. EMBO Rep 9 (12):1193–1195
75. Goral A et al (2016) Calcyclin binding protein/Siah-1 interacting protein is a Hsp90 binding chaperone. PLoS One 11(6): e0156507
76. Echeverria PC, Briand PA, Picard D (2016) A remodeled Hsp90 molecular chaperone ensemble with the novel cochaperone Aarsd1 is required for muscle differentiation. Mol Cell Biol 36(8):1310–1321
77. Mandal AK et al (2007) Cdc37 has distinct roles in protein kinase quality control that protect nascent chains from degradation and promote posttranslational maturation. J Cell Biol 176(3):319–328
78. Vaughan CK et al (2008) Hsp90-dependent activation of protein kinases is regulated by chaperone-targeted dephosphorylation of Cdc37. Mol Cell 31(6):886–895
79. Roe SM et al (2004) The mechanism of Hsp90 regulation by the protein kinase-specific cochaperone p50(cdc37). Cell 116 (1):87–98
80. Panaretou B et al (2002) Activation of the ATPase activity of hsp90 by the stress-regulated cochaperone aha1. Mol Cell 10 (6):1307–1318
81. Lotz GP et al (2003) Aha1 binds to the middle domain of Hsp90, contributes to client protein activation, and stimulates the ATPase activity of the molecular chaperone. J Biol Chem 278(19):17228–17235
82. Meyer P et al (2004) Structural basis for recruitment of the ATPase activator Aha1 to the Hsp90 chaperone machinery. EMBO J 23 (6):1402–1410
83. Wolmarans A et al (2016) The mechanism of Hsp90 ATPase stimulation by Aha1. Sci Rep 6:33179
84. Nathan DF, Vos MH, Lindquist S (1999) Identification of SSF1, CNS1, and HCH1 as multicopy suppressors of a Saccharomyces cerevisiae Hsp90 loss-of-function mutation. Proc Natl Acad Sci U S A 96(4):1409–1414
85. Armstrong H et al (2012) The co-chaperone Hch1 regulates Hsp90 function differently than its homologue Aha1 and confers sensitivity to yeast to the Hsp90 inhibitor NVP-AUY922. PLoS One 7(11):e49322
86. Horvat NK et al (2014) A mutation in the catalytic loop of hsp90 specifically impairs ATPase stimulation by aha1p, but not hch1p. J Mol Biol 426(12):2379–2392
87. Johnson JL et al (2014) Mutation of essential Hsp90 co-chaperones SGT1 or CNS1 renders yeast hypersensitive to overexpression of other co-chaperones. Curr Genet 60(4):265–276
88. Zuehlke AD et al (2017) An Hsp90 cochaperone protein in yeast is functionally replaced by site-specific posttranslational modification in human. Nat Commun 8:15328
89. Koulov AV et al (2010) Biological and structural basis for Aha1 regulation of Hsp90 ATPase activity in maintaining proteostasis in the human disease cystic fibrosis. Mol Biol Cell 21(6):871–884
90. Wang X et al (2006) Hsp90 cochaperone Aha1 downregulation rescues misfolding of CFTR in cystic fibrosis. Cell 127(4):803–815
91. Peng YJ et al (2016) Regulation of CLC-1 chloride channel biosynthesis by FKBP8 and Hsp90beta. Sci Rep 6:32444
92. Dunn DM et al (2015) c-Abl mediated tyrosine phosphorylation of Aha1 activates its co-chaperone function in cancer cells. Cell Rep 12(6):1006–1018
93. Sun L, Hartson SD, Matts RL (2015) Identification of proteins associated with Aha1 in HeLa cells by quantitative proteomics. Biochim Biophys Acta 1854(5):365–380
94. Scheufler C et al (2000) Structure of TPR domain-peptide complexes: critical elements in the assembly of the Hsp70-Hsp90 multichaperone machine. Cell 101(2):199–210
95. Alvira S et al (2014) Structural characterization of the substrate transfer mechanism in Hsp70/Hsp90 folding machinery mediated by Hop. Nat Commun 5:5484
96. Li J, Richter K, Buchner J (2011) Mixed Hsp90-cochaperone complexes are important for the progression of the reaction cycle. Nat Struct Mol Biol 18(1):61–66
97. Assimon VA, Southworth DR, Gestwicki JE (2015) Specific binding of tetratricopeptide repeat proteins to heat shock protein 70 (Hsp70) and heat shock protein 90 (Hsp90) is regulated by affinity and phosphorylation. Biochemistry 54 (48):7120–7131
98. Brinker A et al (2002) Ligand discrimination by TPR domains. Relevance and selectivity of EEVD-recognition in Hsp70 x Hop x Hsp90

complexes. J Biol Chem 277 (22):19265–19275
99. Millson SH et al (2008) Chaperone ligand-discrimination by the TPR-domain protein Tah1. Biochem J 413(2):261–268
100. Prodromou C et al (1999) Regulation of Hsp90 ATPase activity by tetratricopeptide repeat (TPR)-domain co-chaperones. EMBO J 18(3):754–762
101. Richter K et al (2003) Sti1 is a non-competitive inhibitor of the Hsp90 ATPase. Binding prevents the N-terminal dimerization reaction during the atpase cycle. J Biol Chem 278(12):10328–10333
102. Wegele H et al (2003) Sti1 is a novel activator of the Ssa proteins. J Biol Chem 278 (28):25970–25976
103. Chen S, Smith DF (1998) Hop as an adaptor in the heat shock protein 70 (Hsp70) and hsp90 chaperone machinery. J Biol Chem 273(52):35194–35200
104. Rohl A et al (2015) Hsp90 regulates the dynamics of its cochaperone Sti1 and the transfer of Hsp70 between modules. Nat Commun 6:6655
105. Lee CT et al (2012) Dynamics of the regulation of Hsp90 by the co-chaperone Sti1. EMBO J 31(6):1518–1528
106. Southworth DR, Agard DA (2011) Client-loading conformation of the Hsp90 molecular chaperone revealed in the cryo-EM structure of the human Hsp90:Hop complex. Mol Cell 42(6):771–781
107. Schmid AB et al (2012) The architecture of functional modules in the Hsp90 co-chaperone Sti1/Hop. EMBO J 31 (6):1506–1517
108. Rohl A et al (2015) Hop/Sti1 phosphorylation inhibits its co-chaperone function. EMBO Rep 16(2):240–249
109. Longshaw VM et al (2004) Nuclear translocation of the Hsp70/Hsp90 organizing protein mSTI1 is regulated by cell cycle kinases. J Cell Sci 117(Pt 5):701–710
110. Chen L et al (2010) The Hop/Sti1-Hsp90 chaperone complex facilitates the maturation and transport of a PAMP receptor in rice innate immunity. Cell Host Microbe 7 (3):185–196
111. Chen S et al (1998) Differential interactions of p23 and the TPR-containing proteins Hop, Cyp40, FKBP52 and FKBP51 with Hsp90 mutants. Cell Stress Chaperones 3 (2):118–129
112. Bergmayr C et al (2013) Recruitment of a cytoplasmic chaperone relay by the A2A adenosine receptor. J Biol Chem 288 (40):28831–28844
113. Romano SA et al (2009) Reciprocal remodeling upon binding of the prion protein to its signaling partner hop/STI1. FASEB J 23 (12):4308–4316
114. Baindur-Hudson S, Edkins AL, Blatch GL (2015) Hsp70/Hsp90 organising protein (hop): beyond interactions with chaperones and prion proteins. Subcell Biochem 78:69–90
115. Chang HC, Nathan DF, Lindquist S (1997) In vivo analysis of the Hsp90 cochaperone Sti1 (p60). Mol Cell Biol 17(1):318–325
116. Beraldo FH et al (2015) Hyperactivity and attention deficits in mice with decreased levels of stress-inducible phosphoprotein 1 (STIP1). Dis Model Mech 8 (11):1457–1466
117. Willmer T et al (2013) Knockdown of Hop downregulates RhoC expression, and decreases pseudopodia formation and migration in cancer cell lines. Cancer Lett 328 (2):252–260
118. Barik S (2006) Immunophilins: for the love of proteins. Cell Mol Life Sci 63 (24):2889–2900
119. Bose S et al (1996) Chaperone function of Hsp90-associated proteins. Science 274 (5293):1715–1717
120. Quinta HR, Galigniana MD (2012) The neuroregenerative mechanism mediated by the Hsp90-binding immunophilin FKBP52 resembles the early steps of neuronal differentiation. Br J Pharmacol 166(2):637–649. https://doi.org/10.1111/j.1476-5381.2011.01783.x
121. Quinta HR et al (2011) Management of cytoskeleton architecture by molecular chaperones and immunophilins. Cell Signal 23 (12):1907–1920. https://doi.org/10.1016/j.cellsig.2011.07.023. Epub 2011 Aug 12
122. Chattopadhaya S, Harikishore A, Yoon HS (2011) Role of FK506 binding proteins in neurodegenerative disorders. Curr Med Chem 18(35):5380–5397
123. Chambraud B et al (2007) The immunophilin FKBP52 specifically binds to tubulin and prevents microtubule formation. FASEB J 21 (11):2787–2797
124. Chambraud B et al (2010) A role for FKBP52 in Tau protein function. Proc Natl Acad Sci U S A 107(6):2658–2663
125. Jinwal UK et al (2010) The Hsp90 cochaperone, FKBP51, increases Tau stability and polymerizes microtubules. J Neurosci 30 (2):591–599

126. Erlejman AG et al (2014) Molecular chaperone activity and biological regulatory actions of the TPR-domain immunophilins FKBP51 and FKBP52. Curr Protein Pept Sci 15 (3):205–215
127. Storer CL et al (2011) FKBP51 and FKBP52 in signaling and disease. Trends Endocrinol Metab 22(12):481–490
128. Zuehlke AD, Johnson JL (2012) Chaperoning the chaperone: a role for the co-chaperone Cpr7 in modulating Hsp90 function in Saccharomyces cerevisiae. Genetics 191:805–814
129. Zuehlke AD et al (2013) Interaction of heat shock protein 90 and the co-chaperone Cpr6 with Ura2, a bifunctional enzyme required for pyrimidine biosynthesis. J Biol Chem 288 (38):27406–27414
130. Mayr C et al (2000) Cpr6 and Cpr7, two closely related Hsp90-associated immunophilins from Saccharomyces cerevisiae, differ in their functional properties. J Biol Chem 275 (44):34140–34146
131. Duina AA et al (1996) A cyclophilin function in Hsp90-dependent signal transduction. Science 274(5293):1713–1715
132. Duina AA et al (1998) The peptidyl-prolyl isomerase domain of the CyP-40 cyclophilin homolog Cpr7 is not required to support growth or glucocorticoid receptor activity in Saccharomyces cerevisiae. J Biol Chem 273 (18):10819–10822
133. Mok D et al (2006) The chaperone function of cyclophilin 40 maps to a cleft between the prolyl isomerase and tetratricopeptide repeat domains. FEBS Lett 580(11):2761–2768
134. Riggs DL et al (2007) Noncatalytic role of the FKBP52 peptidyl-prolyl isomerase domain in the regulation of steroid hormone signaling. Mol Cell Biol 27(24):8658–8669
135. Cheung-Flynn J et al (2005) Physiological role for the cochaperone FKBP52 in androgen receptor signaling. Mol Endocrinol 19 (6):1654–1666
136. Hartmann J et al (2012) Fkbp52 heterozygosity alters behavioral, endocrine and neurogenetic parameters under basal and chronic stress conditions in mice. Psychoneuroendocrinology 37(12):2009–2021
137. O'Leary JC III et al (2011) A new antidepressive strategy for the elderly: ablation of FKBP5/FKBP51. PLoS One 6(9):e24840
138. Touma C et al (2011) FK506 binding protein 5 shapes stress responsiveness: modulation of neuroendocrine reactivity and coping behavior. Biol Psychiatry 70(10):928–936
139. Tranguch S et al (2005) Cochaperone immunophilin FKBP52 is critical to uterine receptivity for embryo implantation. Proc Natl Acad Sci U S A 102(40):14326–14331
140. Tranguch S, Smith DF, Dey SK (2006) Progesterone receptor requires a co-chaperone for signalling in uterine biology and implantation. Reprod Biomed Online 13 (5):651–660
141. Warrier M et al (2010) Susceptibility to diet-induced hepatic steatosis and glucocorticoid resistance in FK506-binding protein 52-deficient mice. Endocrinology 151 (7):3225–3236
142. Yong W et al (2007) Essential role for Co-chaperone Fkbp52 but not Fkbp51 in androgen receptor-mediated signaling and physiology. J Biol Chem 282(7):5026–5036. Epub 2006 Dec 1
143. Tranguch S et al (2007) FKBP52 deficiency-conferred uterine progesterone resistance is genetic background and pregnancy stage specific. J Clin Invest 117(7):1824–1834
144. Hartmann J et al (2012) The involvement of FK506-binding protein 51 (FKBP5) in the behavioral and neuroendocrine effects of chronic social defeat stress. Neuropharmacology 62(1):332–339
145. Maiaru M et al (2016) The stress regulator FKBP51 drives chronic pain by modulating spinal glucocorticoid signaling. Sci Transl Med 8(325):325ra19. https://doi.org/10.1126/scitranslmed.aab3376
146. Smith DF, Toft DO (2008) The intersection of steroid receptors with molecular chaperones: observations and questions. Mol Endocrinol 22:2229–2240
147. Hinds TD Jr, Sanchez ER (2008) Protein phosphatase 5. Int J Biochem Cell Biol 40:2358–2362
148. Wandinger SK et al (2006) The phosphatase Ppt1 is a dedicated regulator of the molecular chaperone Hsp90. EMBO J 25(2):367–376
149. Schreiber TB et al (2012) Global analysis of phosphoproteome regulation by the Ser/Thr phosphatase Ppt1 in Saccharomyces cerevisiae. J Proteome Res 11(4):2397–2408
150. Zhao R et al (2005) Navigating the chaperone network: an integrative map of physical and genetic interactions mediated by the hsp90 chaperone. Cell 120(5):715–727
151. Rohl A, Rohrberg J, Buchner J (2013) The chaperone Hsp90: changing partners for demanding clients. Trends Biochem Sci 38 (5):253–262
152. Lee P et al (2002) The Cdc37 protein kinase-binding domain is sufficient for protein kinase

activity and cell viability. J Cell Biol 159 (6):1051–1059

153. Mandal AK et al (2008) Ydj1 protects nascent protein kinases from degradation and controls the rate of their maturation. Mol Cell Biol 28 (13):4434–4444
154. Dey B, Caplan AJ, Boschelli F (1996) The Ydj1 molecular chaperone facilitates formation of active p60v-src in yeast. Mol Biol Cell 7(1):91–100
155. Nathan DF, Lindquist S (1995) Mutational analysis of Hsp90 function: interactions with a steroid receptor and a protein kinase. Mol Cell Biol 15(7):3917–3925
156. Louvion JF, Abbas-Terki T, Picard D (1998) Hsp90 is required for pheromone signaling in yeast. Mol Biol Cell 9(11):3071–3083
157. Abbas-Terki T, Donze O, Picard D (2000) The molecular chaperone Cdc37 is required for Ste11 function and pheromone-induced cell cycle arrest. FEBS Lett 467(1):111–116
158. Flom GA et al (2008) Farnesylation of Ydj1 is required for in vivo interaction with Hsp90 client proteins. Mol Biol Cell 19 (12):5249–5258
159. Mandal AK et al (2010) Hsp110 chaperones control client fate determination in the hsp70-Hsp90 chaperone system. Mol Biol Cell 21(9):1439–1448
160. Lee P et al (2004) Sti1 and Cdc37 can stabilize Hsp90 in chaperone complexes with a protein kinase. Mol Biol Cell 15 (4):1785–1792
161. Donze O, Abbas-Terki T, Picard D (2001) The Hsp90 chaperone complex is both a facilitator and a repressor of the dsRNA-dependent kinase PKR. EMBO J 20 (14):3771–3780
162. Donze O, Picard D (1999) Hsp90 binds and regulates Gcn2, the ligand-inducible kinase of the alpha subunit of eukaryotic translation initiation factor 2 [corrected]. Mol Cell Biol 19(12):8422–8432
163. Whitesell L et al (1994) Inhibition of heat shock protein HSP90-pp60v-src heteroprotein complex formation by benzoquinone ansamycins: essential role for stress proteins in oncogenic transformation. Proc Natl Acad Sci U S A 91(18):8324–8328
164. Xu W et al (2001) Sensitivity of mature Erbb2 to geldanamycin is conferred by its kinase domain and is mediated by the chaperone protein Hsp90. J Biol Chem 276 (5):3702–3708
165. Schulte TW et al (1998) Antibiotic radicicol binds to the N-terminal domain of Hsp90 and shares important biologic activities with geldanamycin. Cell Stress Chaperones 3 (2):100–108
166. An WG, Schulte TW, Neckers LM (2000) The heat shock protein 90 antagonist geldanamycin alters chaperone association with p210bcr-abl and v-src proteins before their degradation by the proteasome. Cell Growth Differ 11(7):355–360
167. Silverstein AM et al (1998) p50(cdc37) binds directly to the catalytic domain of Raf as well as to a site on hsp90 that is topologically adjacent to the tetratricopeptide repeat binding site. J Biol Chem 273(32):20090–20095
168. Xu W et al (2012) Dynamic tyrosine phosphorylation modulates cycling of the HSP90-P50(CDC37)-AHA1 chaperone machine. Mol Cell 47(3):434–443
169. Arlander SJ et al (2006) Chaperoning checkpoint kinase 1 (Chk1), an Hsp90 client, with purified chaperones. J Biol Chem 281 (5):2989–2998
170. Kost SL et al (1989) Binding of heat shock proteins to the avian progesterone receptor. Mol Cell Biol 9(9):3829–3838
171. Hutchison KA, Dittmar KD, Pratt WB (1994) All of the factors required for assembly of the glucocorticoid receptor into a functional heterocomplex with heat shock protein 90 are preassociated in a self-sufficient protein folding structure, a "foldosome". J Biol Chem 269(45):27894–27899
172. Smith DF et al (1990) Reconstitution of progesterone receptor with heat shock proteins. Mol Endocrinol 4(11):1704–1711
173. Smith DF et al (1992) Assembly of progesterone receptor with heat shock proteins and receptor activation are ATP mediated events. J Biol Chem 267:1350–1356
174. Dittmar KD et al (1996) Reconstitution of the steroid receptor.hsp90 heterocomplex assembly system of rabbit reticulocyte lysate. J Biol Chem 271(22):12833–12839
175. Kosano H et al (1998) The assembly of progesterone receptor-hsp90 complexes using purified proteins. J Biol Chem 273 (49):32973–32979
176. Hernandez MP, Sullivan WP, Toft DO (2002) The assembly and intermolecular properties of the hsp70-Hop-hsp90 molecular chaperone complex. J Biol Chem 277 (41):38294–38304
177. Morishima Y et al (2000) Stepwise assembly of a glucocorticoid receptor.hsp90 heterocomplex resolves two sequential ATP-dependent events involving first hsp70 and then hsp90 in opening of the steroid binding pocket. J Biol Chem 275 (24):18054–18060

178. Hernandez MP, Chadli A, Toft DO (2002) HSP40 binding is the first step in the HSP90 chaperoning pathway for the progesterone receptor. J Biol Chem 277 (14):11873–11881
179. Murphy PJ et al (2003) Visualization and mechanism of assembly of a glucocorticoid receptor.Hsp70 complex that is primed for subsequent Hsp90-dependent opening of the steroid binding cleft. J Biol Chem 278 (37):34764–34773
180. Kimura Y, Yahara I, Lindquist S (1995) Role of the protein chaperone YDJ1 in establishing Hsp90-mediated signal transduction pathways. Science 268(5215):1362–1365
181. Johnson JL, Craig EA (2000) A role for the Hsp40 Ydj1 in repression of basal steroid receptor activity in yeast. Mol Cell Biol 20 (9):3027–3036
182. Bohen SP (1998) Genetic and biochemical analysis of p23 and ansamycin antibiotics in the function of Hsp90-dependent signaling proteins. Mol Cell Biol 18(6):3330–3339
183. Hildenbrand ZL et al (2011) Hsp90 can accommodate the simultaneous binding of the FKBP52 and HOP proteins. Oncotarget 2(1–2):45–58
184. Cheung J, Smith DF (2000) Molecular chaperone interactions with steroid receptors: an update. Mol Endocrinol 14(7):939–946
185. Davies TH, Ning YM, Sanchez ER (2005) Differential control of glucocorticoid receptor hormone-binding function by tetratricopeptide repeat (TPR) proteins and the immunosuppressive ligand FK506. Biochemistry 44(6):2030–2038
186. Riggs DL et al (2003) The Hsp90-binding peptidylprolyl isomerase FKBP52 potentiates glucocorticoid signaling in vivo. EMBO J 22 (5):1158–1167
187. Galigniana MD et al (2002) Binding of hsp90-associated immunophilins to cytoplasmic dynein: direct binding and in vivo evidence that the peptidylprolyl isomerase domain is a dynein interaction domain. Biochemistry 41(46):13602–13610
188. Galigniana MD et al (2001) Evidence that the peptidylprolyl isomerase domain of the hsp90-binding immunophilin FKBP52 is involved in both dynein interaction and glucocorticoid receptor movement to the nucleus. J Biol Chem 276(18):14884–14889
189. Echeverria PC et al (2009) Nuclear import of the glucocorticoid receptor-hsp90 complex through the nuclear pore complex is mediated by its interaction with Nup62 and importin beta. Mol Cell Biol 29(17):4788–4797
190. Pratt WB et al (2004) Role of hsp90 and the hsp90-binding immunophilins in signalling protein movement. Cell Signal 16 (8):857–872
191. Htun H et al (1999) Direct visualization of the human estrogen receptor alpha reveals a role for ligand in the nuclear distribution of the receptor. Mol Biol Cell 10(2):471–486
192. Lim CS et al (1999) Differential localization and activity of the A- and B-forms of the human progesterone receptor using green fluorescent protein chimeras. Mol Endocrinol 13(3):366–375
193. Freeman BC, Yamamoto KR (2002) Disassembly of transcriptional regulatory complexes by molecular chaperones. Science 296 (5576):2232–2235
194. Silverstein AM et al (1999) Different regions of the immunophilin FKBP52 determine its association with the glucocorticoid receptor, hsp90, and cytoplasmic dynein. J Biol Chem 274(52):36980–36986
195. Storer Samaniego C et al (2015) The FKBP52 Cochaperone Acts in Synergy with beta-Catenin to Potentiate Androgen Receptor Signaling. PLoS One 10(7):e0134015
196. Cluning C et al (2013) The helix 1-3 loop in the glucocorticoid receptor LBD is a regulatory element for FKBP cochaperones. Mol Endocrinol 27(7):1020–1035
197. Iki T et al (2012) Cyclophilin 40 facilitates HSP90-mediated RISC assembly in plants. EMBO J 31(2):267–278
198. Stuttmann J, Parker JE, Noel LD (2008) Staying in the fold: the SGT1/chaperone machinery in maintenance and evolution of leucine-rich repeat proteins. Plant Signal Behav 3(5):283–285
199. Willhoft O et al (2017) The crystal structure of the Sgt1-Skp1 complex: the link between Hsp90 and both SCF E3 ubiquitin ligases and kinetochores. Sci Rep 7:41626
200. Bansal PK, Abdulle R, Kitagawa K (2004) Sgt1 associates with Hsp90: an initial step of assembly of the core kinetochore complex. Mol Cell Biol 24(18):8069–8079
201. Noel LD et al (2007) Interaction between SGT1 and cytosolic/nuclear HSC70 chaperones regulates Arabidopsis immune responses. Plant Cell 19(12):4061–4076
202. Hong TJ, Hahn JS (2016) Application of SGT1-Hsp90 chaperone complex for soluble expression of NOD1 LRR domain in E. coli. Biochem Biophys Res Commun 478 (4):1647–1652

203. Whitesell L, Lindquist SL (2005) HSP90 and the chaperoning of cancer. Nat Rev Cancer 5 (10):761–772
204. Butler LM et al (2015) Maximizing the therapeutic potential of HSP90 inhibitors. Mol Cancer Res 13(11):1445–1451
205. McDowell CL, Bryan Sutton R, Obermann WM (2009) Expression of Hsp90 chaperome proteins in human tumor tissue. Int J Biol Macromol 45(3):310–314
206. Neckers L, Workman P (2012) Hsp90 molecular chaperone inhibitors: are we there yet? Clin Cancer Res 18(1):64–76
207. Koga F, Kihara K, Neckers L (2009) Inhibition of cancer invasion and metastasis by targeting the molecular chaperone heat-shock protein 90. Anticancer Res 29(3):797–807
208. Sawai A et al (2008) Inhibition of Hsp90 down-regulates mutant epidermal growth factor receptor (EGFR) expression and sensitizes EGFR mutant tumors to paclitaxel. Cancer Res 68(2):589–596
209. Veri A, Cowen LE (2014) Progress and prospects for targeting Hsp90 to treat fungal infections. Parasitology 141(9):1–11
210. Wang W et al (2016) Y-632 inhibits heat shock protein 90 (Hsp90) function by disrupting the interaction between Hsp90 and Hsp70/Hsp90 organizing protein, and exerts antitumor activity in vitro and in vivo. Cancer Sci 107(6):782–790
211. Patwardhan CA et al (2013) Gedunin inactivates the co-chaperone p23 protein causing cancer cell death by apoptosis. J Biol Chem 288(10):7313–7325
212. He Y et al (2016) Ailanthone targets p23 to overcome MDV3100 resistance in castration-resistant prostate cancer. Nat Commun 7:13122
213. Smith JR et al (2015) Restricting direct interaction of CDC37 with HSP90 does not compromise chaperoning of client proteins. Oncogene 34(1):15–26
214. Periyasamy S et al (2007) The immunophilin ligands cyclosporin A and FK506 suppress prostate cancer cell growth by androgen receptor-dependent and -independent mechanisms. Endocrinology 148 (10):4716–4726
215. De Leon JT et al (2011) Targeting the regulation of androgen receptor signaling by the heat shock protein 90 cochaperone FKBP52 in prostate cancer cells. Proc Natl Acad Sci U S A 108(29):11878–11883
216. Suh JH et al (2015) Similarities and distinctions in actions of surface-directed and classic androgen receptor antagonists. PLoS One 10 (9):e0137103
217. Liang S et al (2016) Solution formulation development and efficacy of MJC13 in a preclinical model of castration-resistant prostate cancer. Pharm Dev Technol 21(1):121–126
218. Zhang L, Hach A, Wang C (1998) Molecular mechanism governing heme signaling in yeast: a higher-order complex mediates heme regulation of the transcriptional activator HAP1. Mol Cell Biol 18(7):3819–3828
219. Nair SC et al (1996) A pathway of multichaperone interactions common to diverse regulatory proteins: estrogen receptor, Fes tyrosine kinase, heat shock transcription factor Hsf1, and the aryl hydrocarbon receptor. Cell Stress Chaperones 1(4):237–250
220. Blagosklonny MV et al (1996) Mutant conformation of p53 translated in vitro or in vivo requires functional HSP90. Proc Natl Acad Sci U S A 93(16):8379–8383
221. Minet E et al (1999) Hypoxia-induced activation of HIF-1: role of HIF-1alpha-Hsp90 interaction. FEBS Lett 460(2):251–256
222. Aligue R, Akhavan-Niak H, Russell P (1994) A role for Hsp90 in cell cycle control: Wee1 tyrosine kinase activity requires interaction with Hsp90. EMBO J 13(24):6099–6106
223. Sato S, Fujita N, Tsuruo T (2000) Modulation of Akt kinase activity by binding to Hsp90. Proc Natl Acad Sci U S A 97 (20):10832–10837
224. Hu J, Toft DO, Seeger C (1997) Hepadnavirus assembly and reverse transcription require a multi-component chaperone complex which is incorporated into nucleocapsids. EMBO J 16(1):59–68
225. Eustace BK et al (2004) Functional proteomic screens reveal an essential extracellular role for hsp90 alpha in cancer cell invasiveness. Nat Cell Biol 6(6):507–514
226. da Silva Correia J et al (2007) SGT1 is essential for Nod1 activation. Proc Natl Acad Sci U S A 104(16):6764–6769
227. Caplan AJ, Mandal AK, Theodoraki MA (2007) Molecular chaperones and protein kinase quality control. Trends Cell Biol 17 (2):87–92
228. Siligardi G et al (2002) Regulation of Hsp90 ATPase activity by the co-chaperone Cdc37p/p50cdc37. J Biol Chem 277 (23):20151–20159

Chapter 29

Clinical Evaluation and Biomarker Profiling of Hsp90 Inhibitors

Akira Yuno, Min-Jung Lee, Sunmin Lee, Yusuke Tomita, David Rekhtman, Brittni Moore, and Jane B. Trepel

Abstract

Inhibitors of the molecular chaperone heat shock protein 90 (Hsp90) have been in clinical development as anticancer agents since 1998. There have been 18 Hsp90 inhibitors (Hsp90i) that have entered the clinic, all of which, though structurally distinct, target the ATP-binding Bergerat fold of the chaperone N-terminus. Currently, there are five Hsp90 inhibitors in clinical trial and no approved drug in this class. One impediment to development of a clinically efficacious Hsp90 inhibitor has been the very low percentage of clinical trials that have codeveloped a predictive or pharmacodynamic marker of the anticancer activity inherent in this class of drugs. Here, we provide an overview of the clinical development of Hsp90 inhibitors, review the pharmacodynamic assays that have been employed in the past, and highlight new approaches to Hsp90 inhibitor clinical development.

Key words Hsp90 inhibitors, Clinical trial, Biomarkers, Pharmacodynamic assessment, HDC (Hsp90 inhibitor-drug conjugate), HSF1, Immunity

1 The Inhibitors and Clinical Trials

1.1 Discovery of a New Molecular Target

In 1962, Ferruccio Ritossa, who was studying puff regions of nucleic acid synthesis in *Drosophila* salivary gland chromosomes, demonstrated that there was increased transcription in new chromosomal puff regions in response to a shift to elevated temperatures, resulting in the production of a number of unknown factors [1]. In 1974, the first of these factors, termed heat shock proteins, were described [2] and subsequently shown to protect cells from various stresses. Over the next 20 years rigorous research demonstrated that two of the most prevalent heat shock-induced proteins, heat shock protein (Hsp)90 and Hsp70, associate with steroid receptors, and that Hsp90 plays a critical role in the maintenance of steroid receptors in readiness for steroid hormone binding [3–6]. It was also observed that Hsp90 could associate with the oncoprotein v-Src [7–9]. In the early

Stuart K. Calderwood and Thomas L. Prince (eds.), *Chaperones: Methods and Protocols*, Methods in Molecular Biology, vol. 1709, https://doi.org/10.1007/978-1-4939-7477-1_29,

1990s at the NCI, Len Neckers and Luke Whitesell began working with a small molecule, geldanamycin, considered at the time to be a tyrosine kinase inhibitor. They demonstrated that, unexpectedly, geldanamycin directly and specifically bound a 90 KD protein, which they showed was Hsp90, and, furthermore, in v-Src-expressing cells, geldanamycin caused the release of v-Src from Hsp90. Additionally, they showed that at low concentrations the ability of geldanamycin to inhibit the tyrosine kinase activity of v-Src was a consequence of loss of binding of v-Src to Hsp90 rather than direct inhibition of v-Src enzymatic activity [10]. This study revealed (1) Hsp90 was a new, druggable molecular target, (2) identification of geldanamycin as the first Hsp90 inhibitor (geldanamycin, radicicol, and a number of other natural products that were ultimately shown to be Hsp90 inhibitors were discovered prior to this work, but at the time were not known to associate with Hsp90 or act as Hsp90 inhibitors), (3) geldanamycin had anticancer activity in v-Src-driven tumor cells, and (4) the data suggested a novel mechanism of anticancer activity, in which the drug acts not by binding to the oncoprotein (i.e., as an inhibitor of the oncoprotein's enzymatic activity), but by binding to a molecular chaperone complex causing dissociation of the oncoprotein from the protective activity of the chaperone.

1.2 Clinical Hsp90 Inhibitors

The NCI Developmental Therapeutics Program tested geldanamycin in preclinical models and found it was too toxic for clinical development. It is worth noting that geldanamycin went on to be an enormously useful bioprobe of Hsp90 structure and function, having been employed in more than 1000 studies as of January 2017. To continue their efforts to identify a clinical candidate Hsp90 inhibitor Len Neckers and his lab capitalized on their observation in the Whitesell et al. study which showed that the 17-position of geldanamycin could be modified without losing anticancer activity. Together with Ed Sausville, an NCI medical oncologist and translational researcher, and Jim Moyer, a biochemist at Pfizer studying benzoquinoid ansamycins, they obtained a compound Pfizer had previously synthesized, geldanamycin modified in the 17-position (17-AAG). They demonstrated that 17-AAG also bound to Hsp90 and shared important biologic activity with geldanamycin [11], and they submitted 17-AAG for preclinical testing including IND-enabling toxicology, which showed acceptable toxicity, leading to the launch in 1999 under the NCI Cancer Therapy Evaluation Program umbrella of four 17-AAG phase I trials, at the Mayo Clinic, Memorial Sloan Kettering Cancer Center, University of Pittsburgh Cancer Institute and the NCI, and, supported by NCI and sponsored by Cancer Research UK, a fifth 17-AAG phase I trial at the Cancer Research UK Centre for Cancer Therapeutics. All of the five trials were completed and published, including a recommended phase II

dose and schedule (see references 2–6, 8, 9 in bibliography at the end of Table 1). 17-AAG was hard to formulate and had some off-target toxicity, in particular hepatotoxicity, due to the quinone ring, but was also reported to cause prolonged disease stabilization in metastatic melanoma patients [12] and to show RECIST-defined responses in patients with HER2-positive metastatic breast cancer previously progressing on trastuzumab [13]. An effort had been initiated to develop a more soluble analogue of 17-AAG, and in 2004, 5 years after 17-AAG entered the clinic, the more water-soluble 17-AAG derivative 17-DMAG, produced by the NCI, began clinical trial. This was followed in 2005 by the Infinity compound IPI-504, which is the reduced quinone form of 17-AAG and can be found *in vivo* in equilibrium with 17-AAG in patients on 17-AAG trials. This was the last natural product Hsp90 inhibitor to be developed to clinical stage. In 2006, Biogen Idec launched the synthetic inhibitor BIIB21, which was also the first orally available Hsp90 inhibitor. This was followed in 2007 by the Novartis compound AUY922, the Kyowa Hakko compound KW2478, and the Serenex compound SNX-5422. In 2008, there were, remarkably, four new Hsp90 inhibitors in clinical trial, BIIB028 from Biogen Idec, IPI-493 from Infinity, STA-9090 (ganetespib) from Synta, and XL888 from Exelixis. This was followed in 2009 by the Aztex compound AT13387, a second inhibitor from Novartis, HSP990, and a Myriad compound MPC3100. In 2010, Debiopharm entered with Debio0932, and PU-H71, developed by Gabriela Chiosis at Memorial Sloan Kettering Cancer Center began first-in-human trials. The last two Hsp90 inhibitors to enter clinical trial were both from Japan, DS-2248, from Daiichi Sankyo, and TAS-116, from Taiho.

Thus, 18 distinct Hsp90 inhibitors have entered clinical trial (for review see Chiosis and colleagues) [14]). Although Hsp90 has multiple domains, notably an N-terminal domain, a flexible linker domain, a middle domain and a C-terminal domain, and at least two distinct drug-binding domains, the N-terminal ATP/ADP--binding domain and a C-terminal nucleotide-binding domain [15], and there have been sustained efforts directed at targeting both the N-terminal and the C-terminal nucleotide-binding sites [16], all of the 18 clinical Hsp90 inhibitors are targeted to the same N-terminal ATP/ADP-binding site. The N-terminal inhibitors have remarkable specificity. In addition to Hsp90 they have been shown to bind, with variable affinity, only two additional proteins, the Hsp90 family members GRP94 and TRAP1, and this binding may be greatly reduced in cells due to the predominantly endoplasmic reticulum and mitochondrial localizations of GRP94 and TRAP1 respectively.

The focus of this overview is on the pharmacodynamic assessments that have been performed in clinical trials to date and

Table 1
Hsp90 inhibitor clinical trials published with biomarker data

Drug	Combined therapy	Methods	Target	Material	Year	NCT No.	Ref
17-AAG		WB	Hsp70, c-RAF-1, LCK, CDK4	PBMC	2005	NCT00003969	1
		WB	Hsp70, c-RAF-1, CDK4	Tumor biopsy samples			
		IHC	Hsp70	Tumor biopsy samples			
		WB	Hsp90, Hsp70, Grp78, Hop, Cdc37, CHIP, FKBP51, FKBP52, and p23	PBMC	2005	NCT00003969	2
		WB	Hsp70, Grp78, Lck, Raf1	PBMC	2005	NCT00003969	3
		WB	Hsp90, Hsp70	PBMC	2005	NCT00003969	4
		WB	Hsp70, ILK	PBMC	2006	NCT00003969	5
		WB	Hsp72, IGF1R, AKT	PBMC	2007	NCT00079404	6
		WB	Hsp90, Hsp70, p-Akt, Akt, Raf-1	PBMC	2007	NCT00003969	7
		ELISA	Hsp70	PBMC			
		WB	Hsp70, Akt, Raf-1	PBMC	2007	NCT00003969	8
		WB	Hsp72, Akt	PBMC	2007	NCT00079404	9
	Trastuzumab	WB	Hsp70, RAF-1, cdk4, AKT	PBMC	2007	Unknown	10
	Irinotecan	IHC	Hsp70, p-Chk1, p-H2AX, p-histone H3, cleaved caspase-3	Tumor biopsy samples	2008	NCT00119236	11
		ELISA	IL-6, IL-8	Serum	2008	NCT00118092	12
		qRT-PCR	maspin	Blood			
		WB	Hsp70, Raf kinases (A, B, C), ERK, pERK, CDK4, cyclin D1	Tumor biopsy samples	2008	NCT00104897	13
		WB	Hsp70	PBMC	2010	Unknown	14
	Sorafenib	WB	Hsp90, Hsp70, CDK4, pAKT, pERK, c-Raf	PBMC	2010	NCT00121264	15
		ELISA	Hsp72	PBMC/plasma			
	Bortezomib	WB	Hsp70	PBMC	2011	NCT00514371	16
		ELISA	Hsp70	Serum			
	Gemcitabine and/or cisplatin	WB	Hsp90, Hsp70, ILK	PBMC	2011	NCT00047047	17
	Cytarabine	WB	Hsp70, Chk1, ILK, c-Raf	BM cells	2011	NCT00098423	18
	Gemcitabine	WB	Hsp70, Akt, c-Raf	PBMC	2012	NCT00093496	19
		WB	Hsp70, Akt, c-Raf, Chk1, IR, Her2				

				Tumor biopsy samples			
		WB	Hsp72	PBMC	2012	NCT00104897	20
	Docetaxel	WB	Hsp70, Akt, Raf1	PBMC	2012	NCT00058253	21
17-DMAG		WB	Hsp90, Hsp70, ILK	PBMC	2010	NCT00089362	22
		WB	Hsp70, Hsp27, CDK4, RAF-1, AKT, ILK	Tumor biopsy samples			
		RT-PCR	Hsp70	PBMC	2010	NCT00088868	23
		FCM	Hsp70	BM cells	2010	NCT00089271 or	24
			p-AKT	PBMC		NCT00088868	
		WB	Hsp72, CDK4, ERBB2	PBMC/tumor biopsy samples	2011	NCT00248521	25
		ELISA	Hsp72	PBMC/plasma			
	Trastuzumab	WB or ELISA	Hsp70, Akt, pAkt	PBMC	2012	Unknown	26
		WB	AKT, IKK-a, IKK-b	B cells isolated from CLL patients	2016	NCT01126502	27
AT13387		RT-PCR	Hsp70, Hsp27	Tumor biopsy samples	2015	NCT01246102	28
		WB	Hsp70	PBMC			
		ELISA	Hsp70, CK18, caspase-cleaved CK18	Serum			
		RPPA analysis	210 client proteins	Tumor biopsy samples			
		ELISA	Hsp70	Plasma	2015	NCT00878423	29
		WB	several HSP90 client proteins	PBMC			
		IHC	Hsp70, CDK4, RAF-1, AKT, S6, pAKT, pS6, caspase-3	Tumor biopsy samples			
AUY922		ELISA	Hsp70	PBMC	2013	Unknown	30
		IHC	Hsp70, AKT	Tumor biopsy samples			
	89Zr-trastuzumab and 89Zr-bevacizumab	ELISA	Hsp70	PBMC	2014	NCT01081613	31
		ELISA	HER2-ECD	Serum		and NCT01081600	

(continued)

Table 1
(continued)

Drug	Combined therapy	Methods	Target	Material	Year	NCT No.	Ref
	Bortezomib	ELISA/WB	Hsp70	PBMC	2015	NCT00708292	32
		IHC	Hsp70	BM			
BIIB021		WB	Hsp70	PBMC	2013	NCT00618319	33
		Unknown	Hsp70	PBMC	2014	NCT00618735 or	34
		Unknown	Hsp70, HER2-ECD, IGFBP-2	Serum		NCT00618735	
		WB	HER2, Hsp70, CDK4, C-RAF, p-AKT, AKT, ERK, p-ERK	Tumor biopsy samples			
BIIB028		Serum HER-2 assay	HER-2	Serum	2013	NCT00725933	35
		BCA assay	Hsp70	PBMC			
Debio0932		Unknown	HER2	Plasma	2015	NCT01168752	36
		Unknown	Hsp70	PBMC			
HSP990		ELISA	Hsp70	PBMC	2015	NCT00879905	37
IPI-504		WB	Hsp70	PBMC	2011	NCT00113204	38
		WB	Hsp70	PBMC	2013	NCT00276302	39
KW-2478		WB	Hsp70	PBMC	2016	NCT00457782	40
SNX-5422		WB	Hsp70	PBMC	2011	NCT00647764 or NCT00644072	41
		Unknown	Hsp70	Unknown	2013	NCT00595686	42
STA-9090		ELISA	Hsp70	Plasma	2013	NCT00687934	43
			EGFR and KRAS mutational status determined for cohort assignment. Retrospective biomarkers, contingent on tissue availability, included gene mutational analysis, EGFR amplification, and ALK rearrangement		2013	NCT01562015	44
		IHC	pERK, Cyclin D1, pAKT, HIF-1a, VEGFR2, HSP70	Tumor biopsy samples	2014	NCT01111838	45
		Genotyping	KRAS, BRAF, PIKC3A				

Docetaxel		PFS versus elevated lactate dehydrogenase and mutant KRAS	N/A	2015	NCT01348126	46
	RT-PCR	CK18, maspin, PSA, IL-6, uPA, and RANK	PBMC	2016	NCT01270880	47

Bibliography for Table 1

1. Banerji U, O'Donnell A, Scurr M et al. (2005) Phase I pharmacokinetic and pharmacodynamic study of 17-allylamino, 17-demethoxygeldanamycin in patients with advanced malignancies. J Clin Oncol 23: 4152–4161
2. Goetz MP, Toft D, Reid J et al. (2005) Phase I trial of 17-allylamino-17-demethoxygeldanamycin in patients with advanced cancer. J Clin Oncol 23: 1078–1087
3. Grem JL, Morrison G, Guo XD et al. (2005) Phase I and pharmacologic study of 17-(allylamino)-17-demethoxygeldanamycin in adult patients with solid tumors. J Clin Oncol 23: 1885–1893
4. Ramanathan RK, Trump DL, Eiseman JL et al. (2005) Phase I pharmacokinetic-pharmacodynamic study of 17-(allylamino)-17-demethoxygeldanamycin (17AAG, NSC 330507), a novel inhibitor of heat shock protein 90, in patients with refractory advanced cancers. Clin Cancer Res 11: 3385–3391
5. Nowakowski GS, McCollum AK, Ames MM et al. (2006) A phase I trial of twice-weekly 17-allylamino-demethoxy-geldanamycin in patients with advanced cancer. Clin Cancer Res 12: 6087–6093
6. Bagatell R, Gore L, Egorin MJ et al. (2007) Phase I pharmacokinetic and pharmacodynamic study of 17-N-allylamino-17-demethoxygeldanamycin in pediatric patients with recurrent or refractory solid tumors: a pediatric oncology experimental therapeutics investigators consortium study. Clin Cancer Res 13: 1783–1788
7. Ramanathan RK, Egorin MJ, Eiseman JL et al. (2007) Phase I and pharmacodynamic study of 17-(allylamino)-17-demethoxygeldanamycin in adult patients with refractory advanced cancers. Clin Cancer Res 13: 1769–1774
8. Solit DB, Ivy SP, Kopil C et al. (2007) Phase I trial of 17-allylamino-17-demethoxygeldanamycin in patients with advanced cancer. Clin Cancer Res 13: 1775–1782
9. Weigel BJ, Blaney SM, Reid JM et al. (2007) A phase I study of 17-allylaminogeldanamycin in relapsed/refractory pediatric patients with solid tumors: a Children's Oncology Group study. Clin Cancer Res 13: 1789–1793
10. Modi S, Stopeck AT, Gordon MS et al. (2007) Combination of trastuzumab and tanespimycin (17-AAG, KOS-953) is safe and active in trastuzumab-refractory HER-2 overexpressing breast cancer: a phase I dose-escalation study. J Clin Oncol 25: 5410–5417
11. Tse AN, Klimstra DS, Gonen M et al. (2008) A phase 1 dose-escalation study of irinotecan in combination with 17-allylamino-17-demethoxygeldanamycin in patients with solid tumors. Clin Cancer Res 14: 6704–6711
12. Heath EI, Hillman DW, Vaishampayan U et al. (2008) A phase II trial of 17-allylamino-17-demethoxygeldanamycin in patients with hormone-refractory metastatic prostate cancer. Clin Cancer Res 14: 7940–7946
13. Solit DB, Osman I, Polsky D et al. (2008) Phase II trial of 17-allylamino-17-demethoxygeldanamycin in patients with metastatic melanoma. Clin Cancer Res 14: 8302–8307
14. Richardson PG, Chanan-Khan AA, Alsina M et al. (2010) Tanespimycin monotherapy in relapsed multiple myeloma: results of a phase 1 dose-escalation study. Br J Haematol 150: 438–445
15. Vaishampayan UN, Burger AM, Sausville EA et al. (2010) Safety, efficacy, pharmacokinetics, and pharmacodynamics of the combination of sorafenib and tanespimycin. Clin Cancer Res 16: 3795–3804
16. Richardson PG, Chanan-Khan AA, Lonial S et al. (2011) Tanespimycin and bortezomib combination treatment in patients with relapsed or relapsed and refractory multiple myeloma: results of a phase 1/2 study. Br J Haematol 153: 729–740
17. Hubbard J, Erlichman C, Toft DO et al. (2011) Phase I study of 17-allylamino-17 demethoxygeldanamycin, gemcitabine and/or cisplatin in patients with refractory solid tumors. Invest New Drugs 29: 473–480
18. Kaufmann SH, Karp JE, Litzow MR et al. (2011) Phase I and pharmacological study of cytarabine and tanespimycin in relapsed and refractory acute leukemia. Haematologica 96: 1619–1626
19. Hendrickson AE, Oberg AL, Glaser G et al. (2012) A phase II study of gemcitabine in combination with tanespimycin in advanced epithelial ovarian and primary peritoneal carcinoma. Gynecol Oncol 124: 210–215

(continued)

Table 1
(continued)

20. Pacey S, Gore M, Chao D et al. (2012) A Phase II trial of 17-allylamino, 17-demethoxygeldanamycin (17-AAG, tanespimycin) in patients with metastatic melanoma. Invest New Drugs 30: 341–349
21. Iyer G, Morris MJ, Rathkopf D et al. (2012) A phase I trial of docetaxel and pulse-dose 17-allylamino-17-demethoxygeldanamycin in adult patients with solid tumors. Cancer Chemother Pharmacol 69: 1089–1097
22. Ramanathan RK, Egorin MJ, Erlichman C et al. (2010) Phase I pharmacokinetic and pharmacodynamic study of 17-dimethylaminoethylamino-17-demethoxygeldanamycin, an inhibitor of heat-shock protein 90, in patients with advanced solid tumors. J Clin Oncol 28: 1520–1526
23. Kummar S, Gutierrez ME, Gardner ER et al. (2010) Phase I trial of 17-dimethylaminoethylamino-17-demethoxygeldanamycin (17-DMAG), a heat shock protein inhibitor, administered twice weekly in patients with advanced malignancies. Eur J Cancer 46: 340–347
24. Lancet JE, Gojo I, Burton M et al. (2010) Phase I study of the heat shock protein 90 inhibitor alvespimycin (KOS-1022, 17-DMAG) administered intravenously twice weekly to patients with acute myeloid leukemia. Leukemia 24: 699–705
25. Pacey S, Wilson RH, Walton M et al. (2011) A phase I study of the heat shock protein 90 inhibitor alvespimycin (17-DMAG) given intravenously to patients with advanced solid tumors. Clin Cancer Res 17: 1561–1570
26. Jhaveri K, Miller K, Rosen L et al. (2012) A phase I dose-escalation trial of trastuzumab and alvespimycin hydrochloride (KOS-1022; 17 DMAG) in the treatment of advanced solid tumors. Clin Cancer Res 18: 5090–5098
27. Maddocks K, Hertlein E, Chen TL et al. (2016) A phase I trial of the intravenous Hsp90 inhibitor alvespimycin (17-DMAG) in patients with relapsed chronic lymphocytic leukemia/small lymphocytic lymphoma. Leuk Lymphoma 57: 2212–2215
28. Do K, Speranza G, Chang LC et al. (2015) Phase I study of the heat shock protein 90 (Hsp90) inhibitor onalespib (AT13387) administered on a daily for 2 consecutive days per week dosing schedule in patients with advanced solid tumors. Invest New Drugs 33: 921–930
29. Shapiro GI, Kwak E, Dezube BJ et al. (2015) First-in-human phase I dose escalation study of a second-generation non-ansamycin HSP90 inhibitor, AT13387, in patients with advanced solid tumors. Clin Cancer Res 21: 87–97
30. Sessa C, Shapiro GI, Bhalla KN et al. (2013) First-in-human phase I dose-escalation study of the HSP90 inhibitor AUY922 in patients with advanced solid tumors. Clin Cancer Res 19: 3671–3680
31. Gaykema SB, Schroder CP, Vitfell-Rasmussen J et al. (2014) 89Zr-trastuzumab and 89Zr-bevacizumab PET to evaluate the effect of the HSP90 inhibitor NVP-AUY922 in metastatic breast cancer patients. Clin Cancer Res 20: 3945–3954
32. Seggewiss-Bernhardt R, Bargou RC, Goh YT et al. (2015) Phase 1/1B trial of the heat shock protein 90 inhibitor NVP-AUY922 as monotherapy or in combination with bortezomib in patients with relapsed or refractory multiple myeloma. Cancer 121: 2185–2192
33. Dickson MA, Okuno SH, Keohan ML et al. (2013) Phase II study of the HSP90-inhibitor BIIB021 in gastrointestinal stromal tumors. Ann Oncol 24: 252–257
34. Saif MW, Takimoto C, Mita M et al. (2014) A phase 1, dose-escalation, pharmacokinetic and pharmacodynamic study of BIIB021 administered orally in patients with advanced solid tumors. Clin Cancer Res 20: 445–455
35. Hong D, Said R, Falchook G et al. (2013) Phase I study of BIIB028, a selective heat shock protein 90 inhibitor, in patients with refractory metastatic or locally advanced solid tumors. Clin Cancer Res 19: 4824–4831
36. Isambert N, Delord JP, Soria JC et al. (2015) Debio0932, a second-generation oral heat shock protein (HSP) inhibitor, in patients with advanced cancer-results of a first-in-man dose-escalation study with a fixed-dose extension phase. Ann Oncol 26: 1005–1011
37. Spreafico A, Delord JP, De Mattos-Arruda L et al. (2015) A first-in-human phase I, dose-escalation, multicentre study of HSP990 administered orally in adult patients with advanced solid malignancies. Br J Cancer 112: 650–659

38. Siegel D, Jagannath S, Vesole DH et al. (2011) A phase 1 study of IPI-504 (retaspimycin hydrochloride) in patients with relapsed or relapsed and refractory multiple myeloma. Leuk Lymphoma 52: 2308–2315
39. Wagner AJ, Chugh R, Rosen LS et al. (2013) A phase I study of the HSP90 inhibitor retaspimycin hydrochloride (IPI-504) in patients with gastrointestinal stromal tumors or soft-tissue sarcomas. Clin Cancer Res 19: 6020–6029
40. Yong K, Cavet J, Johnson P et al. (2016) Phase I study of KW-2478, a novel Hsp90 inhibitor, in patients with B-cell malignancies. Br J Cancer 114: 7–13
41. Rajan A, Kelly RJ, Trepel JB et al. (2011) A phase I study of PF-04929113 (SNX-5422), an orally bioavailable heat shock protein 90 inhibitor, in patients with refractory solid tumor malignancies and lymphomas. Clin Cancer Res 17: 6831–6839
42. Reddy N, Voorhees PM, Houk BE et al. (2013) Phase I trial of the HSP90 inhibitor PF-04929113 (SNX5422) in adult patients with recurrent, refractory hematologic malignancies. Clin Lymphoma Myeloma Leuk 13: 385–391
43. Goldman JW, Raju RN, Gordon GA et al. (2013) A first in human, safety, pharmacokinetics, and clinical activity phase I study of once weekly administration of the Hsp90 inhibitor ganetespib (STA-9090) in patients with solid malignancies. BMC Cancer 13: 152–161
44. Socinski MA, Goldman J, El-Hariry I et al. (2013) A multicenter phase II study of ganetespib monotherapy in patients with genotypically defined advanced non-small cell lung cancer. Clin Cancer Res 19:3068–3077
45. Cercek A, Shia J, Gollub M et al. (2014) Ganetespib, a novel Hsp90 inhibitor in patients with KRAS mutated and wild type, refractory metastatic colorectal cancer. Clin Colorectal Cancer 13:207–212
46. Ramalingam S, Goss G, Rosell R et al. (2015) A randomized phase II study of ganetespib, a heat shock protein 90 inhibitor, in combination with docetaxel in second-line therapy of advanced non-small cell lung cancer (GALAXY-1). Ann Oncol 26:1741–1748
47. Thakur MK, Heilbrun LK, Sheng S et al. (2016) A phase II trial of ganetespib, a heat shock protein 90 Hsp90) inhibitor, in patients with docetaxel-pretreated metastatic castrate-resistant prostate cancer (CRPC)-a prostate cancer clinical trials consortium (PCCTC) study. Invest New Drugs 34: 112–118

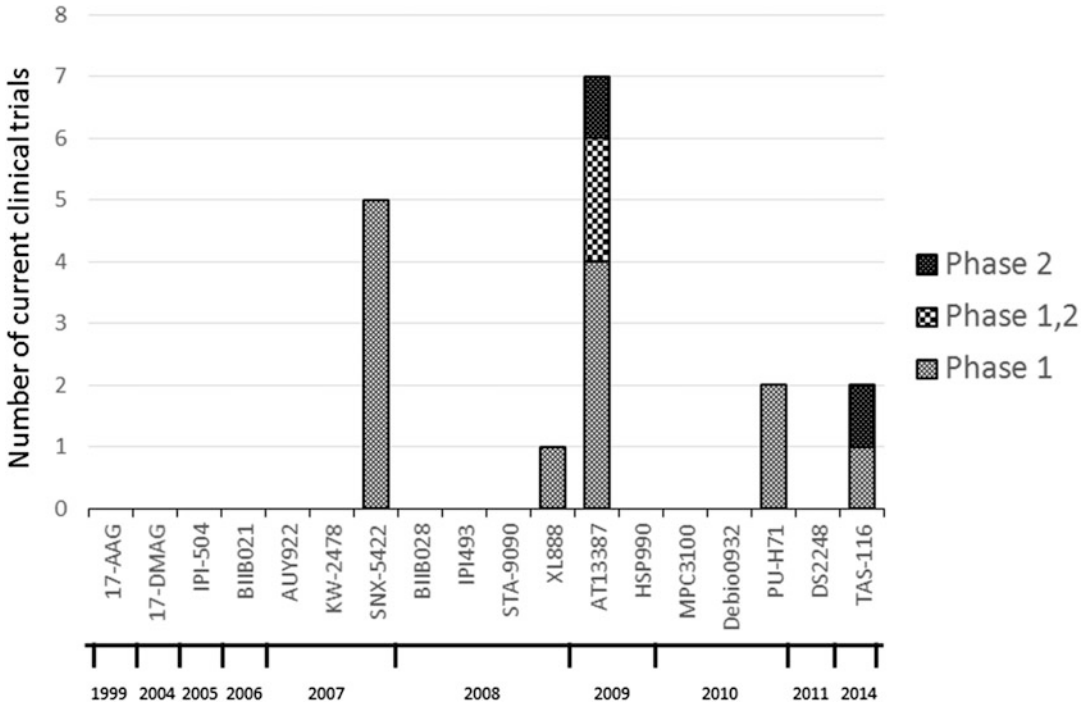

Fig. 1 A timeline of the year each Hsp90 inhibitor entered clinical trial and the current status of clinical development

potential new approaches to clinical development of Hsp90 inhibitors that leverage the unique biology of the Hsp90 chaperone.

1.3 Hsp90 Inhibitor Clinical Trials

It is clear from Fig. 1 that although 18 Hsp90 inhibitors entered clinical development there are many fewer that are currently undergoing clinical evaluation (see also Table 2). There are various possible reasons for this contraction in the field, including that Hsp90 may not be a viable anticancer target. It is still possible however that the N-terminal Hsp90 inhibitors can be successfully developed. The most intensively studied Hsp90 inhibitor, 17-AAG, was terminated for non-clinical reasons, which may have included rapidly expiring patent life and anticipated competition from synthetic Hsp90 inhibitors. A noteable commentary by Carlos Arteaga of the Vanderbilt-Ingram Cancer Center entitled "Why is this effective HSP90 inhibitor not being developed in HER2+ breast cancer?" [17] was published in *Clinical Cancer Research* primarily directed at the drug sponsor, who had closed down the 17-AAG (tanespimycin) program shortly after the completion of a promising trial in HER2+ breast cancer at Memorial Sloan Kettering Cancer Center reported in the same issue of *Clinical Cancer Research* [13]. The author goes on to say "With the positive outcome of this trial, it is then disappointing to read in the report by Modi et al. that 'the development of tanespimycin as a cancer

Table 2
Active HSP90 inhibitor clinical trials

Trial No.	Inhibitor	Combined therapy	Phase	Status	Indication
NCT02973399	SNX-5422	Ibrutinib	I	Recruiting	Chronic lymphocytic leukemia
NCT02914327	SNX-5422	Ibrutinib	I	Recruiting	Chronic lymphocytic leukemia
NCT02063958	SNX-5422	Everolimus	I	Active, not recruiting	Neuroendocrine tumors
NCT01635712	SNX-5422		I	Active, not recruiting	Refractory hematological malignancies
NCT01892046	SNX-5422	Carboplatin and paclitaxel	I	Active, not recruiting	Solid tumors
NCT02721459	XL888	Vemurafenib, cobimetinib	I	Recruiting	Unresectable BRAF mutated stage III/IV melanoma
NCT01712217	AT13387	Crizotinib	I,II	Active, not recruiting	Non-small cell lung cancer (NSCLC)
NCT02503709	AT13387	CDKI AT7519	I	Recruiting	Solid tumors that are metastatic or unresectable
NCT02097225	AT13387	Dabrafenib, trametinib	I	Recruiting	Recurrent melanoma or solid tumors that are metastatic or unresectable
NCT02572453	AT13387		II	Recruiting	Relapsed or refractory anaplastic large cell lymphoma, mantle cell lymphoma, or diffuse large B-cell lymphoma
NCT02381535	AT13387	Radiation therapy and cisplatin	I	Active, not recruiting	Advanced squamous cell carcinoma of the head and neck
NCT02535338	AT13387	Erlotinib hydrochloride	I,II	Recruiting	Recurrent or metastatic EGFR-mutant non-small cell lung cancer
NCT02474173	AT13387	Paclitaxel	I	Recruiting	Advanced triple negative breast cancer
NCT01393509	PU-H71		I	Recruiting	Advanced malignancies
NCT01269593	PU-H71		I	Recruiting	Non-Hodgkin's lymphoma, myeloma, active solid malignancy
JapicCTI-142444	TAS-116		I	Recruiting	Advanced solid tumors
JapicCTI-163182	TAS-116		II	Recruiting	Advanced gastrointestinal stromal tumors (GIST)

therapy has been suspended by the sponsor for non-clinical reasons." Arteaga adds "Through federal grants to academia and/or tax breaks to industry to support the entrepreneurial pursuit of projects that should help society like the one discussed herein, (tax-paying) patients, advocates, and cancer care providers contribute to this research and, therefore, deserve a better explanation as to why the development of this useful therapy is now truncated."

2 Hsp90 Inhibitor Pharmacodynamics

Some additional factors that may have contributed to the inability thus far to bring an Hsp90 inhibitor to regulatory approval are closely connected to the pharmacodynamic markers used in Hsp90 clinical trials. Table 1 compiles the published Hsp90 inhibitor clinical trials and the pharmacodynamic markers analyzed. The most common cells analyzed for biomarkers were peripheral blood mononuclear cells (PBMCs). It is understandable why this tumor surrogate was used, because in patients with locally advanced or metastatic cancer it is very difficult to obtain biopsies pre- and post-therapy, while obtaining peripheral blood samples pre- and post-therapy is almost always feasible. There are, however, several reasons why PBMCs are not an optimal surrogate for Hsp90 inhibitor clinical trials [18]. One is that Hsp90 inhibitors accumulate in tumor while they are rapidly cleared from plasma and normal tissue. Thus, the pharmacokinetics (PK) of Hsp90 inhibitors differs significantly between tumor and normal tissue [19, 20]. In addition, certain tumor cells appear to be more sensitive to N-terminal Hsp90 inhibitors than normal cells [21, 22]. As reported by Kamal et al. [21] the Hsp90 complex in cancer cells is biochemically distinct from nontransformed cells, contributing to a high affinity binding state for certain Hsp90 inhibitors. As expanded upon by Chiosis and colleagues [23, 24], in approximately 50% of cancer cells, especially in MYC-fueled tumors, Hsp90 and Hsc70 can act as nucleation sites for functionally integrated complexes termed the epichaperome, which, can confer sensitivity to Hsp90 inhibitors.

2.1 Client Protein Degradation and Imaging

An additional reason why PBMCs are not optimal as a surrogate is that many of the most sensitive Hsp90 client proteins are putative tumor drivers that are not expressed in PBMCs, including ALK fusion proteins and HER2. Since most studies of PBMCs have looked at client protein degradation, the differential PK and client protein expression between PBMCs and tumor, together with the generally low response rate, may explain why PBMC studies of client proteins have not significantly correlated with dose, response, or survival.

The great majority of samples analyzed for the pharmacodynamic end point of client protein degradation were PBMCs. Although tumor was obtained pre- and post-therapy in a number of trials, the number of samples was very small. The response of client protein degradation in tumor samples was variable, with reports of variability among patients in a trial, intrapatient variability at different time points, and variability depending on the client chosen for analysis. In a trial of 17-AAG reported by Solit and Rosen and collaborators in which pharmacodynamic assessment of tumor was a major goal, 15 patients with metastatic melanoma had evaluable pretreatment and posttreatment tumor, which was analyzed by western blot for cyclin D1, tyrosinase, Hsp70, B-RAF, c-RAF, ERK, and phospho-ERK. No objective clinical responses were observed. The western blot analysis showed an increase in Hsp70, a decrease in cyclin D1, but no significant effect on RAF kinases or phospho-ERK, even among the nine patients with tumor *BRAF* mutations. This failure to impact B-RAF and phospho-ERK was interpreted as lack of target engagement. The authors stated "Rather than simply rejecting hsp90 inhibition as a strategy, we are able to report that we did not adequately "hit the target"; thus, hsp90 inhibition remains an appealing approach" [25]. They concluded that a better Hsp90 inhibitor or a better 17-AAG formulation was needed. A new 17-AAG formulation was developed and shown to be well tolerated with similar pharmacokinetics to the less tolerable Cremophor formulation in a clinical trial published contemporaneously with the closure of the 17-AAG program [26].

Hsp90 inhibitor trials are amenable to multiple noninvasive imaging approaches. These include imaging of tumor burden and pharmacodynamic response with FDG-PET to assess metabolism, particularly in highly glycolytic tumors, 89Zr-trastuzumab to monitor levels of HER2 protein, 89Zr-bevacizumab to detect antiangiogenic activity, and 124I-PU-H71, to image levels of the Hsp90 inhibitor PU-H71 [14].

2.2 Hsp70, HSF1 and Resistance

N-terminal Hsp90 inhibitors induce expression of Hsp70 mRNA and protein. This activity is thought to be mediated by the transcription factor heat shock factor (HSF)1, acting at heat shock response elements in the Hsp70 promoter. Measurement of the induction of Hsp70 has proven to be one of the most reliable Hsp90 inhibitor pharmacodynamic markers. Although used in many trials as a marker of target engagement, it was later appreciated that HSF1 is a master regulator of malignancy [27, 28], and activation of Hsp70 is likely to be a central mechanism of resistance to Hsp90 N-terminal inhibitors. Thus, dosing to the maximum tolerated dose, frequently with concomitant high levels of expression of Hsp70, would be counterproductive, and, conversely, a low level non-heat shock response-inducing Hsp90 inhibitor regimen in a combination therapy trial may function to inhibit the emergence of resistance [29]. A number of efforts are now underway to

develop small molecules that block the cytoprotective HSF1 stress response, including drugs targeted at the Hsp70 chaperone [30–32].

2.3 Nuclear Functions of Hsp90

There are an ever-expanding number of critical nuclear events regulated by Hsp90 [18], including transcriptional regulation, RNA polymerase II pausing [33], mRNA splicing, and induction of apoptosis [34]. One reason these events have been underappreciated may relate to the specific posttranslational modifications that drive the chaperone cycle and modulate Hsp90 function [35–38]. For example, DNA damage can induce phosphorylation of threonines 5 and 7 of Hsp90 alpha and facilitate assembly of the nuclear apoptotic ring, DNA fragmentation, and apoptotic body formation, but without a phosphosite-specific antibody it is difficult to detect DNA damage-induced phospho-threonine 5/7 [34]. Hsp90 is subject to and regulated by multiple posttranslational modifications (PTMs), including serine, threonine and tyrosine phosphorylation, acetylation, SUMOylation, O-linked glycosylation, and S-nitroylation, and many of these PTMs occur at multiple sites and different site-specific PTMs have been shown to control diverse aspects of chaperone function. Thus, there are pivotal functions of Hsp90 that may not be detected unless interrogated with an antibody that is both site- and PTM-specific. As proposed by Sawarkar and Paro, the Hsp90 interactome, which can be examined in a database of interactors maintained by Didier Picard and colleagues at the University of Geneva (http://www.picard.ch/Hsp90Int/index.php), suggests that in addition to direct involvement in chromatin, there is a nidus of Hsp90 interactors among RNA processing/spicing proteins and DNA replication/damage-response proteins, and, given the diversity of its clients, Hsp90 may functionally coordinate processes such as the DNA damage response, splicing, replication, transcription, and nuclear architecture [39].

2.4 Hsp90 and Immunity

There is a long history of studying the role of Hsp90 in immunity (for review see [40]). It is surprising, therefore, that there have been no studies of Hsp90 inhibitors on immunity in the tumor microenvironment or on systemic immunity in patients on clinical trial, and there have been no studies to date combining an Hsp90 inhibitor with an immune-targeted therapy, including vaccines and checkpoint inhibitors. An interesting new approach to understanding anticancer immunity that incorporates analysis of Hsp90 is immunogenic cell death (ICD), which posits that tumor can die in a mode that will induce tolerance and inhibition of antitumor immunity, or in a manner that gives rise to increased cell surface expression of Hsp90, Hsp70, and calreticulin, as well as secretion of ATP and HMGB1, leading to induction of adaptive immunity and immunologic memory [41]. It is critical to understand how to make therapy less toleragenic and to enhance anticancer immunity, with the goal of inducing an abscopal, sustained systemic antitumor

response. Knowledge gained of the role of Hsp90 in the ICD process will greatly enhance the value of targeting Hsp90 as a component of a multipronged therapeutic regimen.

3 Future of Hsp90 Inhibitor Clinical Development

3.1 New N-terminal Hsp90 Inhibitor

The latest Hsp90 inhibitor to enter clinical trial is the Taiho compound TAS-116. Interestingly, TAS-116 appears to be one of the less potent and most selective Hsp90 inhibitors, i.e., it inhibits Hsp90 alpha and beta but not Hsp90 family members GRP94 and TRAP1, while retaining the property of the N-terminal inhibitors of selective accumulation in tumor [42]. It remains to be seen if TAS-116 has improved efficacy, but it is possible that a less potent, more selective inhibitor may be less likely to trigger resistance mechanisms, while having a blunted negative impact on host homeostasis, including systemic immunity.

3.2 Hsp90 Inhibitor-Drug Conjugates

Hsp90 inhibitor-drug conjugates (HDC) are a potentially exciting new approach to leveraging the biology of Hsp90 and small-molecule Hsp90 inhibitors. The HDC concept of linking an Hsp90 inhibitor via a cleavable linker to a cytotoxic payload, allowing the Hsp90 inhibitor to mediate tumor-selective targeting and retention of the payload, was developed at Synta Pharmaceuticals. In 2013, Synta opened a randomized Phase 3 trial of docetaxel versus docetaxel plus ganetespib in second-line treatment of non-small cell lung adenocarcinoma. In 2015, a planned interim analysis suggested the addition of ganetespib was unlikely to demonstrate a statistically significant improvement in overall survival compared to docetaxel alone. This had severe financial repercussions for Synta, who then merged with Madrigal Pharmaceuticals, resulting in termination of ganetespib development. They also chose not to further develop the HDC platform, which they licensed to Tarveda Therapeutics. The first-in-human clinical trial is scheduled to open at the NIH Clinical Center in the second quarter of 2017. The trial will be of PEN-866 (formerly known as STA-8666), which consists of an Hsp90 inhibitor, STA-8663, attached via a cleavable linker to SN-38, the active metabolite of the topoisomerase I inhibitor irinotecan. SN-38 cannot be administered directly to patients, due to poor solubility and toxicity. Conversion of irinotecan to SN-38, which is 100–1000 times more potent than irinotecan, is inefficient and variable in human patients. In a recent study in pediatric sarcoma models short-term treatment with the STA-8666 HDC induced prolonged complete tumor regression that was superior to irinotecan [43].

3.3 New Indications

Hsp90 inhibitors have shown preclinical activity in a variety of non-oncologic model systems, including neurodegenerative

disease, where Hsp90 clients play an important role in regulating protein folding and aggregation, including polyglutamine repeat expansions of the androgen receptor in spinal and bulbar muscular atrophy, huntingtin in Huntington's disease, tau in Alzheimer's disease, and α-synuclein in Parkinson's disease (for review see [44]). In the protein conformational disease cystic fibrosis, it has been shown that the most common mutation, a deletion of phenylalanine 508 in the cystic fibrosis transmembrane conductance regulator (CFTR), drives the proteasomal degradation of the CFTR. Hsp90 and its co-chaperones have been shown to play an important role in triage of the mutant CFTR to the proteasome, and targeting the chaperone may facilitate rescue of misfolded CFTR [45, 46]. The dependence of viruses on Hsp90, and their concomitant sensitivity to Hsp90 inhibitors has been studied by Frydman and colleagues [47, 48]. Mollapour et al. recently reviewed Hsp90 as a target in non-oncology indications [49], focusing on viral (HIV, Kaposi's sarcoma-associated herpes virus), fungal, and parasitic (parasitic nematodes, leishmaniasis, trypanosomiasis, and malaria) disease.

Kenney and colleagues have been studying the potential strategy of using Hsp90 inhibitor therapy to prevent the outgrowth of EBV-infected malignant cells via Hsp90 inhibitor-induced degradation of EBNA1, an Hsp90 client and the only EBV protein required for sustained latent EBV infection of host cells [50]. Recently, Jeff Cohen of the National Institute of Allergy and Infectious Diseases, NIH treated a patient with T cell chronic active EBV infection with an Hsp90 inhibitor, the first patient treated with an Hsp90 inhibitor outside a cancer indication. He was able to show that in response to Hsp90 inhibitor treatment there was a reduced percentage of EBV-positive cells in blood [51].

4 Concluding Remarks

Several N-terminal Hsp90 inhibitors remain in clinical development and a novel Hsp90 inhibitor-drug conjugate is due to enter clinical trial in the first half of 2017. Biomarker studies to date have tended to focus on a limited vision of Hsp90 function. As highlighted by Picard and colleagues, there is a tendency to look at the "usual suspects," and ignore a multitude of Hsp90 interaction partners and clients that are drivers in diverse aspects of malignancy, and which may provide new biomarkers of target engagement and potentially new therapeutic targets [52]. A more comprehensive approach to biomarker development and implementation, incorporating recent discoveries in Hsp90 biology, would facilitate progress in Hsp90 inhibitor and Hsp90 inhibitor drug conjugate clinical development. The biomarker profiling of Hsp90 inhibitors has tended to overlook the host, even though the induction of Hsp70

in PBMCs demonstrates that both tumor and host are being exposed to drug levels sufficient to modulate transcriptional programs and impact phenotype. Within the cell, analysis has focused on regulation of client protein levels, while other critical activities of Hsp90 that may be associated with the malignant phenotype, including, among an array of nuclear activities [39, 53], RNA polymerase II pausing [33] and mRNA splicing [54, 55] have not been considered in understanding clinical response. Considerable research has been directed at understanding the role of Hsp90 in immunity [40, 56]. However, in Hsp90 inhibitor clinical studies this critical aspect of host response, i.e., the analysis of Hsp90 inhibitor impact on systemic immunity and the tumor microenvironment [57] has been neglected. Incorporating these pharmacodynamic endpoints will help to advance understanding of the role of Hsp90 in immune cell regulation and facilitate combination of Hsp90 inhibitors with immunotherapy. There have been advances in understanding of the Hsp90 chaperone machinery and the epichaperome [24] and relationship of Hsp90 inhibition to the oncogenic program regulated by HSF1 [28]. Realization of the full potential of Hsp90 inhibitors will be facilitated by translation of this new understanding into biomarker analysis of target engagement in patients in Hsp90 inhibitor and Hsp90 inhibitor drug conjugate clinical trials.

Acknowledgments

This work was supported by the Intramural Research Program, Center for Cancer Research, National Cancer Institute, National Institutes of Health.

References

1. Ritossa F (1962) New puffing pattern induced by temperature shock and Dnp in Drosophila. Experientia 18:571–573
2. Tissieres A, Mitchell HK, Tracy UM (1974) Protein synthesis in salivary glands of Drosophila melanogaster: relation to chromosome puffs. J Mol Biol 84:389–398
3. Pratt WB (1987) Transformation of glucocorticoid and progesterone receptors to the DNA-binding state. J Cell Biochem 35:51–68
4. Smith DF, Whitesell L, Nair SC et al (1995) Progesterone receptor structure and function altered by geldanamycin, an hsp90-binding agent. Mol Cell Biol 15:6804–6812
5. Pratt WB, Toft DO (1997) Steroid receptor interactions with heat shock protein and immunophilin chaperones. Endocr Rev 18:306–360
6. Scheibel T, Buchner J (1998) The Hsp90 complex—a super-chaperone machine as a novel drug target. Biochem Pharmacol 56:675–682
7. Brugge JS, Erikson E, Erikson RL (1981) The specific interaction of the Rous sarcoma virus transforming protein, pp60src, with two cellular proteins. Cell 25:363–372
8. Oppermann H, Levinson W, Bishop JM (1981) A cellular protein that associates with the transforming protein of Rous sarcoma virus is also a heat-shock protein. Proc Natl Acad Sci U S A 78:1067–1071

9. Xu Y, Lindquist S (1993) Heat-shock protein hsp90 governs the activity of pp60v-src kinase. Proc Natl Acad Sci U S A 90:7074–7078
10. Whitesell L, Mimnaugh EG, De Costa B et al (1994) Inhibition of heat shock protein HSP90-pp60v-src heteroprotein complex formation by benzoquinone ansamycins: essential role for stress proteins in oncogenic transformation. Proc Natl Acad Sci U S A 91:8324–8328
11. Schulte TW, Neckers LM (1998) The benzoquinone ansamycin 17-allylamino-17-demethoxygeldanamycin binds to HSP90 and shares important biologic activities with geldanamycin. Cancer Chemother Pharmacol 42:273–279
12. Banerji U, O'Donnell A, Scurr M et al (2005) Phase I pharmacokinetic and pharmacodynamic study of 17-allylamino, 17-demethoxygeldanamycin in patients with advanced malignancies. J Clin Oncol 23:4152–4161
13. Modi S, Stopeck A, Linden H et al (2011) HSP90 inhibition is effective in breast cancer: a phase II trial of tanespimycin (17-AAG) plus trastuzumab in patients with HER2-positive metastatic breast cancer progressing on trastuzumab. Clin Cancer Res 17:5132–5139
14. Jhaveri K, Taldone T, Modi S et al (2012) Advances in the clinical development of heat shock protein 90 (Hsp90) inhibitors in cancers. Biochim Biophys Acta 1823:742–755
15. Marcu MG, Chadli A, Bouhouche I et al (2000) The heat shock protein 90 antagonist novobiocin interacts with a previously unrecognized ATP-binding domain in the carboxyl terminus of the chaperone. J Biol Chem 275:37181–37186
16. Donnelly A, Blagg BS (2008) Novobiocin and additional inhibitors of the Hsp90 C-terminal nucleotide-binding pocket. Curr Med Chem 15:2702–2717
17. Arteaga CL (2011) Why is this effective HSP90 inhibitor not being developed in HER2+ breast cancer? Clin Cancer Res 17:4919–4921
18. Trepel J, Mollapour M, Giaccone G et al (2010) Targeting the dynamic HSP90 complex in cancer. Nat Rev Cancer 10:537–549
19. Xu L, Eiseman JL, Egorin MJ et al (2003) Physiologically-based pharmacokinetics and molecular pharmacodynamics of 17-(allylamino)-17-demethoxygeldanamycin and its active metabolite in tumor-bearing mice. J Pharmacokinet Pharmacodyn 30:185–219
20. Chiosis G, Neckers L (2006) Tumor selectivity of Hsp90 inhibitors: the explanation remains elusive. ACS Chem Biol 1:279–284
21. Kamal A, Thao L, Sensintaffar J et al (2003) A high-affinity conformation of Hsp90 confers tumour selectivity on Hsp90 inhibitors. Nature 425:407–410
22. Woodford MR, Truman AW, Dunn DM et al (2016) Mps1 mediated phosphorylation of Hsp90 confers renal cell carcinoma sensitivity and selectivity to Hsp90 inhibitors. Cell Rep 14:872–884
23. Moulick K, Ahn JH, Zong H et al (2011) Affinity-based proteomics reveal cancer-specific networks coordinated by Hsp90. Nat Chem Biol 7:818–826
24. Rodina A, Wang T, Yan P et al (2016) The epichaperome is an integrated chaperome network that facilitates tumour survival. Nature 538:397–401
25. Solit DB, Osman I, Polsky D et al (2008) Phase II trial of 17-allylamino-17-demethoxygeldanamycin in patients with metastatic melanoma. Clin Cancer Res 14:8302–8307
26. Burris HA III, Berman D, Murthy B et al (2011) Tanespimycin pharmacokinetics: a randomized dose-escalation crossover phase 1 study of two formulations. Cancer Chemother Pharmacol 67:1045–1054
27. Dai C, Whitesell L, Rogers AB et al (2007) Heat shock factor 1 is a powerful multifaceted modifier of carcinogenesis. Cell 130:1005–1018
28. Mendillo ML, Santagata S, Koeva M et al (2012) HSF1 drives a transcriptional program distinct from heat shock to support highly malignant human cancers. Cell 150:549–562
29. Whitesell L, Santagata S, Mendillo ML et al (2014) HSP90 empowers evolution of resistance to hormonal therapy in human breast cancer models. Proc Natl Acad Sci U S A 111:18297–18302
30. Brodsky JL, Chiosis G (2006) Hsp70 molecular chaperones: emerging roles in human disease and identification of small molecule modulators. Curr Top Med Chem 6:1215–1225
31. Whitesell L, Lindquist S (2009) Inhibiting the transcription factor HSF1 as an anticancer strategy. Expert Opin Ther Targets 13:469–478
32. Patury S, Miyata Y, Gestwicki JE (2009) Pharmacological targeting of the Hsp70 chaperone. Curr Top Med Chem 9:1337–1351
33. Sawarkar R, Sievers C, Paro R (2012) Hsp90 globally targets paused RNA polymerase to regulate gene expression in response to environmental stimuli. Cell 149:807–818
34. Solier S, Kohn KW, Scroggins B et al (2012) Heat shock protein 90alpha (HSP90alpha), a

substrate and chaperone of DNA-PK necessary for the apoptotic response. Proc Natl Acad Sci U S A 109:12866–12872

35. Mollapour M, Neckers L (2012) Post-translational modifications of Hsp90 and their contributions to chaperone regulation. Biochim Biophys Acta 1823:648–655
36. Zuehlke AD, Beebe K, Neckers L et al (2015) Regulation and function of the human HSP90AA1 gene. Gene 570:8–16
37. Woodford MR, Dunn D, Miller JB et al (2016) Impact of Posttranslational Modifications on the Anticancer Activity of Hsp90 Inhibitors. Adv Cancer Res 129:31–50
38. Prodromou C (2017) Regulatory mechanisms of Hsp90. Biochem Mol Biol J 3:2
39. Sawarkar R, Paro R (2013) Hsp90@chromatin. nucleus: an emerging hub of a networker. Trends Cell Biol 23:193–201
40. Graner MW (2016) HSP90 and immune modulation in cancer. Adv Cancer Res 129:191–224
41. Galluzzi L, Buque A, Kepp O et al (2017) Reply: the complement system is also important in immunogenic cell death. Nat Rev Immunol 17:143
42. Ohkubo S, Kodama Y, Muraoka H et al (2015) TAS-116, a highly selective inhibitor of heat shock protein 90alpha and beta, demonstrates potent antitumor activity and minimal ocular toxicity in preclinical models. Mol Cancer Ther 14:14–22
43. Heske CM, Mendoza A, Edessa LD et al (2016) STA-8666, a novel HSP90 inhibitor/SN-38 drug conjugate, causes complete tumor regression in preclinical mouse models of pediatric sarcoma. Oncotarget 7:65540–65552
44. Pratt WB, Gestwicki JE, Osawa Y et al (2015) Targeting Hsp90/Hsp70-based protein quality control for treatment of adult onset neurodegenerative diseases. Annu Rev Pharmacol Toxicol 55:353–371
45. Wang X, Venable J, LaPointe P et al (2006) Hsp90 cochaperone Aha1 downregulation rescues misfolding of CFTR in cystic fibrosis. Cell 127:803–815
46. Okiyoneda T, Barriere H, Bagdany M et al (2010) Peripheral protein quality control removes unfolded CFTR from the plasma membrane. Science 329:805–810
47. Geller R, Vignuzzi M, Andino R et al (2007) Evolutionary constraints on chaperone-mediated folding provide an antiviral approach refractory to development of drug resistance. Genes Dev 21:195–205
48. Geller R, Taguwa S, Frydman J (2012) Broad action of Hsp90 as a host chaperone required for viral replication. Biochim Biophys Acta 1823:698–706
49. Woodford MR, Dunn DM, Ciciarelli JG et al (2016) Targeting Hsp90 in non-cancerous Maladies. Curr Top Med Chem 16:2792–2804
50. Sun X, Barlow EA, Ma S et al (2010) Hsp90 inhibitors block outgrowth of EBV-infected malignant cells in vitro and in vivo through an EBNA1-dependent mechanism. Proc Natl Acad Sci U S A 107:3146–3151
51. Shatzer A, Ali MA, Chavez M et al (2017) Ganetespib, an HSP90 inhibitor, kills Epstein-Barr virus (EBV)-infected B and T cells and reduces the percentage of EBV-infected cells in the blood. Leuk Lymphoma 58:923–931
52. Vartholomaiou E, Echeverria PC, Picard D (2016) Unusual Suspects in the twilight zone between the Hsp90 interactome and carcinogenesis. Adv Cancer Res 129:1–30
53. Calderwood SK, Neckers L (2016) Hsp90 in cancer: transcriptional roles in the nucleus. Adv Cancer Res 129:89–106
54. Lu Y, Xu W, Ji J et al (2015) Alternative splicing of the cell fate determinant Numb in hepatocellular carcinoma. Hepatology 62:1122–1131
55. Ferraldeschi R, Welti J, Powers MV et al (2016) Second-generation HSP90 inhibitor onalespib blocks mRNA splicing of androgen receptor variant 7 in prostate cancer cells. Cancer Res 76:2731–2742
56. Murshid A, Gong J, Calderwood SK (2010) Heat shock protein 90 mediates efficient antigen cross presentation through the scavenger receptor expressed by endothelial cells-I. J Immunol 185:2903–2917
57. Alarcon SV, Mollapour M, Lee MJ et al (2012) Tumor-intrinsic and tumor-extrinsic factors impacting hsp90-targeted therapy. Curr Mol Med 12:1125–1141

INDEX

A

Annexin V 108, 110, 111, 113, 122
Anti-cancer therapy 120, 190, 378, 380, 384–388
Antigen cross-presentation 332, 347, 350, 352, 353, 360, 386
Apoptosis 110–113, 115–117, 121, 124, 142, 151, 152, 359, 372, 374–378, 380–382, 384, 412, 436
ATPase 77, 79, 88, 93, 179–186, 189, 199–203, 205, 206, 209, 254, 256, 275, 359, 373–376, 378, 381–383, 387, 398, 401–404, 406, 409, 410, 412
ATP hydrolysis 75, 76, 179, 180, 182, 183, 185, 186, 189, 200, 203–206, 254, 256, 373, 376, 397, 398, 403, 409, 410
Autoimmunity molecular mimicry 294, 383

B

Bag1 ..... 76, 186
Binding free energy simulations 258
Biomarkers 294, 315–317, 388, 423–439

C

Cancer 2, 36, 87, 97, 112, 129, 140, 190, 221, 293, 307, 322, 334, 345, 359, 372, 405, 424
Caspase 78, 108, 109, 116–118, 124, 174, 374–378, 381
Cell fusion 362, 364
Chaperone 1, 44, 47, 60, 75, 88, 97, 112, 164, 179, 189, 199, 209, 221, 233, 253, 275, 295, 321, 333, 345, 359, 372, 398, 424
Chaperone/client interactions 47–58, 413
Chaperone network 383
Chaperone vaccine 345–355
Chaperonin 97, 210, 293–295, 346, 350, 378, 384, 410
ChIP-seq 31, 223, 226, 229
Chromatin immunoprecipitation (ChIP) 26, 29–32, 76, 221–226, 228–230
Clients 47, 60, 78, 93, 129, 139, 163, 189, 199, 209, 222, 253, 321, 346, 359, 373, 397, 427
Clinical trial 77, 78, 88, 97, 308, 380, 382, 383, 387, 412, 423–439
Co-chaperones 47, 48, 76, 78, 93, 180–182, 189, 190, 195, 199, 200, 209, 210, 234, 253–262, 266–269, 276, 277, 321, 373, 374, 376, 382–384, 397–414, 438
Colony formation assay 107

D

Dendritic cells (DC) 17, 18, 63, 72, 332, 336, 337, 346, 350, 352, 355, 387
Differential protein expression 140, 151
DnaK 182, 184, 185, 200–203, 205, 373
Drosophila Schneider (S2) cells 223, 226
Drug discovery 79, 382
Drug screen 130, 131, 134

E

Epitope 48, 49, 213, 222, 229, 310, 312, 337, 387
Experimentally-guided protein docking 258, 260
Extracellular heat shock protein 384
Extracellular Heat Shock Protein 90 (eHsp90) 321–328
Extraction of Hsp70 peptide complexes (Hsp70.PC) 333, 359–365

F

Filter retardation assay 60
Firefly luciferase 36, 42, 44, 48, 93
Flow cytometry 17, 18, 58, 100, 102, 111, 112, 122, 307–318, 335, 337, 352, 354
Fluorescence linked enzyme chemoproteomic strategy (FLECS) 75–77, 79–85
Formalin fixed paraffin embedded (FFPE) sections 296, 310, 312
Functional enrichment 289
Fusion mass spectrometer 159

G

Gel-LC 140, 154, 155, 159, 160
Genetic interactions (GI) 276–283, 286, 288
Glioblastoma multiforme (GBM) 315–317

Stuart K. Calderwood and Thomas L. Prince (eds.), *Chaperones: Methods and Protocols*, Methods in Molecular Biology, vol. 1709, https://doi.org/10.1007/978-1-4939-7477-1, © Springer Science+Business Media, LLC 2018

Glucocorticoid receptor (GR) 189–197, 399, 403, 406, 408, 409, 411, 412
Grp170 ..... 181, 186, 338, 346, 348–352, 354
GrpE 181, 182, 186, 200

H

Heat shock factor 1 (HSF1) 23, 24, 26–30, 32, 35, 37, 39, 222, 380, 381, 435, 436, 439
Heat shock factor 2 (HSF2) 24–28
Heat shock protein 70 (Hsp70) 16, 24, 36, 75, 121, 164, 179, 189, 199, 234, 275, 307, 331, 359, 371, 398, 423
Heat shock protein 90 (Hsp90) 24, 35, 47, 76, 87, 97, 112, 129, 139, 164, 189, 199, 209, 221, 234, 253, 275, 321, 332, 360, 372, 397, 423
Heat shock proteins (HSP) 331, 341
Heat shock response (HSR) 14, 23, 35–44, 139, 372, 380
High-throughput screen 42, 87–95, 382
Hop .. 76, 189, 200, 209, 255, 373, 382, 401, 402, 404, 405, 407–410, 412, 413
Hsf1 ..... 1–5, 7–9, 11, 14, 17–19
Hsf2 ..... 1–5, 7–9, 11, 14, 17–19
Hsf4 ..... 1–5, 7–9, 11, 14, 17–19
Hsf4-EGFP 17, 18
Hsp27/B1 168
Hsp60 antibodies 164, 275, 293–301, 331, 372
Hsp70 antibodies 310, 331, 335
Hsp90 ..... 332, 335, 338
Hsp90 Co-chaperones 190, 195, 402, 412
Hsp90 inhibitor-drug conjugate (HDC) 437, 438
Hsp90 inhibitors 77, 87, 88, 112, 129, 130, 139–144, 146–160, 209, 210, 221, 223, 258, 322, 381–384, 398, 399, 408, 412, 413, 433, 439
Hsp110 ..... 24, 181, 182, 186, 338, 346, 348, 350, 351, 354, 373, 383
HspBP1 ..... 181, 186, 373
Huntington's disease (HD) 59, 60, 438

I

Immunity 332, 337, 338, 346, 359, 360, 387, 436, 437, 439
Immunohistochemistry (IHC) 293–301, 310–315
Immunomodulator 371
Immunophilins 405, 409–411, 413
Immunostaining 18, 117, 297, 300, 301
Intracellular and membrane-bound heat shock protein 70 (Hsp70) 307–318

K

Knockout mice 2, 14, 17, 332, 337

L

Lactate dehydrogenase (LDH) release assay 109, 120
Large heat shock protein 338, 350, 354, 355
LC-MS/MS 139–141, 144, 149–160, 284
Luciferase assay 38, 41, 48, 51, 52, 54, 57
LUMIER 47–58, 408

M

MaxQuant 159
Molecular chaperones 1, 97, 164, 189, 199, 200, 209, 253, 275, 276, 321, 331–342, 345, 359, 360, 372, 373, 384, 397, 398, 401, 405–407

N

Necrosis 108, 111, 113, 121, 122, 124, 376
Nuclear run on 31
Nucleotide exchange factor (NEF) 78, 179–186, 200, 373
Nucleotide release 181, 184–186

O

Oligomerization 163–175, 310

P

p23 ..... 189, 200, 209, 223, 254–256, 401–403, 409–413
Perseus 159
Pharmacodynamic assessment 425, 435
Phosphorylation 24, 163–175, 210, 211, 378, 400, 403, 404, 408, 436
Physical interactions 276, 277, 398
Polyglutamine diseases 59–73
PolyQ-peptides 61, 63, 73
Polytherapy 130
Post-translational modification (PTM) 37, 44, 209–214, 216, 222, 321, 398, 404, 408, 436
Prion-like seeding 59
Protein aggregation 59–73, 164, 349, 359, 372
Protein client interactions 164, 173, 255, 256
Protein complexes 75, 285, 286, 352, 354, 373, 376
Protein homeostasis 289, 345, 372
Protein-ligand interactions 259–265
Protein–protein interactions (PPIs) 276, 277, 284, 285, 288
Protein refolding 87

Protein structure network analysis 256, 257, 266–269
Proteomics 47–49, 139–144, 146–160, 172, 276, 277, 284, 402
Protocol techniques 139
Purification 25–28, 48, 79, 82, 149, 150, 186, 228, 238, 284, 335, 348, 363, 409

R

Real-time 35–44, 341
RIPA 142–144, 153, 154, 159
RNA-seq 233–238, 250

S

Saccharomyces cerevisiae 189, 209, 210, 275, 399, 406, 407
Scavenger receptor (SR) 315, 336–338
Senescence 109, 120, 121, 124, 380
Small-molecule inhibitors ... 39, 253–262, 266–269, 322, 381, 412
Small stress proteins (sHsp) 164–166, 171, 172, 174, 275
Steady-state 181, 182, 186, 408
Steady-state ATPase 181–183, 185, 186, 202
Stopped-flow 181, 184–186
SUMOylation 210, 436
Synergy 101, 129–132, 134–137, 200, 205, 382, 411
Systems biology 248

T

Tandem mass spectrometry (TMS) 167
Targeting vector 2–5, 7–9, 11, 12, 14, 15, 18–20
T cell 17, 18, 332, 337, 341, 346, 352, 354, 360, 376, 385–387, 438
T-cell activation 352, 354
Tetrazolium assay 117
Transcription 1, 17, 18, 23–32, 35–37, 42, 79, 190, 209, 221, 222, 234, 238, 253, 331, 348, 372, 376, 379, 380, 384, 399, 400, 404, 410, 411, 423, 435, 436
Tumor vaccine 346, 360
TUNEL 108, 111, 113, 114, 118, 122

U

Ubiquitination 210, 373

V

Viability assays 100, 102, 129–132, 134–137, 322